frontiers | Research Topics

Dynamics of land use and carbon emissions in the context of carbon neutrality and carbon peaking

Edited by
Chenxi Li, Ayyoob Sharifi and Bao-Jie He

Coordinated by
Zhiheng Yang

Published in
Frontiers in Environmental Science

ISSN 1664-8714
ISBN 978-2-8325-5904-8
DOI 10.3389/978-2-8325-5904-8

About Frontiers

Frontiers is more than just an open access publisher of scholarly articles: it is a pioneering approach to the world of academia, radically improving the way scholarly research is managed. The grand vision of Frontiers is a world where all people have an equal opportunity to seek, share and generate knowledge. Frontiers provides immediate and permanent online open access to all its publications, but this alone is not enough to realize our grand goals.

Frontiers journal series

The Frontiers journal series is a multi-tier and interdisciplinary set of open-access, online journals, promising a paradigm shift from the current review, selection and dissemination processes in academic publishing. All Frontiers journals are driven by researchers for researchers; therefore, they constitute a service to the scholarly community. At the same time, the *Frontiers journal series* operates on a revolutionary invention, the tiered publishing system, initially addressing specific communities of scholars, and gradually climbing up to broader public understanding, thus serving the interests of the lay society, too.

Dedication to quality

Each Frontiers article is a landmark of the highest quality, thanks to genuinely collaborative interactions between authors and review editors, who include some of the world's best academicians. Research must be certified by peers before entering a stream of knowledge that may eventually reach the public - and shape society; therefore, Frontiers only applies the most rigorous and unbiased reviews. Frontiers revolutionizes research publishing by freely delivering the most outstanding research, evaluated with no bias from both the academic and social point of view. By applying the most advanced information technologies, Frontiers is catapulting scholarly publishing into a new generation.

What are Frontiers Research Topics?

Frontiers Research Topics are very popular trademarks of the *Frontiers journals series*: they are collections of at least ten articles, all centered on a particular subject. With their unique mix of varied contributions from Original Research to Review Articles, Frontiers Research Topics unify the most influential researchers, the latest key findings and historical advances in a hot research area.

Find out more on how to host your own Frontiers Research Topic or contribute to one as an author by contacting the Frontiers editorial office: frontiersin.org/about/contact

Dynamics of land use and carbon emissions in the context of carbon neutrality and carbon peaking

Topic editors
Chenxi Li — Xi'an University of Architecture and Technology, China
Ayyoob Sharifi — Hiroshima University, Japan
Bao-Jie He — Chongqing University, China

Topic coordinator
Zhiheng Yang — Shandong University of Finance and Economics, China

Citation
Li, C., Sharifi, A., He, B.-J., Yang, Z., eds. (2025). *Dynamics of land use and carbon emissions in the context of carbon neutrality and carbon peaking*.
Lausanne: Frontiers Media SA. doi: 10.3389/978-2-8325-5904-8

Table of contents

frontiers | Frontiers in Environmental Science

TYPE Editorial
PUBLISHED 06 January 2025
DOI 10.3389/fenvs.2024.1546729

OPEN ACCESS

EDITED AND REVIEWED BY
Riccardo Buccolieri,
University of Salento, Italy

*CORRESPONDENCE
Chenxi Li,
lichenxi@xauat.edu.cn

RECEIVED 17 December 2024
ACCEPTED 24 December 2024
PUBLISHED 06 January 2025

CITATION
Yang Z and Li C (2025) Editorial: Dynamics of land use and carbon emissions in the context of carbon neutrality and carbon peaking.
Front. Environ. Sci. 12:1546729.
doi: 10.3389/fenvs.2024.1546729

Editorial: Dynamics of land use and carbon emissions in the context of carbon neutrality and carbon peaking

Zhiheng Yang[1] and Chenxi Li[2]*

[1]Institute of Regional Economics, Shandong University of Finance and Economics, Jinan, China, [2]School of Public Administration, Xi'an University of Architecture and Technology, Xi'an, China

KEYWORDS

dynamics, carbon neutrality, carbon peaking, land use, carbon emissions

Editorial on the Research Topic
Dynamics of land use and carbon emissions in the context of carbon neutrality and carbon peaking

In pursuing carbon neutrality and carbon peak targets, understanding the complex relationship between land use and carbon emissions has become crucial. Changes in land use have significant impacts on carbon emissions/absorption in terrestrial ecosystems, with complex mechanisms, diverse spatial characteristics, and numerous uncertainties, necessitating profound transformations in our approaches to land use and carbon emission management. The research topics covered in this Research Topic encompass the influence of various land use practices associated with different production activities on the carbon cycle from ten national research centers, providing abundant empirical cases and theoretical support for exploring strategies for the sustainable use of land resources and the synergistic optimization of carbon emissions.

Multiple analyses of land use: exploring the cornerstone of sustainable development

Land use trade-offs under the 1.5°C temperature control target

van der Ploeg and Haigh explored the land use competition situation under the 1.5°C climate stabilization scenario, proposed to jointly formulate strong policies and regulations to comprehensively promote the efficient use of land in fields such as food, energy, and nature conservation.

Precise deconstruction of natural land carbon sinks

Qu et al. took the dominant position of forests in the absorption of carbon dioxide on land as the core basis, skillfully integrated the MIT carbon cycle model simulation with the

Shell Energy Security Scenarios emission pathways, and constructed a precise analysis framework for national net-zero emission targets under different scenarios.

Deep exploration of the carbon sink potential in ecologically fragile areas

Wang et al. focused on the Luan River Basin, a typical ecologically fragile area, and used the PLUS-INVEST model to simulate he corresponding carbon sink potential of the land use/land cover change patterns under three different scenarios in 2030, providing scientific guidance for land use planning in ecologically fragile areas.

Industrial transformation: insights into opportunities and challenges of green transformation

The green transformation path of the pulp and paper industry

Laberge et al. took a pulp mill in southern Quebec, Canada as a vivid example and found that through the key strategy of optimizing the utilization of by-products, such as skillfully converting biosolids into fertilizers, providing a valuable reference model for the green transformation of the entire industry.

Examination of the sustainable development of the hemp industry

Meffo Kemda et al. deeply explored the performance of the hemp cultivation process and the seed-based food production process, and accurately evaluated its carbon storage capacity in strict accordance with the IPCC guidelines.

Deciphering the spatiotemporal code of carbon emissions in Jiangsu Province

Cai and Li analyzed the spatiotemporal distribution of carbon emissions based on detailed land use and energy consumption data, the main influencing factors are economic development, industrial structure, energy intensity, etc.

Urban development: exploration of space optimization and green space carbon sinks

Exploration of a new path for urban green space carbon sink accounting

Dong et al. combined meteorology with plant physiology and innovatively proposed a photosynthetic rate estimation method to estimate urban green space carbon sinks, aimed to promote energy conservation and emission reduction through nature-based solutions.

The reorientation strategy for rural industrial parks in Nanhai District

Liu et al. took the redevelopment project of rural industrial parks in Nanhai District as an important breakthrough for phasing out high-polluting industries, proposed to resist the temptation of short-term land transfer revenues to achieve long-term development.

Regional coordinated development: the exploration journey of the integration of carbon emissions and ecology

Coordinated development of carbon emissions and ecosystem health

Qu et al. focused on the spatiotemporal distribution characteristics of carbon emissions and ecosystem health in the southern hilly and mountainous regions of China, found that the imbalance phenomenon still generally existed.

Analysis of the evolution of production-living-ecological space in the Taihang mountain poverty belt

Chen et al. analyzed the evolution process of the production-living-ecological space in the Taihang Mountain poverty belt, found the net carbon emissions due to terrestrial transfers increased over time.

Carbon dynamic tracking of land use in the Baiyangdian Basin

Gao et al. traced back the change tracks of land use and carbon emissions in the Baiyangdian Basin, deeply analyzed the carbon conduction effect with the help of the land transfer matrix, and looked forward to the future trends of land use and carbon emissions under four different scenarios in 2035.

In addition, there are also some new trends, such as digital empowerment to improve the emission reduction efficiency of resource-based cities

Qian and Luo found that digital transformation can significantly improve the land green use efficiency of resource-based cities through multiple paths such as driving technological innovation, promoting industrial structure upgrading, and alleviating the problem of land factor mismatch.

Land systems possess both carbon sequestration and emission functions, and transitioning to carbon neutrality requires maintaining a delicate balance between these two roles. By making conscious and sustainable choices in land use, we can make significant progress in addressing climate change and creating a more resilient and low-carbon future for future generations.

Protecting natural ecosystems

Improve the carbon storage capacity by protecting natural ecosystems such as forests, grasslands, farmlands and wetlands. This includes delimiting and managing ecological protection red lines and nature reserves to make effective use of the carbon sequestration capacity of natural ecosystems.

Optimizing human activities space

With the goal of low carbon emissions, the rational distribution of population and industries should be guided. By optimizing the quantitative structure and spatial pattern of land use, it will be beneficial to adjust the industrial layout, reduce the land use types mainly relying on fossil energy consumption, and improve energy utilization efficiency.

Strengthening land use regulation

Strictly control the expansion of construction land and deforestation to reduce carbon emissions from land use. It is crucial to monitor the carbon emissions and carbon emission intensity of major land use types and strengthen policy interventions in the process of carbon emissions from land use.

Innovating land management measures

Economic and policy incentives can be used to guide farmers to cultivate high-carbon sequestration crops, thereby increasing the carbon storage of farmland and grasslands.

In general, this series of colorful, diverse, and in-depth studies in this issue reveals the complex relationships among land use, carbon emissions, and sustainable development. The various research results echo and closely connect with each other, just like the pieces of a jigsaw puzzle, jointly piecing together a magnificent blueprint for sustainable development. Achieving carbon neutrality and reaching peak emissions is a complex and long-term endeavor, with the dynamics of land use and carbon emissions being integral components of its success. Through measures such as scientific planning, rational layout, technological innovation, and policy guidance, we can promote a virtuous cycle between economic and social development and ecological environmental protection, contributing to the harmonious coexistence between humanity and nature.

Author contributions

ZY: Conceptualization, Writing–original draft, Writing–review and editing. CL: Supervision, Writing–review and editing.

Funding

The author(s) declare that no financial support was received for the research, authorship, and/or publication of this article.

Conflict of interest

The authors declare that the research was conducted in the absence of any commercial or financial relationships that could be construed as a potential conflict of interest.

Generative AI statement

The author(s) declare that no Generative AI was used in the creation of this manuscript.

Publisher's note

frontiers | Frontiers in Environmental Science

TYPE Original Research
PUBLISHED 21 December 2023
DOI 10.3389/fenvs.2023.1289531

OPEN ACCESS

EDITED BY
Ayyoob Sharifi,
Hiroshima University, Japan

REVIEWED BY
Rubing Ge,
Chinese Academy for Environmental Planning, China
Junsong Jia,
Jiangxi Normal University, China

*CORRESPONDENCE
Luo Guo,
guoluo@muc.edu.cn

RECEIVED 06 September 2023
ACCEPTED 08 December 2023
PUBLISHED 21 December 2023

CITATION
Qu H, You C, Wang W and Guo L (2023), Exploring coordinated development and its driving factors between carbon emission and ecosystem health in the southern hilly and mountainous region of China.
Front. Environ. Sci. 11:1289531.
doi: 10.3389/fenvs.2023.1289531

Exploring coordinated development and its driving factors between carbon emission and ecosystem health in the southern hilly and mountainous region of China

Hongjiao Qu[1,2], Chang You[1,2], Weiyin Wang[1,2] and Luo Guo[2]*

[1]School of Ethnology and Sociology, Minzu University of China, Beijing, China, [2]College of Life and Environmental Sciences, Minzu University of China, Beijing, China

Achieving "carbon neutrality" is an inevitable requirement for tackling global warming. As one of the national ecological barriers, the southern hilly and mountainous region (SHMR) shoulder the important mission of taking the lead in achieving "carbon peak" and "carbon neutrality". Thus, it has important scientific significance to explore and analyze how to coordinate ecological development under the background of "double carbon action", and it is a key step to ensure that the region achieves synergistic development of promoting economic development and improving ecosystem health. Therefore, in this study, we aimed to address these gaps by adopting a refined grid scale of 10 km × 10 km to explore the spatial-temporal distribution characteristics of carbon emissions and ecosystem health. Additionally, we established a coupling coordination model of carbon emissions intensity (CEI) and ecosystem health index (EHI) to assess the impact of natural and socio-economic factors on the coupling coordination degree (CCD) in different regions. Our findings are as follows: 1) In the SHMR region, the EHI exhibited a progressive development trend, with spatially increasing values from the south to the north. 2) The spatial discrepancy in CEI has been on the rise, which assumed an increase of 4.69 times, and with an increasingly pronounced pattern of spatial imbalance. Carbon emissions tend to concentrate more in the eastern and northern areas, while they are comparatively lower in the western and southern regions. 3) The R^2 of geographical weighted regression model (GWR) is all above 0.8, and the CCD between CEI and EHI demonstrated a positive developmental state. However, most regions still displayed an imbalanced development, albeit with a slight increase in areas exhibiting a more balanced development state. 4) The driving forces of natural and socio-economic factors had a dual-factor and non-linear enhancement effect on the CCD. The influence of natural factors on CCD has gradually diminished, whereas the influence of socio-economic factors has progressively strengthened.

KEYWORDS

southern hilly and mountai-nous region (SHMR), carbon emission intensity (CEI), ecosystem health index (EHI), coupling coordination degree (CCD), geodetector model

1 Introduction

In the context of the 2030 Agenda for Sustainable Development, the achievement of the Sustainable Development Goals (SDGs) necessitates a comprehensive consideration of the social, economic, and environmental dimensions (UNFCCC, 2015; ICSU, 2017). Sustainable Development Goal number 11 aims to promote the establishment of inclusive, secure, resilient, and sustainable cities and human settlements. This implies the need for harmonized progress in both economic development and ecological environmental protection. Consequently, how to mitigate the significant impact of rapid urbanization on the ecological environment and achieve a green and sustainable path of development is a pivotal concern demanding attention from all nations during the process of urbanization (Ayre and Landis, 2012; Bayliss et al., 2012; Awuah et al., 2020). China, with its rapid urbanization and industrialization, has emerged as the largest global emitter of carbon. The rapid economic growth has notably influenced carbon emissions from ecosystems due to frequent land use changes. Consequently, alterations in land use patterns exert significant effects on ecosystems, which subsequently impact the services they provide. It is important to note that land use changes not only affect the spatial distribution, extent, and intensity of carbon emissions but also modify ecosystem health by altering the spatial distribution of biodiversity, regional resources, and ecosystem types. Thus, achieving a balance between socio-economic development and ecosystem health has become a universal and critical challenge, particularly for China (Lin and Christina, 2019). The Southern Hilly and Mountainous Region (SHMR) represents a crucial component of China's ecological security, playing a fundamental role in regulating local and even global climate, facilitating vegetation restoration, and conserving soil and water resources (Tian et al., 2022). However, due to the concentration of population, land resources in this region have been excessively exploited over an extended period. The long-standing irrational utilization of land resources has resulted in both a low regional production level and a deterioration of the ecological environment. Hence, investigating the spatiotemporal interplay between carbon emissions and ecosystem health in the SHMR holds immense significance for achieving green and sustainable development within this region. Furthermore, it has far-reaching implications for guiding the healthy and sustainable green development of the national ecosystem as a whole.

Both domestic and international research has extensively scrutinized the decoupling effects of carbon emissions and economic growth across various scales, including national levels (Liu et al., 2023), provincial (Zhang et al., 2019), urban (Mcgeeid and York, 2019) and regional (Khan et al., 2020) carbon emissions (Munir et al., 2020), an explanation of the mechanism of carbon emissions from a single land class (Chen et al., 2019b), influencing factors (Xie et al., 2020; Jia et al., 2023), change rules (Yu et al., 2018), efficiency (Zhang et al., 2022), and the relationship between land class change and carbon source/sink (Zhang et al., 2013). A large number of studies have been conducted from the perspectives of spatial differences and associations of carbon emissions (Zhao et al., 2022).

As a crucial focus of macroecology research, the concept of ecosystem health possesses distinct characteristics pertaining to spatial and temporal scales. Among the various scales considered for the study of macro ecosystem management, the region emerges as the most appropriate spatial scale for investigating and evaluating ecosystem health. Regional ecosystem health refers to the capacity of each regional ecosystem to consistently and sustainably provide ecosystem service functions within a specific spatial and temporal framework, while maintaining its own health (Yan et al., 2016). Regional ecosystem health assessment has increasingly gained importance as a research direction within the field of ecosystem health assessment. It amalgamates the evaluation of type quality, quantitative structure, and spatial pattern, with a central focus on ecosystem service functions. Several studies have already been conducted on ecosystem health assessment, encompassing different spatial-temporal and regional scales (Chen et al., 2018), such as provinces (Peng et al., 2017), urban agglomerations (Peng et al., 2018), rivers (Zheng et al., 2008; Xia et al., 2019), and wetlands (Wu and Ding, 2019). The evaluation index system for ecosystem health comprises a set of interconnected and mutually constrained indicators, necessitating the selection of indicators that are both relevant and independent. These indicators should comprehensively reflect the level of health and its changing trends in the ecosystem, while accurately reflecting the objectives of ecosystem management and evaluation. Two main models have been employed in constructing the index system: the pressure-state-response (PSR) model (Shear et al., 2003) and the vigor-organization-resilience (VOR) model (Borja et al., 2006). Additionally, the vigor-organization-resilience-ecosystem service (VORS) model has been developed to address the limitations of the previous two models, as they only measure the state of the ecosystem and external disturbances, disregarding the ability to evaluate the provisioning of ecosystem services (Shen et al., 2016; Chen et al., 2019a). Consequently, this study establishes a comprehensive index framework for evaluating ecosystem health in the SHMR region based on the VORS model.

Few studies have explored the spatial relationship between carbon emissions and ecosystem health. Coupling coordination means that two or more systems interact with each other or within the system and affect and restrict each other, and finally reach a benign interaction of coordinated development relationship, the basic premise of which is that there is a certain connection between the factors coupled with each other (Tian et al., 2022). In other words, carbon emission and ecosystem health form a closely related complex coupled system in the competition and cooperation of mutual support and mutual restriction. By regulating subsystems that have a great influence on the overall evolution of the coupled system, all subsystems are promoted to tolerate each other in the unity of oppositions and eventually tend to coordinate development. Thus, this study constructed a coupling coordination model based on carbon emission and ecosystem health to explore the coupling effect and coordination development level between carbon emission intensity (CEI) and ecosystem health index (EHI) on a spatiotemporal scale. What's more, the heterogeneity or non-stationarity of spatial data relationship is one of the research hotspots in the field of spatial statistics and related applications, and the development of local spatial statistical analysis technology is the key link. Geographically weighted regression (GWR) analysis method was used to solve the geographically weighted regression analysis model, so as to quantitatively reflect the heterogeneity or

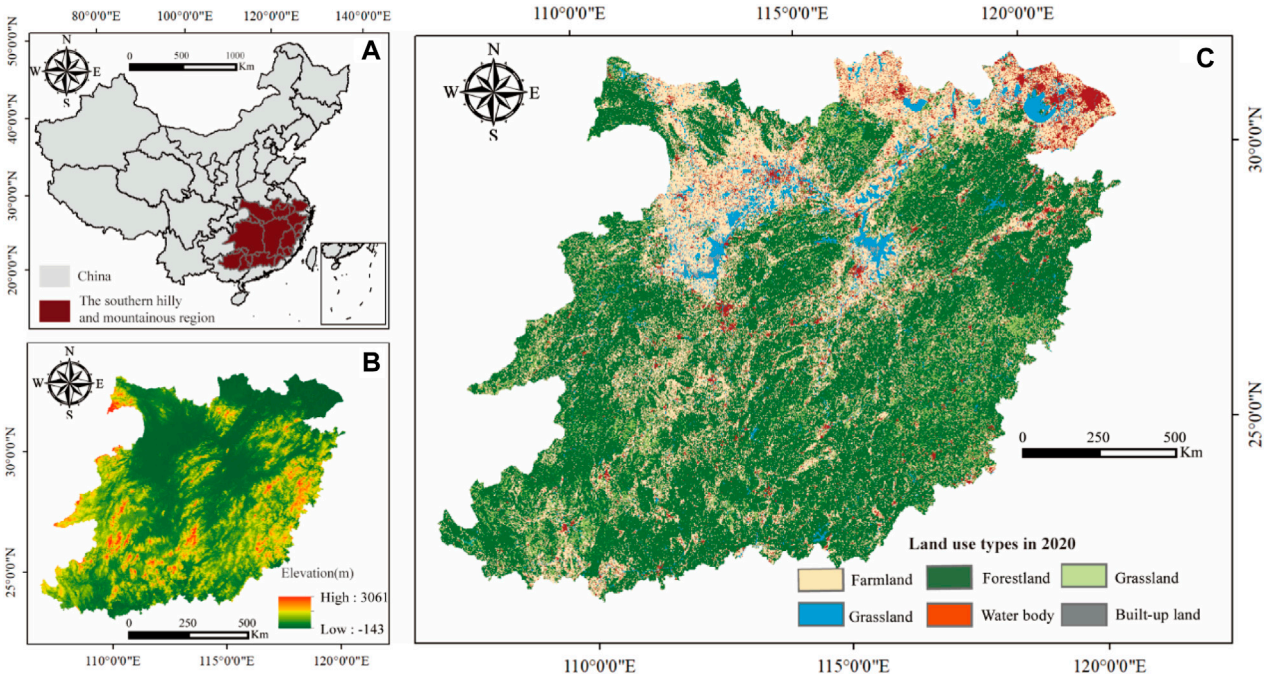

FIGURE 1
(A) Map of study area; **(B)** The DEM of the area; **(C)** The Land use and land cover in 2020.

non-stationary characteristics of spatial data relations by estimating parameters that vary with different spatial locations. Thus, this study further introduced GWR model to explore the spatial heterogeneity of EHI and CEE. In addition, with SHMR ecosystem health as the core, this study aims to propose a new method that can directly verify the specific extent of carbon emission's negative effects on SHMR ecosystem. What's more, the influencing factors of EHI and CEI coupling systems are also discussed. Traditional methods such as the regression model (Chi et al., 2018b), correlation analysis (Bae et al., 2010) and principal component analysis (Cheng et al., 2018) are usually used for this. However, due to the intricate nature of geographical processes, it is not feasible to quantify the interaction and interplay between influencing factors that contribute to spatial differentiation of CCD using traditional statistical regression analysis methods (Ye et al., 2012). In contrast, the geographical detector model offers a unique analytical approach that not only assesses the individual contribution of each factor to the coupled system but also examines the interactive influence of multiple factors on the coupled system (Wang et al., 2016). This interactive analysis aspect is notably absent in other existing studies. Thus, building upon these considerations, this study employed the geodetector model to quantitatively analyze the influencing factors of the CEI and EHI coupling system.

Within the mentioned context, this study primarily investigates the following issues concerning carbon emission and ecosystem health in the SHMR region: 1) What are the spatial-temporal patterns of heterogeneity exhibited by the CEI and EHI within the SHMR region? 2) How does the EHI respond to changes in the CEI during the study period in the SHMR? 3) How does the state of coupling and coordination between the CEI and EHI vary across different regions within the SHMR during the study period? 4) What are the primary drivers that influence the development of coupling systems between the CEI and EHI during the study period? Are there any regional disparities observed in this regard?

1.1 Study area

In Figure 1, the topography of the SHMR exhibits an undulating terrain, complemented by a well-developed water system, numerous rivers, and abundant water resources. This region boasts a wealth of biological species and a diverse array of soil types. The SHMR harbors a flourishing ecosystem, comprising forests, wetlands, grasslands, and more. These ecosystems are characterized by their remarkable biodiversity and impressive carbon storage capacity, rendering them of paramount importance in the context of land use carbon emissions. The SHMR encompasses a diverse range of land use types, including farmland, woodland, and urban areas. It stands out as a vital ecological sanctuary in China, necessitating urgent measures for ecosystem preservation and the attainment of sustainable development. Over the past two decades, the SHMR has encountered significant transformations in land use patterns and ecological landscapes due to intensified human intervention. As a consequence, ecosystems have experienced a precipitous decline, leading to the deterioration of their critical functions pertaining to ecosystem services. These changes bear profound implications for the overall wellbeing of the ecosystems. Concurrently, the surge in carbon emissions has engendered environmental predicaments that pose a substantial threat to social productivity and introduce considerable risks to the natural ecosystem within the SHMR region. The stark contrast between ecological health and economic development has garnered

widespread attention. Therefore, enhancing the ecosystem health of the SHMR and achieving carbon peaking and carbon neutrality assume paramount significance in pursuit of green and sustainable development.

It is noteworthy that, in comparison to certain urban conglomerations, the SHMR exhibits a more intricate interplay of topographic and geomorphic features, thereby endowing its ecosystem with complexity and diversity. Moreover, the SHMR's warm and humid climate, abundant vegetation, and diverse land use types distinguish it from grasslands and plateaus, which tend to possess relatively homogenous ecosystems. Consequently, the SHMR exerts a more pronounced influence on land use carbon emissions. In summary, the SHMR presents an ideal milieu for investigating the correlation between ecosystem health and carbon emissions.

1.2 Data sources and processing

The spatial datasets employed in this investigation were primarily sourced from the esteemed Resources and Environmental Science Data Centre and National Academy of Sciences of China, accessible at the URL http://www.resdc.cn. These datasets encompassed a comprehensive land use classification framework, delineated into six distinct categories, namely cultivated land, forest land, grassland, water bodies, construction land, and unused land. The resolution of these datasets was finely delineated at 1 km × 1 km, ensuring a meticulous and granular analysis. Furthermore, the study also integrated climate data of equally impressive resolution (1 km × 1 km), encapsulating average annual precipitation and average annual temperature. Additionally, datasets pertaining to net primary productivity (NPP), digital elevation model (DEM), population density (PD), and gross domestic product density (GDPD) were also included, all meticulously resolved at the spatial resolution of 1 km × 1 km. To augment the comprehensive analysis, various statistical metrics were culled from the esteemed Statistical Yearbook of the SHMR provinces, spanning the time frame from 1990 to 2020. These encompassed vital aspects such as food production, energy consumption, and other pertinent variables, thereby enriching the comprehensiveness and robustness of the investigation.

1.3 Methods

1.3.1 Quantifying carbon emission efficiency (CEI)

The calculation of carbon emission is to multiply the area of each land use type with its corresponding carbon emission coefficient, and then carry out the sum calculation. The calculation formula is below (Zhang et al., 2014):

$$E_K = \sum e_i = \sum S_i \times \delta_i \quad (1)$$

In this equation, the variable E_K represents the direct carbon emissions, while e_i signifies the carbon emissions associated with each land use type. Moreover, S_i and δ_i represent the area and carbon emission coefficient of land use type i, respectively, indicating the carbon emission coefficient specific to each land-use type. To establish the carbon emission coefficients for each land use type, relevant literature and the specific conditions of the study area were meticulously examined. The carbon emission coefficients were determined as follows: cultivated land (0.422), forest land (−0.644), grassland (−0.022), water bodies (−0.253), and unused land (−0.005) (Cai et al., 2005). The carbon emissions attributed to build-up land were calculated based on fossil energy consumption and subsequently divided by the area to derive the carbon emission intensity of such land. The estimation of carbon emissions from build-up land was accomplished through an indirect estimation method, wherein data from the China Energy Statistical Yearbook were integrated along with various energy consumption patterns and corresponding carbon emission coefficients (Table 1) (Lai et al., 2016).

Carbon emission calculation formula of build-up land (Wu et al., 2022):

$$E_\eta = \sum e_i = \sum E_i \times \mu_i \times \varepsilon_i \quad (2)$$

In this equation, the variable E_η represents the carbon emission emanating from built-up land, whereas e_i signifies the carbon emission generated by the consumption of energy i. Furthermore, E_i denotes the consumption of energy i, while μ_i represents the conversion coefficient of energy i consumption into standard coal. Additionally, the carbon emission coefficient of energy i is signified by ε_i.

The CEI of land use is established by considering both the area and carbon emission coefficient associated with each land use type within a grid. Consequently, a higher carbon emission intensity implies a greater carbon emission within the cell (Friedlingstein et al., 2010).

$$C_{lucc} = \sum_{i=1}^{n} \frac{S_i P_i}{S} \quad (3)$$

In this equation, denoted by C_{lucc}, the CEI is calculated. The variables S_i and P_i correspond to the area and carbon emission coefficient, respectively, of land use type i within the grid. Additionally, the total area of the grid is represented by the variable S. The CEI of build-up land is the value of carbon emissions of build-up land within each grid.

1.3.2 Constructing the ecosystem health assessment framework

An ecologically robust regional ecosystem should uphold its integrity, exhibit inherent self-regulatory capabilities, and offer consistent and sustainable ecosystem services to humanity. Drawing upon a comprehensive review of existing research findings, the vigor-organization-resilience-services (VORS) model has been chosen as the foundation for developing the EHI evaluation framework within the context of the SHMR. The EHI is expressed as (He et al., 2019):

$$EHI = \sqrt[4]{V^* O^* R^* S} \quad (4)$$

Wherein, EHI denotes the ecosystem health index, while V, O, R, and S represent ecosystem vigor, ecosystem organization, ecosystem resilience, and ecosystem service, respectively. Employing the range

TABLE 1 Standard coal coefficient and carbon emission coefficient of different energy source.

Energy types	Standard coal coefficient	Carbon emission coefficient	Energy types	Standard coal coefficient	Carbon emission coefficient
Raw coal	0.7143	0.7559	Diesel oil	1.4571	0.5921
Hard coke	0.9714	0.8550	Fuel oil	1.4286	0.6185
Natural gas	1.2143	0.4483	Kerosene	1.4714	0.5714
Crude oil	1.4286	0.5857	Electricity	0.4040	0.7935
Gasoline	1.4714	0.5538	—	—	—

standardization method, the EHI, V, O, R, and S were standardized on a scale of 0–1 (Mingde et al., 2010).

$$A_i = \frac{X_i - min\ (X_i)}{max\,(X_i) - min\left(X_i^{'}\right)} \tag{5}$$

In this equation, A_i represents the dimensionless value of the ith indicator, and max (X_i) signifies the maximum value of the ith indicator.

1) Ecosystem vigor is a vital ecosystem function, representing a key manifestation of system metabolism or primary productivity. The Normalized Vegetation Index (NDVI) serves as a valuable indicator of vegetation's productive capacity. Moreover, the strong correlation between NDVI and Net Primary Productivity (NPP) means that NPP serves as an ideal metric for characterizing ecosystem vigor in the present study.
2) Ecosystem organization is the interaction between various components of a system, reflecting the stability and complexity of the system structure. The more complex the structure, the healthier the ecosystem. Furthermore, this index layer is subject to the influence of landscape heterogeneity, the configuration of the landscape, and the degree of landscape connectivity. The utilization of the Shannon Diversity Index (SHDI) and Shannon Evenness Index (SHEI) was employed to effectively capture and elucidate the intricate patterns of spatial heterogeneity. That is, the higher the spatial heterogeneity, the more stable the landscape structure, the stronger the landscape organization ability. To encapsulate the landscape connectivity, the Interspersion and Juxtaposition Index (IJI), Division Index (DIVISION), and Contagion Index (CONTAG) were employed as insightful metrics. The higher the landscape connectivity, the more favorable the inter-species migration and the communication between different patches, the stronger the landscape organization. The index of perimeter-area fractal dimension (PAFRAC) was used to express the landscape shape. Thus, the formula is as follows (Chi et al., 2018a):

$$O = 0.4^{*}LH + 0.4^{*}LC + 0.2^{*}IC = (0.2^{*}LC_1 + 0.2^{*}LC_2) + (0.1^{*}LC_3 + 0.15^{*}LC_4 + 0.15^{*}LC_5) + 0.2^{*}PAFRA \tag{6}$$

Where LH alludes to the intricate landscape heterogeneity, LC signifies the profound landscape connectivity, and IC pertains to the captivating landscape shape. Additionally, LC_1 and LC_2 correspond to the succinct acronyms "SHDI" and "SHEI" respectively, while LC_3, LC_4, and LC_5 elegantly represent the metrics of Interspersion and Juxtaposition Index (IJI), Division Index (DIVISION), and Contagion Index (CONTAG) in that order.

3) Ecosystem resilience epitomizes the inherent ability of an ecological system to uphold its structural equilibrium in the face of perturbations caused by human activities. Past investigations have established that land utilization can serve as a reliable gauge of ecosystem resilience. To quantify this resilience, we assign Resilience Coefficients based on the distinct land use categories. The comprehensive measure of ecosystem resilience is then computed through the weighted aggregation of both the spatial extent and ecological resilience coefficients associated with diverse land use classifications within the given region, as delineated below (Kang et al., 2018):

$$R = \sum_{i=1}^{n} \frac{A_i}{A_I} \times RC_i \tag{7}$$

In this equation, R symbolizes the resilience of the urban ecosystem within the district under examination. A_I corresponds to the total land area encompassed by the study region, whereas A_i represents the specific area occupied by the respective land use types. Furthermore, RC_i denotes the ecological restoration coefficient associated with the ith land use classification. Drawing upon prior research findings, the ecological resilience coefficients for cultivated land, forest land, grassland, water bodies, built-up land, and unused land are documented as 0.3, 0.8, 0.7, 0.8, 0.2, and 1, respectively.

4) Ecosystem services encompass an array of invaluable products and advantages bestowed upon human society by the natural ecological environment. These services are quantified through the measure of ecosystem service power, which highlights the monetized value attributed to said services. In this study, the revised calculation of ecosystem services per unit area was undertaken by integrating the land use types specific to the SHMR region, utilizing Xie Gaodi's refined scale of ecological services in Chinese ecosystems. Incorporating the ESV per unit area scale proposed and updated in 2017, the economic value corresponding to grain production per unit area of farmland was adopted as the benchmark ESV, representing a standard equivalent factor of 1.

$$ESV = \sum_{i=1}^{n} A_i \times VC_i \tag{8}$$

In the equation, ESV represents the total value of ecosystem services analyzed in this study, A_i denotes the area (in hectares) of

the *i*th type of land use, and VC_i represents the ecosystem service value coefficient for the *i*th type of land use.

1.3.3 Geographically weighted regression model

Based on the fact that random distribution of variables in the classical OLS model does not have independent spatial characteristics, also required a high degree of mutual independence between regions. Thus, the classical model is modified by introducing spatial differences and spatial correlations. That is, geographical weighted regression (GWR) introduced the spatial attributes of data, and explores the heterogeneity of spatial data through the estimation of different spatial relations of geographic space and regional parameters with spatial dependency (Chris et al., 1996). In the pursuit of investigating the spatial heterogeneity of the CEI on the EHI from a global standpoint, this study employed a GWR model. The formulation utilized in this analysis can be expressed as follows (Sciences et al., 2017):

$$\boldsymbol{Y_i = \beta_0 (\mu_i, \nu_i) + \sum_k \beta_k (\mu_i, \nu_i) X_{ik} + \varepsilon_i} \tag{9}$$

In this equation, we denote Y_i as the dependent variable, representing the observed values of interest. The explanatory variable, X_{ik}, signifies the covariates considered in the analysis. The position function, (μ_i, ν_i), captures the spatial coordinates of each observation i. The constant term of regression, β_0, represents the intercept, while β_k denotes the vector of parameters to be estimated. Lastly, ε_i represents the random error term accounting for unobserved factors.

1.3.4 Coupling coordination analysis of carbon emission and ecosystem health

"Coupling" is a physical concept that means the phenomenon in which two (or more) systems or forms of motion affect each other through various interactions. The phenomenon of "coupling" exists in all fields of society and has universal significance. In economics, coupling refers to the phenomenon that two or more economic subsystems influence each other and even cooperate through various interactions. The concept of coupling degree pertains to the extent of interaction and interconnectivity within a system or its constituent elements. Specifically, coupling coordination degree (CCD) serves as an indicator of the level of interaction and interdependence among subsystems, underpinned by the underlying coupling degree. Therefore, the CCD model of CEI and EHI coupling development is constructed based on the following formulas (He et al., 2017):

$$\boldsymbol{C = \left\{ \frac{U(\alpha) \times U(\beta)}{\left[\frac{U(\alpha)+U(\beta)}{2}\right]^2} \right\}^{\frac{1}{2}}} \tag{10}$$

$$\boldsymbol{T = aU(\alpha) + bU(\beta)} \tag{11}$$

$$\boldsymbol{CCD = \sqrt{C \times T}} \tag{12}$$

In the given equation, the variable D represents the value of CCD, where $U(\alpha)$ denotes the value of EHI and $U(\beta)$ signifies the value of CEI. The variable C signifies the coupling degree of the aforementioned subsystems, while T represents the comprehensive level of coordination between these subsystems. Lastly, the variables a and b refer to the respective contributions made by the two subsystems.

The study recognizes the paramount significance of both economic development and ecological protection. Hence, the CEI and EHI subsystems were accorded equal importance, with the values of a and b being set at 0.5 each.

To enhance the evaluation of the coupling development state between CEI and EHI in SHMR, the classification criteria and types of CCD were established, drawing upon earlier research works (Table 2) (Cui et al., 2019).

1.3.5 Geographical detector model (GDM)

As a statistical method used to reveal the driving factors of spatial differentiation, geographic detector is an important new method to detect the spatial pattern and causes of geographical elements, and has been gradually applied to the research in various fields such as urban development. This study mainly adopted factor detection and interaction detection to measure the effect intensity of driving factors on CCD in SHMR. The formula is as follows (Wang et al., 2020):

$$\boldsymbol{q = 1 - \frac{\sum_{h=1}^{L} N_h \sigma_h^2}{N_\sigma^2}} \tag{13}$$

In the given equation, the q value, ranging from 0 to 1, serves to unveil the degree of contribution of independent variable factors to dependent variable factors, thereby enabling the identification of the dominant factor of CCD in this study. A higher q value suggests a greater influence of the independent variable on the dependent variable. L represents the layer of independent variable. N_h and N denote the number of unit grids of layer h and the entire region, respectively. σ_h^2 and σ^2 represent the variance of CCD in layer h and the entire region, respectively.

The level of economic development exerts a substantial impact on regional land use carbon emissions, necessitating a heightened focus on ecological preservation during urban land expansion. The intricate operation mechanism of ecosystems is influenced by a multitude of natural and socio-economic factors, thereby shaping ecosystem health. Consequently, this study aims to elucidate the influencing factors within the coupling coordination system of carbon emissions and ecosystem health, as illustrated in Table 3. Natural influencing factors were characterized through the selection of climate, topographic factors, geology, and resource endowments. Climatic conditions were specified by indicators such as annual average temperature, annual average humidity, and annual average precipitation. Topographic conditions were represented by elevation and relief degree of the land surface. Resource endowment was assessed through the selection of indicators such as net primary productivity (NPP), forest coverage, and biological abundance index. Human activities and the level of economic development primarily characterized socio-economic factors. To be more precise, the level of human activity was gauged through the human disturbances index, GDP density, and population density.

The computation methodology for determining the relief degree of the land surface in this study draws upon established and pertinent research in the field. The formula is below (Qiao et al., 2018):

TABLE 2 The coupling coordination types and characteristic of CEI and EHI.

CCD range	CCD level	Subsystem characteristic	Coordinated characteristic	Type
$0 < CCD \leq 0.2$	Seriously unbalanced development	$f(\alpha) - f(\beta) > 0.1$	EHI significantly lagged	11
		$f(\beta) - f(\alpha) > 0.1$	CEI significantly lagged	12
		$\lvert f(\alpha) - f(\beta)\rvert \leq 0.1$	Synchronously development	13
$0.2 < CCD \leq 0.4$	Slightly unbalanced development	$f(\alpha) - f(\beta) > 0.1$	EHI significantly lagged	21
		$f(\beta) - f(\alpha) > 0.1$	CEI significantly lagged	22
		$\lvert f(\alpha) - f(\beta)\rvert \leq 0.1$	Synchronously development	23
$0.4 < CCD \leq 0.6$	Slightly balanced development	$f(\alpha) - f(\beta) > 0.1$	EHI significantly lagged	31
		$f(\beta) - f(\alpha) > 0.1$	CEI significantly lagged	32
		$\lvert f(\alpha) - f(\beta)\rvert \leq 0.1$	Synchronously development	33
$0.6 < CCD \leq 0.8$	Moderately balanced development	$f(\alpha) - f(\beta) > 0.1$	EHI significantly lagged	41
		$f(\beta) - f(\alpha) > 0.1$	CEI significantly lagged	42
		$\lvert f(\alpha) - f(\beta)\rvert \leq 0.1$	Synchronously development	43
$0.8 < CCD \leq 1.0$	Highly balanced development	$f(\alpha) - f(\beta) > 0.1$	EHI significantly lagged	51
		$f(\beta) - f(\alpha) > 0.1$	CEI significantly lagged	52
		$\lvert f(\alpha) - f(\beta)\rvert \leq 0.1$	Synchronously development	53

TABLE 3 Index system of influencing factors.

Influencing factor	Factors	Code	Indicators
Natural factors	Climatic conditions	X1	Annual mean temperature
		X2	Annual average humidity
		X3	Annual mean precipitation
	Topographic and geological conditions	X4	Elevation
		X5	Relief degree of land surface
	Resource endowments	X6	NPP
		X7	Biodiversity index
		X8	Forest coverage
Human factors	Human activities	X9	Human disturbances index
		X10	GDP density
		X11	Population density

$$\boldsymbol{RDLS} = \{[\boldsymbol{Max}(\boldsymbol{H}) - \boldsymbol{Min}(\boldsymbol{H})] \times [\mathbf{1} - \boldsymbol{P}(\boldsymbol{A})/\boldsymbol{A}]\}/\mathbf{500} \quad (14)$$

In the above equation, the relief degree of the land surface (RDLS) is computed using the following parameters: $Max(H)$ and $Min(H)$ represent the uppermost and lowermost elevations within the region, respectively. $P(A)$ denotes the extent of flat land area in square kilometers (km^2), while A encompasses the overall area of the research unit, measuring 64 km^2. For the purpose of this investigation, we have classified any land area with a slope equal to or less than 2° as flat terrain.

The computation methodology for the biodiversity index in this investigation aligns with established and pertinent scholarly inquiries. The formula is below (Fitter, 2012):

$$\mathbf{BI} = \mathbf{A}_{\text{bio}} \times (\mathbf{0.11} \times \mathbf{A}_1 + \mathbf{0.35} \times \mathbf{A}_2 + \mathbf{0.21} \times \mathbf{A}_3 + \mathbf{0.28} \times \mathbf{A}_4 + \mathbf{0.04} \times \mathbf{A}_5 + \mathbf{0.01} \times \mathbf{A}_6)/\mathbf{A}_{\text{total}} \quad (15)$$

$$\mathbf{A}_{\text{bio}} = \mathbf{100}/\mathbf{MAX} = \mathbf{100}/\mathbf{0.35} = \mathbf{285.71} \quad (16)$$

Here, the biodiversity index (BI) is determined by the normalized coefficient (A_{bio}) derived from the areas of cultivated land, forestland, grassland, water body, build-up land, and unused land ($A_1 - A_6$), all within the confines of the research unit. The total area of the research unit is denoted as A_{total}.

The calculation model of human disturbances index is established based on a large amount of data of human disturbances and land use, thereby the quantitative description of human disturbance in a certain area was realized. To reflect the spatial characteristics of human

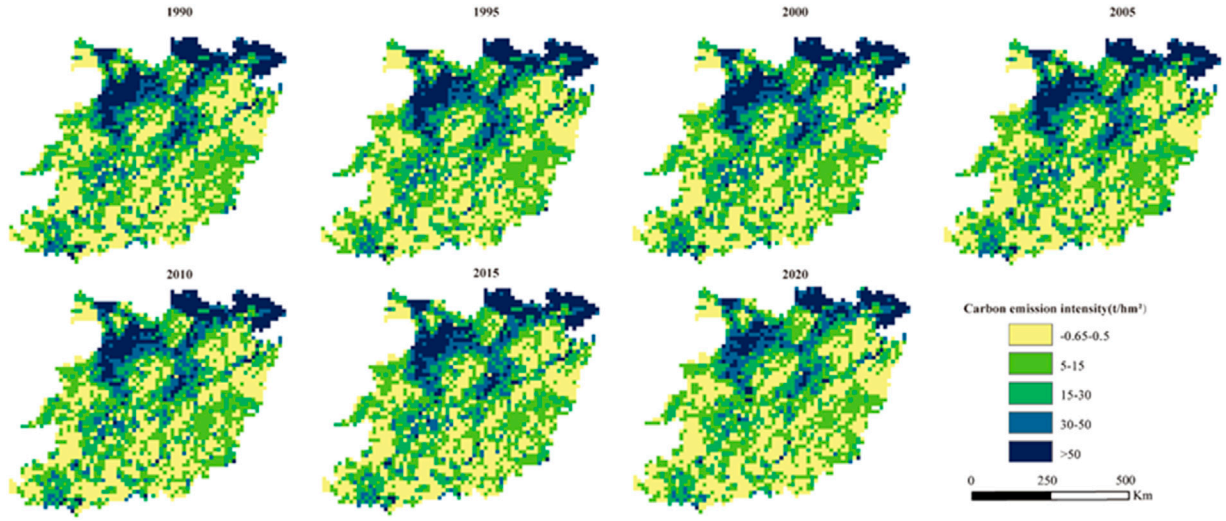

FIGURE 2
The spatial-temporal distribution of carbon emission intensity (CEI) in SHMR, 1990–2020.

disturbances, the human disturbances values were divided into 5 levels by Jenks natural breaks method. The human disturbances index formula is as follows (Chen et al., 2010):

$$HD = \frac{\sum_{i=1}^{m} W_i \times S_i}{S} \quad (17)$$

Here, the human disturbances value (HD) for each grid is determined by the human disturbances index (W_i) associated with each land use type (i), as established in prior research. The area of each land use type (i) is denoted as S_i, while the total area of the grid is represented by S.

2 Results

2.1 Dynamic changes of carbon emission intensity

The CEI in SHMR exhibited a consistent upward trajectory from 1990 to 2020, as depicted in Figure 2. Throughout the duration of the study, the CEI demonstrated a remarkable degree of stability, with minimal drastic fluctuations. From 1990 to 2020, CEI in the northern region of SHMR showed a gradual upward trend. For each region, the CEI decreases from north to south. The overall economic strength of the northern region is increasing at the same time, the CEI is also increasing. The low value of CEI is mostly distributed in the south, showing an overall increase. The maximum carbon emission intensity increases from 3.61 t/hm^2 in 1990 to 101.42 t/hm^2 in 2020, an increase of 4.69 times. The number of grids falling in the I region decreased year by year, especially from 2000 to 2005 decreased by 78.3%, and there was a shift to the II region. The grids in the second zone increased first and then decreased, and the southern region, where the land use type is mainly cultivated land, has been stable in this zone since 2010. The growth rate of grid number in the III region is the highest, accounting for 46.36% of the total grid number in 2020, which is mostly consistent with the distribution range of cultivated land. The grids in the Sections 4, 5 increased year by year and were in clumps, mainly concentrated in the construction land with active human activities.

2.2 Dynamics of ecosystem health

Figure 3 depicted the spatial-temporal distribution of indicators that represent the health of ecosystems in SHMR. These indicators encompass ecosystem vigor (EV), ecosystem organization (EO), ecosystem resilience (ER), and ecosystem services (ES). Notably, the regions exhibiting the most pronounced changes in EV were predominantly situated in the northwestern part of SHMR, displaying a gradual decline in magnitude from north to south. In terms of temporal progression, EV demonstrated an upward trend from 1990 to 2005, followed by a gradual decline from 2005 to 2020. Regarding EO, the regions with notable variations were primarily concentrated in the northwestern part of SHMR, although discernible changes were also evident in the southern region. Over the course of the study period, SHMR as a whole exhibited an increasing trend in EO from 1990 to 2020. However, from 2000 to 2020, the southeastern region experienced a declining trend in EO. In terms of spatial scale, both ER and ES exhibited a comparable distribution pattern. The values of ER and ES were notably higher in regions characterized by abundant forest coverage, whereas regions encompassing vast areas of construction land and unused land demonstrated lower levels of ER and ES. Considering the temporal dimension, ER and ES displayed a gradual decline throughout the SHMR from 1990 to 2020. However, a noteworthy decrease in ER and ES was observed from 2005 to 2020, particularly in the northern and northeastern regions of SHMR.

The spatiotemporal distribution of EHI in the SHMR region was shown in Figure 4. Specifically, in spatial scale, EHI showed a trend of increasing gradually from north to south. The distribution area of high EHI value areas showed an increasing trend, mainly distributed

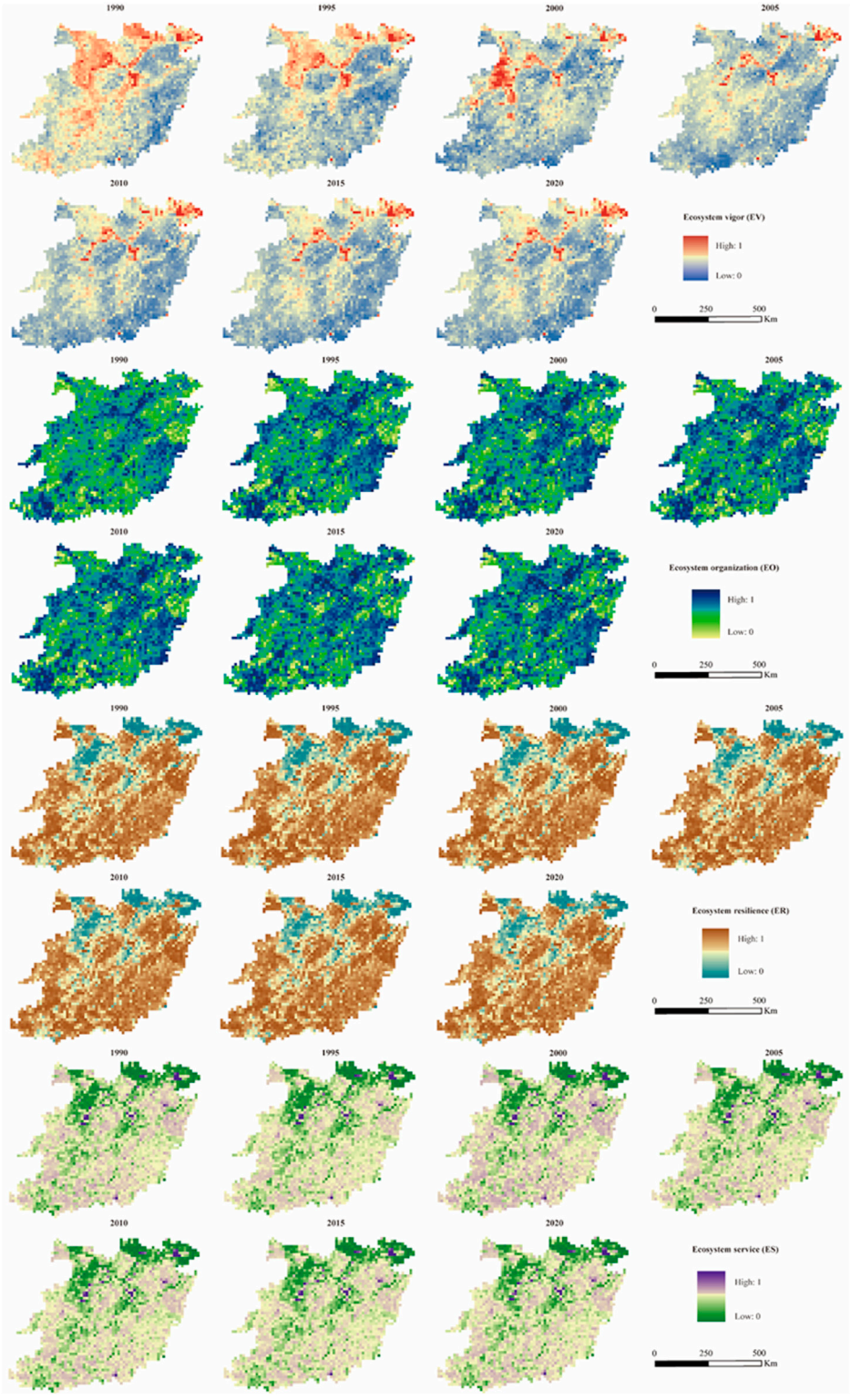

FIGURE 3
The ecosystem health index (EHI) at grid scale, 1990–2020. EV is ecosystem vigor, EO is ecosystem organization, ER is ecosystem resilience, and ES is ecosystem service.

in the southern region with high forest coverage and wide water distribution. The distribution area of high EHI value area showed a decreasing trend, mainly distributed in the northern build-up land and unused land distribution area. In terms of time scale, the overall EHI of SHMR showed a significant increase trend from 1990 to 2005, but showed a gradually decreasing trend after 2005 to 2020.

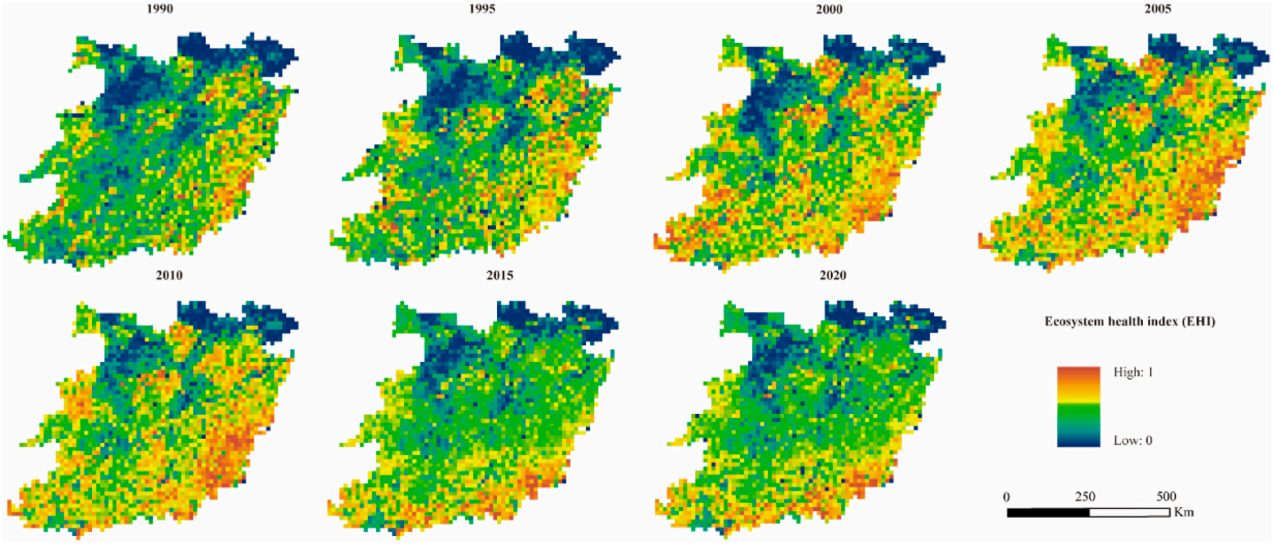

FIGURE 4
The ecosystem health index (EHI) in SHMR, 1990–2020.

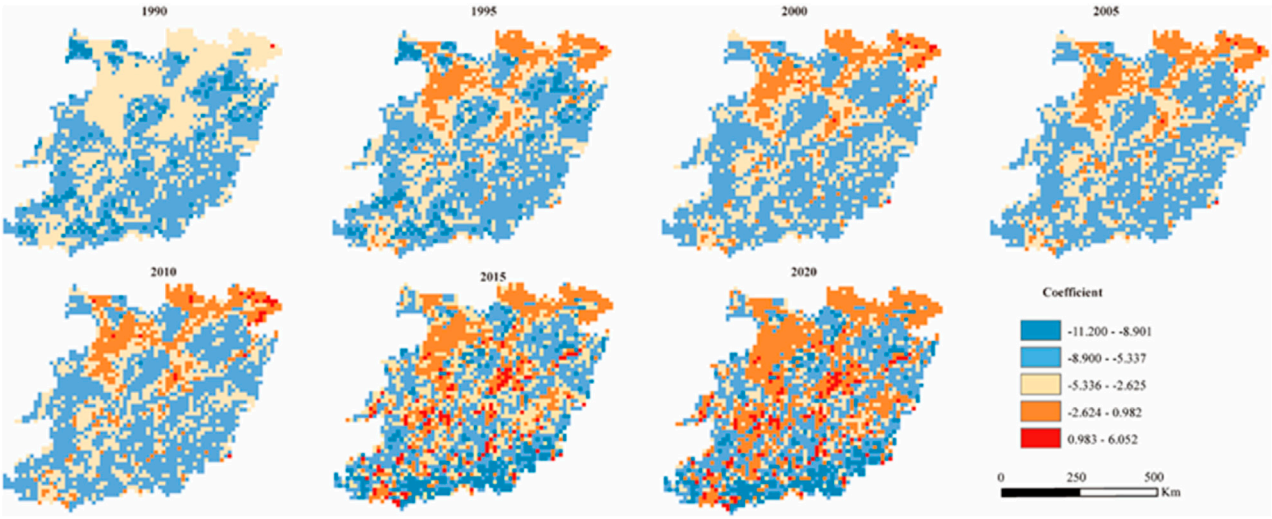

FIGURE 5
Spatial distribution of regression coefficients for the carbon emission intensity (CEI) and ecosystem health index (EHI), 1990–2020.

2.3 Spatial correlation analysis between carbon emission and ecosystem health

In this study, geographical weighted regression model (GWR) was selected to analyze the spatial impacts of carbon emissions on ecosystem health in SHMR (Figure 5), which with the consideration of spatial spillover effects between the above subsystem. Table 4 listed the parameters in the GWR model, we found that R^2 is all above 0.8, which indicated that GWR model has a good fitting effect, and EHI and CEI both showed obvious clustering phenomenon.

What's more, in SHMR from 1990 to 2005, the regression coefficients of CEI and EHI were negative on the whole, and the negative effect between CEI and EHI was dominant. This revealed that with the increase of CEI value, there was a large negative impact in SHMR regional ecosystem. In other words, with the acceleration of regional urbanization, a higher CEI value has been generated, which has a more significant interference with EHI value and a more prominent damage to ecosystem health. It is worth noting that the regression coefficient began to show a positive value from 2010, indicating that the spatial spillover effect of CEI on EHI began to show a positive effect. Moreover, the positive distribution area of the regression coefficient showed an increasing trend from 2010 to 2020, and it was mainly distributed in the areas with more distribution of forest land and water body. Although these regions have higher CEI value, the spatial spillover

TABLE 4 Estimation parameters for GWR models, 1990–2020.

Year	Parameters				
	Residual squares	Sigma	AICc	R^2	Adjusted R^2
1990	313.766	0.403	3714.890	0.873	0.823
1995	346.075	0.431	3872.901	0.883	0.865
2000	387.903	0.423	3903.092	0.892	0.872
2005	398.092	0.401	4012.764	0.883	0.863
2010	414.783	0.523	4298.903	0.891	0.871
2015	463.903	0.521	4382.342	0.902	0.892
2020	488.563	0.515	4450.092	0.912	0.899

effect of CEI on EHI began to show a positive effect. But at the same time, forest land and water body can provide higher EHI value, so CEI and EHI will have a positive relationship.

2.4 Quantification of the coupling coordination degree between carbon emission and ecosystem health

2.4.1 Temporal changes of coupling coordination degree levels

Against the backdrop of rapid globalization, the relentless expansion of urban land and the accelerated surge in carbon emissions have exerted immense pressure on the local ecological milieu. Consequently, for the realization of regional green and sustainable development, it becomes imperative to attain a harmonious and symbiotic relationship between carbon emissions and ecological health while striving for high-caliber economic progress. To this end, the CCD model is employed to quantitatively analyze the coupling and coordination levels and patterns of CEI and EHI across spatial and temporal dimensions (Figure 6). Specifically, a higher CCD value signifies a more robust coupling degree between the two subsystems of carbon emission and ecosystem health, thereby facilitating the emergence of a novel, organized structure. Conversely, a lower CCD value indicates a less desirable state of coordination. In this regard, within the context of advanced carbon emission development, it becomes crucial to curtail the level of EHI to the utmost extent. Thus, the "EHI significantly lagged" CCD type represents the optimal state of coordination. Significantly, as outlined in Table 2, it is imperative for the CCD value to exceed 0.4 to achieve a somewhat balanced equilibrium between ecosystem services and carbon emissions.

2.4.2 Spatial distribution of coupling coordination degree types

Figure 7 showed the CCD values and types from 1990 to 2020 in SHMR. As can be seen from Figure 7, CCD types in SHMR present obvious differences in spatial-temporal distribution. From 1990 to 1995, the main types of CCD were "21" and "22", that is, the CEI and EHI of SHMR showed a slightly unbalanced development state. Specifically, during 1990–1995, CEI lagged behind in most southern regions of SHMR, while EHI lagged behind in most northern regions. This is consistent with the spatial-temporal distribution of CEI and EHI described above, in the northern region of SHMR, the level of economic development in the northern region is more advanced, whereas the southern region lags behind in comparison. Moreover, from 1990 to 1995, there were more "32" type of CCD, and the distribution area of "22" type showed a decreasing trend, which indicates that CEI and EHI showed a slightly balanced development state in the development process of SHMR. In 2000, the distribution of CCD types changed significantly, the distribution area of "21" and "22" types were greatly reduced, and a new CCD distribution type "31" appeared, that is, in the

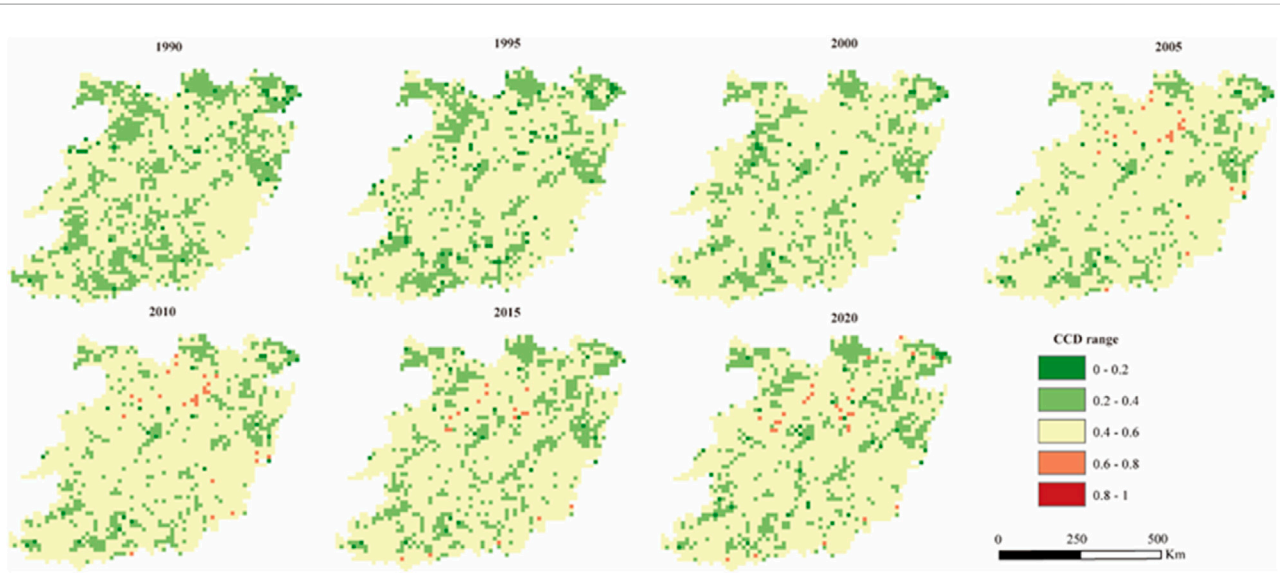

FIGURE 6
The Spatial-temporal characteristic of coupling coordination degree (CCD), 1990–2020.

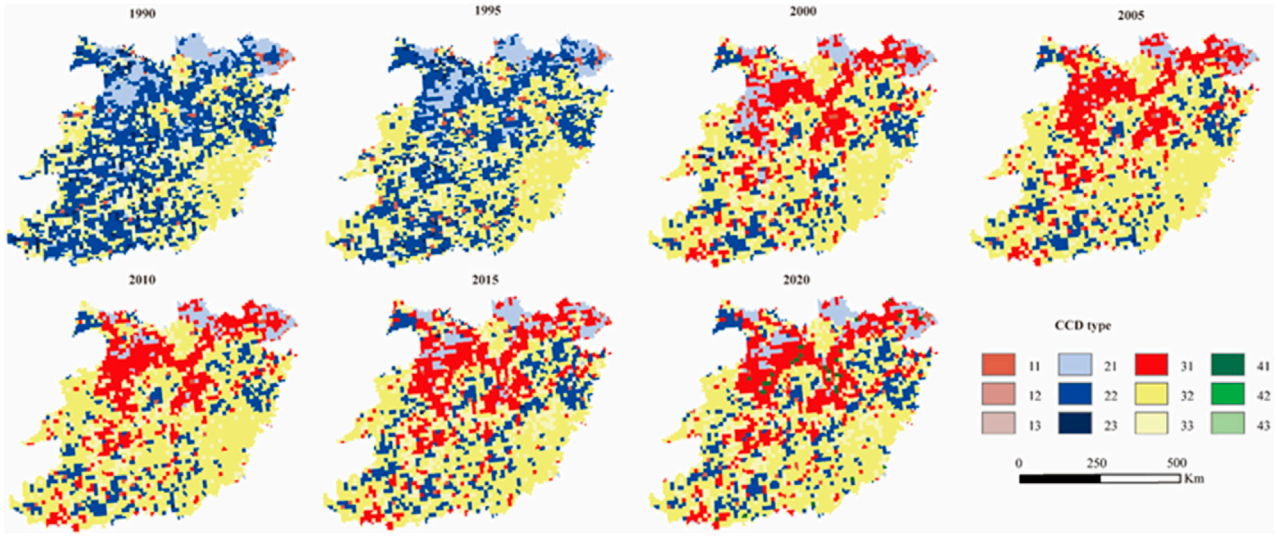

FIGURE 7
Spatial distribution pattern of the coupling coordination degree (CCD) type, 1990–2020 (Seriously unbalanced development: "11", "12", "13"; Slightly unbalanced development: "21", "22", "23"; Slightly balanced development: "31", "32", "33"; Moderately balanced development: "41", "42", "43").

state of CEI and EHI slightly balanced development, EHI showed a lagging development state. Moreover, from 2000 to 2020, the distribution area of "31" type showed an obvious trend of increase, indicating that during this period, SHMR paid more attention to economic development, and the development of EHI was significantly affected, showing a significant lag state. We must ardently foster the advancement of ecological civilization, enhance the quality and resilience of the ecosystem, and propel the SHMR regions towards a trajectory of green and sustainable development.

2.5 Driving factors of regional differences in coupling coordination degree

2.5.1 Single factor detector analysis of coupling coordination degree

The q value, as gauged by the geographic detector, serves as a metric for quantifying the impact of each influencing factor. Notably, a higher q value corresponds to a greater degree of influence exerted by the factor on the spatial differentiation of CCD, as elucidated in Table 5. Furthermore, statistical analysis reveals significant disparities among the factors, affirming the relative soundness of the factors chosen for this study. Moreover, discernible discrepancies emerge in terms of the influence various factors wield on the spatial differentiation of CCD between 1990 and 2020.

As depicted in Table 5, it is evident that the q value associated with forest coverage consistently ranks highest between 1990 and 2010, underscoring its pivotal role in determining the spatial distribution of CCD (Table 3). In fact, its explanatory power with respect to the spatial pattern of CCD escalated to 61.8% by 2020. Notably, the q value linked to the human disturbances index (X9) underwent substantial changes during the period spanning from 1990 to 2020, surging from 0.225 to 0.423. This signifies a bolstering influence of the human disturbances index in elucidating the spatiotemporal characteristics of CCD, surpassing even the significance of forest coverage. Additionally, the q values associated with GDP density (X10) and population density (X11) exhibited an upward trajectory, with explanatory powers of 55.34% and 10.05% respectively, by 2020. Conversely, the q values pertaining to annual average humidity and elevation remained consistently low, signaling their limited capacity to explicate the temporal and spatial dynamics of CCD, and thus their marginal role in the observed changes.

2.5.2 Interaction detector analysis of coupling coordination degree

The interaction detector allowed for the identification of interactions between distinct influencing factors, X, and evaluated whether their combined presence amplifies or diminishes the explanatory capacity of the dependent variable, Y. It also determined if the influence of these factors on Y was independent of each other. The detection results were obtained through a comparison of the individual q values and the interaction q values [q (X1∩X2)]. These results can be broadly categorized into three types: weakening, mutual enhancement, and nonlinear enhancement (Figure 8).

The Figure 8 vividly depicted the enhanced interaction between the two distinct influencing factors. This enhancement was primarily characterized by the augmentation of the two factors, as well as a nonlinear amplification. Notably, no weakening or independent relationship was observed. Specifically, the period spanning 1990–2020 has witnessed a diminishing effect of most natural factors on CCD, while the influence of socio-economic factors has steadily intensified. For example, annual mean precipitation (X3) decreases from 0.341 to 0.280, and NPP (X6) decreases from 0.419 to 0.367, and the influence on CCD shows a weakening trend. Human disturbances index (X9) increased from

TABLE 5 q statistic and p values of detection factors, 1990–2020.

	X1	X2	X3	X4	X5	X6	X7	X8	X9	X10	X11
qs-1990	0.243	0.189	0.341	0.078	0.245	0.419	0.389	0.459	0.225	0.188	0.367
pv-1990	0.000	0.000	0.000	0.000	0.000	0.000	0.000	0.000	0.000	0.000	0.000
qs-2000	0.229	0.191	0.224	0.091	0.256	0.432	0.398	0.409	0.349	0.291	0.298
pv-2000	0.000	0.000	0.000	0.000	0.000	0.000	0.000	0.000	0.000	0.000	0.000
qs-2010	0.201	0.203	0.309	0.089	0.257	0.388	0.409	0.411	0.493	0.389	0.311
pv-2010	0.000	0.000	0.000	0.000	0.000	0.000	0.000	0.000	0.000	0.000	0.000
qs-2020	0.216	0.197	0.281	0.092	0.253	0.367	0.419	0.418	0.423	0.421	0.408
pv-2020	0.000	0.000	0.000	0.000	0.000	0.000	0.000	0.000	0.000	0.000	0.000

Note: qs represents the statistical value of q, pv represents the value of p.

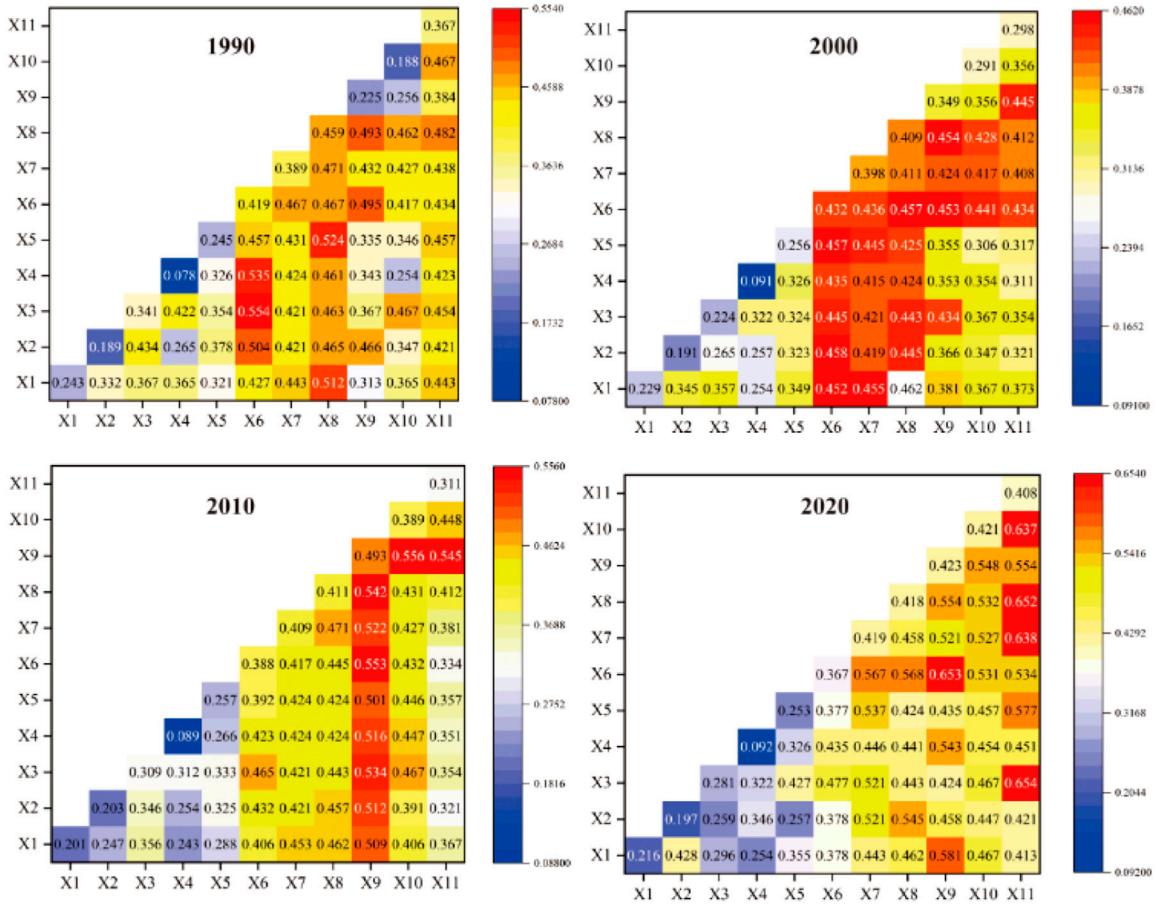

FIGURE 8
Interaction detection of factors, 1990–2020.

0.225 to 0.423, and GDP density (X10) increased from 0.188 to 0.421, gradually becoming a high impact factor promoting the coordinated development of CEI and EHI system coupling. It is worth mentioning that forest coverage (X8) has maintained a relatively significant effect from 1990 to 2020, which may be related to the high forest coverage in SHMR. Further, in 2020, the absolute value of interaction between NPP (X6) and human disturbances index X9 reaches 0.653, higher than the single interaction of X6 and X9; The absolute value of the interaction between NPP (X6) and GDP density (X10) is 0.531, which is higher than the single interaction of X6 and X10. The absolute value of the interaction between annual mean temperature (X1) and population

TABLE 6 Percentages of different types of LISA clusters, 1990–2020.

Type	1990 (%)	1995 (%)	2000 (%)	2005 (%)	2010 (%)	2015 (%)	2020
Low-high	24.01	24.90	25.17	25.20	25.29	25.67	26.60%
High-low	7.89	8.01	8.67	8.90	9.97	10.34	9.84%
High-High	0.30	0.39	0.42	0.51	0.58	0.59	0.62%
Low-low	10.90	9.88	9.25	8.90	8.10	7.89	8 .25%
Not significant	54.89	55.03	56.48	56.89	57.17	54.32	53.70%

density (X11) reached 0.413, which was higher than the single interaction value of X1 and X11. This indicated that with the rapid economic development, the influence and limitation of natural conditions such as precipitation and humidity on CCD in the SHMR region were gradually weakened.

3 Discussion

3.1 Staged response of ecosystem health to carbon emission

The precise delineation of the spatial-temporal progression of ecosystem health, along with a comprehensive comprehension of its dynamic association with the carbon emission process, lies at the crux of achieving a harmonious and sustainable nexus between regional environmental preservation and the enhancement of ecosystem wellbeing (Ran et al., 2021; Song et al., 2015). Moreover, in order to assess the extent of the influence of carbon emission on ecosystem health within the study area, as well as the potential spatial spillover effects, the spatial-temporal response characteristics of carbon emission to ecosystem health in the SHMR region were ascertained through the utilization of the GWR model (Table 6).

The urban agglomerations are undergoing a rapid and transformative phase of social and economic development, where frequent land use changes exert a direct influence on carbon emission dynamics. Alterations in land use patterns, spatial arrangements, and management strategies not only impact the ecosystem, but also disrupt the delicate equilibrium of the carbon cycle system, thereby affecting the CEI. During the initial stage of carbon emission, specifically from 1990 to 2005, the CEI did not exhibit a substantial impact on the EHI. Throughout this period, the spatial distribution proportions of the "Low-high" and "High-low" types experienced marginal shifts, increasing from 24.10% to 25.20% and from 7.89% to 8.90%, respectively. This gradual progression suggests that higher CEI values gradually demonstrate a more pronounced interference on EHI values. From 2005 to 2015, the influence of CEI on EHI became notably significant. The proportion of the "Low-high" spatial distribution rose from 25.20% to 25.67%, while the proportion of the "High-low" spatial distribution increased from 8.90% to 10.34%. Concurrently, swift and efficient carbon emission reduction efforts resulted in an 11.34% decline in the proportion of the "Low-low" spatial distribution, while the proportion of the "High-high" spatial distribution witnessed a 15.69% increase. This pattern emerges due to the rapid urbanization in the SHMR region, wherein population siphoning leads to a substantial influx of rural residents into urban areas, causing congestion. Vigorous human activities act as drivers for accelerated carbon emission, while the expansion of construction land and heightened energy consumption result in significant encroachments upon forested and cultivated lands. Consequently, carbon emissions from construction land experience a noteworthy surge. Previous studies have already indicated that continuous population growth plays a pivotal role in propelling carbon emission dynamics, with the expanding proportion of construction land holding significance in this process (Liu et al., 2023). However, in reality, the vast expansion of urban land fails to align harmoniously with the demands of urban production and living, and the growth rate of the population evidently lags behind the expansion of regional urban land. This contradiction is not exclusive to China alone but is a common phenomenon in the developmental trajectory of global cities (Zhao et al., 2022). In 2020, our country proactively pursued the goal of "Carbon peaking and carbon neutrality," implementing a series of measures across various domains of life, production, and ecology. Consequently, the nation's economic development has transitioned towards a stage of high-quality growth, signifying a transitional phase in carbon emission dynamics. During this period, the influence of CEI on EHI has diminished within the SHMR region. The proportion of the "Low-high" spatial distribution has reached its pinnacle at 26.60%, marking the highest value throughout the study period, while the proportion of the "High-low" spatial distribution stands at 9.84%. This finding further underscores the fact that SHMR's urbanization process is transitioning towards a high-quality, green, and sustainable phase, thereby mitigating the impact of rapid carbon emission on the ecosystem's green and sustainable development. In essence, during the pursuit of high-quality economic development, greater attention should be directed towards the expansion of urban construction land and the enhancement of the development mode. Macro-level land use control should be strengthened, and a concerted effort should be made to promote the efficient, collaborative, and sustainable development of carbon emission and ecosystem services within the SHMR region.

3.2 The influence mechanism of control variables on coupling coordinated degree

The findings of this study revealed significant regional variations in the driving forces of CCD within the SHMR. At the regional level,

during the year 1990, the pivotal factors influencing the coupling system between carbon emission and ecosystem health were identified as forest coverage, net primary productivity (NPP), and biodiversity index. This can be attributed, in part, to the inherent natural endowment of the SHMR itself, with forested land covering a remarkable 70% of the total area. The region also displays conspicuous spatial heterogeneity in its ecosystems (Ren et al., 2018). Furthermore, ecological management initiatives in the SHMR, such as reforestation efforts, land consolidation, and afforestation programs, have contributed to the expansion of forested areas, thereby augmenting the proportion of broadleaf and coniferous forests (Sohil and Sharma, 2020). Furthermore, it is worth noting that the topography of the SHMR exhibits noticeable fluctuations, with vegetation coverage surpassing 60% in the region. This abundant vegetation plays a pivotal role in climate regulation. Several studies have indicated that climatic factors serve as the primary determinants of regional ecological sensitivity (Yao et al., 2012). Through the intricate interplay between precipitation patterns and land use intensity, these factors influence the growth and distribution of vegetation within the region. However, it is crucial to acknowledge that with the rapid economic development and continuous urbanization in the SHMR, socio-economic factors, such as GDP and the human disturbance index, will emerge as the principal drivers influencing the coupling system of carbon emission and ecosystem health in the year 2020. Particularly in the central and eastern regions of the SHMR, population density has increased significantly, accompanied by dense population distribution and a robust GDP. Unfortunately, this dense population distribution and rapid economic progression have given rise to a series of issues, including environmental pollution and ecosystem degradation, resulting in a high CEI value and a low EHI value. Consequently, these regions exhibit a lagging state of development in terms of EHI.

Remarkably, the development of CCD in the SHMR is significantly influenced by both natural and socioeconomic factors, and their interaction yields intriguing outcomes. Previous research has established that alterations in wetland, grassland, and forest ecosystems are intricately shaped by a combination of intricate climatic forces and human activities (Wang et al., 2022). In the year 2020, the distribution area of CCD types in the SHMR region displayed a moderately balanced pattern, with the “31” type experiencing a substantial upward trajectory. This further underscores the prevailing state of lagging development in terms of EHI. Concurrently, the q-values for natural factors, such as forest coverage (X8), annual mean precipitation (X3), and the relief degree of the land surface (X5), were all 0.45. Similarly, the socioeconomic factors of human disturbances index (X9) and GDP density (X10) yielded q-values of −0.34. Notably, the absolute value of the interaction between forest coverage (X8) and human disturbances index (X9) was found to be 0.23. Likewise, the absolute value of the interaction between annual mean precipitation (X3) and GDP density (X10) reached 0.45 The continuous expansion of urbanized areas has led to the encroachment upon vast stretches of farmland and forested land within the region, resulting in the direct attenuation of regional biodiversity and the fragmentation of ecosystem structures. The q-value for the biodiversity index (X7) has exhibited a decline from 0.12 in 1990 to 0.34 in 2020. Consequently, it is imperative to prioritize the preservation of the natural advantages inherent to the SHMR, consistently upholding the region’s high vegetation coverage. Moreover, meticulous attention must be directed towards addressing extreme climatic events. Concurrently, the administrative authorities must proactively recalibrate the regional economic industries and guide the judicious distribution of the population to mitigate the adverse consequences of human interference.

3.3 Implications for ecosystem management and sustainable development

Determining the regional differences of the coupling coordination degree of carbon emission and ecosystem service subsystems in SHMR region and their driving factors will not only provide important guidance and suggestions for the development of differentiated ecosystem protection and ecosystem health improvement in SHMR region. In addition, it can scientifically reduce carbon emission and improve ecosystem health under the background of ensuring the current high-quality economic development. It is usually in the high CEI value regions, which have low EHI values and are mostly in a slightly coupling coordinated development state with lagging ecosystem health.

Owing to the siphon effect, a substantial concentration of high-caliber workforce and advanced production technology converges within this particular region, enabling effective management of the input-output relationship during the process of urban land expansion. This allows for seizing policy opportunities to drive the transformation and upgrading of the industrial structure, optimizing the allocation of land inputs, and ultimately achieving the green and sustainable development of various urban sectors. Simultaneously, the pace of urban land expansion can be judiciously regulated to prevent the destruction of the ecosystem’s landscape organization resulting from imprudent reclamation of cultivated land. This ensures a harmonious development trajectory, striking a balance between high-quality economic growth and ecological environmental preservation. Moreover, the implementation of ecological protection and restoration initiatives, such as land reforestation, assumes great significance as it improves vegetation coverage and mitigates ecological and environmental predicaments like soil erosion, thereby enhancing the overall health of the ecosystem. These projects are particularly crucial in regions boasting high EHI values and relatively lower CEI values. Consequently, it is imperative to curtail the influence of natural factors on the coupling system of carbon emission and ecosystem services. This necessitates comprehensive consideration of the natural endowment conditions within the SHMR region, empowering the strengthening of protective functions such as meteorological disaster monitoring and fostering the implementation of ecological protection and restoration initiatives. Furthermore, urban development within these regions should exhibit reduced reliance on construction land investments, thereby significantly bolstering the efficiency of regional resource integration and utilization.

3.4 Future work

The examination of ecosystem contributions and their potential ramifications on carbon emissions has been the subject of numerous investigations, employing both empirical measurement and simulation analyses. Notably, these studies have shed light on the commendable carbon storage capacity of forest ecosystems, while also identifying wetlands and marine ecosystems as capable carbon sinks. Concomitantly, addressing the issue of land use carbon emissions has also been a focal point of research endeavors, with a particular emphasis on devising strategies to curtail such emissions and safeguard the integrity of ecosystems. Prominent measures include the enhancement of agricultural practices, the adoption of sustainable urban planning and construction models, and the promotion of ecological restoration and conservation efforts. These studies serve as a foundational bedrock for the formulation of policies geared towards carbon reduction and sustainable development. Thus, the nature of land use holds considerable sway over ecosystem robustness and carbon emissions. Subsequent investigations could delve into unraveling the repercussions of diverse land use types on ecosystem functions and services, as well as assessing the corresponding levels of carbon emissions. Moreover, agriculture, as a pivotal terrestrial endeavor, bears substantial influence on ecosystem welfare and carbon emissions. Prospective research endeavors could be steered towards ground-breaking agricultural technological innovations, aiming to curtail agricultural carbon emissions through the implementation of scientific farming methods and the optimization of agricultural production chains. Furthermore, a comprehensive analysis could be conducted on the intricate carbon cycle processes within agro-ecosystems, seeking ways to enhance the carbon storage capacity of farmland by improving soil quality, judicious crop selection, and rational fertilization practices. Lastly, urbanization, an indisputable force in land use dynamics, bears profound ramifications for both ecosystem health and carbon emissions. Future research undertakings could concentrate on fostering ecological restoration and protection amidst the urbanization process, while also endeavoring to diminish carbon emissions in urban planning and construction. This would concomitantly enhance the stability and perpetuation of urban ecosystems. Additionally, novel strategies pertaining to urban greening, urban agriculture, and urban water resources management can be explored as viable approaches to ameliorate urban carbon emissions and bolster ecosystem wellbeing.

5 Conclusion

In this study, carbon emission and ecosystem health evaluation index systems were established respectively, and dynamically evaluated the carbon emission intensity (CEI) and ecosystem health level (EHI) in SHMR. Utilizing the Global Geographically Weighted Regression (GWR) model, this study extended our understanding of the spatial ramifications of carbon emissions on ecosystem health within the SHMR region. Furthermore, a comprehensive coupling system encompassing CEI and the EHI has been devised, enabling a quantitative assessment of the development level and nature of this coupling system. This approach allowed for a more nuanced examination of the intricate interplay between carbon emissions and ecosystem health in the SHMR area. Ultimately, the geodetector model was employed to quantitatively analyze the spatially differentiated influencing factors impacting the coupling system between ecosystem health and carbon emissions. The resulting insights can be summarized as follows:

(1) Within the SHMR region, spanning the period from 1990 to 2020, the EHI has shown a discernible northward spatial increase, accompanied by marked global spatial autocorrelation and localized spatial agglomeration. Concurrently, the CEI has exhibited an escalating level of spatial differentiation, manifesting a conspicuous spatial imbalance. The distribution pattern of carbon emissions can be described as "predominantly eastern and lesser in the western regions, and more pronounced in the northern areas while relatively diminished in the southern regions."
(2) Over the period spanning from 1990 to 2020, the coupling coordination degree (CCD) between the CEI and the EHI within the SHMR region has exhibited a gradual, yet promising, increase. However, upon scrutinizing the spatial distribution of the coupling coordination type pertaining to carbon emission and ecosystem health, an unbalanced development still dominates most of the SHMR, with slightly unbalanced development being the prevalent type. Nevertheless, the area manifesting slightly balanced development is observed to be on the rise. Notably, the CEI and EHI in the northwest and southwest regions of the SHMR are relatively high, with the majority exhibiting CEI lag and a coupling coordinated development type of CEI and EHI synchronous lag.
(3) Our single factor analysis revealed that the human disturbance index, forest coverage, GDP density, and biodiversity index were vital factors contributing to the spatial differentiation of the carbon emission and ecosystem health coupling system in the SHMR region. The factor interaction test further demonstrated that natural and socio-economic factors were not mutually exclusive and, in fact, exhibited a dual-factor and non-linear enhancement effect on the CCD. Over time, as the social and economic landscape has evolved, the influence of natural factors on CCD has weakened, while the influence of social and economic factors has gradually intensified. In other words, our findings suggest that in ecologically vulnerable regions like the SHMR, socio-economic factors play an increasingly catalytic role in augmenting the impact of natural factors.

Data availability statement

The raw data supporting the conclusions of this article will be made available by the authors, without undue reservation.

Author contributions

HQ: Conceptualization, Data curation, Formal Analysis, Investigation, Methodology, Project administration, Resources, Software, Supervision, Validation, Visualization, Writing–original draft, Writing–review and editing. CY: Data curation, Writing–review and editing. WW: Data curation, Writing–review

and editing. LG: Conceptualization, Funding acquisition, Writing–review and editing.

Funding

The author(s) declare financial support was received for the research, authorship, and/or publication of this article. This work was supported by the National Key Research and Development Program of China (2022YFF1303001).

Acknowledgments

We would like to thank the National Key Research and Development Program of China.

Conflict of interest

The authors declare that the research was conducted in the absence of any commercial or financial relationships that could be construed as a potential conflict of interest.

Publisher's note

References

Awuah, K. F., Jegede, O., Hale, B. A., and Siciliano, S. D. (2020). Introducing the adverse ecosystem service pathway as a tool in ecological risk assessment. *Environ. Sci. Technol.* 54, 8144–8157. doi:10.1021/acs.est.9b06851

Ayre, K. K., and Landis, W. G. (2012). A bayesian approach to landscape ecological risk assessment applied to the upper grande ronde watershed, Oregon. *Hum. Ecol. Risk Assess.* 18, 946–970. doi:10.1080/10807039.2012.707925

Bae, D. Y., Kumar, H. K., Han, J. H., Kim, J. Y., Kim, K. W., Kwon, Y. H., et al. (2010). Integrative ecological health assessments of an acid mine stream and *in situ* pilot tests for wastewater treatments. *Ecol. Eng.* 36, 653–663. doi:10.1016/j.ecoleng.2009.11.027

Bayliss, P., Dam, R. A. V., and Bartolo, R. E. (2012). Quantitative ecological risk assessment of the magela creek floodplain in kakadu national park, Australia: comparing point source risks from the ranger uranium mine to diffuse landscape-scale risks. *Hum. Ecol. Risk Assess.* 18, 115–151. doi:10.1080/10807039.2012.632290

Borja, Á., Galparsoro, I., Solaun, O., Muxika, I., Tello, E. M., Uriarte, A., et al. (2006). The European Water Framework Directive and the DPSIR, a methodological approach to assess the risk of failing to achieve good ecological status. *Estuar. Coast. Shelf Sci.* 66, 84–96. doi:10.1016/j.ecss.2005.07.021

Cai, Z., Kang, G., Tsuruta, H., and Mosier, A. (2005). Estimate of CH4 emissions from year-round flooded rice fields during rice growing season in China. *Pedosphere* 15, 66–71.

Chen, A., Zhu, B.-Q., Chen, L.-D., Wu, Y.-H., and Sun, R.-H. (2010). Dynamic changes of landscape pattern and eco-disturbance degree in Shuangtai estuary wetland of Liaoning Province, China. *Chin. J. Appl. Ecol.* 21, 1120–1128.

Chen, C., Wang, Y., and Jia, J. (2018). Public perceptions of ecosystem services and preferences for design scenarios of the flooded bank along the Three Gorges Reservoir: implications for sustainable management of novel ecosystems. *Urban For. Urban Green.* 34, 196–204. doi:10.1016/j.ufug.2018.06.009

Chen, C., Wang, Y., Jia, J., Mao, L., and Meurk, C. D. (2019a). Ecosystem services mapping in practice: a Pasteur's quadrant perspective. *Ecosyst. Serv.* 40, 101042. doi:10.1016/j.ecoser.2019.101042

Chen, D., Lu, X., Liu, X., and Wang, X. (2019b). Measurement of the eco-environmental effects of urban sprawl: theoretical mechanism and spatiotemporal differentiation. *Ecol. Indic.* 105, 6–15. doi:10.1016/j.ecolind.2019.05.059

Cheng, X., Chen, L., Sun, R., and Kong, P. (2018). Land use changes and socio-economic development strongly deteriorate river ecosystem health in one of the largest basins in China. *Sci. Total Environ.* 616-617, 376–385. doi:10.1016/j.scitotenv.2017.10.316

Chi, Y., Shi, H., Zheng, W., Sun, J., and Fu, Z. (2018a). Spatiotemporal characteristics and ecological effects of the human interference index of the Yellow River Delta in the last 30years. *Ecol. Indic.* 39, 1219–1220.

Chi, Y., Zheng, W., Shi, H., Sun, J., and Fu, Z. (2018b). Spatial heterogeneity of estuarine wetland ecosystem health influenced by complex natural and anthropogenic factors. *Sci. Total Environ.* 634, 1445–1462. doi:10.1016/j.scitotenv.2018.04.085

Chris, H., Brunsdon, A., Stewart, F., Martin, E., and Charlton, L. (1996). Geographically weighted regression: a method for exploring spatial nonstationarity. *Geogr. Anal.* 28, 281–298. doi:10.1111/j.1538-4632.1996.tb00936.x

Cui, D., Chen, X., Xue, Y., Li, R., and Zeng, W. (2019). An integrated approach to investigate the relationship of coupling coordination between social economy and water environment on urban scale - a case study of Kunming. *J. Environ. Manage.* 234, 189–199. doi:10.1016/j.jenvman.2018.12.091

Fitter, N. A. H., Norris, K., and Fitter, A. H. (2012). Biodiversity and ecosystem services: a multilayered relationship. *Trends Ecol. Evol.* 27, 19–26. doi:10.1016/j.tree.2011.08.006

Friedlingstein, P., Houghton, R. A., Marland, G., Hackler, J., Boden, T. A., Conway, T. J., et al. (2010). Update on CO2 emissions. *Nat. Geosci.* 3, 811–812. doi:10.1038/ngeo1022

He, J., Pan, Z., Liu, D., and Guo, X. (2019). Exploring the regional differences of ecosystem health and its driving factors in China. *Sci. Total Environ.* 673, 553–564. doi:10.1016/j.scitotenv.2019.03.465

He, J., Wang, S., Liu, Y., Ma, H., and Liu, Q. (2017). Examining the relationship between urbanization and the eco-environment using a coupling analysis: case study of Shanghai, China. *Ecol. Indic.* 77, 185–193. doi:10.1016/j.ecolind.2017.01.017

ICSU (2017). *A guide to SDG interactions: from science to implementation*. USA: International Council for Science ICSU.

Jia, J., Xin, L., Lu, C., Wu, B., and Zhong, Y. (2023). China's CO2 emissions: a systematical decomposition concurrently from multi-sectors and multi-stages since 1980 by an extended logarithmic mean divisia index. *Energy Strategy Rev.* 49, 101141. doi:10.1016/j.esr.2023.101141

Kang, P., Chen, W., Hou, Y., and Li, Y. (2018). Linking ecosystem services and ecosystem health to ecological risk assessment: a case study of the Beijing-Tianjin-Hebei urban agglomeration. *Sci. Total Environ.* 636, 1442–1454. doi:10.1016/j.scitotenv.2018.04.427

Khan, M. K., Khan, M. I., and Rehan, M. (2020). The relationship between energy consumption, economic growth and carbon dioxide emissions in Pakistan. *FIN* 6, 1. doi:10.1186/s40854-019-0162-0

Lai, L., Huang, X., Yang, H., Chuai, X., Zhang, M., Zhong, T., et al. (2016). Carbon emissions from land-use change and management in China between 1990 and 2010. *Sci. Adv.* 2, e1601063. doi:10.1126/sciadv.1601063

Lin, H., and Christina, Q. (2019). Urban sprawl in provincial capital cities in China: evidence from multi-temporal urban land products using Landsat data. *Environ. Sci. Technol.* 64, 3.

Liu, H., Wong, W.-K., The Cong, P., Nassani, A. A., Haffar, M., and Abu-Rumman, A. (2023). Linkage among Urbanization, energy Consumption, economic growth and carbon Emissions. Panel data analysis for China using ARDL model. *Fuel* 332, 126122. doi:10.1016/j.fuel.2022.126122

Mcgeeid, J. A., and York, R. (2019). *Asymmetric relationship of urbanization and co 2 emissions in less developed countries*.

Mingde, X. U., Jing, L. I., Jing, P., and Jian, N. (2010). Ecosystem health assessment based on RS and GIS. *Eco. Envir. Sci.*

Munir, Q., Lean, H. H., and Smyth, R. (2020). CO2 emissions, energy consumption and economic growth in the ASEAN-5 countries: a cross-sectional dependence approach. *ENERG Econ.* 85, 104571. doi:10.1016/j.eneco.2019.104571

Peng, J., Liu, Y. X., Li, T. Y., and Wu, J. S. (2017). Regional ecosystem health response to rural land use change: a case study in Lijiang City, China. *Ecol. Indic.* 72, 399–410. doi:10.1016/j.ecolind.2016.08.024

Peng, J., Peng, K., and Li, J. (2018). Climate-growth response of Chinese white pine (Pinus armandii) at different age groups in the Baiyunshan National Nature Reserve, central China. *Dendrochronologia* 49, 102–109. doi:10.1016/j.dendro.2018.02.004

Qiao, X., Gu, Y., Zou, C., Xu, D., Wang, L., Ye, X., et al. (2018). Temporal variation and spatial scale dependency of the trade-offs and synergies among multiple ecosystem services in the Taihu Lake Basin of China. *Sci. Total Environ.* 651, 218–229. doi:10.1016/j.scitotenv.2018.09.135

Ren, W., Ji, J., Chen, L., and Zhang, Y. (2018). Evaluation of China's marine economic efficiency under environmental constraints—an empirical analysis of China's eleven coastal regions. *J. Clean. Prod.* 184, 806–814. doi:10.1016/j.jclepro.2018.02.300

Sciences, S. o.G., Geosciences, S. O. G., and Andrews, U. O. S. (2017). *Multiscale geographically weighted regression (MGWR)*. Ann: Am. Assoc. Geogr.

Shear, H., Stadler-Salt, N., Bertram, P., and Horvatin, P. (2003). The development and implementation of indicators of ecosystem health in the Great Lakes basin. *Environ. Monit. Assess.* 88, 119–152. doi:10.1023/a:1025504704879

Shen, C., Shi, H., Zheng, W., and Ding, D. (2016). Spatial heterogeneity of ecosystem health and its sensitivity to pressure in the waters of nearshore archipelago. *Ecol. Indic.* 61, 822–832. doi:10.1016/j.ecolind.2015.10.035

Sohil, A., and Sharma, N. (2020). Assessing the bird guild patterns in heterogeneous land use types around Jammu,Jammu and Kashmir,India. *Ecol. Process.* 9, 49. doi:10.1186/s13717-020-00250-9

Tian, J. L., Peng, Y., Huang, Y. H., Bai, T., Liu, L. L., He, X. A., et al. (2022). Identifying the priority areas for enhancing the ecosystem services in hilly and mountainous areas of southern China. *JMS* 19, 338–349. doi:10.1007/s11629-021-6672-z

UNFCCC (2015). *Enhanced actions on climate change: China's intended nationally determined contributions*. New York: United Nations.

Wang, B., Ding, M., Li, S., Liu, L., and Ai, J. (2020). Assessment of landscape ecological risk for a cross-border basin: a case study of the Koshi River Basin, central Himalayas. *Ecol. Indic.* 117, 106621. doi:10.1016/j.ecolind.2020.106621

Wang, J. F., Zhang, T. L., and Fu, B. J. (2016). A measure of spatial stratified heterogeneity. *Ecol. Indic.* 67, 250–256. doi:10.1016/j.ecolind.2016.02.052

Wang, Z., Liu, Y., Li, Y., and Su, Y. (2022). *Response of ecosystem health to land use changes and landscape patterns in the karst mountainous regions of southwest China*, 19. China: INT J ENV RES PUB HE.

Wu, H., and Ding, J. (2019). Global change sharpens the double-edged sword effect of aquatic alien plants in China and beyond. *Front. Plant Sci.* 10, 787. doi:10.3389/fpls.2019.00787

Wu, Y., Shi, K., Chen, Z., Liu, S., and Chang, Z. (2022). Developing improved time-series DMSP-OLS-like data (1992–2019) in China by integrating DMSP-OLS and SNPP-viirs. *IEEE T Geosci. REMOTE* 60, 1–14. doi:10.1109/tgrs.2021.3135333

Xia, H., Qin, Y., Feng, G., Meng, Q., Liu, G., Song, H., et al. (2019). Forest phenology dynamics to climate change and topography in a geographic and climate transition zone: the qinling mountains in Central China. *Forests* 10, 1007. doi:10.3390/f10111007

Xie, Z., Gao, X., Yuan, W., Fang, J., and Jiang, Z. (2020). Decomposition and prediction of direct residential carbon emission indicators in Guangdong Province of China. *Ecol. Indic.* 115, 106344. doi:10.1016/j.ecolind.2020.106344

Yan, Y., Zhao, C., Wang, C., Shan, P., Zhang, Y., and Wu, G. (2016). Ecosystem health assessment of the Liao River Basin upstream region based on ecosystem services. *Acta Ecol. Sin.* 36, 294–300. doi:10.1016/j.chnaes.2016.06.005

Yao, Y., Shi-Xin, W., Yi, Z., Rui, L., and Xiang-Di, H. (2012). The application of ecological environment index model on the national evaluation of ecological environment quality. *Remote Sens*.

Ye, C., Li, C., Wang, Q., and Chen, X. (2012). Driving forces analysis for ecosystem health status of littoral zone with dikes: a case study of Lake Taihu. *Acta ecolo. Sin.* 32, 3681–3690. doi:10.5846/stxb201201180111

Yu, C., Kangjuan, L., Jian, W., and Hao, X. (2018). Energy efficiency, carbon dioxide emission efficiency and related abatement costs in regional China: a synthesis of input-output analysis and DEA. *ENERG Econ.* 12, 1–15.

Zhang, H., Qi, Z. F., Ye, X. Y., Cai, Y. B., Ma, W. C., and Chen, M. N. (2013). Analysis of land use/land cover change, population shift, and their effects on spatiotemporal patterns of urban heat islands in metropolitan Shanghai, China. *Appl. Geogr.* 44, 121–133. doi:10.1016/j.apgeog.2013.07.021

Zhang, W., Shen, Y., and Zhou, Y. (2014). Increased CO2 emissions from energy consumption based on three-level nested I-O structural decomposition analysis for beijing. *J. Resour. Eco.* 5, 115–122. doi:10.5814/j.issn.1674-764x.2014.02.003

Zhang, X., Shen, M., Luan, Y., Cui, W., and Lin, X. (2022). Spatial evolutionary characteristics and influencing factors of urban industrial carbon emission in China. *Int. J. Environ. Res. Public Health* 19, 11227. doi:10.3390/ijerph191811227

Zhang, X., Zhang, H., and Yuan, J. (2019). Economic growth, energy consumption, and carbon emission nexus: fresh evidence from developing countries. *Environ. Sci. Pollut. R.* 26, 26367–26380. doi:10.1007/s11356-019-05878-5

Zhao, X., Xu, H., and Sun, Q. (2022). Research on China's carbon emission efficiency and its regional differences. *Sustain* 14, 9731. doi:10.3390/su14159731

Zheng, B., Duan, J., Jia, J., Liu, F., and Yan, Y. (2008). Assessment of ecosystem services of Lugu Lake watershed. *Int. J. Sustain. Dev. World Ecol.* 15, 62–70. doi:10.1080/13504500809469770

frontiers | Frontiers in Environmental Science

TYPE Original Research
PUBLISHED 26 January 2024
DOI 10.3389/fenvs.2024.1339928

OPEN ACCESS

EDITED BY
Chenxi Li,
Xi'an University of Architecture and Technology, China

REVIEWED BY
Xin Long Xu,
Hunan Normal University, China
Yuanyuan Hao,
Jiangsu University of Technology, China

*CORRESPONDENCE
Shuangcheng Luo,
luo_sc@163.com

RECEIVED 17 November 2023
ACCEPTED 15 January 2024
PUBLISHED 26 January 2024

CITATION
Qian Q and Luo S (2024), The dilemma of land green use efficiency in resource-based cities: a perspective based on digital transformation. *Front. Environ. Sci.* 12:1339928. doi: 10.3389/fenvs.2024.1339928

The dilemma of land green use efficiency in resource-based cities: a perspective based on digital transformation

Qiulan Qian[1] and Shuangcheng Luo[2]*

[1]Hunan Vocational College of Commerce, Changsha, China, [2]School of Economics, Hunan Agricultural University, Changsha, China

Introduction: Improving land use efficiency is a necessary way to promote sustainable urban development. The objective of this study is to examine the issue of land green use efficiency (LGUE) in resource-based cities and analyze the impact of digital transformation on LGUE. The research utilizes data from 113 resource-based cities in China spanning from 2008 to 2020.

Methodology: Firstly, using the stochastic frontier analysis (SFA) to measure LGUE in China cities, this paper investigates the spatial and temporal evolution of LGUE in different cities. Then, this paper explores the impact of digital transformation on the LGUE of resource-based cities based on the broadband China policy using the DID method.

Findings: According to the data measured by the SFA, it is found that resource-based cities are 20.4% lower than non-resource-based cities. An in-depth study found that digital transformation significantly improves LGUE, and the effect is greater in resource-based cities, which is a powerful tool to solve the difficulty of LGUE in resource-based cities. Specifically, digital transformation helps to improve the LGUE of resource-based cities enhance by technological innovation and industrial structure upgrading, and alleviating land factor mismatch.

Discussion: It is not only necessary to guide and encourage the in-depth integration of traditional industries with digital technology to enhance the digital transformation of resource-based cities, but also to continuously optimize the allocation of land resources between regions and narrow the gap in LGUE between cities.

KEYWORDS

land green use efficiency, digital transformation, resource-based cities, "Broadband China" policy, stochastic frontier analysis

1 Introduction

With the continuous development of industrialization and urbanization, countries have intensified the use of land resources. However, the transformation of land resources from their natural state to urban construction land is usually irreversible (Torrey and Jolly, 1993), which has triggered a great deal of attention to the rational and full utilization of land resources. China is a populous country, and China's urbanization rate has grown from 17.9% in 1978 to 65.2% in 2022. The massive rural-urban migration and industrial development have exacerbated the

consumption of land resources and triggered serious land-use problems, including the loss of arable land, inefficient allocation of land resources, land resource tension, and unbalanced urban-rural development (Liu et al., 2014; Huang and Song, 2019), which has attracted extensive attention from the political and academic circles. How to coordinate land use, promote the effective distribution of land resources, and improve the efficiency of land use has become the key to alleviate land use problems.

Resource-based cities are formed and developed through the development and processing of abundant natural resources (Martinez-Fernandez et al., 2012), and urban development is often characterized by a high degree of dependence on resource-based industries, a single industrial structure, and distorted factor allocation. According to the definition of resource-based cities in the National Sustainable Development Plan for Resource-Based Cities (2013–2020), there are 262 resource-based cities in China (116 of which are prefecture-level cities), accounting for 30% of all cities in developing countries (Li et al., 2021). Resource-based cities provide a variety of basic raw materials for economic growth and contribute greatly to economic development. However, the development of resource-based cities is constrained by the characteristics of industrial structure and the dependence on the environment, and the land green use efficiency (LGUE) is often low. Some research has been found that land use problems are more prominent in resource-based cities because of their higher degree of resource dependence and more serious ecological damage (Chen et al., 2019a; Ge and Liu, 2021). According to the data measured by the stochastic frontier analysis (SFA) in this paper, on average, the LGUE of resource-based cities is 20.4% lower than that of non-resource-based cities. The study in this paper confirms the land use dilemma in resource-based cities.

How to improve the LGUE of resource-based cities is a top priority for alleviating land tension and developing green economy. Most of the existing studies have explored how to improve land use efficiency from the aspects of economic development and industrial structure (Masini et al., 2019; Koroso et al., 2020; Liu et al., 2021), and few studies have explored the impact of digital transformation on LGUE. Tang et al. (2022) found that the efficiency of technology use is the main constraint on land use efficiency (Tang and Chen, 2022).Tang and Chen (2022) found that digital construction can effectively improve the green use efficiency of regional cropland, confirming the favorable contribution of digital transformation to land use (Tang et al., 2022). Some studies have also explored the economic effects of digital land use planning (Hersperger et al., 2022; Adade and Vries, 2023; Kyriakopoulou and Picard, 2023). However, there is a lack of research on the factors influencing the LGUE of resource cities, and how digital transformation affects the LGUE of resource-based cities is still unknow.

The innovations of this paper compared to the existing studies are as follows. Firstly, based on the SFA, we measured the LGUE of resource-based cities and non-resource-based cities, and explored the spatial and temporal evolution characteristics of the LGUE of resource-based cities. Secondly, we explore the mechanism of improving LGUE from the aspects of technological innovation and technological application capacity, and the mechanism of digital transformation affecting LGUE, which supplements the existing literature. Thirdly, in combination with the "Broadband China" policy, we use the differences-in-differences (DID) method to empirically test the impact and mechanism of digital transformation on LGUE, which effectively overcomes the bias of the estimation caused by the endogeneity problem.

The next part of this paper is arranged as follows. The second part is a literature review, combing the relevant literature from the measurement of LGUE and its influencing factors, and pointing out the deficiencies and gaps in the existing literature. The third part theoretically analyzes how to improve the LGUE, and combs through the mechanism of the impact of digital transformation on the LGUE. The fourth part utilizes the SFA approach to measure the LGUE, and analyzes the spatial and temporal evolution characteristics of LGUE in Chinese cities. The fourth part is data description and research methods, and the fifth part is the empirically results, analyzes the impact of digital transformation on LGUE based on the Broadband China policy. The sixth part is the conclusion.

2 Literature review

From the existing literature, relevant studies have done a lot of analysis mainly from the aspects of land use efficiency measurement and its influencing factors, but there are not many studies exploring the impact of LGUE from the perspective of digital transformation.

Regarding land use efficiency, studies have pointed out that the development of urbanization and industrialization needs to consume a large amount of land resources, resulting in urban land resources becoming more scarce, and how to improve land use efficiency and promote the sustainable use of land is the key to solving the land problem (Liu, 2018). Therefore, the study of land use efficiency is of great significance for high-quality urban development. Some research pointed out that the rapid process of China's urbanization has really increased the scarcity of urban construction land (Liu and Ravenscroft, 2017). In terms of urban land use efficiency measurement, mainstream methods include SFA, data envelopment analysis (DEA), and SBM model (Chen et al., 2016; Jia et al., 2017; Yu et al., 2019). Compared with other methods, the advantage of the SFA is that it can separate the random interference term from the technical inefficiency term and reduce the influence of random factors, and for the selection of the production function, it can use the transcendental logarithmic function that is more flexible, easy to estimate and inclusive. So it is widely used in the measurement of land use efficiency (Liu et al., 2020). This provides the theory and methodology for the study in this paper.

Since land use efficiency affects resource consumption and environmental pollution, people have begun to pay more attention to LGUE. Relevant studies have pointed out that because urban industrial development can create tax revenue for the government, industrial land is often oversupplied in urban construction land and the price of the land is low, resulting in a mismatch of land resources. The oversupply of industrial land reduces enterprise costs, squeezes the resources of emerging enterprises, and reinforces the structural rigidity of low-end industries, which together form a crude economic development model that exacerbates resource consumption and environmental pollution in the long run (Xie et al., 2022). Improving land use efficiency not only improves the efficiency of industrial inputs and facilitates the treatment of industrial pollutants (Peng et al., 2017; Li et al., 2021), but also ameliorates environmental pollution and CO2 emissions by shortening commuting distances, promoting industrial transformation, and improving transportation efficiency (Zhang et al., 2018; Dong et al., 2020). On this basis, some studies have considered the comprehensive benefits of economy, ecology, and society when analyzing land use efficiency (Lu et al., 2020; Tan et al., 2021), and focused on the LGUE.

For this reason, this paper focuses on the LGUE from an environmental perspective.

Regarding the influencing factors of land use efficiency, most of the existing literature discusses how to improve land use efficiency from the aspects of economic development, residents' income, industrial structure, etc. Some scholars studied the land use efficiency of 417 metropolitan cities in Europe, and found that residents' income and wealth affect land use efficiency, and, specifically, wealthier cities tend to have higher land use efficiency (Masini et al., 2019). Some scholars studied land use efficiency in Ethiopia from the perspective of urban land lease policy and concluded that factors such as increasing land productivity and ensuring sustainable urban growth are key to improving land use efficiency (Koroso et al., 2020). In addition, some research have found that industrial restructuring not only promotes intensive land use in local areas, but also has a large radiation effect on other areas (Peng et al., 2017), while affecting urban land use efficiency by changing the urban land use structure and promoting the reconfiguration of land resources in various industrial sectors (Liu et al., 2021). Some research also explored the impact of urban land use efficiency from the perspective of factor mobility, and found that labor and capital factor mobility has a promotional effect on land use efficiency (Lu et al., 2022).

In recent years, more and more literature has begun to focus on the value of digital technology applications, exploring the relationship between digital transformation and business performance and technological innovation from a micro perspective (Bouwman et al., 2019; Ribeiro-Navarrete et al., 2021; Wu et al., 2023), and analyzing the digital economy from a macro perspective impact on macroeconomic stability, carbon emissions (Bertani et al., 2021; Li and Wang, 2022; Ma et al., 2022; Luo and Yuan, 2023). In addition, digital transformation contributes to green technological innovation and industrial structure transformation, thus affecting green economic growth (Hao et al., 2023). Thus, digital transformation plays an important role in technological innovation and improving environmental performance, and influences the regional industrial structure, which in turn has a profound impact on the efficiency of green land use. However, the existing literature lacks to explore the impact of LGUE from the perspective of digital transformation, and its transmission mechanism is not yet clear. The study in this paper will be a useful addition to the field.

3 Theoretical analysis

3.1 Theoretical analysis of LGUE

The SFA was first proposed by Aigner (Aigner et al., 1977), aiming to explore the gap between the actual output of each unit within the economic system and the optimal output, so as to characterize the ability to achieve optimal production under the given conditions. In reality, due to various frictions and impediments, production subjects often deviate from the optimal production state in practice, resulting in inefficiency. Therefore, the production subject in the given conditions, through continuous adjustment of production inputs, technology application, etc. to ensure that the production process of output maximization and profit maximization goals.

As far as land use is concerned, land and factors such as capital and labor are used as actual inputs for production, and the output component includes both the actual outputs of various sectors of the economy (desired outputs) and the pollution emissions caused by production (non-desired outputs). Under the conditions of comprehensive consideration of desired and non-desired outputs, the efficiency of green land use, can be measured. This is done by considering pollution emissions as a consumption of environmental resources, i.e., pollution emissions are included in the super-efficient production function as a production input. From the existing studies, they included energy and other raw materials as intermediate inputs (Jorgenson and Stiroh, 2000), together with capital and labor, into the production function to analyze the economic growth and productivity of the United States in the post-World War II period. Some research included energy and emissions together as inputs into the production function (Ramanathan, 2005; Lu et al., 2006). In addition, there are some studies that directly introduce both desired and non-desired outputs into the production process at the same time and analyze them using the directional distance function (Chung et al., 1997).

According to the SFA, it is difficult to guarantee that land will achieve the optimal output under the given conditions in the actual development. Referring to the related research (Liu et al., 2021), a theoretical model is constructed to analyze the technical inefficiency situation in the LGUE (as shown in Figure 1).

Assuming that F_1 is the stochastic frontier boundary of land use input and output, the actual land input is C_1 and the actual output is y_1 under the established conditions, at this time, y_1 has not yet reached the optimal output scale, and there exists the phenomenon of inefficiency ($\mu_1 \neq 0$). When the economic agents continue to improve the ability to apply technology, improve technical efficiency to fully efficient, $\mu_1 = 0$, the actual output then grows to y_2. At this time the actual output may be subject to stochastic disturbances, that is, it may be higher than the optimal output (i.e., $v < 0$), may also be lower than the optimal output (i.e., $v > 0$). The SFA separates the stochastic disturbing factors from the technical inefficiency, and analyzes the gap between the actual output and the optimal output after the elimination of the stochastic disturbing factors. Ratio of y_1 to y_2 can reflect the technical efficiency of the land use (taking the value between 0 and 1), and when the value is equal to 1, it means that the input and output of the land use at this time reaches the fully efficient state.

In the case of technology and other conditions remain unchanged, when the land use from C_1 to C_2, the actual output from y_1 to y_3, assuming that the random interference factors have been removed, the actual output y3 and technically efficient output gap is μ_2. With the increasing inputs of land and other factors, external competition gradually intensified, the economic agents can promote production by improving the ability to apply the technology to improve technical efficiency. That is, the actual output of land use increases from y_3 to y_4, and the gap between the actual output of land use and the technologically effective output is narrowing ($\mu_3 < \mu_2$). If technological progress occurs, frontier production increases from F_1 to F_2 levels, and real output increases accordingly ($y_5 > y_4$). To summarize, the main channels to increase real output can be to improve technology application capabilities and to promote technological progress. If technology application capacity and technological progress occur simultaneously, the technical efficiency of land use and real output will be greatly enhanced.

3.2 Analysis of the role of digital transformation on LGUE

According to the theoretical analysis in the previous section, the impact of digital transformation on the LGUE in resource-based cities is also mainly reflected in the promotion of technological innovation, enhancement of technological application capacity, and improvement of land resource mismatch.

Firstly, digitalization helps technological innovation, especially for green innovation that reduces the consumption of environmental resources plays a significant role. For one thing, digital transformation helps to reduce R&D costs, shorten the R&D cycle, consumer participation in product development, etc., and improve the level of enterprise innovation (Tan and Zhan, 2017). Digital transformation can effectively alleviate information asymmetry and improve the matching efficiency of supply and demand of innovation factors such as R&D capital and innovation talents, which play a key role in industrial structure upgrading and technological innovation. Secondly, digital finance based on information technology can reduce information asymmetry and improve the efficiency of capital allocation, thus effectively solving the problem of "difficult and expensive financing" of enterprises. Third, digital transformation can help enterprises grasp market demand in a timely manner, integrate internal and external data resources to improve the efficiency of collaboration, and promote R&D innovation (Kleis et al., 2012), and can also encourage enterprises to cooperate with consumers to enrich the idea of new product development (Hoyer et al., 2010; Schweisfurth, 2017).

Secondly, digital transformation helps to enhance the ability to apply technology and drives the transformation of industrial structure. Digital transformation promotes the intelligence, automation and informatization of enterprise production and services, and enhances the enterprise's technological application capabilities. In terms of production, digital technologies can increase the intelligent and flexible design of products to meet the diversified and customized product needs of consumers and reduce the manufacturing costs and selling prices of products. In terms of service, intelligent back-end production, customer service and software systems can provide users with diversified and constantly upgraded services, such as personalized customization, system solutions, product performance maintenance and optimization, which greatly improves the types of services and efficiency of manufacturing enterprises. With the deep integration of digital technology and the real economy, new industries such as intelligent transportation and intelligent energy have been spawned, as well as new modes and new business forms such as online education, Internet healthcare, online office, digital governance, etc., which eliminate backward and inefficient production capacity and promote the transformation and upgrading of the real industry. Some research applied the data of Brazilian SMEs and found that automation technology is a key factor in upgrading the value chain of enterprises (Oliveira et al., 2021). Some scholars also found that digital economic development and technological innovation are important driving forces in promoting the upgrading of industrial structure (Su et al., 2021).

Finally, digital transformation also helps to improve the mismatch of land resources, thus enhancing the LGUE. In China, with the increasing level of urbanization and industrialization, the demand for construction land for urban development continues to grow, while the transformation of land from agricultural land to urban construction land requires planning and approval by the central and provincial governments. This may lead to two scenarios: urbanization of population is greater than urbanization of land or urbanization of land is greater than urbanization of population. The former may create a "congestion effect", resulting in traffic jams and high land prices, while the latter may lead to the disorderly spread of cities, resulting in "empty cities", "ghost cities", and "ghost towns", thus leading to the spatial mismatch of land resources. Digital transformation mainly improves the land resources mismatch phenomenon from two aspects. On the one hand, digital transformation has the function of discovering the transaction object and transaction value, which can reduce the information asymmetry and transaction cost, so as to enhance the actual utilization value of land. On the other hand, digital technology enables the government to grasp more data on land use, traffic operation, population flow, etc., which helps the government to adjust the land policy in a timely manner, and improves the governmental governance capacity and transparency (Erkut, 2020). Based on the above analysis, this paper proposes the following hypotheses.

H1: Digital transformation enhances the LGUE in resource-based cities by promoting green technology innovation, industrial structure upgrading and improving land resource allocation.

4 LGUE measurement and spatial and temporal evolution

4.1 Measurement methods

Currently, the methods used to measure land use efficiency mainly include SFA, SBM, DEA, etc. Compared with other non-parametric methods, the SFA has the advantage of separating the stochastic factors in the composite error, which reduces the bias caused by deviation from the optimum due to the stochastic factors in the efficiency measurement. Therefore, this paper adopts the SFA to measure the LGUE. The SFA can generally take the form of Cobb-Douglas function and super-efficiency function. The former function form is too simplified and difficult to reflect the reality. Therefore, this paper adopts the latter, and constructs the stochastic frontier production function model that takes logarithm on both sides beyond the logarithmic production function, as shown in Eq. 1.

$$\begin{aligned}\ln Y_{it} = {} & \beta_0 + \beta_K \ln K_{it} + \beta_L \ln L_{it} + \beta_P \ln P_{it} + \beta_C \ln C_{it} + \beta_t t \\ & + \frac{1}{2}\beta_{KK} (\ln K_{it})^2 + \frac{1}{2}\beta_{LL} (\ln L_{it})^2 + \frac{1}{2}\beta_{PP} (\ln P_{it})^2 + \frac{1}{2}\beta_{CC} (\ln C_{it})^2 \\ & + \frac{1}{2}\beta_{tt} t^2 + \beta_{Kt} (\ln K_{it}) t + \beta_{Lt} (\ln L_{it}) t + \beta_{Pt} (\ln P_{it}) t + \beta_{Ct} (\ln C_{it}) t \\ & + \beta_{KL} (\ln K_{it}) (\ln L_{it}) + \beta_{KP} (\ln K_{it}) (\ln P_{it}) + \beta_{KC} (\ln K_{it}) (\ln C_{it}) \\ & + \beta_{LP} (\ln L_{it}) (\ln P_{it}) + \beta_{LC} (\ln L_{it}) (\ln C_{it}) \\ & + \beta_{PC} (\ln P_{it}) (\ln C_{it}) + v_{it} - u_{it} \end{aligned} \quad (1)$$

Y is real output. K, L, and P denote capital, labor, and land, respectively. C denotes pollution emissions, measured by sulfur dioxide emissions from urban industries. Pollution emission is actually a non-desired output, which is included as an input factor in the super-efficient production function, this is because

the emission is a consumption of the natural environment, which can increase the level of output given the other input factors, and thus can be considered as one of the input factors. The subscript i denotes the city, t denotes the year, and β denotes the parameter to be estimated. v_{it} and u_{it} are the random error term and inefficiency term, respectively.

The LGUE can be expressed as the ratio of the actual output of urban land use to the expected value of the output under the fully efficient technology, and the specific calculation formula is shown in Eq. 2.

$$LGUE_{it} = \frac{E(y_{it} \mid u_{it}, X_{it})}{E(y_{it} \mid u_{it} = 0, X_{it})} = \exp(-u_{it}) \quad (2)$$

4.2 Construction of input-output indicators

Input indicators mainly include capital, labor, and land factor inputs (as shown in Table 1). The capital input adopts the perpetual inventory method to calculate the fixed capital stock of the municipal district. The calculation method is as follows: $K_{it} = K_{i,t-1}(1-\delta) + I_{it}$. Referring to the existing studies, the depreciation rate $\delta = 9.6\%$. I_{it} is the total investment in the current period. And the year 2000 is chosen as the base period. Labor input is expressed by the number of people employed in secondary and tertiary industries in the municipal area, and land input is expressed by the area of urban construction land in the municipal district.

Output indicators include desired output and non-desired output. Desired output is the level of economic growth and is expressed by the real value added of the secondary and tertiary industries in the municipal district. Taking 2008 as the base period, the actual output value is calculated by adjusting the value added index of the secondary and tertiary industries. In this paper, the non-desired output is regarded as the input variable introduced into the super-efficient production function, in which the non-desired output is the pollution emission, which is expressed by the urban sulfur dioxide emission.

4.3 Spatial and temporal evolution of LGUE

(1) Temporal change characteristics

According to the availability of data, this paper selects the data of 282 prefecture-level cities in China (including 113 resource-based cities and 169 non-resource-based cities), and uses the SFA to measure the LGUE. In terms of time, the main features are as follows. First, in general, the LGUE of both resource-type cities and non-resource-type cities improved significantly from 2008 to 2020. After removing the random disturbance term, China's technological progress as well as its technological application capacity are improved, reducing the degree of inefficiency, thus greatly improving the LGUE. Second, compared with non-resource-based cities, the LGUE of resource-based cities is much lower than that of non-resource-based cities, and on average, the LGUE of resource-based cities is 20.4% lower than that of non-resource-based cities. The higher degree of dependence on resource-based industries and the unitary industrial structure of resource-based cities, and the greater consumption of environmental resources and land elements by this economic structure and the consequent lower efficiency, which is one of the key factors constraining the improvement of LGUE in resource-based cities.

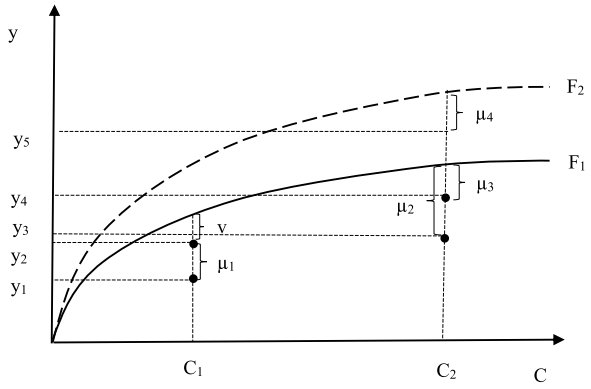

FIGURE 1
Theoretical analysis of LGUE. Note: The horizontal axis C denotes the land input, and the vertical axis y denotes the actual output under the corresponding land input; v denotes the stochastic disturbance term, where v > 0 means that the stochastic disturbance term negatively affects the output, and *vice versa* positively. μ_1, μ_2, μ_3, and μ_4 denote technological inefficiencies. F_1 and F_2 denote the optimal output scenarios under the different technological conditions, with the output of F_2 having a higher technological level.

(2) Spatial structure characteristics

According to the availability of data, resource-based cities in the sample are mainly concentrated in the central, northeastern and western regions. Using Arcgis software, this paper observe the spatial distribution of LGUE in resource-based cities and use non-resource-based cities as the comparative object (as shown in Figures 2, 3). In resource-based cities, LGUE is higher in the Northeast region, followed by the Central region, and lowest in the West region, i.e., showing a decreasing trend of Northeast > Central > West. In terms of time, compared with 2008, the LGUE of resource-based cities in 2020 has improved significantly, still showing a decreasing trend of Northeast > Central > West. Due to the serious missing data of some prefecture-level cities and states in the west, the observed non-resource-based cities are distributed in both the east, center and west regions. For non-resource-based cities, the LGUE in the eastern region is significantly higher than that of other cities, and the number of cities with higher LGUE in the eastern region increases significantly over time. By 2020, Chengdu-Chongqing, the middle reaches of the Yangtze River, and other cities in central and western in China also show a significant increase in LGUE.

5 Data description and research methods

5.1 Background of "Broadband China" policy

In order to solve the problems of slow network speed and unbalanced regional network development, and to promote the

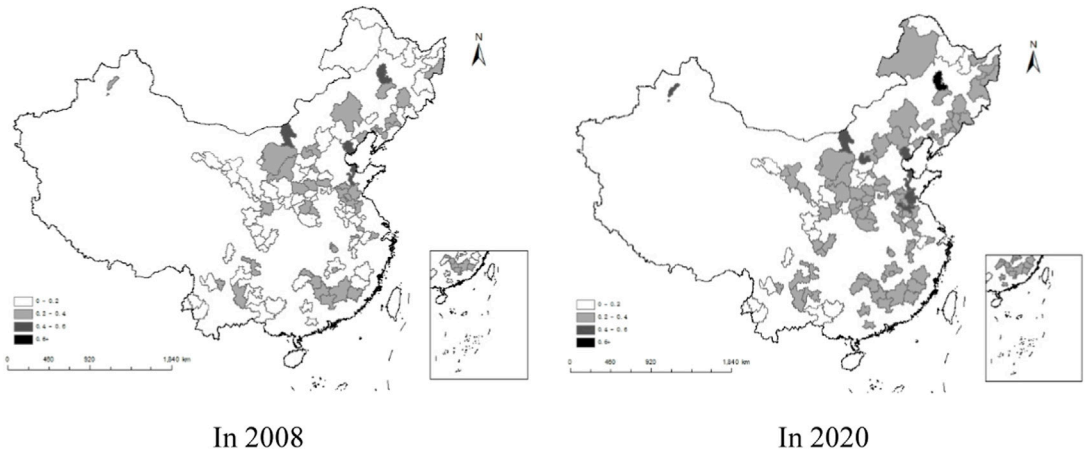

FIGURE 2
Evolution of the LGUE in resource-based cities.

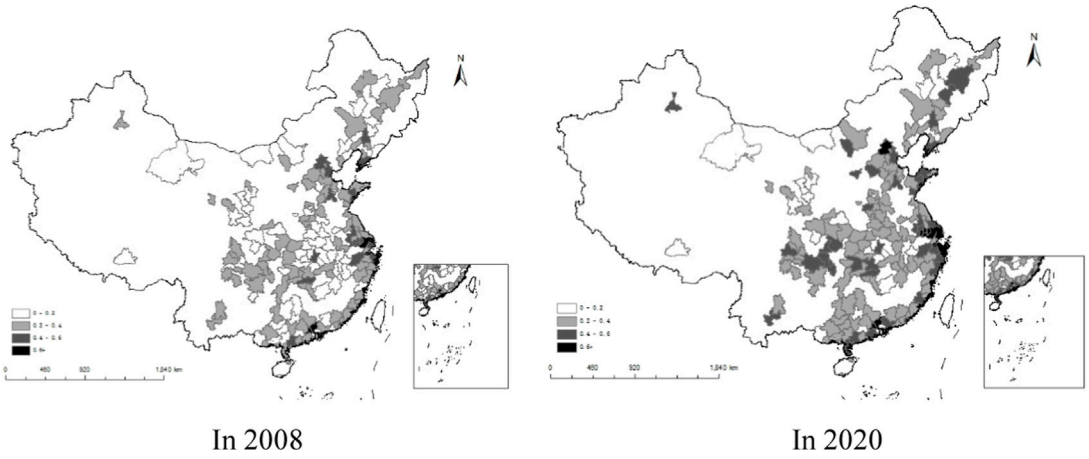

FIGURE 3
Evolution of the LGUE in non-resource-based cities. Note: Resource-based cities are established according to the National Sustainable Development Plan for Resource-based Cities (2013–2020) in China. The LGUE is divided into four grades based on 0–0.2, 0.2–0.4, 0.4–0.6, and 0.6+, and the darker the color indicates the higher the LGUE. Blank areas are areas with missing data.

construction and development of network infrastructure, China's State Council issued the "Broadband China" Strategy and Implementation Plan in August 2013, thus elevating broadband network construction to a national strategy. Subsequently, the Ministry of Industry and Information Technology (MIIT) and the National Development and Reform Commission (NDRC) jointly issued the Measures for the Administration of the Work of Creating "Broadband China" Demonstration Cities (City Clusters) (hereinafter referred to as the Measures), which were based on the indicators of household broadband access capacity, broadband penetration, cell phone penetration, and broadband subscriber penetration, etc., and were issued in three batches in 2014, 2015 and 2016. Finally, 120"Broadband China" demonstration cities (clusters) were selected in three batches.

The Measures clearly point out that "Broadband China" demonstration cities (city clusters) refer to those cities (city clusters) that have a good foundation for broadband development, have realized a significant increase in the level of broadband development in the region through the creation of demonstrations, and have a greater role in demonstrating and leading the overall level and mode of broadband development for the same kind of regions in the country. The focus of the construction of demonstration cities includes improving the speed and application level of broadband networks, promoting the continuous improvement of the broadband network industry chain, and enhancing the security guarantee capability of broadband networks, so as to promote the digital transformation of the cities through the construction of network infrastructures. Therefore, the "Broadband China" policy can be regarded as a quasi-natural experiment for this paper to analyze the impact of digital transformation on the LGUE.

TABLE 1 Input-output related indicators and their definitions.

Category	Indicator	Indicator definition
Input Indicators	Capital (*K*)	Fixed capital stock of the municipal district (million RMB)
	Labor Force (*L*)	Employed population in secondary and tertiary industries under the municipal district (10,000 people)
	Land (*P*)	Urban construction land area under the municipal district (km^2)
Output Indicators	Desired Outputs: Economic Growth (*Y*)	Value added of secondary and tertiary industries in the municipal district (million RMB)
	Non-desired output: Pollution emissions (*C*)	Industrial sulfur dioxide emissions in the municipal district (10,000 tons)

TABLE 2 Descriptive statistics results of variables for resource-based cities.

Variable	N	Mean	SD	p50	Min	Max
LGUE	1,469	0.241	0.0890	0.226	0.0610	0.621
Digit	1,469	0.140	0.347	0	0	1
Popu	1,241	0.0770	0.0830	0.0480	0.00100	0.793
GDPr	1,469	0.0860	0.0320	0.0870	−0.0500	0.165
Struc	1,469	0.499	0.130	0.504	0.130	0.854
FDI	1,225	4.306	1.508	4.468	−1.369	7.351
Aggl	1,356	0.946	0.318	0.989	0.156	1.650
Land	1,349	0.0700	0.0860	0.0380	0.00100	0.800
Envi	1,241	0.100	0.0620	0.0880	0.00800	0.560

5.2 DID model

In order to explore the impact of digital transformation of resource-based cities on the LGUE, the multi-period differences-in-differences model (DID) is constructed as shown in Eq. 3.

$$LGUE_{it} = \beta_0 + \beta_1 Digit_{it} + \beta_2 \sum Controls_{it} + \mu_i + \delta_t + \varepsilon_{it} \quad (3)$$

Where, i denotes city, t denotes year, μ_i and δ_t denotes city fixed effect and year fixed effect respectively. $LGUE_{it}$ denotes the LGUE, which is calculated according to the SFA method. $Digit_{it}$ is a digital transformation indicator, if the city i is recognized as a "Broadband China" demonstration city, then the city is recognized in that year and the following period $Digit_{it} = 1$, otherwise $Digit_{it} = 0$. β_1 is a parameter to be estimated, if $\beta_1 > 0$, then it means that the LGUE is significantly improved after the implementation of the "Broadband China" policy, implying that the digital transformation promotes the improvement of LGUE.

5.3 Data sources and treatment of variables

This paper selects Chinese cities as the initial sample of the study, deletes some cities with serious data missing, considers data availability, and finally obtains 113 resource-based cities from 2008 to 2020. The land green utilization efficiency was measured by the SFA method, some missing values were filled in by linear interpolation, and all variables were shrink-tailed at the bilateral 1% level in order to avoid the interference of extreme values on the empirical results. All data were obtained from the China Urban Statistical Yearbook.

In this paper, the relevant variables affecting the efficiency of green land use are controlled as follows. Population density is one of the key factors affecting the LGUE, and urban construction land resources should match the population flow, otherwise it may cause the problem of spatial mismatch of urban construction land. Therefore, this paper uses the number of population per square kilometer of urban area to reflect the population density (Popu). Economic growth also affects the LGUE, and the faster the economic growth rate, the greater the consumption of land resources and environmental resources by urbanization and industrialization. This paper uses the GDP growth rate (GDPr) to measure the economic growth rate. Industrial development is a direct factor affecting LGUE, which is measured by the proportion of the secondary industry in GDP in this paper (Struc). The degree of industrial agglomeration is also directly related to the LGUE, therefore the entropy of secondary industry location, i.e., the ratio of the proportion of city secondary industry employment to the regional total employment and the proportion of national secondary industry employment to the national total employment, is used to reflect the level of regional industrial agglomeration (Aggl). Whether foreign direct investment (FDI) affects land use has received extensive attention from scholars (Vongpraseuth and Choi, 2015; Wu and Heerink, 2016), and in order to control for its potential impact, a foreign direct investment indicator (FDI) is added to the regression model and measured by the intensity of actual utilization of foreign capital. In addition, this paper also controls for variables related to land use and environmental resources, including two indicators of the breadth of land development and utilization (Land) and the level of human habitat (Envi). Table 2 reports the results of descriptive statistics for the main variables for resource-based cities.

The left three columns of Table 3 report the mean values of the indicators and the significance of the differences between resource-based cities and non-resource-based cities. The results show that compared with non-resource-based cities, the LGUE of resource-based cities is low and significant at the 1% level. The population density, foreign direct investment, and breadth of land development and utilization in resource-based cities are lower than those in non-resource-based cities, but the average value of resource-based cities is higher in the proportion of secondary industry and industrial agglomeration, indicating that resource-based cities mainly develop the secondary industry and the industrial structure is relatively concentrated.

TABLE 3 Comparison of group differences of main variables.

	(1) Resource-based cities	(2) Non-resource-based cities	MeanDiff	(3) Experimental group	(4) Control groups	MeanDiff
LGUE	0.303	0.241	0.062***	0.285	0.220	0.065***
Popu	0.098	0.077	0.021***	0.087	0.072	0.015***
GDPr	0.088	0.086	0.002	0.087	0.086	0.001
Struc	0.457	0.499	−0.042***	0.522	0.488	0.034***
FDI	5.054	4.306	0.749***	4.651	4.132	0.519***
Aggl	0.914	0.946	−0.033***	1.032	0.906	0.126***
Land	0.097	0.070	0.026***	0.083	0.064	0.018***
Envi	0.103	0.100	0.003	0.113	0.0940	0.020***

Note: *, **, *** indicate 10%, 5%, and 1% significance levels, respectively. The left three columns are categorized according to whether they are resource-based cities; the right three columns are categorized according to whether they are "Broadband China" demonstration cities.

The right three columns of Table 3 report the means and significance of differences between the experimental and control groups of resource-based cities. Depending on whether the city is recognized as a "Broadband China" city or not, the resource-based cities are divided into a digital transformation experimental group (Digit = 1) and a control group (Digit = 0). The results show that the mean value of the indicators of the experimental group is significantly higher than that of the control group, indicating that digital transformation has a significant impact on the LGUE, economic growth, industrial agglomeration and so on.

6 Results

6.1 Benchmark regression results

Table 4 reports the estimation results of the impact of digital transformation on LGUE. Column (1) does not control the relevant control variables, and column (2) adds control variables based on column (1). The results show that the coefficients of the impact of digital transformation on LGUE are significantly positive, indicating that the implementation of the "Broadband China" policy promotes the digital transformation of cities and improves the LGUE of resource-based cities. As a comparison, this paper also estimates the impact of digital transformation on LGUE in non-resource-based cities. The results of columns (3) and (4) in Table 4 show that the coefficients of digital transformation impact on LGUE in non-resource-based cities are significantly positive, but the coefficients are smaller than that of resource-based cities (0.000864 < 0.00118), which indicates that the effect of digital transformation on the improvement of LGUE is universal, but has a greater impact on resource-based cities. Therefore, it is particularly important for resource-based cities to accelerate the promotion of city digital transformation.

From the perspective of control variables, the influence coefficient of the proportion of the secondary industry in GDP on the LGUE is positive, indicating that industrial production consumes more environmental resources, and promoting the upgrading of the industrial structure is crucial for the green utilization of urban land. For resource-based cities, the increase in population density inhibits the improvement of LGUE, but industrial agglomeration can improve LGUE. For non-resource-based cities, economic growth has a significant contribution to the improvement of LGUE, indicating that the output per unit of land resources increases significantly under certain other conditions, which helps to improve LGUE.

6.2 Parallel trend test and its dynamic effect analysis

Taking the "Broadband China" policy as the background, this paper uses the DID to test whether the digital transformation affects the LGUE, which needs to satisfy the parallel trend assumption. It needs to test that before the implementation of the "Broadband China" policy, the treatment group and the control group have a consistent trend of change in the LGUE. The parallel trend hypothesis test is carried out using the event study method, and the regression model is shown in Eq. 4.

$$LGUE_{it} = \beta_0 + \sum_{d=-7}^{6} \beta_d Post_{dt} + \beta_2 \sum Controls_{it} + \mu_i + \delta_t + \varepsilon_{it} \quad (4)$$

Where, $Post_{dt}$ denotes the dummy variable for the implementation of "Broadband China" policy at different event points. The range of values is $-8 \le d \le 6$, d equal to 0 means that the city in the year of the implementation of "Broadband China" policy, at this time the dummy variable actually takes the value of 1, otherwise it is 0. The time period $d = -8$ as the control group for the estimation of the double-fixed-effects model. If the estimated coefficients β_d fluctuate around 0 and do not pass the significance test before the implementation of the "Broadband China" policy, it can be said that the parallel trend is satisfied.

Figure 4 shows the parallel trend test, the vertical axis is the size of the estimated coefficient of the impact of the "Broadband China" policy on LGUE in different periods, the horizontal axis is the relative time before and after the implementation of the "Broadband China" policy. 0 indicates the initial period of the implementation of the "Broadband China" policy, and the dotted lines above and below the hollow circles are the 95% confidence intervals. The results in the figure show that before the implementation of the "Broadband

TABLE 4 Baseline regression results of digital transformation on LGUE.

	Resource-based cities		Non-resource-based cities	
	(1)	(2)	(3)	(4)
	LGUE	LGUE	LGUE	LGUE
Digit	0.00119***	0.00118***	0.000838***	0.000864***
	(0.000)	(0.000)	(0.000)	(0.000)
Popu		−0.00342**		−0.00332
		(0.002)		(0.003)
GDPr		−0.00416		0.0143**
		(0.006)		(0.006)
Struc		−0.00397***		−0.00324***
		(0.001)		(0.001)
FDI		−0.0000166		−0.0000797
		(0.000)		(0.000)
Aggl		0.00101**		0.000214
		(0.000)		(0.001)
Land		0.00192		−0.00226
		(0.001)		(0.002)
Envi		−0.00398		0.000524
		(0.003)		(0.007)
Constant	0.247***	0.249***	0.310***	0.311***
	(0.000)	(0.001)	(0.000)	(0.001)
City FE	Yes	Yes	Yes	Yes
Year FE	Yes	Yes	Yes	Yes
Adj. R^2	0.99	0.99	0.99	0.99
F	34.50	6.632	18.37	9.663
N	1,128	1,128	1,693	1,693

Note: ***, **, and * denote significance at the 1%, 5%, and 10% levels, respectively; robustness standard errors are in parentheses below the coefficients.

China" policy, the coefficients of the estimates is around the value of 0, which indicates that the parallel trend is satisfied. After the implementation of the "Broadband China" policy, digital transformation has a sustained positive impact on LGUE, and there is a lag in this impact.

6.3 PSM-DID estimation

The difference-in-difference based on propensity score matching (PSM-DID) can alleviate the problem of "selective bias" of the pilot policy to a certain extent, so this paper conducts a robustness test through the PSM-DID model. In order to avoid the loss of sample size after matching, this paper adopts one-to-two caliper nearest neighbor matching (Luo and Yuan, 2023). Estimation using this model needs to satisfy the balance test, i.e., after matching, the relevant control variables are not significantly different between the treatment and control groups. The results of the balance test in Figure 5 show that after matching, the difference in the means of the control variables between the treatment and control groups is not significant, implying that the balance test condition is satisfied.

Table 5 shows the estimation results under the conditions that the matching meets the com-mon support hypothesis and the weight is not null after matching. The estimated coefficients, significance, and direction of action of the model are in high agreement with the previous results, which indicates that the previous estimation results are robust.

6.4 Robustness tests

In order to test the robustness of the benchmark regression results, this paper also conducts robustness estimation in terms of replacing variables and replacing samples.

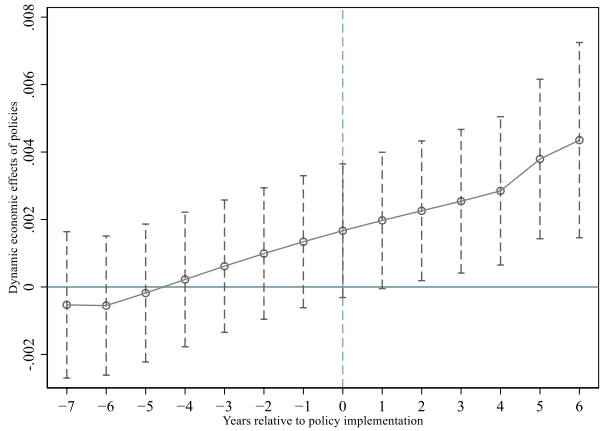

FIGURE 4
Parallel trend test for "Broadband China" policy.

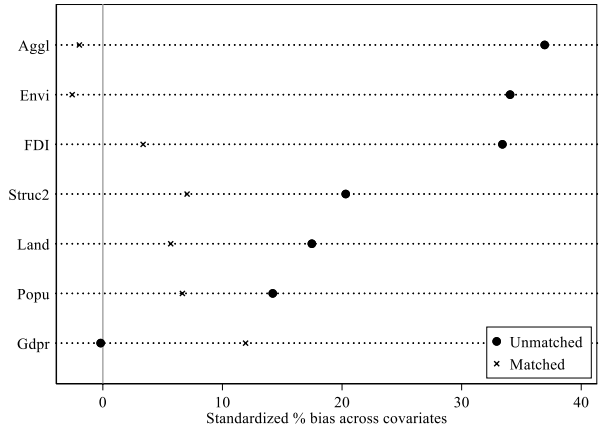

FIGURE 5
Balance test for propensity score matching.

6.4.1 Replacement variables

For the explanatory variables, we use the Cobb-Douglas function to measure to get the LGUE (*LGUE_cd*) as a replacement variable. For the core explanatory variable digital transformation, reference to relevant studies (He et al., 2022), we adopt the PKU-DFIIC as a proxy variable to measure the level of digital transformation of each city (*Digit_PKU*), which is compiled by a joint research team composed of the Peking University Digital Financial Inclusion Index of China. Table 6 columns (1) and (2) report the estimation results after replacing the explanatory variables, respectively, which show that the coefficient of the effect of digital transformation on the LGUE remains significantly positive. Columns (3) and (4) of Table 6 report the estimation results after replacing the explanatory variables for digital transformation, which shows that the baseline regression results are robust after replacing the variables.

6.4.2 Replacement sample

Influenced by the subprime crisis in 2008, the Chinese government introduced macro-control policies of countercyclical adjustment in 2009, which had far-reaching impacts on both the real estate market and land use. In order to minimize the interference of the relevant policies on the regression results, this paper will keep the sample after 2011 for re-estimation. The estimation results after replacing the sample are reported in columns (5) and (6) of Table 6, which shows that the coefficient of the impact of digital transformation on the LGUE is still significantly positive.

6.5 Mechanism analysis of digital transformation affecting LGUE

The interaction term between digital transformation and mechanism variables is added to the baseline regression model as a way to test the impact of digital transformation on LGUE through mechanism variables, and the interaction term econometric model is constructed as shown in Eq. 5.

$$LGUE_{it} = \beta_0 + \beta_1 Digit_{it} + \beta_2 Digit_{it} * M_{it} + \beta_3 M_{it} + \beta_4 \sum Controls_{it} + \mu_i + \delta_t + \varepsilon_{it} \quad (5)$$

Where M_{it} is the mechanism variable, including technological innovation, industrial structure upgrading and land resource mismatch. If the coefficient of the interaction term between the core explanatory variable digital transformation and the mechanism variable is significant, it means that digital transformation has an impact on LGUE through this mechanism.

6.5.1 Technological innovation

Theoretical analysis finds that the key to improve the LGUE is technological innovation and technological application capacity, and digital transformation plays an important role in reducing costs and increasing efficiency, thus contributing to technological innovation and the improvement of LGUE. In this paper, the number of patent applications is used to reflect the level of regional innovation. Column (1) of Table 7 reports the estimation results of the interaction term econometric model of digital transformation affecting LGUE through the mechanism of technological innovation. The result shows that the coefficient of the interaction term between digital transformation and technological innovation is significantly positive, indicating that the higher the level of technological innovation is, the greater the impact of digital transformation on LGUE, which means that the digital transformation significantly improves LGUE through technological innovation. Column (2) of Table 7 reports the estimated results of the interaction term between digital transformation and green innovation, and it can be seen that the coefficient of the interaction term is also significantly positive, which indicates that the digital transformation also affects the green innovation and reduces the consumption of the environmental resources by the economic agents, and in this way, enhances the LGUE.

6.5.2 Industrial structure upgrading

The theoretical analysis points out that digital transformation not only drives new industries and new business forms such as intelligent transportation and digital governance, but also eliminates backward production capacity by improving efficiency, thus optimizing industrial structure and improving LGUE. Industrial structure upgrading is a dynamic process of rational allocation of resources among industries,

TABLE 5 PSM-DID estimation results.

	The weight meeting the common support	Weight is not null
	(1)	(2)
	LGUE	LGUE
Digit	0.00106***	0.000742***
	(0.000)	(0.000)
Popu	−0.00327**	−0.00238
	(0.001)	(0.002)
GDPr	−0.00205	0.000774
	(0.006)	(0.008)
Struc	−0.00422***	−0.00410**
	(0.001)	(0.002)
FDI	−0.0000585	−0.0000855
	(0.000)	(0.000)
Aggl	0.00109**	0.00120*
	(0.000)	(0.001)
Land	0.00196	0.00201
	(0.001)	(0.002)
Envi	−0.00669**	−0.00595
	(0.003)	(0.004)
Constant	0.250***	0.252***
	(0.001)	(0.001)
City FE	Yes	Yes
Year FE	Yes	Yes
Adj. R^2	0.99	0.99
F	6.002	2.251
N	1,104	713

Note: ***, **, and * indicate significant at the 1%, 5%, and 10% levels, respectively; robustness standard errors are in parentheses under the coefficients.

i.e., the reallocation of resources from low-productivity sectors to high-productivity sectors. Under the condition of free flow of production factors, the higher the degree of coupling between input and output structures, the higher the resource allocation effect, which is often manifested in more mature industrial development stages and higher productivity levels. Therefore, industrial structure rationalization index is generally used to characterize industrial structure upgrading. In this paper, the degree of industrial structure rationalization is measured by the Theil index, and the specific calculation formula is shown in Eq. 6.

$$SR = -TL = -\sum_j^n \left(\frac{Q_j}{Q}\right) \ln\left(\frac{Q_j}{L_j} \Big/ \frac{Q}{L}\right) \quad (6)$$

Where j denotes the industrial classification by three sub-industries, n = 1,2,3. Q_j and L_j denote the value added and employment of industry j respectively. TL denotes the Theil index, which is calculated by the deviation of the labor productivity of each industry from the average productivity. When the productivity level of each sector is the same, the economy reaches the equilibrium state, and the rationalization level of industrial structure reaches the highest, at which time TL = 0. On the contrary, the more the economy deviates from the equilibrium state, and the more irrational the industrial structure is, at which time the TL is larger. Therefore, in order to positively characterize the degree of industrial structure rationalization (SR), the negative value of the Theil index. When the value of SR is larger, it means that the industrial structure is more rational. On the contrary, the industrial structure is more irrational.

Column (3) of Table 7 reports the estimation results of the interaction term econometric model of digital transformation affecting the LGUE through the mechanism of industrial structure upgrading. It is found that the coefficient of the interaction term between digital transformation and industrial structure upgrading is significantly positive, indicating that the more reasonable the industrial structure is, the greater the impact of digital transformation on LGUE, which implies that digital

TABLE 6 Robustness test estimation results.

	(1)	(2)	(3)	(4)	(5)	(6)
	LUE_cd	LUE_cd	LUE	LUE	LUE	LUE
Digit	0.000347***	0.000341***			0.00131***	0.00134***
	(0.000)	(0.000)			(0.000)	(0.000)
Digit_PKU			0.000951***	0.000899***		
			(0.000)	(0.000)		
Popu		−0.000777		−0.00283**		−0.0031***
		(0.001)		(0.001)		(0.001)
Gdpr		−0.00551		0.00983*		0.0116**
		(0.004)		(0.006)		(0.006)
Struc		0.000666		−0.00171		−0.00143
		(0.001)		(0.002)		(0.002)
Aggl		−0.000486*		−0.000581		−0.000469
		(0.000)		(0.001)		(0.001)
Land		0.000494		0.00234*		0.00299***
		(0.000)		(0.001)		(0.001)
Envi		−0.00285**		−0.00647***		−0.0074***
		(0.001)		(0.002)		(0.002)
Constant	0.297***	0.298***	0.245***	0.246***	0.246***	0.247***
	(0.000)	(0.001)	(0.001)	(0.001)	(0.000)	(0.001)
City FE	Yes	Yes	Yes	Yes	Yes	Yes
Year FE	Yes	Yes	Yes	Yes	Yes	Yes
r2_a	0.99	0.99	0.99	0.99	0.99	0.99
F	9.630	2.579	14.65	5.323	46.26	10.41
N	1,236	1,236	1,010	1,010	1,010	1,010

Note: ***, **, and * indicate significant at the 1%, 5%, and 10% levels, respectively; robustness standard errors are in parentheses under the coefficients.

transformation promotes the improvement of LGUE through industrial structure upgrading.

6.5.3 Land resource mismatch

To a large extent, land policy directly affects land allocation and land utilization efficiency. In most areas of China, the power of land use approval is concentrated in the central and provincial governments, which makes it difficult for local governments to effectively allocate land resources according to their own level of economic development and population resources, thus forming a spatial mismatch of land resources. Therefore, this paper constructs the index of the misallocation of land resources (MLS), as shown in Eq. 7.

$$MLS_{it} = \left| \frac{1}{S_t} \left(\frac{L_{it}}{L_t} S_t - S_{it} \right) \right| \tag{7}$$

where S_t and L_t denote the total urban construction land and the total population in all cities. S_{it} and L_{it} denote the urban construction land and the population in i city, respectively.

Column (4) of Table 7 reports the estimation results of the interaction term econometric model of digital transformation and land resource mismatch. The results show that the coefficient of the interaction term is significantly negative, indicating that the larger the land resource mismatch is, the smaller the effect of digital transformation on the LGUE is, which means that the land resource mismatch inhibits the promotion effect of digital transformation on the LGUE. Therefore, improving land resource mismatch by increasing the level of digital transformation is the key to improving the LGUE. Digital transformation not only reduces the transaction costs of land transactions, but also provides the ability to improve government governance to adjust land policies as a way to improve the spatial mismatch of land resources.

7 Discussion

In this paper, the SFA method is used to measure the LGUE of resource-based cities in China, and it is found that compared with

TABLE 7 Mechanism analysis of digital transformation affecting LGUE.

	(1)	(2)	(3)	(4)
	LGUE	LGUE	LGUE	LGUE
Digit	−0.00415***	−0.00346***	0.00154***	0.00154***
	(0.001)	(0.001)	(0.000)	(0.000)
Inno	−0.000829***			
	(0.000)			
Digit * Inno	0.000682***			
	(0.000)			
Greeni		−0.000425***		
		(0.000)		
Digit *Greeni		0.000846***		
		(0.000)		
SR			−0.00157**	
			(0.001)	
SR*Digit			0.00804***	
			(0.001)	
MLS				0.000765***
				(0.000)
MLS*Digit				−0.00117***
				(0.000)
Popu	−0.00302**	−0.00334**	−0.00361***	−0.00247*
	(0.001)	(0.001)	(0.001)	(0.001)
GDPr	−0.00717	−0.00598	−0.00479	−0.00519
	(0.006)	(0.006)	(0.006)	(0.006)
Struc	−0.00250*	−0.00294**	−0.00426***	−0.00292**
	(0.001)	(0.001)	(0.001)	(0.001)
FDI	−0.00000634	0.0000323	0.0000122	−0.0000271
	(0.000)	(0.000)	(0.000)	(0.000)
Aggl	0.000960**	0.000840*	0.00141***	0.00102**
	(0.000)	(0.000)	(0.000)	(0.000)
Land	0.00111	0.00190	0.00280**	0.00143
	(0.001)	(0.001)	(0.001)	(0.001)
Envi	−0.00390	−0.00352	−0.00379*	−0.00331
	(0.002)	(0.002)	(0.002)	(0.003)
Constant	0.254***	0.251***	0.250***	0.248***
	(0.001)	(0.001)	(0.001)	(0.001)
City FE	Yes	Yes	Yes	Yes
Year FE	Yes	Yes	Yes	Yes
Adj. R^2	0.99	0.99	0.99	0.99

(Continued on following page)

TABLE 7 (*Continued*) Mechanism analysis of digital transformation affecting LGUE.

	(1)	(2)	(3)	(4)
	LGUE	LGUE	LGUE	LGUE
F	11.67	10.20	15.30	11.64
N	1,128	1,125	1,096	1,128

Note: ***, **, and * indicate significant at the 1%, 5%, and 10% levels, respectively; robustness standard errors are in parentheses below the coefficients.

non-resource-based cities, the LGUE of resource-based cities is even lower, which is 20.4% lower than that of non-resource cities on average. This indicates that it is urgent to improve the green land use efficiency of resource cities. Chen et al. (2019) also obtained similar conclusions and found that industrial land in resource cities faces the problem of inefficient utilization (Chen et al., 2019b). Ge and Liu (2021) study also concluded that the land use problem of resource cities is more prominent because of the more extensive use of land and serious deterioration of the ecological environment (Ge and Liu, 2021). The study in this paper further explores how to improve the dilemma of land use efficiency based on measuring the LGUE in resource-based cities.

Theoretically, based on the stochastic frontier model, this paper constructs a theoretical framework for analyzing LGUE, and explores how to improve LGUE from the perspective of digital transformation. It is found that the factors driving land green utilization efficiency mainly include technology application capacity and technological progress. In a related study, Tang et al. (2022) also found that technology utilization efficiency is the main constraint on land use efficiency (Tang et al., 2022). Tang and Chen (2022) found that digital construction can effectively improve the green use efficiency of regional arable land, confirming the favorable contribution of digital transformation to land use (Tang and Chen, 2022). In addition, some studies have found that digitization of land use planning affects the level of stakeholder engagement and influence, and influences the innovation efficiency and productivity of cities (Hersperger et al., 2022; Adade and Vries, 2023; Kyriakopoulou and Picard, 2023), exploring the impact of digitization on innovation. On this basis, this paper further analyzes and finds that digital transformation is not only conducive to technological innovation and technological application capabilities, but also helps to improve the efficiency of land allocation, which is an advantageous factor to alleviate the dilemma of LGUE in resource-based cities.

Empirically, this paper takes the "Broadband China" model city policy as a quasi-natural experiment, and uses the DID method to identify the impact of digital transformation on LGUE, and the results confirm that digital transformation effectively improves the land utilization efficiency of resource cities. Wang et al. (2023) used the DID model to analyze the impact of the construction of new energy demonstration cities on land use efficiency, and found that this policy mainly enhances land use efficiency through the upgrading of industrial structure (Wang et al., 2023). Liu et al. (2021) study also explored the impact of industrial structure optimization on land use efficiency (Liu et al., 2021). Unlike these studies, which analyze based on the industrial structure perspective, this paper explores and discusses the impact of digital transformation on the LGUE through technological advancement, technological application capacity and land allocation.

8 Conclusion

Enhancing LGUE in resource-based cities is an important way to alleviate land resource tension and guarantee food security. This paper utilizes the SFA to measure the LGUE of resource-based cities in China, and finds that overall the LGUE of resource-based cities in China has gradually improved, but there is still a certain gap with non-resource-based cities. There is still a large room for improvement in the LGUE of resource-based cities. From a spatial point of view, the LGUE of resource-based cities shows a decreasing trend of Northeast > Central > West. Enhancing the land-use efficiency of resource-based cities is crucial for developing countries, especially China, which has a large population and tight land resources. Therefore, resource-based cities should pay more attention to land utilization efficiency, on the one hand, exchange idle land with developed provinces in the east to improve the value of land utilization. On the other hand, resource-based cities should learn from the development experience of the eastern developed region, and improve the efficiency of green land utilization in terms of industrial structure, regional planning and other aspects.

Based on the realistic problem of how to improve the land use efficiency of resource cities, this paper explores the impact of digital transformation on the LGUE of resource-based cities based on the broadband China policy using the DID method. It is found that digital transformation significantly improves the LGUE of resource-based cities. In terms of the mechanism of action, digital transformation affects the LGUE of resource-based cities by promoting technological innovation, upgrading industrial structure, and mitigating land factor mismatch. The conclusion is an important revelation for how to realize industrial structure upgrading and improve land resource allocation efficiency in resource-based cities. This paper argues that it is important to increase continue to increase the construction of digital infrastructure and promote the digital industrialization of cities and the digitalization of industries. It is necessary to guide and encourage the in-depth integration of traditional industries with digital technology, attract more investment in digital enterprises, and vigorously improve the digitalization level of resource-based cities, so as to promote the industrial transformation of resource-based cities and improve the efficiency of land use.

Existing studies have focused more on the impact of digitization on the utilization efficiency of arable land, as well as the economic effects brought about by the digitization of land use planning (Hersperger et al., 2022; Tang and Chen, 2022; Adade and Vries, 2023; Kyriakopoulou and

Picard, 2023), and there is a lack of studies that explore resource-based cities' industrial transformation and improvement of land use efficiency from a digital transformation perspective to explore land use in resource-based cities. This paper uses the SFA model to measure the LGUE in resource-based cities, and explores the impact of digital transformation on the LGUE based on the Broadband China policy, which bridges the research gap in this field. However, this paper has not yet explored in depth how resource-based cities realize digital transformation and lacks research on the micro-mechanisms to improve land use efficiency. In the next study, we will measure the digitalization indicators more accurately from the micro enterprise level and the macro city level, examine the heterogeneity analysis of digital transformation on land green use efficiency from the digitalization type, industrial structure, policy factors, etc., and summarize the experience of digital transformation in resource cities through case studies.

Data availability statement

Publicly available datasets were analyzed in this study. This data can be found here: http://www.stats.gov.cn/ and the China Urban Statistical Yearbook.

Author contributions

QQ: Conceptualization, Resources, Supervision, Writing–original draft. SL: Conceptualization, Methodology, Software, Supervision, Visualization, Writing–original draft, Writing–review and editing.

Funding

The author(s) declare financial support was received for the research, authorship, and/or publication of this article. This study was supported by the National Social Science Foundation of China (21CJY041), the Social Science Foundation of Hunan Province of China (21YBQ120).

Conflict of interest

The authors declare that the research was conducted in the absence of any commercial or financial relationships that could be construed as a potential conflict of interest.

Publisher's note

References

Adade, D., and Vries, W. T. d. (2023). Digital twin for active stakeholder participation in land-use planning. *Land* 12 (3), 538. doi:10.3390/land12030538

Aigner, D., Lovell, C. K., and Schmidt, P. (1977). Formulation and estimation of stochastic frontier production function models. *J. Econ.* 6 (1), 21–37. doi:10.1016/0304-4076(77)90052-5

Bertani, F., Ponta, L., Raberto, M., Teglio, A., and Cincotti, S. (2021). The complexity of the intangible digital economy: an agent-based model. *J. Bus. Res.* 129, 527–540. doi:10.1016/j.jbusres.2020.03.041

Bouwman, H., Nikou, S., and de Reuver, M. (2019). Digitalization, business models, and SMEs: how do business model innovation practices improve performance of digitalizing SMEs? *Telecommun. Policy* 43 (9), 101828. doi:10.1016/j.telpol.2019.101828

Chen, W., Chen, W., Ning, S., Liu, E. n., Zhou, X., Wang, Y., et al. (2019b). Exploring the industrial land use efficiency of China's resource-based cities. *Cities* 93 (93), 215–223. doi:10.1016/j.cities.2019.05.009

Chen, W., Chen, W., Ning, S., Liu, E.-n., Zhou, X., Wang, Y., et al. (2019a). Exploring the industrial land use efficiency of China's resource-based cities. *Cities* 93, 215–223. doi:10.1016/j.cities.2019.05.009

Chen, Y., Chen, Z., Xu, G., and Tian, Z. (2016). Built-up land efficiency in urban China: insights from the general land use plan (2006–2020). *Habitat Int.* 51, 31–38. doi:10.1016/j.habitatint.2015.10.014

Chung, Y. H., Färe, R., and Grosskopf, S. (1997). Productivity and undesirable outputs: a directional distance function approach. *J. Environ. Manag.* 51 (3), 229–240. doi:10.1006/jema.1997.0146

Dong, Y., Jin, G., and Deng, X. (2020). Dynamic interactive effects of urban land-use efficiency, industrial transformation, and carbon emissions. *J. Clean. Prod.* 270, 122547. doi:10.1016/j.jclepro.2020.122547

Erkut, B. (2020). From digital government to digital governance: are we there yet? *Sustainability* 12 (3), 860. doi:10.3390/su12030860

Ge, X. J., and Liu, X. (2021). Urban land use efficiency under resource-based economic transformation—a case study of Shanxi Province. *Land* 10 (8), 850. doi:10.3390/land10080850

Hao, X., Li, Y., Ren, S., Wu, H., and Hao, Y. (2023). The role of digitalization on green economic growth: does industrial structure optimization and green innovation matter? *J. Environ. Manag.* 325, 116504. doi:10.1016/j.jenvman.2022.116504

He, C., Qiu, W., and Yu, J. (2022). Clinical efficacy and safety of surgery combined with 3D printing for tibial plateau fractures: systematic review and meta-analysis. *Front. Environ. Sci.* 10, 403. doi:10.21037/atm-21-7008

Hersperger, A. M., Thurnheer-Wittenwiler, C., Tobias, S., Folvig, S., and Fertner, C. (2022). Digitalization in land-use planning: effects of digital plan data on efficiency, transparency and innovation. *Eur. Plan. Stud.* 30 (12), 2537–2553. doi:10.1080/09654313.2021.2016640

Hoyer, W. D., Chandy, R., Dorotic, M., Krafft, M., and Singh, S. S. (2010). Consumer cocreation in new product development. *J. Serv. Res.* 13 (3), 283–296. doi:10.1177/1094670510375604

Huang, X., and Song, Y. (2019). Evaluation model of regional resource and environment comprehensive carrying capacity based on the conjugation-wrestling mechanism. *J. Nat. Resour.* 34, 2103. doi:10.31497/zrzyxb.20191007

Jia, S., Wang, C., Li, Y., Zhang, F., and Liu, W. (2017). The urbanization efficiency in Chengdu City: an estimation based on a three-stage DEA model. *Phys. Chem. Earth, Parts A/B/C* 101, 59–69. doi:10.1016/j.pce.2017.05.003

Jorgenson, D. W., and Stiroh, K. J. (2000). US economic growth at the industry level. *Am. Econ. Rev.* 90 (2), 161–167. doi:10.1257/aer.90.2.161

Kleis, L., Chwelos, P., Ramirez, R. V., and Cockburn, I. (2012). Information technology and intangible output: the impact of IT investment on innovation productivity. *Inf. Syst. Res.* 23 (1), 42–59. doi:10.1287/isre.1100.0338

Koroso, N. H., Zevenbergen, J. A., and Lengoiboni, M. (2020). Urban land use efficiency in Ethiopia: an assessment of urban land use sustainability in Addis Ababa. *Land Use Policy* 99, 105081. doi:10.1016/j.landusepol.2020.105081

Kyriakopoulou, E., and Picard, P. M. (2023). The Zoom city: working from home, urban productivity and land use. *J. Econ. Geogr.* 23 (6), 1397–1437. doi:10.1093/jeg/lbad025

Li, J., Huang, X., Chuai, X., and Yang, H. (2021b). The impact of land urbanization on carbon dioxide emissions in the Yangtze River Delta, China: a multiscale perspective. *Cities* 116, 103275. doi:10.1016/j.cities.2021.103275

Li, Q., Liu, S., Yang, M., and Xu, F. (2021a). The effects of China's sustainable development policy for resource-based cities on local industrial transformation. *Resour. Policy* 71, 101940. doi:10.1016/j.resourpol.2020.101940

Li, Z., and Wang, J. (2022). The dynamic impact of digital economy on carbon emission reduction: evidence city-level empirical data in China. *J. Clean. Prod.* 351, 131570. doi:10.1016/j.jclepro.2022.131570

Liu, J., Hou, X., Wang, Z., and Shen, Y. (2021a). Study the effect of industrial structure optimization on urban land-use efficiency in China. *Land Use Policy* 105, 105390. doi:10.1016/j.landusepol.2021.105390

Liu, P., and Ravenscroft, N. (2017). Collective action in implementing top-down land policy: the case of Chengdu, China. *Land Use Policy* 65, 45–52. doi:10.1016/j.landusepol.2017.03.031

Liu, S., Xiao, W., Li, L., Ye, Y., and Song, X. (2020). Urban land use efficiency and improvement potential in China: a stochastic frontier analysis. *Land Use Policy* 99, 105046. doi:10.1016/j.landusepol.2020.105046

Liu, S., Ye, Y., Li, L., and Xiao, W. (2021b). Research on urban land use efficiency in China based on the stochastic frontier analysis. *J. Nat. Resour. Chin.* 36 (5), 1268–1281. doi:10.31497/zrzyxb.20210514

Liu, Y. (2018). Introduction to land use and rural sustainability in China. *Land use policy* 74, 1–4. doi:10.1016/j.landusepol.2018.01.032

Liu, Y., Fang, F., and Li, Y. (2014). Key issues of land use in China and implications for policy making. *Land use policy* 40, 6–12. doi:10.1016/j.landusepol.2013.03.013

Lu, X., Pan, J., and Chen, Y. (2006). Sustaining economic growth in China under energy and climate security constraints. *China and World Econ.* 14 (6), 85–97. doi:10.1111/j.1749-124x.2006.00047.x

Lu, X., Qu, Y., Sun, P., Yu, W., and Peng, W. (2020). Green transition of cultivated land use in the Yellow River Basin: a perspective of green utilization efficiency evaluation. *Land* 9 (12), 475. doi:10.3390/land9120475

Lu, X., Shi, Z., Li, J., Dong, J., Song, M., and Hou, J. (2022). Research on the impact of factor flow on urban land use efficiency from the perspective of urbanization. *Land* 11 (3), 389. doi:10.3390/land11030389

Luo, S., and Yuan, Y. (2023). The path to low carbon: the impact of network infrastructure construction on energy conservation and emission reduction. *Sustainability* 15 (4), 3683. doi:10.3390/su15043683

Ma, Q., Tariq, M., Mahmood, H., and Khan, Z. (2022). The nexus between digital economy and carbon dioxide emissions in China: the moderating role of investments in research and development. *Technol. Soc.* 68, 101910. doi:10.1016/j.techsoc.2022.101910

Martinez-Fernandez, C., Wu, C. T., Schatz, L. K., Taira, N., and Vargas-Hernández, J. G. (2012). The shrinking mining city: urban dynamics and contested territory. *Int. J. Urban Regional Res.* 36 (2), 245–260. doi:10.1111/j.1468-2427.2011.01094.x

Masini, E., Tomao, A., Barbati, A., Corona, P., Serra, P., and Salvati, L. (2019). Urban growth, land-use efficiency and local socioeconomic context: a comparative analysis of 417 metropolitan regions in Europe. *Environ. Manag.* 63, 322–337. doi:10.1007/s00267-018-1119-1

Oliveira, L., Fleury, A., and Fleury, M. T. (2021). Digital power: value chain upgrading in an age of digitization. *Int. Bus. Rev.* 30 (6), 101850. doi:10.1016/j.ibusrev.2021.101850

Peng, C., Song, M., and Han, F. (2017). Urban economic structure, technological externalities, and intensive land use in China. *J. Clean. Prod.* 152, 47–62. doi:10.1016/j.jclepro.2017.03.020

Ramanathan, R. (2005). An analysis of energy consumption and carbon dioxide emissions in countries of the Middle East and North Africa. *Energy* 30 (15), 2831–2842. doi:10.1016/j.energy.2005.01.010

Ribeiro-Navarrete, S., Botella-Carrubi, D., Palacios-Marqués, D., and Orero-Blat, M. (2021). The effect of digitalization on business performance: an applied study of KIBS. *J. Bus. Res.* 126, 319–326. doi:10.1016/j.jbusres.2020.12.065

Schweisfurth, T. G. (2017). Comparing internal and external lead users as sources of innovation. *Res. policy* 46 (1), 238–248. doi:10.1016/j.respol.2016.11.002

Su, J., Su, K., and Wang, S. (2021). Does the digital economy promote industrial structural upgrading? a test of mediating effects based on heterogeneous technological innovation. *Sustainability* 13 (18), 10105. doi:10.3390/su131810105

Tan, K. H., and Zhan, Y. (2017). Improving new product development using big data: a case study of an electronics company. *R&D Manag.* 47 (4), 570–582. doi:10.1111/radm.12242

Tan, S., Hu, B., Kuang, B., and Zhou, M. (2021). Regional differences and dynamic evolution of urban land green use efficiency within the Yangtze River Delta, China. *Land Use Policy* 106, 105449. doi:10.1016/j.landusepol.2021.105449

Tang, X., Sheng, L., and Zhou, Y. (2022). Exploring complex urban growth and land use efficiency in China's developed regions: implications for territorial spatial planning. *Front. Earth Sci.* 16 (4), 1040–1051. doi:10.1007/s11707-022-0973-6

Tang, Y., and Chen, M. (2022). The impact mechanism and spillover effect of digital rural construction on the efficiency of green transformation for cultivated land use in China. *Int. J. Environ. Res. Public Health* 19 (23), 16159. doi:10.3390/ijerph192316159

Torrey, B. B., and Jolly, C. L. (1993). *Population and land use in developing countries: report of a workshop*. Washington, DC: National Academy Press.

Vongpraseuth, T., and Choi, C. G. (2015). Globalization, foreign direct investment, and urban growth management: policies and conflicts in Vientiane, Laos. *Land Use Policy* 42, 790–799. doi:10.1016/j.landusepol.2014.10.003

Wang, M., Lin, N., Dong, Y., and Tang, Y. (2023). How does new energy demonstration city policy promote urban land use efficiency in China? The mediating effect of industrial structure. *Land* 12 (5), 1100. Ethics approval and consent to participate Not applicable. Consent for publication Not applicable. doi:10.3390/land12051100

Wu, H., Hu, S., and Hu, S. (2023). How digitalization works in promoting corporate sustainable development performance? The mediating role of green technology innovation. *Environ. Sci. Pollut. Res.* 30 (8), 22013–22023. doi:10.1007/s11356-022-23762-7

Wu, Y., and Heerink, N. (2016). Foreign direct investment, fiscal decentralization and land conflicts in China. *China Econ. Rev.* 38, 92–107. doi:10.1016/j.chieco.2015.11.014

Xie, R., Yao, S., Han, F., and Zhang, Q. (2022). Does misallocation of land resources reduce urban green total factor productivity? An analysis of city-level panel data in China. *Land Use Policy* 122, 106353. doi:10.1016/j.landusepol.2022.106353

Yu, J., Zhou, K., and Yang, S. (2019). Land use efficiency and influencing factors of urban agglomerations in China. *Land Use Policy* 88, 104143. doi:10.1016/j.landusepol.2019.104143

Zhang, R., Matsushima, K., and Kobayashi, K. (2018). Can land use planning help mitigate transport-related carbon emissions? A case of Changzhou. *Land Use Policy* 74, 32–40. doi:10.1016/j.landusepol.2017.04.025

frontiers | Frontiers in Environmental Science

TYPE Original Research
PUBLISHED 15 February 2024
DOI 10.3389/fenvs.2024.1347723

OPEN ACCESS

EDITED BY
Ayyoob Sharifi,
Hiroshima University, Japan

REVIEWED BY
Qinglei Zhao,
Qufu Normal University, China
Zhiheng Yang,
Shandong University of Finance and Economics, China
Fangli Ruan,
China University of Mining and Technology, China
Sarika Bahadure,
Visvesvaraya National Institute of Technology, India

*CORRESPONDENCE
Hongmei Wang,
hmwang@scau.edu.cn

RECEIVED 01 December 2023
ACCEPTED 05 February 2024
PUBLISHED 15 February 2024

CITATION
Liu Z, Fang H, Xu S, Wu Y, Wen K, Shen Z and Wang H (2024), Retain or remove? Decision-making of rural industrial park redevelopment in Nanhai District, China.
Front. Environ. Sci. 12:1347723.
doi: 10.3389/fenvs.2024.1347723

Retain or remove? Decision-making of rural industrial park redevelopment in Nanhai District, China

Zhuojun Liu[1,2], Hongjia Fang[1,3], Shanshan Xu[1,3], Yilin Wu[1,4], Keyin Wen[1], Zitong Shen[5,6] and Hongmei Wang[1]*

[1]School of Public Administration, South China Agricultural University, Guangzhou, China, [2]Key Laboratory of Natural Resources Monitoring in Tropical and Subtropical Area of South China, Ministry of Natural Resources, Guangzhou, China, [3]School of Public Administration, China University of Geosciences, Wuhan, China, [4]Guangdong Urban and Rural Societal Risk and Emergency Governance Research Center, Guangzhou, China, [5]School of Government, Sun Yat-Sen University, Guangzhou, China, [6]Guangdong Poverty Alleviation Governance and Rural Vitalization Institute, Guangzhou, China

Introduction: In both of China and other industrializing countries, improving the efficiency of degraded industrial land use will help control urban sprawl brought about by rapid urbanization. The redevelopment of industrial parks in the countryside is becoming a starting point for phasing out high-polluting industries and an important source of land supply for high-end and green industries. The objective of this paper is to identify how the local state of China determines the necessity for the demolition of rural industrial parks (RIPs) and how this process reflects the underlying decision-making mechanisms.

Methodology: This paper carries out descriptive spatial analysis by combining the economic and social development cross-sectional data in 2019 and extracts data from the Baidu Map to calculate the traffic network density. Cluster analysis is also used to group the RIPs according to their data characteristics. In order to provide an in-depth discussion of the cases, the authors also overlay the results of the spatial and cluster analyses.

Results: The spatial distribution of RIPs is closely related to their location and transportation conditions. Failure of the market has resulted in large tracts of advantageous land being taken up by inefficient industrial parks. Cluster analysis and overlay analysis have evaluated the difficulty of redevelopment and divided the industrial parks into three clusters: retained RIPs, medium-term removed RIPs, and near-term-removed RIPs. The authors put forward that different strategies should be adopted for the future renovation of medium-term-removed and near-term-removed RIPs.

Discussion: This paper argues that proper categorization is the beginning of feasible RIP redevelopment. Local governments should resist the temptation of short-term land transfer revenues to achieve long-term growth. The significant differences in concerns between the grassroots and the higher levels of government also require that the effects of bottom-up influence and top-down intervention should be balanced.

KEYWORDS

rural industrial park, urban renewal, decision-making mechanism, cluster analysis, China

1 Introduction

Urban sprawl is threatening the preservation of agricultural land and the security of ecosystems worldwide (Admasu et al., 2021). Controlling disorderly urban expansion is crucial to social and ecological sustainability (Peng et al., 2017). According to Allred et al. (2015), the net primary productivity (NPP) of central North American ecosystems was significantly reduced by the industrialization of landscape in the Great Plains from 2000 to 2012. Hence, the development of degraded land is becoming the key to realizing sustainable land use (Cowie et al., 2018). Since the promulgation of the 1949 Housing Act, the United States carried out a large-scale urban renewal movement to promote the redevelopment of old urban areas (Staples, 1970). Similarly, China has paid more attention to urban renewal projects in the recent decade, including making full use of urban degraded land and reconstructing inefficient industrial land in both urban and rural areas (Yao and Tian, 2017; Liang et al., 2021). Such means are expected to tackle the problem of inefficiency in industrial land use and to avoid the environmental risks caused by the excessive expansion of urban boundaries. In both of China and other industrializing countries, improving the efficiency of degraded industrial land use will help control urban sprawl brought about by rapid urbanization. Against this background, the redevelopment of industrial parks in the countryside is becoming a starting point for phasing out high-polluting industries and an important source of land supply for high-end and green industries. The objective of this paper is to identify how the local state of China determines the necessity for the demolition of rural industrial parks (RIPs) and how this process reflects the underlying decision-making mechanisms.

Generally, RIP refers to those industrial parks established on collectively owned rural land at the early stage of economic reform, which are managed and operated by rural collectives or town-level governments. Due to vague property rights and spatial fragmentation, RIPs are usually filled with small factories and workshops. Initially, RIPs played a crucial role in the rise of the manufacturing industry. This has promoted the transformation of the Pearl River Delta from a coastal and agricultural area to a famous "world factory" (Zhou et al., 2018). However, as China pays more attention to the upgrading of industry and people's demand for a better living environment gradually increases, RIPs with low efficiency and high carbon dioxide emissions are in urgent need of renovation. In the past 5 years, a number of local governments have successfully carried out large-scale transformations of RIPs and achieved remarkable results. For example, Shunde District of Foshan City, a traditional industrial town where the home appliance giant Midea Group is located, launched the renewal of 231 parks from 2018 to 2022, accounting for 60.5 percent of the total number of parks while 80,000 mu (around 13,200 acres) of inefficient industrial land was vacated (Xiong et al., 2020). Meanwhile, not every city has a drastic renovation plan like Foshan. According to a document issued by the municipal government, the city of Dongguan merely planned to complete the demolition of 30,000 mu (around 4,900 acres) of rural industrial land during the same period, accounting for only 36.1 percent of that of Shunde District and 9.6 percent of that of Foshan City (People's Government of Dongguan City, 2020). Why is the redevelopment of RIPs in some areas so difficult? How can we decide which park should be retained while the other should be removed? Understanding the decision-making mechanism during the redevelopment process would be the key to the successful transformation of land use patterns and the reduction of carbon emissions in the future.

According to the new institutional economics (NIE) theory, lowering transaction costs is the motive of institutional changes (North, 1990). Hence identifying "easily demolished industrial parks" has become a priority for local planning authorities. In order to uncover more details of the redevelopment process, this paper selected Nanhai District of Foshan City for further case study. RIPs of Nanhai are typical for three reasons: First of all, it is a district-level area with the largest number of RIPs in the Pearl River Delta. According to the working plan issued by Foshan City, there are 612 RIPs in Nanhai, involving a land area of more than 189 thousand mu, which is equivalent to the area of nearly 20 Zhujiang New Towns, the central business district (CBD) of Guangzhou City. Second, Nanhai has been designated as a pilot area for the provincial urban renewal policy. In July 2019, Nanhai District was approved to build the "Guangdong Provincial Experimental Zone for Urban–Rural Integration," which is tasked with exploring a new model for the upgrading of urban agglomerations in the Guangdong–Hong Kong–Macao Greater Bay Area. Local officials are encouraged to draft innovative policies to promote urban–rural integration. Last but not least, the redevelopment of Nanhai is rather industry-oriented, which is in line with the Chinese government's thirst for economic development in the post-epidemic era. Most of the vacated areas can only be used to develop industrial projects instead of profitable commercial or residential projects. In May 2021, Nanhai District even directly revised the plans of three land parcels released from urban renewal projects, changing them from residential land to industrial land, in an attempt to improve the financial sustainability of the city.

This paper attempts to classify the existing RIPs of Nanhai by applying an analytical framework generated from NIE theories and examines how the local state of China determines the necessity for the demolition of different types of RIPs. In Section 2, a literature review is provided to clarify the relationship between RIP redevelopment, transaction costs, and property rights. Section 3 introduces the study area and how the empirical study is conducted. Section 4 shows the results of spatial analysis and cluster analysis. Section 5 is an independent discussion beyond the local case itself, while the last section concludes this paper.

2 Literature reviews

2.1 RIP development and redevelopment in China

Existing research confirms that rural industrialization was a major driver of China's economic reform to achieve high growth rates, but it also critiques the myriad environmental risks brought by rural industrialization. For example, Zhang et al. (2021) point out that the area of rural industrial land in China has quadrupled since the 1990s and poses a serious threat to protected farmland. As the earliest region in China to carry out rural industrialization, the local states of Guangdong Province have also been the first to put forward the redevelopment of rural industrial parks, which has attracted extensive attention from scholars. Zhou et al. (2018) argue that the success of RIP at the initial stage was a continuation of the traditional cooperative

agricultural production model, and the subsequent renovation needs to fully respect the willingness of the small landlords. Other scholars try to categorize RIPs based on the analysis of multiple samples. They believe that typical difficulties in the redevelopment include fragmented land ownership, difficulties in sectoral collaboration, and attachment to short-term benefits (Cai et al., 2021; Liang et al., 2021; Meng et al., 2022). In order to overcome these obstacles, researchers propose that an appropriate degree of local government involvement can partially solve the problem of fragmented property rights (Liang et al., 2021; Zhang et al., 2023). According to the performance of RIPs, strategies such as demolition, upgrading, and ecological rehabilitation can also be flexibly used (Cai et al., 2021; Jiang et al., 2022; Meng et al., 2022). Due to extensive media coverage, there has been a significant amount of empirical research on RIPs in Shunde District, Foshan City (Zhou et al., 2018; Zhang et al., 2021; Cai et al., 2021; Liang et al., 2021). On the other hand, RIPs in other regions of China have received relatively less attention due to a lack of micro-level data.

2.2 Transaction costs and property rights in urban renewal

Decision-making in urban renewal is highly complex as multiple stakeholders are involved (Wang et al., 2021). Therefore the ideas of transaction costs and property rights are introduced as powerful tools in the field. It is argued that the initial distribution of property rights is a crucial constraint on the urban renewal process, while allocation is also significantly affected by transaction costs (Coase, 1960; Buitelaar and Segeren, 2011). When transaction costs are high, it may be more efficient to allocate property rights to a single party rather than to multiple parties (Coase, 1960). Some other scholars have deemed that institutions play a key role in shaping economic behavior and outcomes (Williamson, 1985; North, 1990). Changes in property rights may have a huge impact on economic development because they can incentivize or discourage investment and innovation (Demsetz, 1967; North, 1990). When transaction costs are high, it may be more difficult to reach an agreement on property rights allocation among stakeholders, which may make the implementation of urban renewal projects more challenging. China's transaction cost in urban redevelopment consists of negotiation costs attributed to the large number of parties involved and the intensified conflicts of interest between the government and the *de facto* land owners under state-led land requisition (Lai and Tang, 2016). As a result, Yang and Xu (2016) proposed that diversified government interventions are needed to reduce interest frictions and lower transaction costs, so as to avoid the emergence of a state of market failure and achieve the effective use of resources. While there is a growing body of research on land development and transaction costs, the adoption of the theory has focused primarily on the implementation process (Lai and Tang, 2016; Lai et al., 2021). In addition, unique cultures and institutions in China, including stakeholder awareness of public projects, state ownership of urban land, and a strong top–down administrative approach are also crucial factors that need to be considered (Enserink and Koppenjan, 2007; Tang et al., 2008; Li et al., 2012). In terms of examining the decision-making mechanism at the early stages of the urban renewal process, the most important part is to identify the initial distribution of property rights. In the next subsection, topical reviews on factors affecting the initial distribution of property rights are provided.

2.3 Factors affecting the initial distribution of property rights in RIP redevelopment

2.3.1 Economic development level

The initial distribution of property rights is closely related to the local economic development level. Economists have long argued that urban renewal contributes to the local economy and human habitat through direct investment in the redevelopment of decaying urban areas and through externalities upon project completion (Schall, 1976; Akita and Fujita, 1982). Areas with high levels of economic development tend to have more urban renewal projects, as they are more likely to attract private investment and generate demand for new development (Couch and Dennemann, 2000). However, economic conditions alone are not always sufficient to drive urban renewal; effective governance structures, stakeholder engagement, and community participation are necessary for meaningful urban renewal outcomes as well (Vallance et al., 2011). When it comes to redevelopment of RIPs, however, the best-developed industrial parks may be the least eager to transform. This can be explained by the concepts of path dependency and transaction costs. Rural industrial park development involves significant sunk costs, such as infrastructure, buildings, and equipment, which are difficult to reverse or modify (Park, 1996). Industrial parks often involve long-term contracts and agreements between factories and park management, which may further limit the parks' ability to change (Haskins, 2006). As a result, the best-developed industrial parks may be locked into their current paths, unable or unwilling to adapt to changing economic or technological conditions. This can lead to a lack of innovation, reduced competitiveness, and a reduced ability to attract new companies and investment. Parks with more flexible contractual arrangements, less rigid physical infrastructure, and a willingness to experiment with new business models may be better able to adapt to changing circumstances and remain competitive. It is therefore important to consider not only the current economic conditions but also the long-term impact of development decisions and investments on the built environment.

2.3.2 Building quality

Architectural quality, including the condition, design, and historical significance of a building or neighborhood, can also affect its value and redevelopment potential (Zhuang et al., 2020). In addition, the quality of the built environment is an important consideration for urban renewal because it can affect the quality of life of residents, attract businesses and investment, and contribute to the overall economic vitality of an area (Chan and Lee, 2008). An urban built environment with better physical conditions of buildings and infrastructure can tackle multiple economic issues and achieve economic sustainability (Zheng et al., 2009; Kylili et al., 2016). Building quality and infrastructure conditions are equally important for achieving long-term economic sustainability. A poorly built environment can reduce the income and consumption levels of local people and lead to business layoffs or closures, which is inconsistent with sustainable economic development. Conversely, better physical conditions of buildings and infrastructure can address these economic issues and achieve

significant economic development (Sui Pheng, 1993). One exceptional case is that buildings with strong historical resonance and community value are less likely to be demolished, even if they are in poor physical condition. Some scholars have argued that site size, location, building condition, and neighborhood context can strongly influence decision-making and lead to significant research costs that are mainly caused by the search for information (Zhuang et al., 2020). Therefore, building quality is an important factor in the decision-making process of urban renewal projects.

2.3.3 Duration of tenancy

Duration of tenancy is another factor that should not be neglected, as urban regeneration and the initial allocation of property rights are also highly governed by rules, instruments, and diverse responsible actors such as tenant organizations (Soltani, 2022). As one of the major groups of participants, tenants are responsible for shaping urban areas and their requirements in urban renewal must be taken into account seriously (Couch et al., 2011; Soltani, 2022). Although some scholars have argued that tenants play an essential role regardless of the duration of their tenancy, fluctuations in demand, and changing household structures, others have discovered that the duration of a lease impacts stakeholder participation and consensus building in the redevelopment process (Couch et al., 2011; Erfani and Roe, 2020). Longer lease terms may necessitate more extensive negotiations and consultation with interested parties, thereby increasing transaction costs and the viability of redevelopment projects (Couch et al., 2011; McTague and Jakubowski, 2013; Erfani and Roe, 2020). A long-remaining lease term can protect tenants from substantial rent increases caused by large-scale or profitable urban renewal projects (Reimann, 1997). From the perspective of building owners, they frequently complain about uncooperative long-term tenants while occupants deny sanction for necessary building improvements. For instance, in the heart of East Berlin, the restoration of a residential area was delayed or even prevented due to conflicts of interest between landlords and tenants (Reimann, 1997). To evict existing tenants, a significant rent increase is effective only when the duration of tenancy is short while other illegal means are also applied on multiple occasions (Reimann, 1997). Therefore, the duration of tenancy is one of the factors that defines the tenants' negotiation power and even the transaction costs of urban renewal projects.

2.3.4 Willingness to renovate

Owners' or residents' willingness is one of the key factors in making decisions in urban renewal projects. Major concerns include compensation plans, quality of facilities, and responses to helping potentially displaced people. Some researchers have argued that developing a detailed compensation plan and reaching an agreement for each residential unit requires significant research and coordination/negotiation costs, especially in areas where there may be hundreds of residents with different needs (Jo Black and Richards, 2020). It has also been shown that substantial improvement in amenities and the size of housing can greatly increase resident satisfaction with the urban renewal process (Skevington et al., 2004; Mohit et al., 2010; Livingstone et al., 2021). The quality of soft resources such as education, healthcare, shopping, and transportation in older communities also affects residential willingness (Guo et al., 2018). An additional hurdle in China is the ambiguity of property rights. In the US and many European countries, property rights are protected by laws such as the Fifth Amendment to the Constitution (US) or the Basic Law (Germany), which guarantees private property rights and limits the government's ability to expropriate residents (Schleich, 1993; Pritchett, 2003; Kelly, 2006; Hoops, 2016). In China, however, all land is owned by the state, but the distribution of property rights at the operational level is ambiguous among different land users and local governments (Zhu, 2002). As a result, current land users have the right to challenge rising redevelopment interests and refuse expropriation or bargaining, which creates a conflict between existing land users and the government–business alliance (Li, 1996). Due to the active role played by nongovernmental land users, demolition and redevelopment in a human-centered and inclusive urban renewal plan are closely linked to the desires and willingness of potentially displaced parties.

2.3.5 Summary

The literature in recent years has shown that the current round of RIP renovation is still ongoing, while a large body of empirical research needs to be supplemented to better explain how China should control the expansion of industrial parks in rural areas. Previous research has also shown that transaction costs and property rights are suitable tools for discussing barriers to successful urban regeneration. By applying these tools, subsections in this review discuss how economic development level, building quality, duration of tenancy, and willingness to renovate affect the initial distribution of property rights in urban renewal. The first two factors are tangible factors that can be measured using economic performance factors and building quality assessment data. The other two factors are intangible ones that affect urban renewal imperceptibly, which can only be ascertained through in-depth investigation. Given the lack of data at the micro level, few existing studies have systematically analyzed these two types of factors. Most scholars have focused on only one or a limited number of projects, while there are few empirical studies for large samples of data (Couch and Dennemann, 2000; Tang et al., 2008; Zhuang et al., 2020; Zhang et al., 2021; Lai et al., 2021; Zhang et al., 2023). Having reviewed more than 160 urban renewal papers in recent years, Wang et al. (2021) suggest that multi-source heterogeneous data should be introduced to develop innovative decision-making support approaches. To further enrich the empirical analysis and to develop a decision-making support toolkit for RIP redevelopment, this paper attempts to provide an analysis based on more than six hundred samples and report the latest urban renewal progress in another typical area other than the frequently mentioned Shunde District.

3 Materials and methods

3.1 Study area and data sources

This paper takes the Nanhai District of Foshan City, which has the longest history of RIP development in the Pearl River Delta region, as a case study. Foshan is located in the center of Guangdong Province and the hinterland of the Pearl River Delta. It is the third largest city of Guangdong after Guangzhou and Shenzhen in terms of economic development. As one of the most active areas in Foshan, Nanhai District has one subdistrict (jiedao) and six towns (zhen) under its jurisdiction, with a total area of 1.072 thousand square kilometers. By the end of 2022, Nanhai District had a population of over 3.65 million people and had generated a GDP of CNY

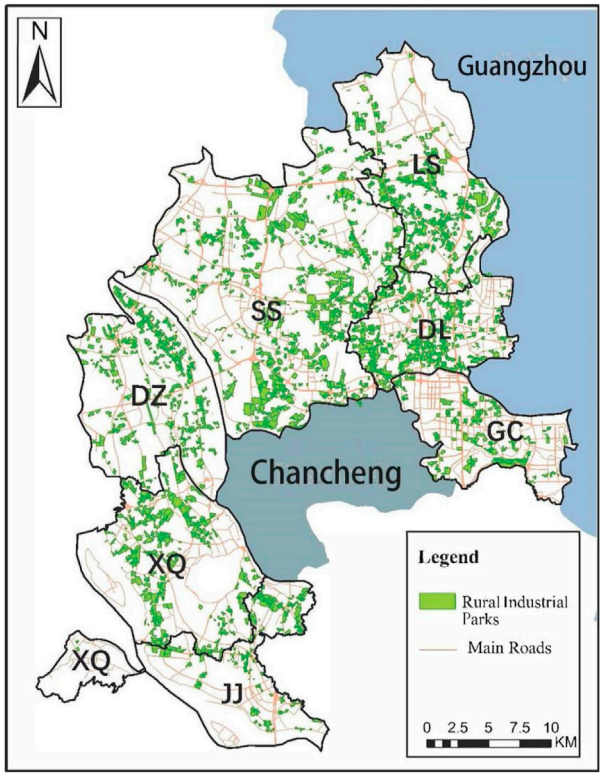

FIGURE 1
Spatial distribution of rural industrial parks in Nanhai District.

373.06 billion (USD 50.98 billion), which is even higher than some provinces like Qinghai and Tibet (Nanhai District Bureau of Statistics, 2023). The study area of this paper is the 612 RIPs delineated by Foshan City, which are distributed in all the town-level units of Nanhai, with a total area of about 189 thousand mu (about 31.14 thousand acres). Although the boundary of an RIP is not officially demarcated, its delineation is the result of a combination of administrative divisions, tenure, and geographic boundaries. In practice, the demolition or reservation of an RIP, regardless of its size, is considered as a whole, which helps to reduce the transaction costs of project implementation.

RIPs in Nanhai District have been built successively since the 1980s and have attracted a large number of factories since their establishment, forming industrial clusters dominated by low- and medium-end industries such as aluminum profiles, furniture, textiles, and footwear, which contributed great value to local economic development and labor employment in the early years. However, industrial development has also intensified the depletion of natural resources, including land, water, and minerals, leading Nanhai to a classic "tragedy of the commons" dilemma, where ambiguous collective property rights arrangements have failed to explicitly define the rights and responsibilities for the use of such public goods. Due to the lack of effective planning control, factory buildings are haphazardly located and poorly licensed. According to the United Front Work Department of CPC Nanhai Committee (2016), pollutant emissions from sixty percent of the enterprises in RIPs did not meet national standards, while some factories even discharged pollutants illegally. The blurred boundaries of land parcels have also hindered the long-term development of factories. In terms of building quality, most of the buildings were poorly designed and constructed at the initial stage. After decades of use, these dilapidated and inefficient factory buildings are leading to the substantial dissipation of rental value. Figure 1 shows the spatial distribution of RIPs in Nanhai District. They are located in all seven town-level units, which are abbreviated as GC, DL, LS, SS, DZ, XQ, and JJ. According to the map, they are either adjacent to the city of Guangzhou or border on Chancheng District, the center of Foshan City. As a place linking Chancheng with Guangzhou, GC Subdistrict is also the seat of Nanhai District Government.

Based on government-sponsored consultancy work launched in late 2019, the authors of this paper spent more than 2 years on building a sound local dataset, aiming to comprehensively reflect the development situation of local RIPs. In addition to compiling data and information provided directly by the local government or other public sources, the authors also visited more than 200 stakeholders, including officials from district- and town-level governments, village cadres, active villagers, entrepreneurs, and residents of neighboring urban communities. More than 2,700 photographs were taken using drones or via onsite shooting. Spatial data include vector data of the boundaries of 612 RIPs in Nanhai District, aerial photography from Baidu Maps (China's largest electronic map provider), results of a building quality survey conducted in early 2020, and land use planning documents, which were provided by the local government authorities or accessed through public channels. Nonspatial data mainly refer to socioeconomic data of the RIPs, such as economic performance data reported annually by RIPs to the Nanhai government, tenancy duration of every park, town-level governments' willingness to renovate, and the proposed acreage for demolition of each RIP.

Table 1 shows a descriptive analysis of fifteen variables collected for further analysis. These variables are organized in accordance with the analytical framework proposed in the next subsection. As the renovation of RIPs has been pushed on continuously in recent years, this paper chooses the year 2019 as the study period, while most of the parks have remained intact and only eleven RIPs have been demolished on a trial basis. Therefore, these removed industrial parks did not produce any output during the study period and all the businesses within them have moved out. Furthermore, there is still a significant proportion of industrial parks with good-quality buildings and high industrial output. The industrial output of RIPs with the best economic performance in 2019 had exceeded CNY 14 billion (USD 1.9 billion). Thus, determining which RIP to be dismantled is a complex issue that requires careful consideration. The reason for not using a more updated panel dataset is that large-scale demolition operations have been carried out since 2020, while the integrity of the dataset has been compromised. In order to maintain the comprehensiveness of the analysis, this paper also attempts to verify the accuracy of the results through a follow-up survey conducted from late 2021 to mid-2023.

3.2 Methodology

Section 2 thoroughly reviews the relationship between urban renewal and NIE theories such as property rights and transaction costs. Previous studies have confirmed that the success of urban

TABLE 1 Descriptive analysis of factors.

Factor	Minimum	Maximum	Mean	Median	Standard deviation
Annual industrial output (CNY million)	0	14,375.00	268.1049	79.50	801.2683
Annual tax generated (CNY million)	0	200.00	9.1882	3.7250	18.7215
Annual industrial output per mu (CNY million)	0	41.3555	1.2244	0.4592	3.0526
Annual rental income (CNY million)	0	65.44	4.6662	3.00	6.3523
Number of industrial enterprises above designated size (IEADS)[a]	0	25.00	1.70	0.00	3.12
Proportion of demolished buildings (%)	0	100.00	27.09	19.30	28.86
Proportion of good quality buildings (%)	0	100.00	46.01	48.89	31.99
Proportion of poor quality buildings (%)	0	93.26	4.29	0.00	13.50
Proportion of area with lease expiration before 2022 (%)	0	100.00	14.89	1.96	27.73
Proportion of area with lease expiration between 2022 and 2025 (%)	0	100.00	9.25	0.2	17.96
Proportion of area with lease expiration after 2025 (%)	0	100.00	6.03	83.12	41.11
Proportion of area proposed for demolition (%)	0	100.00	10.00	0.00	25.50
Proportion of area not proposed for demolition (%)	0	100.00	17.14	0.00	32.87
Proportion of area that cannot be rebuilt after demolition (%)	0	100.00	22.90	0.00	35.30
Willingness of town-level government[b]	1	5	4.11	5	1.65

[a]IEADS refers to industrial enterprises with annual business revenue of CNY 20 million (USD 2.76 million) or more. IEADS are the leading force in regional economic development and the main monitoring object of the statistical department.
[b]A five-point Likert scale was used here: "5" represents the removal of specific RIP being "strongly recommended" while "1" stands for "strongly not recommended."

renewal depends on a range of tangible and intangible factors such as economic development, building quality, duration of tenancy, and stakeholders' willingness to renovate. How do these factors as a whole influence the decision-making process for urban renewal projects? In particular, how do local government authorities determine which existing RIPs should be demolished and which should be preserved? To better answer these questions, the authors of this paper formed an analytical framework, as shown in Table 1. Fifteen specific factors were distributed in four classes. These factors were retrieved from annual statistical reports of local governments and the subsequent onsite investigations. Economic development level is reflected in five factors related to the performance of industrial development. Building quality was determined by the proportion of well-maintained and poorly-maintained buildings. Using the year 2020 as the base period, the years 2022 and 2025 were identified as the dividing lines of tenancy duration. Leases expiring before 2022 were considered to have less resistance to redevelopment while those expiring after 2025 were difficult to repudiate. Last but not least, the overall willingness of town-level government to renovate was collected via onsite interviews with local officials. They were also invited to indicate the acreage to be demolished and the acreage to be reserved. Furthermore, some of the industrial buildings built in the early 1990s are unauthorized structures and have been in use for decades. To maintain social stability, local governments in multiple places generally acquiesce in the continuous use of these industrial buildings, as they cannot be rebuilt after demolition.

This paper applies a mixed use of spatial, quantitative, and qualitative analytical tools. Using the software ArcMap 10.2, this paper summarizes the spatial distribution pattern of RIPs in the Nanhai District and carries out descriptive spatial analysis by combining the economic and social development cross-sectional data in 2019. To further demonstrate the location conditions of the parks in different areas, the authors also extracted the traffic network data from Baidu Map and calculated the traffic network density. The spatial analysis is mainly presented in the form of kernel density maps. A method of natural breaks classification (Jenks method) was applied, in which similar values are grouped together and differences between classes are maximized.

Cluster analysis, as an exploratory analysis that aims to organize the data based on similarity and measure the similarity between different data sources, was also used to group the RIPs according to their data characteristics. Before beginning the main computational steps, the factors shown in Table 1 went through collinearity diagnostics and were standardized using the Z-score method. Subsequent clustering was conducted using the K-means method. The analytical tool in ArcGIS uses the Pseudo F Index to calculate the optimal number of clusters and proposes the grouping plan with higher F-statistics. Having imported the variables in Figure 2 into the analytical tool, the optimal number of clusters was set and all industrial parks were successfully categorized. In order to provide an in-depth discussion of the cases, the authors also overlayed the results of the spatial and cluster analyses. Refinement of the characteristics of different types of RIPs also helps better understand how governments make decisions in the urban renewal process. Although some factors used in spatial and cluster analyses are geographically specific, similar data for other cities are likely to be available through official or public sources. The authors hope that the primary and secondary classifications in Figure 2 will serve as a reference for other studies.

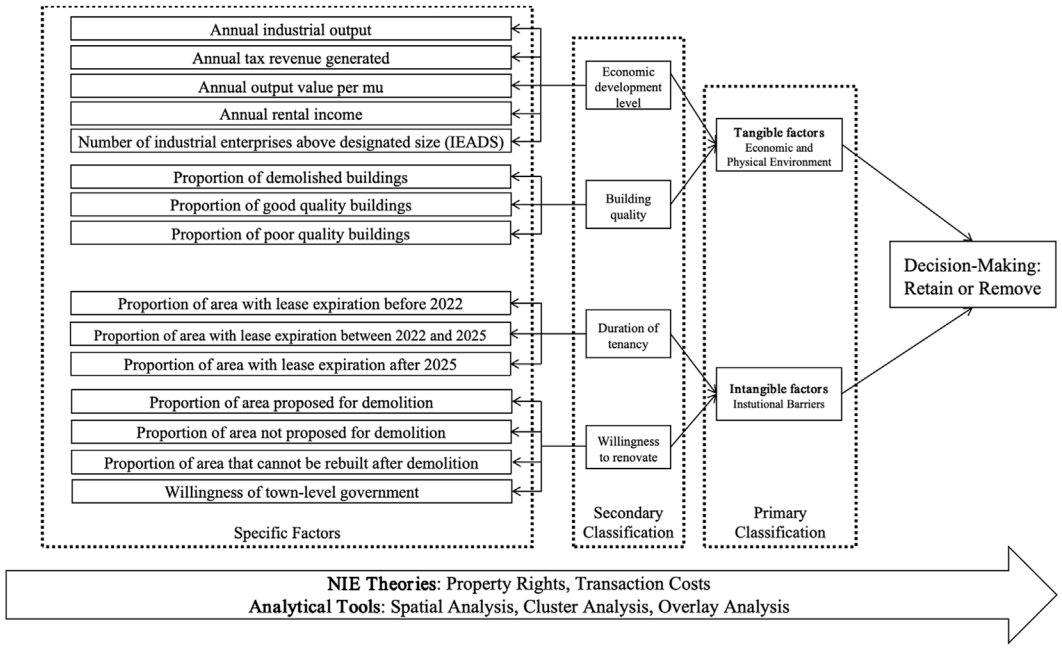

FIGURE 2
Analytical framework.

4 Results

4.1 Spatial characteristics of RIPs

Descriptive spatial analysis shows that most of the rural industrial parks are concentrated in the eastern part of Nanhai District, which has better transportation and location advantages. Figure 3 illustrates the spatial distribution and the transportation conditions of the 601 tested RIPs, combining information on road density, land area, rental income, and number of workers employed. The approximate geographic locations of all the seven town-level units are also labeled with codes in the figure. Nanhai District borders the city of Guangzhou in the east and Chancheng District, the seat of the Foshan government, in the center. After years of infrastructure development, the transportation accessibility between Guangzhou City and Nanhai District is already at a reasonably high level. Therefore, Part A of Figure 3 shows that GC and DL near Guangzhou have the highest road density, followed by SS in the center and LS in the northeast. Owing to the improved transportation conditions, Part B of Figure 3 shows that the intersection of LS, DL, and SS clusters the largest area of RIPs in the whole district. As a highly urbanized subdistrict, the land area of GC RIPs is relatively small. In terms of rental incomes and number of employees, Part C and D of Figure 3 show that RIPs in the eastern part have higher rental income and employ more workers than other parts. For example, it is demonstrated that LS Town has the highest rental incomes and provides the largest number of jobs.

However, the better-located RIPs do not bring the highest economic returns. According to Figure 4, RIPs contributing the highest industrial output and tax revenue are concentrated in the northern towns of SS and LS. This indicates that RIPs in the east are rather inefficient and are in urgent need of renovation. SS is the largest town of Nanhai in terms of both land area and economic development. It also has the largest number of RIPs and contributes the highest industrial output and tax revenue in the region. Another town with better RIP economic performance is LS, which is also located immediately to the east of Guangzhou. In contrast, RIPs in the three western towns of DZ, XQ, and JJ are less effective and have difficulty attracting a sizable employment population. Their road network density is low, and they are far away from Guangzhou and the city center of Foshan. In addition, the southwestern part of Nanhai District has a favorable ecological environment. It has a large area for agricultural production and a national ecological reserve. Some of the RIPs in these three towns have great potential for ecological restoration.

The results of the spatial analysis preliminarily show the characteristics of the spatial distribution of RIPs in Nanhai District. First, RIP development is concentrated in the eastern part of the district. The towns of LS, DL, GC, and SS gather the majority of industrial parks and employment, as well as being the major contributors to industrial output and tax revenues. This feature coincides with the location characteristics of Nanhai District, which is adjacent to Guangzhou to the east. Second, the low efficiency of industrial parks and low industrial output in DL and GC indicate a mismatch of precious land resources. GC and DL are considered the best-located districts in Nanhai. However, their RIPs generate very little industrial output and few job opportunities, while land rents are at a comparatively high level. It is evident that there is a path dependency phenomenon in the development of RIPs in these two towns, and market forces cannot play an effective role in the allocation of land resources.

4.2 Results of K-mean cluster analysis and overlay analysis

According to the pseudo-F value, the cluster analysis based on fifteen factors divides the 601 RIPs into three clusters. Figure 5 shows

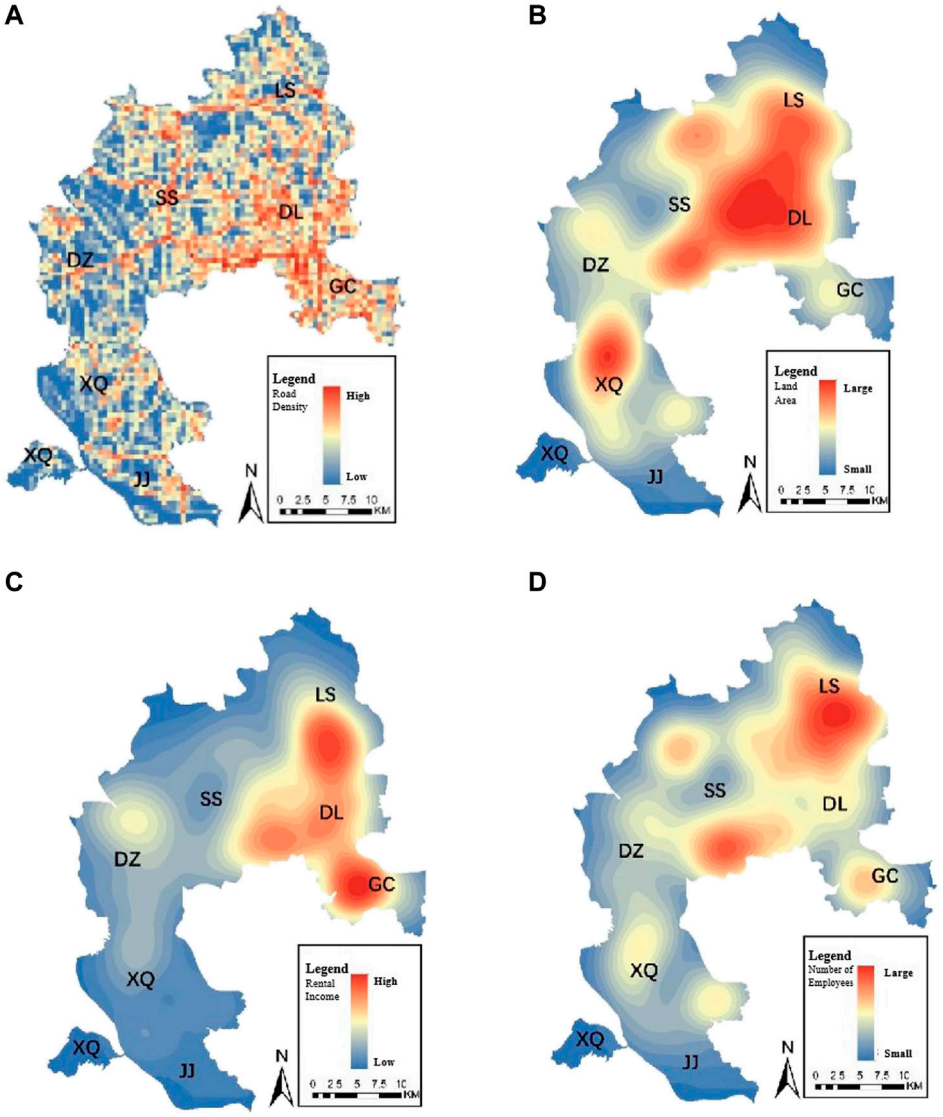

FIGURE 3
Kernel density diagram of road density **(A)**, industrial park land area **(B)**, rental income of industrial park **(C)**, and employment distribution in industrial park **(D)**.

that the three clusters are well differentiated from each other, indicating that all the RIPs have been successfully classified in different clusters. ArcGIS 10.2 software was used to temporarily name the three clusters as Cluster A, B, and C. They, respectively, contain 104, 98, and 399 RIPs, which is a reasonable distribution. Table 2 and Figure 6 show the geographical distribution of the three types of RIPs. The data show that SS has the largest number (47) of RIPs in Cluster A. DZ has the largest concentration of Cluster B RIPs (39), while there are 99 and 91 Cluster C RIPs in DL and SS, respectively.

By overlaying the results of spatial and cluster analysis, Figure 7 shows the detailed data characteristics of the three groups of RIPs. In addition to showing the specific scores for tangible and intangible factors specified in Table 1, two factors for spatial analysis were incorporated into the comprehensive evaluation of the three types of RIPs. "Geographical location" refers to the distance from the RIP to the city centers of Foshan and Guangzhou. "Traffic accessibility" measures the distance to major roads from the RIP. The economic performance of RIPs in Cluster A is at the highest level among the three groups, as measured by factors such as industrial output, tax generated, rent income, and the number of IEDAS. On the other hand, the quality of the existing buildings in this group is relatively good and most existing leases would expire long after 2025, making the town-level government have a strong will to retain them. Therefore, the authors propose naming Cluster A industrial parks "retained RIP."

The economic performance of Cluster B RIPs is generally poor. In terms of land use, a considerable portion of the old factory buildings have already been demolished, and the lease terms of the remaining buildings are still long. Hence, most of the local managers do not recommend demolishing the properties, which makes the necessity for renovating these RIPs in the near

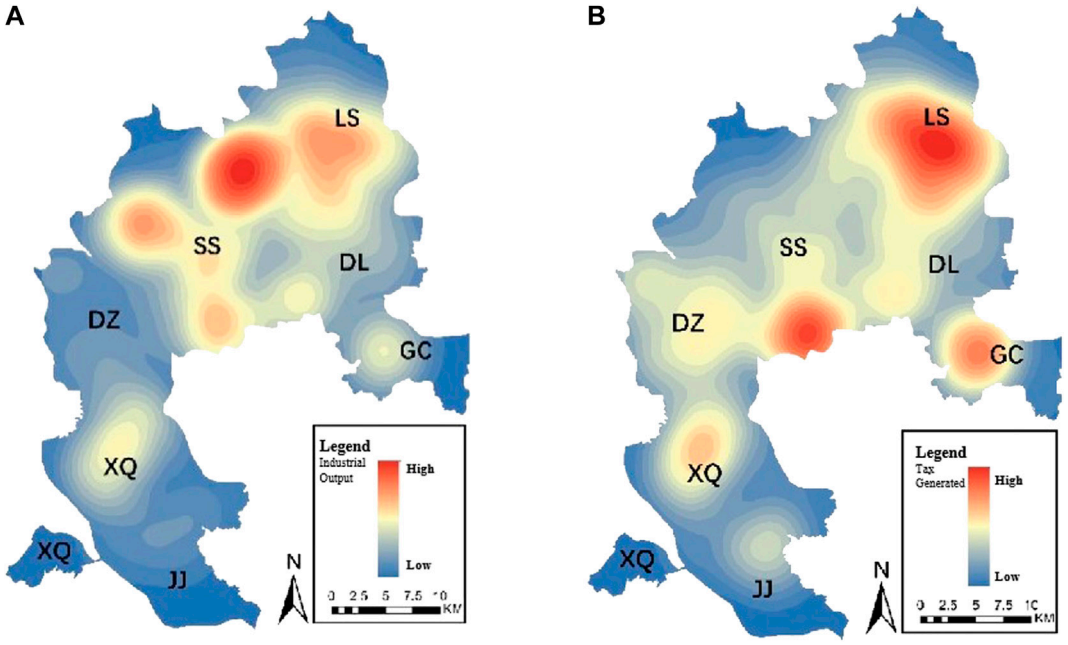

FIGURE 4
Kernel density diagram of industrial output **(A)** and tax generated **(B)**.

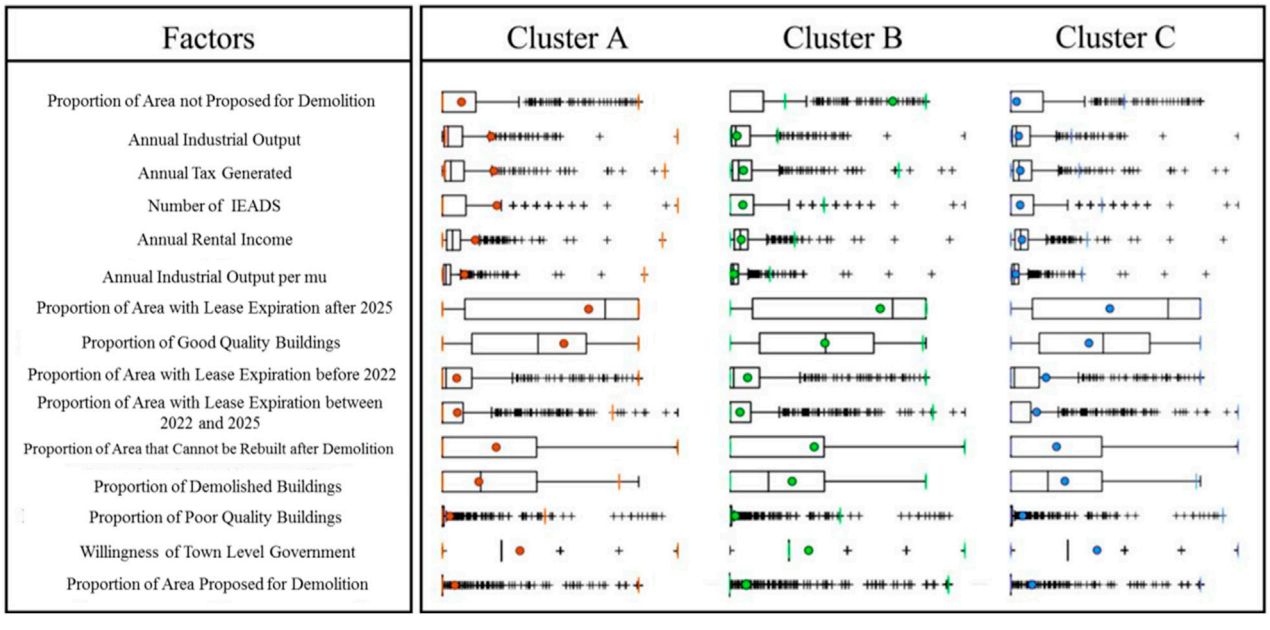

FIGURE 5
Box plot showing comparison of fifteen factors of three cluster groups.

future relatively low. Since these RIPs would not be renovated until years later, they can be defined as "medium-term-removed RIPs."

Cluster C RIPs accounted for 66.4% of the 601 industrial parks and were widely distributed throughout Nanhai District. These parks fully demonstrate the typical characteristics of RIPs, which are small in scale, low in industrial output, and poor in building quality. Moreover, a Cluster C RIP generally has better transportation and location conditions, and the remaining tenancy period of the factory buildings is relatively short, so the town government's willingness to renovate is strong. Based on the above features, the renovation of Cluster C industrial parks is rather

TABLE 2 Distribution of clustering results in each town-level unit.

Cluster	DL	DZ	GC	JJ	LS	SS	XQ	Total
A	6	9	6	2	24	47	10	104
B	6	39	2	12	31	0	8	98
C	99	56	57	9	47	91	39	399
Total	111	104	65	23	102	138	57	601

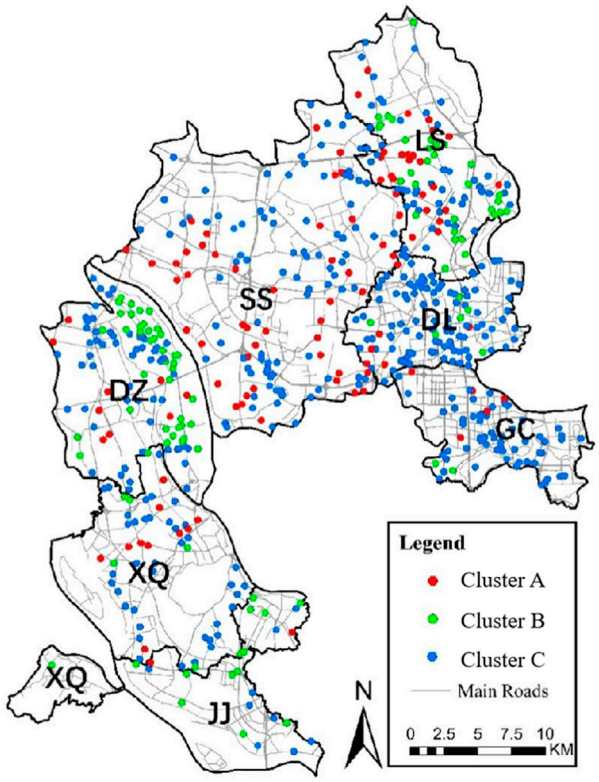

FIGURE 6
Geographical distribution of three types of RIPs.

necessary, as the transaction cost is comparatively low. In summary, they can be called "near-term-removed RIPs."

4.3 Explaining the decision-making for the redevelopment of different types of RIPs

4.3.1 Retained RIP: Shannan industrial park

The representative park of Cluster A is Shannan Industrial Park in SS Town, which is also one of the most developed parks in SS. This RIP covered an area of 1556.15 mu (256.36 acres) and its industrial output in 2019 was CNY 1.449 billion (USD 202.6 million), generating tax revenue of CNY 53.76 million (USD 7.51 million). Shannan Industrial Park is home to eleven IEDAS, which is 6.5 times the average level of Nanhai District. Figure 8 shows that the distribution of factory buildings is dense with a relatively low plot ratio. The quality of the factory buildings is acceptable and there has been a high degree of industrial agglomeration of mold manufacturing, metal processing, door and window manufacturing, and other industries. Driven by industrial development, the industrial park has gathered a large population, and the public facilities are mainly built around the core area of the industrial park. Despite facing problems such as industrial pollution and low-quality facilities, the town-level government still recommends retaining Shannan Industrial Park in order to maintain local employment and economic development.

4.3.2 Medium-term-removed RIP: Donglian Jincheng industrial park

Medium-term-removed RIPs are mainly located in DZ and LS, with a total number of 98. The economic development of Cluster B parks is rather poor in terms of industrial output, average industrial output per mu, and annual tax revenue. However, the redevelopment of such parks needs to overcome multiple obstacles, including a high proportion of area that cannot be demolished and a long remaining tenancy period. Donglian Jincheng Industrial Park in DZ is a typical "medium-term-removed RIP." Its industrial output in 2019 was merely CNY 55 million (USD 7.69 million), with tax revenue of CNY 5.68 million (USD 794 thousand) and only one IEDAS, all of which are lower than the average level of Nanhai District. Although the park is located along a major road, it is far from the city center of Guangzhou. It lacks quality public facilities and the scale of industrial enterprises is small. Scattered small factory buildings are interspersed with rural dwellings. The existing buildings in the industrial park are of low quality, while as many as 97% of the factory buildings have a remaining tenancy term of more than 5 years (Figure 9). To generate rental income, some vacant factory buildings have been converted into apartment buildings for the migrant population. In addition, 64% of the Donglian Jincheng Industrial Park's land violated land use planning and could only be restored to agricultural or ecological land after demolition. Since illegal buildings have been used for many years, the demolition of illegal construction was not enforced due to high transaction costs. Taking factors such as social stability and transaction costs into account, the town government tends to renovate such industrial parks only in the medium or even long term.

4.3.3 Near-term-removed RIP: Dienan Linchang industrial park

"Near-term-removed RIPs" have the worst economic performance. The 399 industrial parks accounted for 63.7% of the total number, making them the majority type of Nanhai's RIPs. This cluster is widely distributed in all towns and is mainly concentrated in GC Subdistrict and DL Town. They are the least developed of the three clusters, with the smallest average size and the lowest development intensity. The average plot ratio is only 1.06. In terms of building quality, a large number of dilapidated buildings have yet to be demolished. The leases of most of their properties would expire within three years. Existing factories are predominantly small and low-end workshops, for most of which the leases would expire within three years. On the positive side, there

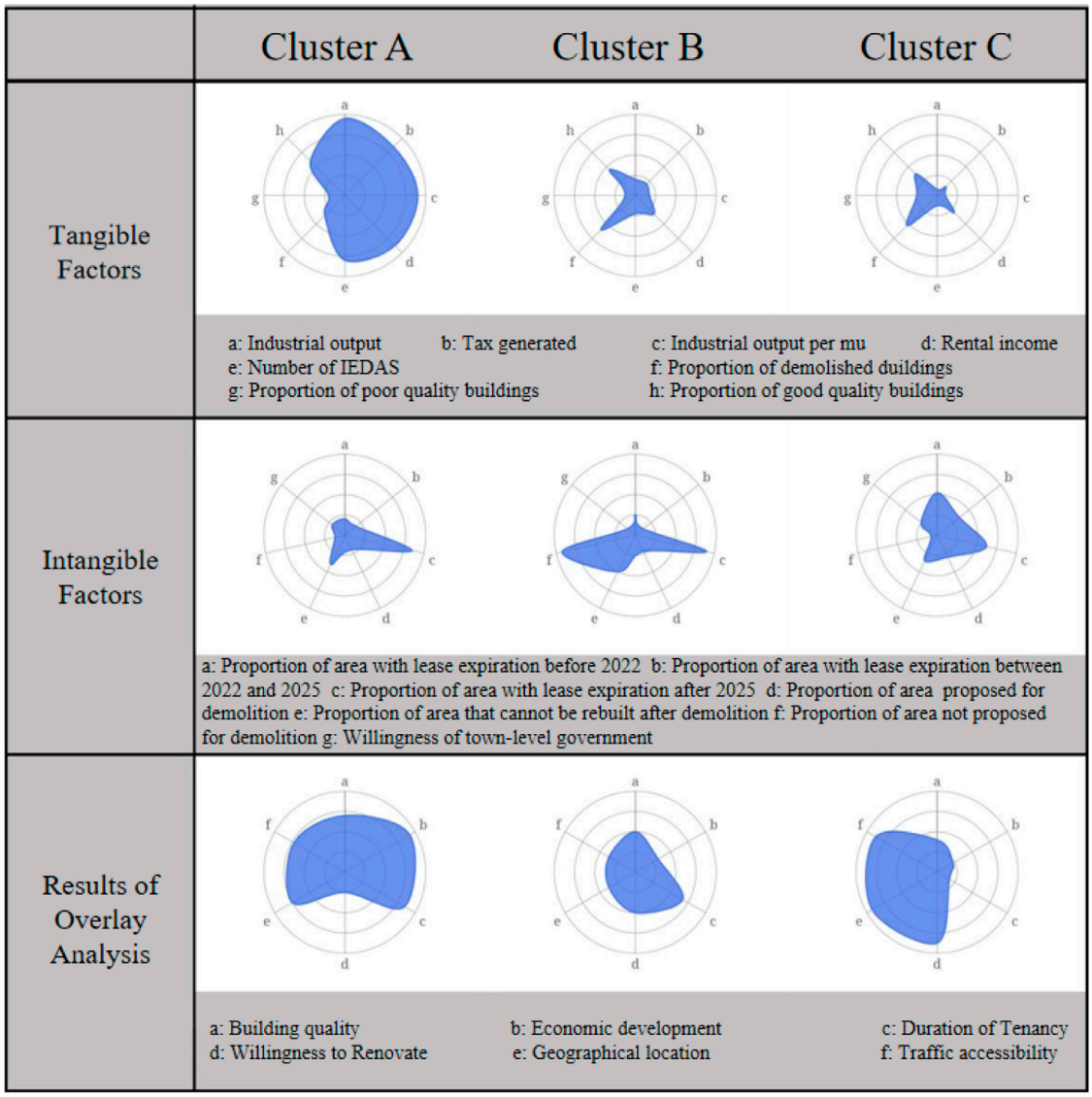

FIGURE 7
Results of overlay analysis.

are fewer institutional impediments to the renewal of near-term-removed RIPs because the transaction costs for demolition and renovation are generally low.

Dienan Linchang Industrial Park, located in GC Subdistrict, is a representative Cluster C RIP. Its land area is only 120.06 mu (19.78 acres). The industrial output and tax revenue generated in 2019 were CNY 31 million (USD 4.34 million) and CNY 500 thousand (USD 69.9), respectively, which are far below the average level of Nanhai District. The factories located in this park are small in scale and are mainly small workshops self-built by individual villagers. The low-rise buildings are outmoded and lack effective land use planning (Figure 10). Most of them are fusions of staff dormitories, workshops, and warehouses. Problems induced by these RIPs include poor working environment, safety issues, serious environmental pollution, poor production efficiency, and lack of market competitiveness. The large number of Cluster C RIPs echoes the necessity of promoting urban renewal in Nanhai. In the very near future, these RIPs would have great potential for large-scale renovation.

5 Discussion

5.1 Proper categorization as the beginning of feasible RIP redevelopment

The above case of Nanhai District demonstrates an example of categorizing RIPs according to their necessity for renovation by spatial analysis, cluster analysis, and overlay analysis of multi-source heterogeneous data provided by local governments. Detailed mapping and classification of the current situation are merely the very first steps in the decision-making process. The complete decision-making mechanism includes steps such as site investigation, identification of targeted RIPs, negotiation with

FIGURE 8
Onsite photos of Shannan Industrial Park.

FIGURE 9
Onsite photos of Donglian Jincheng Industrial Park.

FIGURE 10
Onsite photos of Dienan Linchang Industrial Park.

stakeholders, policy making, and implementation of policies. Wang et al. (2021) point out that policies and strategies, stakeholders, and approaches and tools are the three main directions of research on decision-making for urban regeneration. In the wealthy Pearl River Delta region, where urban boundaries are strictly controlled by ecological considerations, the transformation of RIPs progresses rather slowly in major industrial cities such as Dongguan and Zhongshan because of the ambiguity of collective property rights and complex local interests. Officials in Nanhai also reported that they felt confused about which parks should be transformed first, which in turn affected the overall progress. The empirical analyses in this paper provide ideas to solve their confusion and suggest that the majority of Nanhai RIP has a need for renovation in the near future. Leaving the "retained RIPs" untouched will help local governments focus on other more viable projects. In the following subsections, the authors will demonstrate how the tangible and intangible factors reflect the different decision-making logics from temporal and administrative perspectives.

5.2 Tangible factors: short-term interests vs. long-term growth

In determining the timeline for projects, it is rational to prioritize the redevelopment of "near-term-removed RIPs." However, while confronting results shown by the tangible factors, some RIPs are "path-dependent" and unwilling to give up the existing rental income. For some RIPs with a low level of economic development, redevelopment represents the loss of existing tenants and the uncertainty of future investment. Conservative RIP managers will be rather hesitant about dismantling their parks. On the other hand, RIPs willing to redevelop also prefer to develop commercial or residential projects, as they have a higher transfer price than factory buildings. According to the authors' observation, the prices of commercial and residential land in Nanhai District are approximately ten and fifty times higher than those of industrial land in the same location. In 2018, 94 percent of RIP redevelopment projects in Guangzhou were converted to commercial or residential projects (Meng et al., 2022). This one-time, short-term behavior is not conducive to the expansion of the tax base and can pose a threat to the city's fiscal sustainability and long-term growth. To safeguard local industrial development and to protect the tax base, the Nanhai District has designated multiple industrial zones, in which old factories can only be redeveloped as industrial buildings. Making such decisions implies that local governments have resisted the temptation of short-term land transfer revenues.

5.3 Intangible factors: bottom-up influence vs. top-down intervention

The attitude towards intangible factors also reflects significant differences in concerns between the grassroots and the higher levels of government. For towns and villages, their priority is to ensure the stability of rental income from RIP. The feasibility of project implementation is also their main concern. At the initial stage of the investigation, factors related to economic development and physical space are major concerns in the model. However, with strong suggestions from grassroots managers, the authors incorporated factors such as tenancy duration and willingness to renovate into the final version of the classification method. Grassroots executives wanted to encounter as little resistance as possible in the process of removing RIPs. For governments at the district level and above, the primary goal is to fulfill the orders given by the prefecture and provincial government and to promote the rapid development of the local economy. From 2020 to 2022, Foshan City has given Nanhai District the task of dismantling at least 20,000 mu (around 3,300 acres) of RIPs each year, which is also their major motivation for categorizing the chaotic RIPs. In terms of economic development, the district government pays more attention to the quality of enterprises rather than the quantity. Some officials even believed that all RIPs containing a large number of factories should be prioritized for demolition because these factories are so small that their potential for upgrading is limited, which is not conducive to the rapid development of the local economy, regardless of how many employment opportunities they have provided. Based on these discrepancies, the approaches proposed in this paper also attempt to balance the effects of bottom-up influence and top-down intervention.

6 Conclusion

Taking the rural industrial parks in Nanhai District of Foshan City as studied cases, this paper has analyzed how the initial distribution of property rights and transaction costs affect the decision-making for RIP redevelopment. In addition, this paper also attempts to propose a toolkit that could support urban renewal decision-making through spatial and quantitative analysis approaches. The conclusions are set out as follows:

(1) Combining new institutional economics and property rights theory, this paper proposes a classification method to assist decision-making for RIP renewal projects, containing 15 tangible and intangible factors. These factors include information on four main areas such as economic development level, building quality, duration of tenancy, and willingness to renovate. Such a method is also designed to accommodate struggles between bottom-up influence and top-down intervention.
(2) The authors pointed out that there is a market failure in RIP development while a vast amount of inefficient industrial parks are occupying large areas of well-located land. This result is generated by the 2019 cross-sectional data and vector data, which have also revealed a close relationship between the development of RIPs and their geographical location.
(3) Cluster analysis and the subsequent overlay analysis have explicitly presented different levels of redevelopment necessary for the RIPs by identifying their economic development level and institutional barriers. The authors proposed that the RIPs of Nanhai be divided into three types: retained, medium-term-removed, and near-term-removed.

After enjoying the dividends of rural industrialization, how to combat the accompanying environmental pollution has been an important issue for developing countries (such as China and Vietnam) in recent years (Dang and Tran, 2020; Jiang et al., 2022). Eliminating high-carbon emitting factories and freeing up land for high-tech industries have become important means of controlling industrial pollution in rural China. This paper has provided some policy-making ideas for the future management of rural industrial land in developing countries. For example, retained RIPs should undergo gradual upgrading to maintain their existing economic vitality. Medium-term-removed RIPs should further straighten out property rights relationships, especially to find a suitable way to eliminate long-standing illegal constructions. Near-term-removed RIPs should accelerate the progress of their renovation to set an example for other districts of cities. The follow-up investigation conducted in early 2022 confirmed the accuracy of the findings of this paper. Local departments of the Nanhai government provided feedback that 81.43 percent of the RIPs were planned for redevelopment following the categorization results of this study. The authors also admit that this study has some limitations. Due to the lack of data on pollution levels, carbon dioxide emissions and, so on, the analysis in this paper fails to include the environmental impacts of RIP. Some factors included in this paper are also inevitably geographically specific. In addition to Nanhai, RIP redevelopment in other cities needs to be further examined. Therefore future research should expand the study area and flexibly make use of local data, while the Chinese government is vigorously searching for industrial space to develop high-tech industries, including chip manufacturing and artificial intelligence.

Data availability statement

The original contributions presented in the study are included in the article/supplementary material, further inquiries can be directed to the corresponding author.

Author contributions

ZL: Conceptualization, Data curation, Formal Analysis, Funding acquisition, Methodology, Resources, Supervision, Validation, Writing–original draft, Writing–review and editing. HF: Formal Analysis, Investigation, Software, Validation, Visualization, Writing–original draft. SX: Investigation, Software, Visualization, Writing–original draft. YW: Investigation, Software, Visualization, Writing–original draft. KW: Investigation, Software, Visualization, Writing–original draft. ZS: Data curation, Software, Writing–review and editing. HW: Conceptualization, Funding acquisition, Supervision, Writing–review and editing.

Funding

The authors declare financial support was received for the research, authorship, and/or publication of this article. This study was supported by the National Office for Philosophy and Social Sciences (21CZZ043), the Guangdong Planning Office of Philosophy and Social Science (GD22XMK01), and the Guangzhou Planning Office of Philosophy and Social Science (2019GZGJ56).

Acknowledgments

The authors would like to thank the editors, reviewers and editorial staff for their thorough and constructive engagement with this article.

Conflict of interest

The authors declare that the research was conducted in the absence of any commercial or financial relationships that could be construed as a potential conflict of interest.

Publisher's note

References

Admasu, W. F., Van Passel, S., Nyssen, J., Minale, A. S., and Tsegaye, E. A. (2021). Eliciting farmers' preferences and willingness to pay for land use attributes in northwest Ethiopia: a discrete choice experiment study. *Land Use Policy* 109, 105634. doi:10.1016/j.landusepol.2021.105634

Akita, T., and Fujita, M. (1982). Spatial development processes with renewal in a growing city. *Environ. Plan. A* 14, 205–223. doi:10.1068/a140205

Allred, B. W., Smith, W. K., Twidwell, D., Haggerty, J. H., Running, S. W., Naugle, D. E., et al. (2015). Ecosystem services lost to oil and gas in north America. *Science* 348, 401–402. doi:10.1126/science.aaa4785

Buitelaar, E., and Segeren, A. (2011). Urban structures and land. The morphological effects of dealing with property rights. *Hous. Stud.* 26, 661–679. doi:10.1080/02673037.2011.581909

Cai, L., He, J., Liang, X., and Zhong, N. (2021). Full cycle monitoring of low efficiency industrial park renovation: Shunde practice (in Chinese). *Planners* 37 (6), 45–49. doi:10.3969/j.issn.1006-0022.2021.06.007

Chan, E., and Lee, G. K. L. (2008). Critical factors for improving social sustainability of urban renewal projects. *Soc. Indic. Res.* 85, 243–256. doi:10.1007/s11205-007-9089-3

Coase, R. H. (1960). The problem of social cost. *J. Law Econ.* 3, 1–44. doi:10.1086/466560

Couch, C., and Dennemann, A. (2000). Urban regeneration and sustainable development in britain: the example of the Liverpool Ropewalks partnership. *Cities* 17, 137–147. doi:10.1016/S0264-2751(00)00008-1

Couch, C., Sykes, O., and Börstinghaus, W. (2011). Thirty years of urban regeneration in Britain, Germany and France: the importance of context and path dependency. *Prog. Plann* 1, 1–52. doi:10.1016/j.progress.2010.12.001

Cowie, A. L., Orr, B. J., Castillo Sanchez, V. M., Chasek, P., Crossman, N. D., Erlewein, A., et al. (2018). Land in balance: the scientific conceptual framework for land degradation neutrality. *Environ. Sci. Policy* 79, 25–35. doi:10.1016/j.envsci.2017.10.011

Dang, T. D., and Tran, T. A. (2020). Rural industrialization and environmental governance challenges in the red River Delta, Vietnam. *J. Environ. Dev.* 29 (4), 420–448. doi:10.1177/1070496520942564

Demsetz, H. (1967). Towards a theory of property rights. *Am. Econ. Rev.* 57, 347–359. doi:10.2307/1821637

Enserink, B., and Koppenjan, J. (2007). Public participation in China: sustainable urbanization and governance. *Manag. Environ. Qual.* 18, 459–474. doi:10.1108/14777830710753848

Erfani, G., and Roe, M. (2020). Institutional stakeholder participation in urban redevelopment in tehran: an evaluation of decisions and actions. *Land Use Policy* 91, 104367. doi:10.1016/j.landusepol.2019.104367

Guo, B., Li, Y., and Wang, J. (2018). The improvement strategy on the management status of the old residence community in Chinese cities: an empirical research based on social cognitive perspective. *Cogn. Syst. Res.* 52, 556–570. doi:10.1016/j.cogsys.2018.08.002

Haskins, C. (2006). Multidisciplinary investigation of eco-industrial parks. *Syst. Eng.* 9, 313–330. doi:10.1002/sys.20059

Hoops, B. (2016). Expropriation procedures in Germany and The Netherlands: ready for the voluntary guidelines on the responsible governance of tenure? *Eur. Prop. Law J.* 5, 3–26. doi:10.1515/eplj-2016-0014

Jiang, H., Zhang, T., Xiao, X., Jie, Q., and Liang, Y. (2022). Ecological network breakpoint identification and industrial renewal design strategy for structure restoration: taking the village-level industrial park in Shunde district of foshan as an example (in Chinese). *Ind. Constr.* 52 (5), 16–23. doi:10.13204/j.gyjzG22011504

Jo Black, K., and Richards, M. (2020). Eco-gentrification and who benefits from urban green amenities: NYC's high line. *Landsc. Urban Plan.* 204, 103900. doi:10.1016/j.landurbplan.2020.103900

Kelly, J. J. (2006). We shall not be moved": urban communities, eminent domain and the socioeconomics of just compensation. *St. John's Law Rev.* 80, 923–990.

Kylili, A., Fokaides, P. A., and Jimenez, P. A. L. (2016). Key performance indicators (KPIs) approach in buildings renovation for the sustainability of the built environment: a review. *Renew. Sustain. Energy Rev.* 56, 906–915. doi:10.1016/j.rser.2015.11.096

Lai, Y., and Tang, B. (2016). Institutional barriers to redevelopment of urban villages in China: a transaction cost perspective. *Land Use Policy* 58, 482–490. doi:10.1016/j.landusepol.2016.08.009

Lai, Y., Tang, B., Chen, X., and Zheng, X. (2021). Spatial determinants of land redevelopment in the urban renewal processes in Shenzhen, China. *Land Use Policy* 103, 105330. doi:10.1016/j.landusepol.2021.105330

Li, D. D. (1996). A theory of ambiguous property rights in transition economies: the case of the Chinese non-state sector. *J. Comp. Econ.* 23, 1–19. doi:10.1006/jcec.1996.0040

Li, T. H. Y., Ng, S. T., and Skitmore, M. (2012). Public participation in infrastructure and construction projects in China: from an EIA-based to a whole-cycle process. *Habitat Int.* 36, 47–56. doi:10.1016/j.habitatint.2011.05.006

Liang, X., Li, H., Zhu, M., Feng, P., and He, J. (2021). Promoting high quality development by upgrading village level industrial park: a planning case in Shunde district, foshan city (in Chinese). *Planners* 4, 51–56. doi:10.3969/j.issn.1006-0022.2021.04.008

Livingstone, N., Fiorentino, S., and Short, M. (2021). Planning for residential "value" ? London's densification policies and impacts. *Build. Cities* 2, 203–219. doi:10.5334/bc.88

McTague, C., and Jakubowski, S. (2013). Marching to the beat of a silent drum: wasted consensus-building and failed neighborhood participatory planning. *Appl. Geogr.* 44, 182–191. doi:10.1016/j.apgeog.2013.07.019

Meng, Q., Wu, Y., and Wu, J. (2022). Exploring temporary regeneration path for stock industrial land of village-level industrial park in Guangzhou (in Chinese). *Planners* 7, 100–108. doi:10.3969/j.issn.1006-0022.2022.07.014

Mohit, M. A., Ibrahim, M., and Rashid, Y. R. (2010). Assessment of residential satisfaction in newly designed public low-cost housing in Kuala Lumpur, Malaysia. *Habitat Int.* 34, 18–27. doi:10.1016/j.habitatint.2009.04.002

Nanhai District Bureau of Statistics (2023). Statistical bulletin on economic and social development of Nanhai District, Foshan City, 2022. Avaliable at: http://www.nanhai.gov.cn/fsnhq/bmdh/zfbm/qtjj/tjgb/content/post_5663588.html (Accessed August 20, 2023).

North, D. C. (1990). *Institutions, institutional change and economic performance*. Cambridge, UK: Cambridge University Press. doi:10.2307/2234910

Park, S. O. (1996). Networks and embeddedness in the dynamic types of new industrial districts. *Prog. Hum. Geogr.* 20, 476–493. doi:10.1177/030913259602000403

Peng, J., Tian, L., Liu, Y., Zhao, M., Hu, Y., and Wu, J. (2017). Ecosystem services response to urbanization in metropolitan areas: thresholds identification. *Sci. Total Environ.* 607-608, 706–714. doi:10.1016/j.scitotenv.2017.06.218

People's Government of Dongguan City (2020). The implementation opinions on accelerating the transformation and upgrading of rural industrial parks in Dongguan. Avaliable at: http://www.dg.gov.cn/zwgk/zfxxgkml/szfbgs/zcwj/qtwj/content/post_3035242.html (Accessed June 1, 2022).

Pritchett, W. E. (2003). The "public menace" of blight: urban renewal and the private uses of eminent domain. *Yale Law Policy Rev.* 21, 1–52.

Reimann, B. (1997). The transition from people's property to private property: consequences of the restitution principle for urban development and urban renewal in east Berlin's inner-city residential areas. *Appl. Geogr.* 17, 301–313. doi:10.1016/S0143-6228(97)00023-4

Schall, L. D. (1976). Urban renewal policy and economic efficiency. *Am. Econ. Rev.* 66, 612–628.

Schleich, L. M. (1993). Takings: the fifth amendment, government regulation, and the problem of the relevant parcel. *J. Land Use Environ. Law* 8, 381–411.

Skevington, S. M., Lotfy, M., and O'Connell, K. A. (2004). The World Health Organization's WHOQOL-BREF quality of life assessment: psychometric properties and results of the international field trial. A report from the WHOQOL group. *Qual. Life Res.* 13, 299–310. doi:10.1023/B:QURE.0000018486.91360.00

Soltani, K. (2022). *Redeveloping Tehran: a study of piecemeal versus comprehensive redevelopment of run-down areas*. Cham, Switzerland: Springer. doi:10.1007/978-3-030-97091-8

Staples, J. H. (1970). Urban renewal: a comparative study of twenty-two cities, 1950-1960. *Polit. Res. Q.* 23, 294–304. doi:10.1177/106591297002300205

Sui Pheng, L. (1993). The conceptual relationship between construction quality and economic development. *Int. J. Qual. Reliab Manag.* 10, 18–30. doi:10.1108/02656719310027939

Tang, B., Wong, S., and Lau, M. C. (2008). Social impact assessment and public participation in China: a case study of land requisition in Guangzhou. *Environ. Impact Assess. Rev.* 28, 57–72. doi:10.1016/j.eiar.2007.03.004

United Front Work Department of CPC Nanhai Committee (2016). Nanhai District held a thematic consultation meeting on environmental improvement of rural industrial parks. Avaliable at: http://tzb.nanhai.gov.cn/cms/html/6074/2016/20160719151557577839420/20160719151557577839420_1.html (Accessed December 15, 2022).

Vallance, S., Perkins, H. C., and Dixon, J. E. (2011). What is social sustainability? A clarification of concepts. *Geoforum* 14, 342–348. doi:10.1016/j.geoforum.2011.01.002

Wang, H., Zhao, Y., Gao, X., and Gao, B. (2021). Collaborative decision-making for urban regeneration: a literature review and bibliometric analysis. *Land Use Policy* 107, 105479. doi:10.1016/j.landusepol.2021.105479

Williamson, O. E. (1985). *The economic institutions of capitalism: firms, markets, relational contracting*. New York, NY: Free Press. doi:10.2307/2233521

Xiong, C., Zhang, P., and Lin, H. (2020). Shunde plans to dismantle more than 80,000 mu of rural industrial parks in three years. Avaliable at: http://www.fsxcb.gov.cn/xwyl/content/post_411117.html (Accessed January 16, 2022).

Yang, G., and Xu, C. (2016). Breakthroughs and limitations of urban renewal marketization - based on the perspective of transaction costs (in Chinese). *City Plan. Rev.* 40, 32–38. doi:10.11819/cpr20160905a

Yao, Z., and Tian, L. (2017). Transition of pattern and modes of governance for urban renewal in Guangzhou since the 21st century (in Chinese). *Shanghai Urban Plan. Rev.* 1, 29–34.

Zhang, C., Kuang, W., Wu, J., Liu, J., and Tian, H. (2021a). Industrial land expansion in rural China threatens environmental securities. *Front. Env. Sci. Eng.* 15, 29. doi:10.1007/s11783-020-1321-2

Zhang, L., Ge, D., Sun, P., and Sun, D. (2021b). The transition mechanism and revitalization path of rural industrial land from a spatial governance perspective: the case of Shunde district, China. *Land* 10 (7), 746. doi:10.3390/land10070746

Zhang, S., Yang, J., Ye, C., Chen, W., and Li, Y. (2023). Sustainable development of industrial renovation: renovation paths of village-level industrial parks in pearl river delta. *Sustainability* 15, 9905. doi:10.3390/su15139905

Zheng, S., Long, F., Fan, C. C., and Gu, Y. (2009). Urban villages in China: a 2008 survey of migrant settlements in Beijing. *Eurasian Geogr. Econ.* 50, 425–446. doi:10.2747/1539-7216.50.4.425

Zhou, X., Yang, J., Wang, S., and Wang, C. (2018). Transformation from mulberry fish pond to industrial park: a case study of Shunde, Guangdong province (in Chinese). *City Plan. Rev.* 42, 33–42. doi:10.11819/cpr20181206a

Zhu, J. (2002). Urban development under ambiguous property rights: a case of China's transition economy. *Int. J. Urban Reg. Res.* 26, 41–57. doi:10.1111/1468-2427.00362

Zhuang, T., Qian, Q. K., Visscher, H. J., and Elsinga, M. G. (2020). An analysis of urban renewal decision-making in China from the perspective of transaction costs theory: the case of Chongqing. *J. Hous. Built Environ.* 35, 1177–1199. doi:10.1007/s10901-020-09733-9

frontiers | Frontiers in Environmental Science

TYPE Review
PUBLISHED 27 February 2024
DOI 10.3389/fenvs.2024.1350185

OPEN ACCESS

EDITED BY
Chenxi Li,
Xi'an University of Architecture and Technology, China

REVIEWED BY
Xiao Liu,
South China University of Technology, China
Linghua Duo,
East China University of Technology, China
Guoen Wei,
Nanchang University, China

*CORRESPONDENCE
Lili Dong,
dongll@cqjtu.edu.cn

†These authors have contributed equally to this work

RECEIVED 05 December 2023
ACCEPTED 07 February 2024
PUBLISHED 27 February 2024

CITATION
Dong L, Wang Y, Ai L, Cheng X and Luo Y (2024), A review of research methods for accounting urban green space carbon sinks and exploration of new approaches.
Front. Environ. Sci. 12:1350185.
doi: 10.3389/fenvs.2024.1350185

A review of research methods for accounting urban green space carbon sinks and exploration of new approaches

Lili Dong[1*†], Yiquan Wang[1†], Lijiao Ai[2,3], Xiang Cheng[4,5] and Yu Luo[6]

[1]School of Architecture and Urban Planning, Chongqing Jiaotong University, Chongqing, China, [2]Chongqing Key Laboratory of Germplasm Innovation and Utilization of Native Plants, Chongqing, China, [3]Chongqing Landscape and Gardening Research Institute, Chongqing, China, [4]School of Architecture and Urban Planning, Chongqing University, Chongqing, China, [5]Key Laboratory of the Ministry of Education of Mountainous City and Towns Construction and New Technology, Chongqing University, Chongqing, China, [6]Department of Architecture, The University of Kitakyushu, Kitakyushu, Fukuoka, Japan

Along with urbanization and industrialization, carbon emissions have been increasing significantly, resulting in global warming. Green space has been widely accepted as a natural element in cities to directly increase carbon sinks and indirectly reduce carbon emissions. The quantification of carbon benefits generated by green space is an important topic. This paper aims to provide a comprehensive review of the methods for measuring carbon sinks of green spaces. The results indicate that existing assessment methods can accurately estimate the carbon sinks in green spaces at large scales. However, existing methods are not fully applicable to studies of urban green spaces, due to the low precision of research results. The assimilation method is the most suitable method to study the carbon sequestration efficiency of plants and can project the carbon sinks of urban green spaces at large scales through macroscopic means. Even though, the results of assimilation experiments are unstable under different weather conditions. To address existing research challenges, this paper proposes a photosynthetic rate estimation method based on the light-response curve which is an efficient method to describe the relationship between light intensity and net photosynthetic rate in studying plant physiological characteristics. The newly proposed method, through integrating net photosynthesis-light response curves and urban light intensity associated with meteorological data, has advantages of short measurement time and ensuring standardized experimental environment for result comparability. Overall, this study is important to combine meteorology and plant physiology to propose a photosynthetic rate estimation method for optimizing carbon sink measurement in urban green spaces. The method is more convenient for application for its simple experimental process and result comparability. In practice, this study provides guidance for low-carbon urban green space planning and design, and helps to promote energy conservation and emission reduction through nature-based solutions.

KEYWORDS

urban green space, carbon sinks accounting, photosynthetic rate estimation, net photosynthetic light-response curve, photosynthetically active radiation

1 Introduction

1.1 Urbanization, greenhouse gas emission, and global warming

With the predominant industrialization and urbanization, the construction of urban infrastructure and land use changes have dramatically replaced natural ecosystem areas (He et al., 2021), resulting in significant environmental deterioration, economic losses, social challenges, and public health issues (Li K. et al., 2023; He, 2023; Wei et al., 2023). Addressing such challenges have been a consensus of the public, governments and organizations (Liu X. et al., 2023). Even though, cities are highly dependent on heavy fossil-fuel use. Authorities estimate that fossil fuel combustion accounts for 90% of total CO_2 emissions in 2023 (Friedlingstein et al., 2023), resulting in a rapid rise in atmospheric concentrations of greenhouse gases on Earth, ultimately causing global warming (Gao et al., 2021; Shen and Zhao, 2024). For example, a 1.1°C increase in global average temperature worldwide presents the largest increase in the last 1,000 years (Intergovernmental Panel On Climate Change, 2023). Furthermore, it is reported that the urbanization has contributed to one-quarter of the average annual temperature increase of Guangdong Province in the last 70 years (Zhong et al., 2023). The atmospheric studies in Guangdong, Hong Kong, and Macao in China have concluded that greenhouse gases are the most important determinants of future average and extreme temperatures (Zheng et al., 2022).

The global atmospheric CO_2 concentration in 2022 will be about 1.5 times that of the pre-industrial revolution, in addition to total global CO_2 emissions of about 40.9 billion tons in 2023, of which China will be the largest emitter, accounting for about 35% of the total emissions (Friedlingstein et al., 2023). Cities only cover 3% of the Earth's surface, but they are now representing more than 55% of the global population. Moreover, the spatial distribution of carbon emissions in cities are much higher than rural counterparts, indicating that cities and their adjacent regions are among the highest contributors to carbon emissions (Figure 1). In China, the situation is more alerting since urban areas contribute as much as 90% of national carbon emissions (Li, 2010). With this background, the United Nations Framework Convention on Climate Change was signed by more than 150 countries in 1992, in order to collectively maintain atmospheric greenhouse gas concentrations at a stable level. The 2015 Paris Agreement requires all signatory nations to reduce their greenhouse gas emissions. In September 2020, China explicitly set a double carbon target for 2030 in order to achieve carbon neutrality by 2060.

1.2 Significance of green spaces for climate change mitigation

Achieving carbon neutrality generally involves two primary approaches: carbon emission reduction and carbon sink augmentation. Carbon reduction is the ability of green spaces to reduce energy consumption in buildings, transportation, etc., by improving the microclimate of the space. The carbon sequestration is to increase the carbon sequestration capacity of greenfield plants, with a focus on strengthening the ecological construction and protection of urban green spaces. The terrestrial biosphere shows significant potential for carbon sequestration. The studies indicate that in China, the terrestrial biosphere annually sequestered an average of approximately 1.11 (±0.38) $\times 10^9$ tons of carbon dioxide between 2010 and 2016, roughly equivalent to 45% of the concurrent annual anthropogenic carbon dioxide emissions (Wang J. et al., 2020). Urban green spaces represent primary green ecological resources in densely populated and economically developed urbanized regions. These spaces also constitute the main natural carbon sinks within urban ecosystems and possess a unique ability for self-purification and self-regulation. It is demonstrated that urban green space contributes to improving urban environmental quality by sequestering carbon (Nowak et al., 2018). This is mainly manifested through vegetation employing photosynthesis to reduce

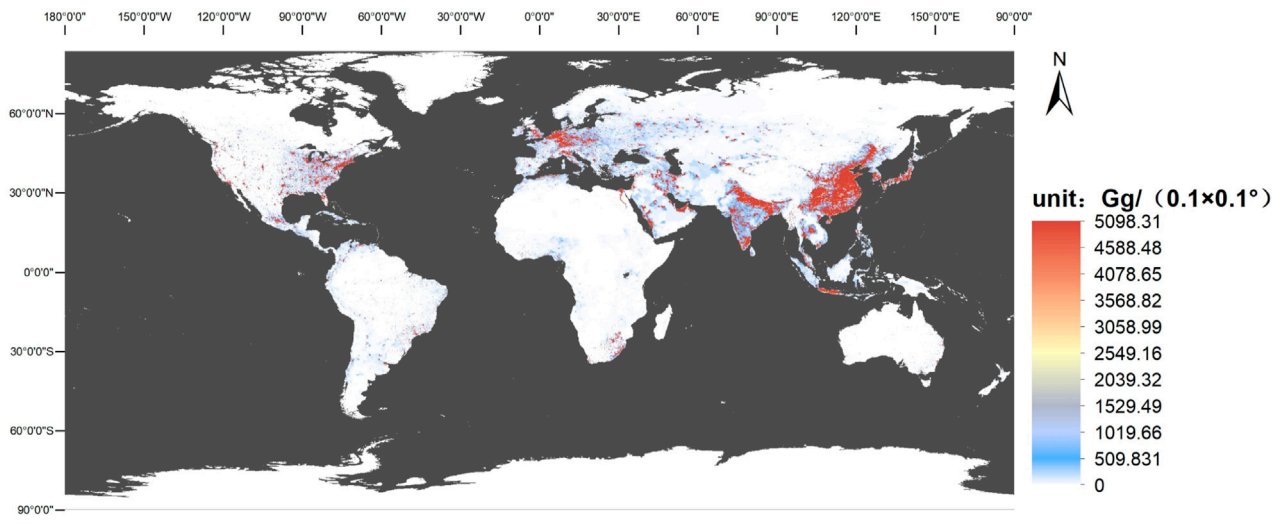

FIGURE 1
Global distribution of total carbon emissions in 2022 (source: Global carbon atlas).

atmospheric CO_2 while releasing O_2 (Russo et al., 2014), playing a crucial role in regulating the balance of atmospheric carbon and oxygen, and enhancing urban environmental quality.

Urban greenspace ecosystem comprises individual plant entities within the city, and its carbon sequestration capacity relies on the carbon sequestration abilities of vegetation. Urban green space vegetation serves as the main component of urban greenspace carbon sinks. Through photosynthesis and respiration within their leaves, plants accumulate a net carbon amount, sequestrating CO_2 within the vegetation, soil, and water bodies, thereby reducing atmospheric CO_2 concentrations (Dong and He, 2023). Moreover, urban green spaces effectively mitigate heat islands (Liu H. et al., 2023), decrease urban energy use, and thereby reduce urban carbon emission. Plants play a dual role of reducing CO_2 emissions and increasing CO_2 sequestration, making them the primary carbon sink in landscape architecture (Bao, 2011). Overall, ecosystem carbon sequestration, including urban greening carbon sinks, has become a focal task in the top-level design of China's efforts toward achieving carbon neutrality. To address warming challenges, it is essential to include more carbon sinks during urban planning and design to sequestrate greenhouse gases such as CO_2 and CH_4, as well as to alleviate environmental deterioration such as urban flooding and heat islands. Quantitative analysis of the carbon sequestration capacity of plants is an important research topic since it not only comprehensively demonstrates their carbon sequestration and oxygen release abilities and influencing factors but also provides the basis for creating, designing, managing, and improving urban natural carbon sinks. Furthermore, the quantitative analysis aids in scientifically selecting tree species for urban green spaces in a low-carbon era, offering theoretical references for strong carbon sink plant configurations, ecological landscape construction, and the development of eco-friendly urban landscapes. Overall, the quantification of green space carbon sink potential is a crucial means for alleviating global greenhouse and heat island effects, serving as a key player in supporting sustainable urban development and mitigating climate change.

2 Green space carbon sink: progress and status

In 1992, the United Nations General Assembly defined the process, activities, and mechanisms to remove CO_2 from the atmosphere as carbon sink. Green carbon sink, accordingly, involves the release of oxygen through plant photosynthesis, absorption of atmospheric CO_2, and its sequestration within vegetation and soil, thereby reducing CO_2 concentration in the atmosphere (Dong and He, 2023). Carbon sequestration is the process of capturing and securely storing carbon, as an alternative to directly emitting CO_2 into the atmosphere. A fundamental principle of plant carbon sequestration is that green plants utilize chlorophyll and other photosynthetic pigments under visible light for their growth requirements, converting CO_2 and H_2O into organic compounds, while releasing O_2 to maintain the balance of carbon and oxygen in the air. Note that plants can absorb only atmospheric CO_2 through photosynthesis (King et al., 2012) so that converting carbon sink quantity into CO_2 absorption is a more direct chemical quantification method. The capacity of plants to absorb atmospheric CO_2 depends primarily on the intensity of their photosynthetic activity which is often represented by the photosynthetic rate. The photosynthetic rate refers to the speed at which photosynthesis sequestrates CO_2 (or generates oxygen). The net photosynthetic rate signifies the organic matter accumulated through plant photosynthesis and is derived by subtracting the respiration rate from the total photosynthetic rate, serving as a determinant of a plant's carbon-fixing ability (Wang et al., 2014). It is commonly measured by a portable photosynthesis system (PPS).

Studies on plant carbon sequestration began in the 1960s and has gradually grown into an important research topic over the past decade, yielding significant accomplishments. For instance, in 1991, Rowntree and Nowak estimated the carbon stock of urban forests across the United States (Rowntree and Nowak, 1991) and concluded that green spaces could sequester CO_2 by regulating local urban conditions such as temperature and humidity. Subsequently, estimates of annual carbon sequestration in urban green spaces were conducted (Nowak et al., 2002; Pataki et al., 2006), enlightening many studies on urban ecosystem carbon storage. Presently, research on the carbon sink potential of garden plants primarily involves macro-scale estimations (i.e., the methods of sample plot measurement, model calculations, remote sensing (RS) estimation, and micrometeorological) and micro-scale measurements (e.g., assimilation) (Figure 2). However, these estimations are different in methods, accuracy levels, and requirements.

At macro scale, the research is primarily focused on carbon sequestration and storage quantification in extensive ecological systems (e.g., forests), from the perspective of plant carbon storage capacity in the agricultural and forestry-related domains (Houghton et al., 1985). Regarding the total carbon storage estimation of urban or natural green spaces, the macro-level approaches allow people to understand the carbon sink benefits of ecosystems, and thereby support and formulate urban forestry policies (Garcia-Gonzalo et al., 2007). Empirically, relevant studies were found before 2010, focusing on quantifying carbon sequestration in vegetation within green spaces (Paw U et al., 2004), yet macroscopic research methods were unable to estimate the net production within ecosystems or plants (López et al., 2010). Nevertheless, these methods are used as a basis for developing process-based simulations and models. Physiological measurements using infrared gas analyzers for CO_2 assimilation in plant leaves and branches, complemented by leveraging Earth observation technologies (e.g., satellite data), are used to extrapolate these measurements to larger scales (Holifield Collins et al., 2008).

At micro scale, primarily from the perspective of plant physiological characteristics, the quantification of carbon sequestration in plants during the process of photosynthesis is carried out by directly measuring flux difference using PPS to quantify their carbon sequestration. Since the 1950s, infrared CO_2 gas analyzers have been widely employed, with a fundamental principle of calculating net photosynthetic rate by measuring the difference in the CO_2 concentration entering the leaf stomata. These analyzers have shown innovation in measurement accuracy, efficiency, applicability, and data storage and are particularly suitable for outdoor measurements. Therefore, the assimilation method has been widely used for quantifying carbon sequestration of individual plants.

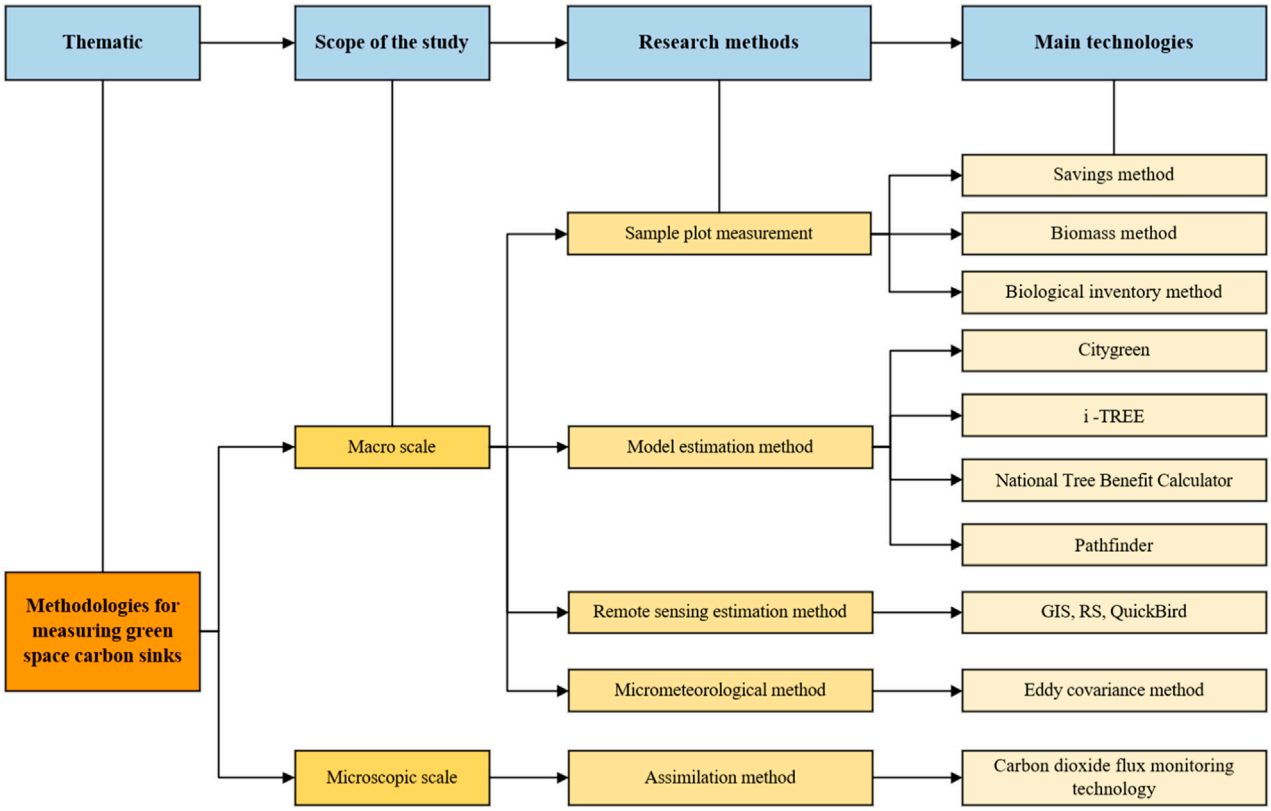

FIGURE 2
Summary of research methods and techniques.

2.1 Sample plot measurement

Sample plot measurement refers to an estimation method of setting up sample plots in typical areas with good forest growth and conducting continuous observation in the sample plots to obtain the changes in carbon stocks per unit time (Zhou et al., 2013). This method quantifies growth over time, considering the time when plants start growing until the time of their harvest. It is mainly applied to investigating the carbon sink potential of macro-scale green spaces. There has been a long history of sample plot measurement application, mainly in forestry and agricultural production, and it is a well suggested method by the IPCC for forest carbon sink assessment (Ouyang et al., 1999). This approach estimates the carbon sequestration of plants by harvesting and weighing all aboveground and belowground organic matter within sampling plots. The average values from these plots were used to estimate the biomass of the entire forest or individual plants, which were then converted into an average annual carbon sequestration rate for green vegetation.

In practical applications, it often involves the use of highly accurate measured data obtained from standard tree analysis to construct ecological indicators and biomass growth equations (Lee et al., 2014). For instance, the relationship between diameter at breast height (DBH), tree height and age indicators of trees was utilized to develop an allometric growth equation to estimate the carbon sequestration capacity of forests (Zhang et al., 2019). The biomass method acquires measured data through extensive field surveys to assess the biomass of plants at different time and measure their photosynthetic intensity. Overall, it is now the most commonly used method for calculating forest carbon storage because of its direct, explicit, and technically straightforward advantages. However, it has several limitations, such as destructive experimentation, inability for continuous observation, difficulty in accounting for root production and litterfall, and complex processing procedures.

2.2 Model estimation method

The model estimation method, based on a plot inventory, is a convenient and precise approach suitable for quantifying carbon sequestration of urban green spaces in large areas or urban regions. By the end of the 21st century, leveraging big data systems, the United States Forest Service, systematically analyzed and developed several convenient plant carbon sequestration calculation systems. At current, the widely utilized systems include Citygreen, the NTBC (National Tree Benefit Calculator), Pathfinder, and the I-Tree Eco. These models receive extensive application in assessing the ecological benefits of urban green spaces. For instance, the Citygreen calculation system, in conjunction with on-site surveys, has been employed to estimate the total carbon sequestration of green spaces in cities like Shenzhen (Chen et al., 2009), Shanghai (Xu, 2010), and Shenyang (Liu et al., 2008). And quantification of carbon sequestration benefits of green space plants in Nanjing residential area using NTBC (Li Q. et al., 2023). The I-Tree Eco module has been

used in cities in the United Kingdom (Monteiro et al., 2019), the United States (Ning et al., 2016), Thailand (Intasen et al., 2017), and Hungary (Kiss et al., 2015) to assess the ecological value of urban green spaces. Moreover, the I-Tree Eco can estimate the carbon sequestration of individual plants based on specific characteristics. Overall, these estimation systems estimate carbon sequestration on a large regional scale by considering vegetation characteristics, meteorological data, site features, greenspace area, and surrounding environments so that the results are comprehensive. However, it is important to note that the physiological, ecological, and climatic parameters of the associated models were calibrated based on the U.S. conditions. Consequently, when such methods are applied to regions with different ecological systems and climatic conditions, substantial errors may occur. Therefore, these models are primarily suitable for use in areas with geographical and climatic conditions similar to those in the United States, upon some essential validation.

2.3 Remote sensing (RS) estimation method

The RS method, using satellite remote sensing to acquire various vegetation status parameters, offers the advantage of rapid, real-time, and large-scale data acquisition. It can well address the limitations of model-based estimations. The basic principle is to obtain various parameters of vegetation within the survey areas by sensing techniques on the basis of ground survey, and to estimate the impact of changes in land use and green space coverage on carbon stocks through spatial classification of vegetation and analysis of time series. Sensing-based assessments of net ecosystem productivity (NEP) are widely applied in carbon sink studies at regional and urban scales, such as some studies utilized QuickBird, RS and GIS to estimate the annual CO_2 uptake per tree in Los Angeles (Mcpherson et al., 2008), and combined LiDAR with QuickBird to estimate carbon stocks in urban trees (Schreyer et al., 2014). Meanwhile, there are studies on the use of remote sensing-based explicit forest carbon stock calculation models to realize high-resolution mapping of forest carbon stocks at large scales and dynamic monitoring of forest carbon sinks globally (Zhu et al., 2024), as well as the combination of ground-based measurements and LiDAR data to estimate the carbon stocks of urban trees (Gülin and Bosch, 2021). Research on the surface carbon storage of urban green spaces in Auckland also used LiDAR data combined with field surveys, suggesting that this approach not only provided more accurate data but also reduced the frequency and cost of actual measurements (Wang V. et al., 2020). This is because the method can offer detailed information on plant biomass in complex urban areas (Alonzo et al., 2014). However, due to the spatial heterogeneity and temporal dynamics of urban green spaces, the use of RS estimation methods for estimating carbon storage may encounter challenges like the inability to accurately determine plant quantity and difficulties in separating overlapping tree canopy boundaries (Richardson and Moskal, 2014). In addition, individual ecological differences among species can also lead to significant errors.

2.4 Micrometeorological method

The micrometeorological method is based on microclimate monitoring and involves continuous dynamic monitoring of near-surface atmospheric flow conditions and atmospheric CO_2 concentrations. This approach indirectly estimates the carbon flux of vegetation (Liu et al., 2018). It focuses on the quantitative study of carbon dioxide and water exchange between the atmosphere and terrestrial ecosystems (Grimmond et al., 2002). In Phoenix, the micrometeorological method was adopted, revealing that CO_2 concentrations at midday were lower than before sunrise mainly due to the strong sunlight at midday which promotes photosynthesis in vegetation (Idso et al., 1998), while in Essen using mobile measurement, it was shown that CO_2 concentrations in the city were lower in summer months given vegetation photosynthesis and other effects (Henninger and Kuttler, 2010). The micrometeorological method can accurately estimate regional-scale carbon fluxes, with eddy covariance being the most commonly used method. For instance, Velasco et al. used the eddy covariance method to show that urban CO_2 concentrations are lower during the daytime during the plant growing season, mainly due to the high photosynthetic capacity of plants at this time of year (Velasco and Roth, 2010), similar to the conclusion reached by Rana et al. (2021). Although the micrometeorological method allows for continuous *in-situ* observations, the unstable near-surface atmosphere and replicated topographic conditions can introduce significant errors into the results (Wilson et al., 2002). For example, atmospheric inversion and data from the Shangri-La observation point in the complex terrain of the Hengduan Mountains resulted in higher estimated data (Wang J. et al., 2020). The micrometeorological method also relies on site-specific observations and cannot represent carbon flux values for the entire region. At the regional scale, there are challenges related to low spatial resolution, making it difficult to differentiate the carbon sink amounts for different ecosystems (Piao et al., 2022).

2.5 Assimilation method

The assimilation method is a micro-scale research method. Since leaves are the most important organs for photosynthesis in trees, the assimilation method calculates plant carbon sequestration by determining the instantaneous net photosynthetic rate per unit of leaf area from the instantaneous CO_2 concentration of the leaves and the change in water content. Infrared Carbon Dioxide Gas Analyzers have been widely used from the 1950s to the present day, and the basic principle of their work is to calculate the net photosynthetic rate by determining the difference in CO_2 concentration entering leaf stomata. Measurements of photosynthesis rates of Wisconsin field species in the 1990s were an early application of the use of PPS to measure net photosynthetic rates of plants (Reich et al., 1995). By the end of 20th century, some studies reported the adoption of a photosynthesis meter to quantify plant photosynthetic intensity in a representative urban green space in Guangzhou and estimated the CO_2 uptake of the plants through the reaction equation of the photosynthesis process (Yang, 1996). Using infrared gas analyzers, measurement of the annual carbon dioxide uptake by urban plants in Korea was conducted, resulting in an empirical formula for future estimation. Furthermore, Han proposed a method for calculating plant carbon sequestration and oxygen release using the net assimilation rate formula (Han, 2005). The assimilation method experiment requires only a small amount of plant leaves, making it friendly to plants and widely applicable, and it has been employed in studies on common garden plants in locations such as West Bengal (Biswas et al., 2014), Rome (Gratani et al., 2016), and Fuzhou (Wang, 2010).

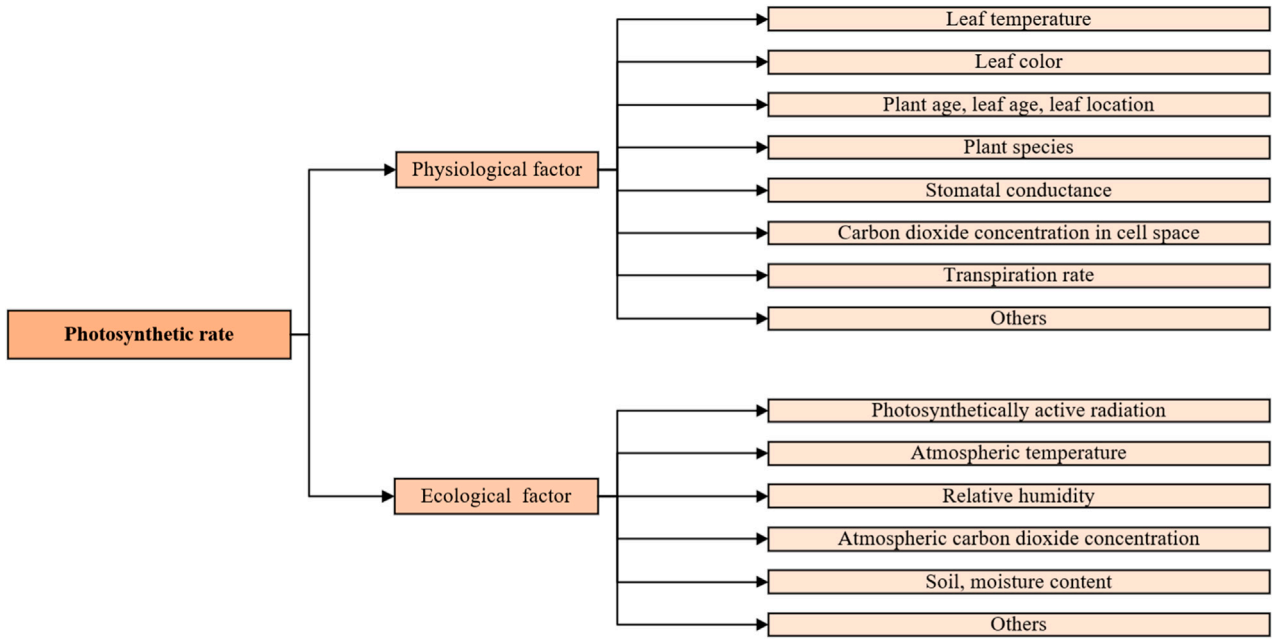

FIGURE 3
Photosynthesis-related influencing factors.

The assimilation method directly measures the carbon sequestration capacity of a single plant, and the results are accurate, allowing a direct comparison of carbon sequestration benefits among different plants. However, its outcomes are significantly influenced by temporal and spatial factors. This is attributed to the rhythmic cyclical variations in the photosynthetic rate of plant leaves, which systematically fluctuate with diurnal and seasonal changes. The primary rationale behind these fluctuations is the close relationship between photosynthetic rates and physiological and ecological environmental conditions such as atmospheric temperature, relative humidity, and solar radiation (Figure 3) (Evans and Santiago, 2011). For instance, the impact of vertical illumination results in peak solar radiation and daylight duration during the summer in the northern hemisphere, leading to a noticeable increase in carbon fixation by plants during this season compared to others. Although winter exhibits relatively weaker carbon fixation capacity throughout the year, the method still remains a high efficiency (Weissert et al., 2017). Moreover, air with higher relative humidity enhances stomatal conductivity in plant leaves, thereby elevating the rate of photosynthesis (Wang et al., 2019). These conditions necessitate labor-intensive hourly measurements of plant photosynthetic rates and impose significant requirements on weather conditions.

2.6 Summary

Whilst there have been many methods for urban green space carbon sink estimation, the advantages and disadvantages of each method are distinct (Table 1). Furthermore, there is no direct way to quantify carbon sinks in urban green spaces, and existing studies on urban green space carbon sink often employ methodologies developed for forest carbon sink (Gratani et al., 2016). Urban green spaces, primarily composed of artificial greenery, differ significantly from natural green spaces such as forests and grasslands. Urban green spaces also exhibit high heterogeneity, with plant species determined by early urban planning, incorporating both local and introduced species. This prominent contrast with naturally evolved green spaces implies that carbon sink in urban green spaces is more complex (Zhao et al., 2023). Therefore, existing methods for green space carbon sequestration may not be entirely applicable to urban settings. The sample plot measurement suitable for large-scale natural environments like forests, faces limitations in regions with diverse tree species distributions, rendering standard plots dissimilar to the entire region. Moreover, its destructive nature, involving irreversible vegetation removal, makes it unsuitable for urban green spaces designed and constructed through human planning. Explorations into non-destructive methods, such as the biomass method, for studying carbon sequestration in Bangkok park green spaces have been undertaken (Singkran, 2022), and the use of remote sensing to quantify and map forest structure to estimate forest above-ground biomass to quantify carbon stocks and fluxes in tropical forests (Mohd Zaki and Abd Latif, 2017), these studies explore additional possibilities for the sample plot inventory method.

Micrometeorological methods demonstrate high accuracy in regional-scale estimations but are sensitive to variations in urban spatial characteristics, leading to significant errors in different regions. Results from these methods reflect carbon sequestration at the regional scale and cannot discern individual plant carbon sequestration at a finer level. Model estimation incorporates green space information from similar regions into the model for estimation, potentially introducing errors due to ecological differences between regions. RS estimates carbon sequestration by calculating various green quantity indicators from satellite imagery, but the considerable variations in carbon sequestration benefits

TABLE 1 Methodologies for estimating carbon sinks in green spaces.

Research scale	Measurement method	Main technologies	Scope	Main indicators	Advantages	Disadvantages
Macroscopic scale	Sample Plot Measurement	Biomass method, Saving method, Biological inventory method	Large-scale forests	Biomass, carbon content, diameter at breast height*etc.*	High accuracy	High cost of data surveys; destructive to samples, unsustainable observations
	Micro-meteorological method	Eddy Covariance Measurements	Large-scale sample plots	Meteorological data	Intuitive observation of the time dynamics of greenfield carbon sinks	Highly influenced by near-surface atmospheric and topographic conditions; difficult to relocate observatories
	Model Estimation method	CITYGREEN	Small or medium scale green spaces	Vegetation information, site information, climate characteristics	Simple and convenient, with many considerations	Different algorithms between models; differences in modeled vegetation parameters and study area parameters
		I -TREE				
		NTBC				
		Pathfinder				
	Remote Sensing method	GIS、RS*etc.*	Large-scale green spaces	Meteorological, soil, and green space ecological indicators	Results are suitable for relative comparisons	Neglect of ecological differences among tree species
Micro scale	Assimilation method	Portable Photosynthesis System	Plant monocultures, small-scale green spaces	Plant physiological data such as net photosynthetic rate, leaf area index*etc.*	Fast estimation of carbon sequestration on a large scale	Results are highly influenced by the experimental environment, and final results are variable

among different plant species result in two-dimensional indicators that may not fully reflect the actual carbon sequestration benefits of urban green spaces. Assimilation method is the most accurate way to quantify the benefits of plant carbon sequestration, but its results may include large errors owning to experimental weather fluctuations. Moreover, scattered distributions of tree species in the experiment require a long period of time, resulting in limitations of labor dependence. The assimilation amount method is only for single plant scale, so that extensive sample plant data should be carried out when facing the large-scale urban green spaces.

3 Proposal of a prediction method for photosynthetic rate

Existing macroscopic studies, except for assimilation quantities, are limited to estimating carbon sinks and stocks for the current green space as a whole. They are unable to quantify and compare the carbon sinks of individual plants within these green spaces. Therefore, the relevant results and findings are of limited significance in providing guidance on construction of urban green spaces. The assimilation method is the most commonly used and accurate method for studying individual plant carbon sequestration. The results can guide the subsequent planning of tree species in urban green spaces. However, the assimilation method is greatly influenced by weather conditions such as light and temperature, and the results under different weather conditions are not comparable. Therefore, ongoing research should explore more convenient and precise measurement methods.

There have been some studies to utilize a photosynthesis model from natural green spaces at similar latitudes to simulate carbon sequestration through photosynthesis (Soegaard and MLler-Jensen, 2003; Helfter et al., 2010). However, results from non-urban green spaces may not be applicable to urban green spaces due to environmental disparities. Moreover, it is also revealed that plant leaf nitrogen concentration (N) is positively proportional to its net photosynthetic rate and leaf area (Mu and Chen, 2021). Since leaf nitrogen measurements require less time and can be amplified to regional and global scales by satellite sensors (Knyazikhin et al., 2012), there are good potentials to use leaf nitrogen concentration as an indirect estimate of photosynthetic carbon sequestration (Giacomo et al., 2005). However, measurements of leaf nitrogen should be conducted in the laboratory and is not suitable for experiments involving a large variety of tree species. A novel approach based on spatial and temporal dynamic analysis was proposed to study the carbon sequestration and oxygen release capacity of tree species (Chen, 2020). This approach reduces the error of the results due to the difference in experimental time and geographical area. However, the indicators required in this method include not only conventional net photosynthetic rates but also light-response curve, chlorophyll content, etc. Although the data accuracy is high, the experimental process is complex and therefore not practical for application.

Since the plant photosynthetic rate has some intrinsic relationships with internal and external factors, an estimation model can be established through the regression relationship between the photosynthetic rate and the main factors. The photosynthetic rate of plants is primarily influenced by intrinsic physiological factors of the plant itself and external ecological variations. However, intrinsic physiological factors are not artificially controllable and can only be simulated and estimated by altering the experimental environment. The annual variation in plant photosynthetic rates is predominantly driven by changes in

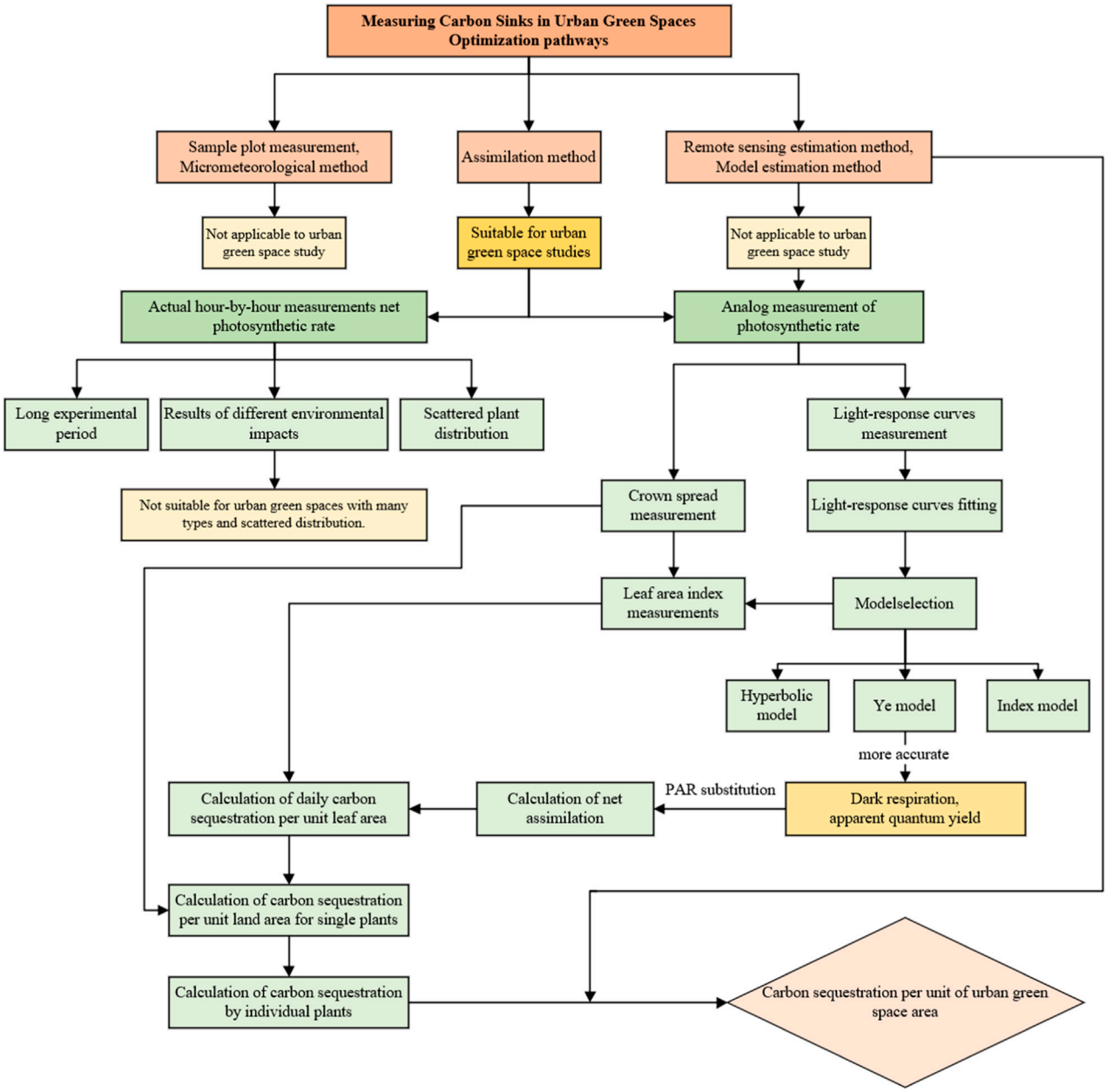

FIGURE 4
Optimization of technical routes.

temperature and light intensity associated with seasons. At diurnal scales, the variation is primarily determined by changes in photosynthetically active radiation (PAR) (Weissert et al., 2017), where in evergreen broadleaf forests, CO_2 concentration decreases with increasing PAR values, and temperature, relative humidity, and CO_2 concentration show insignificant relationships with plant photosynthetic rates. Among these factors, PAR stands out as the most significant factor, while temperature and relative humidity are also greatly influenced by light intensity (Guo, 2012).

Some studies adopt the Farquhar model to fit data and demonstrate an empirical model based on the significant linear relationships between net photosynthetic rate and PAR, deriving (Zhang et al., 2013). Given the maturity of studies on PAR in meteorology, it can be calculated from meteorological observation station data. Accordingly, PAR can be derived as a singular influential factor for predicting plant photosynthetic rates, serving as the basis for a photosynthetic rate prediction model. Specific methods include manual control of light intensity in the leaf chamber, using the light control accessory of the Photosynthesis Measurement System (PMS) to measure the photosynthetic rate of the plant at different light intensities, in order to establish a regression relationship. Typically, existing studies show that there is a significant correlation between the test results of artificially controlled light intensity and actual light intensity under different light geographic conditions (He, 2010). Therefore,

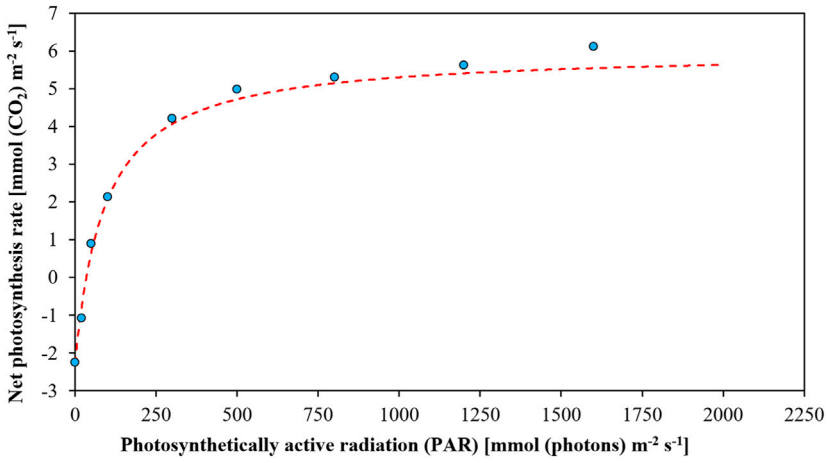

FIGURE 5
The light-response curve to demonstrate the relationship between net photosynthesis rate and photosynthetically active radiation (PAR).

this approach can obtain the photosynthetic rate estimation model through a short testing time, which solves the problems of long hourly testing cycle and distinct results in different testing environments. As a result, this paper proposes to simplify the calculation of plant carbon sequestration benefits by establishing a predictive model through the regression relationship between photosynthesis rate and PAR (Figure 4).

3.1 Modeling

The relationship between net photosynthesis rate and PAR can be described by the net photosynthesis-light response curve which refers to the tendency of the photosynthetic rate of plant leaves to change with the change in the PAR intensity when other environmental conditions are kept unchanged (Figure 5). The light response curves are mainly derived by fitting the photosynthetic rate values exhibited by the plants at different levels of light intensity. In essence, the light response curves show a functional relationship between the photosynthetic rate and light intensity, so that it can be used as a model to predict photosynthetic rate.

Many models have been used to fit net photosynthetic light-response curves, such as exponential model (Eq. 1) (Bassman and Zwier, 1991), rectangular hyperbolic model (Eq. 2) (Baly, 1997), non-rectangular hyperbolic model (Eq. 3) (Gates, 1977; Hardwick, 1977), and mechanistic model (Eq. 4) (Ye, 2007). These models describe photosynthetic physiology and can reasonably analyze the whole process of the light response curve so that they are capable of obtaining accurate data and fitting curves with high reliability. However, there are no models suitable for all situations. For instance, the data fitted by the non-rectangular hyperbolic model and the exponential model are more in line with actual data, but the prediction results of the mechanistic model were more accurate and realistic (de Lobo et al., 2013). Accordingly, the mechanistic model was later modified and simplified as Eq. 5 (Ye et al., 2013). In practice, the fitting can be done by Ye's photosynthetic computational model and the computational model built upon Microsoft Excel (de Lobo et al., 2013).

$$Pn = P\,max\,(1-e^{-\frac{\alpha I}{Pmax}}) - Rd \quad (1)$$

$$Pn = \frac{\alpha I Pmax}{\alpha I + Pmax} - Rd \quad (2)$$

$$Pn = \frac{\alpha I + P\,max\, - \sqrt{(\alpha I + Pmax)^2 - 4\theta\alpha I Pmax}}{2\theta} - Rd \quad (3)$$

$$Pn = \alpha \times \frac{1-\beta \times I}{1+\gamma \times I} \times \left(I - I_{comp}\right) \quad (4)$$

$$Pn = \alpha \times \frac{1-\beta \times I}{1+\gamma \times I} \times I - Rd \quad (5)$$

where Pn represents the net photosynthetic rate [μmol (CO_2) $m^{-2}{\cdot}s^{-1}$], which is the difference between the overall photosynthetic rate and the dark respiration rate of the plant; $Pmax$ is the maximum net photosynthetic rate [μmol (CO_2)$m^{-2}{\cdot}s^{-1}$]; θ is the curvature of the curve; I is the photosynthetic photon flux density; α is the initial slope of the light response curve at $I = 0$, representing the initial quantum efficiency of the photosynthetic process [μmol (CO_2) $(photon)^{-1}$]; Rd is the dark respiration, the amount of carbon dioxide released by the plant in dark [μmol (CO_2) $(photon)^{-1}$]. I_{comp} is the light compensation point [μmol $(photon)m^{-2}{\cdot}s^{-1}$], and β and γ are adjustment factor.

3.2 PAR value estimation

Solar radiation is the primary energy source of the Earth's surface, where the portion of solar radiation that can be utilized by green plants for photosynthesis is defined as PAR, also known as light intensity. PAR serves as the energy source for plant biomass and constitutes a crucial parameter for assessing plant photosynthetic potential (Zhou and Xiang, 1996). The current measurement methods for PAR include the energy system ($W{\cdot}m^2$) for determining PAR illuminance (Q_{PAR}) and the quantum system ($\mu mol{\cdot}m^{-2}{\cdot}s^{-1}$) for determining PAR density (U_{PAR}). The PAR density is also known as the photosynthesis

photon flux density (PPFD), presenting the number of photons incident on a unit surface per unit time (Sun et al., 2017). Under illumination by light sources with different spectral structures, the ratio between leaf photosynthetic rate and photosynthetically active quantum flux density exhibits minimal variation (McCree, 1972). Compared with the energy system, the quantum system for determining the photosynthetically active quantum flux density U_{PAR} is more reasonable. Therefore, quantum measurement systems are increasingly prevalent in fields such as agriculture and ecology.

However, U_{PAR} depends on wavelength and therefore cannot be derived directly from solar irradiance (Wang et al., 2021). Instruments specifically designed for directly measuring the light quantum flux U_{PAR} are not widespread, and most meteorological stations lack regular observation platforms for PAR. As a result, U_{PAR} is generally calculated in an indirect way, such as using UV-visible band fluxes to estimate (Sun et al., 2017), or using meteorological datasets to develop models (García-Rodríguez et al., 2021). On the meteorological conversion, the conventional unit for solar radiation in meteorological parameters is horizontal total radiation ($W{\cdot}m^{-2}$), which can be quantitatively converted into light quantum flux ($\mu mol{\cdot}m^{-2}{\cdot}s^{-1}$) (Wang et al., 2005). More importantly, meteorological research indicates a stable proportion of PAR in total solar radiation. Therefore, the meteorological conversion relationship involves calculations of the photosynthetically active coefficient and quantum conversion coefficient, which are usually calculated by the following empirical formula (Zhou et al., 1984).

$$Q_{PAR=}\eta Q \tag{6}$$

$$U_{PAR} = \mu Q_{PAR} \tag{7}$$

$$U_{PAR} = \mu\eta Q \tag{8}$$

where η is the photosynthetic efficiency coefficient, representing the proportion of photosynthetically active radiation energy in the total solar radiation; μ is the quantum yield indicating the number of quanta per unit photosynthetically active radiation energy, with units of $\mu mol{\cdot}J^{-1}$; Q is the total horizontal solar radiation flux, measured in $W{\cdot}m^{-2}$; Q_{PAR} is the photosynthetically active radiation intensity, measured in $W{\cdot}m^{-2}$; U_{PAR} is the photon flux of photosynthetically active radiation, measured in $\mu mol{\cdot}m^{-2}{\cdot}s^{-1}$.

The current annual average value of η in Eq. 6 is between 0.409 and 0.477 worldwide (Akitsu et al., 2022). Observational studies indicate that η is influenced by both astronomical and meteorological factors. Long-term continuous synchronous observations of Q and PAR in locations such as Beijing, Yantai, and Zhengzhou revealed the stability of η values (Wang and Shui, 1988). A suitable calculation formula for plains was derived as Q_{PAR} = 0.42 Q, where η = 0.42. Subsequent research on cities like Chengdu, Kunming, and Guangzhou yielded similar conclusions (Wang and Shui, 1990), and other scholars found similar results that η is 0.39 ± 0.04 (Zhou et al., 1984). Consequently, the quantum conversion coefficient for China can be established as 0.42.

There is no systematic climatological research result about the value of the quantum conversion factor μ. McCree concluded μ = 4.57 $\mu mol\ J^{-1}$ (McCree, 1972), but the value of μ in Eq. 7 is inconsistent in different regions of China, and at present the intermediate value is 4.55 $\mu mol\ J^{-1}$ (Dong et al., 2011) so based on Eq. 8 that the conversion relationship between Q and PAR is $U_{PAR} = \mu{\times}\eta$ = 4.55 × 0.42 Q = 1.911 Q.

3.3 Experimental procedure

Although no study has found a significant relationship between plant net photosynthetic rate and its size (Weissert et al., 2017), it is advisable to select healthy tree species with a planting age between 3 and 10 years for experiment. Since it is always challenging to measure the height of large deciduous trees using *in-situ* methods, auxiliary measurements are often carried out by tools such as cherry pickers and tower cranes (Chen et al., 2003; Zhao et al., 2008). However, this approach is applicable to only a few tree species with short measurement cycles. Given the diverse and scattered distribution of plant species in urban green spaces, as well as constraints posed by topography, the feasibility of this method is low. Alternatively, *in vitro* measurements are generally adopted. Whilst the photosynthetic rate of some plants may slightly decrease shortly after detachment, most tree species exhibit a high and stable photosynthetic rate within the first hour after detachment (Tang and Wang, 2011). As a result, the light response curves of plants measured within the first hour of leaf detachment can largely represent *in situ* measurements.

Currently, the main method for *in vitro* measurements is to restore the water supply to detached branches and leaves to alleviate water stress, thereby restoring their photosynthetic capacity to the *in situ* level (Qiang et al., 2017). Typically, plant branches are cut and immediately immersed in water, and the cut surface is maximized by making a second diagonal cut in the water, and subtracting excess foliage from the branches will reduce water loss (Xu, 2006). After measurements, the mechanism model of light response through photosynthesis such as leaf floating was adopted to fit formula (Ye et al., 2013), with the initial values of each parameter: α = 0.06, β = 0.002, γ = 0.01, and Rd = 1, and the limiting range of $0 < \alpha < 0.1$, $0.002 < \beta < 0.01$, $0.01 < \gamma < 0.03$, and $0 < Rd < 3$. The measurement steps are as follows:

(1) Prune the middle branches of the plant canopy by pruning shears, and place the cut ends into water quickly. Afterwards, make another diagonal cut approximately 3 cm from the initial cut to increase the water absorption area of the branches, during which remove the majority of leaves or leaflets from the branches to minimize water loss from detached plant materials.
(2) Select the fifth to seventh mature leaves from the top of the branches and wipe them clean.
(3) Place the leaves in a controlled light chamber with an LED red-blue light source, and tight up the chamber to ensure airtightness.
(4) Install a CO_2 injection system and set it to the same average concentration as the test area.
(5) Adjust the light intensity in the chamber to 1,600 $\mu mol\ m^{-2}{\cdot}s^{-1}$ using the red-blue light source, and expose the leaves to internal illumination for approximately 10 min for activation.

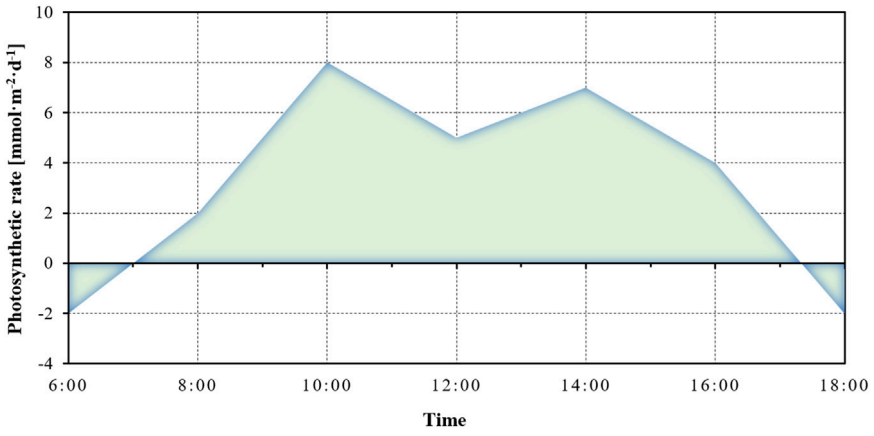

FIGURE 6
Daily assimilation of plant photosynthesis.

(6) Control the light intensity sequentially to 1,600, 1,200, 800, 500, 200, 100, 50, 20 and 0 μmol $m^{-2}·s^{-1}$ using the light intensity controller. After adjusting the light intensity, allow the leaves to adapt for stabilizing about 3 minutes before recording the photosynthetic rate.

3.4 Calculation

3.4.1 Calculation of net assimilation

For the daily assimilation, it is defined as the area enclosed by the net photosynthetic rate curve and the time (Figure 6). The net assimilation refers to the difference between the organic substances formed during photosynthesis and those consumed during respiration within a unit of time, and this value is directly proportional to plant photosynthetic capacity and carbon sequestration (Chen, 2020). Assuming that the PAR is 10 h per day, the net assimilation of the plant on the day of measurement can be calculated by Eq. 9 (Han, 2005).

$$P = \sum i\left[\frac{(P_{i+1} + P_i)}{2} \times \frac{(t_{i+1} - t_i) \times 3600}{1000}\right] \quad (9)$$

where P represents the net assimilation total per unit leaf area determined on the measurement day, with units of mmol·m^{-2}·s^{-1}; P_i denotes the instantaneous photosynthetic rate at the initial measurement point, and P_{i+1} represents the instantaneous photosynthetic rate at the $i+1$ measurement point, both in units of μmol·m^{-2}·s^{-1}; t_i is the instantaneous time at the initial measurement point, t_{i+1} is the time at the $i+1$ measurement point, and $t_{i+1} - t_i$ is the test interval time, measured in hours [h]; j signifies the number of test repetitions; 3,600 corresponds to the conversion factor from seconds to hours; 1,000 is the conversion factor between mmol and μmol.

3.4.2 Daily carbon sequestration per unit leaf area of plants

Daily carbon sequestration per unit leaf area refers to the amount of carbon dioxide absorbed by a single leaf area in a unit of time, commonly expressed in kg·m^{-2}·a^{-1}. The nocturnal respiratory release of carbon dioxide is generally calculated as 20% of the assimilation amount during the day. The calculation of the daily carbon sequestration per unit leaf area, based on the reaction equation of photosynthesis (CO_2+4H_2O→CH_2O+3H_2O + O_2), is expressed by Eq. 10.

$$W_{co2} = P \times (1 - 0.2) \times \frac{44}{1000} \quad (10)$$

where 44 represents the molar mass of carbon dioxide; W_{co2} denotes the mass of CO_2 sequestrated per unit area of leaves [g·m^{-2} d^{-1}]. Based on Eqs 5, 9, 10, 11 can be derived for predicting the plant-specific carbon fixation per unit leaf area according to PAR.

$$W_{co2} = 0.06336 \times \sum i\left[\alpha \times \left(\frac{1 - \beta \times PAR_i}{1 + \gamma \times PAR_i} + \frac{1 - \beta \times PAR_{i+1}}{1 + \gamma \times PAR_{i+1}}\right) - 2Rd\right] \quad (11)$$

where PAR_i represents the instantaneous PAR at the initial moment [μmol·m^{-2}·s^{-1}]; PAR_{i+1} represents the PAR at the next moment [μmol·m^{-2}·s^{-1}].

3.4.3 Carbon sequestration per unit land area by individual plants

Carbon sequestration per unit land area by an individual plant, also known as daily carbon sequestration per unit coverage area, represents the mass of carbon dioxide sequestrated by all leaves on the entire projected area of a landscaping plant in a unit of time, as described by Eq. 12.

$$Q_{co2} = LAI \times W_{co2} \quad (12)$$

where LAI is the leaf area index of a single plant; Q_{co2} is the amount of CO_2 fixed per unit of land area per day by a single plant.

Most previous studies regarded the carbon sequestration benefits of plants as total biomass, including leaves, stem diameter, roots, and rhizomes. This benefit is often determined by measuring the absolute greenness of a certain area (Profous et al., 1988). However, the photosynthesis intensity primarily depends on the effective surface area of leaves involved in photosynthesis. Therefore, the LAI, the total

TABLE 2 Estimation methods for leaf area index of green urban vegetation.

Measurement methods	Main technologies	Main indicators	Advantage	Disadvantage
Leaf area Method	Digital software, Portable leaf are meter, standard branch method	Single leaf area, single plant leaf volume	Relatively accurate results	Complex experimental methods and individual differences in leaf volume and leaf area
Photogrammetry	Plant canopy analyzer instruction	Forest crown clearance score	Simple and convenient, relatively accurate results	Discrepancies may exist between strains
Leaf area regression model	Mathematical model	Crown height, shade coefficient of crown width	Low cost, simple, obtaining results quickly	Individual differences may exist in generic formulas

plant leaf area per unit land area as a multiple of land area, is an important indicator reflecting the density of tree leaves and plant carbon sequestration capacity. A higher LAI indicates a greater leaf area per unit land area and a higher degree of leaf overlap (Ma et al., 2023). Plant growth and carbon sequestration increase with the LAI. The LAI determination can be influenced plant growth period and plant condition. In actual applications, three methods such as leaf area method, instrument measurement method, and regression equation method are commonly employed (Table 2).

The leaf area method calculates the average area of individual plant leaves using devices like portable leaf are meter. The standard single-leaf area should be obtained using the standard branch method based on the entire leaf quantity of an individual plant. Photogrammetry can directly calculate the LAI of plants using plant canopy analyzer instruction, typically selecting the average of the LAI values from multiple directions as the final LAI. The regression model is derived based on physiological indicators such as DBH and tree height (TH) to derive the total leaf area of individual plants (Goude et al., 2019). For example, the urban tree leaf area regression model for Chicago, which was developed on information based on multiple species, ages, DBH and TH, is generalizable because the overall error due to the parameters is not too large, and has been widely used in other regions as well (Mcpherson et al., 1994). Regression models specific to different regions have also been developed based on local tree species characteristics. For example, the LAI of 40 common garden plants in Beijing was determined by a canopy analyzer and a regression model of LAI was established based on the relationship between crown width, DBH, plant height and LAI (Shen, 2007).

3.4.4 Daily carbon sequestration of individual plants

Daily carbon sequestration of individual plants refers to the total amount of carbon dioxide sequestration by an individual plant within a daily time, as described by Eq. 13.

$$M_{co2} = W_{co2} \times S(LAI \times C) \tag{13}$$

where W_{co2} represents the mass of CO_2 sequestrated per unit leaf area of an individual plant [g/d]; S denotes the total leaf area of an individual plant; C is the plant canopy area (vertical projection area).

3.4.5 Daily carbon sequestration per unit of green space area

Urban green space is composed of a large number of individual plants so that daily carbon sequestration per unit of green space area can be calculated by the daily carbon sequestration of each individual plant within the unit of green space. Total carbon sinks in urban green spaces can be quantified using the methodology of plant communities, as expressed by Eq. 14 (Sultana et al., 2021).

$$C_{Sij} = C_{Aij} \times N_{Sij} \tag{14}$$

where i represents the specification; j is the tree species; C_{Sij} is the sum of daily carbon sequestration per unit of green space area; C_{Aij} is the daily carbon sequestration by a single plant of the type; N_{Sij} is the number of plants of the type.

4 Discussion

4.1 Significance of accounting carbon sinks in urban green spaces

It is a consensus embraced by governments and organizations worldwide that urban green spaces are efficient natural carbon sinks and a crucial strategy for mitigating climate change. The loss of carbon sinks due to built-up area increase during urbanization should be compensated by urban green spaces (Nowak et al., 2013). In this context, the carbon offsetting capacity (COC), the ratio between carbon emissions from human activities and the carbon sink of green spaces, has been attracting attention (Chen, 2015). Accordingly, quantitative studies on urban green space carbon sinks not only elucidate their paramount significance for cities but also clarify their ecological value, providing a foundation for subsequent management endeavors. At present, research mainly focuses on the indirect quantification of carbon sinks, holding crucial implications for investigating carbon offset capabilities, as well as ecological and economic benefits. In comparison and more importantly, directly quantifying the individual carbon sequestration capacity of urban green space allows the identification of locally suitable high-efficiency carbon sequestration plants, which can guide future urban green space construction and maximize ecological benefits (Table 3). Despite urban green spaces contributing a fraction of carbon sink capacity compared to urban carbon emissions, appropriate design and management of vegetation, as the primary component of urban green spaces, can significantly enhance future carbon sink capacity. This enhancement must be based

TABLE 3 Comparison of research methods for calculating carbon sinks in urban green spaces.

Research methodology	Measurement method	Estimation method	Object	Current significance	Future significance
Sample Plot Measurement	Indirect	Indirect	Current Green Space	Quantifying ecological benefits	——
Model Estimation Method	Indirect	Indirect			——
Remote Sensing	Indirect	Indirect			——
Micro-meteorological method	Indirect	Indirect			——
Assimilation	Direct	Direct			Guidance for future tree selection

on an understanding of differences in carbon sequestration benefits among various plant species. In addition, the ecological benefits of plants, such as cooling and fire prevention, hold equal importance in climate change mitigation (Murray et al., 2018; Liu X. et al., 2023). In future research, integrating studies on plant carbon sequestration with quantifications of other ecological benefits may prove more advantageous for the sustainable development of cities.

4.2 Trends in research methods for measuring greenfield carbon sinks

Methodologies for quantifying carbon sequestration in urban green spaces exhibit a diverse trend, and existing methods tailored to different scales and types of green spaces are predominantly concentrated in fields such as forests, grasslands, and agricultural areas. Concurrent studies are exploring the integration of various research methods. For instance, employing the accumulation method principle, directly utilized ArcGIS to estimate the carbon sequestration in Russian forests (Malysheva et al., 2018) and used the IUEMS carbon sequestration and oxygen release model to study forest carbon sequestration in the Qinling Mountains based on net ecosystem productivity (Ma et al., 2022). The CASA model was adopted to estimate the carbon sinks of greenfield vegetation in some major cities in China based on satellite images, meteorological data and vegetation data (Xu et al., 2023), or extracting plant species and leaf area indices from large green spaces by satellite and RS correlation techniques to estimate carbon sink benefits (Johnson et al., 2023). In future, more fusion methods should be explored for simpler and more accurate studies.

4.3 Limitations of the photosynthetic rate estimation

To address the challenges of experimental requirements in the assimilation method, this study proposes a method by establishing a model for estimating photosynthetic rate based on light-response curves. This involves measuring the net photosynthetic rate of plants under different levels of light intensity and utilizing mechanistic model of light-response of photosynthesis to fit the light -response curve. The actual hourly PAR is incorporated to simulate the plant's hourly net photosynthetic rate on corresponding dates. The carbon sequestration of plants can be finally quantified using the formula for calculating plant carbon sequestration. This standardized external environment setting allows for the carbon sequestration comparison among different plants under the same conditions, enabling more accurate selection of plants with high carbon sink. The study presents controlled adjustments to the light intensity environment, CO_2 concentration and other conditions in the leaf chamber of the photosynthesis measurement instrument to ensure a consistent experimental environment. Although light intensity and atmospheric CO_2 concentration have the most significant impact on plant photosynthetic rates (Xiao et al., 2019), other external factors can also influence photosynthetic rates. Therefore, in future experiments, there is a need to control the other conditions to make the data more accurate.

There have been many models for net photosynthesis-light response curve fitting, and studies have shown that there are uncertainties in the fitting models (Fang et al., 2015). Moreover, the calculation results of some data of these models may be out of the normal range, this study, to use the light response curve fitting model, follows the mechanism model of photosynthesis response to light. It is a modified model for the rectangular hyperbolic model, having some advantages compared with previous models, and more accurate and real data can be obtained when calculating α. However, the data such as P_{max} will be out of the normal physiological range under some circumstances (de Lobo et al., 2013), which should be overcome to increase the accuracy of the results in the future research. Finally, although the predicted net photosynthetic rate values based on the light response curve exhibit a strong correlation with the actually measured values, this does not mean that the results of the two experimental methods are consistent. The photosynthetic rate estimation method based on the light response curve is only applicable to preliminary research on quantifying carbon sequestration in a large number of urban green spaces. More precise carbon sequestration data requires actual hourly measurements.

4.4 Future research

Quantifying carbon sink in urban green spaces is crucial for guiding future urban green space planning and management efforts. Therefore, research should not only concentrate on the direct carbon

sink capacity of plants but should also comprehensively explore aspects such as the reduction in carbon emissions, self-generated carbon emissions, and factors influencing carbon sink. This will provide clearer paths for the future construction of urban green space, and help to promote the limited urban green space to play the greatest carbon sink benefits. Regarding carbon emissions, urban green spaces, through shading and transpiration, can lower the overall temperature of the city, thereby reducing building energy consumption and indirectly decreasing urban carbon emissions (Dong and He, 2023). Studies indicate that trees in urban centers indirectly absorb more CO_2 than they do directly (McHale et al., 2007). Concerning self-generated carbon emissions, although urban green space vegetation can sequester carbon through photosynthesis, the carbon emissions generated throughout its entire lifecycle, including production, transportation, and management can offset a portion of the carbon sequestration (Park et al., 2021). Deducting the total carbon emissions from the overall carbon sequestration quantity is meaningful for understanding the net carbon sequestration benefits of plants.

On carbon sinks, their influencing factors can be categorized into plants themselves, and planning and design. Regarding plants, indicators such as LAI, size, tree age, tree diameter, and tree height have a significant impact (Othman et al., 2019; Shadman et al., 2022). Moreover, the amount of carbon sequestered by plants varies geographically. Native plants can also show better carbon sequestration efficacy given their local adaptability that means small carbon emissions from maintenance management (Wang et al., 2015). Additionally, past research has predominantly focused on trees and shrubs, neglecting the substantial carbon sink role played by extensive lawns in urban green spaces (Amoatey and Sulaiman, 2020), thus necessitating a quantitative study. On planning and design, plants show different carbon sink abilities with different planting designs. Quantifying the carbon sink capacity variation under different planning and design schemes is important to provide guidance for optimization. Planting density of plant communities had a significant positive relationship with their carbon sequestration (O'Donoghue and Shackleton, 2013), but excessively high density can have opposite effects (Mexia et al., 2018). The proportion of trees and shrubs, plant community hierarchy, biodiversity and vegetation spatial types also significantly affect the carbon sink capacity. Meanwhile, there is a spatial correlation between human activities and greenfield carbon sinks (Dong et al., 2023). On management, digital means can be used to realize the analysis and accurate management of urban green spaces. For example, a digital platform for high carbon sequestering plant communities developed by Python and other programming software in Xi'an provided a scientific guidance for decision-making in plant community design (Wang et al., 2023).

Overall, increasing the carbon sink of green space cannot be only considered in an individual aspect, but should be considered comprehensively from the whole life cycle of plant selection, community design, and maintenance management. However, only from the construction perspective to study the carbon sink of urban green space has a temporary nature. In future, there is a need to study the influencing factors to optimization carbon sink of urban green space so that it can play long-term and better carbon sink benefits. It is also possible to form evaluation standards and systems related to carbon sinks on the basis of carbon sink measurement and quantification, so as to provide a practical basis for evaluating various types of urban green areas.

5 Conclusion

Carbon sink function is one of the most important ecological benefits of urban green space. The associated quantification is not only important for carbon sink measurement, but also important for the future construction of urban low-carbon green space. In this study, we clarified the existing green space carbon sink assessment methods, divided them into macro and micro scales, and analyzed their advantages and disadvantages. It is found that macroscopic methods can accurately estimate the carbon sink benefits of large-scale green spaces, but they cannot be completely applied to urban green spaces and cannot distinguish the carbon sequestration benefits of individual plants. The assimilation method as a research method of carbon sequestration by individual plants can make up for these shortcomings. The assimilation method is more favorable for quantifying the carbon sequestration benefits of individual plants in urban green space. This method can better support the construction of low carbon green space, and can be combined with other tools to accurately estimate carbon sequestration benefits of large-scale green space. However, the assimilation method is affected by the weather and the data comparability is limited by measurement conditions. Therefore, this study proposed to measure net photosynthesis-light response curves in a uniform experimental environment, estimate the net photosynthesis rate by using the photosynthesis-photorespiration-response model of leaf drift as a single-factor variable, and finally calculate carbon sequestered by plants. Moreover, future studies should in-depth explore plant indirect emission reduction benefits and the whole life cycle carbon emissions, and explore the impact of different plant community design and plant indicators on the carbon sink of urban green spaces. Overall, this paper is important to provide a good methodological reference for quantifying carbon sinks in urban green spaces.

Author contributions

LD: Funding acquisition, Methodology, Resources, Supervision, Writing–review and editing. YW: Conceptualization, Investigation, Writing–original draft. LA: Funding acquisition, Writing–review and editing. XC: Methodology, Writing–review and editing. YL: Writing–review and editing.

Funding

The author(s) declare financial support was received for the research, authorship, and/or publication of this article. This work was supported by the Chongqing city management academic

project: Study on Optimization of Plant Configuration Patterns in Chongqing Residential Green Areas Based on High Carbon Sink Efficiency (Grant Number: Urban-Management Kezi 2023·No. (33)). Meanwhile, this work was supported by the Chongqing Graduate Student Research and Innovation Program Funding: Study on Optimization of Plant Configuration Patterns in Chongqing Residential Green Areas Based on High Carbon Sink Efficiency (Grant Number: CYS23513).

Acknowledgments

The authors would like to thank reviewers' constructive comments in improving the paper quality.

Conflict of interest

The authors declare that the research was conducted in the absence of any commercial or financial relationships that could be construed as a potential conflict of interest.

Publisher's note

All claims expressed in this article are solely those of the authors and do not necessarily represent those of their affiliated organizations, or those of the publisher, the editors and the reviewers. Any product that may be evaluated in this article, or claim that may be made by its manufacturer, is not guaranteed or endorsed by the publisher.

References

Akitsu, T. K., Nasahara, K. N., Ijima, O., Hirose, Y., Ide, R., Takagi, K., et al. (2022). The variability and seasonality in the ratio of photosynthetically active radiation to solar radiation: a simple empirical model of the ratio. *Int. J. Appl. Earth Observation Geoinformation* 108, 102724. doi:10.1016/j.jag.2022.102724

Alonzo, M., Bookhagen, B., and Roberts, D. A. (2014). Urban tree species mapping using hyperspectral and lidar data fusion. *Remote Sens. Environ.* 148, 70–83. doi:10.1016/j.rse.2014.03.018

Amoatey, P., and Sulaiman, H. (2020). Quantifying carbon storage potential of urban plantations and landscapes in Muscat, Oman. *Environ. Dev. Sustain* 22, 7969–7984. doi:10.1007/s10668-019-00556-5

Baly, E. C. C. (1997). The kinetics of photosynthesis. *Proc. R. Soc. Lond. Ser. B - Biol. Sci.* 117, 218–239. doi:10.1098/rspb.1935.0026

Bao, Z. (2011). On the design and construction of low-carbon plant landscape. *Chin. Landsc. Archit.* doi:10.3969/j.issn.1000-6664.2011.01.003

Bassman, J. H., and Zwier, J. C. (1991). Gas exchange characteristics of Populus trichocarpa, Populus deltoides and Populus trichocarpa x P. deltoides clones. *Tree Physiol.* 8, 145–159. doi:10.1093/treephys/8.2.145

Biswas, S., Bala, S., and Mazumdar, A. (2014). Diurnal and seasonal carbon sequestration potential of seven broadleaved species in a mixed deciduous forest in India. *Atmos. Environ.* 89, 827–834. doi:10.1016/j.atmosenv.2014.03.015

Chen, D., Li, Y., Luo, T., Chen, B., and Lin, M. (2003). Study on photosynthetic physiological ecology of Cryptocarya chinensis in tropical montane rain forest in Jianfengling, Hainan Island. *For. Res.* 16, 540–547. doi:10.1016/S0142-9418(02)00003-X

Chen, L. (2020). Study on carbon fixation and oxygen release ability of urban greening tree species based on spatial and temporal dynamic analysis. *Glob. Energy Issues* 42, 244–258. doi:10.1504/IJGEI.2020.108960

Chen, L., Li, P., Li, G., Su, D., and Yuan, Y. (2009). Application of CITYGREEN model in air purification, carbon fixation and oxygen release by greenbelt system of Shenzhen City. *Acta Ecol. Sin.* 29, 272–282. doi:10.3321/j.issn:1000-0933.2009.01.033

Chen, W. Y. (2015). The role of urban green infrastructure in offsetting carbon emissions in 35 major Chinese cities: a nationwide estimate. *Cities* 44, 112–120. doi:10.1016/j.cities.2015.01.005

de Lobo, F. A., de Barros, M. P., Dalmagro, H. J., Dalmolin, Â. C., Pereira, W. E., de Souza, É. C., et al. (2013). Fitting net photosynthetic light-response curves with Microsoft Excel - a critical look at the models. *Photosynthetica* 51, 445–456. doi:10.1007/s11099-013-0045-y

Dong, H., Chen, Y., and Huang, X. (2023). A new framework for analysis of the spatial patterns of 15-minute neighbourhood green space to enhance carbon sequestration performance: a case study in Nanjing, China. *Ecol. Indic.* 156, 111196. doi:10.1016/j.ecolind.2023.111196

Dong, X., and He, B.-J. (2023). A standardized assessment framework for green roof decarbonization: a review of embodied carbon, carbon sequestration, bioenergy supply, and operational carbon scenarios. *Renew. Sustain. Energy Rev.* 182, 113376. doi:10.1016/j.rser.2023.113376

Evans, J., and Santiago, L. (2011). Gas exchange and chlorophyll fluorescence Prometheus. Available at: https://prometheusprotocols.net/function/gas-exchange-and-chlorophyll-fluorescence/ (Accessed August 14, 2023).

Fang, L., Zhang, S., Zhang, G., Liu, X., Xia, X., Zhang, S., et al. (2015). Application of five light-response models in the photosynthesis of *Populus x euramericana* cv. "Zhonglin46" leaves. *Appl. Biochem. Biotechnol.* 176, 86–100. doi:10.1007/s12010-015-1543-0

Friedlingstein, P., O'Sullivan, M., Jones, M. W., Andrew, R. M., Bakker, D. C. E., Hauck, J., et al. (2023). Global carbon budget 2023. *Earth Syst. Sci. Data* 15, 5301–5369. doi:10.5194/essd-15-5301-2023

Gao, F., Wu, T., Zhang, J., Hu, A., and Meehl, G. A. (2021). Shortened duration of global warming slowdowns with elevated greenhouse gas emissions. *J. Meteorol. Res.* 35, 225–237. doi:10.1007/s13351-021-0134-y

Garcia-Gonzalo, J., Peltola, H., Zubizarreta Gerendiain, A., and Kellomäki, S. (2007). Impacts of forest landscape structure and management on timber production and carbon stocks in the boreal forest ecosystem under changing climate. *For. Ecol. Manag.* 241, 243–257. doi:10.1016/j.foreco.2007.01.008

García-Rodríguez, A., Granados-López, D., García-Rodríguez, S., Díez-Mediavilla, M., and Alonso-Tristán, C. (2021). Modelling Photosynthetic Active Radiation (PAR) through meteorological indices under all sky conditions. *Agric. For. Meteorology* 310, 108627. doi:10.1016/j.agrformet.2021.108627

Gates, D. M. (1977). *Mathematical Models in plant physiology. A quantitative Approach to Problems in Plant and crop Physiology.*J. H. M. Thornley. *Q. Rev. Biol.* 52, 97. doi:10.1086/409778

Giacomo, G., Elisa, V., Francesca, P., Lucia, C., and Federico, M. (2005). Seasonal and interannual variability of photosynthetic capacity in relation to leaf nitrogen in a deciduous forest plantation in northern Italy. *Tree Physiol.* 25, 349–360. doi:10.1093/treephys/25.3.349

Goude, M., Nilsson, U., and Holmström, E. (2019). Comparing direct and indirect leaf area measurements for Scots pine and Norway spruce plantations in Sweden. *Eur. J. Forest. Res.* 138, 1033–1047. doi:10.1007/s10342-019-01221-2

Gratani, L., Varone, L., and Bonito, A. (2016). Carbon sequestration of four urban parks in Rome. *Power urban social-ecological Syst.* 19, 184–193. doi:10.1016/j.ufug.2016.07.007

Grimmond, C. S. B., King, T. S., Cropley, F. D., Nowak, D. J., and Souch, C. (2002). Local-scale fluxes of carbon dioxide in urban environments: methodological challenges and results from Chicago. *Environ. Pollut.* 116, S243–S254. doi:10.1016/S0269-7491(01)00256-1

Gülin, D., and Bosch, C.C.K.V.D. (2021). Assessment of above-ground carbon storage by Urban trees using LiDAR Data: the case of a university campus. *Forests*. doi:10.3390/F12010062

Guo, X. (2012). *Study on the evaluation method of carbon sequestration capacity of greening plants in residential areas*. ChongQing: Chongqing University.

Han, H. (2005). Effect of carbon fixation and oxygen release about urban greening plants. *J. Northeast For. Univ.* 33, 68–70. doi:10.1360/biodiv.050121

Hardwick, R. C. (1977). Mathematical models in plant physiology. By J. H. M. Thornley. London: academic press (1976), PP. 331, £9.80. *Exp. Agric.* 13, 112. doi:10.1017/S0014479700007675

He, B.-J. (2023). Cause-related injustice, process-related injustice, effect-related injustice and regional heat action planning priorities: an empirical study in Yangtze River Delta and Chengdu-Chongqing urban agglomerations. *Landsc. Urban Plan.* 237, 104800. doi:10.1016/j.landurbplan.2023.104800

He, B.-J., Wang, J., Liu, H., and Ulpiani, G. (2021). Localized synergies between heat waves and urban heat islands: implications on human thermal comfort and urban heat management. *Environ. Res.* 193, 110584. doi:10.1016/j.envres.2020.110584

He, H. (2010). *Study on the role of green space carbon sinks in residential areas in South China and its application to the evaluation of carbon P&L over the whole life cycle*. ChongQing: Chongqing University.

Helfter, C., Famulari, D., Phillips, G. J., Barlow, J. F., Wood, C. R., Grimmond, C. S. B., et al. (2010). Controls of carbon dioxide concentrations and fluxes above central London. *Atmos. Chem. Phys.* 11, 1913–1928. doi:10.5194/acp-11-1913-2011

Henninger, S., and Kuttler, W. (2010). Near surface carbon dioxide within the urban area of Essen, Germany. *Phys. Chem. Earth* 35, 76–84. doi:10.1016/j.pce.2010.03.006

Holifield Collins, C. D., Emmerich, W. E., Moran, M. S., Hernandez, M., Scott, R. L., Bryant, R. B., et al. (2008). A remote sensing approach for estimating distributed daily net carbon dioxide flux in semiarid grasslands. *Water Resour. Res.* 44. doi:10.1029/2006WR005699

Houghton, R. A., Boone, R. D., Melillo, J. M., Palm, C. A., Woodwell, G. M., Myers, N., et al. (1985). Net flux of carbon dioxide from tropical forests in 1980. *Nature* 316, 617–620. doi:10.1038/316617a0

Idso, C. D., Idso, S. B., and Balling, R. C., Jr. (1998). The urban Co2 dome of Phoenix, Arizona. *Phys. Geogr.* 19, 95–108. doi:10.1080/02723646.1998.10642642

Intasen, M., Hauer, R. J., Larsen, E., and Werner, L. P. (2017). Urban forest assessment in Bangkok, Thailand. *J. Sustain. For.* 36, 148–163. doi:10.1080/10549811.2016.1265455

Intergovernmental Panel On Climate Change (IPCC) (2023). *Climate change 2022 – impacts, adaptation and vulnerability: working group II contribution to the sixth assessment report of the intergovernmental Panel on climate change*. 1st ed. Cambridge University Press. doi:10.1017/9781009325844

Johnson, A. J., Davidson, C. I., Cibelli, E., and Wojcik, A. (2023). Estimating leaf area index and coverage of dominant vegetation on an extensive green roof in Syracuse, NY. *Nature-Based Solutions* 3, 100068. doi:10.1016/j.nbsj.2023.100068

King, A. W., Hayes, D. J., Huntzinger, D. N., West, T. O., and Post, W. M. (2012). North American carbon dioxide sources and sinks: magnitude, attribution, and uncertainty. *Front. Ecol. Environ.* 10, 512–519. doi:10.1890/120066

Kiss, M., Takács, Á., Pogácsás, R., and Gulyás, Á. (2015). The role of ecosystem services in climate and air quality in urban areas: evaluating carbon sequestration and air pollution removal by street and park trees in Szeged (Hungary). *Morav. Geogr. Rep.* 23 (3), 36–46. doi:10.1515/mgr-2015-0016

Knyazikhin, Y., Schull, M., Stenberg, P., Myneni, R. B., Rautiainen, M., Yang, Y., et al. (2012). Hyperspectral remote sensing of foliar nitrogen content. *Proc. Natl. Acad. Sci. U. S. A.* 110, E185–E192. doi:10.1073/pnas.1210196109

Li, K., Liu, X., Zhang, H., Ma, J., and He, B.-J. (2023). Evaluating and improving the adaptability of commonly used indices for predicting outdoor thermal sensation in hot and humid residential areas of China. *Dev. Built Environ.* 16, 100278. doi:10.1016/j.dibe.2023.100278

Li, Q., Zhu, Y., and Zhu, Z. (2023). Calculation and optimization of the carbon sink benefits of green space plants in residential areas: a case study of suojin village in nanjing. *Sustainability* 15, 607. doi:10.3390/su15010607

Li, Y. (2010). The development path options and policy proposals of low-carbon economic in China. *Urban Stud.* doi:10.3969/j.issn.1006-3862.2010.02.008

Liu, C., Zhao, S., Li, L., Li, X., XingYuan, X., and Wei, W. (2008). Difference analysis of carbon fixation and pollution removal of urban forest in Shenyang. *Chin. J. Appl. Ecol.* doi:10.3724/SP.J.1005.2008.01033

Liu, H., Huang, B., Cheng, X., Yin, M., Shang, C., Luo, Y., et al. (2023). Sensing-based park cooling performance observation and assessment: a review. *Build. Environ.* 245, 110915. doi:10.1016/j.buildenv.2023.110915

Liu, X., He, J., Xiong, K., Liu, S., and He, B.-J. (2023). Identification of factors affecting public willingness to pay for heat mitigation and adaptation: evidence from Guangzhou, China. *Urban Clim.* 48, 101405. doi:10.1016/j.uclim.2022.101405

Liu, Y., Zhou, G., Du, H., Berninger, F., Mao, F., Li, X., et al. (2018). Response of carbon uptake to abiotic and biotic drivers in an intensively managed Lei bamboo forest. *J. Environ. Manag.* 223, 713–722. doi:10.1016/j.jenvman.2018.06.046

López, F. R., Rubio, E., and Moya, D. (2010). *Los bosques como sumideros de co2: incertidumbre en los cálculos y necesidad de potenciar la investigación*, 74–81.

Ma, H., Li, X., Ji, J., Cui, H., Shi, Y., Li, N., et al. (2023). Monitoring indicators for comprehensive growth of summer maize based on UAV remote sensing. *Agronomy* 13, 2888. doi:10.3390/agronomy13122888

Ma, X., Li, J., Zhao, K., Wu, T., and Zhang, P. (2022). Simulation of spatial Service range and value of carbon sink based on intelligent urban ecosystem management system and net present value models-an example from the qinling Mountains. *Forests* 13, 407. doi:10.3390/f13030407

Malysheva, N., Filipchuk, A., Tsyplenkov, A., and Zolina, T. (2018). "Gis support of carbon sequestration, emissions and balance assessment for Russian forests," in International Conference on Cartography and GIS. Presented at the 8th International Conference on Cartography and GIS, Nessebar, BULGARIA.

McCree, K. J. (1972). Test of current definitions of photosynthetically active radiation against leaf photosynthesis data. *Agric. Meteorol.* 10, 443–453. doi:10.1016/0002-1571(72)90045-3

McHale, M. R., Gregory McPherson, E., and Burke, I. C. (2007). The potential of urban tree plantings to be cost effective in carbon credit markets. *Urban For. Urban Green.* 6, 49–60. doi:10.1016/j.ufug.2007.01.001

Mcpherson, E., Nowak, D., Gordon, H., Grimmond, C., Souch, C., Grant, R., et al. (1994). "Chicago's urban forest ecosystem: results of the Chicago urban forest climate project," in Proceedings of the 7th national urban forest conference.

Mcpherson, E. G., Simpson, J. R., Xiao, Q., and Wu, C. (2008). *Los Angeles 1-Million tree canopy cover assessment*. doi:10.2737/PSW-GTR-207

Mexia, T., Vieira, J., Príncipe, A., Anjos, A., Silva, P., Lopes, N., et al. (2018). Ecosystem services: urban parks under a magnifying glass. *Environ. Res.* 160, 469–478. doi:10.1016/j.envres.2017.10.023

Mohd Zaki, N.A., and Abd Latif, Z. (2017). Carbon sinks and tropical forest biomass estimation: a review on role of remote sensing in aboveground-biomass modelling. *Geocarto. International.* 32, 701–716. doi:10.1080/10106049.2016.1178814

Monteiro, M. V., Handley, P., and Doick, K. J. (2019). An insight to the current state and sustainability of urban forests across Great Britain based on i-Tree Eco surveys. *For. J.*, 1–17. Estimating in situ maximum net photosynthetic rate of Larix olgensis based on abscised measurement. doi:10.1093/forestry/cpz054

Mu, X., and Chen, Y. (2021). The physiological response of photosynthesis to nitrogen deficiency. *Plant Physiology Biochem.* 158, 76–82. doi:10.1016/j.plaphy.2020.11.019

Murray, B. R., Martin, L. J., Colin Brown, D. W. K., Phillips, M. L., and Phillips, M. (2018). Selecting low-flammability plants as green firebreaks within sustainable urban garden design. *Switzerl.* 1, 15. doi:10.3390/fire1010015

Ning, Z. H., Chambers, R., and Abdollahi, K. (2016). Modeling air pollutant removal, carbon storage, and CO2 sequestration potential of urban forests in Scotlandville, Louisiana, USA. *iForest - Biogeosciences For.* 9, 860–867. doi:10.3832/ifor1845-009

Nowak, D. J., Crane, D. E., Stevens, J. C., and Ibarra, M. (2002). "Brooklyn's urban forest,". Gen. Tech. Rep. NE-290 (Newtown Square, PA: U. S. Department of Agriculture, Forest Service, Northeastern Forest Experiment Station), 290. doi:10.2737/NE-GTR-290

Nowak, D. J., Greenfield, E. J., Hoehn, R. E., and Lapoint, E. (2013). Carbon storage and sequestration by trees in urban and community areas of the United States. *Environ. Pollut.* 178, 229–236. doi:10.1016/j.envpol.2013.03.019

Nowak, D. J., Hirabayashi, S., Doyle, M., McGovern, M., and Pasher, J. (2018). Air pollution removal by urban forests in Canada and its effect on air quality and human health. *Urban For. Urban Green.* 29, 40–48. doi:10.1016/j.ufug.2017.10.019

O'Donoghue, A., and Shackleton, C. M. (2013). Current and potential carbon stocks of trees in urban parking lots in towns of the Eastern Cape, South Africa. *Urban For. Urban Green.* 12, 443–449. doi:10.1016/j.ufug.2013.07.001

Othman, R., Suid, S., Mohd Noor, N. F., Baharuddin, Z. M., Hashim, K. S. H. Y., and Lukman Hakim Mahamod, L. H. (2019). The influence of urban park green spaces, plant material specifications and spatial design organization and pattern towards carbon sequestration rate. *Appl. Ecol. Environ. Res.* 17, 8079–8088. doi:10.15666/aeer/1704_80798088

Ouyang, Z., Wang, X., and Miao, H. (1999). A primary study on Chinese terrestrial ecosystem services and their ecological-economic values. *Acta Ecol. Sin.* 5, 607–613. doi:10.1088/0256-307X/15/12/025

Park, H. M., Jo, H. K., and Kim, J. Y. (2021). Carbon footprint of landscape tree production in Korea. *Sustainability* 13, 5915. doi:10.3390/su13115915

Pataki, D. E., Alig, R. J., Fung, A. S., Golubiewski, N. E., Kennedy, C. A., Mcpherson, E. G., et al. (2006). Urban ecosystems and the North American carbon cycle. *Glob. Change Biol.* 12, 2092–2102. doi:10.1111/j.1365-2486.2006.01242.x

Paw U, K. T., Falk, M., Suchanek, T. H., Ustin, S. L., Chen, J., Park, Y. S., et al. (2004). Carbon dioxide exchange between an old-growth forest and the atmosphere. *Ecosystems* 7. doi:10.1007/s10021-004-0141-8

Piao, S., He, Y., Wang, X., and Chen, F. (2022). Estimation of China's terrestrial ecosystem carbon sink: methods, progress and prospects. *Sci. China-Earth Sci.* 65, 641–651. doi:10.1007/s11430-021-9892-6

Profous, G. V., Rowntree, R. A., and Loeb, R. E. (1988). The urban forest landscape of athens, Greece: aspects of structure, planning and management. *Arboric. Assoc. J.* 12, 83–107. doi:10.1080/03071375.1988.9756380

Qiang, L., Feng-Ri, L. I., Wei, P., and University, N. F. (2017). Estimating *in situ* maximum net photosynthetic rate of Larix olgensis based on abscised measurement. *Chin. J. Appl. Ecol.* 28, 3208–3216. doi:10.13287/j.1001-9332.201710.020

Rana, G., Martinelli, N., Famulari, D., Pezzati, F., Muschitiello, C., and Ferrara, R. M. (2021). Representativeness of carbon dioxide fluxes measured by eddy covariance over a mediterranean urban district with equipment setup restrictions. *Atmosphere* 12, 197. doi:10.3390/atmos12020197

Reich, P. B., Walters, M. B., Kloeppel, B. D., and Ellsworth, D. S. (1995). Different photosynthesis-nitrogen relations in deciduous hardwood and evergreen coniferous tree species. *Oecologia* 104, 24–30. doi:10.1007/BF00365558

Richardson, J. J., and Moskal, L. M. (2014). Uncertainty in urban forest canopy assessment: lessons from Seattle, WA, USA. *Urban For. Urban Green.* 13, 152–157. doi:10.1016/j.ufug.2013.07.003

Rowntree, R. A., and Nowak, D. J. (1991). Quantifying the role of urban forests in removing atmospheric carbon dioxide. *J. Arboric.* 7, 269–275. doi:10.48044/jauf.1991.061

Russo, A., Escobedo, F. J., Timilsina, N., Schmitt, A. O., Varela, S., and Zerbe, S. (2014). Assessing urban tree carbon storage and sequestration in Bolzano, Italy. *Int. J. Biodivers. Sci. Ecosyst. Serv. Manag.* 10, 54–70. doi:10.1080/21513732.2013.873822

Schreyer, J., Jan, T., Lakes, T., and Churkina, G. (2014). Using airborne LiDAR and QuickBird data for modelling urban tree carbon storage and its distribution—a case study of berlin. *Remote Sens.* 6, 10636–10655. doi:10.3390/rs61110636

Shadman, S., Khalid, P. A., Hanafiah, M. M., Koyande, A. K., Islam, M. A., Bhuiyan, S. A., et al. (2022). The carbon sequestration potential of urban public parks of densely populated cities to improve environmental sustainability. *Sustain. Energy Technol. Assessments* 52, 102064. doi:10.1016/j.seta.2022.102064

Shen, P., and Zhao, S. (2024). Intensifying urban imprint on land surface warming: insights from local to global scale. *iScience*, 109110. doi:10.1016/j.isci.2024.109110

Shen, X. (2007). Researches on the model of Leaf Area Index of common Landscape Plants in Beijing. Beijing: Beijing Forestry University.

Singkran, N. (2022). Carbon sink capacity of public parks and carbon sequestration efficiency improvements in a dense urban landscape. *Environ. Monit. Assess.* 194, 750. doi:10.1007/s10661-022-10432-x

Soegaard, H., and Mller-Jensen, L. (2003). Towards a spatial CO2 budget of a metropolitan region based on textural image classification and flux measurements. *Remote Sens. Environ.* 87, 283–294. doi:10.1016/S0034-4257(03)00185-8

Sultana, R., Ahmed, Z., Hossain, M. D. A., and Begum, B. A. (2021). Impact of green roof on human comfort level and carbon sequestration: a microclimatic and comparative assessment in Dhaka City, Bangladesh. *Urban Clim.* 38, 100878. doi:10.1016/j.uclim.2021.100878

Sun, Z., Liang, H., Liu, J., and Shi, G. (2017). Estimation of photosynthetically active radiation using solar radiation in the UV–visible spectral band. *Sol. Energy* 153, 611–622. doi:10.1016/j.solener.2017.06.007

Tang, Y., and Wang, C.-K. (2011). A feasible method for measuring photosynthesis *in vitro* for major tree species in northeastern China: a feasible method for measuring photosynthesis *in vitro* for major tree species in northeastern China. *Chin. J. Plant Ecol.* 35, 452–462. doi:10.3724/SP.J.1258.2011.00452

Velasco, E., and Roth, M. (2010). Cities as net sources of CO_2: review of atmospheric CO_2 exchange in urban environments measured by eddy covariance technique. *Geogr. Compass* 4, 1238–1259. doi:10.1111/j.1749-8198.2010.00384.x

Wang, B., Liu, Z., Qi, Y., and Jin, G. (2014). Seasonal dynamics of leaf area index using different methods in the Korean pine plantation. *Acta Ecol. Sin.* 34. doi:10.5846/stxb201306181727

Wang, B., and Shui, Y. (1988). Study on the calculation of the photosynt- hetically active radiation. *Acta Energiae Solaris Sin.*, 59–65. doi:10.19912/j.0254-0096.1988.01.010

Wang, B., and Shui, Y. (1990). Study on the calculation of the photosynthetically active radiation. *J. Appl. Meteorological Sci.* 6.

Wang, C., Du, J., Liu, Y., and Chow, D. (2021). A climate-based analysis of photosynthetically active radiation availability in large-scale greenhouses across China. *J. Clean. Prod.* 315, 127901. doi:10.1016/j.jclepro.2021.127901

Wang, J., Fan, L., Han, D., and Chen, L. (2023). Study on carbon-sink matrix quantization and allocation pattern of GreenSpace plants in xi'an under targets of carbon peak and carbon meutrality. *Chin. Landsc. Archit.* 39, 108–113. doi:10.19775/j.cla.2023.02.0108

Wang, J., Feng, L., Palmer, P. I., Liu, Y., Fang, S., Bösch, H., et al. (2020). Large Chinese land carbon sink estimated from atmospheric carbon dioxide data. *Nature* 586, 720–723. doi:10.1038/s41586-020-2849-9

Wang, Q., Chen, J., and Sun, Z. (2005). Application of quantum unit conversion in solar radiation measurement using Li-cor instruments. *dbkxxb* 21, 140–144. doi:10.3321/j.issn:1002-6819.2005.04.031

Wang, V., Gao, J., and Luitgard, S. (2020). Assessing changes of urban vegetation cover and aboveground carbon stocks using LiDAR and Landsat imagery data in Auckland, New Zealand. *Int. J. Remote Sens.* 41, 2140–2158. doi:10.1080/01431161.2019.1685716

Wang, X., Wang, X., Su, Y., and Zhang, H. (2019). Land pavement depresses photosynthesis in urban trees especially under drought stress. *Sci. Total Environ.* 653, 120–130. doi:10.1016/j.scitotenv.2018.10.281

Wang, Y., Liu, W., Ko, S., and Lin, J. (2015). Tree species diversity and carbon storage in air quality enhancement zones in taiwan. *Aerosol Air Qual. Res.* 15, 1291–1299. doi:10.4209/aaqr.2015.02.0110

Wang, Z. (2010). Research on vegetation quantity and carbon-fixing and oxygen-releasing effects of Fuzhou botanical garden. *Chin. Landsc. Archit.* doi:10.3969/j.issn.1000-6664.2010.12.001

Wei, G., Bi, M., Liu, X., Zhang, Z., and He, B.-J. (2023). Investigating the impact of multi-dimensional urbanization and FDI on carbon emissions in the belt and road initiative region: direct and spillover effects. *J. Clean. Prod.* 384, 135608. doi:10.1016/j.jclepro.2022.135608

Weissert, L. F., Salmond, J. A., and Schwendenmann, L. (2017). Photosynthetic CO2 uptake and carbon sequestration potential of deciduous and evergreen tree species in an urban environment. *Urban Ecosyst.* 20, 663–674. doi:10.1007/s11252-016-0627-0

Wilson, K., Goldstein, A., Falge, E., Aubinet, M., Baldocchi, D., Berbigier, P., et al. (2002). Energy balance closure at FLUXNET sites. *Agric. For. Meteorology* 113, 223–243. doi:10.1016/S0168-1923(02)00109-0

Xiao, M., Li, Y., and Lu, B. (2019). Response of net photosynthetic rate to environmental factors under water level regulation in paddy field. *Pol. J. Environ. Stud.* 28, 1433–1442. doi:10.15244/pjoes/81694

Xu, D. (2006). Some noteworthy problems in measurement and investigation of photosynthesis. *Plant Physiol. Commun.* 42, 1163–1167. doi:10.13592/j.cnki.ppj.2006.06.054

Xu, F. (2010). Effects of community structure on carbon fixation of urban forests in Shanghai, China. *Chin. J. Ecol.* 29, 439. doi:10.13292/j.1000-4890.2010.0090

Xu, F., Wang, X., and Li, L. (2023). NPP and vegetation carbon sink capacity estimation of urban green space using the optimized CASA model: a case study of five Chinese cities. *Atmosphere* 14, 1161. doi:10.3390/atmos14071161

Yang, S. (1996). Primary study on effect of C-O balance of afforestatal trees in cities. *Urban Environ. Urban Ecol.*

Ye, Z. (2007). A new model for relationship between irradiance and the rate of photosynthesis in Oryza sativa. *Photosynthetica* 45, 637–640. doi:10.1007/s11099-007-0110-5

Ye, Z., Suggett, D. J., Robakowski, P., and Kang, H. (2013). A mechanistic model for the photosynthesis–light response based on the photosynthetic electron transport of photosystem II in C3 and C4 species. *New Phytol.* 199, 110–120. doi:10.1111/nph.12242

Zhang, H., Feng, Z., Chen, P., and Chen, X. (2019). Development of a tree growth difference equation and its application in forecasting the biomass carbon stocks of Chinese forests in 2050. *Forests* 10, 582. doi:10.3390/f10070582

Zhang, J., Shi, Y., Zhu, Y., Liu, E., Li, M., Zhou, J., et al. (2013). The photosynthetic carbon fixation characteristics of common tree species in northern Zhejiang. *Acta Ecol. Sin.* 33, 1740–1750. doi:10.5846/stxb201207130989

Zhao, D., Cai, J., Xu, Y., Liu, Y., and Yao, M. (2023). Carbon sinks in urban public green spaces under carbon neutrality: a bibliometric analysis and systematic literature review. *Urban For. Urban Green.* 86, 128037. doi:10.1016/j.ufug.2023.128037

Zhao, X., Wang, C., and Huo, H. (2008). Variations in photosynthetic capacity and associated factors for Larix gmelinii from diverse origins. *Shengtai Xuebao/ Acta Ecol. Sin.* 28, 3798–3807. doi:10.3321/j.issn:1000-0933.2008.08.036

Zheng, Z., Yan, D., Wen, X., Wei, Z., Chou, J., Guo, Y., et al. (2022). The effect of greenhouse gases concentration and urbanization on future temperature over Guangdong-Hong Kong-Macao Greater Bay Area in China. *Clim. Dyn.* 58, 3369–3392. doi:10.1007/s00382-021-06103-1

Zhong, R., Song, S., Zhang, J., and Ye, Z. (2023). Spatial–temporal variation and temperature effect of urbanization in Guangdong Province from 1951 to 2018. *Environ. Dev. Sustain.* doi:10.1007/s10668-023-03113-3

Zhou, J., Zhuang, C., and Deng, Y. (2013). Urban forest carbon sink and its estimation methods: a review. *Chin. J. Ecol.* doi:10.13292/j.1000-4890.2013.0514

Zhou, Y., and Xiang, Y. (1996). Climatological estimation of quantum flux densities. *ACTA METEOROL. SIN.* doi:10.11676/qxxb1996.046

Zhou, Y., Xiang, Y., and Shan, F. (1984). A climatological study on the photosynthetically active radiation. *Acta Meteorol. Sin.* doi:10.11676/qxxb1984.046

Zhu, N., Yang, B., and Dong, Z. (2024). The explicit model of forest carbon storage based on remote sensing. *Acta Geodaetica et Cartographica Sinica* 53, 36. doi:10.11947/j.AGCS.2024.20230089

frontiers | Frontiers in Environmental Science

TYPE Original Research
PUBLISHED 13 March 2024
DOI 10.3389/fenvs.2024.1374383

OPEN ACCESS

EDITED BY
Chenxi Li,
Xi'an University of Architecture and Technology, China

REVIEWED BY
Stanley Mubako,
California Department of Water Resources, United States
Zhe Feng,
China University of Geosciences, China
Siyuan Liang,
Zhengzhou University, China
Zhang Pengtao,
Hebei Agricultural University, China

*CORRESPONDENCE
Meiran Zhao,
zhaomr_an@126.com

†These authors have contributed equally to this work and share first authorship

RECEIVED 22 January 2024
ACCEPTED 05 March 2024
PUBLISHED 13 March 2024

CITATION
Gao X, Zhao M, Zhang M, Guo Z, Liu X and Yuan Z (2024), Carbon conduction effect and multi-scenario carbon emission responses of land use patterns transfer: a case study of the Baiyangdian basin in China.
Front. Environ. Sci. 12:1374383.
doi: 10.3389/fenvs.2024.1374383

Carbon conduction effect and multi-scenario carbon emission responses of land use patterns transfer: a case study of the Baiyangdian basin in China

Xing Gao[1,2,3†], Meiran Zhao[1*†], Mengmeng Zhang[1], Zhongyuan Guo[1], Xiao Liu[1] and Zihua Yuan[1]

[1]School of Public Administration, Hebei University of Economics and Business, Shijiazhuang, China, [2]Hebei Collaborative Innovation Center for Urban-Rural Integrated Development, Hebei University of Economics and Business, Shijiazhuang, China, [3]Center for Urban Sustainability and Innovation Development (CUSID), Hebei University of Economics and Business, Shijiazhuang, China

Carbon pooling and release occur all the time in all corners of the earth, where the land use factor is key to influencing the realization of carbon peaking and neutrality. Land use patterns and carbon emissions change under different scenarios and analyzing the correlation will help formulate scientific land use policies for the future. In this study, through remote sensing data, we investigated the changes in land use patterns and carbon emissions in the Baiyangdian basin in China from 2000 to 2020 and analyzed the carbon conduction effect with the help of a land transfer matrix. The geographical simulation and optimization system-future land use simulation (GeoSOS-FLUS) and Markov models were used to predict the land use changes and carbon emissions under the four different scenarios for the region in 2035. The results indicated that 1) the net land use carbon emissions increased from 52,163.03 × 10^3 to 260,754.91.28 × 10^3 t from 2000 to 2020, and the carbon source-sink ratio exhibited a general uptrend; 2) the net carbon emissions due to terrestrial transfers increased over time. The carbon conduction effects due to the transfer of forests, grasslands, water areas, and unused lands to built-up lands also showed a rising trend, albeit the latter two exhibited only small changes; 3) in 2035, the net carbon uptake under the four development scenarios was predicted to be 404,238.04 × 10^3, 402,009.45 × 10^3, 404,231.64 × 10^3, and 404,202.87×10^3 t, respectively, with all values much higher than that of the study area in 2020. The maximum carbon sink capacity was 817.88 × 10^3 t under the double-carbon target scenario, and the maximum carbon source emission was 405,033.61 × 10^3 t under the natural development scenario. The above results provide an essential reference for low carbon-based urban land use regulations for the Baiyangdian basin and other similar projects in the future.

KEYWORDS

land use, carbon source-sink ratio, carbon conduction effects, Markov prediction, Baiyangdian basin

1 Introduction

Global climate change poses a significant threat to sustainable development and the survival of humans (Rong et al., 2022). The terrestrial carbon system is an important component of the global carbon cycle, which plays a critical role in mitigating global warming by effectively regulating the regional climate through the absorption and release of greenhouse gases from the atmosphere (Yu et al., 2022). Land use activities primarily affect the carbon cycle of the ecosystem (Mendelsohn and Sohngen, 2019), with their carbon emissions being second only to the burning of fossil fuels (Wang Z. et al., 2022). Thus, regulating land use activities to reduce carbon emissions is an important means of promoting carbon neutrality from a practical perspective (Carpio et al., 2021). Therefore, several studies have aimed to demonstrate how carbon emissions from land use can help achieve a range of low carbon development goals, particularly carbon peak and neutrality (Yang and Liu, 2022).

Most studies on land use carbon emissions focus on accounting, mechanisms and consequences, projections, and impact factors (Le Quéré et al., 2012; Houghton and Nassikas, 2017; Yu et al., 2022). The accounting of land use carbon emissions mainly involves assessing the emissions by using bookkeeping, the Intergovernmental Panel on Climate Change (IPCC) inventory, the Carnegie-Ames-Stanford approach (CASA) model, the global production efficiency model (GLO-PEM), and the integrated valuation of ecosystem services and tradeoffs (InVEST) model (Piao et al., 2022; Raihan et al., 2022; Walker et al., 2022). Houghton and Nassikas (2017) used a bookkeeping model and estimated the average global net carbon fluxes induced by land use and coverage change (LUCC) from 2006 to 2015 to be 1.11 ± 0.35 Pg C yr^{-1}; Ghosh et al. (2022) proposed a method to establish a low-carbon city by extensively analyzing land use carbon emissions and sequestration potential using the InVEST model. Regarding the land use carbon emission effects, it primarily investigates the impact of vegetation and soil carbon storage, as well as the dynamic evolution characteristics (Wang et al., 2020; Wolswijk et al., 2022). Affuso and Hite (2013) showed that participatory decision-making on land use can triple the net energy value of biofuels and reduce carbon emissions by 20%; Ghorbani et al. (2023) showed that soil carbon storage and atmospheric carbon dioxide (CO_2) emissions were directly affected by the changes in the soil characteristics and land use; rising pastures and forests increased the soil organic carbon and microbial biomass carbon in both topsoil and subsoil. For the prediction of land use carbon emissions, Cellular Automata-Markov (CA-Markov), Conversion of Land Use and its Effects at Small regional extent (CLUE-S), Future Land Use Simulation (FLUS), and Patch-generating Land Use Simulation (PLUS) models were used to predict the land use spatial layout for carbon emission analysis (Wang H. et al., 2022; Wu et al., 2022). Liu et al. (2018) used a system dynamics approach to establish a multi-perspective integrated measurement model to quantitatively predict new towns on a sector-by-sector basis. They showed that cities need to rely on regional green spaces to mitigate carbon emissions; Yao et al. (2023) proposed a bottom-up cadastral land scale carbon emission prediction framework based on vector cellular automata. Although the aforementioned works serve as excellent examples for the study of land use carbon emissions, only a few studies have focused on carbon emission conduction due to the change in land type (Li et al., 2023). Investigating the effects of land type changes on carbon emissions under various scenarios can provide new perspectives to formulate appropriate land regulation and carbon emission reduction policies (Ke Y. et al., 2022). However, most of the existing research is based on past land use data, and there remains a lack of studies predicting changes in future land use patterns under multiple scenarios and the resultant carbon emissions (Chuai et al., 2019).

Therefore, the objectives of this study were 1) Based on the land use data, combined with the carbon emission estimation model, obtain the carbon emission characteristics of the Baiyangdian basin from 2000 to 2020. 2) Use the land transfer matrix to analyze the carbon transfer effect caused by land use transfer in each period 3) Predict the land use pattern under four different development scenarios in 2035, as well as the resulting carbon emissions, to provide a reference for the city to assess the pressure of carbon emission reduction (Harper et al., 2018).

The rest of the paper is as follows: Section 2 presents an overview of the study area and data sources, Section 3 describes the empirical methodology, Section 4 is the results and analyses section, and Section 5 provides the discussion and conclusions.

2 Study area overview and data sources

2.1 Study area overview

The Xiong'an New Area, China, as a hub to relieve Beijing of non-capital functions, is critical to accelerating the synergistic development of the Beijing-Tianjin-Hebei region, with its land use changes being typical of the current era (Zhou et al., 2021). The Baiyangdian basin, as the ecological hinterland of the Xiong'an New Area, is a prime example of healthy synergies between the carbon system and the development of the city (Li et al., 2008; Zhao et al., 2021; Xia et al., 2023). The study area is situated in the northern part of the North China Plain, between 113°45′–116°26′ eastern longitudes and 37°51′–40°39′ northern latitudes (Figure 1), which belongs to a warm-temperate monsoon climate. The Baiyangdian basin in this study refers to the administrative area of Hebei Province flowing through nine branches such as the Zuma Long River, the Cao River, and the Zhao Wang Xin River, involving 35 counties (cities and districts) under the jurisdiction of Baoding City, Zhangjiakou City, Shijiazhuang City and Cangzhou City, with a total land area of 34,353.07 km^2. The basin exhibits an intricate geography, with highlands in the west (mountains) and lowlands in the east (plains). The mountainous area mainly comprises forests and grasslands (17.79% and 19.69% of the total basin area, respectively), and the plains are primarily cultivable land (46.25% of the total basin area).

2.2 Data sources

In this study, we employed remote sensing image data, Digital Elevation Model (DEM) data, slope data, meteorological data, and fossil energy data as follows:

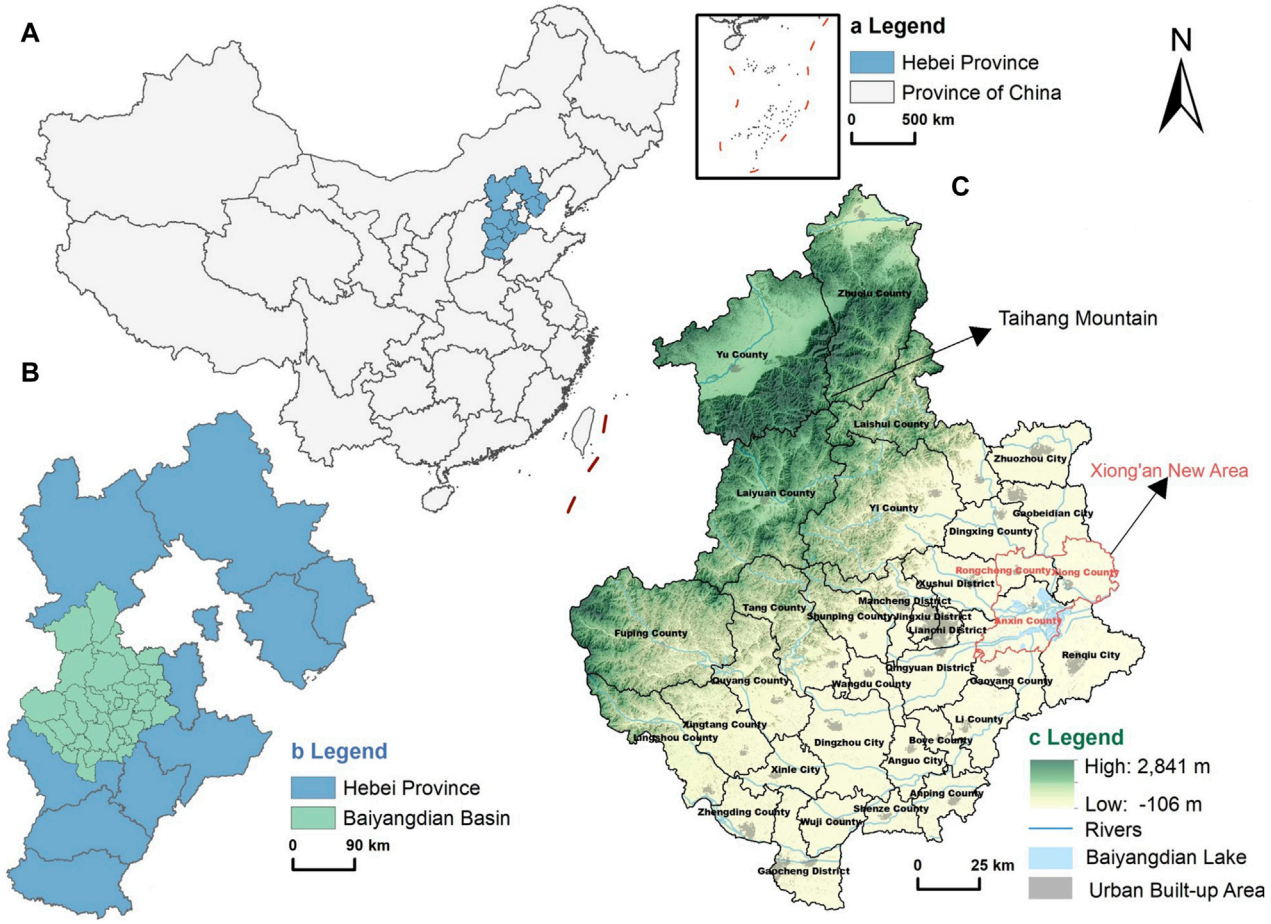

FIGURE 1
Spatial location of the study area. **(A)** China scope; **(B)** Hebei Province; **(C)** Baiyangdian Basin.

(1) The Landsat4-5/Thematic Mapper (TM) and Landsat8/Operational Land Imager (OLI) remote sensing images used in this study were obtained from the Chinese Academy of Sciences Geospatial Data Cloud (https://www.gscloud.cn/). The data identifiers and dates of the selected images are LT51230332000145BJC00 2000-05-24, LT51230322010156IKR00 2010-06-05, and LC81230332020120LGN00 2020-4-29, respectively. Concerning previous classification standards and combined with research needs, the land was divided into cultivable land, forest, grassland, built-up land, unused land, and water area, with a 30-m spatial resolution.

(2) The DEM data were obtained from the Chinese Academy of Sciences Geospatial Data Cloud (https://www.gscloud.cn/), and further, the slope data was extracted from the DEM data, with an initial resolution of 30 m.

(3) Annual average precipitation and average temperature for the basin study area were collected from the China Meteorological Data Network (https://data.cma.cn/), the spatial resolution is 0.5° × 0.5°.

(4) Data on the consumption of the eight main fossil energy sources used to indirectly estimate carbon emissions from built-up land were obtained from the statistical yearbooks of counties and cities and the National Bureau of Statistics (http://www.stats.gov.cn/) for the years 2000–2020. The corresponding energy carbon emission coefficients were the missing values recommended by the Intergovernmental Panel on Climate Change (IPCC).

3 Research methods

3.1 Land use carbon emission calculations

Carbon sinks include grasslands, forests, unused lands, and water areas (Guo and Fang, 2021). Cultivable land can act as both a carbon source and sink due to its different functions (Ma and Wang, 2015). Therefore, this paper accurately measured the carbon emission values for these five land use types by the direct estimation method. Equation 1 is calculated as follows:

$$C_i = S_i * V_i \quad (1)$$

where i = 1, 2, 3, 4, and 5 represent cultivatable land, forest, grassland, water area, and unused land, respectively (Yue et al., 2020); C_i is i land type carbon emissions; S_i is i land type area; and V_i is i land type carbon emission coefficient (Table 1).

TABLE 1 Land use carbon emission coefficients.

Land type	Definition	Carbon emission coefficient [kg·(m^2·a)$^{-1}$]	Reference source
Grassland	Refers to land where herbaceous plants grow predominantly	−0.0021	Jingyun Fang (2001)
Forest	Refers to forestry land where trees, shrubs, bamboo, and coastal mangroves grow	−0.0578	Jingyun Fang (2001)
Cultivable land	Refers to land on which crops are grown, including ripe cropland, new land, recreational land, and rotational land. rest land, grass field rotational crop land; agricultural fruit, agricultural mulberry, and agricultural forest land; beach land, and mudflats that have been ploughed for more than 3 years	0.0422	Ying Li (2013)
Water area	Refers to natural terrestrial waters and water facility land	−0.0252	Ying Li (2013)
Unused land	Refers to land that is currently unutilized, including hard-to-utilize land	−0.0005	Li Lai (2012)

TABLE 2 Standard coal conversion and carbon emission coefficients for the energy sources.

Energy category	Fuel oil	Coke	Natural gas	Crude oil	Diesel oil	Raw coal	Kerosene	Gasoline
Conversion coefficient	1.4286	0.9714	1.3300	1.4286	1.4571	0.7143	1.4714	1.4714
Carbon emission coefficient	0.61850	0.8550	0.4483	0.5857	0.5538	0.5921	0.5714	0.5538

TABLE 3 Indicator system for the allocation of carbon emissions.

Principle	Index	Metrics	Indicator direction	Data source
Fairness	Population	Population size	Positive	Hebei Statistical Yearbook, Baoding Economic Statistical Yearbook
	GDP	GDP numeric value	Positive	Hebei Statistical Yearbook, Baoding Economic Statistical Yearbook
	Historical carbon emissions	Fossil fuels produce carbon emissions	Positive	Hebei Statistical Yearbook, Hebei Economic Statistical Yearbook
Efficiency	Carbon productivity	GDP/carbon emissions	Positive	China Energy Statistical Yearbook
Feasibility	Carbon emission reduction potential	Tertiary industry proportion	Negative	Hebei Statistical Yearbook, Hebei Economic Statistical Yearbook

Carbon emissions from built-up land occur mainly from human activities and the energy production and industrial processes they host (Zhang et al., 2021). This paper indirectly estimated the carbon emissions of the eight main fossil fuel sources through their consumption. Equation 2 is calculated as follows:

$$E_c = \sum E_j * \theta_j * f_j \quad (2)$$

where E_c is built − up land carbon emission, j is the energy source type; E_j is the energy consumption; θ_j is the energy to standard coal factor; and f_j is the carbon emission (Lu et al., 2022) (Table 2).

According to the principle of indicator system construction, this paper selects five indicators, including population, carbon emission intensity, gross domestic product (GDP), historical carbon emissions, and the proportion of the tertiary industry, to construct the Baiyangdian Basin Carbon Emission Indicator System from the perspective of fairness, efficiency, and feasibility (Table 3). The entropy value technique was initially applied to calculate the weights of individual indicators. Subsequently, this method was supplemented by a total carbon emission measurement model to ultimately quantify the indirect carbon emissions originating from the different land types in the study region (Tang et al., 2022).

3.2 Estimation of land transfer-based carbon emission conduction

Land use changes can cause carbon transfer, which is defined as the carbon conduction effect of land use carbon emissions. Two factors, the difference between the level of carbon sequestration and carbon emissions following a change in land class and the area of change, mainly determine the amount of carbon emissions they transmit (Qiao et al., 2016). The area of land class conversion can be calculated from a land use transfer matrix indicating the amount of change and the direction of transfer, and its Eq. 3 is:

TABLE 4 Land use change rules for different scenarios.

Scenario type	Scenario description
Natural development	This reference scenario does not impose any restrictions on the transformation between various land types, nor does it comprise any government or market interventions
Balanced development	In accordance with planning policies and drawings, such as the Planning Outline of Xiong'an New Area in Hebei Province and the Control Planning of the Starting Area of Xiong'an New Area in Hebei Province, the quantity requirements of different land types in different planning directions in the future are determined. The land use structure of the other areas in the basin is consistent with the natural development scenario
Cultivable land protection	The quality and quantity of basic cultivable land are associated with national food security, so the land use change simulation needs to accommodate the concept of cultivable land protection under the baseline scenario. This scenario protects cultivable land in the basin by strictly controlling its total area and conversion to other types, providing a reference for future regional planning of the basin on the premise of farmland protection
Double-carbon target	This scenario incorporates ecological conservation into the baseline. Ecologically protected areas are defined based on factors, such as the ecosystem structure and resource-carrying capacity of urban agglomerations, to prevent the disordered expansion of urban areas from damaging the environment

$$S_{ij} = \begin{bmatrix} s_{11} & \cdots & s_{1N} \\ \cdots & \ddots & \cdots \\ s_{N1} & \cdots & s_{NN} \end{bmatrix} \quad (3)$$

where N is the number of land use types; and S_{ij} is the area transferred from land type i to land type j. The carbon transmission due to the interconversion between land categories other than built-up land (C_t) can be estimated from the transfer matrix and the difference between the carbon emission coefficients ($\delta_{i1} - \delta_{i2}$) of each category using Eq. 4:

$$C_t = S_{ij} \times (\delta_{i1} - \delta_{i2}) \quad (4)$$

This paper considers the built-up land within the Baiyangdian basin to be spatially homogeneous, neglecting the carbon emission differences that may arise in distinct spatial scenarios per unit area. Therefore, during the study period T1~T2, the carbon emissions transferred from built-up land to the other types of land can be calculated by Eq. 5:

$$C_t = S_{bi} \times (\delta_{T1} - \delta_i) = S_{bi} \times \left(E_{b1}/S_{b1} - \delta_i\right) \quad (5)$$

In contrast, Eq. 6 is used to calculate the transfer of carbon emissions from other land types to built-up land:

$$C_t = S_{ib} \times (\delta_i - \delta_{T2}) = S_{ib} \times \left(\delta_i - E_{b2}/S_{b2}\right) \quad (6)$$

Where C_t is the Carbon emission transmission; δ_i is the carbon emission coefficient (δ_{i1}) or carbon absorption coefficient (δ_{i2}) for land use types other than built-up land; δ_{T1} and δ_{T2} are the carbon emission generated on the unit area of built-up land in T1 and T2 years, respectively (Zhang et al., 2014b), and the unit is $t\cdot(km^2\cdot a)^{-1}$. E_{b1} and E_{b2} are the carbon emissions generated by built-up land in T1 and T2 years, respectively; S_{bi} and S_{ib} are the areas of built-up land in years T1 and T2; S_{bi} and S_{ib} are the areas of interconversion of built-up land and other land types, respectively (Zhang et al., 2014a).

3.3 GeoSOS-FLUS model

In this study, the GeoSOS-FLUS model was used to simulate future land use change in the Baiyangdian basin. The model has two main components, scenario setting and model building (Sun et al., 2021). As a resource on which human activity depends, changes in land use and spatial distribution characteristics essentially depend on a tradeoff between economic development and ecological protection. Therefore, based on previous studies and specific planning policies of each city in the Baiyangdian basin, we established four development scenarios, namely, natural development, balanced development, cultivable land protection, and double-carbon target, and analyzed their effects (Tao et al., 2015; Hong et al., 2021; Wang Z. et al., 2022). The different scenario settings and corresponding scenario descriptions are shown in Table 4.

The *GeoSOS-FLUS model* includes the following two framework contents:

(1) The study identified six key factors, namely, elevation, slope, temperature, precipitation, distance to the road, and distance to the railway, responsible for driving land use changes in the Baiyangdian basin. To evaluate the probability of each land use type suitability, we employed an artificial neural network (ANN) algorithm (Wang et al., 2019). To verify the accuracy of the calculations, we simulated a land use distribution map for 2020 using the land use types of the study region in 2010 and matched the findings with the land use distribution map for the same year. The Kappa coefficient is 0.7464 and has an overall accuracy of 84.20%, demonstrating good simulation results.

(2) The model sampled the first-stage land use distribution data and proposed an adaptive inertia competitive roulette mechanism to simulate the land use scenario distribution. A degree of uncertainty and complexity in land use conversion remained, influenced by a variety of factors. Due to the application of the sampling method and competitive mechanism, the proposed model could effectively avoid error transmission, along with the adverse effects of uncertainty and complexity. In other words, the GeoSOS-FLUS model exhibited good accuracy and enabled the simulation predictions to be consistent with the actual data.

TABLE 5 Changes in carbon source emissions, sink absorption, and its ratio in the Baiyangdian basin.

Year	Carbon sink absorption (10^3t)	Carbon source emissions (10^3t)	Net carbon emissions (10^3t)	Carbon source-sink ratio
2000	−782.48	52,945.51	52,163.03	67.66
2010	−795.30	229,974.20	229,178.90	289.17
2020	−792.07	261,546.99	260,754.91	330.21
2000–2020	9.59	208,601.48	208,591.88	4.9 times

3.4 Markov prediction

The Markov process can predict the possible state of an event at any particular instance in the future according to the current state of the event by following the "no aftereffect" principle (Yang et al., 2020). In this study, the transfer probability matrix was solved by a Markov process according to the change relation of time series to make an energy knot prediction. The Markov model was employed to predict future land use patterns in the Baiyangdian basin energy structure based on historical energy data from 2000 to 2020. Let us assume that at time m, the state vector of the energy consumption structure in the basin can be expressed as Eq. 7:

$$S(m) = \left\{S_r(m), S_c(m), S_o(m), S_g(m), S_k(m), S_d(m), S_f(m), S_n(m),\right\} \tag{7}$$

where $S_r(m)$, $S_c(m)$, $S_o(m)$, $S_g(m)$, $S_k(m)$, $S_d(m)$, $S_f(m)$, and $S_n(m)$ are the proportions of raw coal, coke, crude oil, gasoline, kerosene, diesel, fuel oil, and natural gas in energy consumption, respectively. The transition matrix at time m~m+1 can be expressed as Eq. 8:

$$P_{i-j}(m) = \begin{bmatrix} p_{r-c}(m) & p_{r-o}(m) & \cdots & p_{r-f}(m) & p_{r-n}(m) \\ p_{c-r}(m) & p_{c-c}(m) & & p_{c-f}(m) & p_{c-n}(m) \\ \vdots & \vdots & & \vdots & \vdots \\ p_{f-r}(m) & p_{f-c}(m) & & p_{f-f}(m) & p_{f-n}(m) \\ p_{n-r}(m) & p_{n-c}(m) & \cdots & p_{n-f}(m) & p_{n-n}(m) \end{bmatrix} \tag{8}$$

where i and j are energy types; and $P_{i-j}(m)$ is the probability of energy i conversion to energy j. The model effect coefficient, w, was used as the criterion to judge the quality of prediction results, which can be computed as Eq. 9:

$$w = 1 - \frac{\sum\left(S_r - S_p\right)^2}{\sum\left(S_r - \overline{S_r}\right)^2} \tag{9}$$

where S_r is the real value, S_p is the predicted value, and $\overline{S_r}$ is the average of the actual values. If the value is closer to 1, the prediction results are close to the actual values and the prediction accuracy is high.

4 Results and analysis

4.1 Changes in land use carbon emissions

Based on the calculations, Table 5 shows land use carbon emissions in the Baiyangdian basin for the years 2000, 2010, and 2020. The net land use carbon emissions in the basin were found to steadily increase over the past two decades, with a total amount of 208,591.88 × 10^3 t and an average annual increase of 10,429.59 × 10^3 t. Grasslands, forests, water areas, and unused lands acted as carbon sinks, increasing the total carbon absorption by 9.59 × 10^3 t. The combined carbon emissions from cultivable and built-up lands as carbon sources increased by 208,601.48 × 10^3 t. The carbon source emission to sink absorption ratio in the basin increased, especially reaching the highest value of 330.21 in 2020, 4.9 times higher than in 2000. This indicated that the carbon sources in the basin were continuously rising, and the carbon sink was continuously declining.

Specifically, carbon emissions from built-up lands were on an upward trend, along with carbon sequestration in forests and water areas were on an upward trend, other land types steadily declined as carbon sources or sinks (Figure 2). In the case of building sites, from 2000 to 2010, rapid urbanization, enhanced land intensification, and a mass of cultivable lands, forests, and grasslands were transformed into built-up lands, resulting in an expansion trend of built-up land, which is manifested in the fact that the rate of transferring in is 18.5 times higher than the rate of transferring out. The land use dynamic attitude (k) reached 0.0087, with the land area expanding by 268.36 km^2. This increase accounted for 94.52% of carbon emissions in 2000, rising to 98.72% in 2020, representing the largest contribution to carbon emissions (Figure 2). Due to the minimal net conversion of land from other categories to built-up land within their respective land usage dynamics between 2000 and 2010, the proportion of carbon emissions attributed to built-up land was the lowest during the entire research period, in 2020 (Table 6). The area of cultivated land has been decreasing from 2000 to 2010, with 637.45 km^2 of cultivated land being transferred out at a rate 12.67 times faster than the rate of transfer in, making it the land category with the largest reduction in area share of any land category.

Among the carbon sinks, grassland and unused land demonstrated a marginal reduction in carbon sequestration, with the corresponding proportion decreasing from 0.54% in 2000 to 0.49% in 2020 (Figure 2B). The fluctuating trends in the carbon uptake ratios of grasslands and unused lands could be attributed to their continued transfer to built-up and cultivable lands. In 2000–2010, 86.64 km^2 of grassland and 5.14 km^2 of unused land were transferred, and in 2010–2020, 1,390.75 km^2 of grassland and 17.98 km^2 of unused land were transferred.

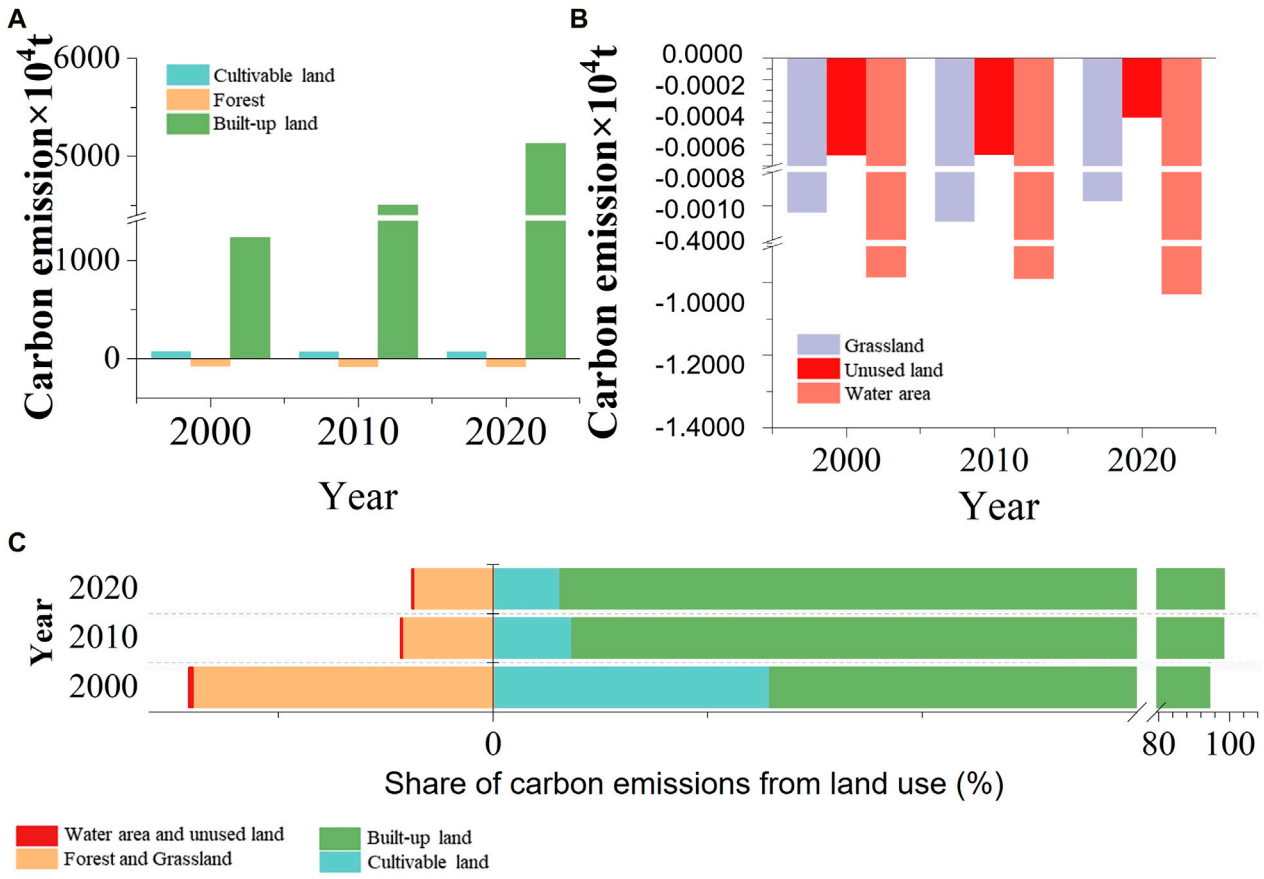

FIGURE 2
Change and proportion of carbon emissions from land use. **(A,B)** Land use carbon emissions; **(C)** Proportion of carbon emissions.

4.2 Carbon conduction effects due to land type changes

To determine the carbon emissions after each stage of land type transfer, we combined the land use transfer matrix with the carbon source/sink capacity of the land type. The values with an asterisk in Table 7 indicate the net carbon emissions from land use transfer at each period of the study period and increased over time. Throughout the entire study period, carbon emissions were determined by the carbon source category. The key role of built-up land was highlighted by the study's finding that built-up land accounted for most carbon emissions from total carbon sources. The transfer of cultivable lands and grasslands to built-up lands had the most significant effect on carbon transfer through the conversion of carbon sinks into sources. This impact is due to the release of carbon stored in the soil, ecosystem, and biomass. This transformation of cultivated land and grassland into built-up land accounted for 84.05% of the total carbon emissions (Table 7). The carbon conduction from cultivable to built-up land was 1.02×10^3 t from 2000 to 2010, which increased to 42.44×10^3 t from 2010 to 2020. The carbon conduction from forests, and grasslands, to built-up land also showed an increasing trend. The carbon conduction effect caused by water area and unused land transfer is the same as that caused by grassland cultivation, which also shows an increasing trend.

4.3 Multi-scenario simulation and prediction of land use structure

In this paper, four scenarios were simulated using the GeoSOS-FLUS model for the prediction of the Baiyangdian basin land use in 2035 (Figure 3). The 2035 balanced development, cultivable land protection, and double-carbon target scenarios were largely consistent, but with differences in certain regions.

In the natural development scenario, the area of forests, water area, grasslands, cultivable lands, and unused lands in 2035 was 12,118.94, 462.03, 1626.05, 15,009.93, and 10.98 km^2, respectively. Compared to 2020, the water area increased by 54.17 km^2 at most; the forest area increased by 39.68 km^2; and the cultivable land reduced by 5.03%, with a reduction of 795 km^2. In the balanced development scenario, compared to 2020, the area of built-up lands, forests, and water bodies increased by 918.30, 260.43, and 119.7 km^2, respectively. Accordingly, the area of the cultivable lands and grasslands was reduced by 1096.82 km^2 and 218.22 km^2, respectively. As urbanization converts large parts of farmlands, food security will be further threatened if the focus remains only on economic development. In the cultivable land protection scenario, the built-up land area was relatively small, close to 5104.76 km^2. Compared with the natural development scenario, the area of forests and grasslands increased by 41.48 and 38.61 km^2, respectively, while the area of

TABLE 6 Land use changes in the Baiyangdian basin from 2000 to 2020.

Year	Land use type	Unchanged	Outflow		Inflow		Net area change	Proportion of land area	k (%)
		Area	Area	Speed	Area	Speed			
2000–2010	Grassland	1911.17	86.64	8.66	209.09	20.91	122.45	47.58%	0.0061
	Cultivable land	16,290.28	637.45	63.75	50.30	5.03	−587.15	35.31%	−0.0035
	Built-up land	3063.80	15.33	1.53	283.69	28.37	268.36	6.17%	0.0087
	Forest	11,918.56	13.47	1.35	207.85	20.78	194.38	9.75%	0.0016
	Water area	356.55	32.71	3.27	34.51	3.45	1.80	1.14%	0.0005
	Unused land	12.68	5.14	0.51	5.30	0.53	0.16	0.05%	0.0009
2010–2020	Grassland	729.52	1390.75	139.07	1717.65	171.77	326.91	46.00%	−0.0134
	Cultivable land	13902.25	2438.33	243.83	3042.70	304.27	604.37	35.16%	−0.0033
	Built-up land	2719.47	628.03	62.80	1703.03	170.30	1075.00	5.35%	0.0259
	Forest	9382.23	2744.18	274.42	730.01	73.00	−2014.17	12.26%	−0.0004
	Water area	289.22	101.83	10.18	116.73	11.67	14.89	1.19%	0.0043
	Unused land	0.01	17.98	1.80	10.98	1.10	−7.00	0.03%	−0.0389

TABLE 7 Carbon conduction effect of land type transfer in the Baiyangdian basin from 2000 to 2020 (10^3 t).

Year	Land use type	Cultivable land	Forest	Grassland	Built-up land	Unused land	Water area	Carbon outflow
2000–2010	Cultivable land	—	−0.71	−0.40	1.02	0.00	−1.59	−1.67
	Forest	16.17	—	3.37	0.03	0.00	0.08	19.64
	Grassland	8.77	−0.12	—	0.25	−0.01	−0.07	8.82
	Built-up land	0.56	−0.49	−0.57	—	−0.01	−0.28	−0.79
	Unused land	0.12	0.00	0.00	0.09	—	0.00	0.20
	Water area	1.62	−0.01	0.20	0.26	−0.01	—	2.07
	Carbon inflow	27.24	−1.33	2.60	1.65	−0.03	−1.86	0.00
	Total	25.56	18.31	11.41	0.86	0.17	0.21	56.53*
2010–2020	Cultivable land		−1.55	−0.44	42.44	0.00	−0.03	40.41
	Forest	0.43		0.19	3.84	0.00	0.00	4.45
	Grassland	0.22	−0.70		7.41	0.00	−0.01	6.92
	Built-up land	−134.83	−29.11	−9.89		−0.48	−3.22	−177.53
	Unused land	0.00	0.00	0.00	0.55		0.00	0.54
	Water area	0.06	0.00	0.00	1.42	0.00		1.48
	Carbon inflow	−134.13	−31.37	−10.14	55.66	−0.48	−3.26	
	Total	−93.72	−26.92	−3.21	−121.87	0.06	−1.78	−247.45*

* Denotes the sum of carbon transferred out and transferred in for all land use types.

cultivable lands and grassland decreased by 65.88 and 10.43 km^2, respectively, indicating a severe deterioration of the Baiyangdian basin ecology. This also suggested that even in the cultivable land protection scenario, only a small portion of cultivable land, grassland, and water area were expanded. It also demonstrated the need to place a higher priority on environmental preservation, rather than economic development in the Baiyangdian basin. In the double-carbon target scenario, the area of cultivable lands, forests, grasslands, water area, unused lands, and built-up lands changed to 14705.15 km^2, 12438.86 km^2, 1615.62 km^2, 527.85 km^2, 6.17 km^2, and 5007.5 km^2, respectively. In comparison to 2020, the grassland area decreased by 190.96 km^2 and the carbon-emitting cultivable land decreased by 1099.78 km^2. Moreover, the area of water area rose by 119.99 km^2, while that of the forests expanded by 359.6 km^2 (Table 8).

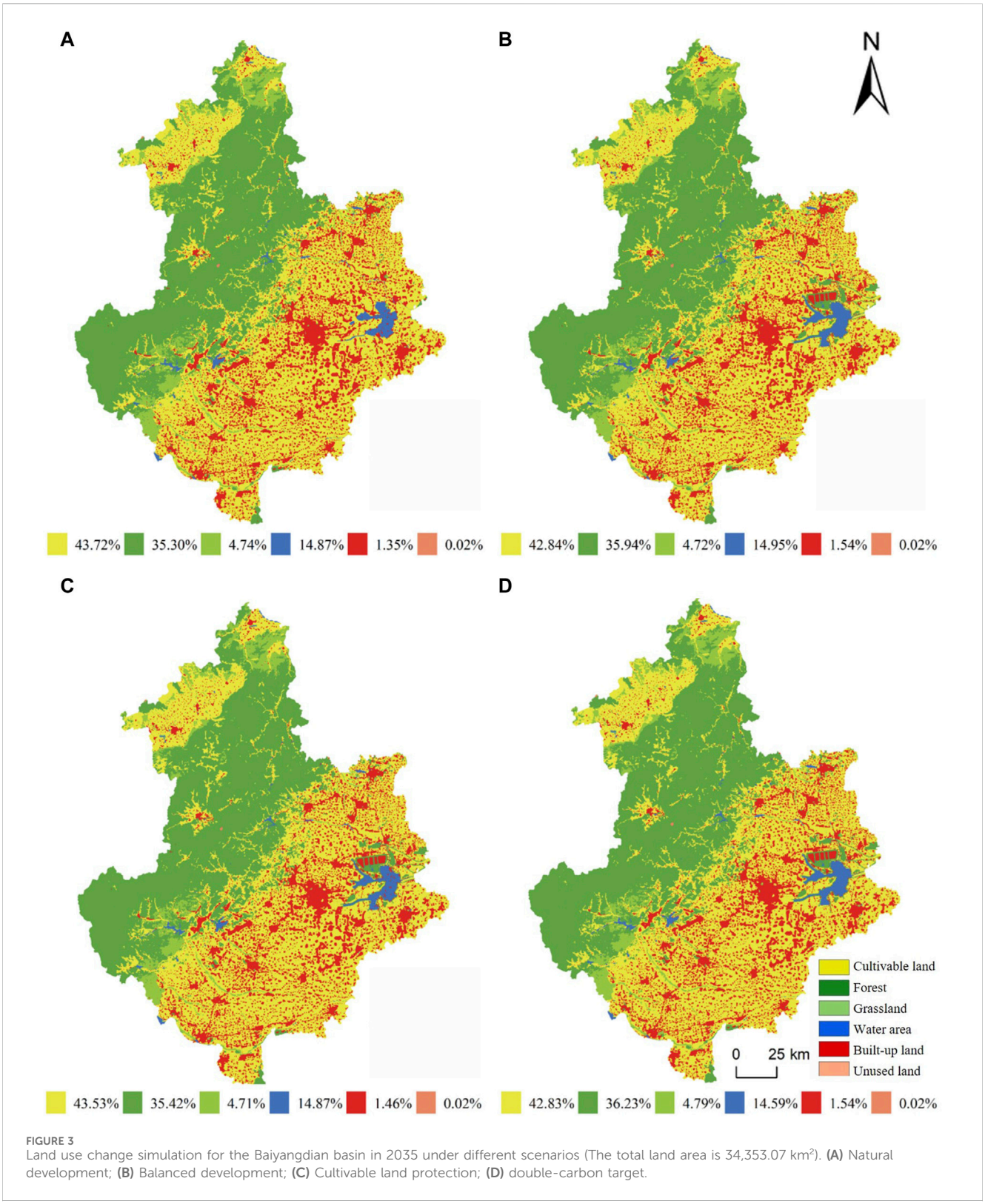

FIGURE 3
Land use change simulation for the Baiyangdian basin in 2035 under different scenarios (The total land area is 34,353.07 km^2). **(A)** Natural development; **(B)** Balanced development; **(C)** Cultivable land protection; **(D)** double-carbon target.

4.4 Prediction of land use carbon emissions

4.4.1 Direct land use carbon emissions

The cultivable land carbon emissions in the Baiyangdian Basin in 2020 were calculated to be 666.97 × 10^3 t, compared to which the emissions in the four scenarios set in 2035 were predicted to decrease slightly (Table 9). In particular, the cultivable land carbon emissions for the balanced development and double-carbon target scenarios were likely to decrease more about 7%. Regarding the carbon sinks, the maximum carbon uptake of the forests under the double-carbon

TABLE 8 Area of each land use type under multi-scenario modeling (km^2).

Land use type	Cultivable land	Forest	Grassland	Built-up land	Water area	Unused land
2020	15804.93	12079.26	1837.08	4212.96	407.86	10.98
Natural development	15009.93	12118.94	1626.05	5105.82	462.03	6.17
Balanced development	14708.11	12339.69	1618.86	5131.26	527.56	6.17
Cultivatable land protection	14944.05	12160.42	1615.62	5104.76	500.64	6.17
Double-carbon target	14705.15	12438.86	1646.12	5007.50	527.85	6.17

TABLE 9 Prediction results of direct carbon emissions from land use under multi-scenario simulation (10^3t).

Land use type	Cultivable land	Forest	Grassland	Water area	Unused land
2020	666.9680	−777.9043	−3.8579	−10.3189	−0.0055
Natural development	633.4190	−780.4597	−3.4147	−11.6894	−0.0031
Balanced development	620.6822	−794.6760	−3.3996	−13.3473	−0.0031
Cultivatable land protection	630.6389	−783.1310	−3.3928	−12.6662	−0.0031
Double-carbon target	620.5573	−801.0626	−3.4569	−13.3546	−0.0031

target scenario was 801.26 × 10^3 t, an increase of 3.1% compared with that in 2020, followed by 794.68 × 10^3 t under the balanced development scenario. The carbon uptake of grasslands remained largely unchanged, with an average value was about 3.5 × 10^3 t. Water areas exhibited the largest carbon uptake in the double-carbon target scenario. Compared with 2020, the water area carbon emissions increased for all four scenarios, with a growth ratio of 23.71%. The unused land area was relatively small, which also remained largely unchanged. The predicted results for the different scenarios are shown in Table 9.

4.4.2 Indirect land use carbon emissions

We chose the energy consumption data of the Baiyangdian basin in 2019 as the initial value and combined it with the average transfer probability matrix P obtained by Eq. 9. We subsequently utilized the Markov model for forecasting the energy composition in 2020 and verified the accuracy by comparing the predictions with the actual data (Figure 4).

According to Eq. 9, the model effect coefficient w is 0.999 close to 1, indicating a good prediction result, and hence, a reasonable and reliable prediction model. Therefore, the energy consumption in 2020 was selected as the initial vector and combined with the average transfer probability matrix, P, obtained from historical energy data from 2000 to 2020, and the energy consumption structure of the Baiyangdian basin in 2035 was predicted (Figure 4).

Using the carbon emissions data from 2000 to 2020 for the Baiyangdian basin, we employed the grey prediction GM (1,1) model to forecast the 2035 emissions and assess the model precision. The carbon emissions due to built-up lands in the basin in 2035 were expected to reach 404,400.19 × 10^3 t.

4.4.3 Summary of land use carbon emissions in the Baiyangdian basin

In this study, we built a Markov model to forecast total terrestrial carbon emissions in the Baiyangdian basin (Table 10). The land use carbon sinks were primarily related to the land type area, and the carbon sources were primarily related to the continuous growth of energy consumption. Compared with 2020, the net land use carbon emissions in the basin were predicted to increase in 2035 for the four scenarios by 143,483.14 × 10^3, 143,454.55 × 10^3, 143,476.74 × 10^3, and 143,447.97 × 10^3 t, respectively. All values were much higher than the net carbon emissions of the study area in 2020. In the natural development scenario, the carbon source emission peaked at 405,033.61 × 10^3 t, increasing by 143,486.62 × 10^3 t, about 55.03%. The lowest carbon sink absorption out of the four scenarios was 795.57 × 10^3 t, with a slight increase of 3.48 × 10^3 t compared with 2020. In the balanced development and cultivable land protection scenarios, carbon emissions increased significantly, carbon sink absorptions increased by 19.34 × 10^3 t and 7.11 × 10^3 t, and carbon source emissions increased by 143,473.89 × 10^3 t and 143,483.84 × 10^3 t, respectively. In the double-carbon target scenario, the lowest carbon source emission was 405,020.75 × 10^3 t and the highest carbon sink absorption was 817.88 × 10^3 t in the fourth scenario, which has a significant increase compared to the other three scenarios. Generally, land use carbon emissions in the natural development scenarios were the highest, followed by the balanced development, cultivable land protection, and double-carbon target scenarios. Therefore, it is worth thinking about how to balance carbon emission and absorption in the Baiyangdian Basin to achieve healthy development (Chuai et al., 2016).

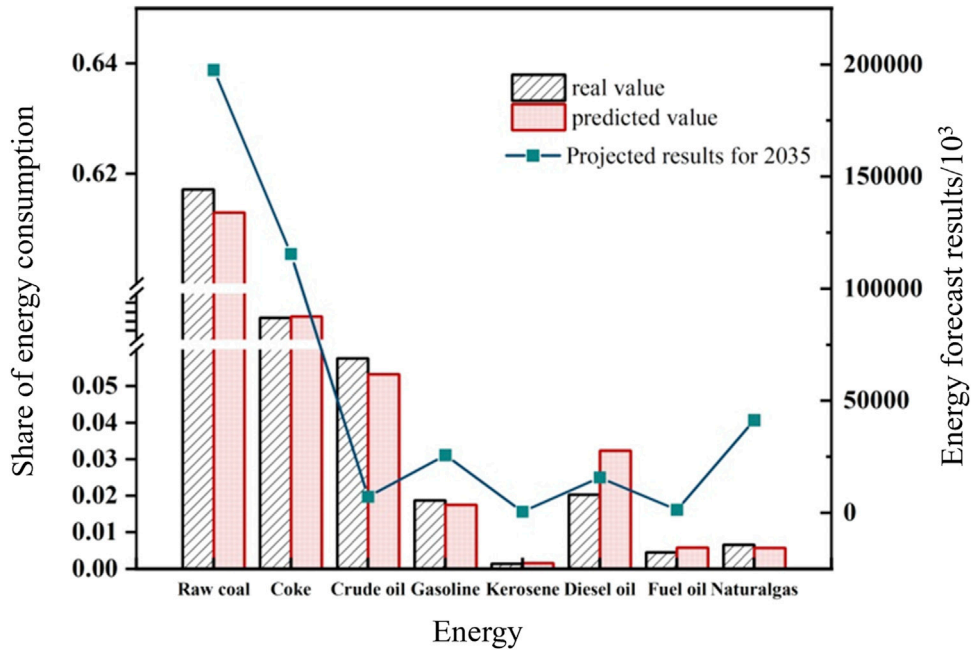

FIGURE 4
Share of energy consumption in the Baiyangdian Basin by energy source and projections.

TABLE 10 Total land use carbon emissions prediction results under multi-scenario simulations (10^3 t).

Land use type	Carbon sink absorption	Carbon source emissions	Net carbon emissions
2020	−792.08	261,546.98	260,754.90
Natural development scenario	−795.56	405,033.60	404,238.04
Balanced development scenario	−811.42	405,020.87	404,209.44
Cultivated land protection scenario	−799.19	405,030.82	404,231.63
Double carbon target scenario	−817.87	405,020.74	404,202.87

5 Conclusion and discussion

5.1 Discussion

The macro-scale carbon sinks in the study area could be rapidly accounted for using the direct carbon emission coefficients of the different land types. The relevant national-scale or regional studies by Fang Jingyun and other scholars (2023) served as the basis for the direct carbon emission coefficients of land use employed in this study. The next step should be to improve the monitoring of ecosystem carbon fluxes across countries and the investigation of carbon density across the various land types to correct the coefficients in a localized manner. Additionally, the GeoSOS-PLUS model combines the transformation, as well as pattern analysis strategies, which can effectively uncover the causes of land type changes and compare the simulation results for various scenarios. This can offer guidance for decision-making and future policy planning. In contrast to Zhou et al. (2020) who used the conventional CA-Markov model to simulate the land use in the built-up land of the urban Shanghai area, our experimental results demonstrated that the GeoSOS-PLUS model significantly improved the simulation and predictions of land use patterns in the Baiyangdian basin, with an overall accuracy of 99%. This addressed the issue of the conventional CA model not adequately accounting for the connection between the influencing variables and spatial changes.

Based on the goal of carbon neutrality, this study makes the following suggestions:

a) The government should strictly regulate the unchecked growth of built-up in developing areas; moderately resume plowing in forests, lakes, and grasslands; and boost the capacity of forests as carbon sinks. They must realize the concept of increasing sinks and reducing sources through the creation of rational and scientific land use policies.
b) Improving the industrial and energy consumption structures; investing more in clean energy resources; and creating a green, diversified energy supply system should be prioritized.
c) When creating the national “dual carbon” roadmap, the unbalanced distribution of regional carbon sources and

sinks must be considered and objectively examined for their growth potential.

It should be noted that this paper uses fixed coefficients to calculate carbon emissions, and the coefficients can be optimized by combining the localized measured data or by using multi-source remote sensing image data to improve the accuracy of the calculation. When analyzing the transmission effect of carbon emissions, this paper does not consider the difference in carbon emission coefficients of the same land use type in different counties and cities, and the same land type in different regions may have differences in carbon emission capacity due to factors such as the degree of land intensification. In the future, we will carry out in-depth research on the refinement of the carbon transmission effect due to the internal transformation of land use types. In addition, there is a long way to go to achieve the goal of "double carbon," and the carbon emission accounting and prediction model established for the characteristics of China's land use has clarified the important paths affecting China's carbon emissions from land use and has been widely applied in cities in the central and eastern parts of China as well as in northern China. For regions outside of China, it is necessary to combine regional characteristics, add more factors describing land characteristics, and continuously improve the accuracy of the model, which can also be committed to the study of carbon emissions in other regions.

5.2 Conclusion

In this study, we first analyzed the land use carbon emissions and subsequent transmissions caused by land use changes in the Baiyangdian basin. We then simulated four scenarios based on the GeoSOS-FLUS model, namely, natural development, balanced development, cultivable land protection, and double-carbon target (Yang et al., 2022), and finally predicted the land use carbon emissions in the Baiyangdian basin in 2035 using a Markov model. The double-carbon target scenario further illustrated the critical position of ecological conservation (Ke N. et al., 2022). In general, from the new direction of carbon emission control, combined with regional land use, our study makes outstanding contributions to regional land rational planning and ecological protection (Chen et al., 2022). The primary conclusions of the study are as follows:

1. The ratio of the Baiyangdian basin carbon source emission to sink absorption has been steadily increasing, especially rapidly in 2020, reaching a maximum of 330.21, 4.9 times higher than in 2000. This shows that the carbon sources (sinks) are consistently rising (declining). Over the past 20 years, the net land use carbon emissions in the basin increased by 208,591.88 × 10^3 t, with an average yearly rise of 10,429.59 × 10^3 t.
2. The net carbon emissions from land transfer in the basin exhibit a clear rising trend between 2000 and 2020. The carbon conduction effect due to forests and grasslands being converted to built-up land also shows an increasing trend, whereas the reverse transfer from built-up land to carbon sinks increases only slightly.
3. After simulating four scenarios in the Baiyangdian basin in 2035, it was found that the net land use carbon emissions under the natural development, balanced development, cultivable land protection, and double-carbon target scenarios are predicted to be 404,238.04 × 10^3, 402,009.45 × 10^3, 404,231.64 × 10^3, and 404,202.87 × 10^3 t, respectively, much higher than the values in 2020. However, carbon emissions from cultivable lands show a decreasing trend; the rate of increase of carbon emissions from built-up lands slowed down, and the carbon absorption by forests and grasslands gradually increased. These trends establish the carbon source-sink ratio as a highly suitable parameter for the future planning of ecological vs economic development.

Data availability statement

The original contributions presented in the study are included in the article/supplementary material, further inquiries can be directed to the corresponding author.

Author contributions

XG: Writing–original draft, Writing–review and editing. MiZ: Writing–original draft, Writing–review and editing. MnZ: Writing–original draft, Writing–original draft. ZG: Writing–review and editing. XL: Writing–review and editing. ZY: Writing–review and editing.

Funding

The authors declare that financial support was received for the research, authorship, and/or publication of this article. This project is supported by the National Natural Science Foundation of China (NSFC): Research on Safety Resilience Evaluation of Critical Infrastructure Systems in Urban Cities and Optimization of Operation (72374063); the National Natural Science Foundation of China (NSFC): Realization Mechanisms, Influencing Factors and Optimization of Urban Ecosystem Service Delivery: A Case Study of Beijing and its Surrounding Areas (42371279); the Social Science Foundation of Hebei Province: Research on Optimization of Ecological Spatial Pattern and Quality Improvement of Baiyangdian Basin Based on Multi-source Data (HB22GL030) Funding Support.

Conflict of interest

The authors declare that the research was conducted in the absence of any commercial or financial relationships that could be construed as a potential conflict of interest.

Publisher's note

References

Affuso, E., and Hite, D. (2013). A model for sustainable land use in biofuel production: an application to the state of Alabama. *Energy Econ.* 37, 29–39. doi:10.1016/j.eneco.2013.01.003

Ali, G., Pumijumnong, N., and Cui, S. (2018). Valuation and validation of carbon sources and sinks through land cover/use change analysis: the case of Bangkok metropolitan area. *Land use policy* 70, 471–478. doi:10.1016/j.landusepol.2017.11.003

Carpio, A., Ponce-Lopez, R., and Lozano-García, D. F. (2021). Urban form, land use, and cover change and their impact on carbon emissions in the Monterrey Metropolitan area, Mexico. *Urban Clim.* 39, 100947. doi:10.1016/j.uclim.2021.100947

Chen, H., Qi, S., and Tan, X. (2022). Decomposition and prediction of China's carbon emission intensity towards carbon neutrality: from perspectives of national, regional and sectoral level. *Sci. Total Environ.* 825, 153839. doi:10.1016/j.scitotenv.2022.153839

Chuai, X., Huang, X., Qi, X., Li, J., Zuo, T., Lu, Q., et al. (2016). A preliminary study of the carbon emissions reduction effects of land use control. *Sci. Rep.* 6, 36901. doi:10.1038/srep36901

Chuai, X., Yuan, Y., Zhang, X., Guo, X., Zhang, X., Xie, F., et al. (2019). Multiangle land use-linked carbon balance examination in Nanjing City, China. *Land Use Policy* 84, 305–315. doi:10.1016/j.landusepol.2019.03.003

Chuai, X. W., Lai, L., Huang, X. J., Zhao, R., Wang, W., and Chen, Z. (2012). Temporospatial changes of carbon footprint based on energy consumption in China. *J. Geogr. Sci.* 22 (1), 110–124. (in Chinese). doi:10.1007/s11442-012-0915-4

Fang, J., Chen, A., Peng, C., Zhao, S., and Ci, L. (2001). Changes in forest biomass carbon storage in China between 1949 and 1998. *Science* 292, 2320–2322. doi:10.1126/science.1058629

Ghorbani, M., Amirahmadi, E., Konvalina, P., Moudry, J., Kopecky, M., and Hoang, T. N. (2023). Carbon pool dynamic and soil microbial respiration affected by land use alteration: a case study in humid subtropical area. *Land* 12, 459. doi:10.3390/land12020459

Ghosh, S., Dinda, S., Das Chatterjee, N., Dutta, S., and Bera, D. (2022). Spatial-explicit carbon emission-sequestration balance estimation and evaluation of emission susceptible zones in an Eastern Himalayan city using Pressure-Sensitivity-Resilience framework: an approach towards achieving low carbon cities. *J. Clean. Prod.* 336, 130417. doi:10.1016/j.jclepro.2022.130417

Guo, X., and Fang, C. (2021). Integrated land use change related carbon source/sink examination in jiangsu province. *Land* 10, 1310. doi:10.3390/land10121310

Harper, A. B., Powell, T., Cox, P. M., House, J., Huntingford, C., Lenton, T. M., et al. (2018). Land-use emissions play a critical role in land-based mitigation for Paris climate targets. *Nat. Commun.* 9, 2938. doi:10.1038/s41467-018-05340-z

Hong, C., Burney, J. A., Pongratz, J., Nabel, J. E., Mueller, N. D., Jackson, R. B., et al. (2021). Global and regional drivers of land-use emissions in 1961–2017. *Nature* 589, 554–561. doi:10.1038/s41586-020-03138-y

Houghton, R. A., and Nassikas, A. A. (2017). Global and regional fluxes of carbon from land use and land cover change 1850–2015. *Glob. Biogeochem. Cycles* 31, 456–472. doi:10.1002/2016gb005546

Ke, N., Lu, X., Zhang, X., Kuang, B., and Zhang, Y. (2022a). Urban land use carbon emission intensity in China under the "double carbon" targets: spatiotemporal patterns and evolution trend. *Environ. Sci. Pollut. Res.* 30 (7), 18213–18226. doi:10.1007/s11356-022-23294-0

Ke, Y., Xia, L., Huang, Y., Li, S., Zhang, Y., Liang, S., et al. (2022b). The carbon emissions related to the land-use changes from 2000 to 2015 in Shenzhen, China: implication for exploring low-carbon development in megacities. *J. Environ. Manag.* 319, 115660. doi:10.1016/j.jenvman.2022.115660

Le Quéré, C., Andres, R. J., Boden, T., Conway, T., Houghton, R. A., House, J. I., et al. (2012). The global carbon budget 1959–2011. *Earth Syst. Sci. Data Discuss.* 5, 165–185. doi:10.5194/essd-5-165-2013

Li, W., Chen, Z., Li, M., Zhang, H., Li, M., Qiu, X., et al. (2023). Carbon emission and economic development trade-offs for optimizing land-use allocation in the Yangtze River Delta, China. *Ecol. Indic.* 147, 109950. doi:10.1016/j.ecolind.2023.109950

Li, Y., Ge, Y. X., and Liang, Y. (2013). Relationship between agricultural carbon emissions and agricultural gross value of output. *Chin. J. Agric. Resour. Regional Plan.* 34, 60–65. doi:10.7621/cjarrp.1005-9121.20130310

Li, Y., Huang, X., Zhen, F., Zhang, H. L., Qi, Y. W., and Wang, T. (2008). Simple sequence repeat analysis of genetic diversity in primary core collection of peach (Prunus persica). *Trans. Chin. Soc. Agric. Eng.* 24 (2), 102–110. doi:10.1111/j.1744-7909.2007.00598.x

Liebmann, H., and Kuder, T. (2012). Pathways and strategies of urban regeneration-deindustrialized cities in eastern Germany. *Eur. Plan. Stud.* 20, 1155–1172. doi:10.1080/09654313.2012.674348

Liu, L. Y., Zheng, B. H., and Bedra, K. B. (2018). Quantitative analysis of carbon emissions for new town planning based on the system dynamics approach. *Sustain. Cities Soc.* 42, 538–546. doi:10.1016/j.scs.2018.08.006

Lu, X., Zhang, Y., Li, J., and Duan, K. (2022). Measuring the urban land use efficiency of three urban agglomerations in China under carbon emissions. *Environ. Sci. Pollut. Res.* 29, 36443–36474. doi:10.1007/s11356-021-18124-8

Ma, X., and Wang, Z. (2015). Progress in the study on the impact of land-use change on regional carbon sources and sinks. *Acta Ecol. Sin.* 35, 5898–5907. doi:10.5846/stxb201312112932

Mendelsohn, R., and Sohngen, B. (2019). The net carbon emissions from historic land use and land use change. *J. For. Econ.* 34, 263–283. doi:10.1561/112.00000505

Piao, S., He, Y., Wang, X., and Chen, F. (2022). Estimation of China's terrestrial ecosystem carbon sink: methods, progress and prospects. *Sci. China Earth Sci.* 65, 641–651. doi:10.1007/s11430-021-9892-6

Qiao, W. F., Mao, G. X., Wang, Y. H., et al. (2016). Research on urban expansion and land use change in Nanjing over the past 32 years. *Journal of Geo-information Science* 18(2), 200–209. doi:10.3724/SP.J.1047.2016.00200

Raihan, A., Muhtasim, D. A., Farhana, S., Hasan, M. A. U., Pavel, M. I., Faruk, O., et al. (2022). Nexus between economic growth, energy use, urbanization, agricultural productivity, and carbon dioxide emissions: new insights from Bangladesh. *Energy Nexus* 8, 100144. doi:10.1016/j.nexus.2022.100144

Rong, T., Zhang, P., Zhu, H., Jiang, L., Li, Y., and Liu, Z. (2022). Spatial correlation evolution and prediction scenario of land use carbon emissions in China. *Ecol. Inf.* 71, 101802. doi:10.1016/j.ecoinf.2022.101802

Sun, Q., Qi, W., and Yu, X. (2021). Impacts of land use change on ecosystem services in the intensive agricultural area of North China based on Multi-scenario analysis. *Alexandria Eng. J.* 60, 1703–1716. doi:10.1016/j.aej.2020.11.020

Tang, W., Cui, L., Zheng, S., and Hu, W. (2022). Multi-scenario simulation of land use carbon emissions from energy consumption in shenzhen, China. *Land* 11, 1673. doi:10.3390/land11101673

Tao, Y., Li, F., Wang, R., and Zhao, D. (2015). Effects of land use and cover change on terrestrial carbon stocks in urbanized areas: a study from Changzhou, China. *J. Clean. Prod.* 103, 651–657. doi:10.1016/j.jclepro.2014.07.055

Walker, W. S., Gorelik, S. R., Cook-Patton, S. C., Baccini, A., Farina, M. K., Solvik, K. K., et al. (2022). The global potential for increased storage of carbon on land. *Proc. Natl. Acad. Sci.* 119 (23), e2111312119. doi:10.1073/pnas.2111312119

Wang, H., Jin, Y., Hong, X., Tian, F., Wu, J., and Nie, X. (2022a). Integrating IPAT and CLUMondo models to assess the impact of carbon peak on land use. *Land* 11, 573. doi:10.3390/land11040573

Wang, W., Wang, W., Xie, P., and Zhao, D. (2020). Spatial and temporal disparities of carbon emissions and interregional carbon compensation in major function-oriented zones: a case study of Guangdong province. *J. Clean. Prod.* 245, 118873. doi:10.1016/j.jclepro.2019.118873

Wang, Y., Shen, J., Yan, W., and Chen, C. (2019). Backcasting approach with multi-scenario simulation for assessing effects of land use policy using GeoSOS-FLUS software. *MethodsX* 6, 1384–1397. doi:10.1016/j.mex.2019.05.007

Wang, Z., Li, X., Mao, Y., Li, L., Wang, X., and Lin, Q. (2022b). Dynamic simulation of land use change and assessment of carbon storage based on climate change scenarios at the city level: a case study of Bortala, China. *Ecol. Indic.* 134, 108499. doi:10.1016/j.ecolind.2021.108499

Wolswijk, G., Barrios Trullols, A., Hugé, J., Otero, V., Satyanarayana, B., Lucas, R., et al. (2022). Can mangrove silviculture Be carbon neutral? *Remote Sens.* 14, 2920. doi:10.3390/rs14122920

Wu, Z., Zhou, L., and Wang, Y. (2022). Prediction of the spatial pattern of carbon emissions based on simulation of land use change under different scenarios. *Land* 11, 1788. doi:10.3390/land11101788

Xia, C., Zhang, J., Zhao, J., Xue, F., Li, Q., Fang, K., et al. (2023). Exploring potential of urban land-use management on carbon emissions-A case of Hangzhou, China. *Ecol. Indic.* 146, 109902. doi:10.1016/j.ecolind.2023.109902

Yang, B., Chen, X., Wang, Z., Li, W., Zhang, C., and Yao, X. (2020). Analyzing land use structure efficiency with carbon emissions: a case study in the Middle Reaches of the Yangtze River, China. *J. Clean. Prod.* 274, 123076. doi:10.1016/j.jclepro.2020.123076

Yang, S., Fu, W., Hu, S., and Ran, P. (2022). Watershed carbon compensation based on land use change: evidence from the Yangtze River Economic Belt. *Habitat Int.* 126, 102613. doi:10.1016/j.habitatint.2022.102613

Yang, X., and Liu, X. (2022). Carbon conduction effect and temporal-spatial difference caused by land type transfer in Chang-Zhu-Tan urban agglomeration from 1995 to 2018. *Acta Ecol. Sin.* 42, 338–347. doi:10.1016/j.chnaes.2022.02.004

Yang, X., and Liu, X. Z. (2023). Path analysis and mediating effects of influencing factors of land use carbon emissions in Chang-Zhu-Tan urban agglomeration. *Technol. Forecast. Soc. Change* 188, 122268. doi:10.1016/j.techfore.2022.122268

Yao, Y., Sun, Z. H., Li, L. L., Cheng, T., Chen, D. S., Zhou, G. X., et al. (2023). CarbonVCA: a cadastral parcel-scale carbon emission forecasting framework for peak carbon emissions. *Cities* 138, 104354. doi:10.1016/j.cities.2023.104354

Yu, Z., Chen, L., Tong, H., Chen, L., Zhang, T., Li, L., et al. (2022). Spatial correlations of land-use carbon emissions in the Yangtze River Delta region: a perspective from social network analysis. *Ecol. Indic.* 142, 109147. doi:10.1016/j.ecolind.2022.109147

Yue, C., Ciais, P., Houghton, R. A., and Nassikas, A. A. (2020). Contribution of land use to the interannual variability of the land carbon cycle. *Nat. Commun.* 11, 3170. doi:10.1038/s41467-020-16953-8

Zhang, D., Wang, Z., Li, S., and Zhang, H. (2021). Impact of land urbanization on carbon emissions in urban agglomerations of the middle reaches of the Yangtze River. *Int. J. Environ. Res. Public Health* 18, 1403. doi:10.3390/ijerph18041403

Zhang, J., Zhang, A., Dong, J., and Basin, E. (2014a). Carbon emission effect of land use and influencing factors decomposition of carbon emission in Wuhan urban agglomeration. *Resour. Environ. Yangtze Basin* 23, 595–602. doi:10.11870/cjlyzyyhj201405001

Zhang, M., Zhang, Z., Huang, X. J., et al. (2014b). Design and development of gis and rs-based land use carbon balance accounting module. *Bulletin of Surveying and Mapping* 2, 101–103. doi:10.13474/j.cnki.11-2246.2014.0065

Zhao, C., Gong, J., Zeng, Q., Yang, M., and Wang, Y. (2021). Landscape pattern evolution processes and the driving forces in the wetlands of lake Baiyangdian. *Sustainability* 13, 9747. doi:10.3390/su13179747

Zhou, L., Dang, X. W., Sun, Q. K., and Wang, S. H. (2020). multi-scenario simulation of urban land change in Shanghai by random forest and CA-Markov model. *Sustain. Cities Soc.* 55, 102045. doi:10.1016/j.scs.2020.102045

Zhou, Y., Chen, M., Tang, Z., and Mei, Z. (2021). Urbanization, land use change, and carbon emissions: quantitative assessments for city-level carbon emissions in Beijing-Tianjin-Hebei region. *Sustain. Cities Soc.* 66, 102701. doi:10.1016/j.scs.2020.102701

frontiers | Frontiers in Environmental Science

TYPE Original Research
PUBLISHED 10 April 2024
DOI 10.3389/fenvs.2024.1347592

OPEN ACCESS

EDITED BY
Chenxi Li,
Xi'an University of Architecture and Technology, China

REVIEWED BY
Zhiheng Yang,
Shandong University of Finance and Economics, China
Arabinda Maiti,
Vidyasagar University, India

*CORRESPONDENCE
Jinying Zhang,
605907211@qq.com

RECEIVED 01 December 2023
ACCEPTED 19 March 2024
PUBLISHED 10 April 2024

CITATION
Chen J, Zhang J, Du H and Zhang T (2024), Evolution characteristics, carbon emission effects and influencing factors of production-living-ecological space in Taihang Mountain poverty belt, China.
Front. Environ. Sci. 12:1347592.
doi: 10.3389/fenvs.2024.1347592

Evolution characteristics, carbon emission effects and influencing factors of production-living-ecological space in Taihang Mountain poverty belt, China

Jing Chen[1,2], Jinying Zhang[3]*, Hui Du[1,2] and Tianmeng Zhang[4]

[1]School of Public Administration, Hebei University of Economics and Business, Shijiazhuang, China, [2]Hebei Collaborative Innovation Center for Urban-rural Integrated Development, Hebei University of Economics and Business, Shijiazhuang, China, [3]Qing Gong College, North China University of Science and Technology, Tangshan, China, [4]Financial Department, Hebei University of Economics and Business, Shijiazhuang, China

The rapid advancement of urbanization and industrialization in China has gradually spread to the poor mountainous areas, which has not only brought about rapid economic development but has also caused the increasing competition for production-living-ecological spaces (PLES) and many ecological and environmental problems, carbon emissions have also increased. As an economically less developed and ecologically fragile area in China, whether the transition of the PLES in the mountain poverty belt has unique characteristics? How the PLES transition in mountainous areas affects carbon emissions and what are the important factors affecting carbon emissions? To explore these issues in depth, we studied the Taihang Mountain area in Shijiazhuang (TMS) using remote sensing image interpretation data from 2000, 2010, and 2020, and we analyzed the PLES evolution characteristics, carbon emission changes, carbon emission effects and its influencing factors of PLES. The results are as follows: 1) The TMS was dominated by ecological and production space. From 2000 to 2020, the production space decreased by 384.66 km^2, the ecological space increased by 123.80 km^2, and the living space increased by 260.86 km^2. Agricultural production space was mainly converted to ecological and rural living space. Industrial and mining productive space was mainly converted to agricultural productive space and urban living space. 2) The study area was in a state of carbon deficit, the transition of ecological space and agricultural productive space to industrial and mining productive space and living space were the main transition types caused the carbon emissions increasing, and that of industrial and mining productive space to agricultural productive space was the main type caused the carbon emissions decreasing. 3) The proportion of construction land, urbanization rate and proportion of secondary industry are the main factors leading to the increase of carbon emissions. Per capita energy consumption, forest coverage and proportion of tertiary industry are the main factors leading to the decrease of

carbon emissions. This can provide new ideas for research on carbon emissions from land-use changes and a theoretical basis for the optimization of territorial space in the mountainous areas of China.

KEYWORDS

carbon emission effects, production-living-ecological space, influencing factors, carbon neutralization, transition

1 Introduction

Recently, China has made significant progress in its economic development. Simultaneously, rapid urbanization and industrialization have led to man–land and production–living–ecological spaces (PLES) conflicts, which have caused many ecological and environmental problems, including rapid increases in carbon emissions. The carbon emissions of China account for about 25% of the global total (Zhou, et al., 2023). The Chinese government has been committed to achieve carbon peak and carbon neutrality by 2030 and 2060. With the implementation of Chinese territorial spatial planning, the priority of China's land management strategy has shifted from land-use patterns to space regulation, that is, the PLES mode (Zhang et al., 2021). PLES transition is a deepening application of land-use transition in the new era. Many studies have shown that land-use transition is an important cause of carbon emissions (Houghton, 2018). It is unknown how the PLES transition affect carbon emissions. Mountainous areas in China are economically less developed and ecologically fragile, as well as important ecological environment protection areas and carbon sink sources. Recently, these areas have faced the dual tasks of economic development and ecological protection, causing a complicated land-use transition (Zhang et al., 2018) and the conflict of PLES, which has induced a series of social, economic, and ecological effects. Therefore, it is important to study PLES transition and its carbon emission effect.

Land use is a hotspot issue facing mankind (Arrow, et al., 1995), and many studies have been carried out on the issue, focusing on land-use transitions (Drummond et al., 2017), land use/cover changes (LUCCs) (Goldewijk, 2001; Winkler et al., 2021), the effects of land use/cover changes on biodiversity (Newbold et al., 2015), ecosystem services (Balthazar et al., 2014), greenhouse gases (de Sousa-Neto et al., 2018), nitrogen (Ojoyi et al., 2017), and the influencing factors of land use change (Weber et al., 2001; Deslatte et al., 2022; Lambin et al., 2011). With the introduction of PLES in China and its gradual evolution into an important theoretical direction land use, many studies have been conducted under the framework of PLES, such as the functional identification and spatial division (Duan et al., 2021; Bai et al., 2022), coupling coordination analysis (Yang et al., 2020; Cui et al., 2022), spatial conflict (Zhao et al., 2022), and spatial pattern optimization (Tian et al., 2020; Liao et al., 2022).Among them, research on the transition of PLES and ecological effects is currently a very important research aspect, involving research on ecosystem service value (Wang et al., 2022), eco-environment quality (Yang et al., 2018), and study areas covering China (Kong et al., 2021), provinces (Chen et al., 2022), and cities (Jiang et al., 2022). As an economically less developed and ecologically fragile area in China, it is worth studying further whether the transition of the PLES in the mountain poverty belt has unique characteristics.

Land-use change is one of the most important causes of carbon emissions. The net carbon emissions from land-use changes accounted for 12.5% of total carbon emissions in the world from 1990 to 2010 (Houghton et al., 2012). About 1/4 of anthropogenic carbon emissions were caused by land-use changes over the past 20 years (Barnett et al., 2005). In tropical Asia, carbon emissions from land-use change accounted for approximately 75% of total carbon emissions (Houghton and Hackler, 1999). Land use changes may emit tens of billions of tons of carbon over the next few centuries (Schimel, 2010). How does PLES transition affect China's carbon emissions? Some researchers pointed out that the spatial evolution of PLES has a negative impact on carbon emissions (Liu et al., 2023). Some researchers pointed out that the expansion of living space leads to an increase in carbon emissions (Li et al., 2023), and some researchers believed that the transition of ecological space to production and living spaces was the main reason for the increase in carbon emissions (Zheng et al., 2022). Mountainous areas in China are important carbon sink sources and play a vital role in protecting the regional ecological environment and reducing carbon emissions. Therefore, the manner in which the PLES transition in mountainous areas affects regional carbon emissions requires further study.

Influencing factors of carbon emissions is another significant research direction of carbon emissions. Many studies point out that economics, population, technology, industrial structures, and energy structures significantly affect carbon emissions (Ang et al., 1998; Chontanawat, 2018; Vujovi et al., 2018). Generally, economic increase and population growth caused the increasing of energy demand, therefore resulting in increased carbon emissions (Henriques and Borowiecki, 2017; Li, 2020). It shows an inverted U-shaped relationship between economic development and carbon emissions (Hidemichi et al., 2018; Arshed et al., 2021). Technological progress and industrial structure optimization are helpful to decreasing carbon emissions (Wang, et al., 2018). Urbanization is also an important reason in regard to the increase in carbon emissions in Asian countries (Shahbaz et al., 2015; Nosheen et al., 2020). Afforestation increases carbon sinks, whereas deforestation increases carbon emissions (Woodbury et al., 2007). Whether the transition of the PLES has a direct impact on carbon emissions requires further investigation. What are the important factors affecting carbon emissions in mountainous areas? It should be noted though that there are few studies on special regions, especially mountain poverty belts.

Based on this, this study takes the Taihang Mountains area of Shijiazhuang (TMS) in China as an example, aimed to deeply analyze the carbon emission effects of the PLES and examine the influencing factors on carbon emissions. The indicators of "Contribution rate of PLES transition to carbon emissions" and "Marginal carbon emissions of PLES" were introduced to describe

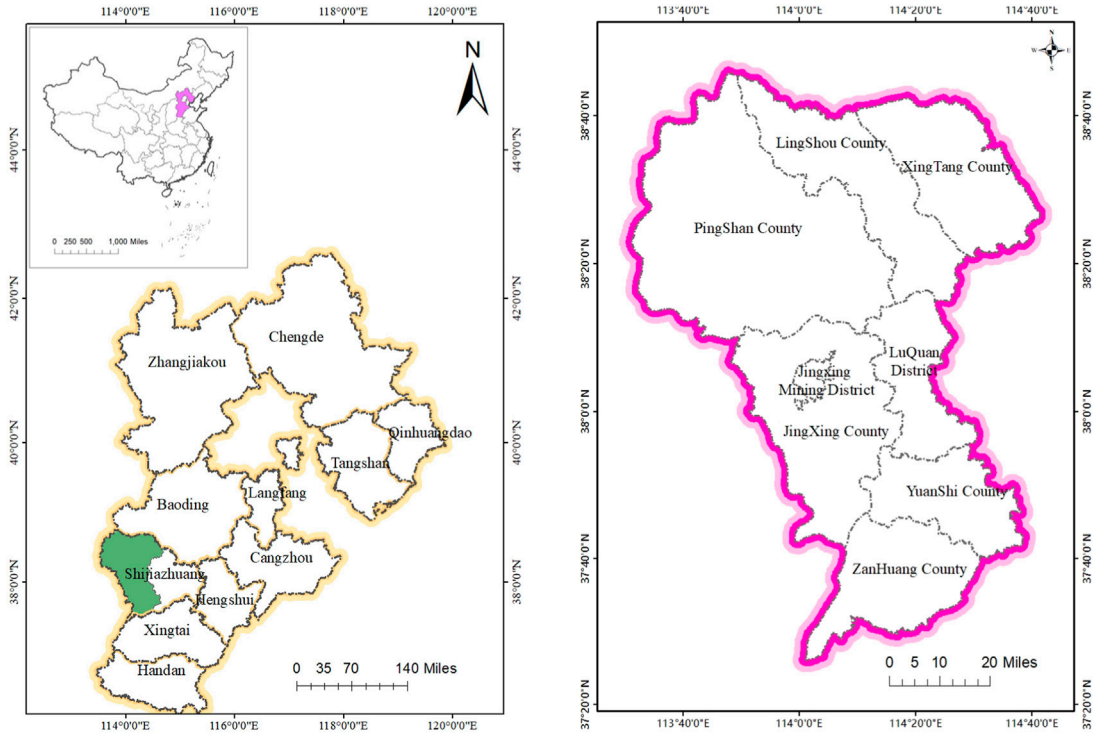

FIGURE 1
The geographical location of TMS.

the carbon emission effects, and the Improved STIRPAT Model was used to examine the influencing factors on carbon emissions. Theoretically, this study can provide new ideas for international research on land-use change and carbon emissions, and enrich international research on the factors influencing carbon emissions. Practically, the results of this study can provide a theoretical basis for the optimization of land space and low-carbon development in mountainous areas of China and provide a reference for the formulation of relevant land space control policies.

According to the purpose, the remaining elements of the paper is arranged as follows. The Materials and Methods are organized in Section 2, and Section 3 is Results analysis. The final Section 4 concludes Discussion, Conclusion and the Policy suggestions.

2 Materials and methods

2.1 Study area

The Taihang Mountain area in the west of Shijiazhuang (TMS) is located in the middle of the Taihang Mountain area in Hebei Province (Figure 1) between 37° 27′-38° 42′N and 113° 31′- 114° 33′E, and it includes Xingtang County, Lingshou County, Pingshan County, Jingxing Mining Area, Luquan District, Jingxing County, Yuanshi County, and Zanhuang County. The terrain of the TMS is high in the west and low in the east, with an altitude of 100–2281 m. The geomorphic types vary and are complicated; there are mid-mountains, low mountains, hills, intermountain basins, and valleys from east to west. The study area is ecologically fragile. The land use pattern has undergone urban expansion, reduction in cultivated land, deforestation to cultivated land abandonment, and recovery growth of forest land. It is the epitome of the transition of PLES in mountainous areas of China.

2.2 Data sources

Land use data (30 m resolution) from 2000, 2010, and 2020 were obtained from the Data Centre for Resources and Environmental Sciences, Chinese Academy of Sciences (https://www.resdc.cn). Socio-economic data and energy data were obtained from the "Shijiazhuang Economic Statistics Yearbook," and soil data from the second national soil survey of Hebei Province.

About the division of PLES, land use types were divided into single functional types (Chen et al., 2015) and composite functional types (Zhang et al., 2017). Based on the classification criteria (Data Center for Resources and Environmental Sciences, 2018), this paper classifies PLES into 3 primary categories, that is Production space (PS), Living space (LS), Ecological space (ES); and 8 subcategories, that is Agricultural productive space (APS), Industrial and mining productive space (IMPS), Urban living space (ULS), Rural living space (RLS), Forest ecological space (FES), Meadow ecological space (MES), Water ecological space (WES) and Other ecological space (OES).

TABLE 1 Carbon density of production—living–ecological spaces (PLES) Unit: t/hm^2.

Year	APS	IMPS	FES	MES	WES	OES	ULS	RLS
2000	−0.09*	402.92	−0.6036	−0.205	−0.238	−0.05	26.04	0.31
2010	−0.09	670.51	−0.6036	−0.205	−0.238	−0.05	123.51	1.21
2020	−0.09	377.70	−0.6036	−0.205	−0.238	−0.05	90.96	3.99

*Negative values represent carbon sink, positive values represent carbon emissions.

2.3 Methods

2.3.1 Transfer matrix of PLES

The transfer matrix of PLES can not only disclose the PLES structure but also quantitatively describe the dynamic evolution of PLES transition from the beginning to the end. The transfer matrixes of 2000–2010, 2010–2020, and 2000–2020 were obtained using the spatial overlay function of ArcGIS. As shown in Formula 1:

$$S_{ij} = \begin{bmatrix} S_{11} & S_{12} & \ldots & S_{1n} \\ S_{21} & S_{22} & \ldots & S_{2n} \\ \ldots & \ldots & \ldots & \ldots \\ S_{m1} & S_{m2} & \ldots & S_{mn} \end{bmatrix} \quad (1)$$

where S is the area of PLES and S_{ij} *is* the area transferred from type i to type j. Each row in the matrix represents the flow direction from type i to other types, and each column represents the source from other types to type j. The transfer-in and transfer-out areas of PLES were calculated based on the transfer matrix, and the percentage of the transferred area was calculated based on PLES in different periods.

2.3.2 Carbon emission calculation of PLES

2.3.2.1 Calculation of carbon emissions

Carbon emissions are calculated by carbon density and corresponding land use area, the expression is as follows:

$$C_s = \sum_{i=1}^{n} S_i * SD_i \quad (2)$$

where C_s is total carbon emission, S_i is the area of PLES, i = 1,2. n represents the type of PLES, SD_i is carbon density, where "−"represents carbon sink, "+" represents carbon emission.

Referring to the carbon density of different land use types by relevant research (Zhu et al., 2019; Yang et al., 2020), we constructed the preliminary carbon density of PLES in the TMS. On this basis, we modified the soil carbon sink density referring to the soil carbon density of each soil type in Hebei Plain (Luan et al., 2011; Gao et al., 2018). The vegetation carbon sink density was modified based on the carbon density of different vegetation types in North China (Chen, 2003). Furthermore, the carbon emissions density was modified referring to the corresponding relationship between industrial space and energy consumption (Zhao et al., 2010). Finally, we determined the carbon density of PLES in the TMS (Table 1).

2.3.2.2 Contribution rate of PLES transition to carbon emissions

Referring to the index of "ecological contribution rate of land use transition (Yang et al., 2018)," we introduce the index of carbon-emissions contribution rate of PLES transition as follows:

$$R = (C_b\text{-}C_e)S_i/\Delta TC \quad (3)$$

where R is the carbon-emissions contribution rate of the PLES transition, C_b is the carbon density in the beginning, C_e is the carbon density in the end, S_i is the area of PLES transition, and ΔTC is the carbon emission changes during the period.

2.3.2.3 Marginal carbon emissions of PLES

Marginal carbon emissions is the change in carbon emissions caused by the change of per unit PLES, which indicates the sensitivity of the area to carbon emissions (Hu et al., 2015). The expression is as follows:

$$MC = TC/S \quad (4)$$

where MC is the marginal carbon emissions, TC is carbon emission changes, and S is area changes.

2.3.3 Analysis of influencing factors of carbon emissions

2.3.3.1 Improved STIRPAT model

The STIRPAT model was firstly proposed by York and Dietz (York et al., 2003) based on the IPAT identity, and it has been applied widely to examine the influence of population, economy and technology on ecological environment. It also been used to estimate the influencing factors of CO_2 emissions and has good scalability. The basic expression is as follows:

$$I = aP^bA^cT^de \quad (5)$$

where I represents the environmental effect, P represents the population, A represents the wealth, T represents technology; a is the dominant coefficient; b, c, and d are Elasticity coefficients; and e is error.

We take the logarithm of the two sides and construct an extended influencing factors, then get Model (6):

$$\ln I = \ln a + b\ln P + c\ln A + d\ln T + \ln e + f\ln O \quad (6)$$

where I represents CO_2 emissions, ln$a$ is a constant term, ln$e$ is a random distractor, O is added factor.

TABLE 2 Indicator of carbon emission influencing.

Target layer	Indicator layer	Variable	Description of independent variables
Population factors	Total population	P_1	10,000 people
	Urbanization rate	P_2	Proportion of urban population (%)
	Population density	P_3	Number of people living on per unit area(person/m^2)
Economic development	Per capita GDP	A_1	GDP to total population ratio (¥/person)
	Proportion of secondary industry	A_2	Proportion of secondary industry in total GDP (%)
	Proportion of tertiary industry	A_3	Proportion of tertiary industry in total GDP (%)
	Foreign direct investment	A_4	Total amount of foreign direct investment (10,000$)
Technological factors	Energy intensity	T_1	Standardized coal consumption per unit GDP (%)
	Per capita energy consumption	T_2	Energy consumption to total population ratio(t/person)
Other factors	Forest coverage rate	O_1	Proportion of forest land in total area (%)
	Proportion of construction land	O_2	Proportion of construction land in total area (%)
	Number of industrial enterprises above scale	O_3	Number of industrial enterprises with annual revenue of more than 20 million ¥ (individual)
	Per capita disposable income	O_4	¥

TABLE 3 Areas and changes in PLES of the TMS during 2000-2020. Unit: km^2.

Year	APS	IMPS	FES	MES	WES	OES	ULS	RLS
2000	3221.16	29.14	2167.36	2131.68	306.08	23.47	48.27	315.15
2010	3032.63	37.74	2414.58	2020.13	219.50	28.34	105.24	384.15
2020	2840.97	24.67	2308.59	2136.31	278.49	29.00	119.56	504.73
2000–2010	−188.53	8.60	247.22	−111.54	−86.58	4.87	56.97	69.00
2010–2020	−191.66	−13.07	−105.99	116.18	58.99	0.66	14.32	120.58
2000–2020	−380.19	−4.47	141.23	4.63	−27.59	5.52	71.28	189.58

2.3.3.2 Variable description

Based on the research of carbon emissions caused by land use changes (Fahey et al., 2010; Zhang et al., 2021), the land use changes of forest land and construction land will cause carbon emission changes, therefore, the paper added the indicators of forest coverage rate and proportion of construction land. As shown in Table.2.

3 Results

3.1 Evolution characteristics of PLES

PLES in the TMS is dominated by ecological space and production space, of which agricultural productive space accounts for the largest proportion, next came forest ecological space and grassland ecological space; the sum of these three spaces accounts for more than 90% in the TMS. The evolution characteristics of PLES are: 1) From 2000 to 2020, the production space decreased by 384.66 km^2, of which agricultural productive space decreased continuously by a total of 380.19 km^2. Industrial and mining productive space first increased by 8.60 km^2 from 2000 to 2010 and then decreased by 13.07 km^2 from 2010 to 2020. 2) From 2000 to 2020, ecological space increased slightly by 123.80 km^2, of which forest ecological space first increased by 247.22 km^2 from 2000 to 2010 and then decreased by 105.99 km^2 from 2010 to 2020. Meadow ecological space first decreased by 111.54 km^2 from 2000 to 2010 and then increased by 116.18 km^2 from 2010 to 2020. 3) From 2000 to 2020, living space significantly increased by 260.86 km^2. Urban and rural living spaces increased continuously by 71.28 km^2 and 189.58 km^2, respectively (Table 3).

With the rapid economic development and urbanization of Shijiazhuang City, urban and rural living spaces increased rapidly. Also, agricultural productive space was occupied, leading to serious contradictions between living and production land. Recently, with the reformation of the energy structure, high-energy-consumption, high-pollution, and high-emissions industries were eliminated, and the growth in industrial and mining productive space was controlled.

As shown in Figure 2, forest and meadow ecological spaces are mainly distributed in Pingshan, Jingxing, Lingshou, and Zanhuang County. Water ecological space includes Hutuo River, Gangnan Reservoir, and Huangbizhuang Reservoir, which are located in

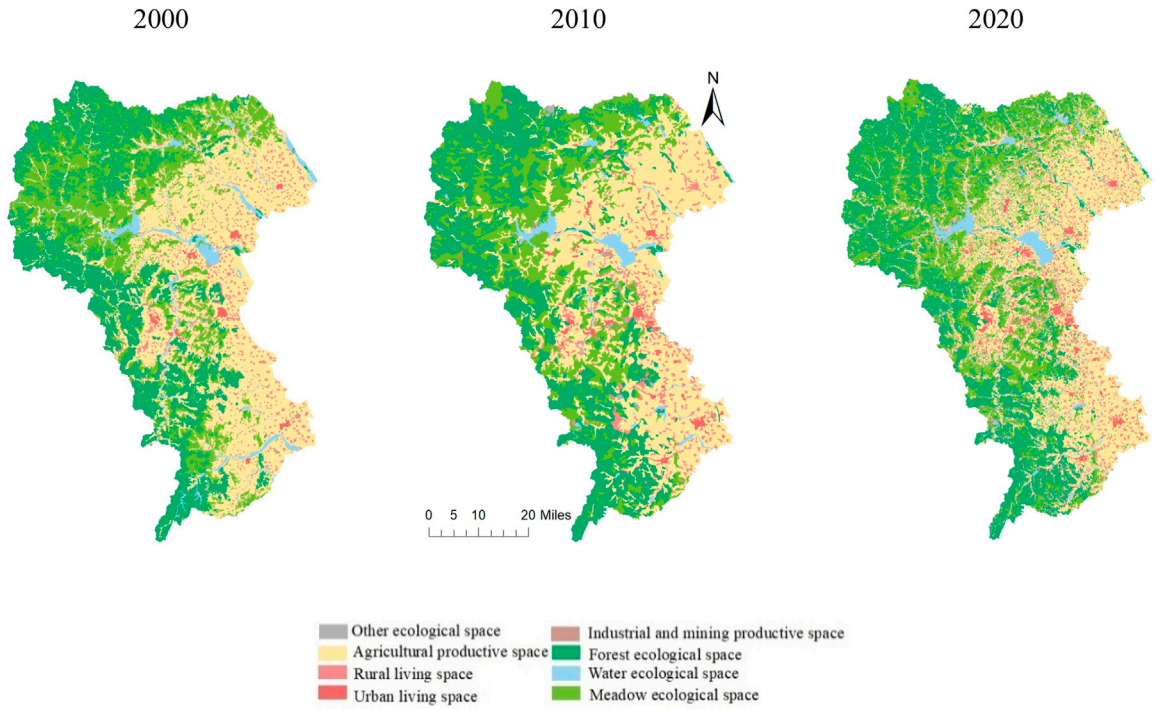

FIGURE 2
PLES distribution of the TMS during 2000-2020.

Pingshan County and Luquan District. Agricultural productive space is mainly located in the east of TMS, such as Xingtang, Luquan, and Yuanshi County. Urban living space is scattered in each county (district) and is concentrated in Luquan District and Jingxing Mining District. Industrial productive space is generally located in the peripheral areas of urban living space, while rural living space is scattered in all counties (districts).

3.2 Transition of PLES

To understand the transition of PLES, we calculated the transition structure and transition rates using Eq. 1, and the results are as follows:

From Table 4 we can see that from the perspective of the transfer-in, agricultural productive space was mainly transferred from meadow ecological space, and industrial and mining productive space was mainly transferred from rural productive land. Forest ecological space was mainly transferred from rural productive space and meadow ecological space, water ecological land was mainly transferred from agricultural productive space, and other ecological space was mainly transferred from forest ecological space and meadow ecological space. Urban living space was mainly transferred from agricultural productive space and rural living space, and rural living space was mainly transferred from agricultural productive space.

From the perspective of the transfer-out, agricultural productive space was mainly converted to forest ecological space, meadow ecological space, and rural living space, and industrial and mining productive space was converted to agricultural productive space and urban living space. Forest ecological space was converted to meadow ecological space, and meadow ecological space was converted to forest ecological space and agricultural ecological space; water ecological space was converted to agricultural productive space and forest ecological space, and other ecological space was converted to agricultural productive space and water ecological space. Finally, urban living space was converted to agricultural productive space, and rural living space was converted to agricultural productive space.

With the rapid urbanization of Shijiazhuang City, huge amounts of agricultural productive space and ecological space was occupied by urban living space. With the implementation of a series of ecological engineering projects such as forest rehabilitation from slope agriculture, the cultivated land with serious soil erosion and obvious ecological vulnerability has gradually transformed into ecological space, further restoring the latter.

3.3 Carbon emission effects of PLES

3.3.1 Spatial-temporal evolution of carbon emission

As shown in Table 5, from 2000 to 2020, carbon emissions were 130.96×10^4 t, 387.69×10^4 t, and 222.06×10^4 t, respectively, and carbon storage was 20.11×10^4 t, 17.33×10^4 t, and 21.55×10^4 t, respectively. The study area has been in a state of carbon deficit. From the perspective of the changing trend, carbon emissions first rapidly increased by 256.73×10^4 t from 2000 to 2010 and then slowly decreased by 165.63×10^4 t from 2010 to 2020. Carbon storage first decreased by 2.78×10^4 t from 2000 to 2010 and then increased by 4.21×10^4 t from 2010 to 2020. The carbon deficit first

TABLE 4 Transition matrix and transition rates of PLES during 2000–2020 Unit: km^2, %.

Year			2020							
	Increase or decrease rate		APS	IMPS	FES	MES	WES	OES	ULS	RLS
2010	APS	Area	—	12.06	153.24	316	99.9	6.88	9.71	134.94
		in	—	0.4	5.4	11.1	3.5	0.2	0.3	4.7
		out	—	0.6	11.2	9.3	2.6	0.1	1.6	9.1
	IMPS	Area	18.59	—	0	0	0	0	0	0
		in	0.6	—	0.0	0.0	0.0	0.0	0.0	0.0
		out	41.4	—	4.8	11.7	0.0	0.0	14.6	6.7
	FES	Area	361.35	1.39	—	660.2	34.05	2.65	0	11.75
		in	15.7	0.1	—	28.6	1.5	0.1	0.0	0.5
		out	7.1	0.0	—	33.9	0.5	0.7	0.0	0.7
	MES	Area	300.32	3.4	735.21	—	14.3	3.86	0	8.62
		in	14.1	0.2	34.4	—	0.7	0.2	0.0	0.4
		out	11.1	0.0	28.6	—	10.7	28.7	4.8	8.1
	WES	Area	83.53	0	11.49	29.76	—	5.75	0	0
		in	30.0	0.0	4.1	10.7	—	2.1	0.0	0.0
		out	3.5	0.0	1.5	0.7	—	0.0	0.0	2.0
	OES	Area	3.9	0	15.58	8.33	0	—	0	0
		in	13.4	0.0	53.7	28.7	0.0	—	0.0	0.0
		out	0.2	0.0	0.1	0.2	2.1	—	1.5	0.3
	ULS	Area	53.05	4.25	0	5.77	0	1.75	—	21.34
		in	44.4	3.6	0.0	4.8	0.0	1.5	—	17.9
		out	0.3	0.0	0.0	0.0	0.0	0.0	—	1.0
	RLS	Area	292.18	1.96	14.64	41	9.88	1.39	5.17	—
		in	57.9	0.4	2.9	8.1	2.0	0.3	1.0	—
		out	4.7	0.0	0.5	0.4	0.0	0.0	17.9	—

* "in" represent Transfer-in rate, "out" represent Transfer-out rate.

10.3389/fenvs.2024.1347592

TABLE 5 Carbon emission structure and changes in PLES. Unit: 10^4 t.

Year	APS	IMPS	FES	MES	WES	OES	ULS	RLS	Total
2000[a]	−2.90	117.41	−13.08	−4.37	−0.73	−0.01	12.57	0.98	109.87
2010[a]	−2.73	253.07	−14.57	−4.14	−0.52	−0.01	129.98	4.65	365.71
2020[a]	−2.56	93.17	−13.93	−4.38	−0.66	−0.01	108.75	20.14	200.51
2000–2010[b]	0.17	135.65	−1.49	0.23	0.21	0.00	117.41	3.67	255.84
2010–2020[b]	0.17	−159.89	0.64	−0.24	−0.14	0.00	−21.23	15.49	−165.20
2000–2020[b]	0.34	−24.24	−0.85	−0.01	0.07	0.00	96.18	19.16	90.64

[a]Negative values represent carbon sink and positive values represent carbon source.
[b]Negative values represent a decrease and positive values represent an increase.

increased by 255.84 × 10^4 t from 2000 to 2010 and then decreased by 165.20 × 10^4 t from 2010 to 2020.

From the perspective of PLES types, agricultural productive space, as well as forest, meadow, water, and other ecological space were carbon sinks, and industrial and mining productive space, urban living space, and rural living space were carbon sources. From 2000 to 2020, the carbon storage of agricultural productive space has been decreasing, with a total reduction of 0.34 × 10^4 t. The carbon storage of ecological space first increased by 1.06 × 10^4 t from 2000 to 2010 and then decreased by 0.26 × 10^4 t from 2000 to 2020, with a total increase of 0.80 × 10^4 t. The carbon emissions of industrial and mining space first increased by 135.65 × 10^4 t from 2000 to 2010 and then decreased by 159.89 × 10^4 t from 2010 to 2020, with a total reduction of 24.24 × 10^4 t. The carbon emissions of urban living space first increased by 117.41 × 10^4 t from 2000 to 2010 and then decreased by 21.23 × 10^4 t from 2010 to 2020, with a total increase of 96.18 × 10^4 t. The emissions of rural residential land increased gradually, with a total increase of 19.16 × 10^4 t. Thus, the carbon emissions have shifted from "high pollution, high emissions" to "low pollution, low emissions." With the implementation of a series of energy conservation policies, coal consumption has dropped significantly and has been replaced by clean energy such as electricity and natural gas, thereby leading to a obviously decrease in carbon emissions.

The data of PLES and carbon density were input into the ArcGIS 10.8 to obtain the carbon emissions pattern (Figure 3). Carbon emissions were divided into high, medium-high, medium, low-medium, and low levels following the equal-interval method by the means of Nature break Point. As shown in Figure 3, low and low-medium levels of carbon emissions belonging to carbon surplus areas were distributed in agricultural productive space and ecological space, mainly in Xingtang, Lingshou, Pingshan, Jingxin, and Zanhuang County. The medium, medium-high, and high levels belonging to carbon emission areas were distributed in industrial and mining productive space, urban living space, and rural living space, mainly in Luquan District, Jingxing Mining District, Yuanshi County. From the perspective of spatial pattern changes, from 2000 to 2010, the low and low-medium levels decreased significantly, whereas the medium level increased obviously. From 2010 to 2020, the low and low-medium levels were further reduced, and the high-level areas increased.

3.3.2 Carbon-emissions contribution rate of PLES

The carbon-emissions contribution rate of PLES was calculated based on Formula 2 (Table 6).

The main transition types of carbon emissions were in agricultural productive space, industrial and mining productive space, urban living space, and rural living space. In the transition types caused the carbon emissions increasing, there are two transition directions. One is from carbon sink to carbon source, such as agricultural production space to industrial and mining productive space, urban living space and rural living space, and meadow ecological space to industrial and mining productive space, accounting for 52.8% of the increase in total carbon emissions. The second is from low-to high-density carbon emissions, such as urban living space to industrial and mining productive space, rural living space to urban living space, and urban living space to urban living space, accounting for 31.9% of the increase in total carbon emissions. In the main transition types caused the carbon emissions reduction, the contribution rate of industrial and mining productive space to agricultural productive space was the highest, followed by industrial and mining productive space to itself, and the third is urban living space to agricultural living space. All three account for 91.5% of the total reduction in carbon emissions.

3.3.3 Marginal change in carbon emissions

The marginal change in carbon emissions can reflect the influence of areas on carbon emissions or sink. The marginal carbon emissions of industrial and mining productive space were the highest at 54231.40 t, followed by urban living space at 13493.02 t; those of rural living space were the lowest at 1010.74 t, indicating that the three PLES types were the main carbon emission sources. The marginal carbon sink of forest ecological space was the highest at 60.36 t, followed by water ecological space and water ecological space at 20.52 t and 23.80 t, respectively, whereas those of agricultural productive space and other ecological space were the lowest at 9.002 t and 5.00 t, indicating that the three PLES types were the main carbon sink sources.

3.4 Influencing factors of carbon emissions

3.4.1 Parameter estimation results of panel data model

Based on panel data from 2000 to 2020, this paper used the improved STIRPAT model to analyze the influencing factors using Stata12.0 software. The results were shown in Table 7.

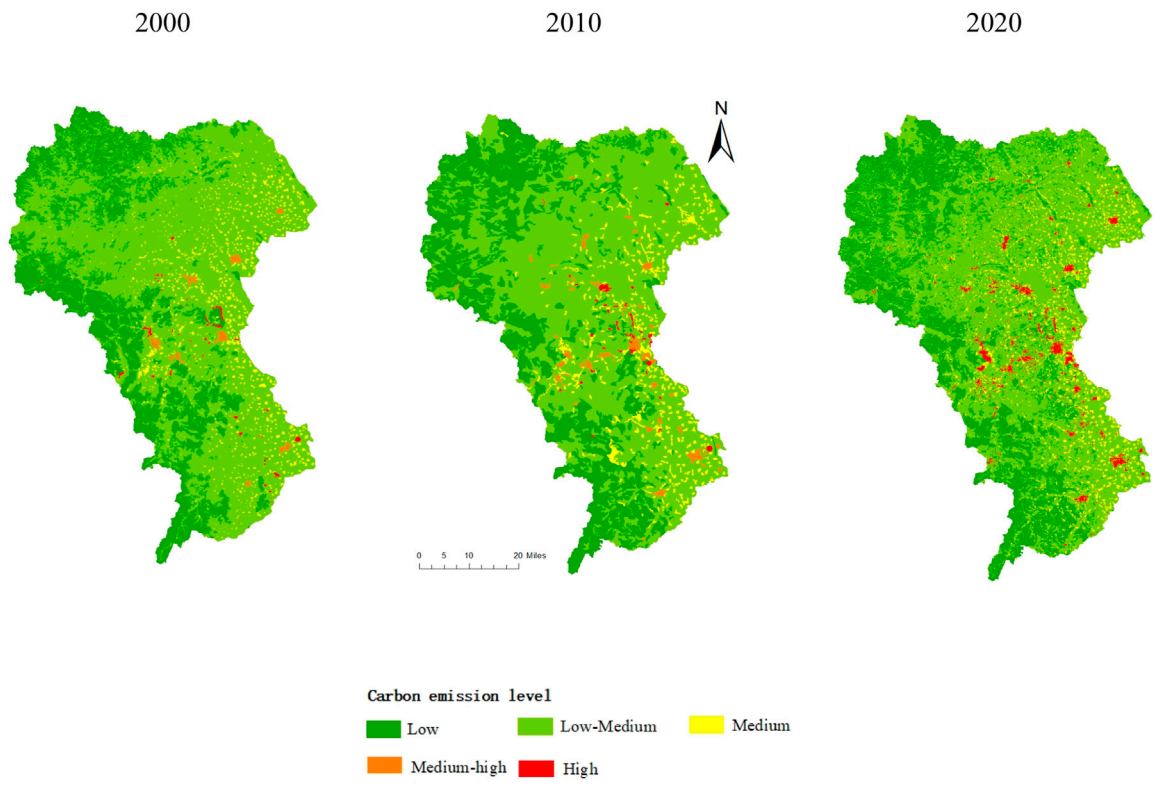

FIGURE 3
Carbon emission pattern of PLES.

It can be seen from Table 7, the coefficient of Total population, Population density, Per capita GDP, Foreign direct investment, Per capita energy consumption, Number of industrial enterprises above scale, Per capita disposable income did not pass the *t*-test, which showed that these indicators did not conform to the Kuznets hypothesis. All the other coefficients passed the *t*-test under the given condition. The baseline regression equation was:

$$\ln C_{it} = 9.535 + 0.956 \ln P_2 + 0.191 \ln A_2 - 0.205 \ln A_3 - 0.986 \ln T_2 - 0.882 \ln O_1 + 0.975 \ln O_2 \quad (7)$$

3.4.2 Analysis of influencing factors

The improved STIRPAT model obtained from the results is shown in Eq. 7. From the fitting results of the model, the order of the effects of the influencing factors was as follows: O_2>P_2>A_2>A_3>O_1>T_2. Among these, the proportion of construction (O_2), land urbanization rate (P_2), and proportion of secondary industry (A_2) were positively correlated with total carbon emissions, while the proportion of tertiary industry (A_3), forest coverage rate (O_1), and *per capita* energy consumption (T_2) were negatively correlated.

The proportion of construction land (O_2) was the strongest factor for the increase of carbon emissions in the TMS, and the elasticity coefficient was found to be 0.975%, indicating that for every 1% increase in the proportion of construction land, the total carbon emissions will increase by 0.975%. This indicates that the transition of the PLES has a direct impact on carbon emissions. For every 1% increase in urbanization rate (P_2), the proportion of secondary industries (A_2), total carbon emissions will increase by 0.956% and 0.191%, respectively. The study area is located in the poverty belt of the Taihang Mountains, and its economic development had low and late starting points. By accelerating industrialization, the economic level has improved, resulting in excessive energy consumption and high carbon emissions.

Per capita energy consumption (T_2) is the strongest factor in regard to the decrease in carbon emissions, and the elasticity coefficient is −0.986%, indicating that for every 1% increase in *per capita* energy consumption, the total carbon emissions will decrease by 0.986%. Therefore, improvements in technology can promote improvements in energy-use efficiency, which is an effective way to reduce total carbon emissions.

The influence coefficient of forest coverage rate (O_1), and Per capita energy consumption (A_3) are −0.882% and −0.205%, respectively, and each increase of 1% will decrease the total carbon emissions by 0.882% and 0.205%, respectively. From 2000 to 2020, the forest coverage rate in the TMS increased from 52.16% to 53.9%, which caused the carbon sink value to increase and the net carbon emissions decreased. It can be seen that the transformation of PLES is an important reason for the decrease of carbon emissions. The tertiary industry in the study area has developed rapidly, from 29.75% in 2000 to 52.62% in 2020. Tertiary industries such as tourism and social services have achieved rapid development. It has low carbon emission intensities, which cause a decrease in carbon emissions.

TABLE 6 Carbon-emissions contribution rate of main PLES transition types Unit: 10^4 t, %.

Types	PLES transition	Carbon emissions	Contribution rate (%)
Increased carbon emissions	APS—IMPS	45.56	33.1
	ULS—ULS	21.68	15.7
	ULS—IMPS	14.95	10.8
	MES—IMPS	12.85	9.3
	APS—ULS	8.84	6.4
	RLS—IMPS	7.4	5.4
	APS—RLS	5.51	4.0
	Total	116.79	84.7
Decreased carbon emissions	IMPS—APS	74.89	50.3
	IMPS—IMPS	47.46	31.9
	ULS—APS	13.86	9.3
	Total	136.21	91.5

TABLE 7 Estimated results of fixed effect model.

Statistics	Coefficient	Standard error
$\ln P_1$	0.105*	0.192
$\ln P_2$	0.956***	12.687
$\ln P_3$	0.852*	1.725
$\ln A_1$	0.108*	0.215
$\ln A_2$	0.191***	6.775
$\ln A_3$	−0.205***	8.355
$\ln A_4$	0.241*	0.441
$\ln T_1$	−0.743*	1.345
$\ln T_2$	−0.986***	7.558
$\ln O_1$	−0.882***	5.993
$\ln O_2$	0.975***	7.921
$\ln O_3$	0.373*	0.721
$\ln O_4$	0.180*	0.354
Time effect	YES	_
Individual effects	YES	_
lna(constant)	9.535***	27.821
R^2	0.652	_
Adjusted R^2	0.613	_
F	12.84	_
NO	24	_

Note: *** and * indicate that the statistical quantity is significance at the significance level of 1% and 10%, respectively. Same as Table 7 and Table 8.

3.4.3 Robustness test

To ensure the reliability of the research results, we conducted a robustness test on the following aspects:

3.4.3.1 Increasing the control variables

To eliminate the influence of the unobservable factors, this study increased the indicator of the proportion of local financial expenditures to GDP and we then conducted a regression analysis once again. In China, the government's macro-control policies can directly affect industrial structure, energy conservation, and emission reduction technology, thus indirectly affecting carbon emissions. With reference to the relevant literature (Zeng et al., 2019), this study selected an indicator of the proportion of local financial expenditure to GDP as the proxy variable for government macro control. The test results indicate that increasing the indicator is consistent with the baseline regression results, which proves the reliability of the regression results (Table 8).

3.4.3.2 Replace the explained variable

The explanatory variables used in the baseline regression were based on carbon emissions from land-use changes. This study used the total carbon emissions of each county obtained from the Statistical Yearbook as explanatory variables. The test results indicated whether the explained variable was replaced, which was consistent with the baseline regression results, thus proving the reliability of the regression results (Table 9).

4 Conclusion and discussion

4.1 Discussion

4.1.1 Comparisons between this paper and previous studies

In terms of the transition of the PLES, the PLES in the TMS experienced the process of first decreasing and then increasing ecological space and continuing to increase the living space, which is consistent with the ecological space changes in the mountainous areas of China (Wang and Liu, 2023) and the trends of forest change in Asia (Hansen, 2013). Driven by rapid industrialization and urbanization, the labor force in the

TABLE 8 Robustness test: increasing control variables.

Statistics	Coefficient	Standard error
lnP_2	0.956***	12.687
lnA_2	0.191***	6.775
lnA_3	−0.205***	8.355
lnT_2	−0.986***	7.558
lnO_1	−0.882***	5.993
lnO_2	0.975***	7.921
the proportion of the local financial expenditure to GDP	0.125*	3.346
Time effect	YES	_
Individual effects	YES	_
lna(constant)	9.535***	27.821
R^2	0.650	_
Adjusted R^2	0.614	_
NO	24	_

TABLE 9 Robustness test: replacing the explained variable.

Statistics	Coefficient	Standard error
lnP_2	0.932***	9.256
lnA_2	0.182***	6.312
lnA_3	−0.197***	7.230
lnT_2	−0.973***	6.903
lnO_1	−0.834***	4.548
lnO_2	0.964***	6.529
Time effect	YES	_
Individual effects	YES	_
lna(constant)	9.361***	25.673
R^2	0.576	_
Adjusted R^2	0.503	_
NO	24	_

mountainous areas has been transferred to cities and towns, leading to natural vegetation restoration and expansion of forestland.

In terms of the carbon emission effects, ecological space is the main source of carbon sinks. The changes seen in the forestland and grassland directly affect the amount of carbon sinks, which is consistent with relevant international research conclusions (Jandl et al., 2007). In recent years, China has vigorously implemented afforestation and strengthened forest management; therefore, the area of ecological space in the TMS has increased, and the carbon sink capacity has improved. The expansion of industrial and mining production and urban living spaces were the main reasons for the increase in carbon emissions, which is consistent with the relevant international research (Grimm et al., 2008; Beesley, 2012; Burgin et al., 2016). However, the difference is that carbon emissions in the study area first increased and then decreased, reflecting it has gone through the process of polluting first and then remediation in the TMS. And it also reflected the conflict in the PLES experienced a process of conflict intensification leading to gradual coordination.

In terms of the factors influencing carbon emissions, urbanization, economic growth, and energy consumption are the main reasons found for the increase in carbon emissions, which is consistent with the research conclusions of developing countries, such as Pakistan and Africa (Aftab et al., 2021; Namahoro et al., 2021). This reflects the enormous pressure on developing countries to reduce carbon emissions. Energy intensity and increased forest area are important reasons for the reduction in carbon emissions, which is consistent with the conclusions of other countries (Ang, 1999; Henriques and Borowiecki, 2017). However, this study argues that the PLES transition, especially the transition between the ecological space and production space, is another important reason for carbon emissions.

4.1.2 Limitations and prospect of this study

Owing to limited data access, this study takes the Taihang Mountain area, located west of Shijiazhuang, as an example to study the transition of the PLES and carbon emissions in the Taihang Mountain area in China, which may not be sufficiently comprehensive.

Due to the complex topography of the TMS, land-use patterns are affected by altitude, slope, aspect, soil erosion, and other factors that may influence carbon emissions. Future studies should consider these factors in relation to carbon emissions.

4.2 Conclusion

In this study, the spatial-temporal evolution characteristics of the PLES transition was explored in the TMS from 2000 to 2020 based on the land-use transfer matrix. Secondly, the carbon effects of the PLES transition were described through the indicators of "Contribution rate" and "Marginal carbon emissions". Finally, the influencing factors were analyzed by the Improved STIRPAT Model. It can provide a theoretical basis for the optimization of territorial space in the mountainous areas of China. The main conclusions are as follows:

(1) The TMS is mainly composed of ecological space and production space. During the study period, the ecological space and living space increased by 123.80 km^2 and 260.86 km^2, respectively, while the production space decreased by 384.66 km^2. The TMS has been in a state of carbon deficit, and it has experienced a process of increasing first and then decreasing. Carbon storage of ecological space increased by 0.80×10^4t, while that of agricultural productive space decreased by 0.34×10^4t. Carbon emissions of industrial and mining productive space decreased by 24.24×10^4t, while that of living space increased by115.30×10^4t.

(2) The transition between agricultural productive space and industrial and mining productive space was the main transition types caused the increase or decrease of carbon

emissions. The marginal carbon emission of industrial and mining productive space was the largest, and the marginal carbon sink of forest ecological space was the largest.

(3) Proportion of construction land was the strongest factor leading to the increase of carbon emissions, with the elasticity coefficient of 0.975%, followed by the factors of urbanization rate and proportion of secondary industry. Per capita energy consumption is the strongest factor leading to the decrease of carbon emissions, with the elasticity coefficient is −0.986%, followed by the factors of forest coverage and proportion of tertiary industry.

4.3 Policy recommendations

Based on the aforementioned analysis, we can formulate different policies according to different territorial space control objectives and gradually coordinate the PLES.

(1) For ecological space, the core is to enhance the carbon sequestration capacity. The carbon storage of forest and meadow ecological space in the TMS is much larger than that of other ecological spaces, so the scale of forestland and grassland can be continuously increased. The vacating space should preferentially restore to forest and meadow ecological space. The carbon sequestration capacity can also be improved by planting local tree species and optimizing the proportion of mixed species.

(2) For agricultural productive space, because it has a certain carbon sequestration capacity, so we should actively develop green agriculture, reduce the application of pesticides and fertilizers, and implement straw returning. Combining with the terrain and climate resources in the study area, develop unique mountain green agriculture. For industrial and mining productive space, reduce pollution energy and increase clean energy to reduce carbon emissions, and establish industrial parks to optimize the layout of industrial production space.

(3) For urban living space, delineate the urban boundary to control the urban expansion. Reasonable arrange the park green space in the urban area to enhance the carbon sequestration capacity. For rural living space, guide moderately intensive arrangement of rural living spaces through village relocation and mergers, and construct modern new rural living space. Increase the area of green land in the village to enhance the carbon sequestration capacity.

Data availability statement

The raw data supporting the conclusion of this article will be made available by the authors, without undue reservation.

Author contributions

JC: Writing–original draft, Writing–review and editing. YZ: Methodology, Writing–review and editing. HD: Data curation, Software, Writing–review and editing. TZ: Supervision, Writing–review and editing.

Funding

The author(s) declare financial support was received for the research, authorship, and/or publication of this article. This research was funded by the Humanities and Social Science Research Project of Hebei Education Department, grant number SQ2023040.

Conflict of interest

The authors declare that the research was conducted in the absence of any commercial or financial relationships that could be construed as a potential conflict of interest.

Publisher's note

All claims expressed in this article are solely those of the authors and do not necessarily represent those of their affiliated organizations, or those of the publisher, the editors and the reviewers. Any product that may be evaluated in this article, or claim that may be made by its manufacturer, is not guaranteed or endorsed by the publisher.

References

Aftab, S., Ahmed, A., Chandio, A. A., Korankye, B. A., and Fang, W. (2021). Modeling the nexus between carbon emissions, energy consumption, and economic progress in Pakistan: evidence from cointegration and causality analysis. *Energy Rep.* 7, 4642–4658. doi:10.1016/j.egyr.2021.07.020

Ang, B. W. (1999). Is the energy intensity a less useful indicator than the carbon factor in the study of climate change. *Energy Policy* 27, 943–946. doi:10.1016/S0301-4215(99)00084-1

Ang, B. W., Zhang, F. Q., and Choi, K. H. (1998). Factorizing changes in energy and environmental indicators through decomposition. *Energy* 23 (6), 489–495. doi:10.1016/S0360-5442(98)00016-4

Arrow, K., Bolin, B., Costanza, R., Dasgupta, P., Folke, C., Holling, C., et al. (1995). Economic growth, carrying capacity, and the environment. *Science* 268, 91–95. doi:10.1016/0921-8009(95)00059-3

Arshed, N., Munir, M., and Iqbal, M. (2021). Sustainability assessment using STIRPAT approach to environmental quality: an extended panel data analysis. *Environ. Sci. Pollut. Res.* 28, 18163–18175. doi:10.1007/s11356-020-12044-9

Bai, R., Shi, Y., and Pan, Y. (2022). Land-use classifying and identification of the Production-Living-Ecological Space of island villages-A case study of islands in the western sea area of Guangdong Province. *Land* 11, 705. doi:10.3390/land11050705

Balthazar, V., Vanacker, V., Molina, A., and Lambin, E. F. (2015). Impacts of forest cover change on ecosystem services in high Andean mountains. *Ecol. Indic.* 48, 63–75. doi:10.1016/j.ecolind.2014.07.043

Barnett, T. P., Adam, J. C., and Lettenmaier, D. P. (2005). Potential impacts of a warming climate on water availability in snow-dominated regions. *Nature* 438, 303–309. doi:10.1038/nature04141

Beesley, L. (2012). Carbon storage and fluxes in existing and newly created urban soils. *J. Environ. Manage.* 104, 158–165. doi:10.1016/j.jenvman.2012.03.024

Burgin, S., Franklin, M. J. M., and Hull, L. (2016). Wetland loss in the transition to urbanisation: a case study from Western Sydney, Australia. *Wetlands* 36, 985–994. doi:10.1007/s13157-016-0813-0

Chen, L., Zhou, Sh. L., Zhou, B. B., Zhao, K., Wu, X., and Xian, Y. (2015). Characteristics and driving forces of regional land use transition based on the leading function classification: a case study of Jiangsu Province. *Econ. Geogr.* 35, 155–162. doi:10.15957/j.cnki.jjdl.2015.02.022

Chen, X. L. (2003). *Research on carbon sequestration functions of main forest types in northern China. Doctor*. Beijing: Beijing Forestry University.

Chen, Z., Liu, Y., and Tu, S. (2022). Comprehensive eco-environmental effects caused by land use transition from the perspective of Production–Living–Ecological Spaces in a typical region: a case study of the Guangxi Zhuang Autonomous Region, China. *Land* 11, 2160. doi:10.3390/land11122160

Chontanawat, J. (2018). Decomposition analysis of CO_2 emission in ASEAN: an extended IPAT model. *Energy Procedia* 153, 186–190. doi:10.1016/j.egypro.2018.10.057

Cui, X., Xu, N., Chen, W., Wang, G., Liang, J., Pan, S., et al. (2022). Spatio-temporal variation and influencing factors of the coupling coordination degree of production-living-ecological space in China. *Int. Environ. Res. Public Health* 19, 10370. doi:10.3390/ijerph191610370

Data Center for Resources and Environmental Sciences, Chinese Academy of Sciences (RESDC) (2018). *China land use/land cover remote sensing monitoring data classification system*. Beijing, China: RESDC.

Deslatte, A., Szmigiel-Rawska, K., Tavares, A. F., Ślawska, J., Karsznia, I., and Łukomska, J. (2022). Land use institutions and social-ecological systems: a spatial analysis of local landscape changes in Poland. *Land Use Policy* 114, 105937. doi:10.1016/j.landusepol.2021.105937

de Sousa-Neto, E. R., Gomes, L., Nascimento, N., Pacheco, F., and Ometto, J. P. (2018). Land use and land cover transition in Brazil and their effects on greenhouse gas emissions. *Soil Manag. Clim. Change*, 309–321. doi:10.1016/B978-0-12-812128-3.00020-3

Drummond, M. A., Griffith, G. E., Auch, R. F., Stier, M. P., Taylor, J. L., Hester, D. J., et al. (2017). Understanding recurrent land use processes and long-term transitions in the dynamic south-central United States, c. 1800 to 2006. *Land Use Policy* 68, 345–354. doi:10.1016/j.landusepol.2017.07.061

Duan, Y., Wang, H., Huang, A., Xu, Y., Lu, L., and Ji, Z. (2021). Identification and spatial-temporal evolution of rural "production-living-ecological" space from the perspective of villagers' behavior-A case study of Ertai Town, Zhangjiakou City. *Land Use Policy* 106, 105457. doi:10.1016/j.landusepol.2021.105457

Fahey, T. J., Woodbury, P. B., Battles, J. J., Goodale, C. L., Hamburg, S. P., Ollinger, S. V., et al. (2010). Forest carbon storage: ecology, management, and policy. *Front. Ecol. Environ.* 8, 245–252. doi:10.1890/080169

Gao, H., Fu, T. G., Liu, J. T., Liang, H., and Han, L. (2018). Ecosystem services management based on differentiation and regionalization along vertical gradient in Taihang Mountain, China. *Sustainability* 10 (4), 986–1000. doi:10.3390/su10040986

Goldewijk, K. K. (2001). Estimating global land use change over the past 300 years: the HYDE Database. *Glob. Biogeochem. Cycles* 15 (2), 417–433. doi:10.1029/1999GB001232

Grimm, N. B., Faeth, S. H., Golubiewski, N. E., Redman, C. L., Wu, J. G., Bai, X. M., et al. (2008). Global change and the ecology of cities. *Science* 319, 756–760. doi:10.1126/science.1150195

Hansen, M. C., Potapov, P. V., Moore, R., Hancher, M., Turubanova, S. A., Tyukavina, A., et al. (2013). High-resolution global maps of 21st-century forest cover change. *Science* 342, 850–853. doi:10.1126/science.1244693

Henriques, T. S., and Borowiecki, K. J. (2017). The drivers of long-run CO_2 emissions in Europe, North America and Japan since 1800. *Energy Policy* 101, 537–549. doi:10.1016/j.enpol.2016.11.005

Hidemichi, F., Kazuyuki, I., Andrew, C., Kagawa, S., and Managi, S. (2018). An analysis of urban environmental Kuznets curve of CO_2 emissions: empirical analysis of 276 global metropolitan areas. *Appl. Energy* 228, 1561–1568. doi:10.1016/j.apenergy.2018.06.158

Houghton, R. A. (2018). Interactions between land-use change and climate-carbon cycle feedbacks. *Curr. Clim. Change Rep.* 4, 115–127. doi:10.1007/S40641-018-0099-9

Houghton, R. A., and Hackler, J. L. (1999). Emissions of carbon from forestry and land-use change in tropical Asia. *Glob. Change Biol.* 5, 481–492. doi:10.1046/j.1365-2486.1999.00244.x

Houghton, R. A., House, J. I., Pongratz, J., van der Werf, G. R., DeFries, R. S., Hansen, M. C., et al. (2012). Carbon emissions from land use and land-cover change. *Biogeosciences* 9 (12), 5125–5142. doi:10.5194/bg-9-5125-2012

Hu, G. X., Lei, G. P., and Zhou, H. (2015). Effects of different land use patterns on carbon emission in heilongjiang province. *Res. Soil Water Conservation* 22 (6), 287–292. doi:10.13869/j.cnki.rswc.2015.06.040

Jandl, R., Lindner, M., Vesterdal, L., Bauwens, B., Baritz, R., Hagedorn, F., et al. (2007). How strongly can forest management influence soil carbon sequestration? *Geoderma* 137, 253–268. doi:10.1016/j.geoderma.2006.09.003

Jiang, X. T., Zhai, S. Y., Liu, H., Chen, J., Zhu, Y., and Wang, Z. (2022). Multi-scenario simulation of production-living-ecological space and ecological effects based on shared socioeconomic pathways in Zhengzhou, China. *Ecol. Indic.* 137, 108750. doi:10.1016/j.ecolind.2022.108750

Kong, D. Y., Chen, H. G., and Wu, K. S. (2021). The evolution of "Production-Living-Ecological" space, eco-environmental effects and its influencing factors in China. *J. Nat. Resour.* 36, 1116–1135. doi:10.31497/zrzyxb.20210503

Lambin, E. F., and Meyfroidt, P. (2011). Global land use change, economic globalization, and the looming land scarcity. *Proceedings of the National Academy of Sciences of the United States of America* 108 (9), 3465–3472. doi:10.1073/pnas.1100480108

Li, X. S., Li, Zh.X., and Xie, X. T. (2023). Analysis of the interaction mechanism of urbanization, carbon emissions, and production-living-ecological space in Henan Province of China. *Trans. CSAE* 39(11), 256–265.

Li, Y. H. (2020). Measure of the impact of fiscal decentralization on carbon emissions based on the STIRPAT model. *Stat. Decis.* 19, 136–140. doi:10.13546/j.cnki.tjyjc.2020.18.031

Liao, G., He, P., Gao, X., Lin, Z., Huang, C., Zhou, W., et al. (2022). Land use optimization of rural production-living-ecological space at different scales based on the BP-ANN and CLUE-S models. *Ecol. Indic.* 137, 108710-. doi:10.1016/j.ecolind.2022.108710

Liu, T. H., Ji, Z. X., Duan, Y. M., and Xu, Y. Q. (2023). Spatial pattern evolution and carbon effect of production-living-ecological space in Zhangjiakou city under carbon peak and carbon neutrality goals. *Acta Sci. Nat. Univ. Pekin.* 59 (3), 513–522. doi:10.13209/j.0479-8023.2023.025

Luan, W. L., Song, Z. F., and Li, S. M. (2011). Changes of soil organic carbon content in Hebei Plain. *Acta Geogr. Sin.* 85, 1528–1535.

Namahoro, J. P., Wu, Q., Zhou, N., and Xue, S. (2021). Impact of energy intensity, renewable energy, and economic growth on CO_2 emissions: evidence from Africa across regions and income levels. *Renew. Sustain. Energy Rev.* 2021, 111233. doi:10.1016/j.rser.2021.111233

Newbold, T., Hudson, L. N., Hill, S. L. L., Contu, S., Lysenko, I., Senior, R. A., et al. (2015). Global effects of land use on local terrestrial biodiversity. *Nature* 520 (7545), 45–50. doi:10.1038/nature14324

Nosheen, M., Abbasi, M. A., and Iqbal, J. (2020). Analyzing extended STIRPAT model of urbanization and CO_2 emissions in Asian countries. *Environ. Sci. Pollut. Res.* 27, 45911–45924. doi:10.1007/s11356-020-10276-3

Ojoyi, M. M., Mutanga, O., Odindi, J., Kahinda, J. M. M., and Abdel-Rahman, E. M. (2017). Implications of land use transitions on soil nitrogen in dynamic landscapes in Tanzania. *Land Use Policy* 64, 95–100. doi:10.1016/j.landusepol.2017.02.023

Schimel, D. S. (2010). Terrestrial ecosystems and the carbon cycle. *Glob. Change Biol.* 1 (1), 77–91. doi:10.1111/j.1365-2486.1995.tb00008.x

Shahbaz, M., Loganathan, N., Sbia, R., and Afza, T. (2015). The effect of urbanization, affluence and trade openness on energy consumption: a time series analysis in Malaysia. *Renew. Sustain. Energy Rev.* 47 (11), 683–693. doi:10.1016/j.rser.2015.03.044

Tian, F., Li, M., Han, X., Liu, H., and Mo, B. (2020). A production-living-ecological space model for land-use optimisation: a case study of the core Tumen River region in China. *Ecol. Model.* 437, 109310. doi:10.1016/j.ecolmodel.2020.109310

Vujovi, T., Petkovi, Z., Pavlovi, M., and Jović, S. (2018). Economic growth based in carbon dioxide emission intensity. *Phys. A Stat. Mech. its Appl. S0378437118305028* 506, 179–185. doi:10.1016/j.physa.2018.04.074

Wang, A., Liao, X., Tong, Z., Du, W., Zhang, J., Liu, X., et al. (2022). Spatial-temporal dynamic evaluation of the ecosystem service value from the perspective of "production-living-ecological" spaces: a case study in Dongliao River Basin, China. *J. Clean. Prod.* 333, 130218. doi:10.1016/j.jclepro.2021.130218

Wang, S., and Liu, F. (2023). Spatiotemporal evolution of land use efficiency in southwest Mountain area of China: a case study of yunnan province. *Agriculture* 13, 1343. doi:10.3390/agriculture13071343

Wang, Y., Yang, G., Dong, Y., Cheng, Y., and Shang, P. (2018). The scale, structure and influencing factors of total carbon emissions from households in 30 provinces of China—based on the extended STIRPAT Model. *Energies* 11, 1125. doi:10.3390/en11051125

Weber, A., Fohrer, N., and Mo¨ller, D. (2001). Long-term land use changes in a mesoscale watershed due to socio-economic factors-effects on landscape structures and functions. *Ecol. Model.* 140 (1-2), 125–140. doi:10.1016/S0304-3800(01)00261-7

Winkler, K., Fuchs, R., Rounsevell, M., and Herold, M. (2021). Global land use changes are four times greater than previously estimated. *Nat. Commun.* 12, 2501. doi:10.1038/s41467-021-22702-2

Woodbury, P. B., Heath, L. S., and Smith, J. E. (2007). Effects of land use change on soil carbon cycling in the conterminous United States from 1900 to 2050. *Glob. Biogeochem. Cycles* 21 (3). doi:10.1029/2007GB002950

Yang, Q. K., Duan, X. J., and Wang, L. (2018). Land use transformation based on ecological-production-living spaces and associated eco-environment effects: a case study in the Yangtze River Delta. *Sci. Geogr. Sin.* 38, 97–106. doi:10.13249/j.cnki.sgs.2018.01.011

Yang, Y., Bao, W., and Liu, Y. (2020). Coupling coordination analysis of rural production-living-ecological space in the Beijing-Tianjin-Hebei region. *Ecol. Indic.* 117 (4), 106512. doi:10.1016/j.ecolind.2020.106512

Yang, Y. Y., Bao, W. K., Li, Y. H., Wang, Y., and Chen, Z. (2020). Land use transition and its eco-environmental effects in the Beijing-Tianjin-Hebei urban agglomeration: a production-living-ecological perspective. *Land* 9, 285. doi:10.3390/land9090285

York, R., Rose, E., and Dietz, T. (2003). STIRPAT, IPAT and Impact: analytic tools for unpacking the driving forces of environmental impacts. *Ecol. Econ.* 46, 351–365. doi:10.1016/S0921-8009(03)00188-5

Zeng, L., Lu, H., Liu, Y., Zhou, and Hu, (2019). Analysis of regional differences and influencing factors on China's carbon emission efficiency in 2005-2015. *Energies12* 16, 3081. doi:10.3390/en12163081

Zhang, B. L., Gao, J. B., Gao, Y., Cai, W. M., and Zhang, F. R. (2018). Land use transition of mountainous rural areas in China. *Acta Geogr. Sin.* 73, 503–517.

Zhang, D., Wang, Z., Li, S., and Zhang, H. (2021). Impact of land urbanization on carbon emissions in urban agglomerations of the middle reaches of the yangtze river. *Int. J. Environ. Res. Public Health* 18, 1403. doi:10.3390/ijerph18041403

Zhang, H. Q., Xu, E. Q., and Zhu, H. Y. (2017). Ecological-Living-Productive land classification system in China. *J. Resour. Ecol.* 8, 121–128. doi:10.5814/j.issn.1674-764x.2017.02.002

Zhao, R. Q., Huang, X. J., and Zhong, T. Y. (2010). Research on carbon emission intensity and carbon footprint of different industrial spaces in China. *Acta Geogr. Sin.* 65, 1048–1057.

Zhao, T., Cheng, Y., Fan, Y., and Fan, X. (2022). Functional tradeoffs and feature recognition of rural Production-Living-Ecological Spaces. *Land* 11, 1103. doi:10.3390/land11071103

Zheng, Y. W., Liu, X. H., Xiong, M. Q., Li, F. J., Fu, Y. J., Zhang, Z. F., et al. (2022). Spatial-temporal characteristics of ecological-living-productive land and its carbon emissions in Xinjiang from 1990 to 2018. *Pratacultural Sci.* 39 (12), 2565–2577. doi:10.11829/j.issn.1001-0629.2022-0294

Zhou, K. L., Yang, J. N., Yang, T., and Ding, T. (2023). Spatial and temporal evolution characteristics and spillover effects of China's regional carbon emissions. *J. Environ. Manage.* 325, 116423. doi:10.1016/j.jenvman.2022.116423

Zhu, W. B., Zhang, J. J., Cui, Y. P., et al. (2019). Assessment of territorial ecosystem carbon storage based on land use change scenario: a case study in Qihe River Basin. *Acta Geogr. Sin.* 74, 446–459.

frontiers | Frontiers in Environmental Science

TYPE Original Research
PUBLISHED 10 May 2024
DOI 10.3389/fenvs.2024.1342330

OPEN ACCESS

EDITED BY
Chenxi Li,
Xi'an University of Architecture and Technology, China

REVIEWED BY
Martí Rufí-Salís,
2.-0 LCA Consultants, Spain
Alexander N. Ignatov,
Peoples' Friendship University of Russia, Russia
Joseph Onyango Gweyi,
Kenyatta University, Kenya

*CORRESPONDENCE
Nadia Marchettini,
nadia.marchettini@unisi.it

RECEIVED 21 November 2023
ACCEPTED 15 April 2024
PUBLISHED 10 May 2024

CITATION
Meffo Kemda M, Marchi M, Neri E, Marchettini N and Niccolucci V (2024), Environmental impact assessment of hemp cultivation and its seed-based food products.
Front. Environ. Sci. 12:1342330.
doi: 10.3389/fenvs.2024.1342330

Environmental impact assessment of hemp cultivation and its seed-based food products

Marlyse Meffo Kemda, Michela Marchi, Elena Neri, Nadia Marchettini* and Valentina Niccolucci

Ecodynamics Group, Department of Physical, Earth and Environmental Sciences, University of Siena, Siena, Italy

Introduction: Hemp is a crop cultivated in Europe since ancient times, with a variety of purposes and products. Despite being known for its positive environmental effects on ecosystems, the impacts of hemp-based food products have not been sufficiently investigated yet. This paper contributed to deepen the knowledge of the hemp industry by focusing on the potential environmental impact of the cultivation phase (under three different agronomic practices in Italy: organic outdoor and conventional outdoor, and indoor) and the production of selected hemp-based goods (seed oil and flour for food purposes and flowers for therapeutic uses).

Methods: The impact was quantified utilizing the life cycle assessment within different impact categories, such as carbon footprint (CF), eutrophication (EP), acidification (AP), and water footprint (WF). For a carbon offset assessment, the carbon storage capability (i.e., the carbon fixed in crop residues left in the field) of hemp was also investigated through the guidelines provided by the Intergovernmental Panel on Climate Change (IPCC).

Results and Discussion: The cultivation phase contributed to a CF that ranged from 1.2 (organic outdoor) to 374 (indoor) kg per kg of grains (conventional outdoor). These results were in line with the literature. Sensitivity scenarios based on hotspot analysis were also presented for CF mitigation for each kind of cultivation. On the other hand, the ability of hemp to sequester carbon in the soil due to crop residues left in the field (i.e., carbon storage) was evaluated (–2.7 kg CO_2 (ha year)$^{-1}$), showing that the CF was fully compensated (–0.27 kg CO_2 (ha year)$^{-1}$ for conventional outdoor and –1.07 kg CO_2 (ha year)$^{-1}$ for organic outdoor). Regarding hemp-based products, only dried flowers showed a negative balance (–0.99 kg CO_2 per kg dry flower), while hemp oil and flour reported 31.79 kg CO_2 per kg flour) when carbon storage was accounted. The results support the idea that the production chain can be sustainable and carbon-neutral only when all the different parts of the plant (flowers, seeds, fibers, leaves, and all residues) were used to manufacture durable goods according to the framework of the circular economy.

KEYWORDS

life cycle assessment, agrifood, hemp (*Cannabis sativa* L.), environmental impact, carbon footprint, carbon storage

1 Introduction

Hemp (*Cannabis sativa* L.) is an annual dicotyledonous angiosperm plant belonging to the order Rosales, suborder Rosidae, and family Cannabaceae (The Angiosperm Phylogeny Group, 1998; Adesina et al., 2020). Hemp is a versatile plant, and it easily adapts to different climatic conditions. It is used today in several agricultural and industrial sectors, such as textiles manufacturing, bio-composite materials, papermaking, construction field, biofuels, personal care, and cosmetics (Salentijn et al., 2015; Campiglia et al., 2017). Hemp is also grown for its therapeutic uses and for food production (i.e., seeds). The seeds are the edible parts of *Cannabis sativa* L. and contain a large amount of macro and micro nutrients, such as proteins, unsaturated fatty acids, dietary fibers, and minerals, making them a good fortifying component in food production (Teterycz et al., 2021). Furthermore, hemp oil shows a growing marketable potential, and hemp flour, a by-product of oil processing, is added in many protein-rich foods and animal feeds (Yano and Fu, 2023). Hemp is an excellent break crop that can improve the soil structure due to its extensive root system (Amaducci et al., 2008); moreover, it also reduces weed pressure and enhances the yield of the subsequent crop (Bocsa et al., 1998; Amaducci et al., 2015; Campiglia et al., 2020). Additionally, hemp shows the ability of absorbing and accumulating heavy metals, such as cadmium, nickel, chromium, lead, mercury, cobalt, and arsenic in contaminated soils (Citterio et al., 2005; Gryndler et al., 2008; Ćaćić et al., 2019). Industrial hemp can be utilized for phytoremediation of heavy metal-polluted soil, while the resulting contaminated biomass can be used as an energy source (Todde et al., 2022). Finally, hemp contributes to the provision of the ecosystem's services by supporting pollination. Late-season crop flowering provides bee communities with supplementary nutritional resources during the months of floral scarcity (i.e., late summer and the beginning of autumn in Italy) (Dowling et al., 2021), thus sustaining pollination and biodiversity richness, with benefits for the other crops in the agroecosystems and the surrounding natural systems (Journals and Dalio, 2014; Flicker et al., 2020).

Hemp has been cultivated since ancient times in many parts of Europe, and among all the possible applications, its use in the production of textile was prevalent for many centuries (Mercuri et al., 2002; Allegret et al., 2013; Skoglund et al., 2013). However, during the 20th century, the increasing use of cotton and synthetic fibers (Allegret et al., 2013) and the rising cost of labor (Campiglia et al., 2020) led to a decline in hemp cultivation. Moreover, the cultivation of hemp was forbidden in many countries due to the delta-9-tetrahydrocannabinol (Δ9-THC) content, i.e., the main psychoactive constituent of *Cannabis* and one of at least 113 total cannabinoids identified in the plant. Nowadays, in several EU countries, hemp with less than 0.3% or 0.2% Δ9-THC does not fall within the drug regulation laws, thus increasing the interest in this crop (Faux et al., 2013; Farinon et al., 2022). Finally, when considering the low content of total Δ9-THC, hemp-based food products do not represent any risk to human and animal health (Kladar et al., 2021).

Since 2017, the demand for hemp-based food has grown by 500% (Sorrentino, 2021), causing the intensification of agricultural practices and a substantial increase in the consumption of resources along the supply chain (Amaducci et al., 2015; Sawler et al., 2015; Petit et al., 2020). In the European community, hemp cultivation is included in the European Green Deal objectives because of its contribution to increasing the carbon storage capacity of the agricultural system, breaking of the diseases cycle, preventing soil erosion, and enhancing biodiversity by reducing the use of pesticides (European Commission, 2023).

Although some information regarding the evaluation of the environmental impact of hemp fiber production can be found in the literature, the environmental assessment under different agronomic conditions and for hemp-derived food products (e.g., seeds, oil, and flour) are not sufficiently investigated. Zampori et al. (2013) provided a "from cradle to gate" life cycle assessment (LCA) of thermal insulators from hemp material, emphasizing the greenhouse gas (GHG) emissions along the overall supply chain and the carbon dioxide (CO_2) uptake by the plant biomass. Heidari et al. (2019) assessed the environmental impact of innovative bio-based materials (such as hemp shiv) for construction, while Andrianandraina et al. (2015) developed a methodological approach to assess the influence of the parameters of elementary processes in the foreground system of an LCA study and utilized hemp-based insulation materials as a case study. Concerning hemp fiber, Patyk and Reinhardt (1998) conducted a preliminary life cycle analysis of hemp products, including the cultivation, harvest, and pressing of oil for biofuel production, decorticating, steam pressure digestion of fiber, and textile production. Van Der Werf (2004) compared the environmental impact of agricultural practices for different crops including hemp in France. González-García et al. (2010) analyzed the impact associated with the production of hemp and flax fibers for paper pulp. Campiglia et al. (2020) evaluated the environmental impacts of different agronomic practices for hemp seed, focusing on three agricultural variables: the genotypes, plant density, and nitrogen content in fertilizers.

The goal of this paper is to contribute to the ongoing research on the sustainability aspects of the hemp industry from the point of view of circular economy. This objective is achieved by carrying out an environmental impact assessment of the cultivation processes of hemp in Italy, according to a "from cradle to farm gate" life cycle approach. The quantified impact categories are carbon footprint (CF), eutrophication (EP), acidification (AP), and water footprint (WF). CF is selected as a reference indicator, focusing on the CF offset (i.e., the distance from the carbon neutral condition) due to the temporary carbon storage in crop residues left in the field to mineralize the soil.

Three different agronomic methods are examined, i.e., conventional (outdoor and indoor) and organic (outdoor). For each of these, primary data are collected, and all emissions, both direct and indirect, are evaluated. This contributes to the completeness and reliability of the results. Furthermore, the ability of hemp to sequester carbon in the soil (i.e., the contribution by crop residues left in the field) is also accounted for. The balance emission vs. storage reveals the position of hemp in the carbon neutrality scale. In addition, the environmental impacts of the manufacturing and packing processes for hemp-based products (seed oil, flour, and dried flowers) are assessed.

Finally, after hotspot identification, some management practices are proposed and analyzed in terms of impact reduction. Such measures include the utilization and market of all parts of the

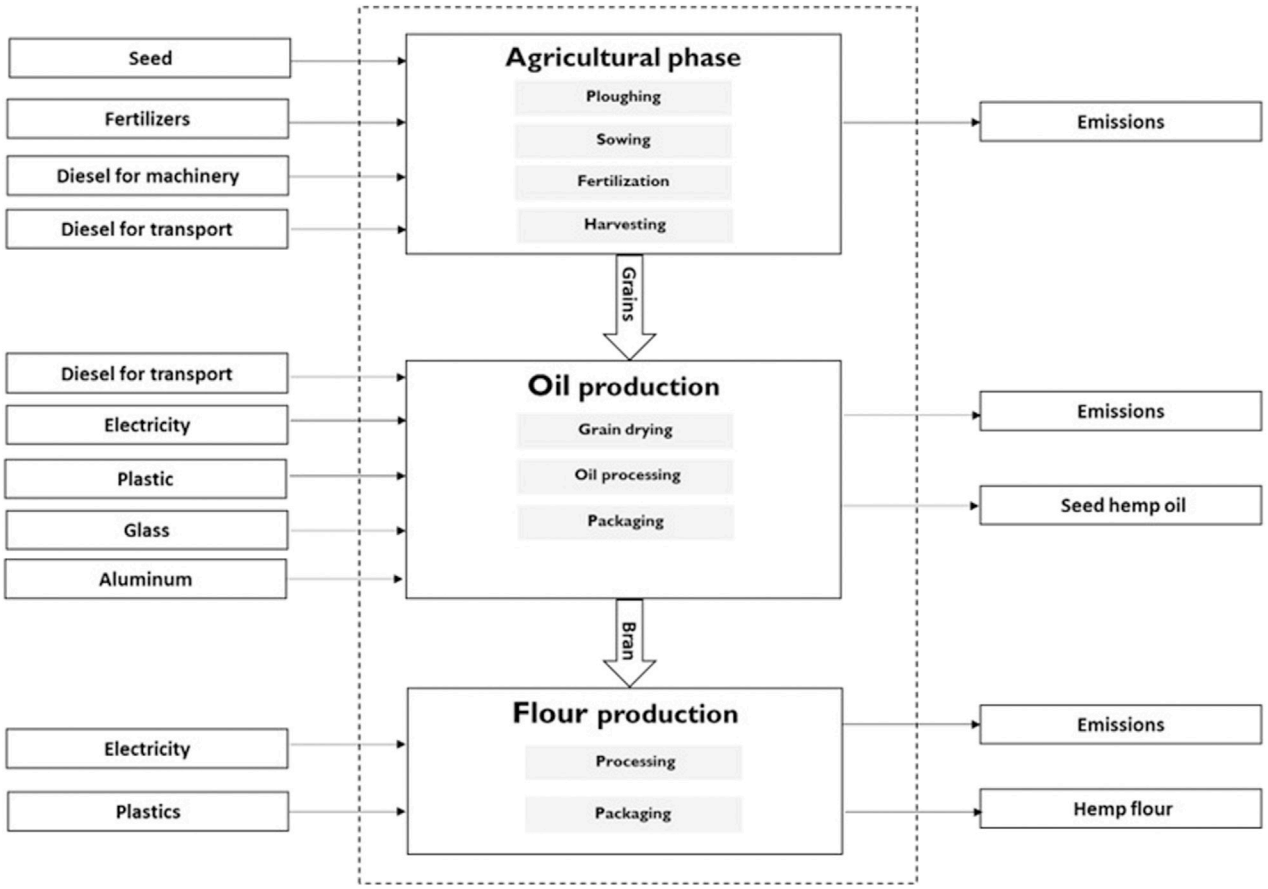

FIGURE 1
Flowchart of conventional outdoor hemp crops from cultivation to products processing and packaging (Tuscany, Italy).

plant, thus reducing waste and promoting a circular and more sustainable production model (Scrucca et al., 2020; Kaur and Kander, 2023).

2 Materials and methods

2.1 Case studies

Three different case studies are used as proxies for the assessment of the environmental impact of the hemp industry. They differ for agronomic methods (i.e., both conventional outdoor and indoor and organic outdoor) and commercial purposes (i.e., flowers for therapeutics uses and grains for hemp-based food products). All the case studies are located in Italy. A brief description of the hemp life cycles with their specific characteristics, management, operational phases, and outputs is provided below. All the system boundaries are "from cradle to farm gate" (i.e., from the resource's extraction to the packaged product leaving the farm), while the temporal boundaries are 1 year of agricultural activity.

Conventional outdoor (Figure 1): a medium-sized farm located in Siena (43°18′13.3″ N and 11°22′57.2″ E, Tuscany, central Italy). The final marketable products are seed oil and flour. The cultivar is Finola, a variety that has been bred specifically to produce grains and sometimes fiber and oilseed for food items (Jasinskas et al., 2020). Cultivation takes place outdoor with conventional management, i.e., using fertilizers and without irrigation, due to the low water requirements of hemp. Sowing is carried out in May, and the biomass with ripe grains is harvested in September. Once collected, the biomass (also containing fibers) is deliberately left in the cropland, while the grains are dried and processed to obtain food products. Hempseed oil is obtained by cold pressing the grains, while hemp flour is obtained by grinding the leftovers of hemp oil production. Hempseed oil is packed in 250-mL glass bottles. A plastic film is used for the packing of 1 kg of flour.

Organic outdoor (Figure 2): a small farm located in Sovicille (43°15′56.2″ N and 11°14′15.7″ E, Tuscany, central Italy) produces *C. sativa* for therapeutic uses. Hemp cultivation (cultivar Carmagnola) happens outdoor without irrigation and with extremely limited use of fertilizers. The sowing takes place in May, and the fresh flowers are harvested manually in September using specific scissors. The unused parts of the plant (i.e., biomass) are left in the fields. Fresh flowers are dehydrated naturally and packed in 1-kg plastic buckets.

Indoor (Figure 3): a farm in Eboli (40°37′01″ N, 15°03′23″ E, Campania, Southern Italy) that produces *C. sativa* in greenhouses for therapeutic uses. Hemp production (cultivar Carmagnola) takes place indoor, quarterly of a year, and requires a lot of resources and energy to recreate the natural external microclimatic conditions.

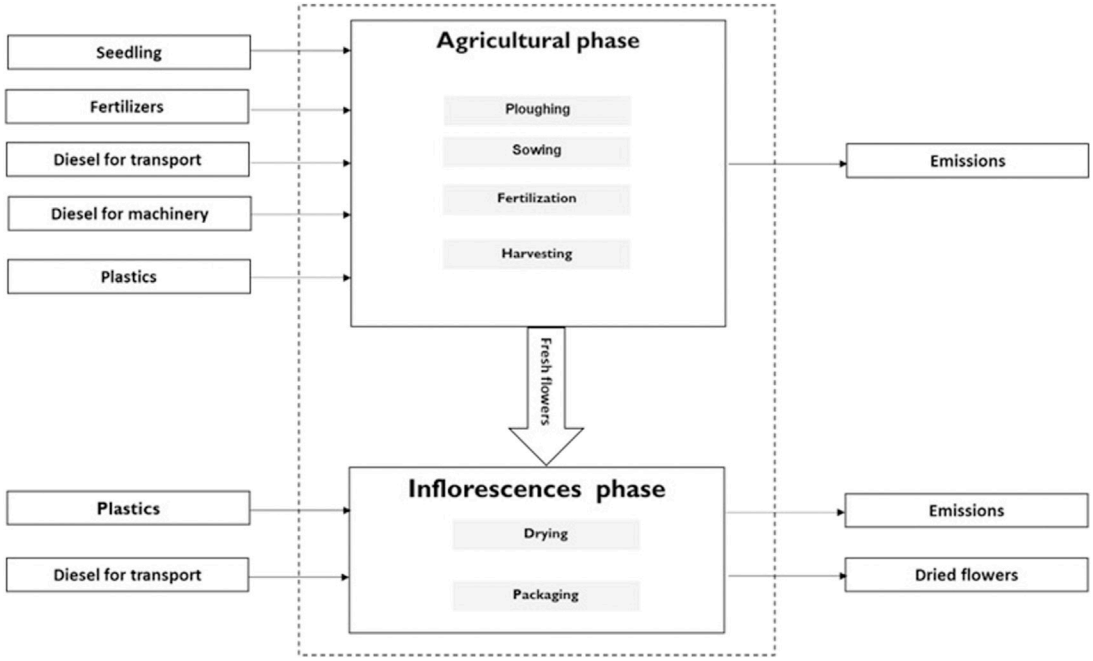

FIGURE 2
Flowchart of organic outdoor hemp crops from cultivation to dried flowers and packaging (Tuscany, Italy).

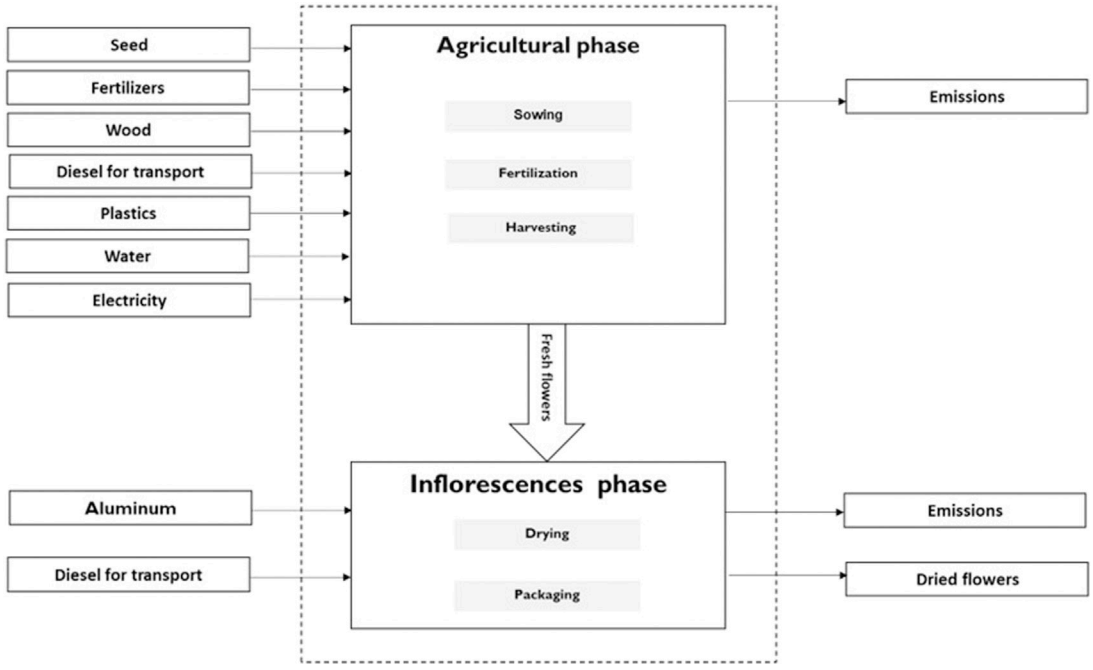

FIGURE 3
Flowchart of indoor hemp crops from cultivation in pots to dried flowers and packaging (Campania, Italy).

Prolonged exposure to LED light (up to 18 h a day) increases the photosynthetic capacity and the possibility of achieving excellent vegetative development. At the end of the growing period, the light hours are reduced to 12 h to recreate the autumn conditions and induce the flowering of the plant. Fresh flowers are harvested manually, and the residual biomass is placed in home composters outside the greenhouse. Once harvested, the fresh flowers are dried naturally and packaged in small aluminum boxes (5 g).

2.2 Data collection and processing

Most of the data about the hemp life cycle were primary, i.e., directly collected from farmers, with the best accuracy, with a bottom-up approach. Data collection referred to: 2018 (conventional outdoor), 2020 (organic outdoor), and 2019 (indoor). The LCA included both direct and indirect GHG emissions due to the upstream processes of obtaining materials, fuels, and all the products used by farmers during 1 year of production (Niccolucci et al., 2021). The calculation was carried out using SimaPro 9.0.0.49 software (Ecoinvent, 2020), Ecoinvent 3.6 database, and by selecting the CML-IA method. The identified impact categories were carbon footprint (CF), eutrophication (EP), acidification (AP), and water footprint (WF).

The following assumptions and approximations made were the following: 1) machinery, equipment, and infrastructures were included in the general cut-off, which ranged from 1% to 5% (Palacios-Munoz et al., 2019). 2) According to the information provided by the owner of the indoor cultivation, agricultural tools (irrigation pipes, wooden poles, and plastic pots) used in the greenhouse were replaced every 3 years (i.e., their lifetime). 3) Diesel consumption for transportation was estimated based on the weight of the carried materials and the traveled distance. 4) Direct emissions deriving from the use of fossil fuels for transport, agricultural machinery, and other devices, as well as due to the fertilizers use and the crop residues left on the field or composted, were included in the calculation by applying the equations framework and emissions factors proposed by the Intergovernmental Panel on Climate Change (IPCC) (IPCC, 2006; IPCC, 2019) and the European Environmental Agency (EMEP/EEA, 2019).

Finally, according to ISO 14044:2006/Amd 2:2020 (ISO, 2020), a mass allocation was adopted to take into account the transformation of hemp seeds into oil (20%) and flour (80%). The inventory was organized in three main phases: 1) agricultural, 2) crop transformation, and 3) product packaging. Two different functional units have been used depending upon the different research question: 1) 1 ha of cultivated land per year; 2) 1 kg of hemp products (i.e., fresh flowers or grains) and relative marketable products (i.e., dried flowers, seed oil, and flour).

The IPCC framework (IPCC, 2006; IPCC, 2019) was adopted as it is a standardized methodology that is valid and replicable at an international level. Carbon footprint offset (CF_{OFFSET}, i.e., the net annual carbon balance) is quantified by subtracting the annual storage (quantified as CO_2 $_{STORAGE}$, i.e., the annual CO_2 stock in cropland soil, as in the case of conventional and organic outdoor) from the anthropogenic GHG emissions (quantified as CF_{TOT} and expressed in tons of equivalent carbon dioxide annually emitted, CO_2eq, due to the agronomic practices and product processing) (see Eqs 1–3).

$$C_{STORAGE} = \left[\frac{SOC_{REF} - (SOC_{REF} \cdot F_{LU} \cdot F_{MG} \cdot F_I)}{20yr}\right] \quad (1)$$

$$CF_{TOT} = \underbrace{\sum_{i=1}^{n} CF_i}_{\text{DIRECT EMISSIONS}} + \underbrace{\sum_{j=1}^{m} CF_j}_{\text{INDIRECT EMISSIONS}} \quad () \quad (2)$$

$$CF_{OFFSET} = -CO_{2STORAGE} + CF_{TOT} = -\left(C_{STORAGE} \times \frac{44}{12}\right) + CF_{TOT} \quad (3)$$

The variation in carbon stock in soil was calculated with Equation 1 (IPCC, 2006), which considers the reference carbon storage in 0–30 cm of soil depth (SOC_{REF}) and the stock change factors for the specific land use (F_{LU}), the management regime (F_{MG}), and the input of organic matter (F_I). The stock change factors represent the carbon fraction released into the atmosphere due to land use practices (e.g., cultivated or uncultivated land), management regimes (e.g., tillage or no-till), and organic matter input into the soil (e.g., low, medium, or high). This study used a reference of carbon storage in soils of 44.33 t C ha^{-1}, which is obtained as an average value for sandy soils and other soils with high-activity clay and low-activity clay in temperate regions, as proposed by the IPCC Guidelines (IPCC, 2006). On the other hand, the stock change factor for land use (F_{LU}, i.e., 0.75) represents the area that has been continuously cultivated for ≥20 years, predominantly for hemp production and other similar annual crops. The stock change factor for management regimes (F_{MG}, i.e., 1) represents substantial soil disturbance with full inversions and/or frequent (within a year) tillage operations. The stock change factor for input of organic matter (F_I, i.e., 1) is representative of annual cropping with cereals, where all crop residues are returned to the field. Biomass decomposition is considered under temperate climate and dry and moist regimes. The values of the available range are chosen, which are in line with the climatic zones and the different options proposed by the IPCC Guidelines (IPCC, 2006).

The carbon stock over time will occur primarily during the first 20 years, following the management field practices. After that, the rates will tend toward a new steady-state level, with little or no change occurring unless further changes in management conditions occur (IPCC, 2006).

3 Results and discussion

3.1 Hemp cultivation

The life cycle inventory (LCI) is elaborated as a quantification of all relevant flows coming from (i.e., energy and raw material) and directed to (i.e., direct emissions) the environment, which are needed to support the overall hemp life cycle. In Table 1 the LCI results are presented focusing on the respective agricultural phase. Although this phase is common for all kinds of hemp-based products (i.e., grains and flowers), the crop transformation and packaging phases depend on the type of the products. The inventory is organized in two different functional units, depending on the addressed research purpose. The first FU is 1 ha of cultivated field, and it provides a local perspective for discussing those impacts that produce emissions in the field. Furthermore, this FU is chosen to be used as a reference in comparison with other similar case studies found in the literature. The second FU is 1 kg of products (grains or flowers), and it has a regional and global relevance and is more convenient when comparing agronomic practices.

The most relevant LCA environmental impact results for the three case studies according to the two functional units are reported in Table 2.

Considering the mass unit as FU, the organic practice shows the lowest impact, while the indoor practice shows the highest, within all the

10.3389/fenvs.2024.1342330

TABLE 1 LCI of the hemp cultivation phase within the three agronomic practices (conventional outdoor, organic outdoor, and indoor) and two functional units (1 ha of cultivated field and 1 kg of grains for conventional outdoor or of flowers for organic outdoor and indoor).

Item	Unit per FU	Conventional outdoor	Organic outdoor	Indoor	Conventional outdoor	Organic outdoor	Indoor	Notes
		FU = 1 ha (cropland)			FU = 1 kg (grains or flowers)			
		Amount	Amount	Amount	Amount	Amount	Amount	
Yield	kg/ha	1.0×10^3 (kg grains)	8.3×10^2 (kg flowers)	1.7×10^3 (kg flowers)				
Seed	kg	2.7×10^1	-	7.2×10^{-3}	2.8×10^{-2}	-	4.2×10^{-6}	Certified seeds of varieties with a THC content <0.2%
Seedlings	n	-	3.3×10^3	-	-	4.0×10^0	-	Seedlings are grown in indoor systems and transported in plastic jars
Diesel for machinery								
Plowing	kg	3.3×10^1	3.7×10^1	-	3.3×10^{-2}	4.5×10^{-2}	-	
Sowing and harrowing	kg	2.1×10^1	-	-	2.1×10^{-2}	-	-	
Fertilization	kg	2.5	-	-	2.5×10^{-3}	-	-	
Threshing	kg	1.7×10^1	-	-	1.7×10^{-2}	-	-	
Diesel for transport (light truck)								
Fertilizer	kg	2.4×10^{-2}	-	-	2.4×10^{-5}	-	-	The source is 10 km away from the field (for conventional outdoor), while it is not available for the other cultivation (i.e., organic outdoor and indoor)
Seedling	kg	-	3.6×10^{-2}	-	-	4.3×10^{-5}	-	Origin of seedlings is 62.4 km away from the site
Seed	kg	-	-	2.1×10^{-5}	-	-	1.2×10^{-8}	Seeds derive from harvest (conventional outdoor) and purchased from a site 245 km away (Indoor)
Fertilizers								
Ammonium nitrate	kg	4.8×10^1	6.1×10^{-1}	6.6×10^2	4.8×10^{-2}	7.4×10^{-4}	3.9×10^{-1}	
Triple superphosphate	kg	6.3×10^1	5.6×10^{-1}	1.0×10^3	6.3×10^{-2}	6.8×10^{-4}	5.9×10^{-1}	
Potassium chloride	kg	-	1.4×10^0	2.5×10^3	-	1.7×10^{-3}	1.5×10^0	

(Continued on following page)

TABLE 1 (*Continued*) LCI of the hemp cultivation phase within the three agronomic practices (conventional outdoor, organic outdoor, and indoor) and two functional units (1 ha of cultivated field and 1 kg of grains for conventional outdoor or of flowers for organic outdoor and indoor).

Item	Unit per FU	Conventional outdoor	Organic outdoor	Indoor	Conventional outdoor	Organic outdoor	Indoor	Notes
		FU = 1 ha (cropland)			FU = 1 kg (grains or flowers)			
		Amount	Amount	Amount	Amount	Amount	Amount	
Plastics	kg	-	4.0×10^{2}	5.7×10^{4}	-	4.8×10^{-1}	8.6×10^{0}	Plastics type: high-density polyethylene. Plastic refers to that used for the transport of seedlings (organic outdoor) or to the materials used in the greenhouse (jars, irrigation pipes, and wires) (indoor.) For indoor, plastic jars were already present in the greenhouse at the time of the start of the cultivation activity
Wood	kg	-	-	1.4×10^{3}	-	-	3.3×10^{1}	Wooden poles are used to support the plants and keep them able to support the load
Water for irrigation	kg	-	-	2.3×10^{4}	-	-	3.6×10^{0}	From the national water network
Electricity								
Electric lamps	kWh	-	-	1.9×10^{6}	-	-	1.3×10^{1}	Italian electricity mix
Fans	kWh	-	-	5.7×10^{5}	-	-	3.3×10^{2}	
Air conditioner	kWh	-	-	6.6×10^{5}	-	-	3.9×10^{2}	
Dehumidifier	kWh	-	-	4.9×10^{5}	-	-	2.9×10^{2}	
Humidifier	kWh	-	-	1.4×10^{5}	-	-	8.2×10^{1}	
Direct emissions								
Carbon dioxide (CO_2)	kg	2.3×10^{2}	1.2×10^{2}	6.8×10^{-5}	2.3×10^{-1}	1.4×10^{-1}	1.0×10^{-8}	Emission factors provided by IPCC (IPCC, 2006; IPCC, 2019)
Methane (CH_4)	kg	1.3×10^{-2}	6.6×10^{-3}	6.5	1.3×10^{-5}	7.9×10^{-6}	9.8×10^{-4}	Emission factors provided by EMEP/EEA (EMEP/EEA, 2019)
Nitrous oxide (N_2O)	kg	4.53	4.3×10^{-1}	7.8×10^{1}	4.5×10^{-3}	5.1×10^{-4}	1.2×10^{-2}	
Carbon oxide (CO)	kg	8.4×10^{-1}	5.4×10^{-4}	1.6×10^{-7}	8.4×10^{-4}	6.4×10^{-7}	2.4×10^{-11}	
Non-methane volatile organic compounds (NMVOCS)	kg	2.6×10^{-1}	1.3×10^{-1}	3.3×10^{-8}	2.6×10^{-4}	1.6×10^{-4}	4.9×10^{-12}	
Ammonia (NH_3)	kg	6.2×10^{-4}	3.5×10^{-4}	3.3×10^{-8}	6.2×10^{-7}	4.2×10^{-7}	4.9×10^{-12}	
Nitrogen oxides (NOX)	kg	2.53	1.28	3.2×10^{-7}	2.5×10^{-3}	1.5×10^{-3}	4.8×10^{-11}	
Sulfur dioxide (SO_2)	kg	4.4×10^{-3}	2.2×10^{-3}	6.4×10^{-7}	4.4×10^{-6}	2.7×10^{-6}	9.7×10^{-11}	

(Continued on following page)

TABLE 1 (*Continued*) LCI of the hemp cultivation phase within the three agronomic practices (conventional outdoor, organic outdoor, and indoor) and two functional units (1 ha of cultivated field and 1 kg of grains for conventional outdoor or of flowers for organic outdoor and indoor).

Item	Unit per FU	Conventional outdoor	Organic outdoor	Indoor	Conventional outdoor	Organic outdoor	Indoor	Notes
		FU = 1 ha (cropland)			FU = 1 kg (grains or flowers)			
		Amount	Amount	Amount	Amount	Amount	Amount	
Black carbon (BC)	kg	3.7×10^{-2}	4.1×10^{-2}	-	3.7×10^{-5}	4.9×10^{-5}		
Particulate matter 10 (PM10)a	kg	1.4×10^{-1}	7.1×10^{-2}	-	1.4×10^{-4}	8.5×10^{-5}	-	
Particulate matter 2.5 (PM2.5)a	kg	1.4×10^{-1}	7.1×10^{-2}	-	1.4×10^{-4}	8.5×10^{-5}	-	
Total suspended particles (TSP)b	kg	1.4×10^{-1}	7.1×10^{-2}	-	1.4×10^{-4}	8.5×10^{-5}	-	
Particulate matter 0.1 (PM0.1)a	kg	3.6×10^{-5}	5.5×10^{-5}	3.3×10^{-8}	3.6×10^{-8}	6.6×10^{-8}	4.9×10^{-12}	
Indeno [1,2,3-cd] pyrene (ID (1,2,3-cd)P)	kg	3.8×10^{-10}	5.7×10^{-10}	3.4×10^{-13}	3.8×10^{-13}	6.9×10^{-13}	5.1×10^{-17}	
Benzo(k) fluoranthene (B(k)F)	kg	2.1×10^{-10}	3.1×10^{-10}	1.9×10^{-13}	2.1×10^{-13}	3.8×10^{-13}	2.8×10^{-17}	
Benzo(b) fluoranthene (B(b)F)	kg	4.0×10^{-10}	6.0×10^{-10}	3.5×10^{-13}	4.0×10^{-13}	7.2×10^{-13}	5.3×10^{-17}	
Benzo(a) fluoranthene (B(a)F)	kg	3.8×10^{-10}	5.7×10^{-10}	3.4×10^{-13}	3.8×10^{-13}	6.9×10^{-13}	5.1×10^{-17}	
Lead (Pb)	kg	1.2×10^{-9}	1.2×10^{-9}	1.1×10^{-12}	1.3×10^{-12}	2.3×10^{-12}	1.7×10^{-16}	

[a]PM_{10} includes airborne particles between 2.5 and 10 μm in diameter, $PM_{2.5}$ includes particles between 0.1 and 2.5 μm in diameter, and $PM_{0.1}$ includes particles <0.1 μm in diameter.
[b]TSP, includes airborne particles >10 μm in diameter.

TABLE 2 Environmental impacts due to hemp production in the three agronomic practices. Results are reported for both the two functional units: 1 ha of cultivated field and 1 kg of grains (conventional outdoor) or flowers (organic outdoor and indoor).

Impact category	Conventional outdoor	Organic outdoor	Organic indoor	Conventional outdoor	Organic outdoor	Organic indoor
	FU: 1 ha (cropland)			FU: 1 kg (grains or flowers)		
Carbon footprint **(CF)** **(kg CO_2eq)**	1.8×10^{3}	1.0×10^{3}	6.2×10^{5}	1.9×10^{0}	1.2×10^{0}	3.7×10^{2}
Eutrophication **(EP)** **(kg PO_4^{3-} eq)**	2.5×10^{0}	5.1×10^{-1}	4.4×10^{2}	2.6×10^{-3}	6.2×10^{-4}	2.7×10^{-1}
Acidification **(AP)** **(kg SO_2 eq)**	4.2×10^{0}	3.7×10^{0}	2.5×10^{3}	4.3×10^{-3}	4.5×10^{-3}	1.53×10^{-1}
Water footprint **(WF)** **(m^3 water eq)**	3.2×10^{2}	2.0×10^{2}	4.2×10^{5}	3.2×10^{-1}	3.1×10^{-1}	2.5×10^{2}

evaluated impact categories. In the case of outdoor practices, the CF is 1.2 kg CO_2eq for organic and 1.9 kg CO_2eq for conventional practices, with a variation of −37%. The indoor practice is two orders of magnitude larger (3.7×10^2 kg CO_2eq), and this is essentially due to the intensive use of fertilizers and, above all, the large electricity requirements. Furthermore, indoor production occurs four times per year.

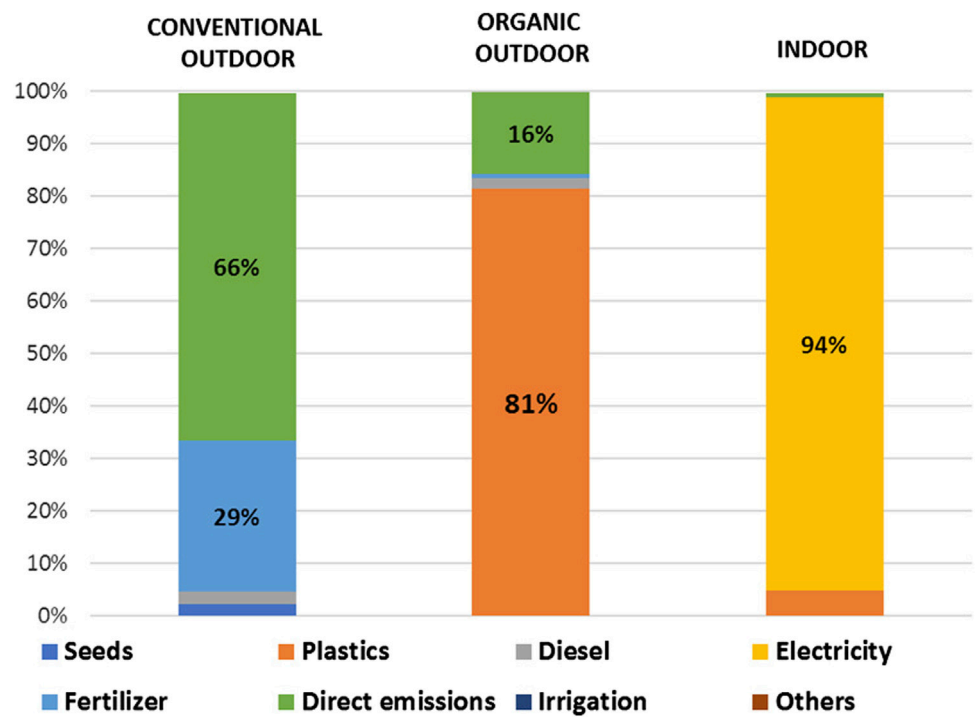

FIGURE 4
Carbon footprint (CF) composition for the considered agronomic practices (conventional outdoor, organic outdoor, and indoor).

The CFs show the following different compositions (Figure 4):

- Conventional outdoor practice is dominated by direct emissions to air (66%) due to residual crops, with a moderate contribution from fertilizer production (29%).
- Organic outdoor practice is characterized by a substantial contribution from plastic jars for seedlings (81%), with a marginal contribution from residual crops as direct emissions (16%).
- Conventional indoor practice is predominantly caused by the energy requirements for the operational and maintenance activities of the greenhouses.

In this study, the emissions are accounted, and the contribution of direct emissions is included for those selected processes from database that do not include them. Direct emissions accounting represents an important added value for this kind of study. Direct contributions from crop residues left in the field or composted, fertilizers, and fossil fuel consumption are separately accounted according to the IPCC framework (IPCC, 2006; IPCC, 2019) and EMEP/EEA (EMEP/EEA, 2019) (see Table 1). This contribution is especially relevant for agricultural products with intensive management, as is also confirmed in this case.

The WF results, calculated as the water scarcity index, show that the water use intensity for indoor practice (250 m^3 water eq) is around three orders of magnitude larger than that of outdoor cultivation (0.3 m^3 water eq). All the selected impact categories explored (EP, AP, and WF) show a similar percentage composition to those of CF.

The results from FU = 1ha are compared with the available recent literature (see Table 3). This was possible only for conventional outdoor practice. In this study, the CF is in line with those shown in the literature for different European countries. Data variability increases when only the outlier is included, but our value still scores among the lowest (Figure 5). The literature (Van Der Werf, 2004; González-García et al., 2010; Andrianandraina et al., 2015) confirms that the main contributors to CF are the production and use of diesel and fertilizers in addition to crop residues (generally neglected). The differences could be, for example, due to the country of origin, system boundaries, the (partial or total) inclusion of direct emissions, the evaluation methods (i.e., endpoint and middle point), weather conditions, and the prevalent management practices (i.e., the choice of cultivar variety, the rate of fertilization, plant density, and the type of production system). The EP and AP results confirm that conventional outdoor practice has the lowest impact like for CF, even if the variability is low (Figure 5).

For the three agronomic practices, various mitigation scenarios are proposed to promote a more efficient use of natural resources and are discussed in terms of CF management (Table 4).

In conventional outdoor practice, crop residues are a hotspot of the system, and as such, it is important to focus preliminarily on their role. Crop residues left in the field (approximately 15 t of dry biomass (ha year)$^{-1}$) have a natural mulching function, protecting the soil from the disruptive effects of rain, wind, and sun. Their presence on the surface of hardened soils increases the soil fertility, reducing the susceptibility to surface compaction. Another important function of crop residues is the supply of organic matter, following their degradation, with the release of nutritive

TABLE 3 Comparison of environmental impacts of the hemp cultivation phase according to conventional outdoor practice (FU 1 ha of cropland) with the existing literature.

Case study	Reference	Carbon footprint	Eutrophication	Acidification	Notes
		kg CO_2eq	kg PO_4^{3-} eq	kg SO_2 eq	
This study		1.8×10^3	2.5×10^0	4.3×10^0	Country: Italy
					System boundaries: from cradle to gate
					Data: primary
					Direct emissions: from fertilizer, transport, and crop residues
					Method: CML, IA baseline
Heidari et al. (2018)	Heidari et al. (2019)	5.1×10^3	-	-	Country: France
					System boundaries: from cradle to gate (include shiv storage)
					Data: primary
					Direct emissions: from the fertilization process
					Method: Re.Ci.Pe endpoint
Campiglia et al. (2020)	Campiglia et al. (2020)	Range from 1.6×10^2 to 1.88×10^4	-	-	Country: France
					System boundaries: from cradle to gate
					Data: primary
					Direct emissions: not included
					Method: Re.Ci.Pe, 2016
Andrianandraina et al. (2015)	Andrianandraina et al. (2015)	1.0×10^3	1.3×10^1	9.9×10^0	Country: France
					System boundaries: not clearly defined
					Data: secondary
					Direct emissions: from the fertilization process
					Method: CML 2021 e CED
Zampori et al. (2013)	Zampori et al. (2013)	6.7×10^2	-	-	Country: France
					System boundaries: from cradle to gate
					Data: primary
					Direct emissions: from the fertilization process
					Methods: GGP, CED, and EcoIndicator H
González-García et al. (2010)	González-García et al. (2010)	2.9×10^3	1.7×10^1	2.7×10^1	Country: Spain
					System boundaries: from cradle to gate
					Data: primary and secondary
					Direct emissions: from the fertilization process
					Method: CML baseline 200

(Continued on following page)

TABLE 3 (*Continued*) Comparison of environmental impacts of the hemp cultivation phase according to conventional outdoor practice (FU 1 ha of cropland) with the existing literature.

Case study	Reference	Carbon footprint	Eutrophication	Acidification	Notes
		kg CO_2eq	kg PO_4^{3-} eq	kg SO_2 eq	
Van der Werf (2004)	Van Der Werf (2004)	2.3×10^3	2.1×10^1	9.8×10^0	Country: France
					System boundaries: from cradle to gate
					Data: secondary
					Direct emissions: from the fertilization process
					Method: personal evaluation from the literature
Patyk and Reinhard (1998)	Patyk and Reinhardt (1998)	1.4×10^3	-	6.6×10^0	Country: Germany
					System boundaries: from cradle to gate
					Data: secondary
					Direct emissions: not specified
					Method: not specified

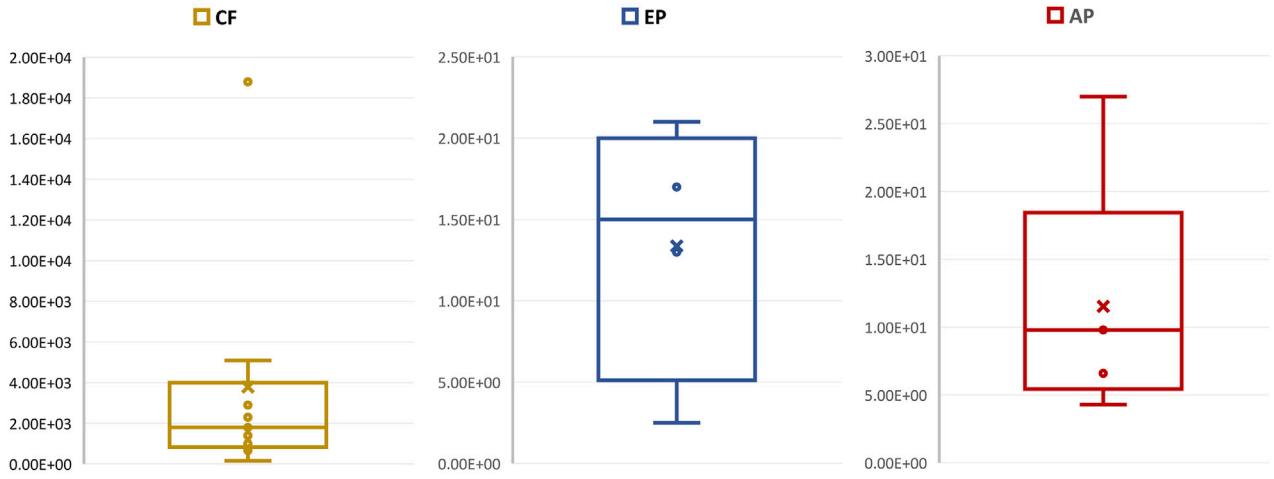

FIGURE 5
Data variability between this study and other research found in the literature. CF is expressed in kgCO_2eq, EP in PO_4^{3-} eq and AP in kg SO_2eq per ha.

TABLE 4 Mitigation scenarios for carbon footprint management for each agronomic practice. Results are expressed per kg CO_2eq/ha of cropland.

Agronomic practice	CF **kg CO_2eq/ha (this study)**	Mitigation scenario	#	CF **kg CO_2eq/ha**	Impact reduction (%)
Conventional outdoor	1.8×10^3	Removal of crop residues (75%) from the field	I	1.3×10^3	−30
Organic Outdoor	1.0×10^3	Use bioplastic jars instead of plastic	IIa	9.4×10^2	−8
		Use of seeds instead of seedlings in plastic jars	IIb	1.9×10^2	−81
Indoor	6.2×10^5	Electricity from photovoltaic panels instead of national mix	III	9.9×10^4	−84

elements, and the stimulation of biological processes by microorganisms. In this regard, it would be interesting to understand and quantify the ability of residual hemp biomass in reducing the use of fertilizer resulting from this practice. The CO_2 stored annually in the soil due to the crop residues left in the field and the CO_2eq net emissions due to agronomic practices are

evaluated. The yearly carbon stock in soil (with more than 30% of hemp residues) is estimated in −2.07 t CO_2 ha^{-1} because tillage practices are carried out for both conventional outdoor practice, in which hemp seeds are strewn in the field, and organic outdoor practice, in which the installation of seedlings is planned. The carbon stored over a period of 20 years of cultivation is −121 t CO_2 ha^{-1}. When considering the conventional and organic outdoor practices, the total CFs of the agricultural phase (1.8 and 1.0 t CO_2eq ha^{-1}, respectively) are fully compensated by the biomass fraction stored annually in the ground (−0.27 and −1.07 t CO_2eq ha^{-1}, respectively). The largest energy and environmental impacts of hemp cultivation are due to the production and use of the fertilizers and pesticides, contributing to most of the CFs, and are consistent with other studies (Pervaiz and Sain, 2003; Scrucca et al., 2020). Therefore, the practice of leaving crop residues in the field could lead to impact mitigation.

Since hemp is a fibrous plant, crop residues can also be harvested and transformed into consumer products such as textiles and building materials. In this sense, the removal of residual biomass from the field, for example, 75% (scenario I in Table 4), produces a significant reduction in gross carbon emissions (−30%) due to the cultivation phase. Furthermore, according to Zampori et al. (2013), the fraction of crop residues collected in the field would lead to the manufacture of 4.4×10^2 insulation panels composed by hemp (85%) and polyester (15%) fibers. The manufacture of all these panels emits 2.0×10^3 kg CO_2eq, accounting for 4.4 kg CO_2eq $(panel)^{-1}$. However, a hemp-based insulating panel impacts 5 times less in terms of CF when compared with a traditional cork one and 10 times less with respect to an expanded clay one (Asdrubali et al., 2015; Essaghouri et al., 2023). The carbon stocked in each hemp-based insulating panel is −8.7 t CO_2, representing a semi-permanent storage throughout their life (≥50 years). The CF offset shows a net negative value (−4.2 t CO_2 per panels), confirming the carbon neutral condition of this production chain, as claimed by other studies (Ingrao et al., 2015; Scrucca et al., 2020; Liu et al., 2023). Based on these estimations, 1 kg of dried hemp biomass contains 1.7 t CO_2 (Struik et al., 2000), and each insulating panel is composed of 5.1 kg of fiber.

For organic outdoor practice, two scenarios are assumed: the use of starch-based bioplastic instead of plastic jars (scenario IIa) for seedlings or the use of seed instead of seedlings (scenario IIb). CF shows a moderate decrease (8%) for starch-based bioplastic and an important reduction (−81%) for seeds.

In the indoor agricultural practice, because of the large contribution of electricity on the overall impact, an agri-voltaic scenario is proposed, i.e., a 100% renewable source (i.e., photovoltaic panels) instead of the current Italian energy mix (almost 40% renewable) (scenario III). To cover the annual energy consumption (3.7×10^6 kWh), the greenhouse would use the electricity produced by 1.1×10^3 photovoltaic panels of 3 kW (taking up approximately 2 ha under the hypothesis to develop a local energy community comprising all the farmers of the area).

3.2 Hemp-based products

A separate inventory for hemp-based products is elaborated, including the processing and packaging phases.

Regarding flour and oil processing (Table 5), two inputs are accounted: diesel (used during the transport of hemp seeds from the field to the processing plant) and electricity (used during the transformation processes). Regarding the packaging, only the raw materials are accounted, for while their transportation is not considered because they are purchased in the same place where the processing and bottling of the final oil product take place.

The dried flowers are packaged using different materials depending on the practice used (i.e., organic outdoor or indoor) (Table 6).

The environmental impacts of the production of 1 kg of hemp-seed oil and 1 kg of flour are shown in Table 7.

The CF is 26 kgCO_2eq kg^{-1} for oil, while it is 33 kgCO_2eq kg^{-1} for flour. Due to the lack of specific literature reports, other kinds of flour and oil are used for comparison (Table 8). The CF of hemp-based food products is one order of magnitude higher than the others. This could be due to a very low yield of hemp seed (1 t ha^{-1}) with respect to winter wheat (yield 9.7 Mt ha^{-1}) and winter rye (8.5 Mt ha^{-1}) (Baldini et al., 2019; Riedesel et al., 2022). In addition, the transformation and processing of hemp oil has a low yield (1 L requires 5 kg of seeds) when compared with other kinds of oil (Rapa et al., 2019). The choice of the packaging format (250 mL bottles) is an important aspect, causing a relevant variation in the total impact. Hemp generally requires low inputs demand but also has a low oil yield (Bernas et al., 2021).

The CF composition of hemp-based food products is dominated by the agricultural phase (90%), with a lower contribution from packaging (10%).

The WF shows the highest value when compared to the literature due to the low yield for both hemp oil and flour.

Regarding flowers, the impacts of the indoor production are slightly larger than that of organic outdoor (Table 9), and our results are a thousand times smaller than the literature. Summers et al. (2021) analyzed the energy and materials required to grow hemp indoors and quantified the corresponding greenhouse gas (GHG) emissions using LCA for a cradle-to-gate system boundary. The analysis was performed across the United States, and the resulting life cycle GHG emissions range from 2.2×10^3 to 5.1×10^3 kg CO_2eq per kg of dried flowers, depending on the location. Mills (2012) estimated that when performed indoor, the production of 1 kg of dried flowers is associated with 4.6×10^3 kg of carbon dioxide emissions into the atmosphere.

The difference between the CF results in our study and in the literature can be justified by considering the following points:

- System boundary: the literature studies include the transport of workers and those of huge quantities of hemp flowers to the warehouses and the redistribution over long distances before the final sale.
- Data source: our study mainly used primary data, while the literature papers are based mostly on secondary (based on public-domain sources) data.
- Kind of indoor production: the case from the United States is much more energy intensive than those in Italy. Production takes place five times a year (four in our case) to obtain high yields (5,000 kg ha^{-1} $year^{-1}$). A larger amount of electricity is

TABLE 5 Data inventory associated with processing and packaging of oil and flour from conventional outdoor practice. Functional unit: 1 kg of oil and flour.

Item	Unit/ FU	Amount	Notes
HEMP-SEED OIL AND FLOUR PROCESSING			
Diesel for transport	kg	1.2×10^{-1}	368 km from the field to the processing site by a light truck
Electricity			
For oil production	kWh	3.2×10^{-2}	Italian energy mix
For flour processing	kWh	6.7×10^{-3}	
HEMP-SEED OIL PACKAGING			
Glass production	kg	7.2×10^{-1}	Transportation not included: bottles, aluminum corks, and plastic films are bought locally
Aluminum production	kg	1.7×10^{-1}	
Plastic production	kg	1.0×10^{-1}	
HEMP FLOUR PACKAGING			
Plastic film production	kg	1.7×10^{-3}	Transportation not included: plastic films are bought locally
DIRECT EMISSIONS ASSOCIATED WITH OIL PROCESSING*			
Carbon dioxide (CO_2)	kg	1.4×10^{-1}	Emission factors provided by IPCC (IPCC, 2006; IPCC, 2019)
Methane (CH_4)	kg	7.8×10^{-3}	
Nitrous oxide (N_2O)	kg	1.1×10^{-3}	
Carbon oxide CO	kg	2.6×10^{-2}	Emission factor provided by EMEP/EEA (EMEP/EEA, 2019)
Non-methane volatile organic compounds ($NMVOC_S$)	kg	5.5×10^{-3}	
Ammonia (NH_3)	kg	5.4×10^{-3}	
Nitrogen oxides (NO_X)	kg	5.3×10^{-2}	
Sulfur dioxide (SO_2)	kg	1.1×10^{-3}	
Black carbon (BC)	kg	6.8×10^{-25}	
Particulate matter $_{10}$ (PM_{10})	kg	4.0×10^{-5}	
Particulate matter $_{2.5}$ ($PM_{2.5}$)	kg	4.0×10^{-5}	
Particulate matter $_{0.1}$ ($PM_{0.1}$)	kg	5.4×10^{-3}	
Total suspended particles (TSP)	kg	4.0×10^{-5}	
Indeno[1,2,3-cd]pyrene (ID(1,2,3-cd)P)	kg	5.6×10^{-8}	
Benzo(k)fluoranthene (B(k)F)	kg	3.1×10^{-8}	
Benzo(b)fluoranthene (B(b)F)	kg	5.9×10^{-8}	
Benzo(a)fluoranthene (B(a)F)	kg	5.6×10^{-8}	

Direct emissions of the flour processing are not calculated because the only input is the electricity from the national grid.

used and is combined with natural gas to ensure suitable conditions in greenhouses. CO_2 is injected to increase foliage growth, and due to the large scale of production, electricity is also used during the drying process (in our case, drying occurs under natural conditions).

Regarding the packaging of the flowers, the impact categories comparison shows that for the packaging of 1 kg of dried flowers, the use of plastic boxes has a slightly higher impact than the use of recycled aluminum boxes.

Moreover, in the case of dried flowers, as for hemp oil and flour, the CF composition is mainly due to the hemp cultivation (about 90%), with a lower contribution of the packaging (10%).

Table 10 shows the CF offset of dried flowers from organic outdoor practice and hemp-based food products from conventional outdoor practice because in these cases, the crop residues are left in the soil, creating a temporary carbon storage. In the indoor condition, on the other hand, biomass residues are composted and then exit the system boundary. The temporary storage is represented by the annual rate of carbon contained in

TABLE 6 Data inventory associated with the processing and packaging of dried flowers. Functional unit: 1 kg of dried flowers.

Item	Unit/ FU	Amount	Amount	Notes
DRIED HEMP FLOWERS PACKAGING				
		Organic outdoor	Indoor	
Transport				
Plastic buckets	kg km	4.0×10^{-4}	-	222 km by a diesel light truck
Aluminum boxes	kg km	-	5.7×10^{-4}	Aluminum boxes arrive from China by kerosene jet-powered aircraft
Plastics production	kg	1.5×10^{-1}	-	Plastic type: high-density polyethylene
Aluminum production	kg	-	2.8×10^{0}	Aluminum from recycled material
DIRECT EMISSIONS				
Carbon dioxide (CO_2)	kg	1.3×10^{-3}	9.7×10^{-3}	Emission factors provided by IPCC (IPCC, 2006; IPCC, 2019)
Methane (CH_4)	kg	6.8×10^{-8}	6.8×10^{-8}	
Nitrous oxide (N_2O)	kg	6.8×10^{-8}	2.7×10^{-7}	
Carbon oxide (CO)	kg	3.0×10^{-6}	3.7×10^{-6}	Emission factor provided by EMEP/EEA (EMEP/EEA, 2019)
Non-methane volatile organic compounds ($NMVOC_S$)	kg	6.6×10^{-8}	3.7×10^{-6}	
Particulate matter $_{0.1}$ ($PM_{0.1}$)	kg	6.2×10^{-7}	-	
Ammonia (NH_3)	kg	6.2×10^{-7}	-	
Indeno[1,2,3-cd]pyrene (ID(1,2,3-cd)P)	kg	6.4×10^{-12}	-	
Benzo(k)fluoranthene (B(k)F)	kg	3.5×10^{-12}	-	
Benzo(b)fluoranthene (B(b)F)	kg	6.7×10^{-12}	-	
Nitrous oxide (NO_X)	kg	6.0×10^{-6}	3.4×10^{-5}	
Benzo(a)fluoranthene (B(a)F)	kg	6.4×10^{-12}	-	
Lead (Pb)	kg	2.1×10^{-11}	-	
Sulfur dioxide (SO_2)	kg	1.2×10^{-8}	-	
Sulfur oxide (SO_X)	kg	-	3.1×10^{-9}	

TABLE 7 Environmental impacts of hemp-seed oil and flour. Functional unit: 1 kg of oil or flour.

Impact category	Seed hemp oil **(FU 1 kg)**	Hemp flour **(FU 1 kg)**
Carbon footprint **(CF)**	2.6×10^{1}	3.3×10^{1}
(kg CO_2eq)		
Eutrophication **(EP)**	3.5×10^{-2}	4.4×10^{-2}
(kg PO_4^{3-} eq)		
Acidification **(AP)**	7.1×10^{-2}	7.5×10^{-2}
(kg SO_2eq)		
Water footprint **(WF)**	4.7×10^{0}	5.6×10^{0}
(m^3 water eq)		

crop residues, which is stabilized in the soil during continuous cultivation cycles (20 years). This value is quantified considering the cropland surface needed to obtain 1 kg of product. The production of 1 kg of dried flowers, cultivated organically outdoor, naturally processed, and packaged in plastic buckets, is carbon-neutral (−0.99 kg CO_2) when the temporary carbon

TABLE 8 Environmental impacts from hemp oil anf flour production, compared with the existing literature referring to other kinds of oils and flours.

	Carbon footprint **(kg CO_2eq kg^{-1})**	Water footprint **(m^3 water eq kg^{-1})**	Reference
OILS			
Hemp-seed oil	26.0	4.7	This study
Palm oil	2.0	0.01	(Schmidt, 2015)
Soybean oil	2.0	0.01	
Rapeseed oil	0.3	-	
Sunflower oil	0.8	0.4	
Peanut oil	4.7	2.5	
Olive oil	From 1.6 to 3.2	-	(Fernández-Lobato et al., 2021)
Olive oil	-	0.04	(Borsato et al., 2019)
FLOURS			
Hemp flour	33.0	5.6	This study
Winter wheat flour	0.3	-	(Riedesel et al., 2022)
Winter rye flour	0.3	-	

TABLE 9 Environmental impacts due to the production of 1 kg of dried flowers.

Impact category	Organic outdoor (FU 1 kg)	Indoor (FU 1 kg)
Carbon footprint **(CF)**	1.5×10^{0}	2.1×10^{0}
(kg CO_2eq)		
Eutrophication **(EP)**	7.1×10^{-4}	1.5×10^{-3}
(kg PO_4^{3-} eq)		
Acidification **(AP)**	5.5×10^{-3}	8.5×10^{-3}
(kg SO_2eq)		
Water footprint **(WF)**	3.2×10^{-1}	1.3×10^{0}
(m^3 water eq)		

TABLE 10 Carbon footprint offset of hemp-seed oil, flour, and dried flowers.

Impact category	Conventional outdoor **(FU: 1 kg seed oil)**	Conventional outdoor **(FU: 1 kg flour)**	Organic outdoor **(FU: 1 kg dried flowers)**
Cropland surface needed to obtain 1 kg product **(ha/FU)**	1.3×10^{-3}	5.9×10^{-4}	1.2×10^{-3}
Carbon storage in soil per FU of product cultivated, processed, and packaged (A)	-2.6×10^{0}	-1.2×10^{0}	-2.5×10^{0}
(kg CO_2 stocked/FU)			
CF (B)	2.6×10^{1}	3.3×10^{1}	1.5×10^{0}
(kg CO_2 eq/FU)			
CF offset per FU of product cultivated, processed, and packaged (A + B)	2.3×10^{1}	3.2×10^{1}	-9.9×10^{-1}
(kg CO_2/FU)			
Emissions reduction **(%)**	−10%	−4%	−166%

storage in soil is included. On the other hand, 1 kg of hemp-seed oil and flour have annual CFs higher than the rate of carbon storage in soil due to the more impactful processes to obtain hemp-based food products (23.41 kg CO_2 and 31.79 kg CO_2, respectively).

When properly arranged, carbon storage represents a useful tool for developing mitigation strategies and guidelines for supporting the consumers' choice. It is opportune to keep in mind that sequestration should be guaranteed over a long period (≥100 years) and not just for 1 year. In many cases, the soil carbon storage could be lost if changes in cropland management or climate effects lead to lower organic matter inputs or increased microbial activity (Paul et al., 2023).

4 Conclusion

The hemp life cycle is quite articulated and complex and provides a number of positive ecosystem services like, among others, carbon uptake and storage, pollination, fertility, heavy-metal absorption, and biodiversity. Furthermore, virtually, every part of the hemp plant has a potential application and can be used to manufacture a variety of marketable products like food items, construction materials, pharmaceuticals, and textiles. Due to the growing importance of hemp in recent years, this paper assesses its environmental potential as a carbon storage plant and the relevance of its production chain.

Three different case studies, representing the Italian industry, are analyzed and compared. An environmental impact profile is then defined through life cycle assessment and a set of mainly primary data.

Considering the mass unit as FU, the organic cultivation practice registers the lowest impact, while the indoor practice shows the highest impact in all the evaluated impact categories (CF, AP, EP, and WF).

Furthermore, carbon footprint offset is evaluated by comparing the carbon footprint (i.e., the direct and indirect emissions in agricultural and transformation phases) with the temporary carbon storage in soil (i.e., the stock due to crop residues in the field when practiced). The cultivation phase provides a CF that ranks from 1.2 (organic outdoor) to 374 (indoor) kg CO_2eq per kg of flowers or 1.9 kg CO_2eq per kg of grains (conventional outdoor). The ability of hemp to sequester carbon in the soil due to crop residues left in the field is evaluated as −2.7 kg CO_2 (ha year)$^{-1}$; this value effectively neutralizes the CF of the agricultural phase for both conventional and organic outdoor practices in the first year.

Dried flowers show a negative balance (−0.99 kg CO_2 per kg dry flower) only when carbon storage due to crop residues in soil is included. Emissions from hemp oil and flour are not compensated, reporting positive values (23.41 kg CO_2 per kg oil and 31.79 kg CO_2 per kg flour).

Under a perspective of circular economy, a scenario based on the use of hemp biomass for insulating panels allows the appreciation of the advantage of fixing carbon in durable goods. As such, the hemp industry can be considered a clear example of a fully circular and sustainable production chain.

Data availability statement

The original contributions presented in the study are included in the article/Supplementary material; further inquiries can be directed to the corresponding author.

Author contributions

MMK: data curation, formal analysis, investigation, methodology, software, visualization, and writing—original draft. MM: conceptualization, data curation, formal analysis, investigation, methodology, writing—original draft, and writing–review and editing. EN: data curation, software, and writing–original draft. NM: conceptualization, supervision, and writing–review and editing. VN: conceptualization, data curation, formal analysis, investigation, methodology, supervision, visualization, writing–original draft, and writing–review and editing.

Funding

The author(s) declare that financial support was received for the research, authorship, and/or publication of this article. This study is carried out within the Agritech National Research Center and received funding from the European Union Next-Generation EU (PIANO NAZIONALE DI RIPRESA E RESILIENZA (PNRR)—MISSIONE 4 COMPONENTE 2, INVESTIMENTO 1.4—D.D. 1032 17/06/2022, CN00000022). This manuscript reflects only the authors' views and opinions, and neither the European Union nor the European Commission can be considered responsible for them. The publication was made possible thanks to the specific contribution of the University of Siena for the support of Open Access and funds from the Department of Physical Sciences, Earth and Environment.

Acknowledgments

The authors thank Gaia Esposito and Cosimo Montefrancesco for their precious support and the three anonymous farmers for providing data and all the precious information.

Conflict of interest

The authors declare that the research was conducted in the absence of any commercial or financial relationships that could be construed as a potential conflict of interest.

Publisher's note

References

Adesina, I., Bhowmik, A., Sharma, H., and Shahbazi, A. (2020). A review on the current state of knowledge of growing conditions, agronomic soil health practices and utilities of hemp in the United States. *Agriculture* 10 (4), 129. doi:10.3390/agriculture10040129

Allegret, S. (2013). "The history of hemp," in *Hemp: industrial production and uses*. Editors P. Bouloc, S. Allegret, and L. Arnaud (UK: CABI), 4–26. Available at: http://www.cabidigitallibrary.org/doi/10.1079/9781845937935.0004.

Amaducci, S., Colauzzi, M., Bellocchi, G., and Venturi, G. (2008). Modelling post-emergent hemp phenology (Cannabis sativa L.): theory and evaluation. *Eur. J. Agron.* 28 (2), 90–102. doi:10.1016/j.eja.2007.05.006

Amaducci, S., Scordia, D., Liu, F. H., Zhang, Q., Guo, H., Testa, G., et al. (2015). Key cultivation techniques for hemp in Europe and China. *Industrial Crops Prod.* 68, 2–16. doi:10.1016/j.indcrop.2014.06.041

Andrianandraina, V. A., Senga Kiessé, T., Cazacliu, B., Idir, R., and Van Der Werf, H. M. G. (2015). Sensitivity analysis of environmental process modeling in a life cycle context: a case study of hemp crop production. *J Industrial Ecol.* 19 (6), 978–993. doi:10.1111/jiec.12228

Asdrubali, F., D'Alessandro, F., and Schiavoni, S. (2015). A review of unconventional sustainable building insulation materials. *Sustain. Mater. Technol.* 4, 1–17. doi:10.1016/j.susmat.2015.05.002

Baldini, M., Zuliani, F., Cattivello, C., and Barbiani, G. (2019). Nuove indicazioni per la coltivazione della canapa in Friuli Venezia Giulia. Available at: https://www.ersa.fvg.it/export/sites/ersa/aziende/in-formazione/notiziario/allegati/2019/1/2_Nuove-coltivazioni-della-canapa.pdf.

Bernas, J., Bernasová, T., Nedbal, V., and Neugschwandtner, R. W. (2021). Agricultural LCA for food oil of winter rapeseed, sunflower, and hemp, based on Czech standard cultivation practices. *Agronomy* 11 (11), 2301. doi:10.3390/agronomy11112301

Bocsa, I., Bosca, I., and Karus, M. (1998). The cultivation of hemp: botany, varieties, cultivation and harvesting. Available at: https://www.semanticscholar.org/paper/The-Cultivation-of-Hemp%3A-Botany%2C-Varieties%2C-and-Bocsa-Bosca/05d7ce569a509e6be4ac2c4b88d2d3e311f93486.

Borsato, E., Giubilato, E., Zabeo, A., Lamastra, L., Criscione, P., Tarolli, P., et al. (2019). Comparison of water-focused life cycle assessment and water footprint assessment: the case of an Italian wine. *Sci. Total Environ.* 666, 1220–1231. doi:10.1016/j.scitotenv.2019.02.331

Ćaćić, M., Perčin, A., Zgorelec, Ž., and Kisić, I. (2019). Evaluation of heavy metals accumulation potential of hemp (Cannabis sativa L.). *J. Cent. Eur. Agric.* 20 (2), 700–711. doi:10.5513/jcea01/20.2.2201

Campiglia, E., Gobbi, L., Marucci, A., Rapa, M., Ruggieri, R., and Vinci, G. (2020). Hemp seed production: environmental impacts of cannabis sativa L. Agronomic practices by life cycle assessment (LCA) and carbon footprint methodologies. *Sustainability* 12 (16), 6570. doi:10.3390/su12166570

Campiglia, E., Radicetti, E., and Mancinelli, R. (2017). Plant density and nitrogen fertilization affect agronomic performance of industrial hemp (Cannabis sativa L.) in Mediterranean environment. *Industrial Crops Prod.* 100, 246–254. doi:10.1016/j.indcrop.2017.02.022

Citterio, S., Prato, N., Fumagalli, P., Aina, R., Massa, N., Santagostino, A., et al. (2005). The arbuscular mycorrhizal fungus Glomus mosseae induces growth and metal accumulation changes in Cannabis sativa L. *Chemosphere* 59 (1), 21–29. doi:10.1016/j.chemosphere.2004.10.009

Dowling, C. A., Melzer, R., and Schilling, S. (2021). Timing is everything: the genetics of flowering time in *Cannabis sativa*. *Biochem.* 43 (3), 34–38. doi:10.1042/bio_2021_138

Ecoinvent (2020). Swiss centre for life-cycle inventories. Ecoinvent database - ecoinvent. Available at: https://ecoinvent.org/the-ecoinvent-database/.

EMEP/EEA (2019). EMEP/EEA air pollutant emission inventory guidebook 2019 — European Environment Agency. Available at: https://www.eea.europa.eu/publications/emep-eea-guidebook-2019.

Essaghouri, L., Mao, R., and Li, X. (2023). Environmental benefits of using hempcrete walls in residential construction: an LCA-based comparative case study in Morocco. *Environ. Impact Assess. Rev.* 100, 107085. doi:10.1016/j.eiar.2023.107085

European Commission (2023). Hemp. Available at: https://agriculture.ec.europa.eu/farming/crop-productions-and-plant-based-products/hemp_en.

Farinon, B., Molinari, R., Costantini, L., and Merendino, N. (2022). "Biotechnological transformation of hempseed in the food industry," in *Cannabis/hemp for sustainable agriculture and materials*. Editors D. C. Agrawal, R. Kumar, and M. Dhanasekaran (Singapore: Springer), 163–202. Available at: https://link.springer.com/10.1007/978-981-16-8778-5_7.

Faux, A. M., Draye, X., Lambert, R., d'Andrimont, R., Raulier, P., and Bertin, P. (2013). The relationship of stem and seed yields to flowering phenology and sex expression in monoecious hemp (Cannabis sativa L.). *Eur. J. Agron.* 47, 11–22. doi:10.1016/j.eja.2013.01.006

Fernández-Lobato, L., García-Ruiz, R., Jurado, F., and Vera, D. (2021). Life cycle assessment, C footprint and carbon balance of virgin olive oils production from traditional and intensive olive groves in southern Spain. *J. Environ. Manag.* 293, 112951. doi:10.1016/j.jenvman.2021.112951

Flicker, N. R., Poveda, K., and Grab, H. (2020). The bee community of cannabis sativa and corresponding effects of landscape composition. *Environ. Entomol.* 49 (1), 197–202. doi:10.1093/ee/nvz141

González-García, S., Hospido, A., Feijoo, G., and Moreira, M. T. (2010). Life cycle assessment of raw materials for non-wood pulp mills: hemp and flax. *Resour. Conservation Recycl.* 54 (11), 923–930. doi:10.1016/j.resconrec.2010.01.011

Gryndler, M., Sudová, R., Püschel, D., Rydlová, J., Janoušková, M., and Vosátka, M. (2008). Cultivation of high-biomass crops on coal mine spoil banks: can microbial inoculation compensate for high doses of organic matter? *Bioresour. Technol.* 99 (14), 6391–6399. doi:10.1016/j.biortech.2007.11.059

Heidari, M. D., Lawrence, M., Blanchet, P., and Amor, B. (2019). Regionalised life cycle assessment of bio-based materials in construction; the case of hemp shiv treated with sol-gel coatings. *Materials* 12 (18), 2987. doi:10.3390/ma12182987

Ingrao, C., Lo Giudice, A., Bacenetti, J., Tricase, C., Dotelli, G., Fiala, M., et al. (2015). Energy and environmental assessment of industrial hemp for building applications: a review. *Renew. Sustain. Energy Rev.* 51, 29–42. doi:10.1016/j.rser.2015.06.002

IPCC (2006). 2006 IPCC guidelines for national greenhouse gas inventories — IPCC. Available at: https://www.ipcc.ch/report/2006-ipcc-guidelines-for-national-greenhouse-gas-inventories/.

IPCC (2019). 2019 refinement to the 2006 IPCC guidelines for national greenhouse gas inventories — IPCC. Available at: https://www.ipcc.ch/report/2019-refinement-to-the-2006-ipcc-guidelines-for-national-greenhouse-gas-inventories/.

ISO (2020). International Standard published. ISO 14044:2006/Amd 2: 2020 Environmental management Life cycle assessment Requirements and guidelines. Available at: https://www.iso.org/standard/76122.html.

Jasinskas, A., Streikus, D., and Vonžodas, T. (2020). Fibrous hemp (Felina 32, USO 31, Finola) and fibrous nettle processing and usage of pressed biofuel for energy purposes. *Renew. Energy* 149, 11–21. doi:10.1016/j.renene.2019.12.007

Journals, I., and Dalio, Dr. J. S. (2014). Cannabis sativa-an important subsistence pollen source for *Apis mellifera*. Available at: http://figshare.com/articles/Cannabis_sativa_An_Important_Subsistence_Pollen_Source_for_Apis_mellifera_/1134447.

Kaur, G., and Kander, R. (2023). The sustainability of industrial hemp: a literature review of its economic, environmental, and social sustainability. *Sustainability* 15 (8), 6457. doi:10.3390/su15086457

Kladar, N., Čonić, B. S., Božin, B., and Torović, L. (2021). European hemp-based food products – health concerning cannabinoids exposure assessment. *Food control.*, 129, 108233. doi:10.1016/j.foodcont.2021.108233

Liu, J., Liu, S., Zhu, L., Sun, L., Zhang, Y., Li, X., et al. (2023). Carbon neutrality potential of textile products made from plant-derived fibers. *Sustainability* 15 (9), 7070. doi:10.3390/su15097070

Mercuri, A. M., Accorsi, C. A., and Mazzanti, M. B. (2002). The long history of Cannabis and its cultivation by the Romans in central Italy, shown by pollen records from Lago Albano and Lago di Nemi. *Veg. Hist. Archaeobotany* 11 (4), 263–276. doi:10.1007/s003340200039

Mills, E. (2012). The carbon footprint of indoor Cannabis production. *Energy Policy* 46, 58–67. doi:10.1016/j.enpol.2012.03.023

Niccolucci, V., Marchi, M., Neri, E., Pulselli, R. M., Bastianoni, S., and Marchettini, N. (2021). Insights into nitrogen footprint accounting for products and application to an organic pig farm. *Ecol. Indic.* 133, 108411. doi:10.1016/j.ecolind.2021.108411

Palacios-Munoz, B., Peuportier, B., Gracia-Villa, L., and López-Mesa, B. (2019). Sustainability assessment of refurbishment vs. new constructions by means of LCA and durability-based estimations of buildings lifespans: a new approach. *Build. Environ.* 160, 106203. doi:10.1016/j.buildenv.2019.106203

Patyk, A., and Reinhardt, G. A. (1998). Life cycle assessment of hemp products. *Life Cycle Assess. hemp Prod.*, 39–44.

Paul, C., Bartkowski, B., Dönmez, C., Don, A., Mayer, S., Steffens, M., et al. (2023). Carbon farming: are soil carbon certificates a suitable tool for climate change mitigation? *J. Environ. Manag.* 330, 117142. doi:10.1016/j.jenvman.2022.117142

Pervaiz, M., and Sain, M. M. (2003). Carbon storage potential in natural fiber composites. *Resour. Conservation Recycl.* 39 (4), 325–340. doi:10.1016/s0921-3449(02)00173-8

Petit, J., Salentijn, E. M. J., Paulo, M. J., Thouminot, C., Van Dinter, B. J., Magagnini, G., et al. (2020). Genetic variability of morphological, flowering, and biomass quality traits in hemp (cannabis sativa L.). *Front. Plant Sci.* 11, 102. doi:10.3389/fpls.2020.00102

Rapa, M., Ciano, S., Rocchi, A., D'Ascenzo, F., Ruggieri, R., and Vinci, G. (2019). Hempseed oil quality parameters: optimization of sustainable methods by miniaturization. *Sustainability* 11 (11), 3104. doi:10.3390/su11113104

Riedesel, L., Laidig, F., Hadasch, S., Rentel, D., Hackauf, B., Piepho, H. P., et al. (2022). Breeding progress reduces carbon footprints of wheat and rye. *J. Clean. Prod.* 377, 134326. doi:10.1016/j.jclepro.2022.134326

Salentijn, E. M. J., Zhang, Q., Amaducci, S., Yang, M., and Trindade, L. M. (2015). New developments in fiber hemp (Cannabis sativa L.) breeding. *Industrial Crops Prod.* 68, 32–41. doi:10.1016/j.indcrop.2014.08.011

Sawler, J., Stout, J. M., Gardner, K. M., Hudson, D., Vidmar, J., Butler, L., et al. (2015). The genetic structure of marijuana and hemp. *PLoS ONE* 10 (8), e0133292. doi:10.1371/journal.pone.0133292

Schmidt, J. H. (2015). Life cycle assessment of five vegetable oils. *J. Clean. Prod.* 87, 130–138. doi:10.1016/j.jclepro.2014.10.011

Scrucca, F., Ingrao, C., Maalouf, C., Moussa, T., Polidori, G., Messineo, A., et al. (2020). Energy and carbon footprint assessment of production of hemp hurds for application in buildings. *Environ. Impact Assess. Rev.* 84, 106417. doi:10.1016/j.eiar.2020.106417

Skoglund, G., Nockert, M., and Holst, B. (2013). Viking and early middle ages northern scandinavian textiles proven to be made with hemp. *Sci. Rep.* 3 (1), 2686. doi:10.1038/srep02686

Sorrentino, G. (2021). Introduction to emerging industrial applications of cannabis (Cannabis sativa L.). *Rend. Fis. Acc. Lincei* 32 (2), 233–243. doi:10.1007/s12210-021-00979-1

Struik, P. C., Amaducci, S., Bullard, M. J., Stutterheim, N. C., Venturi, G., and Cromack, H. T. H. (2000). Agronomy of fibre hemp (Cannabis sativa L.) in Europe. *Industrial Crops Prod.* 11 (2–3), 107–118. doi:10.1016/s0926-6690(99)00048-5

Summers, H. M., Sproul, E., and Quinn, J. C. (2021). The greenhouse gas emissions of indoor cannabis production in the United States. *Nat. Sustain* 4 (7), 644–650. doi:10.1038/s41893-021-00691-w

Teterycz, D., Sobota, A., Przygodzka, D., and Łysakowska, P. (2021). Hemp seed (Cannabis sativa L.) enriched pasta: physicochemical properties and quality evaluation. *PLoS ONE* 16 (3), e0248790. doi:10.1371/journal.pone.0248790

The Angiosperm Phylogeny Group (1998). An ordinal classification for the families of flowering plants. *Ann. Mo. Botanical Gard.* 85 (4), 531–553.

Todde, G., Carboni, G., Marras, S., Caria, M., and Sirca, C. (2022). Industrial hemp (Cannabis sativa L.) for phytoremediation: energy and environmental life cycle assessment of using contaminated biomass as an energy resource. *Sustain. Energy Technol. Assessments* 52, 102081. doi:10.1016/j.seta.2022.102081

Van Der Werf, H. M. G. (2004). Life Cycle Analysis of field production of fibre hemp, the effect of production practices on environmental impacts. *Euphytica* 140 (1–2), 13–23. doi:10.1007/s10681-004-4750-2

Yano, H., and Fu, W. (2023). Hemp: a sustainable plant with high industrial value in food processing. *Foods* 12 (3), 651. doi:10.3390/foods12030651

Zampori, L., Dotelli, G., and Vernelli, V. (2013). Life cycle assessment of hemp cultivation and use of hemp-based thermal insulator materials in buildings. *Environ. Sci. Technol.* 47 (13), 7413–7420. doi:10.1021/es401326a

frontiers | Frontiers in Environmental Science

TYPE Perspective
PUBLISHED 14 May 2024
DOI 10.3389/fenvs.2024.1381141

OPEN ACCESS

EDITED BY
Chenxi Li,
Xi'an University of Architecture and Technology, China

REVIEWED BY
Andreas Magerl,
University of Natural Resources and Life Sciences Vienna, Austria
Leonardo Clavijo,
Universidad de la República, Uruguay

*CORRESPONDENCE
Nicolas Bélanger,
nicolas.belanger@teluq.ca

RECEIVED 02 February 2024
ACCEPTED 29 April 2024
PUBLISHED 14 May 2024

CITATION
Laberge S, Courcot B, Lagarde A, Lebel Desrosiers S, Lafore K, Thiffault E, Thiffault N and Bélanger N (2024), Opportunities and challenges to improve carbon and greenhouse gas budgets of the forest industry through better management of pulp and paper by-products. *Front. Environ. Sci.* 12:1381141. doi: 10.3389/fenvs.2024.1381141

Opportunities and challenges to improve carbon and greenhouse gas budgets of the forest industry through better management of pulp and paper by-products

Sharlène Laberge[1,2], Blandine Courcot[1,2], Andréanne Lagarde[1,2], Simon Lebel Desrosiers[1,2], Karima Lafore[1,2], Evelyne Thiffault[3], Nelson Thiffault[4,5] and Nicolas Bélanger[1,2]*

[1]Département Science et Technologie, Téluq, Université du Québec, Québec, QC, Canada, [2]Centre d'étude de la Forêt, Université du Québec à Montréal, Montréal, QC, Canada, [3]Centre de Recherche sur les Matériaux Renouvelables, Département des Sciences du bois et de la forêt, Université Laval, Québec, QC, Canada, [4]Canadian Wood Fibre Centre, Canadian Forest Service, Natural Resources Canada, Québec, QC, Canada, [5]Centre d'étude de la forêt, Faculté de Foresterie, de Géographie et de Géomatique, Université Laval, Québec, QC, Canada

Developing land use strategies to optimize carbon sinks and improve carbon footprints involves proposing efficient nature-based solutions that industries and businesses can implement while considering financial and legislative constraints. The pulp and paper industry is associated with significant greenhouse gas (GHG) emissions, primarily due to the substantial carbon dioxide (CO_2) footprint of its mills. Also, some forestry operations contribute to the release of carbon to the atmosphere in the form of CO_2 and methane (CH_4). Conversely, this industry could potentially be a significant ally in the fight against climate change by favoring forestry practices that reduce carbon emissions and increase its sequestration, namely, by adding value to industrial by-products (e.g., biosolids) instead of treating them as wastes and landfilling them. Notably, the pulp and paper industry has been seeking alternative uses of its by-products, such as fertilizers to maximize tree growth. In this paper, we identify opportunities and challenges that exist for the pulp and paper industry in regard to recycling industrial by-products to: 1) lower GHG emissions directly at the mill and 2) improve its GHG budget by increasing carbon sequestration in forests and plantations. We illustrate our analyses by describing a case study of a pulp and paper mill in southern Quebec, Canada, that uses its biosolids and other by-products as fertilizers. This case study highlights that this strategy could not only contribute to the reduction of GHGs but could also create added value and improve economic returns of forest operations.

KEYWORDS

biosolids, greenhouse gases, landfilling, methane, nature-based climate solutions, pulp and paper industry

1 Introduction

Other than innovative technologies such as carbon capture (Kätelhön et al., 2021) and utilization (Jeffry et al., 2021) as well as charge carrier dynamics (Sun et al., 2023), nature-based climate solutions (NCS) are proposed to reduce atmospheric greenhouse gases (GHGs) and mitigate climate change (Griscom et al., 2017; Seddon, 2022). Nature-based climate solutions include efforts that aim to increase the ability of ecosystems to sequester carbon and decrease GHG emissions. Applying NCS may include land-use practices such as protecting forests or proceeding to afforestation of abandoned farmlands, decommissioned mine sites or abandoned industrial fields (Bastin et al., 2019; Lewis et al., 2019; Kaarakka et al., 2021). Nature-based climate solutions may also include more subtle changes in cultural practices such as reducing the use of synthetic fertilizers and using biochar, lime, green crops and crop rotation, and mycorrhizae to reduce nitrous oxide (N_2O) emissions, a potent GHG (Forster et al., 2021; Hassan et al., 2022). In agricultural contexts, implementing such NCS could also imply using less intensive tilling practices to reduce carbon loss from soils (Maia et al., 2022). Similarly, the forest industry can modify forest management practices with the goal of sequestering more carbon and lowering GHG emissions (Drever, 2021).

The pulp and paper industry, known for its energy-intensive operations (either as electricity, heat for steam production and fuel), is closely tied to a substantial carbon dioxide (CO_2) footprint, contributing to 2% of direct industrial CO_2 emissions in 2022 (Szabó et al., 2009; Del Rio et al., 2022; IEA, 2023), even though this industry often self-generates its electricity and heat using its residues as fuel. In the US, for example, Tomberlin et al. (2020) estimated that one metric ton of paper creates a production weighted average of 942 kg of CO_2 equivalent, with 50% coming from fuels (Tomberlin et al., 2020). Globally in 2021, the pulp and paper industry emitted an average of 0.45 t of CO_2 per tonne of paper produced, whereas projections suggest emissions of 0.31 t CO_2 per tonne of paper by 2030 (IEA, 2022).

Moreover, the industry faces emissions from by-products such as paper biosolids (PBs) and de-inking sludges, with landfilling and incineration recognized as sources of CO_2 and methane (CH_4) emissions (Faubert et al., 2016). With the aim of developing a circular economy and mitigating climate change more efficiently, the pulp and paper industry has been looking at alternatives to landfilling and incineration of PBs. Notably, the industry has been using its biosolids as a soil amendment for silvicultural, agricultural and ecological restoration purposes, as well as for biorefinery products such as wood adhesives and fillers, thermoplastic composites, and sorbent materials (Pervaiz and Sain, 2015; Bilodeau-Gauthier et al., 2022; Chen et al., 2023; Grimond et al., 2023). Recycling of PBs in silviculture could increase carbon sequestration by maximizing tree growth (Bilodeau-Gauthier et al., 2022) and promoting a stable form of carbon in soils (Khlifa et al., 2023), as well as reducing GHG emissions compared to synthetic fertilizers (Chen et al., 2023). Additionally, it could avoid a significant CO_2-equivalent flux to the atmosphere associated with the landfilling or incineration of PBs. This avoidance could also be conducted in a cost-effective way, while fast-growing tree plantations receiving PBs could contribute to fibre supply and help conserve habitats and biodiversity (Himes et al., 2022). In this perspective paper, we aim to identify opportunities and challenges for the pulp and paper industry in recycling its PBs to: 1) lower GHG emissions directly at the mill site, 2) improve its GHG budget by increasing carbon sequestration in forests and plantations, and 3) favor a forest land management scheme for the preservation of natural habitats and biodiversity.

2 The world problem of biosolids, with emphasis on paper biosolids

Quantifying global waste generation proves challenging due to varied definitions and methodologies. Current estimates indicate waste production at 19.8 billion tonnes annually, with 15% comprising biomass like solid wood, construction wood, paper and cardboard (Maalouf and Mavropoulos, 2023). Despite uncertainties, projections suggest a global increase to 28 and 46 billion tonnes per year by 2030 and 2050, respectively (Di Giacomo and Romano, 2022). Managing these wastes poses a significant environmental challenge, with 40% being landfilled, 19% recycled or composted, and 11% incinerated (Kaza et al., 2018). As the global population continues to grow, waste management emerges as one of the greatest environmental challenges of the 21st century (Vaverková, 2019).

Effective waste management should be guided by policies that promote reducing at the source, reusing, recycling and recovering (i.e., the 4R principle; Rada et al., 2018). However, more often than not, it involves landfilling or incineration. Because incineration is costly and a direct and significant source of GHGs, landfilling is the preferred method and is expected to increase in the coming decades. Nonetheless, the expansion of landfill sites brings environmental challenges, including increased hydraulic loads of leachates on adjacent watercourses, air quality issues (e.g., odors and suspended particles) and GHG emissions (Wang et al., 2014; Zhang et al., 2019; Siddiqua et al., 2022).

Sewage sludge, a by-product of municipal wastewater treatment, is termed municipal biosolids (MBs) when meeting certain criteria for land application. These must exhibit low levels of pathogens and other contaminants such as metals, although criteria vary from country to country (LeBlanc et al., 2009; Lowman et al., 2013; Popoola et al., 2023). Global production of biosolids is projected to reach 200 million tonnes annually by 2025 (Mohajerani et al., 2017), with the pulp and paper industry being a major contributor. In 2020, 34 countries accounted for 82% of the global paper and paperboard production (402 million tonnes) (FAO, 2023), set to increase to 550 million tonnes by 2050 (Mabee and Roy, 2003). As such, the production of PBs is expected to increase proportionally. In Quebec, Canada, for example, paper mill biosolids amounted to 1 million tonne in 2018 (RECYC-QUÉBEC, 2018). The pulp and paper production process generates wastes and by-products, of which 87% is classified as pulp and paper mill sludge, whereas the remaining is considered as impurities, waste chemicals and gaseous emissions (Turner et al., 2022).

The pulp and paper industry is regulated for wastewater discharge from pulp and paper mills into surface waters. Paper biosolids, similar to MBs, are disposed by landfilling, incineration, or are applied to land for various purposes (e.g., agriculture, forestry, ecological restoration). In addition to environmental impacts,

landfilling and incineration of biosolids face limited social acceptance and economic challenges, such as substantial fees. These fees aim, in part, to incentivize industries to adhere to the 4R principle before resorting to elimination (Primeau, 2014; Faubert et al., 2015). While landfilling is cost-effective compared to incineration, cost recovery options (e.g., biogas recovery for energy production) remains challenging. Consequently, the use of MBs and PBs as soil amendments or materials for reconstructing soils in restoration projects is gaining popularity.

3 Landfilling of paper biosolids

Landfilling of PBs is the most widely used disposal method, and the pulp and paper industry generally manages its own landfilling facilities (Haile et al., 2021). In addition to hazardous substances reaching adjacent watercourses and causing air quality issues (Haile et al., 2021; Siddiqua et al., 2022), landfilling sites generate large amounts of GHGs under various conditions (Wang et al., 2014; Zhang et al., 2019). However, estimates of the proportion of landfill sites dedicated to PB disposal relative to landfill sites as a whole and empirical estimates of GHG emissions from them are non-existent, making it difficult to assess their contribution to GHG emissions globally (Primeau, 2014; Faubert et al., 2016; MELCC, 2020). Faubert et al. (2016) suggested from modelling and theory that 2.69 tonnes of CO_2 and 0.24 tonne of CH_4 could be emitted to the atmosphere for every tonne of PBs that is landfilled. Methane emissions are a primary concern for climate change due to its high global warming potential (GWP) compared to CO_2, i.e., 28 to 32 times higher over 100 years as initially suggested by Byrne and Goldblatt (2014). However, a new model (GWP*) has recently been proposed to improve calculations of warming-equivalent emissions since GWP can overestimate the cumulative effect of short-lived climate pollutants, such as CH_4, by not properly considering the short-term and long-term effects of these pollutants in the atmosphere (Cain et al., 2019; Lynch et al., 2020). Methane from landfilled PBs is considered the main GHG because most of CO_2 emissions could be offset by the main constituent of PBs, i.e., short lignin fibers derived from photosynthesis (Camberato et al., 2006). However, landfilled biosolids can also generate N_2O through the cooxidation of ammonia by methanotrophic soil bacteria in cover soils (Zhang et al., 2009).

Methanogenesis occurs during the anaerobic mineralization of organic matter (Le Mer and Roger, 2001). Anaerobic conditions in landfill cells are created over time through the compaction of layers of organic matter (Olivier, 2013). Because PBs are rich in wood fibers and organic matter, they provide a significant carbon source for methanogenic microbes (Camberato et al., 2006). During the fermentation process, methanogenic microbes transform organic matter into CH_4 and some CO_2 (Le Mer and Roger, 2001). Landfill cells are typically covered with an engineered cap comprising a clay layer to limit water infiltration and gas exchange. This cap is further covered by a sandy mineral soil with low organic matter content (Handel et al., 1997; Fraser-McDonald et al., 2022). A portion of the CH_4 produced is then oxidized through methanotrophy to CO_2 and water in the cover soil layer, facilitated by its high oxygen levels (Boeckx et al., 1996; Le Mer and Roger, 2001) and low organic matter content (Handel et al., 1997). Methane that remains unaffected in the cover soil layer is released to the atmosphere by diffusion and plant gas exchange (Le Mer and Roger, 2001).

Cover soils thus aim to reduce CH_4 emissions by creating oxygenated conditions where CH_4 transforms into CO_2 and water before reaching the atmosphere. However, fissures, cracks and holes in the mineral cap often form, creating preferential channels for CH_4 from the organic layer to bypass oxidation and be released directly to the atmosphere (Schroth et al., 2012). Also, highly porous material can allow CH_4 to flow through the cover soil too quickly for oxidation to occur before reaching the atmosphere (Wang et al., 2022). The heterogeneous nature of the cover soil often leads to high spatial variability in CH_4 fluxes across a landfill site (Schroth et al., 2012). Estimates of CH_4 emissions from PB landfill sites, assuming that 10% of CH_4 is oxidized in the cover soil, may therefore be underestimated (Chanton et al., 2009; Schroth et al., 2012). However, membrane gas permeation has been used in recent years to channel biogas for energy use or to transform it into CO_2 through flaring (Makaruk et al., 2010; Chmielewski et al., 2019). To our knowledge, however, this method has only been used in municipal landfills.

4 Paper biosolids as fertilizers

Application of MBs and PBs to agricultural soils can positively impact soil fertility and crop yields (Gagnon and Ziadi, 2012; Lu et al., 2012; Ziadi et al., 2013; Abdi et al., 2016; Sharma et al., 2017). Other than providing nitrogen and phosphorus, PBs: 1) are rich in calcium, thus addressing soil acidity issues, 2) enhance soil structure by providing organic matter (or carbon), 3) increase nutrient cycling by improving soil microbial biomass and activity and 4) increase soil cation exchange capacity due to the added organic matter and increased pH. Paper biosolids are less enriched in nitrogen and phosphorus compared to MBs and contain fewer contaminants, thus reducing environmental risks (Charbonneau et al., 2001; Gagnon et al., 2013). The high fiber content of PBs also imparts slow-nitrogen-release fertilizer properties (Gagnon and Ziadi, 2012). In forestry, the use of PBs can be particularly significant for carbon sequestration. It has the potential to stimulate tree growth by improving foliar nutrition and, consequently, accelerating carbon capture through photosynthesis (Lteif et al., 2007; Rodriguez et al., 2018; Bilodeau-Gauthier et al., 2022). However, further work is necessary to assess how fertilization with PBs can influence carbon sequestration of forest plantations under different climates, site conditions (e.g., soils), site (mechanical) preparation and weed management. To our knowledge, no effort was made in synthesizing such data.

Fertilization with PBs can decrease GHG emissions when compared to synthetic fertilizers such as urea (Chen et al., 2023). Furthermore, the use of PBs in agriculture and forestry diverts biosolids from landfills, thereby reducing associated CH_4 emissions (Faubert et al., 2019). Considering these factors, repurposing PBs from the pulp and paper industry as fertilizers in silviculture emerges not only as a theoretical concept but also as a practical NCS. To illustrate this potential, we present a case study from

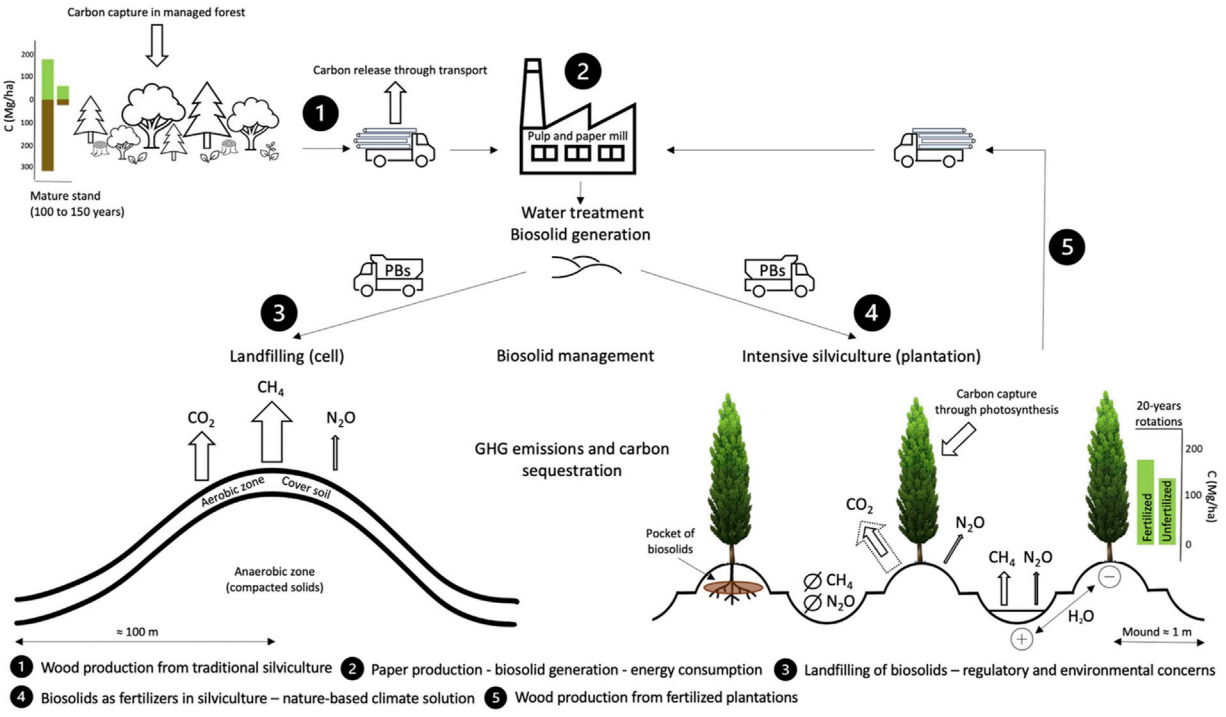

FIGURE 1
Conceptual diagram of paper biosolids management methods. The size of GHG emissions arrows does not accurately represent differences between disposal methods but indicates variations within each method. Solid arrows refer to greenhouse gases emitted from biosolids, whereas the dotted arrow for CO_2 represents emitted by background (natural) soil respiration. Soil and tree biomass carbon stocks from unpublished data for mature managed deciduous forests (K. Lafore) and hybrid poplar plantations (S. Lebel-Desrosiers) in southern Quebec, Canada. For the latter, soil carbon stocks are not yet available.

southern Quebec. This case study demonstrates how the purposeful use of PBs in silvicultural treatments can effectively contribute to sustainable waste management practices and significantly enhance carbon sequestration efforts (Figure 1).

In this case study, PBs are specifically used to fertilize fast-growing hybrid poplar (e.g., *Populus* x *canadensis* × *P. maximowiczii*) plantations, classified as an intensive silvicultural practice. Trees are planted on mound which are created with an excavator (Figure 1). Using allometric equations from the R software package "allodb" (Gonzalez-Akre et al., 2022), it was estimated that, over a 20-year period, plantations receiving industrial by-products could sequester up to 26.7% more carbon than unfertilized plantations (treated: 171 Mg C ha^{-1}; unfertilized: 134 Mg C ha^{-1}). Achieving a target of 200 m^3 ha^{-1} for merchantable wood could be realized, on average, in about 20 years in fertilized plantations (compared to 140 m^3 ha^{-1} in unfertilized plantations), allowing faster rotations and higher carbon sequestration in the long term. In comparison, wood biomass (aboveground) in twenty-one mature (~100–150 years) deciduous forests and mixedwood stands in southern Quebec holds between 38 and 184 Mg ha^{-1} of carbon (K. Lafore, unpublished data).

It could be argued that this wood biomass is destined for paper, a product with a short life span and limited recycling cycles, resulting in fewer benefits in terms of carbon emission mitigation. Yet, augmenting yields in forest plantations destined for paper production also has the added benefit of relieving pressure on other forests for wood supply. This, in turn, leads to the protection of larger swaths of forest landscapes supporting the provision of other ecosystem services (Wang et al., 2022).

Soil carbon stocks are expected to substantially increase after PB application due to their high organic carbon content and carbon: nitrogen ratio (Henry et al., 1994; Gagnon and Ziadi, 2012). At an application rate of about 125 Mg ha^{-1}, the newly added carbon (approximately 50–60 Mg C ha^{-1}) is anticipated to become a stable long-term storage in forest soils, similar to observations in ecological restoration projects, some being afforestation efforts, using MBs for soil reconstruction (Trlica and Teshima, 2011; Carbassa et al., 2020; Khlifa et al., 2023). These afforestation projects can also lead to significant tree growth and carbon sequestration as well (e.g., Grimond et al., 2023; Bélanger et al., 2024). Soil carbon improvement results from 'pockets' of PBs trapped at the base of the mounds during their creation and due to limited mixing, along with the aggregation of organic carbon to clay-mineral particulates. The stability of these carbon pools is largely influenced by the chemical signature of the carbon forms in the PBs, particularly the presence of more labile carbohydrates (Gagnon and Ziadi, 2022).

In the mid-term, increased tree growth is expected to further enhance soil carbon stocks via increased litter flux, including roots, to the soil (Thevathasan and Gordon, 1997; Arevalo et al., 2011), promoting forest floor development and carbon accumulation in mineral horizons. Preliminary data suggest that forest floor depth of the southern Quebec case study sites increased from an average of 1.7–5 cm in just 12 years for plantations receiving PBs, while no

change in forest floor depth was observed in unfertilized plantations over 14 years. The soil organic content of boreal, mixed and deciduous forest soils in Quebec is, on average, 44 Mg C ha^{-1} (Tremblay and Ouimet, 2000). Less than 3% of the forests exhibited soil organic content (SOC) above 100 Mg C ha^{-1} in this study. Similarly, a very large variation in soil carbon stocks (2–315 Mg ha^{-1}) was measured for old-growth forest stands in southern Quebec (K. Lafore, unpublished data). Although estimating the amount of this new carbon is challenging, a forest floor in steady state in these temperate forests typically reaches a depth of 5–15 cm and is 25%–40% of the soil carbon stock. The expectation is that this steady state will be reached more rapidly in the plantations receiving PBs.

Another key, yet complex aspect to consider, is the potential reduction in GHG emissions by diverting PBs from landfills and applying them to plantations. It is anticipated that applying relatively small amounts of PBs at the soil surface, without or with very limited compaction and under well-aerated soil conditions, will significantly lower overall CH_4 and N_2O emissions compared to landfilling. However, spatial variation in fluxes is expected to be large, correlating with field microtopography associated with mounding. Mounding creates a heterogeneous soil surface with: 1) dry zones characterized by lower litter accumulation (mounds), 2) unaltered areas with soil moisture levels and litter accumulation rates expected from a well-drained forest soil (ground level), and 3) wetter zones with substantial litter accumulation (depressions) that could contribute to CH_4 and N_2O emissions. In fact, like methanogenesis, denitrification rates are higher in compacted and poorly drained soils (Beare et al., 2009). Considering that wet depressions represent about one-third of the planted landscape, GHG emissions under this microtopography should be assessed. Preliminary summer sampling at the case study site suggests that CH_4 fluxes are present in only some depressions and CO_2 fluxes were lower in (wet) depressions and on (dry) mounds (287–356 mg m^{-2} h^{-1}) than on unaltered soil (701 mg m^{-2} h^{-1}).

The values above suggest no significant change in CO_2 fluxes due to mounding or PB application, as they are within the range of those measured in comparable forest stands under the same soil temperatures (Bélanger et al., 2021). Similarly, our preliminary data suggest that PB application does not lead to the production of N_2O across the mounding microtopography. Chen et al. (2023) observed the opposite after PB application in hybrid poplar plantations in Alberta, i.e., a 21% and 17% increase in CO_2 and N_2O emissions, but no change in CH_4 emissions. These sites appear to show less microtopography (prepared by one-way cultivation). Measurements of the southern Quebec case study sites were taken 3 years after PB application, while fresh and wet biosolids are known to be significant sources of N_2O (Roman-Perez and Hernandez-Ramirez, 2022). The duration of these large emissions is not well known, especially in forest soils; this deserves our full attention because the benefits that could be gained by reducing landfill CH_4 emissions and increasing carbon sequestration with the use of PBs in hybrid poplar plantations could be offset if this practice also causes N_2O emissions for a prolonged period. Further monitoring of soil conditions and gas efflux is thus required to determine if carbon accumulates in the new soils and to assess GHG dynamics to fully evaluate their potential as a climate solution.

5 Conclusion

Management of waste materials from the pulp and paper industry often involves landfilling. However, our preliminary results offer a promising perspective for the enhanced recovery and recycling of PBs, leading to reduced GHG emissions and improved carbon sequestration when combined with appropriate silvicultural practices. As more field data are collected to better quantify landfill CH_4 emissions, diverting PBs from landfills to plantations could prove valuable for the forest sector to contribute to CH_4 emissions mitigation targets.

Despite the promising benefits of applying biosolids in forestry, challenges must be addressed. Environmental and regulatory concerns, including the potential for heavy metal accumulation and pathogen transmission, require careful management (Pöykiö et al., 2007; Lu et al., 2012). Among the pollutants of concerns are perfluoroalkylated substances, synthetic chemicals such as perfluorooctane sulfonate and perfluorooctanoic acid (PFAS), which pose health risks (Kirk et al., 2018; Ehrlich et al., 2023; van Larebeke et al., 2023). Communities near landfill sites have raised public health concerns, including quality-of-life impacts due to odors (Lowman et al., 2013). Moreover, it is not yet clear how the wastewater treatment processes impact the concentration of PFAS in sludges and biosolids (Behnami et al., 2024; Gewurtz et al., 2024). Therefore, the development of guidelines and monitoring systems is essential to ensure that the use of biosolids adheres to environmental safety standards and does not adversely affect forest ecosystems or human health.

Data availability statement

The datasets presented in this article are not readily available because this is a perspective paper only and we report preliminary data only. When full data are published, they will be made available publicly. Requests to access the datasets should be directed to nicolas.belanger@teluq.ca.

Author contributions

SL: Conceptualization, Data curation, Formal Analysis, Investigation, Methodology, Writing–original draft, Writing–review and editing. BC: Conceptualization, Formal Analysis, Investigation, Methodology, Writing–original draft, Writing–review and editing. AL: Conceptualization, Investigation, Methodology, Writing–original draft, Writing–review and editing. SL: Conceptualization, Formal Analysis, Investigation, Methodology, Writing–original draft, Writing–review and editing, Data curation. KL: Data curation, Conceptualization, Formal Analysis, Investigation, Methodology, Writing–original draft, Writing–review and editing. ET: Funding acquisition, Project administration, Resources, Supervision, Conceptualization, Formal Analysis, Investigation, Methodology, Writing–original draft, Writing–review and editing. NT: Funding acquisition, Project administration, Resources, Supervision, Conceptualization, Formal Analysis, Investigation, Methodology, Writing–original draft, Writing–review and editing. NB: Validation,

Conceptualization, Investigation, Methodology, Writing–original draft, Writing–review and editing, Data curation, Formal Analysis, Funding acquisition, Project administration, Resources, Supervision.

Funding

The authors declare that financial support was received for the research, authorship, and/or publication of this article. This research was funded by the Natural Sciences and Engineering Research Council of Canada through an Alliance grant (reference ALLRP 572865-22) to NB, ET, and NT as well as by the Fonds de recherche du Québec Science et technologie through an Appui aux réseaux d'innovation grant (reference 2020-RI-278290) to NB and NT.

Conflict of interest

The authors declare that the research was conducted in the absence of any commercial or financial relationships that could be construed as a potential conflict of interest.

Publisher's note

References

Abdi, D., Ziadi, N., Shi, Y., Gagnon, B., Lalande, R., and Hamel, C. (2016). Residual effects of paper mill biosolids and liming materials on soil microbial biomass and community structure. *Can. J. Soil Sci.* doi:10.1139/CJSS-2016-0063

Arevalo, C. B. M., Bhatti, J. S., Chang, S. X., and Sidders, D. (2011). Land use change effects on ecosystem carbon balance: from agricultural to hybrid poplar plantation. *Agric. Ecosyst. Environ.* 141, 342–349. doi:10.1016/j.agee.2011.03.013

Bastin, J.-F., Finegold, Y., Garcia, C., Mollicone, D., Rezende, M., Routh, D., et al. (2019). The global tree restoration potential. *Science* 365 (6448), 76–79. doi:10.1126/science.aax0848

Beare, M. H., Gregorich, E. G., and St-Georges, P. (2009). Compaction effects on CO_2 and N_2O production during drying and rewetting of soil. *Soil Biol. Biochem.* 41 (3), 611–621. doi:10.1016/j.soilbio.2008.12.024

Behnami, A., Zoroufchi Benis, K., Pourakbar, M., Yeganeh, M., Esrafili, A., and Gholami, M. (2024). Biosolids, an important route for transporting poly- and perfluoroalkyl substances from wastewater treatment plants into the environment: a systematic review. *Sci. total Environ.* 925, 171559. doi:10.1016/j.scitotenv.2024.171559

Bélanger, N., Collin, A., Khlifa, R., and Lebel-Desrosiers, S. (2021). Balsam fir and American beech influence soil respiration rates in opposite directions in a sugar maple forest near its northern range limit. *Front. For. Glob. Change* 4, 664584. doi:10.3389/ffgc.2021.664584

Bélanger, N., Grimond, L., Khlifa, R., Bilodeau-Gauthier, S., and Rivest, D. (2024). "Afforestation of former asbestos mines in Quebec, Canada: an efficient nature-based climate solution that also leads to gains in biodiversity. Chapter 8," in *Biodiversity and ecosystem services on post-industrial land* (New Jersey, U.S: Wiley publisher).

Bilodeau-Gauthier, S., Palma Ponce, G., Miquel, J.-C., Lafleur, B., Brais, S., and Bélanger, N. (2022). Growth and foliar nutrition of a hybrid poplar clone following the application of a mixture of papermill biosolids and lime mud. *Can. J. For. Res.* 52 (1), 117–128. doi:10.1139/cjfr-2021-0086

Boeckx, P., Cleemput, O. V., and Villaralvo, I. (1996). Methane emission from a landfill and the methane oxidising capacity of its covering soil. *Soil Biol. Biochem.* 28, 1397–1405. doi:10.1016/S0038-0717(96)00147-2

Byrne, B., and Goldblatt, C. (2014). Radiative forcing at high concentrations of well-mixed greenhouse gases. *Geophys. Res. Lett.* 41 (1), 152–160. doi:10.1002/2013GL058456

Cain, M., Lynch, J., Allen, M. R., Fuglestvedt, J. S., Frame, D. J., and Macey, A. H. (2019). Improved calculation of warming-equivalent emissions for short-lived climate pollutants. *Npj Clim. Atmos. Sci.* 2 (1), 29. doi:10.1038/s41612-019-0086-4

Camberato, J. J., Gagnon, B., Angers, D. A., Chantigny, M. H., and Pan, W. L. (2006). Pulp and paper mill by-products as soil amendments and plant nutrient sources. *Can. J. Soil Sci.* 86 (4), 641–653. doi:10.4141/S05-120

Carabassa, V., Domene, X., Díaz, E., and Alcañiz, J. M. (2020). Mid-term effects on ecosystem services of quarry restoration with Technosols under Mediterranean conditions: 10-year impacts on soil organic carbon and vegetation development. *Restor. Ecol.* 28 (4), 960–970. doi:10.1111/rec.13072

Chanton, J. P., Powelson, D. K., and Green, R. B. (2009). Methane oxidation in landfill cover soils, is a 10% default value reasonable? *J. Environ. Qual.* 38 (2), 654–663. doi:10.2134/jeq2008.0221

Charbonneau, H., Hébert, M., and Jaouich, A. (2001) *Portrait de la valorisation agricole des Matières résiduelles fertilisantes au Québec – partie 2: contenu en éléments fertilisants et qualité environnementale. VECTEUR environnement, novembre 2000.*

Chen, X., Thomas, B. R., Pattison, S., An, Z., and Chang, S. X. (2023). Pulp mill biosolids mitigate soil greenhouse gas emissions from applied urea and improve soil fertility in a hybrid poplar plantation. *J. Environ. Manag.* 344, 118474. doi:10.1016/j.jenvman.2023.118474

Chmielewski, A., Urbaniak, A., Palige, J., Roubinek, O., Wawryniuk, K., and Dobrowolski, A. (2019). Membrane installation for biogas enrichment – field tests and system simulation. *Chem. Process Eng.* 40 (2), 235–260. doi:10.24425/cpe.2019.126116

Del Rio, F., Sovacool, B. K., Griffiths, S., Bazilian, M., Kim, J., Foley, A. M., et al. (2022). Decarbonizing the pulp and paper industry: a critical and systematic review of sociotechnical developments and policy options. *Renew. Sustain. Energy Rev.* 167, 112706. doi:10.1016/j.rser.2022.112706

Di Giacomo, G., and Romano, P. (2022). Evolution and prospects in managing sewage sludge resulting from municipal wastewater purification. *Energies* 15 (15), 5633. doi:10.3390/en15155633

Drever, C. R., Cook-Patton, S. C., Akhter, F., Badiou, P. H., Chmura, G. L., Davidson, S. J., et al. (2021). Natural climate solutions for Canada. *Sci. Adv.* 7, eabd6034. doi:10.1126/sciadv.abd6034

Ehrlich, V., Bil, W., Vandebriel, R., Granum, B., Luijten, M., Lindeman, B., et al. (2023). Consideration of pathways for immunotoxicity of per- and polyfluoroalkyl substances (PFAS). *Environ. Health* 22 (1), 19. doi:10.1186/s12940-022-00958-5

FAO. (2023). *Pulp and paper capacities, survey 2022–2024/Capacités de la pâte et du papier, enquête 2022-2024/Capacidades de pulpa y papel, estudio 2022-2024.*

Faubert, P., Barnabé, S., Bouchard, S., Côté, R., and Villeneuve, C. (2016). Pulp and paper mill sludge management practices: what are the challenges to assess the impacts on greenhouse gas emissions? *Resour. Conservation Recycl.* 108, 107–133. doi:10.1016/j.resconrec.2016.01.007

Faubert, P., Bélisle, C. L., Bertrand, N., Bouchard, S., Chantigny, M. H., Paré, M. C., et al. (2019). Land application of pulp and paper mill sludge may reduce greenhouse gas emissions compared to landfilling. *Resour. Conservation Recycl.* 150, 104415. doi:10.1016/j.resconrec.2019.104415

Faubert, P., Lemay-Bélisle, C., Bertrand, N., and Bouchard, S. (2015). La gestion des biosolides des papetières au Québec: quelle serait la meilleure option pour réduire les émissions de gaz à effet de serre? *Vecteur Environ.*

Forster, P., Storelvmo, T., Armour, K., Collins, W., Dufresne, J.-L., Frame, D., et al. (2021). "The Earth's energy budget, climate feedbacks, and climate sensitivity (Chapter 7)," in *Climate change 2021: the physical science basis. Contribution of working group I to the sixth assessment report of the intergovernmental panel on climate change* (Cambridge: Cambridge University Press).

Fraser-McDonald, A., Boardman, C., Gladding, T., Burnley, S., and Gauci, V. (2022). Methane emissions from trees planted on a closed landfill site. *Waste Manag. Res. J. a Sustain. Circular Econ.* 40 (11), 1618–1628. doi:10.1177/0734242X221086955

Gagnon, B., and Ziadi, N. (2012). Papermill biosolids and alkaline residuals affect crop yield and soil properties over nine years of continuous application. *Can. J. Soil Sci.* 92 (6), 917–930. doi:10.4141/cjss2012-026

Gagnon, B., and Ziadi, N. (2022). Soil carbohydrate and aggregation as affected by carbohydrate composition of paper mill biosolids. *Can. J. Soil Sci.* 102 (2), 371–384. doi:10.1139/cjss-2021-0136

Gagnon, B., Ziadi, N., Robichaud, A., and Karam, A. (2013). Metal availability following paper mill and alkaline residuals application to field crops. *J. Environ. Qual.* 42 (2), 412–420. doi:10.2134/jeq2012.0310

Gewurtz, S. B., Auyeung, A. S., Silva, De, Teslic, S., and Smyth, S. A. (2024). Per- and polyfluoroalkyl substances (PFAS) in Canadian municipal wastewater and biosolids: recent patterns and time trends 2009 to 2021. *Sci. Total Environ.* 912, 168638. doi:10.1016/j.scitotenv.2023.168638

Gonzalez-Akre, E., Piponiot, C., Lepore, M., Herrmann, V., Lutz, J. A., Baltzer, J. L., et al. (2022). *Allodb*: an R package for biomass estimation at globally distributed extratropical forest plots. *Methods Ecol. Evol.* 13 (2), 330–338. doi:10.1111/2041-210X.13756

Grimond, L., Rivest, D., Bilodeau-Gauthier, S., Khlifa, R., Elferjani, R., and Bélanger, N. (2023). Novel soil reconstruction leads to successful afforestation of a former asbestos mine in southern Quebec, Canada. *New For.* 55, 477–503. doi:10.1007/s11056-023-09989-3

Griscom, B. W., Adams, J., Ellis, P. W., Houghton, R. A., Lomax, G., Miteva, D. A., et al. (2017). Natural climate solutions. *Proc. Natl. Acad. Sci.* 114 (44), 11645–11650. doi:10.1073/pnas.1710465114

Haile, A., Gelebo, G. G., Tesfaye, T., Mengie, W., Mebrate, M. A., Abuhay, A., et al. (2021). Pulp and paper mill wastes: utilizations and prospects for high value-added biomaterials. *Bioresour. Bioprocess.* 8 (1), 35. doi:10.1186/s40643-021-00385-3

Handel, S. N., Robinson, G. R., Parsons, W. F. J., and Mattei, J. H. (1997). Restoration of woody plants to capped landfills: root dynamics in an engineered soil. *Restor. Ecol.* 5 (2), 178–186. doi:10.1046/j.1526-100X.1997.09721.x

Hassan, M. U., Aamer, M., Mahmood, A., Awan, M. I., Barbanti, L., Seleiman, M. F., et al. (2022). Management strategies to mitigate N_2O emissions in agriculture. *Life* 12 (3), 439. doi:10.3390/life12030439

Henry, C. L., Cole, D. W., Hinckley, T. M., Harrison, R. B., and Features Submission, H. C. (1994). The use of municipal and pulp and paper sludges to increase production in forestry. *J. Sustain. For.* 1 (3), 41–55. doi:10.1300/J091v01n03_04

Himes, A., Betts, M., Messier, C., and Seymour, R. (2022). Perspectives: thirty years of triad forestry, a critical clarification of theory and recommendations for implementation and testing. *For. Ecol. Manag.* 510, 120103. doi:10.1016/j.foreco.2022.120103

IEA (2022) *Pulp and paper emissions intensity in the net zero scenario, 2018-2030*. Paris: IEA.

IEA (2023) *Pulp and paper - tracking report. (last updated July 2023)*.

Jeffry, L., Ong, M. Y., Nomanbhay, S., Mofijur, M., Mubashir, M., and Show, P. L. (2021). Greenhouse gases utilization: a review. *Fuel* 301, 121017. doi:10.1016/j.fuel.2021.121017

Kaarakka, L., Cornett, M., Domke, G., Ontl, T., and Dee, L. E. (2021). Improved forest management as a natural climate solution: a review. *Ecol. Solutions Evid.* 2 (3), e12090. doi:10.1002/2688-8319.12090

Kätelhön, A., Meys, R., Deutz, S., Suh, S., and Bardow, A. (2021). Climate change mitigation potential of carbon capture and utilization in the chemical industry. *PNAS* 116 (23), 11187–11194. doi:10.1073/pnass.1821029116

Kaza, S., Yao, L. C., Bhada-Tata, P., and Van Woerden, F. (2018) *What a waste 2.0: a global snapshot of solid waste management to 2050*. Washington, DC: World Bank. doi:10.1596/978-1-4648-1329-0

Khlifa, R., Rivest, D., Grimond, L., and Bélanger, N. (2023). Stability of carbon pools and fluxes of a Technosol along a 7-year reclamation chronosequence at an asbestos mine in Canada. *Ecol. Eng.* 186, 106839. doi:10.1016/j.ecoleng.2022.106839

Kirk, M., Smurthwaite, K., Braunig, J., Trevenar, S., D'Este, C., Lucas, R., et al. (2018) *The PFAS health study: systematic literature review [Application/pdf], 256 pages*. doi:10.25911/KW6T-7H44

LeBlanc, R. J., Matthews, P., and Richard, R. P. (2009). Global atlas of excreta, wastewater sludge, and biosolids management: moving forward the sustainable and welcome uses of a global resource/. Greater Moncton Sewerage Commission. Available at: https://digitallibrary.un.org/record/660552/files/un_habitat_atlas_excreta_wastewater_sludge.pdf.

Le Mer, J., and Roger, P. (2001). Production, oxidation, emission and consumption of methane by soils: a review. *Eur. J. Soil Biol.* 37 (1), 25–50. doi:10.1016/S1164-5563(01)01067-6

Lewis, S. L., Wheeler, C. E., Mitchard, E. T. A., and Koch, A. (2019). Restoring natural forests is the best way to remove atmospheric carbon. *Nature* 568 (7750), 25–28. doi:10.1038/d41586-019-01026-8

Lowman, A., McDonald, M. A., Wing, S., and Muhammad, N. (2013). Land application of treated sewage sludge: community health and environmental justice. *Environ. Health Perspect.* 121 (5), 537–542. doi:10.1289/ehp.1205470

Lteif, A., Whalen, J. K., Bradley, R. L., and Camiré, C. (2007). Mixtures of *papermill biosolids* and pig slurry improve soil quality and growth of hybrid poplar. *Soil Use Manag.* 23 (4), 393–403. doi:10.1111/j.1475-2743.2007.00103.x

Lu, Q., He, Z. L., and Stoffella, P. J. (2012). Land application of biosolids in the USA: a review. *Appl. Environ. Soil Sci.* 2012, 1–11. doi:10.1155/2012/201462

Lynch, J., Cain, M., Pierrehumbert, R., and Allen, M. (2020). Demonstrating GWP*: a means of reporting warming-equivalent emissions that captures the contrasting impacts of short- and long-lived climate pollutants. *Environ. Res. Lett.* 15, 044023. doi:10.1088/1748-9326/ab6d7e

Maalouf, A., and Mavropoulos, A. (2023). Re-assessing global municipal solid waste generation. *Waste Manag. Res. J. a Sustain. Circular Econ.* 41 (4), 936–947. doi:10.1177/0734242X221074116

Mabee, W., and Roy, D. N. (2003). Modeling the role of papermill sludge in the organic carbon cycle of paper products. *Environ. Rev.* 11 (1), 1–16. doi:10.1139/a03-001

Maia, F., De Souza Medeiros, A., Santos, D., Lyra, G. B., Lal, R., Assad, E. D., et al. (2022). Potential of no-till agriculture as a nature-based solution for climate-change mitigation in Brazil. *Soil Tillage Res.* 220, 105368. doi:10.1016/j.still.2022.105368

Makaruk, A., Miltner, M., and Harasek, M. (2010). Membrane biogas upgrading processes for the production of natural gas substitute. *Sep. Purif. Technol.* 74 (1), 83–92. doi:10.1016/j.seppur.2010.05.010

Ministère de l'environnement et de la lutte contre les changements climatiques (2020). Stratégie de valorisation de la matière organique. Available at: http://www.environnement.gouv.qc.ca/matieres/organique/strategie-valorisation-matiere-organique.pdf.

Mohajerani, A., Lound, S., Liassos, G., Kurmus, H., Ukwatta, A., and Nazari, M. (2017). Physical, mechanical and chemical properties of biosolids and raw brown coal fly ash, and their combination for road structural fill applications. *J. Clean. Prod.* 166, 1–11. doi:10.1016/j.jclepro.2017.07.250

Olivier, M. J. (2013) *Matières résiduelles et 3RV-E (4e éd). Les Productions Jacques Bernier*.

Pervaiz, M., and Sain, M. (2015). Recycling of paper mill biosolids: a review on current practices and emerging biorefinery initiatives. *Clean. – Soil, Air, Water* 43 (6), 919–926. doi:10.1002/clen.201400590

Popoola, L. T., Olawale, T. O., and Salami, L. (2023). A review on the fate and effects of contaminants in biosolids applied on land: hazards and government regulatory policies. *Heliyon* 9 (10), e19788. doi:10.1016/j.heliyon.2023.e19788

Pöykiö, R., Nurmesniemi, H., and Keiski, R. L. (2007). Environmental risk assessment of heavy metal extractability in a biosludge from the biological wastewater treatment plant of a pulp and paper mill. *Environ. Monit. Assess.* 128, 153–164. doi:10.1007/s10661-006-9301-y

Primeau, C. (2014). Modes de gestion des biosolides des usines de pâtes et papiers au Québec: Analyse comparative. Université de Sherbrooke.

Rada, E. C., Ragazzi, M., Torretta, V., Castagna, G., Adami, L., and Cioca, L. I. (2018). "Circular economy and waste to energy. Technologies and materials for renewable energy," in *Environment and sustainability: tmrees18* (Beirut: Lebanon), 030050. doi:10.1063/1.5039237

RECYC-QUÉBEC (2018). Bilan 2018 de la gestion des matières résiduelles. Available at: https://www.recyc-quebec.gouv.qc.ca/sites/default/files/documents/bilan-gmr-2018-complet.pdf.

Rodriguez, O., de Castro Andrade, G., Bellote, J., and Tomazello-Filho, M. (2018). Effect of pulp and paper mill sludge on the development of 17-year-old loblolly pine (*Punus taeda* L.) trees in southern Brazil. *For. Ecol. Manag.* 422, 179–189. doi:10.1016/j.foreco.2018.04.016

Roman-Perez, C. C., and Hernandez-Ramirez, G. (2022). Nitrous oxide production and nitrogen transformations in a soil amended with biosolids. *Can. J. Soil Sci.* 102 (2), 505–518. doi:10.1139/cjss-2021-0064

Schroth, M. H., Eugster, W., Gómez, K. E., Gonzalez-Gil, G., Niklaus, P. A., and Oester, P. (2012). Above- and below-ground methane fluxes and methanotrophic activity in a landfill-cover soil. *Waste Manag.* 32 (5), 879–889. doi:10.1016/j.wasman.2011.11.003

Seddon, N. (2022). Harnessing the potential of nature-based solutions for mitigating and adapting to climate change. *Science* 376 (6600), 1410–1416. doi:10.1126/science.abn9668

Sharma, B., Sarkar, A., Singh, P., and Singh, R. P. (2017). Agricultural utilization of biosolids: a review on potential effects on soil and plant grown. *Waste Manag.* 64, 117–132. doi:10.1016/j.wasman.2017.03.002

Siddiqua, A., Hahladakis, J. N., and Al-Attiya, W. A. K. A. (2022). An overview of the environmental pollution and health effects associated with waste landfilling and open dumping. *Environ. Sci. Pollut. Res.* 29 (39), 58514–58536. doi:10.1007/s11356-022-21578-z

Sun, M., Hanif, A., Wang, T., Gu, Q., and Shang, J. (2023). Ambient temperature NO_2 removal by reversible NO_2 adsorption on copper-based metal-organic frameworks (MOFs)-derived nanoporous adsorbents. *Sep. Purif. Technol.* 314, 123563. doi:10.1016/j.seppur.2023.123563

Szabó, L., Soria, A., Forsström, J., Keränen, J. T., and Hytönen, E. (2009). A world model of the pulp and paper industry: demand, energy consumption and emission scenarios to 2030. *Environ. Sci. Policy* 12 (3), 257–269. doi:10.1016/j.envsci.2009.01.011

Thevathasan, N. V., and Gordon, A. M. (1997). Poplar leaf biomass distribution and nitrogen dynamics in poplar-barley intercropped system in southern Ontario, Canada. *Agrofor. Syst.* 37 (1), 79–90. doi:10.1023/A:1005853811781

Tomberlin, K., Venditti, R., and Yao, Y. (2020). Life cycle carbon footprint analysis of pulp and paper grades in the United States using production-line-based data and integration. *BioRes.* 15 (2), 3899–3914. doi:10.15376/biores.15.2.3899-3914

Tremblay, S., and Ouimet, R. (2000). A model for predicting organic carbon stocked in the forest floor of mineral forest soils in Quebec. *Note de recherche forestière no. 104. Direction de la recherche forestière, Ministère des ressources naturelles du Québec.*

Trlica, A., and Teshima, M. (2011). Assessing soil carbon storage and climate change mitigation in biosolids mine reclamation projects. *Sixth Int. Conf. Mine Clos.*, 551–558. doi:10.36487/acg_rep/1152_123_trlica

Turner, T., Wheeler, R., and Oliver, I. W. (2022). Evaluating land application of pulp and paper mill sludge: a review. *J. Environ. Manag.* 317, 115439. doi:10.1016/j.jenvman.2022.115439

Van Larebeke, N., Koppen, G., De Craemer, S., Colles, A., Bruckers, L., Den Hond, E., et al. (2023). Per- and polyfluoroalkyl substances (PFAS) and immune system-related diseases: results from the Flemish Environment and Health Study (FLEHS) 2008–2014. *Environ. Sci. Eur.* 35 (1), 28. doi:10.1186/s12302-023-00731-6

Vaverková, M. D. (2019). Landfill impacts on the environment— review. *Geosciences* 9 (10), 431. doi:10.3390/geosciences9100431

Wang, C., Zhang, W., Li, X., and Wu, J. (2022). A global meta-analysis of the impacts of tree plantations on biodiversity. *Glob. Ecol. Biogeogr.* 31 (3), 576–587. doi:10.1111/geb.13440

Wang, Q., Gu, X., Tang, S., Mohammad, A., Singh, D. N., Xie, H., et al. (2022). Gas transport in landfill cover system: a critical appraisal. *J. Environ. Manag.* 321, 116020. doi:10.1016/j.jenvman.2022.116020

Wang, X., Jia, M., Chen, X., Xu, Y., Lin, X., Kao, C. M., et al. (2014). Greenhouse gas emissions from landfill leachate treatment plants: a comparison of young and aged landfill. *Waste Manag.* 34 (7), 1156–1164. doi:10.1016/j.wasman.2014.02.004

Zhang, C., Guo, Y., Wang, X., and Chen, S. (2019). Temporal and spatial variation of greenhouse gas emissions from a limited-controlled landfill site. *Environ. Int.* 127, 387–394. doi:10.1016/j.envint.2019.03.052

Zhang, H., He, P., and Shao, L. (2009). N_2O emissions at municipal solid waste landfill sites: effects of CH_4 emissions and cover soil. *Atmos. Environ.* 43 (16), 2623–2631. doi:10.1016/j.atmosenv.2009.02.011

Ziadi, N., Gagnon, B., and Nyiraneza, J. (2013). Crop yield and soil fertility as affected by papermill biosolids and liming by-products. *Can. J. Soil Sci.* 93 (3), 319–328. doi:10.4141/cjss2012-129

frontiers | Frontiers in Environmental Science

TYPE Original Research
PUBLISHED 16 May 2024
DOI 10.3389/fenvs.2024.1368205

OPEN ACCESS

EDITED BY
Chenxi Li,
Xi'an University of Architecture and Technology, China

REVIEWED BY
Yang Wang,
Yunnan Normal University, China
Jing Liu,
China University of Mining and Technology, China

*CORRESPONDENCE
Kongqing Li,
likq@njau.edu.cn

RECEIVED 11 January 2024
ACCEPTED 15 April 2024
PUBLISHED 16 May 2024

CITATION
Cai Y and Li K (2024), Spatiotemporal dynamic evolution and influencing factors of land use carbon emissions: evidence from Jiangsu Province, China.
Front. Environ. Sci. 12:1368205.
doi: 10.3389/fenvs.2024.1368205

Spatiotemporal dynamic evolution and influencing factors of land use carbon emissions: evidence from Jiangsu Province, China

Yaxuan Cai and Kongqing Li*

College of Humanities and Social Development, Nanjing Agricultural University, Nanjing, Jiangsu, China

Land use/cover change has an important impact on global climate change and carbon cycle, and it has become another major source of carbon emission after energy consumption. Therefore, this study focuses on the main line of "land use carbon emissions-spatial and temporal patterns-influencing factors," and selects 13 cities in Jiangsu Province as the research object. Based on the data of land use and energy consumption, combined with the method of land use carbon emissions and ArcGIS technology, this study conducted a quantitative analysis of the spatio-temporal distribution of carbon emissions in Jiangsu Province. The factors affecting the spatial distribution of carbon emissions from land use in Jiangsu Province were discussed by using Geographic detector. The results show that: 1) Carbon emissions in Jiangsu Province showed an overall growth trend, from 16215.44 $\times 10^4 tC$ in 2010–23597.68 $\times 10^4 tC$ in 2020, with an average annual growth rate of 4.55%, of which the construction land and watersheds had a greater impact on carbon sources and sinks, respectively. 2) During the period, there were significant differences in carbon emission levels among different cities in Jiangsu Province, and the land use carbon emission in Jiangsu Province showed a stable spatial pattern of "northwest—southeast." The southern part of Jiangsu is always the hot area of carbon emission, while the cold spot area is mainly distributed in the northern and central parts of Jiangsu. 3) The interaction of factors such as economic development, industrial structure, energy intensity, land use and human activities is an important reason for the spatio-temporal differences of land use carbon emissions in Jiangsu Province. Among them, the level of urbanization, population size and economic aggregate have significant effects on carbon emissions.

KEYWORDS

carbon emissions, spatio-temporal evolution characteristics, influencing factors, hot spot analysis, geographic detector

1 Introduction

In recent years, environmental changes have become more and more drastic as global warming and its negative effects on the ecological environment have gradually intensified (Wang et al., 2014; Pechanec et al., 2018; Zhang et al., 2022). Environmental problems have become one of the major issues of common concern to all countries in the world. At present, global environmental problems are highlighted by climate change triggered by massive

greenhouse gas emissions (Zhang et al., 2022). After the industrial revolution, the widespread use of fossil fuels led to the production of large quantities of carbon dioxide, which triggered a rise in global temperatures (Nicholls et al., 2020). In the last decade, the global average temperature has been increasing rapidly. According to the projections of some scholars, by 2050 the global average surface temperature could increase by more than 1.5°C over the period from 1850 to 1990 (Zhu et al., 2022). If the world does not act quickly and aggressively, the global average temperature will continue to rise, which could raise the future sea level by tens of meters (DeFries et al., 2002). This disaster will not only lead to the disappearance of nearly half of the biological species on Earth, but also pose a serious threat to the sustainable development of society, economy and environment, which will in turn jeopardize the security and wellbeing of all humankind (DeFries et al., 2002; Meehl et al., 2014; Waheed et al., 2019; Jiang and Hao, 2022).

According to CO_2.earth, China's current historical cumulative energy consumption and carbon dioxide emissions rank second only to the United States in the world, and it is projected that by 2025, China's emissions will exceed those of the United States. Therefore, there is an urgent need to regulate CO_2 emissions in China (Zhang and Cheng, 2009; Zheng et al., 2019). For this end, in order to achieve carbon emission reduction, China has proposed a "dual-carbon" strategy, in which carbon peaking and carbon neutrality are regarded as new development trends, and low-carbon development will be the dominant direction in the future (Fu et al., 2022). The Fifth Report of the United Nations Special Committee on Climate Change (IPCC) states that carbon dioxide levels in the air have risen since the beginning of the industrialization process, largely due to the burning of fossil fuels and changes in land use patterns. Between 1850 and 1998, direct carbon emissions due to land use and its changes accounted for one-third of the total carbon emissions from human activities, which had a profound impact on the global carbon cycle (Chuai et al., 2015). Therefore, the study of land use carbon emissions from the perspective of land use and its control is of great significance for perfecting China's low-carbon development model and achieving the "dual-carbon" goal (Meng et al., 2023).

Changes in land use will have a great impact on the material cycle and energy flow of the ecosystem, which will not only change the structure, process and function of the ecosystem, but also lead to changes in carbon emissions in the ecosystem (Rong et al., 2022). Different types of land have obvious differences in biomass. When one type of land is transformed into another type of land, it will inevitably cause fluctuations in biomass and lead to changes in carbon storage (Lai et al., 2016; Zhang et al., 2020). In addition, land use change can also affect the regional microclimate to some extent, which can lead to changes in the respiration and decomposition rates of plants and soils in this area, and can also have an impact on the carbon cycle of ecosystems (Zhang et al., 2018). Against this background, many scholars have conducted in-depth discussions on carbon emissions from land use. These studies mainly focus on the calculation method of carbon emissions, the scale of the study, and the various factors affecting carbon emissions (Stuiver, 1978; Breetz, 2017).

The main methods currently used to calculate carbon emissions are the sample land inventory method, the emission inventory method, the mechanistic model simulation method and the carbon emission factor method. The sample land inventory method has relatively few intermediate steps and produces fairly accurate results, however, the obvious drawbacks of this method are the difficulty and high cost of obtaining resource data (Fischer et al., 2011). The emission inventory approach also has its limitations, mainly because it is not comprehensive and fails to accurately reflect emissions from a wide range of activities and consumption patterns, while also lacking sufficient transparency in terms of assumptions, data inputs and emission factors (Leao et al., 2020). Although the mechanistic model simulation method can accurately simulate the carbon cycle process with a high degree of precision, the complexity of the simulation process and the numerous parameters make it difficult for this method to be widely applied (Wu et al., 2019). In contrast, the carbon emission factor method can be widely applied at multiple scales (e.g., macro, meso, and micro scales, etc.) due to its simple formulae and principles (Hu et al., 2023).

In terms of research scale, most of the existing studies use the national and provincial scales to analyze carbon emissions, mainly because the statistics of carbon emissions are carried out at the provincial scale, while studies at the municipal scale are lacking, which makes the research at the municipal scale still a relatively blank stage (Wang et al., 2019; Cai et al., 2021). In fact, the spatial distribution of carbon emissions is jointly determined by the dynamic spatial effects of itself and its neighboring units. Carbon emissions may vary at different spatial scales. By analyzing carbon emissions at the provincial and municipal scales on a spatial scale, we can gain a more comprehensive understanding of the characteristics of carbon emissions in the region.

From the perspective of influencing factors, traditional research methods, such as LMDI, Kaya or STIRPAT models, only reveal the direct effect of each variable on the dependent variable, and then calculate the corresponding influence coefficients. For example (Zhao et al., 2018), conducted an in-depth study on the matching between agricultural carbon emissions and soil and water resources at the provincial level and used the LMDI model for estimation in order to explore how the development of soil and water resources affects agricultural carbon emissions (Wu et al., 2016); used the optimized Kaya constant equation to study the various influencing factors of carbon emissions in China and observed that the growth of the urbanization rate, the energy carbon emission coefficient, and the increase in energy intensity all have a contributing effect on the increase in carbon emissions (Yang and Liu, 2023); used Toronto City in Inner Mongolia as an example, and used the STIRPAT model to conduct linear regression analyses of several indicators, including population, in order to explore the influencing factors of land-based carbon emissions in the city. Typically, various drivers affecting carbon emissions are interconnected, and the interactions between the factors can have different impacts on carbon emissions (Jiang et al., 2018). In many previous studies related to carbon emissions, researchers have identified the relationship between many different drivers and carbon emissions. However, most of the current studies have not considered the interaction between the drivers behind carbon emissions. In addition, most of the models used in the current literature are based on data-based assumptions and do not delve into the interaction between the factors. Therefore, this paper proposes a framework for the study of the interactions among the drivers of carbon emissions based on the geographic detector model. The geographic detector model is a research method that quantifies the spatial heterogeneity of a study object by analyzing the

differences between intra- and inter-stratum variances. This model does not need to rely on data assumptions and thus has been widely used in studies related to impact mechanisms (Wang et al., 2010; Jiang et al., 2018; Yang et al., 2019). More importantly, the model is not only able to identify the key drivers that manifest specific spatio-temporal phenomena, but also to explore the interactions among the influencing factors (Wang et al., 2010).

At the same time, with the in-depth study of carbon emissions from land use, more and more scholars have begun to recognize that carbon emissions show significant spatial variability. In recent years, some scholars have even focused on the spatial correlation and spatial aggregation characteristics of carbon emission research. Using spatial autocorrelation (Sun et al., 2020) and hotspot analysis methods (Allaire et al., 2012), some studies have explored the spatial and temporal distribution and agglomeration effects of urban carbon emissions in different regions. For example (Xu et al., 2019), discussed the influence of social ties and economic activities on the spatial and temporal distribution characteristics of carbon emissions in the Pearl River Delta (PRD) (Wu et al., 2021); revealed the spatial and temporal distribution pattern of carbon emissions from industrial land in China during 1997–2016 (Zhang Q. et al., 2017; Wang and He, 2019). conducted an analysis using the Moran index, and the results showed that there was a significant spatial positive correlation between the carbon emissions of various provinces in China, which further revealed the characteristics of spatial agglomeration. From previous studies on the spatial characteristics of carbon emissions, it is clear that China's carbon emissions do exhibit significant spatial autocorrelation. The researchers also emphasize that understanding the differences in the spatial characteristics of carbon emissions among different cities plays a crucial role in reducing carbon emissions (Tian and Zhou, 2019).

In general, domestic and foreign studies have focused on the accounting of carbon sources, sinks and net carbon emissions from land use, the spatial and temporal distribution characteristics of carbon emissions, and the analysis of factors influencing carbon emissions. These studies are relatively comprehensive, but there are still some limitations: the analyses of the spatial agglomeration characteristics of energy consumption and carbon emissions by the previous researchers mostly stayed at the national and provincial scales, while studies on the spatial and temporal analysis at the provincial and municipal level only focus on the comparison of results from year to year, unable to reveal the inherent law of spatio-temporal changes in carbon emissions, and it is difficult to formulate emission reduction policies based on the spatio-temporal characteristics (Pei et al., 2018); Secondly, in terms of content, there are fewer in-depth discussions on the interactions between neighboring regions, but the revelation of the degree of inter-regional dependence and interactions is helpful to achieve the complementary advantages and coordinated development of the regions; then, most of the studies on the driving factors of carbon emissions have ignored the spatial differences of various influencing factors and the effects of different driving factors on the spatial distribution of carbon emissions from land use.

Situated along the eastern coastal belt, Jiangsu Province is not only one of the most economically prosperous regions in China, but also the center of the Yangtze River Delta region. Since the reform and opening up, Jiangsu's export-oriented industrialization strategy and accelerated urbanization have led to the province's rapid economic development, population explosion, intensified energy use and rapid expansion of urban construction land area (Guo and Fang, 2021). Accordingly, the remarkable land-use changes in Jiangsu Province will inevitably affect the local carbon cycle. Therefore, in order to investigate the spatial and temporal dynamic evolution of land use of carbon emissions and its driving factors in Jiangsu Province, this paper selects 13 prefectural-level cities in Jiangsu Province as the research object, and estimates the land use carbon emissions of 13 municipal-level cities and administrative districts in Jiangsu Province from 2010 to 2020 by using the energy consumption data and land use data extracted from remote sensing imagery, and analyzed the spatial and temporal distribution characteristics of their carbon emissions; then, based on the results of carbon emission estimation, the spatial and temporal patterns were further revealed from different perspectives by using exploratory spatial and temporal data analysis (ESTDA) and standard deviation ellipse (SDE). Finally, the geographical detector model was applied to identify the main influencing factors and their interactions, and to reveal the spatial differences of carbon emission drivers in different regions of Jiangsu Province. The conclusions of this study help to clarify the spatial distribution characteristics and influencing factors of carbon emissions from land use in the 13 municipal administrative regions of Jiangsu Province, and also provide a reference for the formulation of regional and differentiated carbon emission reduction policies.

2 Data and methodology

2.1 Representative case

Jiangsu is located in the middle of the eastern coastal region of mainland China, downstream of the Yangtze River and Huaihe River (116°18′-121°57′E, 30°45′-35°20′N), which is an important part of the Yangtze River Delta region. It has jurisdiction over 13 prefecture-level administrative regions, including Nanjing, Suzhou, Wuxi, Changzhou, Zhenjiang, Nantong, Yangzhou, Taizhou, Lianyungang, Yancheng, Huai'an, Suqian and Xuzhou, accounting for 1.12% of China's total land area (Figure 1). Geographically, it straddles the north and south, and therefore the climate and vegetation have characteristics of both the south and the north. Jiangsu's *per capita* GDP, comprehensive competitiveness, and regional development and livelihood index (DLI) all rank first among all provinces in China, making it the province with the highest level of comprehensive development in China, and it has already stepped into the level of an "upper-middle-class" developed country. However, in recent years, the conflict between rapid development and spatial carrying capacity in Jiangsu Province has become increasingly acute, with drastic changes in land resources and an increasing scarcity of available land resources, triggering a series of ecological and environmental problems such as water pollution and land degradation (He et al., 2022). As an important support and carrier for social and economic development of Jiangsu Province, land use affects the realization of regional carbon balance. Exploring the carbon emission reduction space in the process of land use is of great significance for realizing

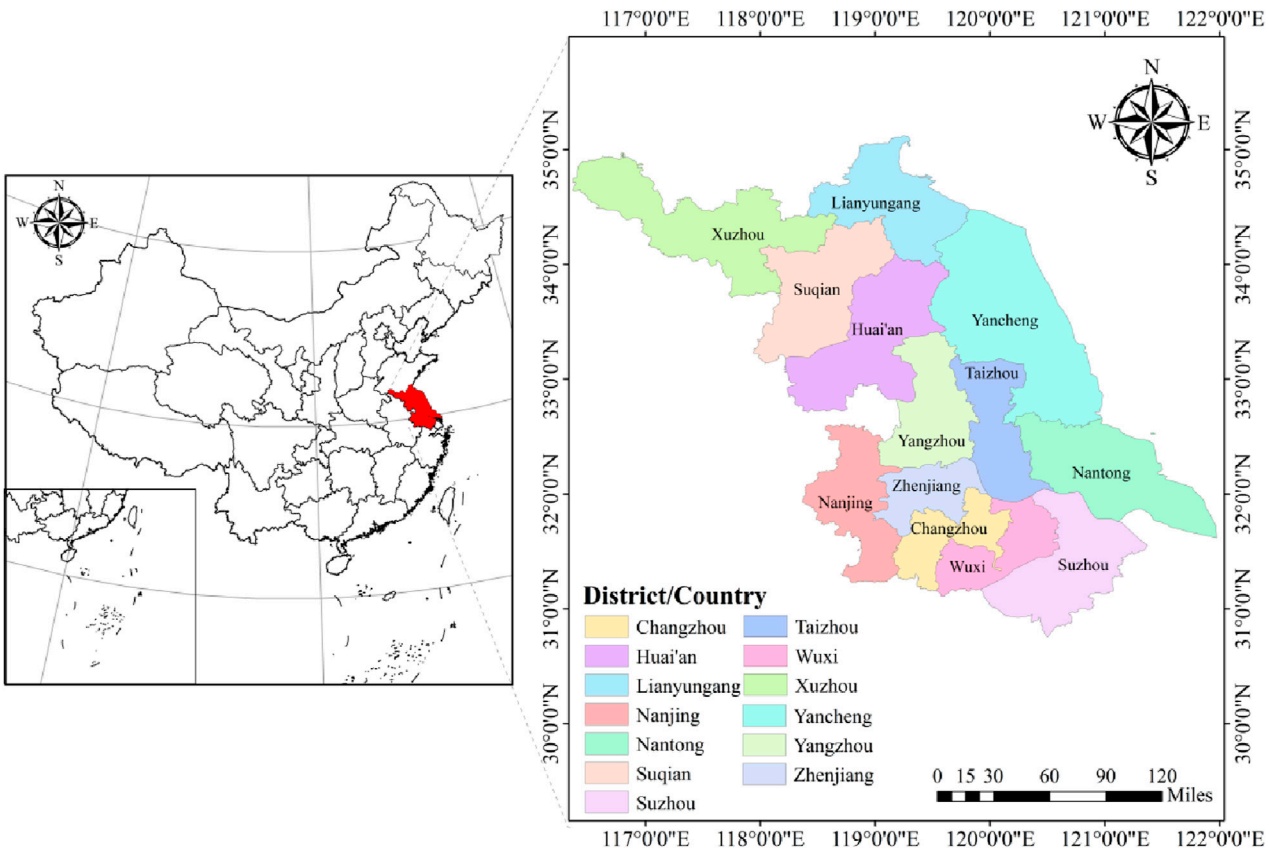

FIGURE 1
Location of study area.

the "double carbon" goal and improving the green and low-carbon development level of Jiangsu Province.

2.2 Data sources and processing

2.2.1 Data sources

The data used in this study include: 1) Land use data. According to the research needs, remote sensing image data with a raster resolution of 30 m × 30 m in 2010, 2015, 2018 and 2020 were obtained and divided into six land use types: arable land, woodland, grassland, water area, construction land and unutilized land, and ArcGIS software was used to extract the area of each land type. The main remote sensing data are from Data Center for Resources and Environmental Sciences, Chinese Academy of Sciences (https://www.resdc.cn/). 2) Fossil energy data. The fossil energy data used in this paper to calculate the carbon emissions from construction land were obtained from the statistical yearbooks of the 13 prefectural-level cities under the jurisdiction of Jiangsu Province. 3) Social economic data, such as population, GDP were obtained from the Centre for Resource and Environmental Science and Data, Chinese Academy of Sciences (https://www.resdc.cn/).

2.2.2 Influencing factor index selection

Based on the existing research results on carbon emission influencing factors (Deng, 2022; Ye et al., 2023), this study constructs an index system of driving factors of carbon emission of land use in Jiangsu Province from various aspects such as economy, land, population and energy, taking into account the specific situation of the region and availability of data. Considering the uniqueness of "collinear immunity" in the geographic detector model, population size, urbanization rate and population density are selected at the population level; economic total and industrial structure are selected at the economic level; land use structure is selected at the land level; and energy intensity is selected at the energy level. The meanings and statistical descriptions of relevant variables are shown in Table 1.

Population: As the dominant land user, the carbon dioxide released from all economic and social activities carried out by human beings on the land will affect the overall carbon balance pattern of the land, and at the same time, the migration in and out of the population will lead to changes in the population size, thus indirectly affecting the carbon emissions of the whole land. Therefore, this paper chooses the total resident population at the end of the year to represent the population size, and the number of people per unit area to represent the population density, so as to explore the interrelationship between them and the carbon emissions from land use in depth.

Urbanization rate: Rapid development, one of the key indicators of rapid social development, has led to a significant increase in the number of people living in cities and towns. This growth has further triggered the intensive use of energy and land resources, with far-

TABLE 1 Influence index selection and construction.

Guideline layer	Indicator layer	Variable meaning	Unit
Population	X1:Population size	Total resident population of prefecture-level cities	$\times 10^4 people$
	X2:Urbanization rate	Proportion of urban resident population in total population of the region	%
	X3:Population density	Unit construction land area Number of permanent residents	$\times 10^4 people/km^2$
Economy	X4:Economic aggregate	The final results of production activities of resident units in a certain period of time	$\times 10^4 yuan$
	X5:Industrial structure	The proportion of the gross domestic product of the secondary industry in the total regional production value	%
Land	X6:Land use structure	The proportion of regional construction land area in total area	%
Energy	X7:Energy intensity	Total energy consumption per unit of GDP	$t/\times 10^4 yuan$

reaching impacts on carbon emissions from land use. In view of this, we use the urbanization rate as an indicator of the level of social development to explore in depth its impact factors on carbon emissions from land use.

Economy: As the economy continues to develop, human consumption of resources such as land and energy gradually increases, which in turn leads to a rise in carbon emissions from land use. At the same time, economic prosperity also promotes the improvement of education and environmental awareness. In this context, the in-depth implementation of carbon emission reduction policies, the continuous innovation of energy-saving and emission reduction technologies and clean energy technologies, as well as the public's growing preference for environmentally friendly lifestyles, all have an impact on carbon emissions. Therefore, there is a close and dynamic correlation between the level of economic development and land use carbon emissions. In this study, gross regional product is taken as one of the important considerations of carbon emission influencing factors.

Industrial structure: In China's economic system, the secondary industry plays an important role in the industrial structure, and compared with the primary and tertiary industries, it is more inclined to the use of energy and the development of the industrial sector, and this industrial characteristic makes it more closely related to the land use carbon emissions. Therefore, the article chooses the proportion of the secondary industry in the regional GDP as the index of industrial structure in this study, in order to explore the interaction between these two variables.

Land use structure: Land use structure refers to the spatial distribution of various land uses in a given time scale in a study area, which can visually reflect the current land-use status of the area. In different periods of social development, the degree and pattern of anthropogenic exploitation and utilization will also lead to differences in carbon emissions from land in different regions. It is worth noting that construction land has seen the most significant changes among all types of land use in recent years, and is also the main source of carbon emissions from land use. Therefore, this study chooses the proportion of construction land to total land use as a proxy for land use structure, aiming to explore in depth the intrinsic link between it and land use carbon emissions.

Energy intensity: The impact of energy use intensity on land use carbon emissions lies mainly in the non-equilibrium of the technological level of resource consumption in different regions. This non-equilibrium makes the energy demand of each region differ geographically when reaching the same level of economic growth, which indirectly affects the distribution and spatial characteristics of total carbon emissions. In view of this, this study considers the total energy consumption per unit of GDP as a key element in the system of impact indicators.

2.3 Calculation method of carbon emissions

Land use carbon emissions refer to the CO_2 generated during land use change or use, which can be categorized into direct carbon emissions and indirect carbon emissions. The former mainly emphasizes carbon emissions caused by land use, while the latter focuses more on anthropogenic carbon emissions from living on the land. Among them, the net carbon emission depends on the

TABLE 2 Carbon emission coefficient of each land use type.

Land-use type	Arable land	Woodland	Grassland	Watershed	Unutilized land
Carbon emission coefficient	0.497	−0.581	−0.021	−0.253	−0.005

TABLE 3 Carbon emission coefficient of each energy source.

Energy type	Raw coal	Coke	Fuel oil	Gasoline	Kerosene	Diesel	Natural gas	Electricity
Carbon emission coefficient	0.7559	0.8550	0.5538	0.5714	0.5921	0.6185	0.4483	0.4040
Standard coal coefficient	0.7143	0.9714	1.4286	1.4714	1.4714	1.4571	1.2143	0.7935

difference between the carbon source and the carbon sink. Combined with the current land use situation in Jiangsu Province, carbon emissions from land use in the region mainly come from six land types: arable land, grassland, woodland, watershed, construction land and unutilized land. Based on the fact that land has the dual roles of "carbon source" and "carbon sink" at the same time, this paper will use construction land as a carbon source to calculate carbon emissions, and woodland, grassland, watersheds, and unutilized land as carbon sinks to calculate carbon sequestration, and it is important to note that arable land has the functions of carbon source and sink at the same time.

2.3.1 Direct carbon emissions accounting

The carbon emission coefficient method is used to directly account for carbon emissions from arable land, woodland, grassland, watersheds and unutilized land, which are aggregated to obtain the direct carbon emissions from land use, and the calculation formula is as follows:

$$E_k = \sum e_i = \sum A_i \times \mu_i \tag{1}$$

Where, E_k represents the direct carbon emission; i represents each land use type, which here represents arable land, woodland, grassland, watershed, and unutilized land; e_i represents the carbon emission/absorption of land type i; A_i represents the area of land of type i; μ_i represents the carbon emission coefficient of land type i. With reference to the research results of relevant scholars (Shi et al., 2012; Sun et al., 2015; Zhang P. Y. et al., 2017; Li et al., 2022; Xu et al., 2022) and combined with the actual situation in Jiangsu, the carbon emission coefficient of each land use type is shown in Table 2.

2.3.2 Indirect carbon emissions accounting

Construction land carries many social and economic activities of human beings, so it is impossible to calculate carbon emission directly according to the area of construction land. Therefore, indirect carbon emissions are mainly the carbon emissions generated by human beings in the process of construction land activities, including fossil energy consumption, electricity consumption and population respiration. The calculation formula is as follows:

$$C_f = \sum n_i \times \varepsilon_i \times \varphi_i \tag{2}$$

$$C_p = P \times \beta \tag{3}$$

$$C_b = C_f + C_p \tag{4}$$

Where, C_b is the indirect carbon emissions; C_f is the carbon emissions from fossil energy consumption; C_p is the carbon emissions from population respiration; n_i represents the annual consumption of different energy sources; ε_i and φ_i represent different energy conversion factors for standard coal and carbon emissions, respectively; P represents the number of population in Jiangsu; β represents the carbon emission's factor of population breathing in Jiangsu, Based on the results of previous studies, the value is 79 kg/person (Zhou, 2011). The energy sources selected in this paper are raw coal, coke, fuel oil, gasoline, kerosene, diesel, natural gas and Electricity, and the specific coefficients are shown in Table 3 (carbon emission coefficients are based on the IPCC2006 inventory; standard coal conversion coefficients are from *the China Energy Statistics Yearbook*).

2.4 Standard deviational ellipse (SDE)

The standard deviation ellipse model proposed by Lefever (1926) is an analytical technique used to accurately characterize the spatial distribution of the research object, which mainly covers core elements such as the center of gravity, the long and short axes and the azimuthal angle (Wang et al., 2020). The primary location of the element in space is known as the center of gravity, which usually coincides with the mean position of the arithmetic. The long axis represents the direction of the data distribution, while the short axis reveals the extent of the data distribution. The azimuth angle reveals the trend of the distribution of the study target. This method will be used in this study to analyze the distribution of carbon emission and its trends over time for each city in Jiangsu Province. The formulas are as follows:

a) Center of gravity coordinates

$$\bar{x}_i = \frac{\sum_{i=1}^{n} w_i x_i}{\sum_{i=1}^{n} w_i}, \bar{y}_i = \frac{\sum_{i=1}^{n} w_i y_i}{\sum_{i=1}^{n} w_i} \tag{5}$$

b) Azimuth

$$\tan\theta = \left(\sum_{i=1}^{n} w_i^2 \bar{x}_i^2 - \sum_{i=1}^{n} w_i^2 \bar{y}_i^2\right) + \sqrt{\left(\sum_{i=1}^{n} w_i^2 \bar{x}_i^2 - \sum_{i=1}^{n} w_i^2 \bar{y}_i^2\right) + 4\left(\frac{\sum_{i=1}^{n} w^2 \bar{x}_i^2 \bar{y}_i^2)^2}{2\sum_{i=1}^{n} w_i^2 \bar{x}_i \bar{y}_i}\right.} \tag{6}$$

c) x-axis standard deviation:

$$\sigma_x = \frac{\sqrt{\sum_{i=1}^{n} \left(w_i \bar{x}_i \cos\theta - w_i \bar{y}_i \sin\theta\right)^2}}{\sum_{i=1}^{n} w_i^2} \tag{7}$$

TABLE 4 The types of independent variable interaction.

Interaction type	Judgment criterion
Nonlinearity attenuation	$q\ (X_i \cap X_j)$<min $[q\ (X_i), q\ (X_j)]$
Unilinear attenuation	min $[q\ (X_i), q\ (X_j)]$<$q\ (X_i \cap X_j)$<max [q (X_i),q (X_j)]
Bilinear reinforcement	$q\ (X_i \cap X_j)$>max $[q\ (X_i), q\ (X_j)]$
Nonlinear reinforcement	$q\ (X_i \cap X_j)$>$q\ (X_i)$+$q\ (X_j)$
independent	$q\ (X_i \cap X_j) = q\ (X_i)$+$q\ (X_j)$

d) y-axis standard deviation:

$$\sigma_y = \frac{\sqrt{\sum_{i=1}^{n} \left(w_i \bar{x}_i \sin\theta - w_i \bar{y}_i \cos\theta\right)^2}}{\sum_{i=1}^{n} w_i^2} \tag{8}$$

Where (x_i, y_i) represents the spatial coordinate position of the research object; w_i stands for weight; $(\bar{x}_i, \bar{y}_i)$ denotes the weighted average center; θ is the azimuth Angle of the ellipse; $\bar{x}_i$ and $\bar{y}_i$ represent the coordinate deviation between the position of the research object and the average center; σ_x and σ_y represent the standard deviation along the x and y-axes.

2.5 Exploratory spatial data analysis (ESDA)

Exploratory spatial data analysis method is actually the comprehensive embodiment of spatial data analysis techniques and methods. This method is often used to describe the distribution characteristics of data in space, and can identify and represent outliers in spatial data in an intuitive manner. In addition, the technique can detect the aggregation effect of certain events in space, provide insights into the spatial layout of the data, and elucidate the spatial interaction mechanisms between different events (Messner et al., 1999). Carbon emissions in space are not randomly distributed, and there may be some correlation between different regions. Through the "cold hot spot analysis" tool in "ArcGIS" software, we can calculate Getis-Ord Gi* for specific weighted elements. Through the calculated z-score and p-value, we can determine the spatial aggregation location of high value areas (hot spots) and low value areas (cold spots), so as to judge the spatial heterogeneity characteristics within the study area (Getis and Ord, 1992). This method is extremely important for the spatial clustering distribution characteristics of the study area.

2.6 The geographical detector model

The Geographical Detector Model is a method of statistical analysis that integrates factors, interactions, risks and ecology, which not only reveals the spatial dissimilarity of a geographic object or phenomenon, but also detects the driving forces generated by the dependent variables (Cheng et al., 2014). Therefore, in this study, we will use the driver detector to quantify the specific influence of each factor on carbon emission, and the result is q. The specific calculation formula is as follows:

$$q = 1 - \frac{\sum_{h=1}^{L} N_h \sigma_h^2}{N\sigma^2} \tag{9}$$

Where q represents the magnitude of influence, with a value ranging from 0–1, and a higher value means that its influence is also stronger; h = 1 2 ..... L represents different classifications or subdivisions of the independent variables; N_h represents the number of samples of class h; σ_h^2 represents the variance of the independent variable of class h; N represents the number of samples of each city; and σ^2 represents the variance.

Among them, the Geographical Detector Model also includes an interaction detection model, which seeks to elucidate whether the independent variables have an independent effect on the dependent variable, or whether there is an enhanced or diminished effect following an interaction. If an interaction has occurred, there may be five cases as shown in Table 4. At the same time, in order to improve the significance of geographical detector analysis, the article adopts the natural breakpoint method in ArcGIS software to grade the features of each indicator (divided into five levels) to achieve the optimal discretization.

3 Results

3.1 Temporal changes in carbon emissions from land use

As can be seen from Table 5, the net carbon emissions in Jiangsu Province during the study period showed a trend of first increasing, then slowly decreasing, and finally rapidly increasing, but in terms of time, the overall net carbon emissions in Jiangsu Province still showed an increasing trend, with an average annual growth rate of 4.55 percent. In 2010–2015, the region's net carbon emissions showed an upward trend, increasing from $16215.44 \times 10^4 tC$ in 2010–$18458.35 \times 10^4 tC$ in 2015. From 2015 to 2018, the net carbon emissions showed a slow downward trend, decreasing by $177.66 \times 10^4 tC$. It can be seen that, with the increased focus on low-carbon development path, a series of measures adopted by Jiangsu Province aimed at promoting sustainable economic and social development measures, has achieved remarkable results in reducing carbon emissions. In 2018–2020, Jiangsu Province's net carbon emissions showed a rapid upward trend again, increasing to $23597.68 \times 10^4 tC$.

In terms of carbon sources, construction land is the primary land type contributing to the increase of carbon emissions in the region, which increased from $15953.78 \times 10^4 tC$ in 2010–$18200.48 \times 10^4 tC$ in 2015, then decreased slightly and then rose rapidly to $23343.63 \times 10^4 tC$ in 2020, which coincides with the trend of net carbon emissions in Jiangsu Province. However, the role of arable land as a carbon source is weakened in this process, and its contribution to the carbon source decreased from 1.95% in 2010 to 1.31% in 2020, which may be related to the shrinkage of arable land in Jiangsu Province due to the rapid expansion of land for construction. From the perspective of carbon sinks, watersheds plays a crucial role in carbon sequestration, with more than 67% of carbon sequestration originating from watersheds, followed by woodland, while grasslands and unutilized land in Jiangsu Province are relatively weak in terms of carbon sequestration capacity. As shown in Table 5, during the period 2010–2020, the amount of carbon absorbed in Jiangsu Province is

TABLE 5 Carbon emissions from land use in Jiangsu Province from 2010 to 2020 (tC).

Carbon emission		2010	2015	2018	2020
Carbon Source	Arable land	3172312.746	3134848.466	3107855.295	3096525.052
	Construction Land	159537764.512	182004841.031	180237891.206	233436276.140
Total		162710077.258	185139689.497	183345746.501	236532801.192
Carbon Sink	Woodland	−180194.425	−179342.152	−155965.278	−176283.604
	Grassland	−1929.456	−1915.243	−2319.242	−2227.511
	Watershed	−373420.030	−374799.710	−380458.146	−377444.856
	Unutilized Land	−113.606	−91.707	−52.825	−79.674
Total		−555657.517	−556148.813	−538795.491	−556035.644
Net carbon emission (10^4tC)		16215.442	18458.354	18280.695	23597.677

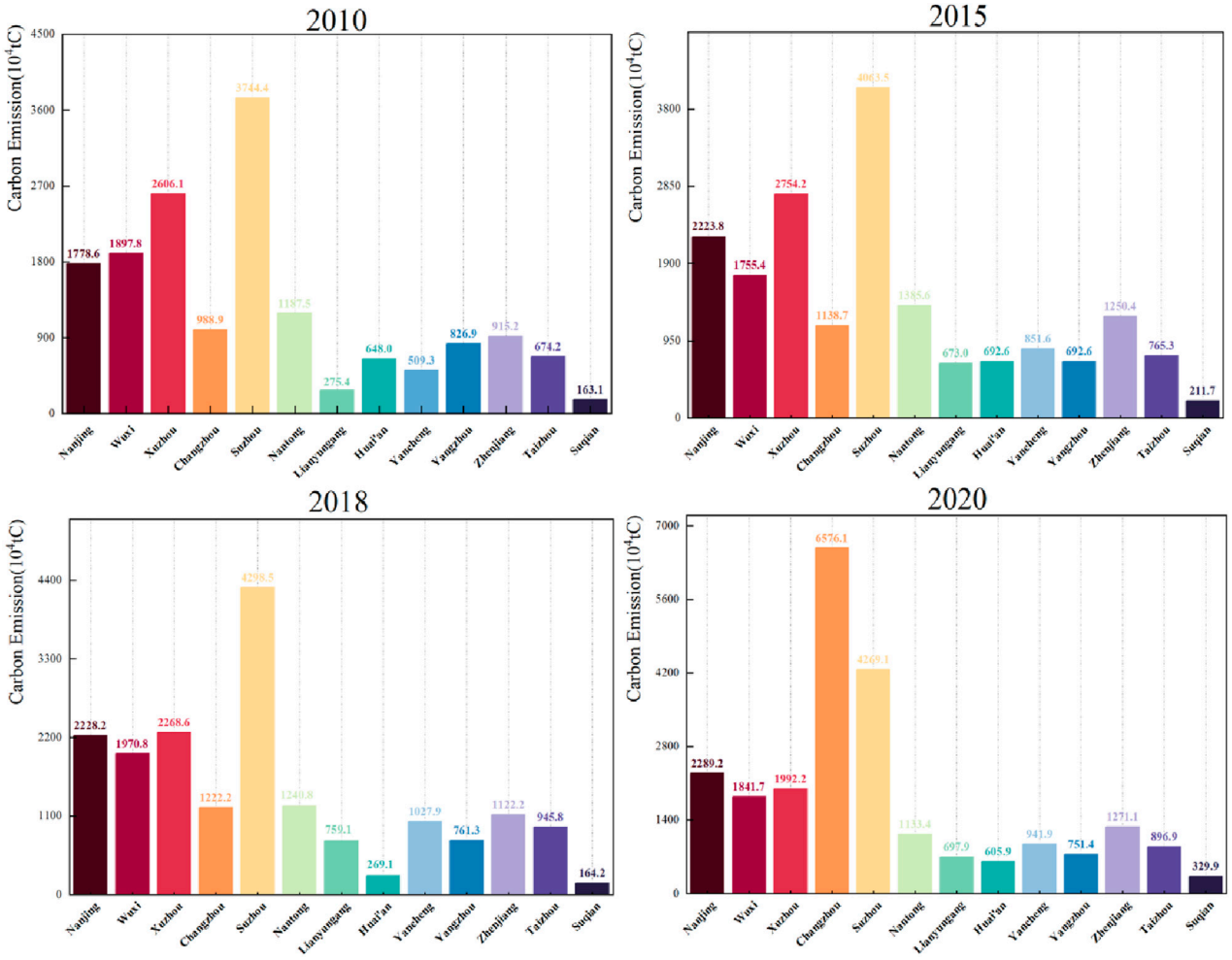

FIGURE 2
Carbon emissions from land use by city in Jiangsu Province (10^4tC).

significantly lower than the carbon emissions in the region. Therefore, the carbon emissions from land use in Jiangsu Province will continue to increase for some time to come, and it will be difficult to rely solely on biological means of carbon sequestration, such as planting trees and grasses, to offset the increase in carbon emissions from land use for construction.

In order to have an in-depth understanding of the changes of land use carbon emissions in each city of Jiangsu Province during the study

TABLE 6 Classification criteria for carbon emission levels (10^4tC).

Type	Carbon emission level	Partition unit
1	Light Emission Zone	(0,2754.160]
2	General Emission Zone	(2754.160,4298.543]
3	Moderate Emission Zone	(4298.543,17650.295]
4	Heavy Emission Zone	(17650.295,17995.090]
5	Extremely Heavy Emission Zone	≧17995.090

period, this paper conducted detailed statistics on the carbon emissions data of each city, and the results are shown in Figure 2. Because the actual situation of each city is different, the change rule of land use carbon emission varies from city to city. From 2010 to 2015, the carbon emissions of all cities in Jiangsu Province showed an upward trend, except for Wuxi and Yangzhou, which decreased. From 2015 to 2020, the carbon emission from land use in most of the cities in Jiangsu Province basically shows an upward trend in the fluctuation. Among them, driven by the radiation of neighboring cities such as Wuxi and Suzhou, Changzhou's economy has entered a period of rapid growth, with the proportion of secondary and tertiary industries gradually increasing, and the manufacturing industry has also achieved rapid development. Therefore, Changzhou's carbon emissions grew most significantly during this period, increasing slowly at first and then rising rapidly in 2018, with a total increase of $5427.468 \times 10^4 tC$. This was followed by Suzhou, Taizhou and Suqian, where net carbon emissions increased by $206.399 \times 10^4 tC$, $131.655 \times 10^4 tC$ and $118.121 \times 10^4 tC$ respectively. During that period, the net carbon emissions of Xuzhou, Nantong and Huai'an showed a downward trend year by year.

3.2 Spatial evolution of carbon emissions from land use

3.2.1 Spatial evolution of land use carbon emissions in Jiangsu Province

In order to more accurately reflect the spatial and temporal distribution characteristics of carbon emissions in each city of Jiangsu Province, this study used the natural segment point method of spatial analysis in ArcGIS software to classify the net carbon emissions of the 13 cities in Jiangsu Province according to different levels (Table 6), which are as follows: light emission zone,

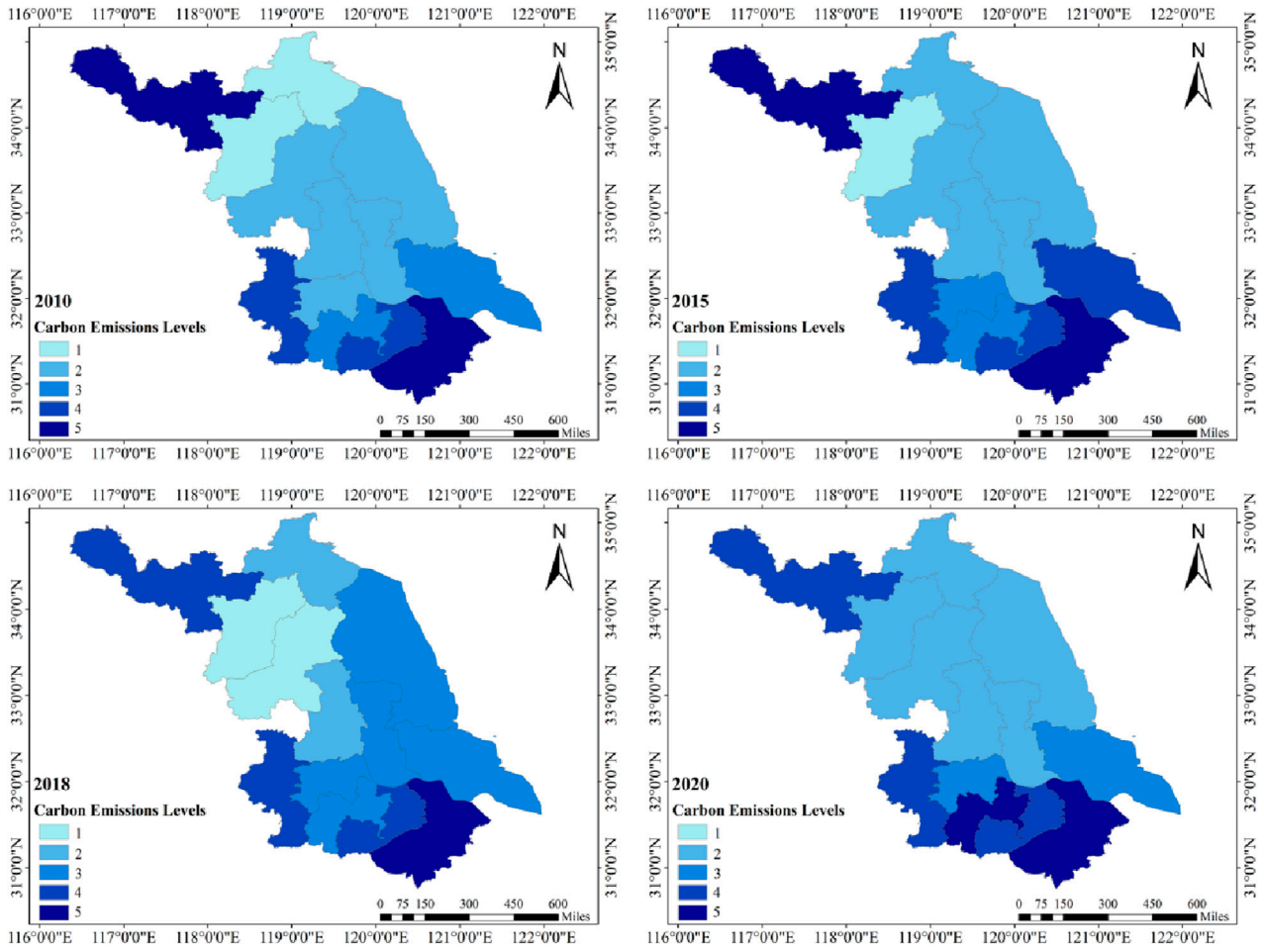

FIGURE 3
Spatial distribution of net carbon emissions by province in the study area by year (10^4tC).

TABLE 7 The General G value of carbon emissions of Jiangsu Province.

Year	General G	z-score	*p*-value
2010	0.423512	2.282405	0.022465
2015	0.425774	2.295431	0.021708
2018	0.425122	2.290657	0.021983
2020	0.423862	2.316825	0.020513

general emission zone, moderate emission zone, heavy emission zone, and extremely heavy emission zone.

As can be seen from Figure 3, from 2010 to 2020, carbon emissions from land use in all cities in the study area show obvious geographical distribution differences. That is, the overall carbon emissions have a trend of weakening from the surrounding areas to the central area and obvious clustering feature.

From 2010 to 2015, the extremely heavy carbon emission zones were mainly distributed in the "two wings" of Jiangsu Province, represented by Xuzhou, Suzhou and other marginal areas with a relatively high degree of industrialization. Because of their rich economic development background and unique geographical location, these areas enjoyed rapid urban construction and economic growth, which also led to the continuous rise of carbon emission. Due to the significant reduction in the use of coal and the transformation and upgrading of five industries, namely, steel, cement, coking, thermoelectric enterprises and chemical industry, the carbon emissions generated in the industrial process have been reduced (Chi et al., 2019), which also makes the carbon emissions of Xuzhou show a significant downward trend in 2018, and gradually exit the extremely heavy carbon emission zone. From 2015 to 2020, as Changzhou's economy enters the stage of rapid development, its carbon emissions increase rapidly and begin to transform into an extremely heavy carbon emission zone.

The general and medium emission zones were mainly located in the central region of Jiangsu Province, mainly including Yancheng, Yangzhou, Taizhou, Zhenjiang and Nantong, etc. Between 2010 and 2015, except for Nantong, which transformed into a heavy carbon emission zone, the carbon emissions of other regions were relatively stable and remained at their original carbon emission levels. In 2018, Yancheng, Taizhou, Zhenjiang and Nantong all shifted to medium emission zone due to accelerated urbanization, but in 2020, the cities reverted back to general emission zone.

In 2010, the light emission zones were mainly concentrated in Suqian and Lianyungang, which lagged behind in terms of relatively slow economic development, and thus had smaller carbon emissions from their energy consumption. Since 2015, the significant expansion of urban construction land under the influence of policies led to an increase in Lianyungang's carbon emissions, crossing over into the general carbon emission zone. In 2018, due to Huaian's stringent control of its carbon emissions, it was successfully transformed into a light emission zone, the number of light carbon emission zones in Jiangsu Province remained at two again. In 2020, the carbon emissions of all cities in Jiangsu Province have increased on the whole, and the light carbon emission zone have disappeared.

3.2.2 Exploratory spatial data analysis of carbon emissions from land use

The "Hot spot Analysis" tool in ArcGIS 10.6 was used to calculate the spatial aggregation degree and change of net carbon emissions in cities of Jiangsu Province, and the results were shown in Table 7. During 2010–2020, the General G value of net carbon emissions from land use in Jiangsu Province was all greater than 0 and showed an overall upward trend, from 0.423512 to 0.423862, indicating that net carbon emissions in this region had an obvious spatial aggregation feature, and the aggregation degree would increase with the evolution of time.

The overall spatial pattern of carbon emissions from land use in Jiangsu Province from 2010 to 2020 is "high in the south and low in the north" (Figure 4). The hot spots of carbon emission are mainly distributed in Suzhou, Wuxi, Changzhou and other southern Jiangsu regions, which are geographically adjacent to Shanghai, with rapid economic development and high urbanization, and are the main economic development force in Jiangsu Province, so it is necessary to focus on the management of carbon emissions in this region. The cold spot zone mainly distributed in the north of Jiangsu Province, such as Huaian, Yancheng, Lianyungang, etc. Although this region has rich natural resources, it is located inland and has a low level of economic development, so the carbon emission is relatively small.

During the study period, the distribution pattern of hotspot high-value zone and cold spot low-value zone were relatively stable in space and time, but the distribution characteristics varied among the stages. Spatio-temporally, the range of hotspot zone in Jiangsu Province remained stable from 2010 to 2018, but the hotspot center had an obvious northward trend, which was mainly manifested in the gradual transition of Nantong as a sub-hotspot zone to a hotspot zone. At the same time, the range of cold spot zone in Jiangsu Province is expanded, and Suqian successfully enters the ranks of sub-hot spot zone. In 2018–2020, the range of hot spot zone in Jiangsu Province showed a shrinking trend, transforming from three hot spot zones and two sub-hot spot zones in 2018 to one hot spot and four sub-hot spot zones in 2020, in which Suzhou and Nantong exit from the hot spot zone. The scope of the cold spot zone in Jiangsu Province during this period showed an expanding trend, and the center of the cold spot showed a tendency to shift to the north-west direction, which is reflected by the fact that Xuzhou also gradually transitions to the sub-hot spot zone during this period. These changes show that Jiangsu Province has made good progress in carbon emission reduction in recent years, but in some areas there is still a need to further strengthen management and control.

3.2.3 The migration of gravity center and SDE analysis of carbon emissions

The SDE model was used to conduct complementarity analysis to reveal the changing law of the location of the center of gravity of regional carbon emissions in Jiangsu Province and the spatial distribution characteristics of high carbon emission areas, as shown in Table 8 and Figure 5.

During the period 2010–2020, the spatial distribution of carbon emissions in Jiangsu Province formed a stable "northwest-southeast" pattern with the change of the length of the axis, and its direction towards the southern part of Jiangsu Province is especially obvious, which indicates that the main driving force for the growth of carbon emissions in Jiangsu Province is the

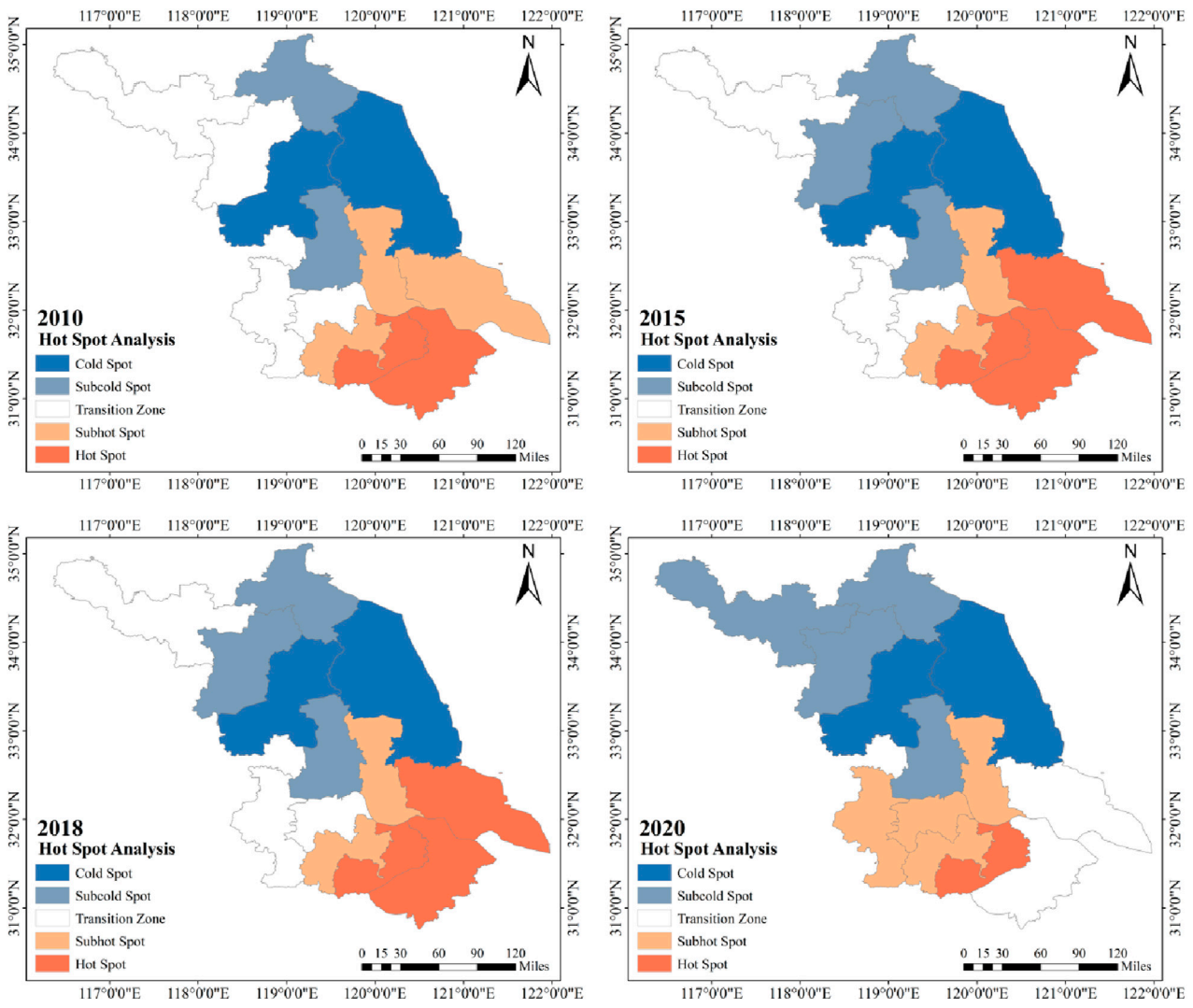

FIGURE 4
Hot spot analysis of carbon emissions in Jiangsu Province.

TABLE 8 Elliptic parameters of standard deviation of carbon emissions in Jiangsu Province.

Year	Barycentric coordinates		Drift direction	Distance (km)	Velocity (km/a)	Macroaxis (km)	Brachyaxis (km)	Azimuth angle (°)
	Longitude (E)	Latitude (N)						
2010	119°34′18.93″	32°23′45.18″	—	—		216.0157	72.9789	144.0230
2015	119°34′06.44″	32°26′46.59″	Northwest	5.6311	1.1262	213.5580	80.5198	145.1754
2018	119°39′26.70″	32°22′10.11″	Southeast	11.9118	3.9706	204.7010	82.5465	146.1783
2020	119°38′46.91″	32°11′37.95″	Southwest	19.5313	9.7656	179.8585	76.7598	148.0974

southern part of Jiangsu Province, such as Suzhou, Wuxi, Nanjing, and so on. In addition, the long and short axes of the standard deviation ellipse are also changed to different degrees. Specifically, the long axis decreased from 216.016 km in 2010 to 179.859 km in 2020, with a change amplitude of 36.157 km, indicating that carbon emissions in Jiangsu Province showed an obvious centripetal accumulation in the "northwest to southeast" direction during this period. During 2010–2018, the short axis increased from 72.979 km to 82.547 km, indicating that the carbon emissions of Jiangsu Province showed a divergence trend in the "northeast-southwest" direction during this period, mainly because the carbon emissions of Yancheng, Huaian, Yangzhou and other

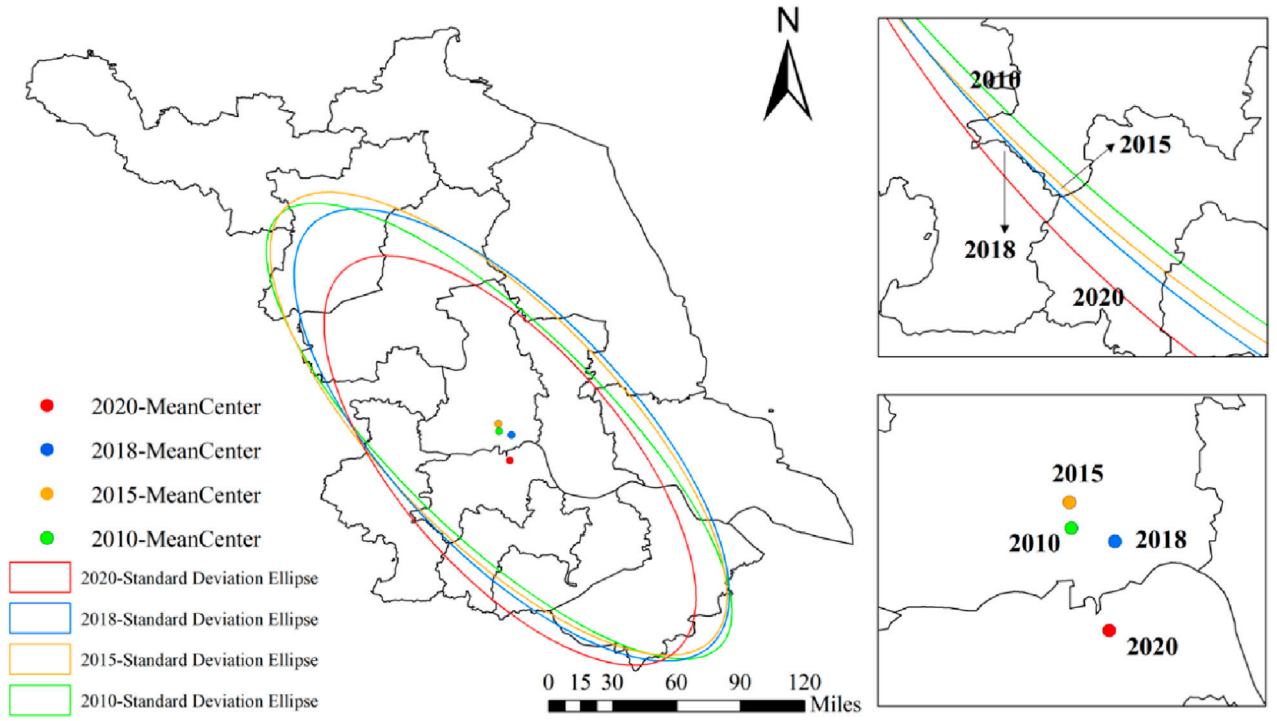

FIGURE 5
Standard deviation elliptic distribution and center of gravity shift trajectory of carbon emissions.

TABLE 9 The q-value for detection analysis of carbon emission factors from land use in Jiangsu Province.

Year	The q-value						
	X1	X2	X3	X4	X5	X6	X7
2010	0.7605	0.5167	0.7693	0.8570	0.4758	0.2319	0.2614
2015	0.8071	0.5618	0.7573	0.8545	0.1232	0.2435	0.5699
2018	0.7589	0.6952	0.4583	0.8308	0.2386	0.5933	0.3586
2020	0.2005	0.5022	0.8824	0.3166	0.6540	0.2407	0.2757
Mean value	0.6317	0.5690	0.7168	0.7147	0.3729	0.3274	0.3664

northern and central Jiangsu regions also increased, narrowing the carbon emission gap between different regions. From 2018 to 2020, the short axis decreases again to 76.760 km, which indicates that the density of carbon emission distribution gradually increases during this period. This is because under the "Southern Jiangsu Model," Nanjing, Changzhou, Wuxi and Suzhou have emerged as the most economically developed regions in Jiangsu Province, and have also become the gathering places of industrial enterprises in Jiangsu Province. As the scale of industry expands and energy consumption increases, carbon emissions also show a faster growth trend, and high carbon emissions further promote the centripetal concentration of carbon emissions.

During the study period, the center of gravity of carbon emissions in Jiangsu Province was distributed between 119°34′06.44"~119°39′26.70″E and 32°11′37.95"~32°26′46.59″N, which is located in the southeast direction of the regional geometric center, which means that the carbon emissions in the eastern and southern regions of Jiangsu Province are relatively high. By observing the trajectory of the change of the center of gravity of carbon emissions in Jiangsu Province, it can be found that the center of gravity of carbon emissions in the province mainly migrates to the southeast, which means that the growth rate of carbon emissions in the eastern and southern regions of Jiangsu Province is above average.

From 2010 to 2020, the center of gravity moved a total of 23.352 km to the south-east, and during this period, there was a backward movement of the center of gravity, which can be divided into three main phases: the first phase was 2010–2015, during which

the center of gravity moved 5.631 km to the north-west, reaching the northernmost point of the study period; The second phase, from 2015 to 2018. The migration direction of the center of gravity in this phase was completely opposite to the first phase. The center of gravity migrated in the south-eastern place, reaching a distance of 11.912 km and the angle of backward migration was the largest during the study period; The third phase was 2018–2020, in which the center of gravity moved north-west by 11.99 km at a rate of 9.766 *km*/*a*, which was the period with the longest distance and the fastest rate of migration of the unit during the study period.

3.3 Geo-detection analyses of the impact of land-use carbon emissions

3.3.1 Detection of single factor

The geographic detector is used for detection and analysis, and the q value of carbon emission for each detection factor is calculated, and then the visual display is carried out. The results show that different influencing factors have certain consistency and difference on land use carbon emissions in Jiangsu Province (Table 9). From the table, it can be seen that in 2010, the order of the q-value of each indicator is: economic total > population density > population size > urbanization rate > industrial structure > energy intensity > land-use structure, in which the sum of the explanatory power of population size, urbanization rate, population density and economic total accounted for 74.97% of the sum of the total explanatory power affecting carbon emissions, and the q-values of these four factors are all greater than 0.5. Therefore, these factors can be regarded as the main driving forces affecting Jiangsu's carbon emissions in that year.

In 2015, the q-value of each indicator is in the following order: economic total > population size > population density > energy intensity > urbanization rate > land use structure > industrial structure, of which economic total, population size, population density, energy intensity and urbanization rate are the dominant factors affecting carbon emissions in Jiangsu Province in that year. Under the background of rapid economic development in Jiangsu Province in 2015, its demand for energy is also rising, and this large-scale energy consumption has led to a significant increase in carbon emissions, so it can be found that energy intensity has also become the dominant factor affecting carbon emissions in Jiangsu Province in that year.

In 2018, the order of the q-value of each indicator is: economic total > population size > urbanization rate > land use structure > population density > energy intensity > industrial structure, in which economic total, population size, urbanization rate and land use structure were the main factors influencing carbon emissions in Jiangsu Province in that year. The influence of land use structure grew rapidly during the period, which was mainly due to the accelerated pace of urbanization driven by population surge, rapid development of secondary and tertiary industries and government policies, which triggered the rapid expansion of construction land. This also indirectly proves that construction land is the main source of carbon emissions, echoing the previous measurements.

In 2020, the q-value of each indicator is in the following order: population density > industrial structure > urbanization rate > economic total > energy intensity > land use structure > population size, of which the factors that play a dominant role in the carbon emissions of Jiangsu Province are population density, industrial structure and urbanization rate. During this period, the influence of each indicator has changed significantly, and population size and economic total are no longer the dominant factors affecting carbon emissions. On the contrary, the industrial structure has gradually increased its strength in explaining carbon emissions. This change may be attributed to the fact that the overall economic growth rate of Jiangsu began to decline due to the impact of the Xin Guan epidemic, and the secondary industry led by industry gradually became the core driving force of local economic growth, which led to the gradual weakening of the influence of the total economic output on carbon emissions in Jiangsu Province, and the gradual increase of the influence of the industrial structure on carbon emissions.

3.3.2 Detection of two-factor interaction

The interaction between the indicators was further explored using the interaction detection method of the geographical detector (Figure 6). The results of the interaction of the influencing factors mainly show two-factor enhancement or non-linear enhancement effects, and there is no mutual independence or weakness, which means that the spatial and temporal differences in land use carbon emissions in the study area is not entirely caused by a single factor, but by the joint action of multiple factors.

Among them, in 2010, the combinations with the most significant interactions are X2∩X3, X2∩X4, X2∩X5, X4∩X5, and their interaction values are 0.9988, 0.9935, 0.9890, 0.9972, respectively; in 2015, the combinations with the most significant interactions are X1∩X3, X2∩X4, X2∩X5, X4∩X5, X4∩X7, with interaction values of 0.9925, 0.9821, 1.0000, 0.9853, and 0.9918, respectively; in 2018, the combinations with the most significant interactions were X1∩X5, X1∩X7, X2∩X3, X2∩X7, and X6∩X7, with interaction values of 0.9989, 0.9999, 0.9886, and 0.9957, respectively; in 2020, the combinations with the most significant interaction are X1∩X2, X1∩X3, X1∩X5, X2∩X4, X3∩X7, and X4∩X5, with interaction values of 0.9981, 0.0081, 0.9982, 0.9820, 0.9820, and 0.9847, respectively.

Observing the whole research cycle, the interaction mechanisms of the indicators in different time periods show obvious differences. In the early part of the study period (2010–2015), the influences of urbanization rate or economic volume interacting with other variable factors are more significant. However, in the middle and late periods of the study (2015–2020), the interactions between population size and other variable factors are more prominent. Overall, the interactions between the three factor combinations of urbanization rate and population density, urbanization rate and total economic value, and total economic value and industrial structure show high explanatory power almost throughout the study period, which strongly indicates that they have the most critical impact on carbon emissions in Jiangsu Province.

4 Discussion

4.1 Analysis of spatio-temporal evolution characteristics of carbon emissions from land use

During the period of 2010–2020, Jiangsu's carbon emissions from land use in general showed a fluctuating upward trend, with a

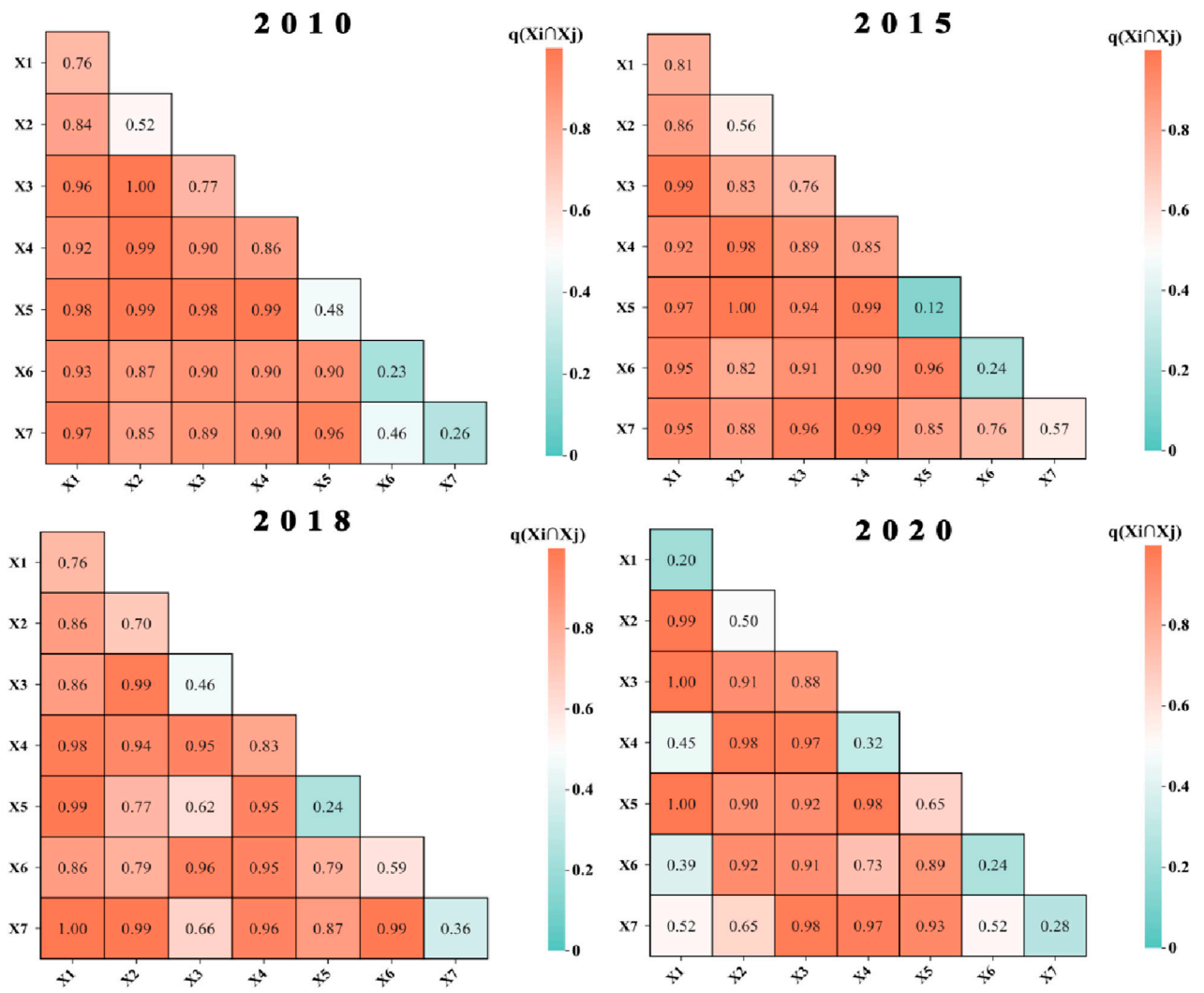

FIGURE 6
Two-factor interaction heat map of carbon emissions from land use in Jiangsu Province.

downward trend in 2015–2018 and a rapid rise in 2018. This is because with the national emphasis on the development of low-carbon economy, Jiangsu Province, in order to ensure the achievement of the "Twelfth Five-Year" energy-saving, emission reduction and carbon reduction targets, has formulated policies such as the "2014–2015 Energy Saving, Emission Reduction and Low-Carbon Development Action Implementation Programme." As a result, in 2015, carbon emissions in Jiangsu Province were under better control, showing a downward trend. However, as the pace of China's urbanization continues to accelerate, Jiangsu Province stepped into the rapid development stage of urbanization in 2018. This has led to the gradual emergence of problems such as inefficient use, inappropriate use and disorderly expansion of construction land, which has triggered a series of ecological and environmental problems, and thus has led to the trend of rapid growth of carbon emissions from land use in Jiangsu Province in 2018.

Overall, about more than half of the carbon sequestration during the study period originated from watersheds (Table 5). It can be seen that the watershed of Jiangsu Province seem to possess higher carbon sequestration potential. One possible explanation for this is that watershed, as the dividing line between land and sea, have large organic carbon reserves (Zhang et al., 2022). Therefore, in order to achieve the goal of reducing carbon emissions, it is also particularly crucial to prevent water bodies from being polluted. In Jiangsu Province, industrial and mining land with high carbon emissions is mainly concentrated in coastal areas near the Yangtze River Basin, where a large number of other pollutants may exist that have not yet been identified (Yuan et al., 2022), therefore, the use of industrial and mining land in areas near the Yangtze River Basin should be strictly controlled, and in the future, it is even more important to prohibit the expansion of industrial land in such areas, as well as consider relocating enterprises elsewhere, and converting industrial and mining land to other uses.

By analyzing the characteristics of the spatial evolution of carbon emissions from land use in Jiangsu Province, it can be found that carbon emissions in Jiangsu Province show a strong spatial focus. It is mainly manifested in the fact that the

surrounding cities of Nanjing, Suzhou, Wuxi and other high carbon emission areas are also always in the hot spot of carbon emission. This phenomenon has a certain connection with the economic development status of each place (Rehman et al., 2021). As we all know, the economic development of Jiangsu Province is very unbalanced, showing significant geographical differences, of which Southern Jiangsu, Central Jiangsu and Northern Jiangsu are the three major economic regions with obvious gradient differences. Southern Jiangsu is located in the hinterland of the "Yangtze River Delta Economic Circle," adjacent to the core city of Shanghai, and has a fast-developing economy; Northern Jiangsu is located in the periphery, farther away from Shanghai, and the attraction and radiation effect of the economic center is very weak. Therefore, the overall spatial distribution pattern of carbon emissions in Jiangsu Province is high in the south and low in the north. However, with the passage of time, the number of areas with high carbon emissions in Jiangsu Province has gradually increased and spread to the central and northern parts of the Jiangsu Province. This is mainly due to the fact that Jiangsu Province has begun to vigorously promote the development and opening up of northern and central Jiangsu in recent years, and has deeply explored and utilized the traditional resources of northern and central Jiangsu. Although the economy has achieved rapid growth, it has also caused a series of ecological and environmental pollution problems.

4.2 Analysis of influencing factors of land use carbon emission in Jiangsu Province

The Carbon emissions from land use in Jiangsu Province are affected by a variety of factors, such as economic development, industrial structure, energy intensity, land use and human activities, and the process has a complex mechanism. Among them, population size, economic aggregate, urbanization rate and population density are not only obviously related to the land use carbon emissions in Jiangsu Province, but also the main driving force of the uneven spatial distribution of land use carbon emissions in Jiangsu Province.

The results of the study show that the demographic factors (population density, population size and urbanization rate) have always had a strong explanatory power for carbon emissions in Jiangsu Province. The reason why carbon emissions have become the focus of global attention is that excessive carbon emissions can cause a series of environmental problems that are closely related to the survival of human beings, in which human beings are both the bearers and generators of carbon emissions (). Against the backdrop of accelerated industrialization and urbanization, the supply and demand relationship between land for living and production and land for construction will become tighter due to the concentration of population, which in turn will lead to a continuous increase in the area of arable land and construction land, and a decrease in the area of carbon sinks, such as woodland, grassland and watersheds. At the same time, as the population grows, we need to consume more energy to make the products we need, which means that more carbon dioxide will be released in people's daily lives and travel.

Secondly, as shown in Table 9, carbon emissions from land use in Jiangsu Province are to a large extent positively driven by the economic aggregate factor. This is mainly because rapid economic growth will bring about a significant "siphon effect," which will attract the inflow of resources and capital from neighbouring regions, leading to an increase in energy consumption in production and life, and ultimately driving the rise of regional carbon emissions. However, as Jiangsu Province's economy continues to improve and its industrial structure transforms, the province's economy will gradually become more intensive, and the efficiency of resource use will continue to increase, which will further lead to a gradual reduction in the intensity of carbon emissions; While the economy is developing, people pay more and more attention to environmental protection, and they begin to pursue more low-carbon living habits, which also leads to the reduction of carbon emissions (Gu et al., 2023). Therefore, it can also be found that the q value of the influence of the total economy is decreasing year by year, and it is only 0.3166 in 2020.

Although the explanatory power of industrial structure on carbon emissions is lower than that of the main drivers mentioned above, we can observe that the influence of industrial structure on the growth of carbon emissions increases significantly at a later stage. Therefore, when it comes to carbon emission reduction in the future, cities and regions in Jiangsu Province need to focus on concentrating on optimizing the industrial layout, strengthening the integration between industries, and integrating the concept of low carbon into the development of industrialization.

It should be emphasized that the effects of pairwise interactions of factors on carbon emissions are more significant than those of single factors (Figure 6). It is clear that carbon dioxide emissions are the product of the combined influence of many factors. Therefore, when formulating strategies to reduce carbon emissions, it is necessary to consider a combination of factors, and the effect of only targeting a single factor may not be satisfactory.

4.3 Low-carbon recommendations

4.3.1 Optimize the land use structure and strictly control new construction land

In order to realize the low-carbon development of land use in Jiangsu Province, it is necessary to pay attention to the strict control of the expansion rate and scale of construction land, and to formulate differentiated carbon emission management strategies at the city and county levels. Firstly, the province should strictly implement the land use control system, strictly divide the scope of urban development, and strictly control the conversion of woodland, watershed and other high carbon sink land into construction land; secondly, it should vigorously advocate afforestation and greening, improve environmental management, vigorously develop low-carbon fisheries, and explore new types of fishery and forestry management methods, so as to achieve win-win results in terms of economy and ecology; lastly, it should strengthen the intensive use of construction land, take the initiative to explore the potentials of its inherent, and advocate three-dimensional construction land use. Finally, it is necessary to strengthen the intensive use of construction land, actively explore its inherent potential, advocate three-

dimensional development of construction land, carry out a reasonable layout of construction land, and strengthen the infrastructure construction of neighboring counties and cities to alleviate the pressure on the land of the central urban area, and promote the outward development of towns and cities.

4.3.2 Strengthening industrial transformation and optimization and upgrading industrial structure

Economic development is an important factor affecting carbon emissions from land use in Jiangsu Province, and the optimization and adjustment of industrial structure is the key to achieving green and low-carbon development. Therefore, in the future, Jiangsu Province should adjust the structure of the three industries, promote the transformation of the economic development mode, change the traditional development mode of "high energy consumption, high pollution and high emission" to "high efficiency, high output and high growth," The traditional development mode of "high energy consumption, high pollution and high emission" should be changed to a new economic growth mode of "high efficiency, high output, high growth" and "low pollution." On the one hand, it is necessary to actively promote the development of low-carbon industries, act in strict accordance with the country's new low-carbon industrial policy, and prioritize the allocation of land resources to innovative industries and modern service industries that are in line with the direction of industrial transformation and upgrading. Land use standards will be more inclined to energy saving, environmental protection, low energy consumption, high economic benefits and low carbon emissions of environmental friendly fields. On the other hand, strengthen the supervision of existing industries, especially industry, strictly control each carbon emission index, and carry out industrial emission reduction layer by layer in the two dimensions of supply and supervision.

4.3.3 Optimizing the structure of energy use and improving the efficiency of energy use

In the context of fossil energy as the largest source of carbon emissions, improving energy efficiency has been recognized by many countries as an effective means of reducing emissions. Therefore, in order to realize the gradual decoupling of economic growth and land use carbon emissions, it is necessary to adjust the economic structure to the direction of capital economy, while improving energy efficiency and reducing energy consumption. This will help Jiangsu Province achieve economical and intensive economic development, thus achieving the goal of reducing emissions. On the one hand, Jiangsu should make use of its unique energy advantages to strengthen cross-regional cooperation with Zhejiang, Anhui and other provinces, deepen energy cooperation relations with neighboring provinces, commit to building high-end energy and chemical industry bases, and comprehensively plan the regional layout of key energy and chemical industry projects, while promoting the protection of ecological environment; On the other hand, it will gradually change the energy consumption structure of Jiangsu Province, which is dominated by fossil fuels such as coal, oil and natural gas, promote the diversified development of energy consumption structure, commit to the development of efficient and green energy resources, and promote the research and development and application of safe, efficient and clean renewable energy and new energy.

4.3.4 Reasonable control of population size

By analyzing the results of the geodetector, we can clearly see that population size has a significant impact on carbon emissions from land use. Jiangsu Province, as an economically developed region, has a huge population base, which will be a key factor for Jiangsu Province to face greater carbon emission pressure in the future. In addition, with the full implementation of the two-child policy, the population size of Jiangsu Province will continue to increase carbon dioxide emissions in the near future. Therefore, there is a need to strengthen the control of the population. The number of household population should be effectively controlled and people should be guided to establish a scientific concept of childbearing to prevent the two-child policy from being implemented without excessive population growth during the peak fertility period. At the same time, it is necessary to effectively control the excessive inflow of migrants and achieve a long-term balance between carbon emission reduction and attracting migrants to develop employment.

5 Conclusion

In this study, carbon emissions from land use in Jiangsu Province during the period 2010–2020 were estimated, and various technical methods such as hotspot analysis, standard deviation ellipse and geo-detector were used to conduct an in-depth study and analysis of their spatial and temporal evolution patterns as well as the factors that affect these changes, and the following results were obtained.

From the perspective of time evolution characteristics, carbon emissions in Jiangsu Province generally show a growth trend, from $16215.44 \times 10^4 tC$ in 2010–$23597.68 \times 10^4 tC$ in 2020, with an average annual growth rate of 4.55 percent. However, in 2018, carbon emissions have experienced a downward trend. Among them, construction land is the primary land type causing the rise of carbon emissions in the region, and the role of carbon sources is increasing, while the role of arable land as a source of carbon is weakening; from the perspective of carbon sinks, watershed play a crucial role in carbon sequestration, whereas the carbon sequestration capacity of grassland and unutilized land in Jiangsu Province is relatively weak. Given that emissions from carbon sources significantly exceed the absorption of carbon sinks, land-use carbon emissions in Jiangsu Province are expected to continue to increase in the coming period.

The Carbon emissions from land use in Jiangsu Province show a spatial trend of weakening from the surrounding regions to the central region. Among them, except for Xuzhou, the high carbon emission areas are mainly concentrated in the southern part of Jiangsu Province near Shanghai. According to the hotspot analysis and the standard deviation ellipse analysis, the land use carbon emissions of each city in Jiangsu Province have obvious distribution characteristics of high in the south and low in the north, and a stable spatial clustering pattern, and the degree of aggregation increases with the evolution of time.

The spatial variability of carbon emissions from land use in Jiangsu Province is the result of a combination of factors such as economic development, industrial structure, energy intensity, and land use. Among them, population size, economic aggregate, urbanization rate and population density all play a decisive role, and the results show that the influence of any two influencing factors after interaction shows different degrees of two-factor enhancement and non-linear enhancement.

Finally, based on the analysis of the whole paper, it puts forward the policy suggestions for low-carbon development in Jiangsu Province, such as strictly controlling the expansion of construction land, optimizing the industrial structure, improving energy efficiency, and controlling population growth.

Overall, this study reveals the relationship of carbon emissions between neighboring regions and the impacts of the interaction of different drivers on carbon emissions, bridges the gap in the existing research literature, and provides a reference for realizing the complementary advantages and coordinated development between regions. At the same time, the study may have deficiencies in the following aspects, which should be avoided as much as possible in future research: (1) When calculating direct carbon emissions from land use in this study, the carbon emission coefficients of all land use types are adopted from previous research results. Due to technical constraints, these coefficients are not fully localized, which may lead to slight deviations between the calculation results and the actual carbon emission characteristics of the study area; nevertheless, these results are still acceptable and understandable. (2) The change process of land use carbon emissions should be continuous, but due to the different uniform calibrations of land area, this paper chooses to use remote sensing image data to account for land use carbon emissions during 2010–2020, which makes the results have a large difference in each time period and the problem of discontinuous changes. It will be further improved in the future research.

Data availability statement

The original contributions presented in the study are included in the article/supplementary material, further inquiries can be directed to the corresponding author.

Author contributions

YC: Writing–original draft. KL: Writing–review and editing.

Funding

The author(s) declare that financial support was received for the research, authorship, and/or publication of this article. This work was supported by General Project of National Social Science Foundation of China (Grant No. 22BGL192).

Conflict of interest

The authors declare that the research was conducted in the absence of any commercial or financial relationships that could be construed as a potential conflict of interest.

Publisher's note

References

Allaire, S. E., Lange, S. F., Lafond, J. A., Pelletier, B., Cambouris, A. N., and Dutilleul, P. (2012). Multiscale spatial variability of CO_2 emissions and correlations with physico-chemical soil properties. *Geoderma* 170, 251–260. doi:10.1016/j.geoderma.2011.11.019

Breetz, H. L. (2017). Regulating carbon emissions from indirect land use change (ILUC): US and California case studies. *Environ. Sci. Policy* 77, 25–31. doi:10.1016/j.envsci.2017.07.016

Cai, M., Shi, Y., Ren, C., Yoshida, T., Yamagata, Y., Ding, C., et al. (2021). The need for urban form data in spatial modeling of urban carbon emissions in China: a critical review. *J. Clean. Prod.* 319, 128792. doi:10.1016/j.jclepro.2021.128792

Cheng, G., Han, J. W., Zhou, P. C., and Guo, L. (2014). Multi-class geospatial object detection and geographic image classification based on collection of part detectors. *Isprs J. Photogrammetry Remote Sens.* 98, 119–132. doi:10.1016/j.isprsjprs.2014.10.002

Chi, W., Li, Y., Cao, Y., and Cao, Y. (2019). Survey analysis and countermeasures research on eco-civilisation construction in Xuzhou city. *Environ. Prot. Circular Econ.* 39, 84–87.

Chuai, X. W., Huang, X. J., Wang, W. J., Zhao, R. Q., Zhang, M., and Wu, C. Y. (2015). Land use, total carbon emission's change and low carbon land management in Coastal Jiangsu, China. *J. Clean. Prod.* 103, 77–86. doi:10.1016/j.jclepro.2014.03.046

DeFries, R. S., Houghton, R. A., Hansen, M. C., Field, C. B., Skole, D., and Townshend, J. (2002). Carbon emissions from tropical deforestation and regrowth based on satellite observations for the 1980s and 1990s. *Proc. Natl. Acad. Sci. U. S. A.* 99, 14256–14261. doi:10.1073/pnas.182560099

Deng, Y. (2022). *Study on land use carbon emission characteristics and influencing factors in the Yangtze River Economic Belt*. Changsha, China: Nanchang University.

Fischer, C., Kleinn, C., Fehrmann, L., Fuchs, H., and Panferov, O. (2011). A national level forest resource assessment for Burkina Faso - a field based forest inventory in a semiarid environment combining small sample size with large observation plots. *For. Ecol. Manag.* 262, 1532–1540. doi:10.1016/j.foreco.2011.07.001

Fu, J., Ding, R., Zhang, Y. L., Zhou, T., Du, Y. M., Zhu, Y. Q., et al. (2022). The spatial-temporal transition and influencing factors of green and low-carbon utilization efficiency of urban land in China under the goal of carbon neutralization. *Int. J. Environ. Res. Public Health* 19, 16149. doi:10.3390/ijerph192316149

Getis, A., and Ord, J. K. (1992). The analysis of spatial association by use of distance statistics. *Geogr. Anal.* 24, 189–206. doi:10.1111/j.1538-4632.1992.tb00261.x

Gu, H., Liu, Y., Xia, H., Tan, X., Zeng, Y., and Zhao, X. (2023). Spatiotemporal dynamic evolution and its driving mechanism of carbon emissions in hunan province in the last 20 years. *Int. J. Environ. Res. public health* 20, 3062. doi:10.3390/ijerph20043062

Guo, X. M., and Fang, C. L. (2021). Integrated land use change related carbon source/sink examination in Jiangsu province. *Land* 10, 1310. doi:10.3390/land10121310

He, W. K., Li, X. S., Yang, J., Ni, H., and Sang, X. J. (2022). How land use functions evolve in the process of rapid urbanization: evidence from Jiangsu Province, China. *J. Clean. Prod.* 380, 134877. doi:10.1016/j.jclepro.2022.134877

Hu, Y., Zhang, K., Hu, N., and Wu, L. (2023). A review of agricultural carbon emission measurement in China. *Chin. J. Eco-Agriculture* 31, 163–176. doi:10.12357/cjea.20220777

Jiang, M. H., and Hao, X. Q. (2022). Adjusting the intermediate input sources for global carbon emission reduction: an input-output optimization model. *Sci. Total Environ.* 835, 155582. doi:10.1016/j.scitotenv.2022.155582

Jiang, X. T., Wang, Q., and Li, R. R. (2018). Investigating factors affecting carbon emission in China and the USA: a perspective of stratified heterogeneity. *J. Clean. Prod.* 199, 85–92. doi:10.1016/j.jclepro.2018.07.160

Lai, L., Huang, X. J., Yang, H., Chuai, X. W., Zhang, M., Zhong, T. Y., et al. (2016). Carbon emissions from land-use change and management in China between 1990 and 2010. *Sci. Adv.* 2, e1601063. doi:10.1126/sciadv.1601063

Leao, E. B. D., do Nascimento, L. F. M., de Andrade, J. C. S., and de Oliveira, J. A. P. (2020). Carbon accounting approaches and reporting gaps in urban emissions: an analysis of the Greenhouse Gas inventories and climate action plans in Brazilian cities. *J. Clean. Prod.* 245, 118930. doi:10.1016/j.jclepro.2019.118930

Li, Y., Shen, Y., and Wang, S. (2022). Temporal and spatial characteristics and effects of terrestrial carbon emissions based on land use change in Anhui Province. *J. soil water conservation* 36, 182–188. doi:10.13870/j.cnki.stbcxb.2022.01.024

Meehl, G. A., Teng, H. Y., and Arblaster, J. M. (2014). Climate model simulations of the observed early-2000s hiatus of global warming. *Nat. Clim. Change* 4, 898–902. doi:10.1038/nclimate2357

Meng, Q. X., Zheng, Y. N., Liu, Q., Li, B. L., and Wei, H. J. (2023). Analysis of spatiotemporal variation and influencing factors of land-use carbon emissions in nine provinces of the yellow River Basin based on the LMDI model. *Land* 12, 437. doi:10.3390/land12020437

Messner, S. F., Anselin, L., Baller, R. D., Hawkins, D. F., Deane, G., and Tolnay, S. E. (1999). The spatial patterning of county homicide rates: an application of exploratory spatial data analysis. *J. Quantitative Criminol.* 15, 423–450. doi:10.1023/a:1007544208712

Nicholls, Z. R. J., Gieseke, R., Lewis, J., Nauels, A., and Meinshausen, M. (2020). Implications of non-linearities between cumulative CO_2emissions and CO_2-induced warming for assessing the remaining carbon budget. *Environ. Res. Lett.* 15, 074017. doi:10.1088/1748-9326/ab83af

Pechanec, V., Purkyt, J., Benc, A., Nwaogu, C., Sterbová, L., and Cudlín, P. (2018). Modelling of the carbon sequestration and its prediction under climate change. *Ecol. Inf.* 47, 50–54. doi:10.1016/j.ecoinf.2017.08.006

Pei, J., Niu, Z., Wang, L., Song, X. P., Huang, N., Geng, J., et al. (2018). Spatial-temporal dynamics of carbon emissions and carbon sinks in economically developed areas of China: a case study of Guangdong Province. *Sci. Rep.* 8, 13383. doi:10.1038/s41598-018-31733-7

Rehman, A., Ma, H. Y., and Ozturk, I. (2021). Do industrialization, energy importations, and economic progress influence carbon emission in Pakistan. *Environ. Sci. Pollut. Res.* 28, 45840–45852. doi:10.1007/s11356-021-13916-4

Rong, T. Q., Zhang, P. Y., Zhu, H. R., Jiang, L., Li, Y. Y., and Liu, Z. Y. (2022). Spatial correlation evolution and prediction scenario of land use carbon emissions in China. *Ecol. Inf.* 71, 101802. doi:10.1016/j.ecoinf.2022.101802

Shi, H., Mu, X. m., Zhang, Y., and L, M. (2012). Effects of different land use patterns on carbon emission in Guangyuan City of Sichuan Province. *Bull. Soil Water Conservation* 32, 101–106. doi:10.13961/j.cnki.stbctb.2012.03.020

Stuiver, M. (1978). Atmospheric Carbon Dioxide and Carbon Reservoir Changes: reduction in terrestrial carbon reservoirs since 1850 has resulted in atmospheric carbon dioxide increases. *Science* 199, 253–258. doi:10.1126/science.199.4326.253

Sun, H., Liang, H., Chang, X., Cui, Q., and Tao, Y. (2015). Land use carbon emissions and their spatial correlation in China. *Econ. Geogr.* 35, 154–162. doi:10.15957/j.cnki.jjdl.2015.03.023

Sun, L. C., Qin, L., Taghizadeh-Hesary, F., Zhang, J. J., Mohsin, M., and Chaudhry, I. S. (2020). Analyzing carbon emission transfer network structure among provinces in China: new evidence from social network analysis. *Environ. Sci. Pollut. Res.* 27, 23281–23300. doi:10.1007/s11356-020-08911-0

Tian, Y. Y., and Zhou, W. Q. (2019). How do CO_2 emissions and efficiencies vary in Chinese cities? Spatial variation and driving factors in 2007. *Sci. Total Environ.* 675, 439–452. doi:10.1016/j.scitotenv.2019.04.239

Waheed, R., Sarwar, S., and Wei, C. (2019). The survey of economic growth, energy consumption and carbon emission. *Energy Rep.* 5, 1103–1115. doi:10.1016/j.egyr.2019.07.006

Wang, J. F., Li, X. H., Christakos, G., Liao, Y. L., Zhang, T., Gu, X., et al. (2010). Geographical detectors-based health risk assessment and its application in the neural tube defects study of the heshun region, China. *Int. J. Geogr. Inf. Sci.* 24, 107–127. doi:10.1080/13658810802443457

Wang, S. J., Fang, C. L., Guan, X. L., Pang, B., and Ma, H. T. (2014). Urbanisation, energy consumption, and carbon dioxide emissions in China: a panel data analysis of China's provinces. *Appl. Energy* 136, 738–749. doi:10.1016/j.apenergy.2014.09.059

Wang, S. J., Huang, Y. Y., and Zhou, Y. Q. (2019). Spatial spillover effect and driving forces of carbon emission intensity at the city level in China. *J. Geogr. Sci.* 29, 231–252. doi:10.1007/s11442-019-1594-1

Wang, W., Samat, A., Abuduwaili, J., and Ge, Y. (2020). Spatio-temporal variations of satellite-based PM2. 5 concentrations and its determinants in Xinjiang, northwest of China. *Int. J. Environ. Res. Public Health* 17, 2157. doi:10.3390/ijerph17062157

Wang, Y. Y., and He, X. B. (2019). Spatial economic dependency in the Environmental Kuznets Curve of carbon dioxide: the case of China. *J. Clean. Prod.* 218, 498–510. doi:10.1016/j.jclepro.2019.01.318

Wu, M. S., Ran, Y. H., Jansson, P. E., Chen, P., Tan, X., and Zhang, W. X. (2019). Global parameters sensitivity analysis of modeling water, energy and carbon exchange of an arid agricultural ecosystem. *Agric. For. Meteorology* 271, 295–306. doi:10.1016/j.agrformet.2019.03.007

Wu, S., Hu, S. G., and Frazier, A. E. (2021). Spatiotemporal variation and driving factors of carbon emissions in three industrial land spaces in China from 1997 to 2016. *Technol. Forecast. Soc. Change* 169, 120837. doi:10.1016/j.techfore.2021.120837

Wu, Y. Z., Shen, J. H., Zhang, X. L., Skitmore, M., and Lu, W. S. (2016). The impact of urbanization on carbon emissions in developing countries: a Chinese study based on the U-Kaya method. *J. Clean. Prod.* 135, 589–603. doi:10.1016/j.jclepro.2016.06.121

Xu, Q., Dong, Y. X., Yang, R., Zhang, H. O., Wang, C. J., and Du, Z. W. (2019). Temporal and spatial differences in carbon emissions in the Pearl River Delta based on multi-resolution emission inventory modeling. *J. Clean. Prod.* 214, 615–622. doi:10.1016/j.jclepro.2018.12.280

Xu, Y., Guo, N., Ru, K., and Fan, S. (2022). Spatial zoning characteristics and optimization strategies of Fujian Province from the perspective of carbon neutrality. *J. Appl. Ecol.* 33, 500–508. doi:10.13287/j.1001-9332.202201.016

Yang, J. T., Song, C., Yang, Y., Xu, C. D., Guo, F., and Xie, L. (2019). New method for landslide susceptibility mapping supported by spatial logistic regression and GeoDetector: a case study of Duwen Highway Basin, Sichuan Province, China. *Geomorphology* 324, 62–71. doi:10.1016/j.geomorph.2018.09.019

Yang, X., and Liu, X. Z. (2023). Path analysis and mediating effects of influencing factors of land use carbon emissions in Chang-Zhu-Tan urban agglomeration. *Technol. Forecast. Soc. Change* 188, 122268. doi:10.1016/j.techfore.2022.122268

Ye, L., Wang, G. L., Zhang, Y. X., Sun, S. N., Qin, Y. P., Sun, L. Y., et al. (2023). Spatiotemporal evolution and driving forcesof the carbon emissions of the Yangtze River DeltaUrban agglomeration. *Pol. J. Environ. Stud.* 32, 2417–2428. doi:10.15244/pjoes/157379

Yuan, Y., Chuai, X. W., Xiang, C. Z., and Gao, R. Y. (2022). Carbon emissions from land use in Jiangsu, China, and analysis of the regional interactions. *Environ. Sci. Pollut. Res.* 29, 44523–44539. doi:10.1007/s11356-022-19007-2

Zhang, C. Y., Zhao, L., Zhang, H. T., Chen, M. N., Fang, R. Y., Yao, Y., et al. (2022). Spatial-temporal characteristics of carbon emissions from land use change in Yellow River Delta region, China. *Ecol. Indic.* 136, 108623. doi:10.1016/j.ecolind.2022.108623

Zhang, D. J., Ge, W. Y., and Zhang, Y. (2020). Evaluating the vegetation restoration sustainability of ecological projects: a case study of Wuqi County in China. *J. Clean. Prod.* 264, 121751. doi:10.1016/j.jclepro.2020.121751

Zhang, L., Jin, G., Wan, Q., Liu, Y. F., and Wei, X. J. (2018). Measurement of ecological land use/cover change and its varying spatiotemporal driving forces by statistical and survival analysis: a case study of yingkou city, China. *Sustainability* 10, 4567. doi:10.3390/su10124567

Zhang, P. Y., He, J. J., Hong, X., Zhang, W., Qin, C. Z., Pang, B., et al. (2017a). Regional-level carbon emissions modelling and scenario analysis: a STIRPAT case study in henan province, China. *Sustainability* 9, 2342. doi:10.3390/su9122342

Zhang, Q., Yang, J., Sun, Z. X., and Wu, F. (2017b). Analyzing the impact factors of energy-related CO_2 emissions in China: what can spatial panel regressions tell us? *J. Clean. Prod.* 161, 1085–1093. doi:10.1016/j.jclepro.2017.05.071

Zhang, X. P., and Cheng, X. M. (2009). Energy consumption, carbon emissions, and economic growth in China. *Ecol. Econ.* 68, 2706–2712. doi:10.1016/j.ecolecon.2009.05.011

Zhao, R. Q., Liu, Y., Tian, M. M., Ding, M. L., Cao, L. H., Zhang, Z. P., et al. (2018). Impacts of water and land resources exploitation on agricultural carbon emissions: the water-land-energy-carbon nexus. *Land Use Policy* 72, 480–492. doi:10.1016/j.landusepol.2017.12.029

Zheng, J. L., Mi, Z. F., Coffman, D., Milcheva, S., Shan, Y. L., Guan, D. B., et al. (2019). Regional development and carbon emissions in China. *Energy Econ.* 81, 25–36. doi:10.1016/j.eneco.2019.03.003

Zhou, J. (2011). *Study on the cointegration and causal relationship between land use change and carbon balance in changsha city* (Changsha, China: Hunan Normal University).

Zhu, E. Y., Qi, Q. Y., Chen, L. S., and Wu, X. H. (2022). The spatial-temporal patterns and multiple driving mechanisms of carbon emissions in the process of urbanization: a case study in Zhejiang, China. *J. Clean. Prod.* 358, 131954. doi:10.1016/j.jclepro.2022.131954

frontiers | Frontiers in Environmental Science

TYPE Original Research
PUBLISHED 24 June 2024
DOI 10.3389/fenvs.2024.1380868

OPEN ACCESS

EDITED BY
Chenxi Li,
Xi'an University of Architecture and Technology, China

REVIEWED BY
Yu Zhu,
Central South University Forestry and Technology, China
Muhammad Ziaul Hoque,
Bangabandhu Sheikh Mujibur Rahman Agricultural University, Bangladesh

*CORRESPONDENCE
Jie Liu,
liujie2004-2007@163.com

RECEIVED 02 February 2024
ACCEPTED 28 May 2024
PUBLISHED 24 June 2024

CITATION
Wang Y, Liu J, Zhang L, Xue Z and Yang Y (2024), Projecting the response of carbon sink potential to land use/land cover change in ecologically fragile regions.
Front. Environ. Sci. 12:1380868.
doi: 10.3389/fenvs.2024.1380868

Projecting the response of carbon sink potential to land use/land cover change in ecologically fragile regions

Ye Wang[1], Jie Liu[2]*, Lirong Zhang[1], Zhongcai Xue[1] and Yue Yang[1]

[1]Colloge of Resources and Environmental Sciences, Hebei Normal University for Nationalities, Chengde, Hebei, China, [2]College of Teacher Education, Hebei Normal University for Nationalities, Chengde, Hebei, China

Introduction: The carbon storage service of ecosystems in ecologically fragile areas is highly sensitive to regional land use/land cover (LULC) changes. Predicting changes in regional carbon storage under different LULC scenarios is crucial for land use management decisions and exploring carbon sink potential. This study focuses on the Luan River Basin, a typical ecologically fragile area, to analyze the impact of LULC changes on carbon storage.

Methods: The PLUS-InVEST model was employed to simulate LULC patterns for the year 2030 under three scenarios: natural development, cropland protection and urban development, and ecological protection. The model projected the future carbon sink potential of the basin under these scenarios.

Results: From 2000 to 2020, carbon storage showed a trend of decrease followed by an increase. By 2030, compared to 2020, carbon storage is projected to increase by 16.97% under the ecological protection scenario and decrease by 22.14% under the cropland protection and urban development scenario. The increase in carbon storage was primarily due to the conversion of cropland and grassland to forestland, while the decrease was mainly associated with the conversion of forestland to grassland and cropland, and the transformation of grassland to cropland and construction land. In the potential LULC scenarios of 2030, certain regions within the basin exhibited unstable carbon sink potential, strongly influenced by LULC changes. These areas were predominantly characterized by artificially cultivated forests, shrubs, and agricultural land. Implementing appropriate forest management measures and optimizing agricultural land management practices are essential to enhance carbon sink potential in these regions. Population density, annual average temperature, and DEM (Digital Elevation Model) were the dominant factors driving the spatial variation of carbon sink potential in the Luan River Basin.

Discussion: The research results provide a theoretical basis for rational planning of land use and the enhancement of carbon sink potential in ecologically fragile regions.

KEYWORDS

LULC, carbon storage, FLUS model, InVEST model, carbon sink potential, multi-scenario simulation

1 Introduction

The global issue of climate change caused by carbon dioxide emissions has received attention from countries worldwide (Sarkodie et al., 2020). With the ongoing process of urbanization, China has become the world's largest emitter of carbon dioxide (Yu et al., 2021). At the 75th session of the United Nations General Assembly in 2020, China pledged to reach its peak carbon emissions by 2030 and achieve carbon neutrality by 2060 (Li et al., 2023). Terrestrial ecosystems play a crucial role in carbon reduction and sequestration, making them important components of the global carbon cycle (Liu et al., 2023). The significance of terrestrial ecosystems in reducing carbon emissions and mitigating global warming has made them a major research hotspot worldwide in recent years (Tang et al., 2018; Piao et al., 2022; Wang H. W. et al., 2023a). Research has shown that LUCC is one of the important factors that influence the carbon cycling process in terrestrial ecosystems and cause regional changes in carbon balance (Zhao M. M. et al., 2019b; Zhu et al., 2019; Aneseyee et al., 2022).

There are multiple methods for estimating regional carbon storage. Traditional estimation methods such as the storage accumulation method and biomass method have demonstrated high accuracy in calculating carbon stocks at small spatial scales (Fang et al., 2001; Brown, 2002; Boothandford et al., 2014). However, traditional methods for estimating carbon stocks have limited accuracy in large-scale studies, and is difficult to analyze the dynamic changes and spatial distribution of regional carbon stocks. As information technology advances, carbon stock estimation methods primarily based on modeling have emerged. In comparison to other model methods (McGuire et al., 1992; Neilson, 1995; Sitch et al., 2003), the InVEST model has the advantage of requiring less input data and having faster computation speed (Bagstad et al., 2013). It allows for the spatial mapping of carbon stock distribution and dynamic changes, providing insights into the relationship between LULC changes and carbon stocks (Posner et al., 2016). Currently, the InVEST model has been widely applied in spatial planning, ecological compensation, risk management, climate change adaptation, and other environmental management decisions in various countries and regions. Scholars have utilized the carbon stock module to explore the impact of LULC changes on carbon stocks in terrestrial ecosystems (He et al., 2016; Li Y. H. et al., 2022a; Xu et al., 2023).

LULC scenario simulation plays a pivotal role in accurately assessing and quantifying the impact of LULC change on ecosystem carbon storage (Liu et al., 2023). Currently, the combination of the InVEST model and LULC data has been used to calculate regional carbon stocks. Furthermore, land prediction models have been employed to forecast future LULC patterns and changes in carbon stocks at the regional level. In existing land prediction models, FLUS (Gu et al., 2022; Xiang et al., 2022), CLUE-S (Islam et al., 2021; Kiziridis et al., 2023), and CA-Markov (Alhameedi et al., 2022; Zhang et al., 2023) have been widely used. However, these models primarily focus on improving modeling techniques, model rules, and accuracy, while paying less attention to exploring the underlying driving forces behind land cover change (Sohl and Claggett, 2013). The PLUS model integrates the Land Expansion Analysis Strategy (LEAS) and a Cellular Automata (CA) model based on multi-type random patch seeds. On one hand, LEAS incorporates the advantages of traditional conversion analysis strategies, allowing for a better exploration of the driving factors behind various LULC changes. On the other hand, the CA model, combined with random seed generation and threshold decay mechanisms, can simulate LULC changes at the patch level more effectively. The PLUS model possesses powerful data mining capabilities and the ability to model land changes at the patch level, offering great potential for applications such as optimizing land resource allocation and defining urban expansion boundaries (Liang et al., 2021). The coupling of the InVEST and PLUS models has been widely used for the calculation and prediction of carbon stocks. Wang R. Y. et al. (2023b) used the PLUS and InVEST models to simulate and predict the spatial development pattern of LULC as well as the changes in carbon stocks in the Greater Bay Area in China in 2030 under multiple scenarios. Kulaixi et al. (2023) utilized the PLUS-InVEST model to examine the spatiotemporal distribution and changing patterns of carbon storage under multiple scenarios in an Arid Inland River Basin in Xinjiang, China. Cui et al. (2023) used the PLUS model to simulate the future four LULC scenarios and the ecosystem carbon storage was assessed by the InVEST model in Guangdong, China.

The Luan River Basin possesses abundant vegetation resources and serves as an important ecological barrier in the Beijing-Tianjin-Hebei region of China (Xu et al., 2020). Moreover, due to its location in the agricultural-pastoral transitional zone and constraints imposed by precipitation and temperature, it has become a typical ecologically fragile area in northern China. Currently, studies on carbon stocks in the Luan River Basin primarily focus on the analysis of historical changes and the prediction of future trends. He et al. (2022) explored and predicted the spatiotemporal link between changes in LULC and carbon storage by coupling the FLUS model and InVEST model in China's Beijing-Tianjin-Hebei region, including the Luan River Basin. Guo et al. (2022) simulated the 2030 carbon storage and explored its spatial-temporal characteristics under three different scenarios. The above results provide scientific knowledge for the study of carbon storage in the Luan River Basin. However, the quantitative impact of LULC change on carbon storage remains uncertain, and there is a lack of discussion on carbon sink potential.

In the above context, this study primarily analyzes the following issues regarding the impact of LULC changes on carbon storage and future carbon sink potential: 1) How will potential LULC changes in 2030 affect the carbon storage in the basin? 2) What impact do transitions between different LULC types have on changes in carbon storage? Which LULC transitions primarily affect changes in carbon storage? 3) Based on the potential future LULC changes, what are the distribution characteristics of carbon sink potential? Considering the different characteristics of carbon sink potential zones, how can carbon storage in ecologically fragile areas be enhanced?

1.1 Study area

The Luan River Basin is situated in the northeast part of the North China Plain, spanning between 39°10′-42°35′ N and 115°20′-

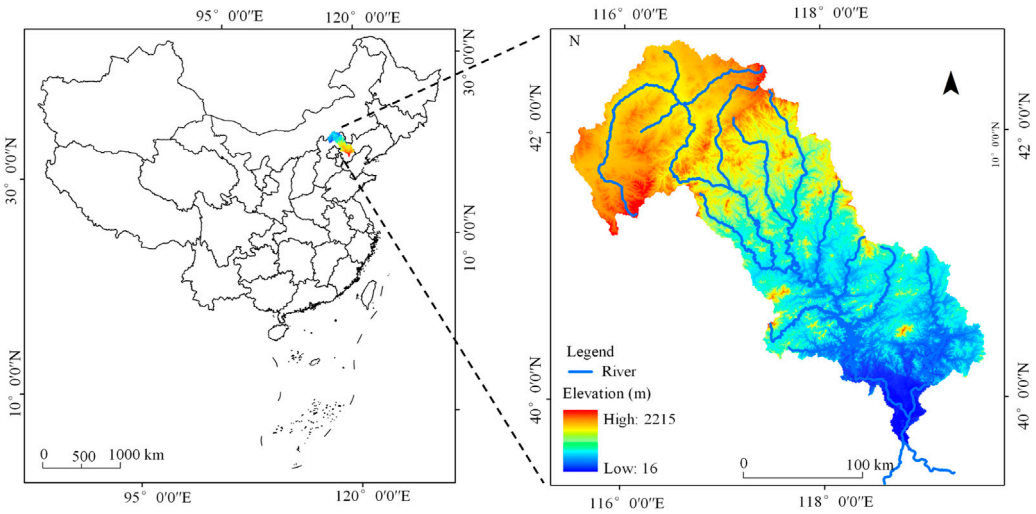

FIGURE 1
The geographical location and elevation map of the Luan River Basin.

TABLE 1 Data and sources.

Data type	Data name	Resolution/m	Data source
Climate environmental factors	DEM	30	Resource and Environment Science and Data Center, Chinese Academy of Sciences (https://www.resdc.cn/)
	Slope	30	
	Annual average precipitation	1,000	
	Annual average temperature	1,000	
	Soil type	1,000	
	Distance to water body system	1,000	
Socio-economic factors	Population density	1,000	Resource and Environment Science and Data Center, Chinese Academy of Sciences (https://www.resdc.cn/)
	GDP	1,000	
	Distance to main road	30	Openstreetmap (https://www.openstreetmap.org/)
	Distance to highway	30	
	Distance to government office	30	

119°15′ E (Figure 1). It originates from Fengning County and flows into the Bohai Sea in Leting County, covering a total length of approximately 877 km and an area of 44,880 square kilometers. The landforms within the basin are diverse and complex, with the upper reaches being dominated by plateaus and mountainous hills, the middle reaches by the Yan Mountains, and the lower reaches by the flat Hebei Plain. The terrain slopes from northwest to southeast, and there is a notable difference in climate between the north and the south. The climate varies notably from north to south, with a transition from cold-temperate arid and semi-arid climate to warm-temperate semi-humid climate. The average annual temperature is between 1°C and 11°C and the average annual precipitation ranges from 400 to 800 mm (Zeng et al., 2012). The Luan River Basin is characterized by interlaced zones of agriculture, pastoralism, and forestry, leading to complex relationships among ecosystem services. It is a typical ecologically fragile area in northern China.

1.2 Data sources and processing

The LULC data for the Luan River Basin in the years 2000, 2005, 2010, 2015, and 2020 were obtained from the Geospatial Data Cloud (https://www.gscloud.cn/), with a spatial resolution of 30 m. After cropping and projection, the LULC data were reclassified into six categories: cropland, forestland, grassland, water body, construction land, and unused land. The ArcGIS 10.0 Hydrology tool was utilized to delineate sub-basins in the Luan River Basin, based on DEM data. Taking into account both natural and socio-economic conditions, and based on the principles of driver accessibility, timeliness, and

TABLE 2 Carbon density of different LULC types (t/ha).

LULC	Aboveground carbon density	Underground carbon density	Soil carbon density	Carbon density of dead organic matter
Cropland	3.21	0.32	50.82	0.00
Forestland	69.63	21.00	133.82	1.95
Grassland	1.18	13.6	79.87	2.00
Water body	3.42	12.1	8.64	0.00
Construction land	0.41	6.91	28.82	0.00
Unused land	9.13	1.82	34.08	0.00

significance, 11 driving factors were selected to predict the LULC distribution in the Luan River Basin under different scenarios for the year 2030 (Table 1).

1.3 Research methodology

1.3.1 Ecosystem carbon storage assessment based on the InVEST model

Carbon storage was calculated based on the InVEST model, which simulates carbon storage based on the LULC data of each period and the corresponding carbon density using the following formula (Li Y. X. et al., 2022b) (see Eqs 1, 2).

$$C_i = C_{ia} + C_{ib} + C_{is} + C_{id} \quad (1)$$

$$C_{tot} = \sum_{i=1}^{n} C_i \times S_i \quad (2)$$

Where i represents the land-use type; Ci indicates the carbon density of land utilization type i; C_{ia}, C_{ib}, C_{is}, and C_{id} indicate the carbon density of terrestrial biogenic carbon, subsurface biogenic carbon, soil carbon, and dead organic carbon of LULC type i, respectively. The unit of all carbon densities is megagrams per hectare (t/ha). C_{tot} indicates the total carbon storage in the region(t); S_i indicates the area of land utilization pattern i (ha); n indicates the total number of LULC types.

The construction of the carbon density database primarily relied on measured data from existing literature. Priority was given to carbon density values obtained from field surveys conducted in the Luan River Basin (Xu et al., 2019). For data where reference literature was lacking, it was supplemented using research literature from neighboring areas (Li et al., 2004; He et al., 2022). If there were still gaps, carbon density data for six land types could be obtained based on the following carbon density correction formula (Zhang and Zhang, 2009; Alam et al., 2013) (see Eqs 3–6).

$$C_{BP} = 6.789 \times e^{0.0054 \times MAP} \quad (3)$$

$$C_{SP} = 3.3968 \times MAP + 3996.1 \quad (4)$$

$$K_{BP} = C_{BP1}/C_{BP2} \quad (5)$$

$$K_{SP} = C_{SP1}/C_{SP2} \quad (6)$$

Where MAP represents the annual average precipitation(mm); C_{BP} represents the biomass carbon density after correction (t/ha); C_{SP} represents the soil carbon density after correction (t/ha); K_{BP} represents the precipitation factor correction coefficient for biomass carbon density; K_{SP} represents the precipitation factor correction coefficient for soil carbon density. By comparing the calibrated carbon density results with actual carbon density, the *RMSE* was 0.83, indicating that the calibration results are fairly accurate and can be used as input for the InVEST model parameters. Finally, the carbon density dataset for land utilization categories in the Luan River Basin was obtained (Table 2).

1.3.2 Future LULC simulation (PLUS) model

The PLUS model is a fine-scale LULC prediction model developed based on the FLUS model, taking into account the policy-driven guidance effect in LULC planning (Liang et al., 2021; Gao et al., 2022). Based on LULC data from 2010 to 2020 in the Luan River Basin, this study utilized the driving factors as predictor variables to calculate the suitability probabilities for different LULC types. Using the 2010 LULC data as the baseline, the PLUS model was employed to simulate the LULC data for 2020. The simulated results were compared with the actual data for 2020, resulting in a Kappa coefficient of 0.81, indicating a high level of reliability in the simulation results (Zadbagher et al., 2018; Liu et al., 2022).

The neighborhood weights represent the expansion capacity of different LULC types. In this study, the neighborhood weights were calculated using the dimensionless values of the LULC-type area changes in the Luan River Basin from 2010 to 2020 (Table 3).

1.3.3 The setting of different future scenarios

The "Land and Spatial Planning Announcement of Hebei Province (2021-2035)" was released in September 2021. It proposed the establisent of the ecological security barrier, implementation of cropland protection measures, and promotion of coordinated urban development. The Luan River Basin has irrigated nearly 21% of the irrigated areas in Hebei Province and has supported about 20% of the population, accounting for nearly 30% of the province's GDP. Therefore, based on the ecological and economic role played by the Luan River Basin, different LULC scenarios for the year 2030 were simulated using the PLUS model to meet various development needs. The LULC transition matrix represented the conversion rules between different LULC types. When one LULC type could be converted into another, the corresponding value in the matrix was 1; otherwise, it was 0. The three scenarios are shown in Table 4. Parameters and weights used in the simulation of suitability maps are shown in Supplementary Table S1. These scenarios are as follows:

TABLE 3 The neighborhood weights of different land use types.

LULC	Cropland	Forestland	Grassland	Water body	Construction land	Unused land
Neighborhood weight	0.50	0.17	0.13	0.18	0.19	0.07

TABLE 4 LULC transfer matrix under different scenarios.

Land use	S1						S2						S3					
	L1	L2	L3	L4	L5	L6	L1	L2	L3	L4	L5	L6	L1	L2	L3	L4	L5	L6
L1	1	1	1	1	1	1	1	0	0	0	1	0	1	1	1	1	0	0
L2	1	1	1	1	1	1	1	1	1	0	1	1	0	1	1	0	0	0
L3	1	1	1	1	1	1	1	1	1	0	1	1	0	1	1	0	0	0
L4	1	1	1	1	1	1	1	0	0	1	1	0	0	1	1	1	0	0
L5	1	1	1	1	1	1	1	0	0	0	1	0	1	1	1	1	1	0
L6	1	1	1	1	1	1	1	0	0	0	1	0	0	1	1	1	1	1

Note: L1: cropland, L2: forestland, L3: grassland, L4: water body, L5: construction land, L6: unused land.

1) Natural Evolution Scenario (S1). Based on the transition probabilities from 2010 to 2020, the LULC structure for the year 2030 was predicted, allowing for free conversion between different LULC types.
2) Cropland Protection and Urban Development Scenario (S2). The priority was given to the development of construction land while strictly controlling the conversion of cropland to LULC types other than construction land. This scenario aimed to meet the demands of economic development while ensuring the protection of agricultural land.
3) Ecological Protection Scenario (S3). Under the requirements of ecological conservation, strict control measures were implemented for the conversion of forestland, grassland, and water bodies. Forestland and grassland could be converted into each other but could not be converted into other land types. On the other hand, other land types could be converted into forestland and grassland.

1.3.4 Driver analysis

The spatial distribution patterns of the input driver parameters for LULC change, along with the corresponding changes in carbon sink, were analyzed using an exploratory spatial data analysis (ESDA) technique, specifically spatial autocorrelation through GeoDa-1.20.0 software (Hoque et al., 2019b; Zhang et al., 2019). Spatial autocorrelation, as assessed by Local Indicators of Spatial Association (LISA), reveals four distinct types of spatial clusters at the local level: High-High (HH), High-Low (HL), Low-High (LH), and Low-Low (LL) (Hoque et al., 2019b; Zhang et al., 2019).

Geodetector is a set of statistical methods used to detect spatial heterogeneity and reveal the underlying drivers. Its core idea is based on the assumption that if a certain independent variable significantly influences a dependent variable, then the spatial distribution of both variables should exhibit similarity (Wang et al., 2016; Lin et al., 2019). Discrimination and factor detection involve comparing the total variance of the study area with the sum of variances in the classified sub-regions to detect spatial heterogeneity in Y or determine the extent to which a factor X explains the spatial heterogeneity of attribute Y. The results are measured using the q-statistic. We utilized discrimination and factor detection in Geodetector to analyze the explanatory power of different drivers on the spatial heterogeneity of carbon sink potential.

2 Results

2.1 Temporal and spatial analysis of LULC

Figures 2, 3 respectively illustrate the overall changes in total area and transfer directions of various LULC types from 2000 to 2020 and in 2030 under different scenarios. From 2000 to 2020, the area of cropland, grassland, water bodies, and unused land decreased, while the area of forestland and construction land increased. During the period from 2000 to 2010, the area of cropland decreased, while the areas of forestland increased. This was mainly due to the implementation of the national policy of the Grain for Green Project (Zhao A. Z. et al., 2019a), which resulted in a notable transfer of cropland to forestland. Additionally, the rapid process of urbanization led to a large-scale encroachment of cropland for construction purposes. From 2010 to 2020, the area of forestland continued to increase, while the area of cropland further decreased. This can be attributed to the further development of the Grain for Green Project and the strong promotion of the "Three-North' Shelterbelt by the government (Mu et al., 2017), which led to a continuous transfer of cropland to forestland. According to the set features of potential LULC scenarios in 2030, S1 continued the LULC change characteristics from 2000 to 2020, with a continuous decrease in cropland and grassland areas and a consistent increase in forestland and construction land. In S2, driven by socio-economic development as a force for LULC change, the areas of cropland and construction

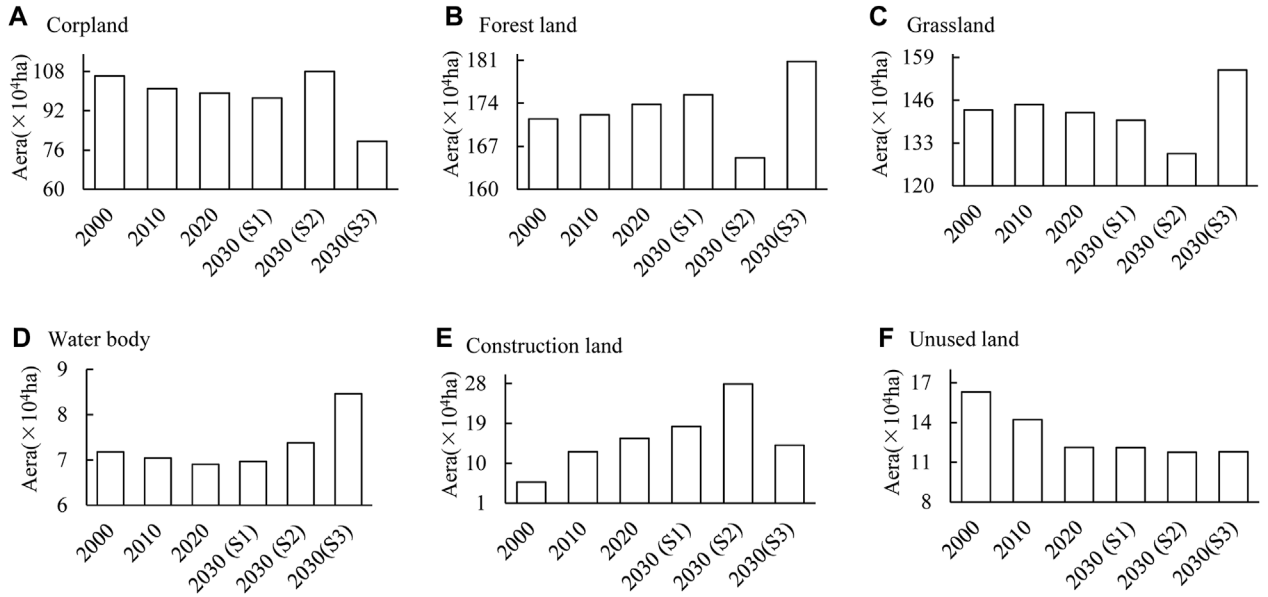

FIGURE 2
The LULC area change from 2000 to 2030. **(A)** Corpland, **(B)** Forest land, **(C)** Grassland, **(D)** Water body, **(E)** Construction land, **(F)** Unused land.

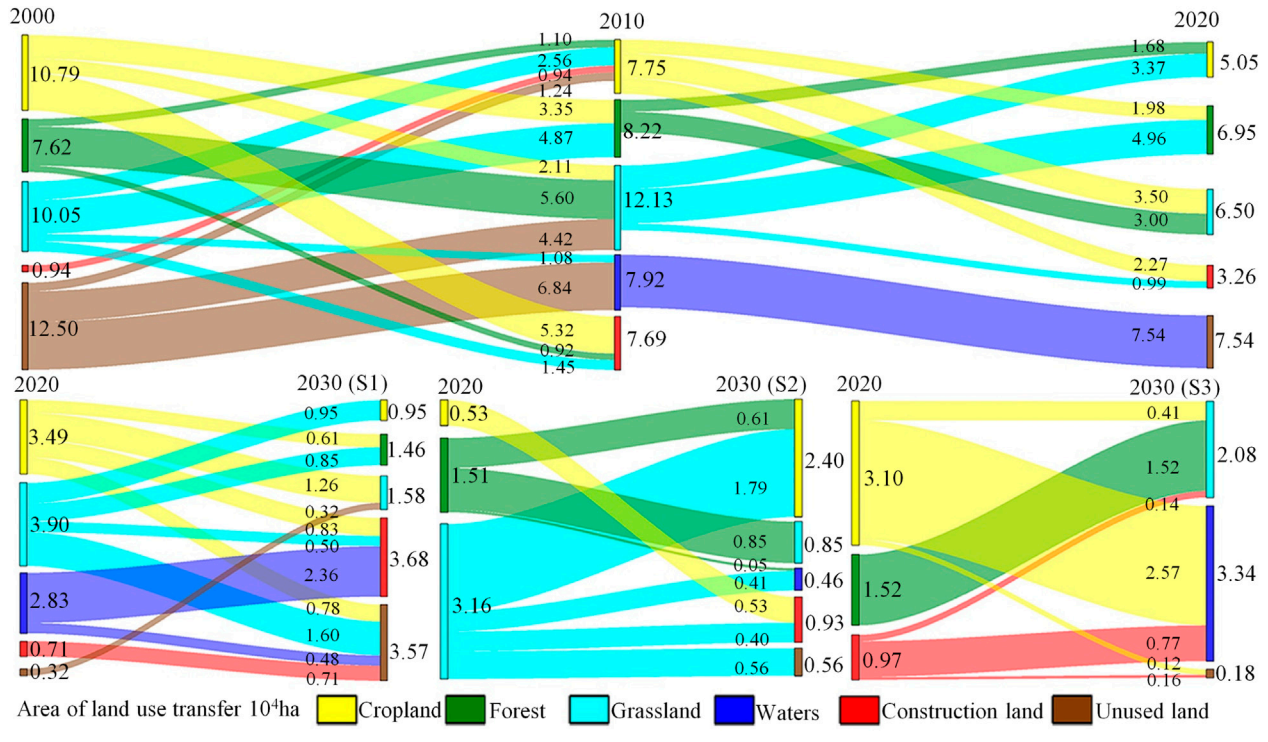

FIGURE 3
Sankey map of LULC type transfer from 2000 to 2030.

land experienced increases, while the areas of forestland and grassland decreased accordingly. In S3, agricultural land and urban land were strictly restricted, and ecological land saw development, mainly reflected in the increase of forestland and grassland areas.

From the spatial distribution perspective (Figure 4), cropland is primarily distributed in the upstream and downstream areas of the basin, specifically in the North China Plain. Grassland is mainly located in the higher-altitude Inner Mongolia Plateau region in the upstream of the basin. Forestland is distributed in the Yan Mountain

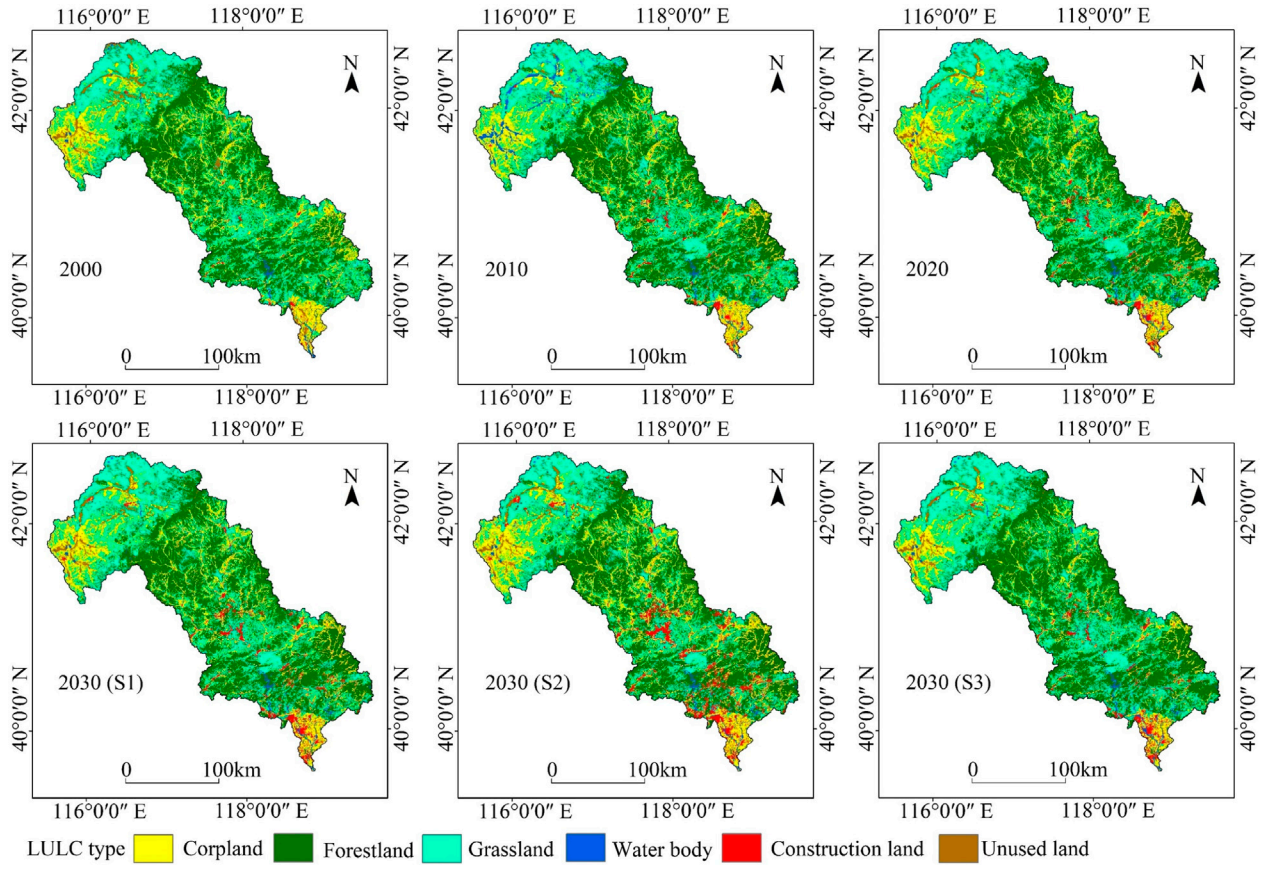

FIGURE 4
Spatial distribution of LUCC from 2000 to 2030.

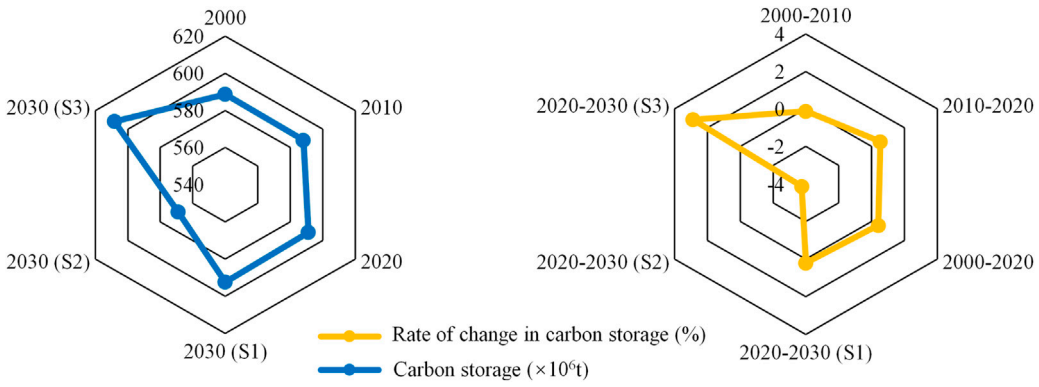

FIGURE 5
The carbon storage changes from 2000 to 2030.

range in the middle reaches of the basin, while construction land is mainly concentrated in the urban clusters in the middle and lower reaches of the basin. In the LULC scenarios for 2030, in S1 and S2, there was a notable expansion of construction land in the central and southern regions of the basin, while grassland exhibited varying degrees of degradation. In S3, grassland in the northern and central parts experienced recovery.

2.2 Temporal and spatial analysis of carbon storage

Figure 5 presents carbon storage and its changes from 2000 to 2030. In the years 2000, 2010, and 2020, carbon storage was 588.79 × 10^6 t, 588.06 × 10^6 t, and 591.17 × 10^6 t, respectively, showing an overall weak trend of change. In 2030, compared to 2020, in S1, carbon storage was

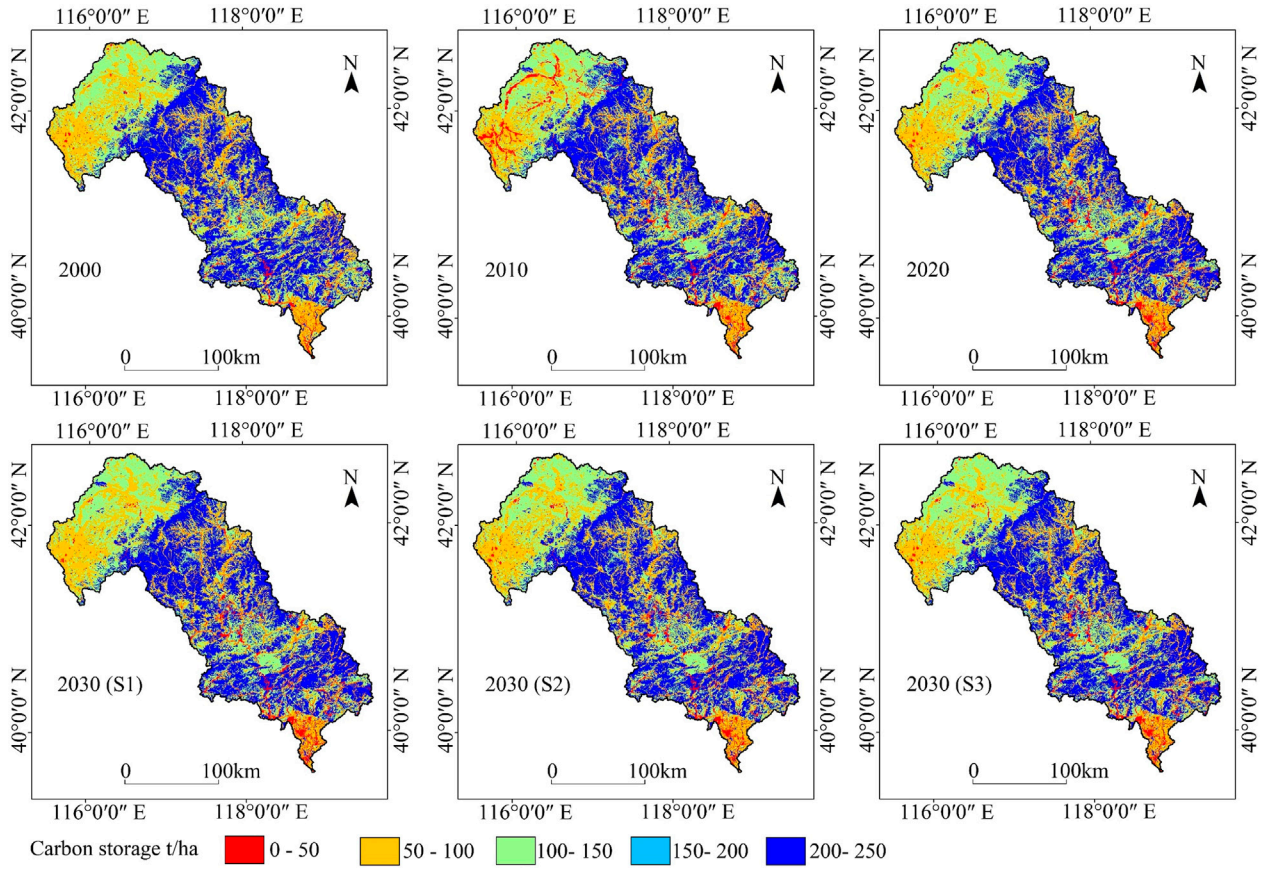

FIGURE 6
Spatial distribution of carbon storage from 2000 to 2030.

592.39 × 10^6 t, with a small change. In S2, carbon storage underwent a decrease to 569.03 × 10^6 t, with a change rate of −22.14%. In S3, carbon storage increased markedly to 608.14 × 10^6 t, with a change rate of 16.97%.

The spatial distribution of carbon storage in the Luan River Basin exhibited a pattern of higher values in the middle region of the basin and lower values in the northern and southern parts (Figure 6). This spatial distribution pattern remained relatively stable over time with minimal changes. The areas with high carbon storage in the Luan River Basin were concentrated in the middle region, specifically in the Yan Mountains. This region experienced slower urban development and lower land development, resulting in higher vegetation coverage.

Conversely, the areas with low carbon storage were concentrated in the northern and southern parts. The northern part, belonging to the southern edge of the Inner Mongolia Plateau, had higher altitudes and lower precipitation. It was economically developed in agriculture and animal husbandry, featuring widespread cropland and grassland. The southern part, mainly situated in the northern part of the North China Plain forming the Luan River Delta, had a flat terrain, high urbanization level, intense land development and utilization, dense population, and high demand for construction land. This region included parts of the Bohai Sea urban agglomerations where ecological space was notably encroached upon due to urbanization. Consequently, areas with high carbon storage, such as forestland, cropland, and grassland, were relatively scarce and scattered in this urbanized region. Taking into account the changes in LULC structure in the Luan River Basin, the spatial distribution pattern of carbon storage was closely related to the LULC types in the region. LULC changes had a substantial impact on regional carbon storage, with ecological land playing a more prominent role in the variation of carbon storage.

To explore spatial autocorrelation, Moran's I values were calculated and found to be 0.5912 (2020), 0.5833 (2010), 0.5921 (2020), 0.5933 (2030-S1), 0.5929 (2030-S2), and 0.5934 (2030-S3). All the computed results are greater than 0, indicating that there is a certain degree of spatial clustering in carbon storage across the Luan River Basin. The distribution of carbon storage hot spots in the Luan River Basin shows minimal variation, with hot spots predominantly found in the middle and upper reaches of the basin, while cold spots are concentrated in the upstream and downstream regions (Figure 7). In 2030, the scenario S3 showed the largest increase in the area of carbon storage hot spots, while the scenario S1 had the smallest increase in the area of carbon storage hot spots.

2.3 Effects of LULC changes on carbon storage

Figure 8 illustrates the proportion and changes in carbon storage of various LULC types from 2000 to 2030 under different scenarios. The sum of carbon storage in forestland, grassland, and cropland

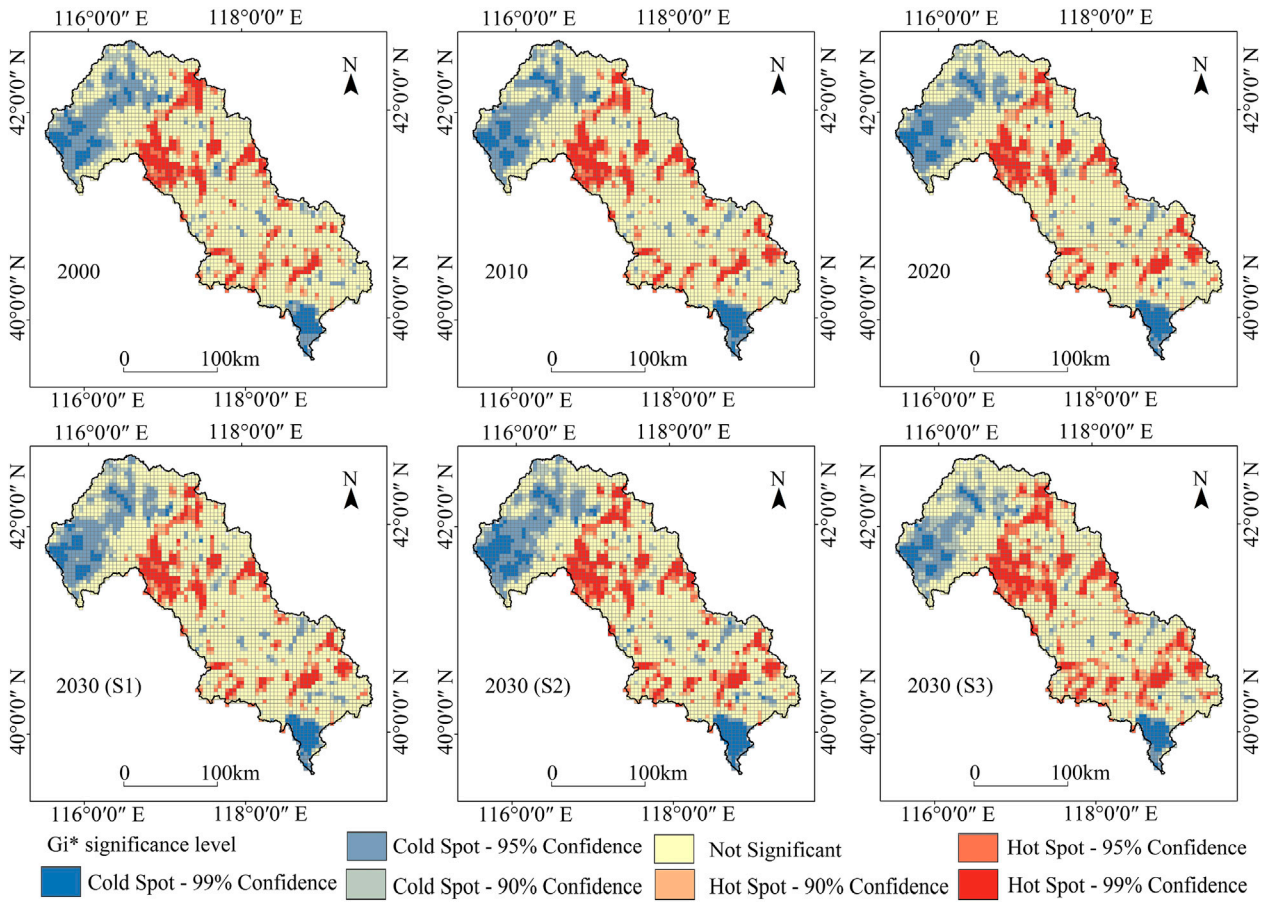

FIGURE 7
Hot spot distribution of carbon storage from 2000 to 2030 in the Luan River Basin.

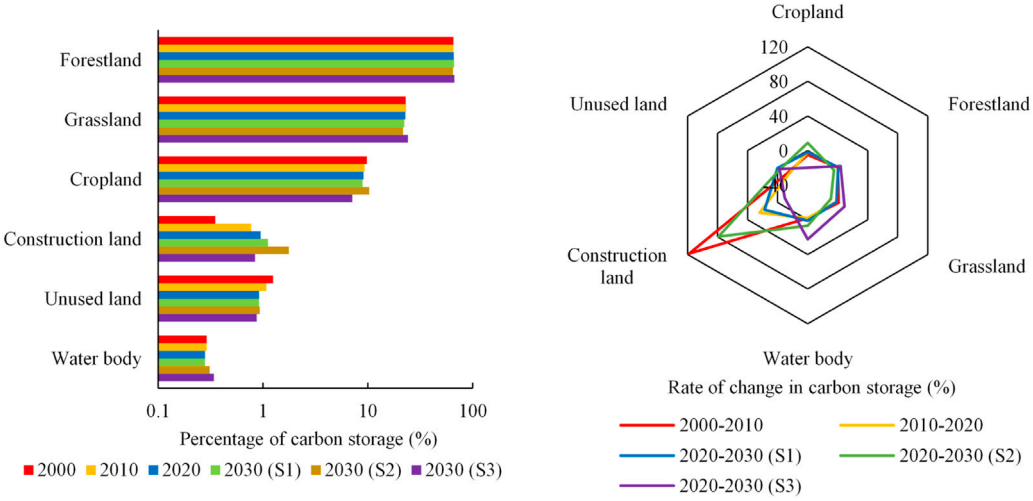

FIGURE 8
Carbon storage percentage and change rate for each LULC type.

10.3389/fenvs.2024.1380868

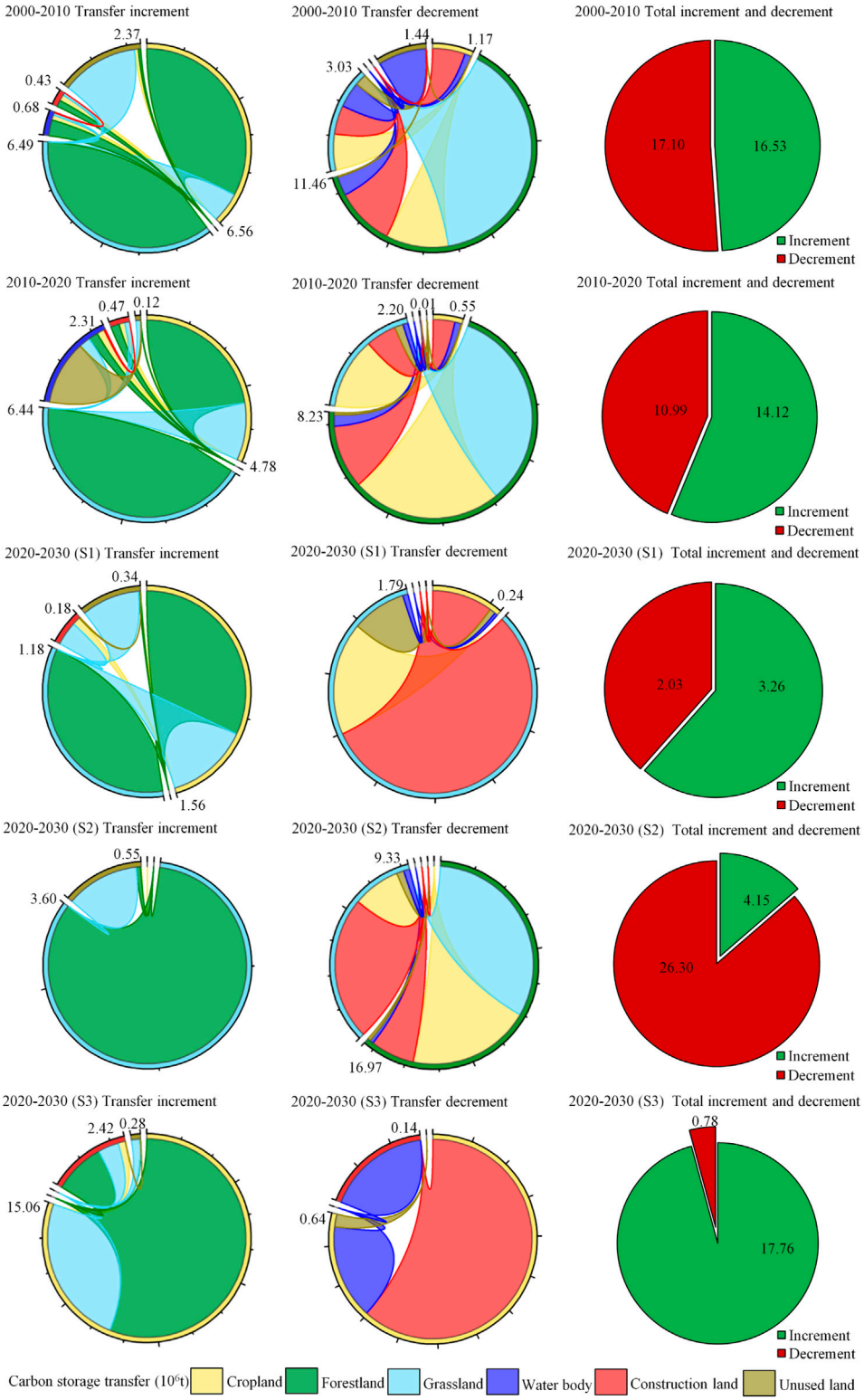

FIGURE 9
Carbon storage transfers between LULC types from 2000 to 2030.

exceeded 96%, making them the main contributors to the basin's carbon storage, while water bodies contributed less than 0.5%. The changes in carbon storage in each period indicated a increase in carbon storage in construction land from 2000 to 2010 and 2010 to 2020, with the most noticeable decrease in carbon storage in unused land. In 2030 under different scenarios, there was a increase in carbon storage in construction land in S1 and S2, while the carbon storage in cropland for S1 and grassland for S2 decreased markedly.

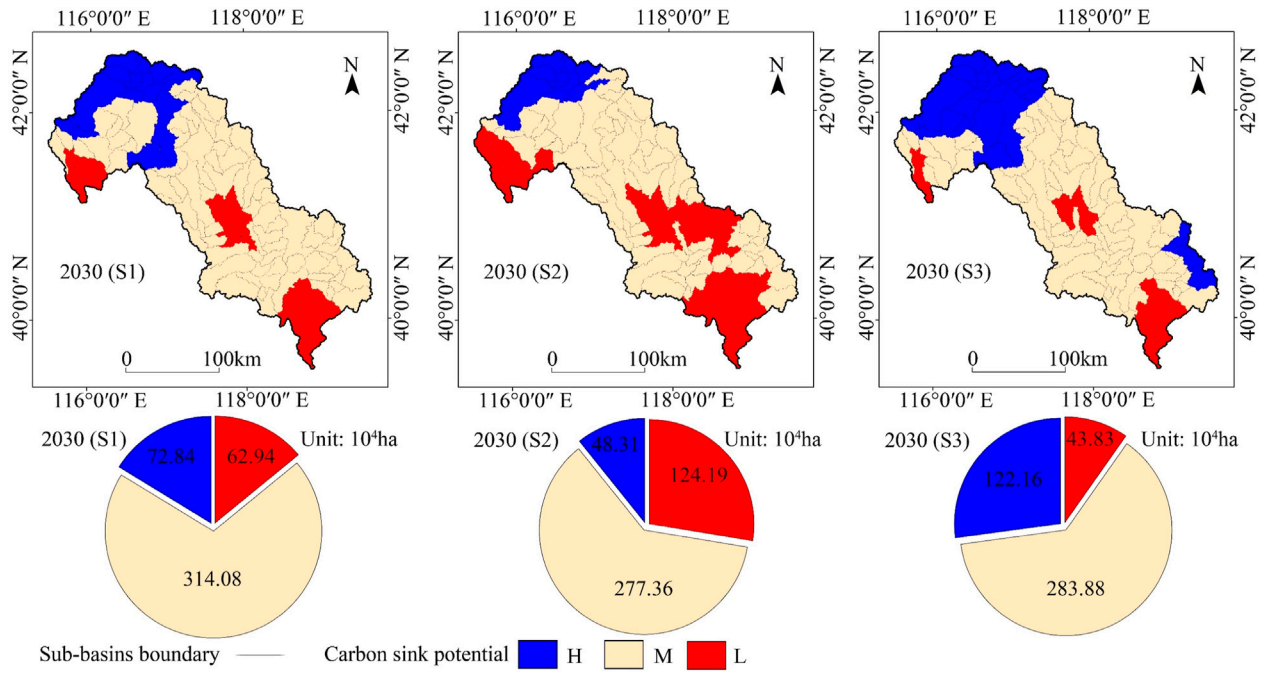

FIGURE 10
Carbon sink potential distribution and area proportions in different scenarios in 2030.

The carbon storage in water bodies increased markedly in S3, while the carbon storage in cropland decreased notably.

The transfer of carbon storage between different LULC types (Figure 9) showed that from 2000 to 2010, the increase in carbon storage mainly came from the conversion of cropland and grassland to forestland, while the decrease was mainly due to the conversion from forestland to grassland. From 2010 to 2020, the increase in carbon storage mainly came from the conversion of grassland to forestland, while the decrease was mainly due to the conversion from forestland to grassland and cropland.

From 2020 to 2030, the increase in carbon storage in S1 mainly came from the conversion of cropland and grassland to forestland, while the decrease was mainly due to the conversion from grassland to construction land. The increase in carbon storage in S2 and S3 mainly came from the conversion of grassland and cropland to forestland. The conversion from forestland to cropland and grassland to construction land was the main reason for the decrease in carbon storage in S2. The main reason for the decrease in carbon storage in S3 was the conversion from cropland to construction land. Overall, the increase in carbon storage at each period mainly came from the conversion of other LULC types to forestland, while the conversion from forestland, grassland, and cropland to other low carbon density LULC types was the main reason for the decrease in carbon storage.

2.4 Prediction of carbon sink potential zoning

At the sub-basin scale, the rate of carbon storage changes between each scenario in 2030 and the year 2020 was calculated (Figure 10). The sub-basins with an average carbon storage change rate exceeding 10% are classified as high carbon sink potential areas (H), those ranging from −10% to 10% are categorized as medium carbon sink potential areas (M), and those below −10% are designated as low carbon sink potential areas (L). By comparing the three scenarios, this study found that the high carbon sink potential area was the largest in S3. This was mainly due to ecological activities such as vegetation restoration and intensive LULC in some sub-basins, increasing the area of forestland and grassland, and consequently an increase in regional carbon storage. On the other hand, the S2 had the smallest high carbon sink potential area, mainly due to drastic LULC changes, extensive vegetation destruction, and continuous expansion of construction land, leading to a reduction in carbon sink areas and a decline in carbon storage.

Based on the carbon sink potential under three potential LULC scenarios in 2030, the Luan River Basin is divided into seven carbon sink potential zones (Table 5). The High Growth Zone (Z1), located in the northern part of the basin, exhibits consistently high carbon sink potential under all scenarios, with a change rate ranging from 13.99% to 21.37%, indicating stable growth in carbon storage in this region. The Moderate Growth Zone (Z2) shows relatively high carbon sink potential under S1 and S3, with a change rate of 10.78%–14.18%. However, excessive expansion of cropland and urban land areas may impact the stability of carbon storage growth in this zone. The Low Growth Zone (Z3) only exhibits high carbon sink potential under S3, with a change rate of 7.66%–13.72%, indicating that an increase in forestland and grassland areas will effectively enhance carbon storage in this region.

The Balance Zone (Z4), located in the central part of the basin, shows a moderate level of carbon sink potential under all scenarios, with a change rate ranging from −9.45% to 12.17%. This suggests that carbon storage in this zone tends to stabilize, with relatively minor impacts from future LULC changes. The Low Decline Zone (Z5) has lower carbon sink potential under S2, with a change rate of −11.77% to −7.31%, indicating a

TABLE 5 Characteristics of carbon sink potential zoning in 2030.

Code	Carbon sink potential zoning	Carbon sink potential			Average carbon storage change rate (%)
		S1	S2	S3	
Z1	High Growth Zone	H	H	H	17.71
Z2	Moderate Growth Zone	H	M	H	12.74
Z3	Low Growth Zone	M	M	H	10.26
Z4	Balance Zone	M	M	M	−0.46
Z5	Low Decline Zone	M	L	M	−9.86
Z6	Moderate Decline Zone	L	L	M	−13.22
Z7	High Decline Zone	L	L	L	−19.92

slight declining trend in carbon storage due to excessive expansion of cropland and urban land areas. The Moderate Decline Zone (Z6) exhibits lower carbon sink potential under S1 and S2, with a change rate of −15.11% to −11.07%. However, an increase in forestland and grassland areas will alleviate the decline in carbon storage in this zone. The High Decline Zone (Z7), mainly located in the central and southern parts of the basin, shows consistently lower carbon sink potential under all scenarios, with a change rate of −25.22% to −16.22%, indicating a continuous decline in carbon storage in this region (Figure 11).

2.5 Analysis of the drivers of carbon sink potential heterogeneity

The spatial auto-correlation analysis (Figure 12) revealed a distribution pattern characterized by clear clustering, with predominant occurrences of High-High (HH) and Low-Low (LL) types of clusters, and only a few instances of High-Low (HL) or Low-High (LH) spatial outliers Supplementary Figure S2).

Figure 13 illustrates the ranking of the importance of driving factors. Except for factors such as soil type, distance to highway, distance to main road, and distance to government office, all other driving factors are greater than 25%. After screening, the driving factors with relatively high importance are obtained: population density, annual average temperature, DEM, GDP, slope, annual average precipitation, and distance to water body system have relatively high q values, with the q value of population density reaching 0.775. This indicates that natural environmental factors such as population density have strong explanatory power for the spatial distribution of carbon sink potential.

3 Discussion

3.1 The impact of LULC changes on the carbon storage

This study indicated that the carbon storage in the Luan River Basin showed an overall increasing trend from 2000 to 2020, primarily due to the conversion of cropland and grassland into forestland. These research findings were consistent with the results of some other scholars' studies. Cui (Cui et al., 2019) showed that although carbon storage in the BTH (Beijing-Tianjin-Hebei) region decreased year by year from 1990 to 2015, there was an increase in the northern part, specifically in the Luan River Basin. He (He et al., 2022) demonstrated through scenario simulations that the main reason for the increase in carbon storage in the BTH region was the expansion of forestland and grassland areas.

Starting from the year 2000, various ecological projects, such as reforestation, protection of natural forests, and afforestation, have been extensively carried out in China. As a result, the forestland vegetation has entered an early stage of succession, leading to a enhancement in carbon storage capacity. With rapid socio-economic development, the expansion of cropland and construction land has led to a decrease in the area of forestland, grassland, and other land types in some areas of the Luan River Basin, resulting in a decline in carbon storage. The lower reaches of the Luan River Basin had lower elevations and gentle slopes, making them suitable for human habitation. However, excessive land development has led to a lower ecological environment quality, consequently reducing carbon storage. In contrast, the middle reaches of the Luan River Basin consisted of higher elevations and steeper slopes in mountainous areas, with less human disturbance and higher vegetation coverage, primarily dominated by forestland. The favorable ecological environment promoted plant growth, leading to higher carbon storage in this region. The upper reaches of the Luan River Basin were characterized by higher elevations, and limited precipitation, and predominantly consisted of shrub forests and grasslands with lower water demands. The rapid development of agriculture and animal husbandry in this area has resulted in a decline in habitat quality, indirectly affecting carbon storage.

3.2 Carbon sink potential zoning based on future LULC changes

Carbon sink potential refers to the potential increase in carbon storage in a given region compared to its historical carbon stocks. Predicting carbon sink potential is beneficial for effective carbon emissions management and plays a crucial role in achieving sustainable development (Meng et al., 2023). This study determined the carbon sink potential of the Luan River Basin for the year 2030 at the sub-basin scale. A sub-basin is a closed area where local surface water and groundwater naturally converge

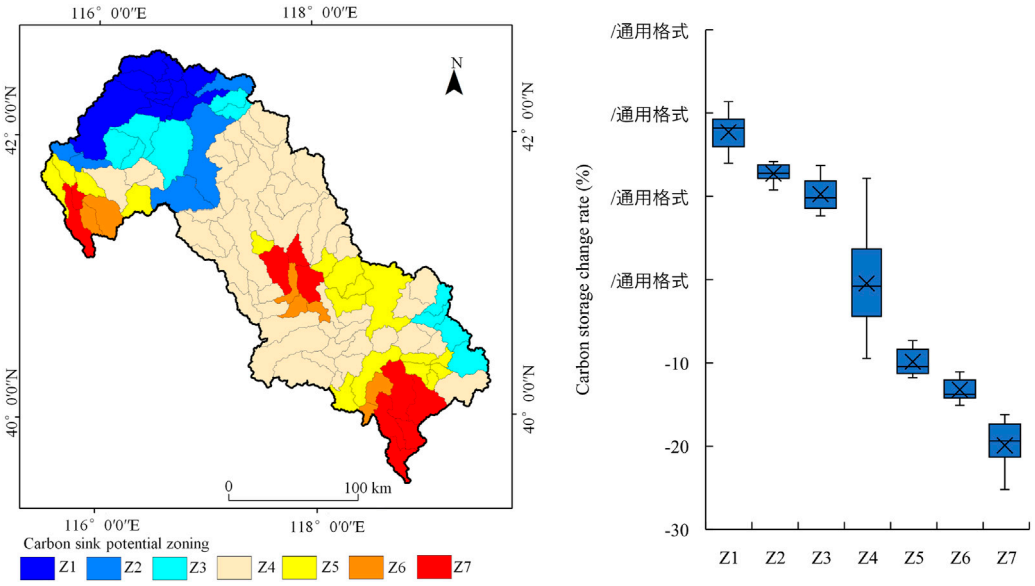

FIGURE 11
Carbon sink potential zones and the change rate of carbon storage in each zone in 2030.

within a watershed. At the sub-basin scale, spatial differences in climate and underlying surface characteristics are relatively small, making it more suitable for managing carbon sink potential compared to administrative divisions. The Luan River Basin is located in the transitional zone between agriculture and animal husbandry in China and is considered an ecologically fragile area. Carbon storage in this region is sensitive to future changes in land-use structures (Vizcaino et al., 2020). Economic development leads to the expansion of agricultural and urban land, resulting in a decline in regional carbon sink potential (He et al., 2016). The increase in ecological land improves regional carbon sink potential but may impact socio-economic development to some extent (Yang et al., 2020). Economic development and population growth should not only pursue speed but also aim for high-quality development, maintaining coordination between the economy and the ecological environment, enhancing the value of regional ecosystem services, and increasing regional carbon sink capacity (Babbar et al., 2021). Therefore, a carbon sink potential zoning based on future land-use changes is conducive to the sustainable development of regional carbon storage services and socio-economics.

This study assessed the carbon sink potential under three typical land-use scenarios for 2030, resulting in the identification of seven carbon sink potential zones. The High Growth Zone exhibited stable growth in carbon storage under all scenarios, but being located in the Inner Mongolia Plateau area, vegetation growth is highly influenced by climate conditions. The Balance Zone, located in the mountainous area in the middle of the basin, has the largest proportion of carbon storage in the basin. With extensive original forests and strict ecological protection policies limiting the conversion of forestland to other LULC types, the carbon storage in this area tends to remain stable. The High Decline Zone showed a declining trend in carbon storage under all scenarios, mainly located in the southern and central parts of the basin, characterized by high population density and economic development. Due to the high proportion of agricultural and construction land, which is expected to further expand in the future, there is a risk of further decline in carbon sink potential in this region. The Moderate Growth Zone and Low Growth Zone, mainly located in the northern part of the basin, feature extensive artificially planted forests and shrubs. They possess a certain potential for improving carbon sequestration and are crucial for raising the upper limit of basin carbon storage (Li et al., 2023; Liu et al., 2023). The Moderate Decline Zone and Low Decline Zone face the risk of declining carbon sink potential, crucial for raising the lower limit of basin carbon storage. This region, mainly located in the central and southern parts of the basin, has a high proportion of agricultural land. Improper measures in the agricultural production process can lead to severe damage to the planting conditions of cultivated land, reducing soil carbon density and, consequently, the carbon sink potential. Although under the policy of returning cropland to forestland, the restoration of vegetation on cultivated land increases both above-ground and below-ground biomass, extensive farming practices still affect the carbon cycling process in cultivated land systems (Wang et al., 2023).

Based on the findings of this study, the following recommendations are provided: The carbon sink potential in the Luan River Basin exhibits uneven spatial distribution, with a significant proportion of forest carbon sinks and high carbon sequestration rates in the upper and middle reaches. Horizontal carbon compensation and trading can be conducted with downstream areas to strengthen low-carbon exchanges and cooperation. While leveraging their own resource advantages for economic benefits, efforts should be made to address potential "ecological deficits' in downstream areas. Conversely, the downstream areas, characterized as low-value carbon sink zones in the Luan River Basin, have fewer forest carbon sinks. Therefore, measures such as afforestation or increasing urban green spaces

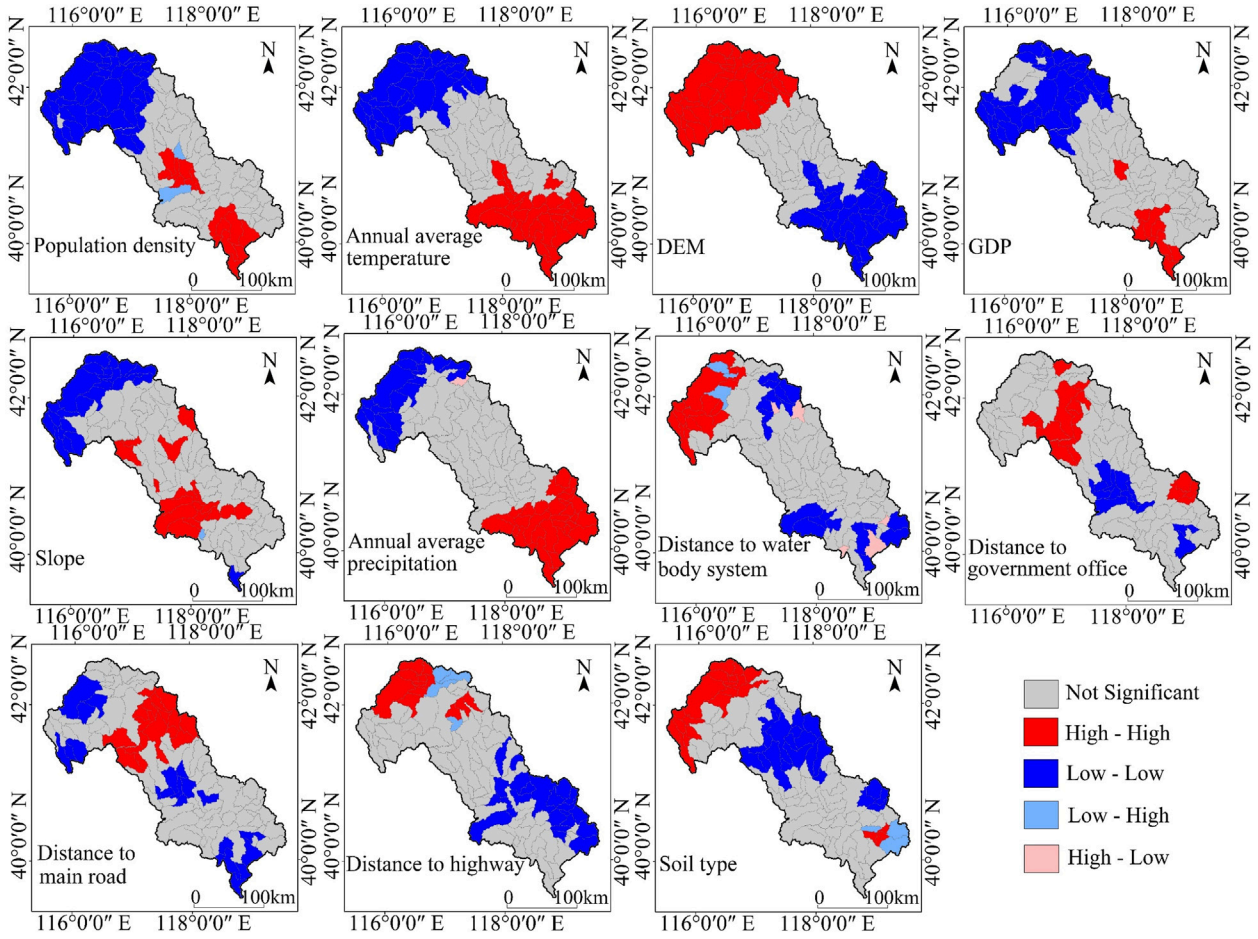

FIGURE 12
Spatial heterogeneity LISA cluster map of drivers.

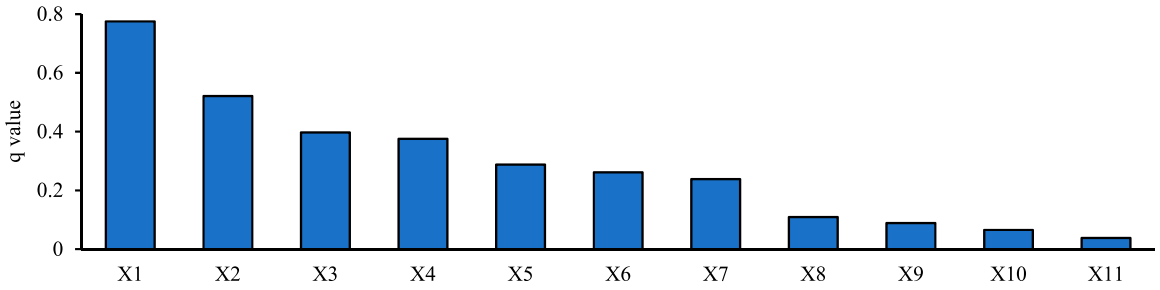

FIGURE 13
Rank of the importance of drivers. Note.X1: Population density, X2: Annual average temperature, X3: DEM, X4: GDP, X5: Slope, X6: Annual average precipitation, X7: Distance to water body system, X8: Distance to government office, X9: Distance to main road, X10: Distance to highway, X11: Soil type.

should be implemented to enhance the region's carbon sequestration capacity. In future scenario projections, there are considerable differences in the carbon sink potential structure of the Luan River Basin, particularly under S2, where there is a notable decline in carbon sink potential. To address this, optimizing the land use structure for carbon sinks and adjusting the proportions of various carbon sink land types are recommended. Forests are the main contributors to carbon sinks in the Luan River Basin but face the risk of shrinking in size. Planning and establishing forest nature reserves, implementing afforestation programs, and practicing reforestation can stabilize and enhance the carbon sequestration capacity of regional forests. Additionally, grassland resources should

be protected to prevent further degradation trends in the northern part of the basin. Unused land, due to its weak carbon sink potential and prevalence in areas unsuitable for large-scale development (such as the Inner Mongolia Plateau), can be managed for sustainable carbon sequestration by restoring vegetation on unused land while simultaneously prioritizing ecological conservation efforts.

3.3 Limitations and future work

Based on the InVEST model to assess carbon storage, the accuracy of its estimates is primarily influenced by input parameters. Selecting appropriate carbon density data is crucial to ensuring the precision of model simulations. In this study, carbon density was corrected based on the research findings of previous scholars. However, due to factors such as climate change and human activities, carbon density values can also change. The correction of carbon density solely based on temperature and precipitation introduces a level of uncertainty (Liu et al., 2021). Therefore, it is necessary to further strengthen the timeliness of acquiring and validating carbon density data, conduct local calibration, perform field measurements of key indicators, accurately estimate regional carbon storage changes, optimize model operating structures, improve model validation accuracy, and ensure the scientific rationality of the data. Based on this foundation, explore internal land structure differences, consider the impact of vegetation temporal scales on carbon storage, select more scientifically reasonable natural and human-driven factors, enhance the predictive accuracy of multi-model simulations, aiming for better maintenance of regional ecosystem carbon balance.

Additionally, while the InVEST model effectively assessed the spatiotemporal changes in carbon storage in the Luan River Basin from 2000 to 2020 and projected scenarios for 2030 in response to land-use changes, it overlooks the impacts of biochemical processes on carbon sequestration capacity. This limitation introduces some errors in the spatial distribution pattern of carbon storage. In future research, a combined macro and micro approach could be employed to provide a data foundation and scientific basis for estimating carbon storage, thereby enhancing the precision of carbon storage assessments.

4 Conclusion

In this study, we assessed the historical changes in carbon storage in the typical ecologically fragile area, the Luan River Basin. Additionally, we predicted the spatial distribution characteristics of carbon sink potential in 2030 based on three potential land-use scenarios. The main conclusions are as follows:

1) From 2000 to 2020, the main LULC changes were characterized by an increase in forestland and construction land, accompanied by a decrease in cropland. By 2030, under the natural development scenario, the areas of forestland and construction land will continue to increase, while cropland and grassland will continue to decrease. Under the urban development and cropland protection scenario, the areas of forestland and grassland will experience a considerable decrease, while cropland and construction land will witness a notable increase. Under the ecological protection scenario, the areas of cropland and construction land will decrease, while forestland and grassland will see a marked increase.
2) From 2000 to 2020, carbon storage showed a trend of decrease followed by an increase. In 2030, under the ecological protection scenario, carbon storage will increase by 16.97%, while under the urban development and cropland protection scenario, carbon storage will decrease by 22.14%.
3) Changes in carbon storage are mainly related to the conversion between forestland, grassland, cropland, and construction land. The increase in carbon storage is mainly caused by the conversion of cropland, grassland, and construction land to forestland, while the conversion of forestland to grassland and cropland, and grassland to cropland and construction land, are the main reasons for the decrease in carbon storage.
4) The distribution of carbon sink potential exhibits spatial heterogeneity, with high-value areas located in the grasslands and mountainous forests of the northern part of the basin, while low-value areas are predominantly urban land and unused land in the southern part of the basin. Therefore, in the future, actions in the Luan River Basin should be based on an ecological protection scenario, optimizing land use structure, protecting forest land within the basin, limiting excessive expansion of urban land and degradation of cropland while ensuring the quantity of basic farmland, and promoting sustainable development in the Luan River Basin.

Data availability statement

The original contributions presented in the study are included in the article/Supplementary Material, further inquiries can be directed to the corresponding author.

Author contributions

YW: Data curation, Formal Analysis, Investigation, Methodology, Project administration, Resources, Software, Supervision, Validation, Visualization, Writing–original draft, Writing–review and editing. JL: Writing–review and editing, Conceptualization, Funding acquisition. LZ: Writing–review and editing, Data curation. ZX: Data curation, Writing–review and editing. YY: Writing–review and editing, Data curation.

Funding

The author(s) declare financial support was received for the research, authorship, and/or publication of this article. This work was supported by the Higher Education Science and Technology Research Project for Hebei Province (No. BJK2023105), and the Chengde National Sustainable Development Agenda Innovation Demonstration Zone Construction Science and Technology Special Programme (No. 202202F001).

Conflict of interest

The authors declare that the research was conducted in the absence of any commercial or financial relationships that could be construed as a potential conflict of interest.

Publisher's note

All claims expressed in this article are solely those of the authors and do not necessarily represent those of their affiliated organizations, or those of the publisher, the editors and the reviewers. Any product that may be evaluated in this article, or claim that may be made by its manufacturer, is not guaranteed or endorsed by the publisher.

Supplementary material

The Supplementary Material for this article can be found online at: https://www.frontiersin.org/articles/10.3389/fenvs.2024.1380868/full#supplementary-material

References

Alam, S. A., Starr, M., and Clark, B. J. F. (2013). Tree biomass and soil organic carbon densities across the Sudanese woodland savannah: a regional carbon sequestration study. *J. Arid Environ.* 89, 67–76. doi:10.1016/j.jaridenv.2012.10.002

Alhameedi, W. M. M., Chen, J., Faichia, C., Nath, B., Alshaibah, B., and Aizari, A. (2022). Geospatial analysis of land use/cover change and land surface temperature for landscape risk pattern change evaluation of baghdad city, Iraq, using CA-markov and ANN models. *Sustainability* 14, 8568. doi:10.3390/su14148568

Aneseyee, A. B., Soromessa, T., Elias, E., Noszczyk, T., Hernik, J., and Benti, N. E. (2022). Expressing carbon storage in economic terms: the case of the upper Omo Gibe Basin in Ethiopia. *Sci. Total Environ.* 808, 152166–166. doi:10.1016/j.scitotenv.2021.152166

Babbar, D., Areendran, G., and Sahama, M. (2021). Assessment and prediction of carbon sequestration using Markov chain and InVEST model in Sariska Tiger Reserve, India. *J. Clean. Prod.* 278, 0959–65296. doi:10.1016/j.jclepro.2020.123333

Bagstad, K. J., Semmens, D. J., Waage, S., and Winthrop, R. (2013). A comparative assessment of decision-support tools for ecosystem services quantification and valuation. *Ecosyst. Serv.* 5, 27–39. doi:10.1016/j.ecoser.2013.07.004

Boothandford, M. E., Abanades, J. C., Anthony, E. J., Blunt, M. J., Brandani, S., Macdowell, N., et al. (2014). Carbon capture and storage update. *Energy & Environ. Sci.* 7, 130–189. doi:10.1039/c3ee42350f

Brown, S. (2002). Measuring carbon in forests: current status and future challenges. *Environ. Pollut.* 116, 363–372. doi:10.1016/s0269-7491(01)00212-3

Cui, L. H., Tang, W. W., Zheng, S., and Singh, R. P. (2023). Ecological protection alone is not enough to conserve ecosystem carbon storage: evidence from Guangdong, China. *Land* 12, 111–11. doi:10.3390/land12010111

Cui, X. L., Wei, X. Q., Liu, W., Zhang, F., and Li, Z. H. (2019). Spatial and temporal analysis of carbon sources and sinks through land use/cover changes in the Beijing-Tianjin-Hebei urban agglomeration region. *Phys. Chem. Earth* 110, 61–70. doi:10.1016/j.pce.2018.10.001

Fang, J. Y., Chen, A. P., Peng, C. H., Zhao, S. Q., and Ci, L. (2001). Changes in forest biomass carbon storage in China between 1949 and 1998. *Science* 292, 2320–2322. doi:10.1126/science.1058629

Gao, L. A., Tao, F., Liu, R. R., Wang, Z. L., Leng, H. J., and Zhou, T. (2022). Multi-scenario simulation and ecological risk analysis of land use based on the PLUS model: a case study of Nanjing. *Sustain. Cities Soc.* 85, 104055. doi:10.1016/j.scs.2022.104055

Gu, M. L., Ye, C. S., Hu, M. S., Lyu, X., Li, X., Hu, H. P., et al. (2022). Multi-scenario simulation of land use change based on MCR-SD-FLUS model: a case study of Nanchang, China. *Trans. Gis* 26, 2932–2953. doi:10.1111/tgis.12986

Guo, W., Teng, Y. J., Yan, Y. G., Zhao, C. W., Zhang, W. Q., and Ji, X. L. (2022). Simulation of land use and carbon storage evolution in multi-scenario: a case study in beijing-tianjin-hebei urban agglomeration, China. *Sustainability* 14, 13436. doi:10.3390/su142013436

He, C. Y., Zhang, D., Huang, Q. X., and Zhao, Y. Y. (2016). Assessing the potential impacts of urban expansion on regional carbon storage by linking the LUSD-urban and InVEST models. *Environ. Model. Softw.* 75, 44–58. doi:10.1016/j.envsoft.2015.09.015

He, Y. T., Xia, C. Y., Shao, Z., and Zhao, J. (2022). The spatiotemporal evolution and prediction of carbon storage: a case study of urban agglomeration in China's beijing-tianjin-hebei region. *Land* 11, 858. doi:10.3390/land11060858

Hoque, M. Z., Cui, S., Xu, L., Islam, I., Tang, J., and Ding, S. (2019b). Assessing agricultural livelihood vulnerability to climate change in coastal Bangladesh. *Int. J. Environ. Res. Public Health* 16, 4552. doi:10.3390/ijerph16224552

Islam, S., Li, Y. C., Ma, M. G., Chen, A. X., and Ge, Z. X. (2021). Simulation and prediction of the spatial dynamics of land use changes modelling through CLUE-S in the southeastern region of Bangladesh. *J. Indian Soc. Remote Sens.* 49, 2755–2777. doi:10.1007/s12524-021-01402-w

Kiziridis, D. A., Mastrogianni, A., Pleniou, M., Tsiftsis, S., Xystrakis, F., and Tsiripidis, I. (2023). Simulating future land use and cover of a mediterranean mountainous area: the effect of socioeconomic demands and climatic changes. *Land* 12, 253. doi:10.3390/land12010253

Kulaixi, Z., Chen, Y. N., Li, Y. P., and Wang, C. (2023). Dynamic evolution and scenario simulation of ecosystem services under the impact of land-use change in an arid Inland River Basin in Xinjiang, China. *Remote Sens.* 15, 2476. doi:10.3390/rs15092476

Li, K. R., Wang, S. Q., and Cao, M. K. (2004). Vegetation and soil carbon storage in China. *Sci. China Ser. D-Earth Sci.* 47, 49–57. doi:10.1360/02yd0029

Li, L., Zayiti, A., and He, X. (2023). Evaluating the stand structure, carbon sequestration, oxygen release function, and carbon sink value of three artificial shrubs alongside the tarim desert highway. *Forests* 14, 2137. doi:10.3390/f14112137

Li, M. lin., Qin, Y. b., Zhang, T. B., Zhou, X. B., Yi, G. H., Bie, X. J., et al. (2023). Climate change and anthropogenic activity Co-driven vegetation coverage increase in the Three-North shelter forest region of China. *Remote Sens.* 15, 1509–1517. doi:10.3390/rs15061509

Li, Y. H., Yao, S., Jiang, H. Z., Wang, H. R., Ran, Q. C., Gao, X. Y., et al. (2022a). Spatial-temporal evolution and prediction of carbon storage: an integrated framework based on the MOP-PLUS-InVEST model and an applied case study in hangzhou, east China. *Land* 11, 2213–2222. doi:10.3390/land11122213

Li, Y. M., Yang, X., Wu, B. W., Zhao, J. Z., Jiang, W. X., Feng, X. J., et al. (2023). Spatio-temporal evolution and prediction of carbon storage in Kunming based on PLUS and InVEST models. *Peerj* 11, 152855–e15328. doi:10.7717/peerj.15285

Li, Y. X., Liu, Z. S., Li, S. J., and Li, X. (2022b). Multi-scenario simulation analysis of land use and carbon storage changes in changchun city based on FLUS and InVEST model. *Land* 11, 647. doi:10.3390/land11050647

Liang, X., Guan, Q. F., Clarke, K. C., Liu, S. S., Wang, B. Y., and Yao, Y. (2021). Understanding the drivers of sustainable land expansion using a patch-generating land use simulation (PLUS) model: a case study in Wuhan, China. *Comput. Environ. Urban Syst.* 85, 101569. doi:10.1016/j.compenvurbsys.2020.101569

Lin, X. B., MacLachlan, I., Ren, T., and Sun, F. Y. (2019). Quantifying economic effects of transportation investment considering spatiotemporal heterogeneity in China: a spatial panel data model perspective. *Ann. Regional Sci.* 63, 437–459. doi:10.1007/s00168-019-00937-8

Liu, C., Xu, L. R., Li, D. L., Huang, Y. R., Kang, J. M., Peng, B., et al. (2023). Spatiotemporal variations and determinants of supply–demand balance of ecosystem service in saihanba region, China. *Forests* 14, 1100–1120. doi:10.3390/f14061100

Liu, K., Zhang, C. Z., Zhang, H., Xu, H., and Xia, W. (2023). Spatiotemporal variation and dynamic simulation of ecosystem carbon storage in the loess plateau based on PLUS and InVEST models. *Land* 12, 1065. doi:10.3390/land12051065

Liu, X. Y., Wei, M., Li, Z. G., and Zeng, J. (2022). Multi-scenario simulation of urban growth boundaries with an ESP-FLUS model: a case study of the Min Delta region, China. *Ecol. Indic.* 135, 108538. doi:10.1016/j.ecolind.2022.108538

Liu, Y., Zhang, J., and Zhou, D. (2021). Temporal and spatial variation of carbon storage in the Shule River Basinbased on InVEST model. *Acta Ecol. Sin.* 41, 4052–4065. doi:10.5846/stxb201911152452

McGuire, A. D., Melillo, J. M., Joyce, L. A., Kicklighter, D. W., Grace, A. L., Moore, B., et al. (1992). INTERACTIONS BETWEEN CARBON AND NITROGEN DYNAMICS IN ESTIMATING NET PRIMARY PRODUCTIVITY FOR POTENTIAL VEGETATION IN NORTH AMERICA. *Glob. Biogeochem. Cycles* 6, 101–124. doi:10.1029/92gb00219

Meng, X. X., Li, J. H., Jin, M., Su, X. P., and Suo, G. B. (2023). Research on forest carbon sink potential in China. *Sustainability* 15, 3589. doi:10.3390/su15043589

Mu, Y., Zhang, C. S., Wang, X. Q., Zhang, J. W., and Zong, X. Y. (2017). Analysis on dynamic change of vegetation coverage based on NDVI: a case study of Beijing-Tianjin-Hebei. *LAND Reclam. Ecol. FRAGILE AREAS*, 179–183. doi:10.1201/9781315166582-35

Neilson, R. P. (1995). A MODEL FOR PREDICTING CONTINENTAL-SCALE VEGETATION DISTRIBUTION AND WATER-BALANCE. *Ecol. Appl.* 5, 362–385. doi:10.2307/1942028

Piao, S. L., He, Y., Wang, X. H., and Chen, F. H. (2022). Estimation of China's terrestrial ecosystem carbon sink: methods, progress and prospects. *Sci. China-Earth Sci.* 65, 641–651. doi:10.1007/s11430-021-9892-6

Posner, S., Verutes, G., Koh, I., Denu, D., and Ricketts, T. (2016). Global use of ecosystem service models. *Ecosyst. Serv.* 17, 131–141. doi:10.1016/j.ecoser.2015.12.003

Sarkodie, S. A., Owusu, P. A., and Leirvik, T. (2020). Global effect of urban sprawl, industrialization, trade and economic development on carbon dioxide emissions. *Environ. Res. Lett.* 15, 034049. doi:10.1088/1748-9326/ab7640

Sitch, S., Smith, B., Prentice, I. C., Arneth, A., Bondeau, A., Cramer, W., et al. (2003). Evaluation of ecosystem dynamics, plant geography and terrestrial carbon cycling in the LPJ dynamic global vegetation model. *Glob. Change Biol.* 9, 161–185. doi:10.1046/j.1365-2486.2003.00569.x

Sohl, T. L., and Claggett, P. R. (2013). Clarity versus complexity: land-use modeling as a practical tool for decision-makers. *J. Environ. Manag.* 129, 235–243. doi:10.1016/j.jenvman.2013.07.027

Tang, X. L., Zhao, X., Bai, Y. F., Tang, Z. Y., Wang, W. T., Zhao, Y. C., et al. (2018). Carbon pools in China's terrestrial ecosystems: new estimates based on an intensive field survey. *Proc. Natl. Acad. Sci. U. S. A.* 115, 4021–4026. doi:10.1073/pnas.1700291115

Vizcaino, B. Q., Williams, L. G., and Asbjornsen, H. (2020). Biodiversity and carbon storage are correlated along a land use intensity gradient in a tropical montane forest watershed, Mexico. *Basic Appl. Ecol.* 44, 24–34. doi:10.1016/j.baae.2019.12.004

Wang, H. W., Jin, H. J., Li, X. Y., Zhou, L., Qi, Y., Huang, C. L., et al. (2023a). Changes in carbon stock in the Xing'an permafrost regions in Northeast China from the late 1980s to 2020. *Giscience Remote Sens.* 60, 1–20. doi:10.1080/15481603.2023.2217578

Wang, J. F., Zhang, T. L., and Fu, B. J. (2016). A measure of spatial stratified heterogeneity. *Ecol. Indic.* 67, 250–256. doi:10.1016/j.ecolind.2016.02.052

Wang, K., Sun, P. L., Wang, X., Mo, J. X., Li, N., and Zhang, J. T. (2023). Impact of the Grain for green project on the well-being of farmer households: a case study of the mountainous areas of northern Hebei province, China. *Land* 12, 1257. doi:10.3390/land12061257

Wang, R. Y., Cai, H. A., Chen, L. K., and Li, T. H. (2023b). Spatiotemporal evolution and multi-scenario prediction of carbon storage in the GBA based on PLUS-InVEST models. *Sustainability* 15, 8421. doi:10.3390/su15108421

Xiang, S. J., Wang, Y., Deng, H., Yang, C. M., Wang, Z. F., and Gao, M. (2022). Response and multi-scenario prediction of carbon storage to land use/cover change in the main urban area of Chongqing, China. *Ecol. Indic.* 142, 109205–109213. doi:10.1016/j.ecolind.2022.109205

Xu, C. L., Zhang, Q. B., Yu, Q., Wang, J. P., Wang, F., Qiu, S., et al. (2023). Effects of land use/cover change on carbon storage between 2000 and 2040 in the Yellow River Basin, China. *Ecol. Indic.* 151, 110345. doi:10.1016/j.ecolind.2023.110345

Xu, K. P., Wang, J. N., Wang, J. J., Wang, X. H., Chi, Y. Y., and Zhang, X. (2020). Environmental function zoning for spatially differentiated environmental policies in China. *J. Environ. Manag.* 255, 109485. doi:10.1016/j.jenvman.2019.109485

Xu, L., He, N. P., and Yu, R. G. (2019). 2010s Chinese terrestrial ecosystem carbon density dataset. *China Sci. Data* 4, 90–96. doi:10.11922/sciencedb.603

Yang, B., Chen, X., Wang, Z. Q., Li, W., Zhang, C., and Yao, X. (2020). Analyzing land use structure efficiency with carbon emissions: a case study in the Middle Reaches of the Yangtze River, China. *J. Clean. Prod.* 274, 123076–126526. doi:10.1016/j.jclepro.2020.123076

Yu, X. H., Liang, Z. F., Fan, J. J., Zhang, J. L., Luo, Y. H., and Zhu, X. Y. (2021). Spatial decomposition of city-level CO2 emission changes in Beijing-Tianjin-Hebei. *J. Clean. Prod.* 296, 126613. doi:10.1016/j.jclepro.2021.126613

Zadbagher, E., Becek, K., and Berberoglu, S. (2018). Modeling land use/land cover change using remote sensing and geographic information systems: case study of the Seyhan Basin, Turkey. *Environ. Monit. Assess.* 190, 494. doi:10.1007/s10661-018-6877-y

Zeng, S. D., Xia, J., She, D. X., Du, H., and Zhang, L. P. (2012). Impacts of climate change on water resources in the Luan River basin in North China. *Water Int.* 37, 552–563. doi:10.1080/02508060.2012.709424

Zhang, B. H., and Zhang, J. P. (2009). "Spatial distribution of soil organic carbon density and storage in shandong province, China," in *International research conference of resources utilization and environmental effectiveness*, 117–121.

Zhang, F., Yushanjiang, A., and Jing, Y. (2019). Assessing and predicting changes of the ecosystem service values based on land use/cover change in Ebinur Lake Wetland National Nature Reserve, Xinjiang, China. *Sci. Total Environ.* 656, 1133–1144. doi:10.1016/j.scitotenv.2018.11.444

Zhang, Z. Y., Hormann, G., Huang, J. L., and Fohrer, N. (2023). A random forest-based CA-markov model to examine the dynamics of land use/cover change aided with remote sensing and GIS. *Remote Sens.* 15, 2128. doi:10.3390/rs15082128

Zhao, A. Z., Zhang, A. B., Liu, J. H., Feng, L. L., and Zhao, Y. L. (2019a). Assessing the effects of drought and "Grain for green" program on vegetation dynamics in China's loess plateau from 2000 to 2014. *Catena* 175, 446–455. doi:10.1016/j.catena.2019.01.013

Zhao, M. M., He, Z. B., Du, J., Chen, L. F., Lin, P. F., and Fang, S. (2019b). Assessing the effects of ecological engineering on carbon storage by linking the CA-Markov and InVEST models. *Ecol. Indic.* 98, 29–38. doi:10.1016/j.ecolind.2018.10.052

Zhu, E. Y., Deng, J. S., Zhou, M. M., Gan, M. Y., Jiang, R. W., Wang, K., et al. (2019). Carbon emissions induced by land-use and land-cover change from 1970 to 2010 in Zhejiang, China. *Sci. Total Environ.* 646, 930–939. doi:10.1016/j.scitotenv.2018.07.317

frontiers | Frontiers in Environmental Science

TYPE Original Research
PUBLISHED 09 August 2024
DOI 10.3389/fenvs.2024.1379046

OPEN ACCESS

EDITED BY
Chenxi Li,
Xi'an University of Architecture and Technology, China

REVIEWED BY
Licheng Liu,
University of Minnesota Twin Cities, United States
Etsushi Kato,
Institute of Applied Energy, Japan

*CORRESPONDENCE
Robin van der Ploeg,
r.vanderploeg@shell.com

RECEIVED 30 January 2024
ACCEPTED 28 June 2024
PUBLISHED 09 August 2024

CITATION
van der Ploeg R and Haigh M (2024), The importance of natural land carbon sinks in modelling future emissions pathways and assessing individual country progress towards net-zero emissions targets.
Front. Environ. Sci. 12:1379046.
doi: 10.3389/fenvs.2024.1379046

The importance of natural land carbon sinks in modelling future emissions pathways and assessing individual country progress towards net-zero emissions targets

Robin van der Ploeg[1]* and Martin Haigh[2]

[1]Shell Global Solutions International B.V., Amsterdam, Netherlands, [2]Shell International Limited, London, United Kingdom

Nature-based solutions (NBS), in the form of active ecosystem conservation, restoration and improved land management, represent a pathway to accelerate net-zero emissions (NZE) strategies and support biodiversity. Meaningful implementation and successful accounting depend on the ability to differentiate between anthropogenic and natural carbon fluxes on land. The United Nations Framework Convention on Climate Change (UNFCCC) land carbon accounting methods currently incorporate all CO_2 fluxes on managed land in country inventories without distinguishing between anthropogenic and natural components. Meanwhile, natural land carbon sinks are modelled by earth system models but are mostly reported at global level. Here we present a simple yet novel methodology to estimate the present and future progression of natural land sinks at the country and regional level. Forests dominate the uptake of CO_2 on land and as such, our analysis is based on allocating global projections of the natural land carbon flux to individual countries using a compilation of forest land areas for a historic and scenario range spanning 1960–2100. Specifically, we use MIT's carbon cycle model simulations that are set in the context of emissions pathways from the Shell Energy Security Scenarios (2023). Our natural land carbon flux estimates for individual countries and regions such as the European Union (EU) show generally good agreement with independent estimates from recent land-use harmonisation studies for 2000–2020. Hence, our approach may also provide a simple, first-order exploration of future natural land fluxes at country level—a potential that other studies do not yet offer. In turn, this enables better understanding of the anthropogenic and natural components contributing to country NZE targets under different scenarios. Nevertheless, our findings also suggest that models such as the Shell World Energy Model (WEM) would benefit from further improvements in the apportionment of land carbon sources and sinks to evaluate detailed actions to meet country targets. More importantly, uncertainties remain regarding the resilience of land ecosystems and their capacity to store increasing amounts of carbon under progressive global warming. Therefore, we recommend that the carbon cycle modelling and energy

modelling research communities continue to collaborate to develop a next generation of relevant data products to distinguish anthropogenic from natural impacts at local, regional and national levels.

KEYWORDS

carbon cycle, greenhouse gases, climate change, CO_2 fertilisation, natural land carbon sink, net-zero emissions, nature-based solutions

1 Introduction

Anthropogenic carbon emissions have increased atmospheric CO_2 concentrations from ~277 ppm in 1760 to ~412 ppm in 2020 (Friedlingstein et al., 2022). At present, the natural land and ocean carbon sinks respectively remove ~29% and ~26% of anthropogenic CO_2 emissions, leaving the remaining ~46% to accumulate in the atmosphere (Friedlingstein et al., 2022). As such, these natural carbon sinks mitigate the rate of greenhouse gas-driven climate change. Increasing CO_2 concentrations have been attributed as the leading driver of this land carbon sink through a mechanism known as CO_2 fertilisation (Ruehr et al., 2023), but other global change factors, including land-use change and recovery, nutrient cycles and climate change, all have confounding effects on land ecosystem carbon storage (Keenan and Williams, 2018; Denning, 2022). Given the increasing importance of land-based climate mitigation in country policies (Roe et al., 2019; Roe et al., 2021), particularly for low-emissions pathways (Hasegawa et al., 2021), it is crucial to develop an understanding of the Earth system dynamics involved, the spatiotemporal scales at which they operate, and the associated uncertainties and knowledge gaps (Denning, 2022; Mo et al., 2023). Furthermore, the resilience of land carbon sinks under progressive global warming is important in the context of tipping points in the Earth System (Duffy et al., 2021; Ritchie et al., 2021), especially in temperature overshoot scenarios.

Good model representation of natural land fluxes at the regional and country level is thus key for the evaluation of country progress towards net-zero emissions climate targets and the associated contributions from energy and land. Earth system models (ESMs) with a terrestrial biosphere component and dynamic global vegetation models (DGVMs) are generally best equipped to simulate the future responses of land ecosystem productivity to global change perturbations. However, these models currently do not resolve future changes in natural land fluxes very well at the regional level and models may even disagree on the sign of change for large parts of the world depending on the emissions pathways used to drive the simulations (Canadell et al., 2021). Furthermore, the land carbon accounting methods from the United Nations Framework Convention on Climate Change (UNFCCC), which countries use in their national greenhouse gas inventories (NGHGIs), were shown to be not fully consistent with estimates from integrated assessment models (IAMs) because of conceptual and methodological differences (Grassi et al., 2017; Grassi et al., 2018). Specifically, country reports count all CO_2 emissions and removals on managed land as anthropogenic, without distinguishing between direct effects (land use and land use change) and indirect effects (human-induced environmental change including, e.g., CO_2 fertilisation), whereas IAMs count indirect anthropogenic effects towards natural emissions and removals. Recent studies have tried to reconcile these model-based and report-based differences through a series of forest-based land adjustments, in which indirect fluxes due to environmental change on managed lands are reclassified from natural to anthropogenic (Grassi et al., 2021). This approach was able to effectively reduce the model-report gaps both at the global level (Grassi et al., 2021) and even at the country level for selected countries (Schwingshackl et al., 2022; Grassi et al., 2023), although the latter remains limited to recent history. Similarly, this adjustment approach also shows promise for improving the global alignment between NGHGIs and future mitigation pathways as assessed by the Intergovernmental Panel on Climate Change (IPCC) (Gidden et al., 2023).

Here, we aim to augment these efforts by presenting a simple but effective methodology that allows both past and future estimates of the global natural land sink from ESMs to be allocated to regional and country levels of interest, using averaged natural land fluxes and a compilation of country forest land areas. This methodology was developed in the context of the new Shell Energy Security Scenarios (Shell, 2023), in which the relevant representations of the carbon cycle and land use have been aligned as best as possible with both historical data from the Global Carbon Project (Friedlingstein et al., 2022) and future projections from MIT's earth systems model (Sokolov et al., 2018) based on the narratives prescribed by the Shell Scenarios pathways. Our forest-based approach allows for a direct comparison of all anthropogenic land fluxes (including both land-use emissions and nature-based solutions; NBS) and natural land fluxes on a like-for-like basis for all 234 countries included in the Shell Scenarios modelling workflow and can be deepened or adapted for other purposes.

2 Literature review

Summarised below are selected findings from recent land carbon literature that provide context for the analysis presented in this paper. This section may be of particular interest for a diverse, general readership.

2.1 The terrestrial carbon cycle

Carbon in terrestrial ecosystems is stored in multiple forms, most notably in vegetation above ground, in soils and in permafrost. Over the 2013–2023 period, global vegetation is estimated to contain about 450 Gt C, whereas permafrost contains 1,400 Gt C and soils contain up to 1700 Gt C (Friedlingstein et al., 2023). For comparison, the atmosphere presently holds 875 Gt C and estimated fossil reserves for gas, oil and coal combined are

905 Gt C (Friedlingstein et al., 2023). Photosynthesis and respiration are the two main processes that control the exchange of carbon between the atmosphere and the biosphere. Within the biosphere, a series of interactions between autotrophic and heterotrophic organisms results in further cycling of organic and inorganic carbon across various food levels and ecosystems. Although the carbon fluxes associated with photosynthesis and respiration are approximately in balance at the global scale [~130 Gt C/year; (Friedlingstein et al., 2023)], the amount of carbon stored in the biosphere grows and shrinks over a range of timescales, from daily and seasonal cycles to inter-annual variability over decades or longer. Some of this terrestrial carbon is sequestered on timescales of centuries to millennia, after which it can eventually be respired or transferred to the geological carbon cycle for burial and storage over millions of years. Given the relative sizes of the various terrestrial carbon reservoirs and differences in their permanence, even slight changes in the amount of carbon stored in soils could have an impact on global atmospheric CO_2 concentrations (Longbottom et al., 2022). At the same time, this implies that strategies aimed at enhancing land carbon storage should focus comprehensively on both vegetation and soils to successfully combat climate change.

Historically, the land carbon reservoir has been considered distinct from the ocean carbon reservoir, with rivers acting as a pathway between the two. However, it has become increasingly clear that there is no clear divide between these reservoirs and that in reality they are connected across the land-to-ocean aquatic continuum [LOAC; (Regnier et al., 2022)]. In this updated continuum view, it becomes apparent that there are two additional short-range loops that carry carbon from land ecosystems to inland waters and from tidal wetlands to the open ocean. The analysis by Regnier et al. (2022) shows that while the majority of the carbon that is fixed by "terra firme" ecosystems becomes part of vegetation and soil carbon stocks, the rest is leached into the LOAC loops and is either outgassed back to the atmosphere or subsequently stored in sediments and the ocean. In future studies of carbon budgets, such evolving insights could result in a different apportionment between land and ocean sinks. However, because the sedimentary and oceanic reservoirs are more stable carbon repositories than biomass and soil carbon, these findings might be beneficial for carbon sequestration in the longer term.

There are four main groups of processes that control the strength of the present-day land carbon sink (Keenan and Williams, 2018; and references therein): 1) direct climate effects through changes in precipitation and temperature (e.g., Jung et al., 2017); 2) atmospheric composition effects such as CO_2 fertilisation and nutrient deposition (e.g., Keenan et al., 2023); 3) land-use change effects including deforestation, reforestation and agricultural management practices (e.g., Yue et al., 2020); and 4) natural disturbance effects from storms, wildfires and pests (e.g., Walker et al., 2019). If any of these processes change over time, land carbon fluxes can change significantly. Notably, increased carbon sequestration on land is generally thought to be beneficial for land-based ecosystems because it promotes soil health (Keenan and Williams, 2018). This contrasts with the impacts of the increasing ocean carbon sink, which are unequivocally negative for marine ecosystems, leading to reduced metabolic rates in marine organisms and widespread coral bleaching caused by ocean acidification (Hughes et al., 2018).

2.2 Quantification of carbon fluxes

The terrestrial carbon sink would be most accurately quantified by considering the net ecosystem carbon balance (NECB) at the scale of interest (Chapin et al., 2006). This balance encompasses net ecosystem production (NEP), defined as gross primary productivity (GPP) minus ecosystem respiration (RE), discounted for additional carbon losses through fire, land-use change emissions and transfer to aquatic ecosystems. However, NECB is difficult to quantify and the conceptual separation between direct and indirect anthropogenic influences on natural ecosystems poses additional problems. As a result, most studies focus on a metric known as the residual land carbon sink, which is estimated by mass balance as the residual of all anthropogenic emissions minus the oceanic sink and atmospheric CO_2 growth. Consequently, the uncertainties associated with the residual land carbon sink are relatively large. This methodology is also employed by the Global Carbon Project and subsequently compared to mean estimates from an ensemble of process-based DGVMs (Friedlingstein et al., 2023).

Data is obtained from a large and increasingly advanced range of technologies, including satellite and near-surface remote sensing methods, distributed and coordinated measurement networks, repeated national inventories, atmospheric observations, inversion capabilities and new modelling strategies (Keenan and Williams, 2018). The eddy-covariance technique is an atmospheric measurement technique that is used for direct, high-frequency measurements of the exchange of carbon, water and energy between ecosystems and the atmosphere, and is particularly important because it has the potential to reduce gaps between field observations, remote sensing and models (Upton et al., 2024).

2.3 Drivers of land carbon change

2.3.1 CO_2 fertilisation effect

Elevated atmospheric CO_2 concentrations are shown to result in increased photosynthesis in many environments, with the potential to increase the total amount of carbon stored in organic matter at the ecosystem scale on decadal to centennial timescales (Canadell et al., 2021). This has led scientists to propose the "CO_2 fertilisation hypothesis," in which photosynthesis responds to increasing CO_2 and acts as a negative feedback mechanism to atmospheric CO_2 growth (see Walker et al., 2021 and references therein). For this hypothesis to be valid, net ecosystem production must be positive on global scales, i.e., gross primary production must exceed the sum of respiration and other losses.

The size of the CO_2-driven increase in land carbon storage and the associated predictive understanding of this process has long remained elusive due to a range of study methods and contrasting outcomes (Walker et al., 2021). Part of the problem is that the size of this global photosynthesis flux cannot be observed directly—instead, it must be estimated by terrestrial biosphere models, predicted from indirect satellite measurements or inferred from proxies (e.g., ice core records of carbonyl

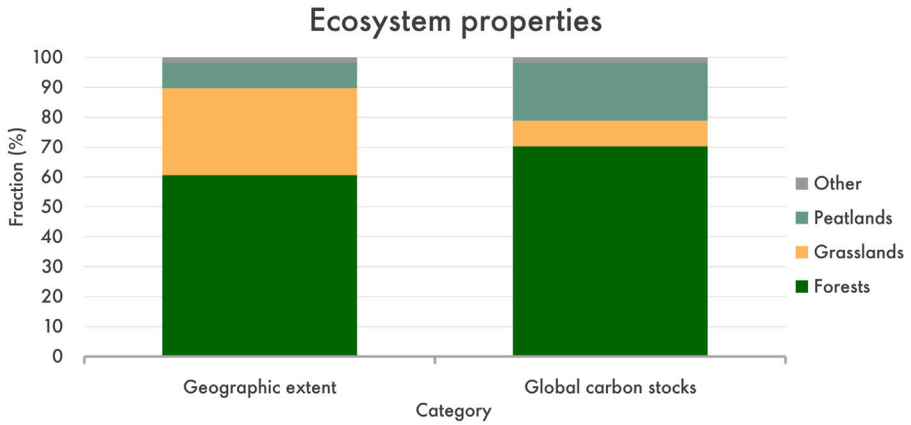

FIGURE 1
Geographic extent and global carbon stocks of major terrestrial ecosystems. Adapted from data reported in Goldstein et al. (2020).

sulphide, deuterium isotopomers in plants and seasonal changes in atmospheric CO_2). A recent study (Keenan et al., 2023) was able to partially resolve the wide range of estimates of historic global changes in photosynthesis by extracting an emerging constraint from an ensemble of models.

2.3.2 Temperature and tipping points

Increasing temperature has a negative effect on the strength of the land carbon sink (Penuelas et al., 2017). Over the past 20–30 years, the sensitivity of the land carbon sink to CO_2 has been much stronger than to temperature (Fernández-Martínez et al., 2018), leading to an overall positive effect—but this could deteriorate in the future under sustained warming. In particular, tipping points in the Earth System involving the biosphere may lead to a reduction or even a reversal of the land carbon sink in critical regions such as the Amazon basin (Gatti et al., 2021). A new synthesis suggests that global warming beyond 1.5 °C could already trigger multiple climate tipping points, although the thresholds of biosphere-related tipping points varies substantially between regions depending on the ecosystems and processes involved (Armstrong McKay et al., 2022).

Furthermore, a recent study (Duffy et al., 2021) constructed temperature response curves for global land carbon uptake using a large-scale carbon flux monitoring network and found that the temperature limit for global photosynthesis in the warmest quarter of the year has already been reached in the past decade. This suggests that further warming may lead to a sharp decline in photosynthesis and an increase in respiration on global scales, for instance through forest dieback. Forest dieback is an example of a fast-onset tipping element compared to, e.g., ice sheet melt, which means that forests are relatively resistant to slow and sustained warming but much more vulnerable to rapid and extreme warming, even if both scenarios would eventually converge at the same temperature. This highlights the importance of timescales and the distinction between fast-onset and slow-onset tipping points in future pathways (Ritchie et al., 2021), particularly when overshoot scenarios are considered.

3 Materials and methods

3.1 Model context

The global carbon cycle and climate evaluations of the Shell Energy Security Scenarios (Shell, 2023) performed by the MIT Joint Program on the Science and Policy of Global Change (Sokolov et al., 2023) are used as the starting point of this analysis. The full narratives for the *Archipelagos* and *Sky 2050* scenarios including all aspects of global change are described in detail in the associated publication (Shell, 2023). In short, the *Sky 2050* scenario explores economic development and transformation of the energy system in line with a global CO_2 NZE target by 2050, whereas the *Archipelagos* scenario is less far-reaching because of short-term geopolitical tensions and security imperatives. Climate model simulations of these scenarios are run on the MIT Integrated Global System Model (IGSM), of which the MIT Earth System Model (MESM) is part (Sokolov et al., 2018). This modelling framework was also used to assess the carbon cycle and climate implications of the Shell Energy Transformation Scenarios *Waves, Islands* and *Sky* 1.5 (Paltsev et al., 2021). In addition, the MIT IGSM has been used in a dedicated study to explore land-use competition under 1.5 °C climate stabilisation for the *Sky 2050* scenario (Gurgel et al., 2024).

Earth system parameters included in the climate evaluation of these Shell scenarios are modelled from 1850 to 2100 and are reported at the global level; the relevant carbon cycle parameters include atmospheric CO_2 concentrations (in ppm), anthropogenic carbon emissions from fossil fuels, industrial processes and land-use, respectively, and carbon uptake by the land and ocean through natural sinks, respectively (all in Gt C yr^{-1}). Although the land and ocean components of the MESM simulate processes at a resolution of several degrees latitude and longitude (Sokolov et al., 2018), the current model design does not allow for a breakdown and reporting of these carbon cycle fluxes at the country level. Rather than performing additional simulations with other ESMs, we set out to design a simple but effective method to

TABLE 1 Data and logic applied for compilation and extrapolation of individual country total forest land areas.

Scenario	Category	Year	Description	Source	Model assumption
History	Total forest land	1960–1989	Estimated	This study	Relative changes prescribed by global trend and scaled to 1990 values
History	Total forest land	1990–2020	Reported annually	FAO	—
Archipelagos and Sky 2050	Total forest land	2021–2100	Modelled	Gurgel et al. (2024)	Relative changes prescribed by regional trends and scaled to 2020 values, areas can decline and regrow
History	Primary forest land	1960–1989	Estimated	This study	Relative changes prescribed by global trend and scaled to 1990 values
History	Primary forest land	1990–2017	Reported annually	FAO	—
Archipelagos and Sky 2050	Primary forest land	2018–2100	Extrapolated	This study	Relative changes prescribed by regional trends and scaled to 2020 values, areas can only decline or remain stable but not regrow

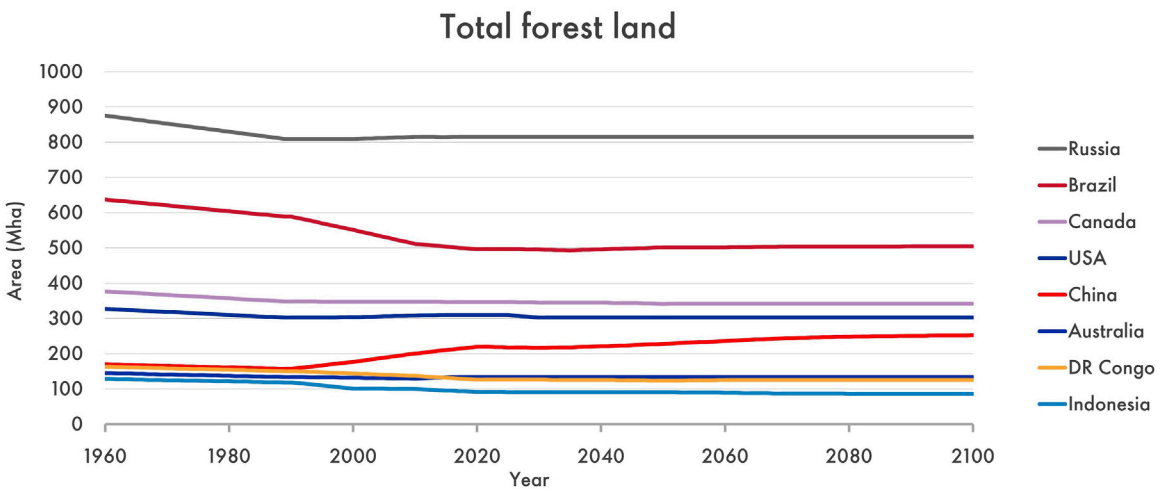

FIGURE 2
Model timeseries of total forest land cover for the top eight countries, representing ~63% of the global total in 2020.

spatially allocate the global natural land sink as modelled by the MESM for use in the Shell World Energy Model (WEM) framework. Hence, the first step in our analysis is identifying the relevant ecosystem processes and data types that would help us to derive averaged natural land fluxes and spatially allocate them in a meaningful way.

3.2 Forests as a proxy for natural land sink allocation

Globally, terrestrial biomass (defined as above-ground and below-ground, including shallow soils) occurs primarily in forest, grassland and peatland ecosystems, with a comparatively small fraction residing in mangroves, seagrasses and marshes. Forests have a typical carbon density of approximately 200–250 t C ha^{-1}, which is intermediate between grasslands (50–100 t C ha^{-1}) and peatlands (500 t C ha^{-1}) (Goldstein et al., 2020). Notably, forests represent ~61% of all land ecosystems with terrestrial biomass by area and ~70% by global carbon stocks (Goldstein et al., 2020) (Figure 1). Grasslands have the second-largest areal extent of land ecosystems (~29%) but have small global carbon stocks by comparison (~8%), whereas peatlands represent only a small fraction (~9%) of land ecosystems by area but have substantial global carbon stocks (~20%) (Goldstein et al., 2020). Carbon cycling across all these ecosystems has been extensively studied, but peatland areal extent has not been mapped to the same extent as forests and grasslands owing to inherent difficulties in observation (Crezee et al., 2022). Modelling studies with DGVMs estimate that forests contributed as much as 81% to the global natural land sink in recent history (Friedlingstein et al., 2022; Schwingshackl et al., 2022). Moreover, the IPCC writes in AR6 WG1 Chapter 5 that, although uncertain, future land carbon sinks are primarily expected to occur in regions with present-day forests (Canadell et al., 2021). Taken together, these lines of evidence would indeed suggest that forest ecosystems are a solid first-order candidate for exploratory natural land sink allocation across the world, but we also explore the effects that an alternative allocation based on peatlands would have on our analysis.

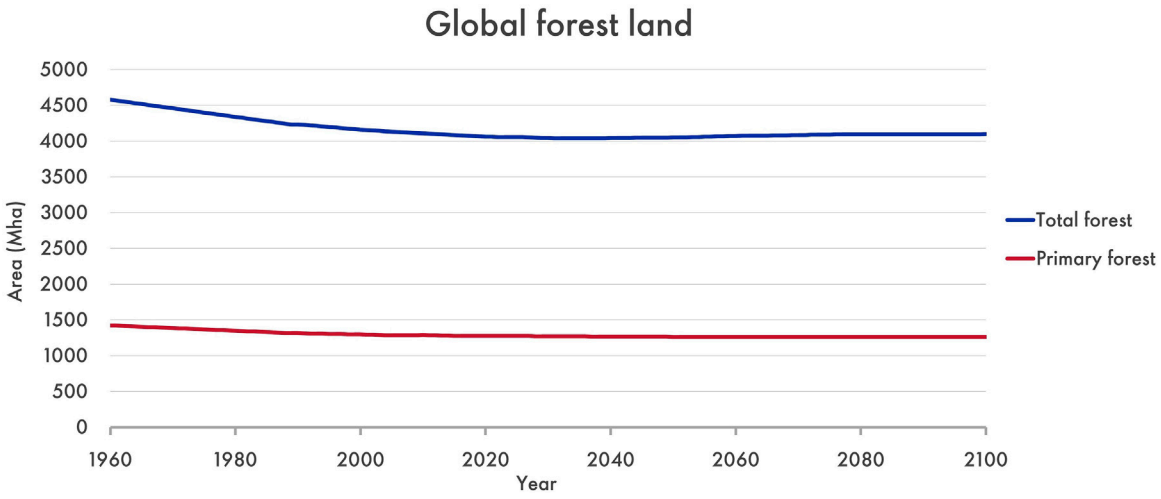

FIGURE 3
Model timeseries of global total forest (blue) and primary forest (red) land cover for the full historic and scenario range of 1960–2100. The timeseries used for Sky 2050 and Archipelagos are identical.

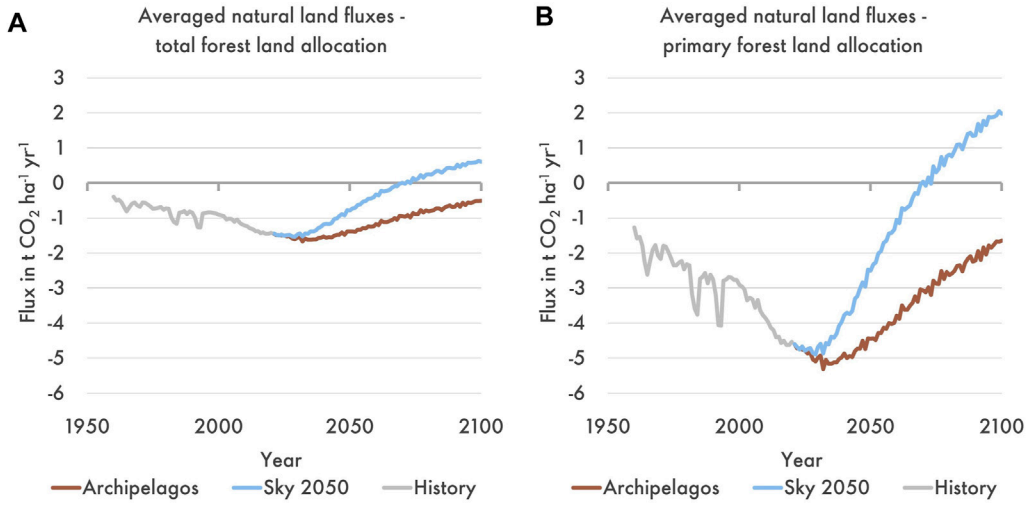

FIGURE 4
Averaged natural land fluxes (in t CO_2 ha^{-1} yr^{-1}) for Archipelagos and Sky 2050 using total forest land allocation **(A)** and primary forest land allocation **(B)**. Flux is relative to the atmosphere, so that a negative sign represents a net sink and a positive sign represents a net source.

3.3 Forest land area data compilation

As a first step, we compiled a forest land cover dataset as a proxy for natural land sink allocation. For recent historical years (1990–2020), we use forest land data sourced from the Food and Agriculture Organisation of the United Nations (FAO) and Global Forest Watch. The FAO dataset is valuable because it has comprehensive coverage of forest land areas and other forest resource parameters for virtually all countries and regions worldwide, assessed in a consistent and transparent reporting process. However, the FAO dataset is updated every 5 years only, its temporal coverage is limited to the 1990–2020 period and a few small countries and regions do not have data entries. By contrast, the Global Forest Watch dataset offers real-time high-resolution forest cover data since the year 2000, based in part on Landsat satellite observations at 30-metre resolution (Hansen et al., 2013). An alternative data resource that could be explored is the LUH2 dataset (Hurtt et al., 2020), which presents harmonised land-use data for the 850–2100 period at a resolution of 0.25° × 0.25° for use in climate model simulations but requires detailed expertise and processing to unlock beyond the global aggregate values. Considering that our study is aimed primarily at understanding country-level changes, we consider the FAO database to be the most pragmatic point of departure. According to the FAO database, global total forest land cover in 2020 was approximately 4,060 Mha of which primary forest cover was approximately 1,280 Mha, respectively equivalent to 38% and 12% of all habitable land (10,600 Mha). We prefer total forest

TABLE 2 Overview of carbon flux estimates for global mature forests per ecosystem type adapted from data reported in Anderson-Teixeira et al. (2021) and comparison to the averaged natural land sinks presented here.

Forest category	Forest ecosystem type	Year	Flux category	Flux in t CO_2 ha^{-1} yr^{-1}	Source
Mature forest	Tropical broadleaf	Recent	Net Ecosystem Production (NEP)	5.42 ± 9.27	Anderson-Texeira et al. (2021)
Mature forest	Temperate broadleaf	Recent	Net Ecosystem Production (NEP)	11.32 ± 6.96	Anderson-Texeira et al. (2021)
Mature forest	Temperate conifer	Recent	Net Ecosystem Production (NEP)	2.53 ± 7.29	Anderson-Texeira et al. (2021)
Mature forest	Boreal conifer	Recent	Net Ecosystem Production (NEP)	3.70 ± 3.26	Anderson-Texeira et al. (2021)
Mature forest	Global mean (area-weighted)	Recent	Net Ecosystem Production (NEP)	4.95 ± 6.89	This study, derived from Anderson-Texeira et al. (2021) using forest areas per ecosystem type from Xu et al. (2018), Xu et al. (2021)
Total forest	Global mean	2020	Averaged natural land flux—total forest land allocation	1.43	This study
Primary forest	Global mean	2020	Averaged natural land flux—primary forest land allocation	4.53	This study

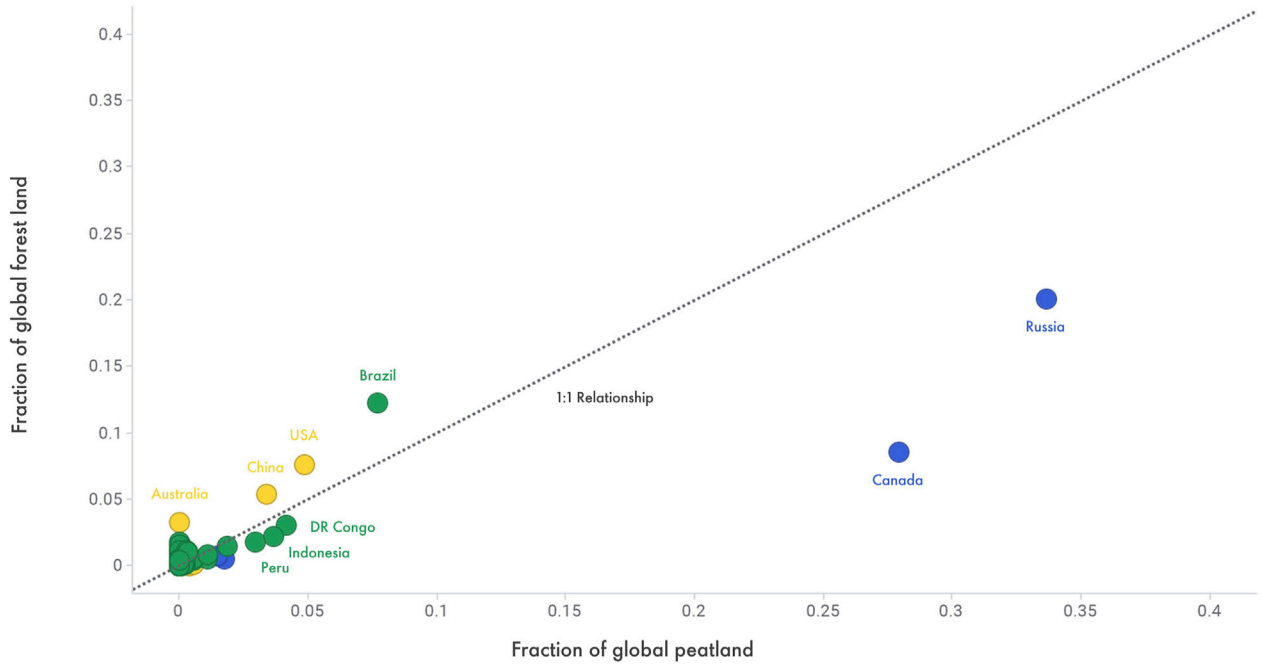

FIGURE 5
Comparison of country fractions of global peatland versus country fractions of global total forest land.

land cover as the method to allocate the natural land sink, but we also discuss the potential implications of using only primary forest land cover.

Primary forests generally have a higher ecosystem integrity than non-primary forests, and have a larger carbon carrying capacity for a given forest ecosystem type (Keith et al., 2024). In this context, depending on the collective land-use histories and the potential differences therein between countries and regions, it may be better to view primary forests as forests that display a high level of maturity with many old-growth characteristics, rather than forests that have never been impacted by human disturbance (Keith et al., 2024). Although primary forests clearly account for a

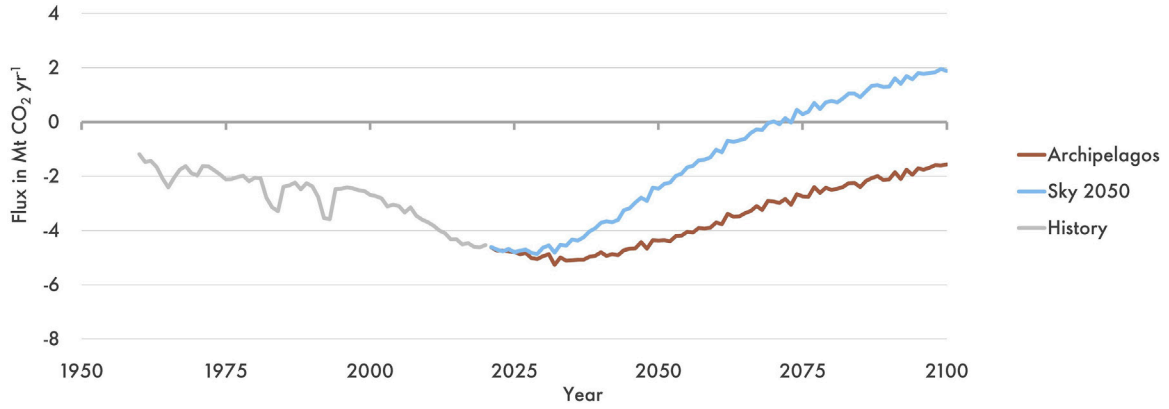

FIGURE 6
Modelled natural land fluxes (in Mt CO_2 yr^{-1}) for the United Kingdom in Archipelagos and Sky 2050 using total forest land allocation.

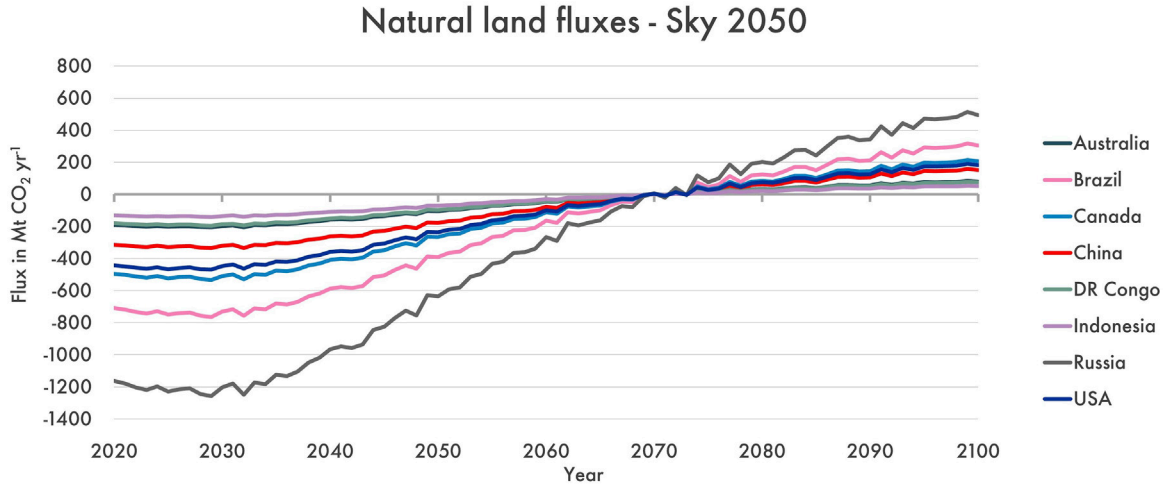

FIGURE 7
Modelled natural land fluxes (in Mt CO_2 yr^{-1}) for the top eight countries in Sky 2050 using total forest land allocation.

much smaller land fraction than total forest land, a natural land sink allocation method based on primary forests would minimise the chance of including managed forest lands in the allocation, because carbon fluxes on managed lands should, in principle, be reported as gross sources and sinks in anthropogenic land-use emissions instead of being counted towards the natural sinks (Grassi et al., 2018; Grassi et al., 2021). Using only primary forests for allocation would further allow us more clearly to set the natural sink apart from NBS potentials at the country level, as primary forests can be protected from deforestation through an NBS avoidance pathway but they cannot be targeted for enhanced carbon uptake through an NBS sequestration pathway. Ultimately, the quality of such an analysis depends on how gross sources and sinks are accounted for, either on the anthropogenic side or on the natural side, and how consistent this approach is between countries (Keith et al., 2021).

3.3.1 Country forest land areas for 1990–2020

In the FAO annual forest land cover database, total forest land areas are available from 1990 to 2020 and primary forest land areas are available from 1990 to 2017. This database was accessed via https://www.fao.org/faostat/en/#data/ and data were last downloaded on 27 September 2022 using the following filters: Countries = ALL; Elements = Area; Items = Primary Forest, Forest Land; Years = 1961–2020. Total forest land data could be successfully extracted from the FAO database for 230 out of 234 countries and regions included in the Shell energy modelling workflow using their corresponding ISO3 codes. Data for the remaining 4 countries and regions were added manually from Global Forest Watch (Hong Kong, Macau and Kosovo) or from the literature (Taiwan) (Tsai, 2020). Primary forest land data had additional data gaps for the following countries and regions: Curaçao, Sint Maarten, Monaco and the Vatican. All countries and regions were assigned a dominant ecosystem

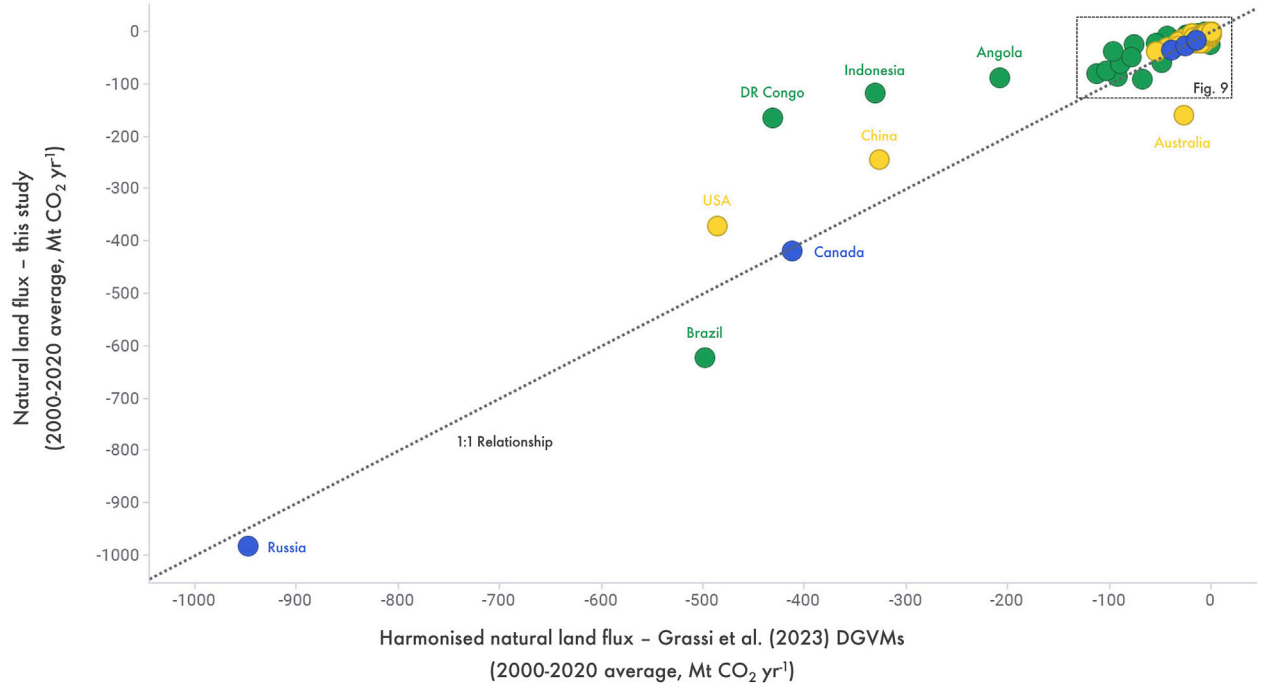

FIGURE 8
Comparison of natural land fluxes for individual countries as modelled in the Shell scenarios and as reported in the land-use flux harmonisation study of Grassi et al. (2023), based on averages for the 2000–2020 period. All units are in Mt CO_2 yr^{-1}. Colours represent the dominant ecosystem classification for each country (green = tropical, yellow = temperate, blue = boreal). The black line represents a 1:1 relationship, which would represent a perfect calibration. Data points in the dashed rectangle are shown in Figure 9 at higher resolution.

classification (boreal, temperate or tropical) based on their prevailing climate regimes. Next, reported forest land cover data were extrapolated outside of the reported FAO range (1990–2020) to cover the full historical and scenario range from 1960 to 2100. A summary of our methods and assumptions is given in Table 1 and explained in detail in the subsequent sections.

3.3.2 Country forest land areas for 2020–2100

For the years 2020–2100, we use forest land areas that were modelled with the MIT IGSM specifically for the *Sky 2050* scenario (Gurgel et al., 2024) and are therefore consistent with the climate model simulations of Sokolov et al. (2023). The estimated evolution of forest land areas in *Sky 2050* (Gurgel et al., 2024) was obtained for the 18 model regions of the global economy included in the MIT IGSM (Chen et al., 2016). All 234 countries and regions included in the Shell WEM were mapped to their corresponding MIT IGSM model regions, after which future changes in forest land areas were prescribed for all individual countries based on the relative changes occurring in their respective model regions. By design of the MIT IGSM, large countries that are modelled individually (e.g., Brazil and India) have unique timeseries of forest land areas, whereas countries that are modelled as part of an aggregate model region (e.g., Europe or Africa) have shared timeseries of forest land areas. Because of small offsets in absolute values of land areas between the FAO data and the data used by Gurgel et al. (2024), all future changes for 2020–2100 were normalised to the year 2020 (the last historical year with reported FAO data) as a model baseline. We apply this approach to both total forest areas and primary forest areas, with the distinction that total forest areas are allowed to regrow over time according to the outcomes of Gurgel et al. (2024) for each region, whereas primary forest areas are conservatively only allowed to decline or remain stable but not regrow.

Given the scope of the study by Gurgel et al. (2024), the future evolution of forest land areas was only modelled for *Sky 2050* and not for *Archipelagos*. Hence, for simplicity we set the country-level forest land area datasets of *Archipelagos* to be identical to those of *Sky 2050*. We consider this approach a reasonable compromise for the purpose of natural land sink allocation because both scenarios invoke minimal global reductions in future forest land cover, despite their different land-use narratives. Moreover, using a shared country forest land area dataset for both scenarios allows for a better comparison of the first-order differences in carbon cycle impacts between the scenarios that were collectively modelled in the MESM. However, additional country-level complexity could be added in future revisions of our forest land area data compilation, for instance based on the presence or absence of NBS avoidance pathways for forest protection and differences in the phasing of deforestation, as well as NBS sequestration pathways for reforestation—all depending on the scenarios used. Examples of compiled total forest land areas for the eight largest countries are shown in Figure 2.

3.3.3 Country forest land areas for 1960–1990

For the years 1960–1990, forest land areas for individual countries and regions are not accessible at the same level of quality as for the more recent historical period of 1990–2020. Consequently, for simplicity, we prescribed the forest land areas in all countries and regions to follow the same trends for 1960–1990 as the global forest land area timeseries that

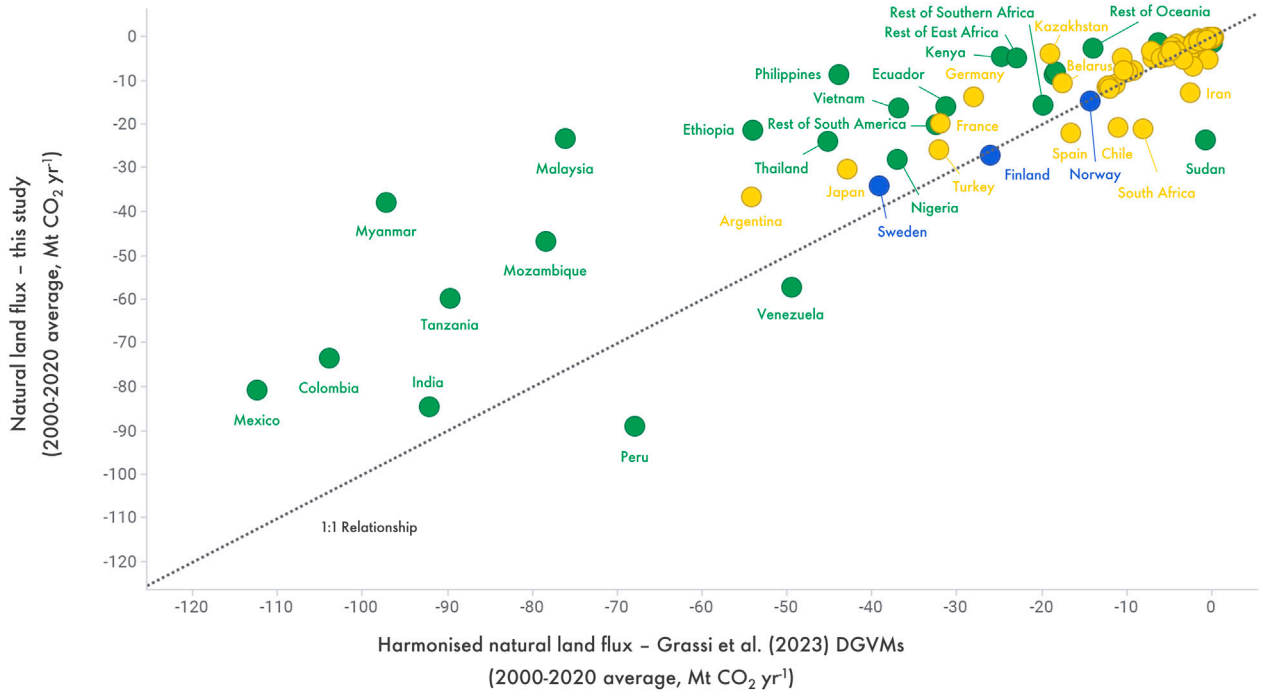

FIGURE 9
Comparison of natural land fluxes for individual countries as modelled in the Shell scenarios and as reported in the land-use flux harmonisation study of Grassi et al. (2023), based on averages for the 2000–2020 period. All units are in Mt CO_2 yr^{-1}. Colours represent the dominant ecosystem classification (green = tropical, yellow = temperate, blue = boreal). The black line represents a 1:1 relationship, which would represent a perfect calibration. Data are identical to Figure 8, but axes are adjusted for visual clarity.

is available from Our World in Data. The history of primary forest cover is less well constrained than for total forest cover, but at the global level the fraction of primary forest relative to total forest appears to be stable at ~0.31 across all years for which the FAO report overlapping data. This fraction also appears to be broadly consistent with the harmonised forest areas presented in the LUH2 dataset of Hurtt et al. (2020) for the 1960–1990 period. Hence, we used this fraction of ~0.31 to derive global primary forest land areas from global total forest land areas for 1960–1990, assuming this fraction has stayed constant through time. The complete timeseries for global primary and total forest land areas for 1960-2100 are shown in Figure 3.

3.4 Averaged natural land fluxes for 1960–2100

Forest land areas from all individual countries and regions were summed in order to obtain an internally consistent timeseries of global forest land areas for the full historical and scenario range of 1960–2100. Next, MIT's model timeseries for global natural land fluxes in *Archipelagos* and *Sky 2050* were divided by the respective timeseries of global forest land areas to obtain averaged natural land fluxes, first for the baseline year 2020 and subsequently for the two scenarios from 1960 to 2100 (Figure 4). For the year 2020, using a global natural land sink of ~5,790 Mt CO_2 (Sokolov et al., 2023), we calculated an averaged natural land flux of −1.4 t CO_2 ha^{-1} yr^{-1} based on total forest land and −4.5 t CO_2 ha^{-1} yr^{-1} based on primary forest land. Because the same global sink value is distributed over land areas of different sizes depending on the allocation method, the averaged fluxes based on total forest land are approximately one-third of the averaged fluxes based on primary forest land. Interestingly, we note that the baseline values of the averaged fluxes using primary forest allocation match well with carbon flux estimates for mature forests on the ecosystem level (Anderson-Teixeira et al., 2021; Table 2). However, because total forest land is representative of a much larger land surface area and data is available for a substantially higher number of countries, we favour that allocation method. It also aligns better with estimates in mainly developed countries with little to no primary forest remaining but demonstrating net natural land carbon uptake today, such as in the European Union (EU). For most countries that have both primary forest and total forest data, there is also a fairly good correlation between the two, suggesting that the allocation method does not impact the overall land sink estimates at the country level too much. Lastly, we combine the calculated, averaged natural land fluxes with forest land areas per country to generate country-specific timeseries of natural land sinks for all countries in the WEM for *Archipelagos* and *Sky 2050*.

3.5 Method sensitivities and limitations

We performed a sensitivity analysis to see if distributing the natural land sink based on peatlands would result in a different

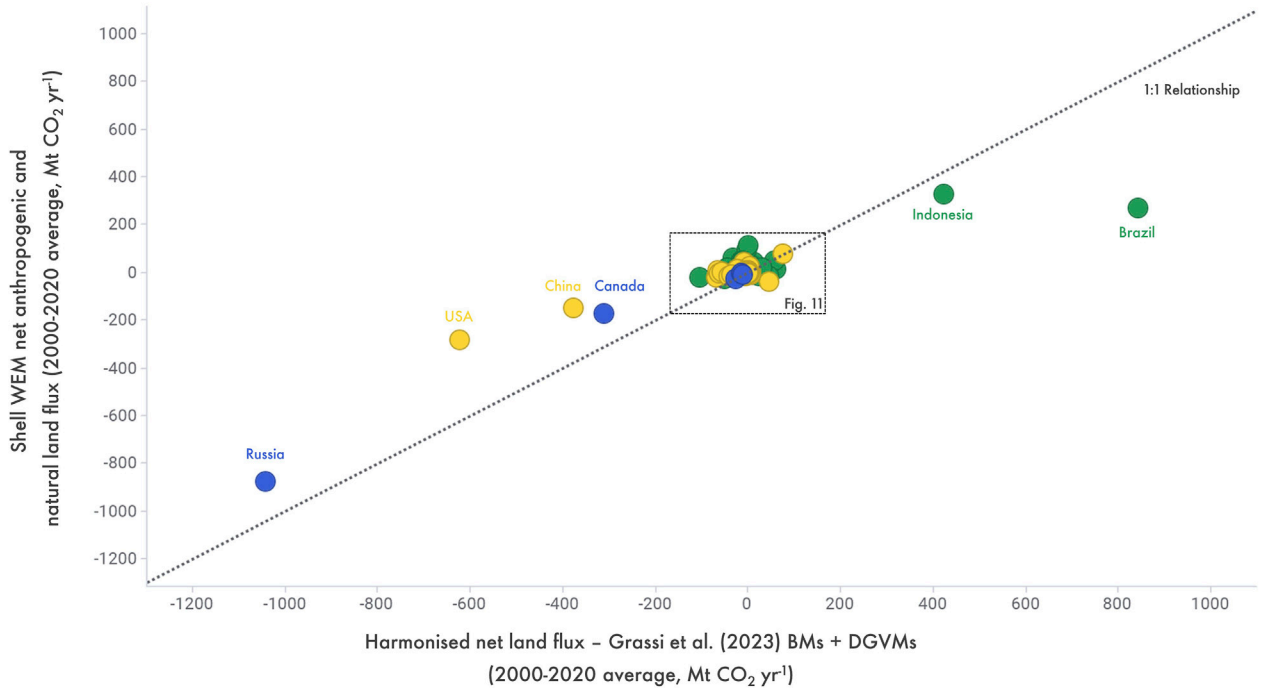

FIGURE 10
Comparison of net land carbon fluxes for individual countries as modelled in the Shell scenarios and as reported in the land-use flux harmonisation study of Grassi et al. (2023), based on averages for the 2000–2020 period. All units are in Mt CO_2 yr^{-1}. Colours represent the dominant ecosystem classification for each country (green = tropical, yellow = temperate, blue = boreal). The black line represents a 1:1 relationship, which would represent a perfect calibration. Data points in the dashed rectangle are shown in Figure 11 at higher resolution.

outcome compared to using forest land. Peatland areas were compiled for as many countries as possible from the literature (Page et al., 2011; Gumbricht et al., 2017; Xu et al., 2018; Crezee et al., 2022), but peatland cover data is significantly sparser than forest cover data. We find that peatland allocation would produce relatively similar results for most countries, as countries with a higher share of forest land typically also have a higher share of peatlands (Figure 5). The two main exceptions to this relationship are Canada and Russia, which harbour a disproportionately large fraction of global peatlands. However, because of their large country and forest land areas, these countries would receive a sizeable share of the natural land sinks in any case. Although peatland extent in tropical countries may not be fully mapped, it is encouraging for the validation of the method that countries such as the Democratic Republic of the Congo and Indonesia plot relatively close to the 1:1 relationship.

We note that our methods are inherently simplified, because we assume that a single flux value can be used to represent carbon sinks in boreal, temperate and tropical forests. However, at first order, this appears to be consistent with a global forest ecosystem review that did not find significant differences in net ecosystem production in mature forests between boreal, temperate and tropical biomes (Anderson-Teixeira et al., 2021; Table 2). Secondly, our method implies that all countries with total forest cover will have a net natural land flux of the same sign and same direction of change as the modelled global natural land flux for any given year. By extension, this also means that countries without present-day forest cover will have a natural land sink equal to 0 for all model years. (Note, however, that if the country undertakes NBS, then the CO_2 impact will be accounted for in the anthropogenic land-use timeseries of the Shell WEM). Although there is growing evidence that the direction of change in natural land sinks will vary between regions (Canadell et al., 2021; Fernández-Martinez et al., 2023), for instance sinks in the tropics are predicted to diminish whereas sinks in the high-latitudes are predicted to grow—here we maintain the assumption of a uniform evolution of the natural land sink so as to stay consistent with the global aggregate values as modelled by MIT (Sokolov et al., 2023). Consequently, our approach may lead to an overestimation of future natural land sinks in tropical countries and an underestimation of future natural land sinks in boreal countries. Going forward, our analysis could be expanded to better represent such regional differences and their driving mechanisms in a more advanced model context. In any case, we see our dataset as a contribution to an increasingly important research area for both the carbon cycle modelling and energy system modelling research communities and thus we recommend that these communities continue to collaborate to further advance similar data products.

4 Results and discussion

4.1 Scenario outcomes for natural land fluxes

The main trends we observe in our averaged natural land sinks for *Archipelagos* and *Sky 2050* (Figure 4) are inherited directly from the

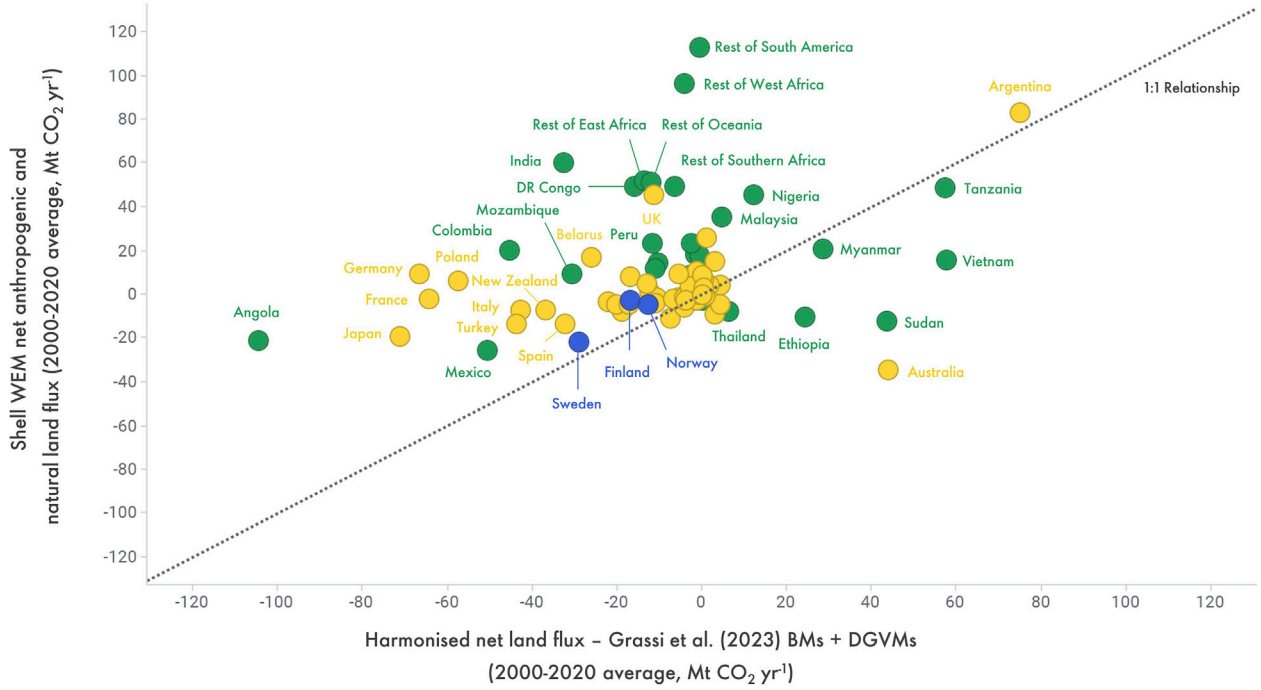

FIGURE 11
Comparison of net land carbon fluxes for individual countries as modelled in the Shell scenarios and as reported in the land-use flux harmonisation study of Grassi et al. (2023), based on averages for the 2000–2020 period. All units are in Mt CO_2 yr^{-1}. Colours represent the dominant ecosystem classification for each country (green = tropical, yellow = temperate, blue = boreal). The black line represents a 1:1 relationship, which would represent a perfect calibration. Data are identical to Figure 10, but axes are adjusted for visual clarity.

respective trends at the global level (Shell, 2023). As such, only key aspects relating to land use emissions and natural land sinks are described here. In *Sky 2050*, as a result of concerted action to follow through on the Glasgow Deforestation Pledge to halt global deforestation by 2023 (Reference), land-use emissions decrease rapidly through a combination of NBS avoidance and sequestration pathways, followed by global total land-use CO_2 emissions reaching net-zero around 2030, and subsequently becoming net-negative. As atmospheric CO_2 growth slows and levels off, the figure for the natural land carbon sink reaches a plateau by ~2030 and then starts to gradually decline. At the global level, MIT's modelling shows that the natural land sink would be expected to transition to a net source by ~2070 because of sustained net-negative emissions and a reversal of the biosphere buffering capacity, as carbon in natural forests is rereleased to the atmosphere—the unwinding of the CO_2 fertilisation effect. This implies that by 2100, negative anthropogenic land-use emissions will be partially offset by positive emissions from natural land ecosystems. Conversely, in *Archipelagos*, land-use emissions become negative at a slower pace, but total anthropogenic CO_2 emissions never reach net-zero. As a result, enhanced and prolonged atmospheric CO_2 growth yields a stronger natural land sink until ~2040 and natural land ecosystems are not expected to become a net source of CO_2 by 2100 at the global level.

Our new dataset allows for the evaluation of natural land sinks between different scenarios for any region of interest, or between different countries or regions in a single scenario (Figures 6, 7; Supplementary Data S1, S2). In our analysis, the natural land sink is dominated by a small number of large countries: Russia, Brazil, Canada, United States and China together account for approximately 54% of the global value because of their equally large share in total forest land area.

4.2 Integration of anthropogenic and natural land fluxes

With a full representation of natural land fluxes at the country level in the WEM, we are now able to compare the evolution of anthropogenic land-use emissions, including NBS pathways, with natural land sinks on spatial and temporal scales of interest and between scenarios. This allows us to compare our modelled results with the emissions that individual countries report, for instance as part of their National Greenhouse Gas Inventories (NGHGIs), as well as their land-based carbon sequestration targets in the years leading up to achieving net-zero emissions. We demonstrate this by adding up the anthropogenic land-use emissions and the natural land sinks to arrive at a total net land flux for each country in the WEM, which we then compare to individual country entries for historic emissions as compiled by the land-use flux harmonisation study of Grassi et al. (2023). Based on averages for the period of 2000–2020 for which both studies overlap, we find a generally good match between natural land fluxes allocated using our methodology and the natural land fluxes estimated from an ensemble of DGVMs as presented in Grassi et al. (2023) (Figures 8, 9). This comparison suggests that our approach may work well for boreal and temperate

TABLE 3 Comparison of land carbon fluxes as reported in land-use flux harmonisation study of Grassi et al. (2023) and as modelled by the Shell scenarios for the European Union (EU).

Country	Year	Anthropogenic land-use flux (Grassi et al., 2023 BMs)	Natural land flux (Grassi et al., 2023 DGVMs)	Net land flux (Grassi et al., 2023 BMs + DGVMs)	LULUCF flux (Grassi et al., 2023 NGHGI data compilation)	Anthropogenic land-use flux (Sky 2050)	Natural land flux (Sky 2050—this study)	Net land flux (Sky 2050—this study)
EU	2000–2020 average	−221	−239	−460	−320	+162	−189	−27
EU	2020	−195	−251	−446	−250	+121	−227	−106
EU	2030	NA	NA	NA	−310	+10	−236	−226

All units in Mt CO_2 yr^{-1}. NA, not available.

countries, but we observe an apparent underestimation of natural land fluxes in many tropical countries (e.g., DR Congo, Indonesia and Angola, but notably excluding Brazil). This could point to additional non-forest land carbon sinks in tropical countries that we currently do not account for in our simple modelling workflow. Nevertheless, the overall agreement is encouraging and suggests that our method may indeed be valuable for exploration of future natural land fluxes at country level.

We find that our combined estimates of net anthropogenic and natural land emissions also display a reasonable agreement with the available land-use harmonisation estimates (Figures 10, 11). Here we specifically compare our net land fluxes with the summed flux estimates of bookkeeping models (BMs) and DGVMs for non-intact forests of Grassi et al. (2023), the modelling metric that is thought to be most compatible to country NGHGI reporting. In our analysis, we find a moderately good agreement between both data sources for the largest countries (Figure 10), but for many smaller countries we observe that our methodology results in slightly higher net land fluxes compared to the estimates of Grassi et al. (2023) (Figure 11). Below we specifically discuss the example of the European Union (EU) in more detail.

The EU report a value of −250 Mt CO_2 yr^{-1} for land-use, land-use change and forestry (LULUCF) emissions for the year 2020 (Grassi et al., 2023). Because this is a negative number, the LULUCF sector is already considered as a net land carbon sink for the EU. By 2030, the EU have the ambition to further increase the magnitude of this net land carbon sink to −310 Mt CO_2 yr^{-1} through NBS (Reference), although this is lower than the 2000–2020 average value of −320 Mt CO_2 yr^{-1} (Grassi et al., 2023). By contrast, the land-use emissions for the EU as estimated in Shell modelling of anthropogenic land-use emissions are +121 Mt CO_2 yr^{-1} in 2020 and +10 Mt CO_2 yr^{-1} in 2030 (based on *Sky 2050*). Notably, these are positive values as they are based only on the anthropogenic components of land-use emissions estimates, whereas the reported EU numbers include both anthropogenic and natural components. We note that the 2020 values of the natural land flux estimates are strikingly similar between both methods [−227 Mt CO_2 yr^{-1} in our analysis and −251 Mt CO_2 yr^{-1} in Grassi et al. (2023)]. This also makes sense conceptually because the two approaches are both forest-based and considering that virtually all forests in the EU can be classified as non-intact. Hence, inclusion of the natural land sink estimates presented here should allow for a more consistent comparison of the two datasets. Our net land fluxes, i.e., the sum of anthropogenic and natural sources and sinks, are estimated at −106 Mt CO_2 yr^{-1} in 2020 and −226 Mt CO_2 yr^{-1} in 2030 at the EU level (Table 3). As such, our net land fluxes for the year 2020 differ substantially from the BMs + DGVMs estimate in Grassi et al. (2023), which is potentially because the apportionment of world land-use emissions in the Shell WEM, which is based on avoidance potentials across NBS types, gives significant land-use emissions in the blue carbon and wetland categories for its model baseline, whereas the EU report negligible numbers for these categories. Yet, for 2020, our net land estimates of −106 Mt CO_2 yr^{-1} appear to be closer to the actual LULUCF fluxes reported in the NGHGIs (−250 Mt CO_2 yr^{-1}) than those compiled in Grassi et al. (2023) (−446 Mt CO_2 yr^{-1}). This improvement could be a coincidence owing to the various uncertainties and methodological differences, and our estimate is still a factor of 2x different from the NGHGI reporting. However, it suggests that our methodology may indeed be effective for the integrated evaluation of land carbon sources and sinks in the context of country-specific NZE targets, particularly if the anthropogenic land-use emissions apportionment in the Shell WEM can also be further improved going forward.

4.3 Outlook for policymakers

To the best of our knowledge, there are no other data products available that allow countries to track their land carbon ambitions with such a first-order evaluation of future natural land flux trends at their respective level. Hence, we see the ability to be able to explore future natural land carbon scenarios as the largest added value for policymakers. Our methodology could also be easily adapted for scenarios developed by other parties or institutes because our approach based on forest land area effectively allocates global projections from earth system model simulations to regions of interest. More generally, our analysis speaks to the role of land in NZE target definitions and whether the NZE scope should include anthropogenic and/or natural land-based carbon removals. The meaning of NZE as a concept is actively being debated at the interface of academia, policy and business, and the exact definitions of NZE targets have important implications for their effectiveness in addressing the causes and consequences of climate change (Fankhauser et al., 2021; Rogelj et al., 2021; Allen et al., 2022). In Article 4 of the Paris Agreement, all parties aim "... to achieve a balance between anthropogenic emissions by sources and removals by sinks of greenhouse gases ...". We note that this ambition only covers

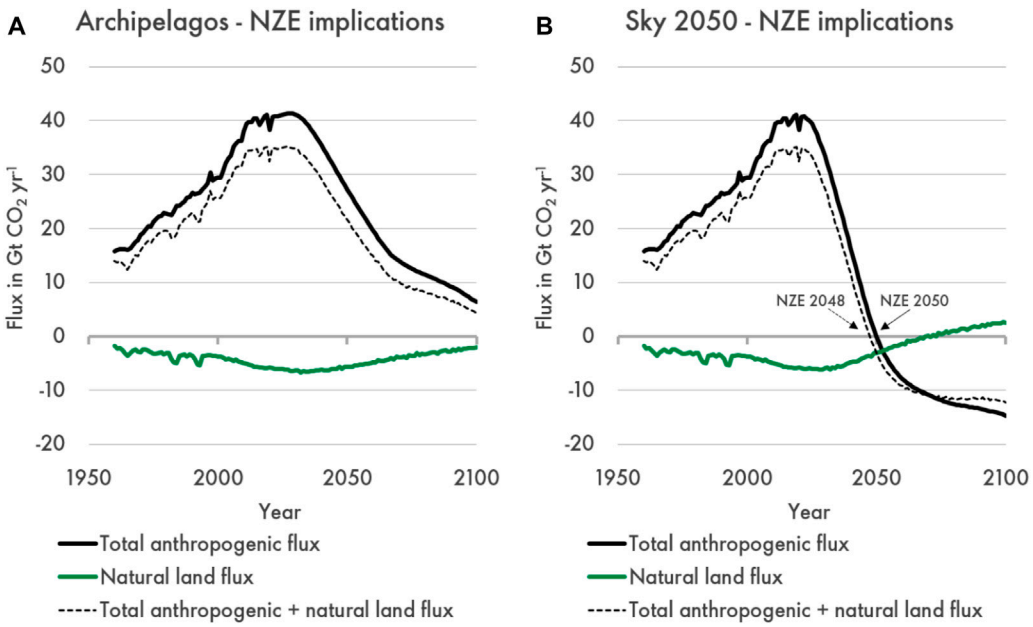

FIGURE 12
The impact of including natural land in a global NZE target for Archipelagos **(A)** and Sky 2050 **(B)**. In Archipelagos, NZE is not reached within the model timeline, whereas in Sky 2050, NZE is reached in 2050 or 2048 depending on the NZE target definition.

anthropogenic fluxes and does not consider natural land sinks. Based on our results and in line with global carbon budget studies we argue that carbon accounting methods for NZE targets should differentiate effectively between anthropogenic and natural effects where possible, to avoid the potential for entities to wrongly claim natural removals as if they were achieved through anthropogenic actions, for instance through NBS. Most NGHGIs cannot fully separate human-induced and natural effects, so it is imperative that pragmatic advances are being made to reconcile different methodologies and provide more complete and transparent reporting (Grassi et al., 2023). Distinguishing between anthropogenic and natural land contributions to land fluxes would also eliminate the risk of inconsistencies across countries in classification of land as "managed" for NGHGI accounting. In our analysis of the Energy Security Scenarios (Shell, 2023), we find that if natural land sinks were allowed to be included in a global NZE target for CO_2, this would accelerate the time needed to reach global NZE by approximately 2 years compared to only counting anthropogenic emissions and removals (total fluxes from energy, anthropogenic land and industrial process combined) (Figure 12). In other words, inclusion of natural land fluxes in the NZE definition in *Sky 2050* would result in reaching global NZE by 2048 instead of 2050, which is not a trivial difference. This outcome is consistent with previous work (Gidden et al., 2023). Similarly, NZE for all greenhouse gases would be reached 2–3 years earlier if natural land fluxes were to be included in that NZE definition. In any case, we argue that land-based carbon removals have an important role to play in NZE ambitions. However, whilst reaching NZE is a highly worthwhile—and highly challenging—pursuit in its own right, it should not be forgotten that sustaining net-negative emissions would be the ambition for at least the second half of this century from a planetary sustainability perspective.

5 Conclusion

This study presents a novel methodology to evaluate the future progression of natural land carbon sinks at the regional and country level, developed in the context of the new Shell Energy Security Scenarios (Shell, 2023). We allocate global projections from earth system model simulations to regions of interest using a compilation of forest land areas sourced from the FAO and other model sources for a historic and scenario range spanning 1960–2100. Our new dataset allows for the evaluation of natural land sinks between different scenarios for any region of interest, or between different countries or regions in a single scenario, which we demonstrate for the Shell scenarios *Sky 2050* and *Archipelagos*. We compare our results to the findings of other studies, including the land-use flux harmonisation study of Grassi et al. (2023), and find a remarkably good match in natural land sink estimates for recent history for individual countries and regions such as the EU. Our total net land flux estimates, combining anthropogenic land-use emissions from the Shell World Energy Model and natural land flux estimates arising from the present study, show a reasonable match for large countries but also show substantial scatter for many smaller countries. This suggests that the allocation of anthropogenic land-use emissions in the Shell World Energy Model (WEM) may potentially be further improved. Lastly, we discuss the importance of accurate land carbon accounting and demonstrate that including natural land fluxes as part of NZE definitions would accelerate reaching global NZE by approximately 2 years in *Sky 2050*. Given the importance of land carbon in mitigating climate change, we recommend that the carbon cycle modelling and energy modelling research communities continue to collaborate to develop relevant data and methods to distinguish anthropogenic and natural land CO_2 fluxes at country level, for both present and future.

Data availability statement

The original contributions presented in the study are included in the article/Supplementary Material, further inquiries can be directed to the corresponding author.

Author contributions

RvP: Conceptualization, Data curation, Formal Analysis, Investigation, Methodology, Visualization, Writing–original draft, Writing–review and editing. MH: Conceptualization, Formal Analysis, Funding acquisition, Methodology, Supervision, Writing–review and editing.

Funding

The authors declare financial support was received for the research, authorship, and/or publication of this article. This research was financially supported by Shell Global Solutions International B.V. and Shell International Limited.

Acknowledgments

We gratefully acknowledge Andy Robertson and Martine Ruigrok for technical discussions on NBS potentials and their implementation in the Shell WEM, as well as Sergey Paltsev, Angelo Gurgel and the other staff at the MIT Joint Program on the Science and Policy of Global Change for their comments on the work and the ongoing collaboration in the climate evaluation of Shell Scenarios. The methods and results remain the responsibility of the authors. Lastly, we acknowledge three independent reviewers for their comments that have improved the quality of the manuscript.

Conflict of interest

The authors declare that financial support was received for the research, authorship and/or publication of this article.

This research was financially supported by Shell Global Solutions International B.V. and Shell International Limited, both wholly owned subsidiaries of Shell plc. The funder was involved in the study design and the decision to submit it for publication.

Publisher's note

Supplementary material

The Supplementary Material for this article can be found online at: https://www.frontiersin.org/articles/10.3389/fenvs.2024.1379046/full#supplementary-material

References

Allen, M. R., Friedlingstein, P., Girardin, C. A. J., Jenkins, S., Malhi, Y., Mitchell-Larson, E., et al. (2022). Net zero: science, origins, and implications. *Annu. Rev. Environ. Resour.* 47 (1), 849–887. doi:10.1146/annurev-environ-112320-105050

Anderson-Teixeira, K. J., Herrmann, V., Banbury Morgan, R., Bond-Lamberty, B., Cook-Patton, S. C., Ferson, A. E., et al. (2021). Carbon cycling in mature and regrowth forests globally. *Environ. Res. Lett.* 16 (5), 053009. doi:10.1088/1748-9326/abed01

Armstrong McKay, D. I., Staal, A., Abrams, J. F., Winkelmann, R., Sakschewski, B., Loriani, S., et al. (2022). Exceeding 1.5°C global warming could trigger multiple climate tipping points. *Science* 377 (6611), eabn7950. doi:10.1126/science.abn7950

Canadell, J. G., Monteiro, P. M. S., Costa, M. H., Cunha, L. C. d., Cox, P. M., Eliseev, A. V., et al. (2021). "Global carbon and other biogeochemical cycles and feedbacks," in *Climate change 2021: the physical science basis. Contribution of working group I to the sixth assessment report of the intergovernmental Panel on climate change*. Editors V. Masson-Delmotte, P. Zhai, A. Pirani, S. L. Connors, C. Péan, S. Berger, et al. (Cambridge University Press), 673–816.

Chapin, F. S., Woodwell, G. M., Randerson, J. T., Rastetter, E. B., Lovett, G. M., Baldocchi, D. D., et al. (2006). Reconciling carbon-cycle concepts, terminology, and methods. *Ecosystems* 9 (7), 1041–1050. doi:10.1007/s10021-005-0105-7

Chen, Y. H. H., Paltsev, S., Reilly, J. M., Morris, J. F., and Babiker, M. H. (2016). Long-term economic modeling for climate change assessment. *Econ. Model.* 52, 867–883. doi:10.1016/j.econmod.2015.10.023

Crezee, B., Dargie, G. C., Ewango, C. E. N., Mitchard, E. T. A., Emba B, O., Kanyama T, J., et al. (2022). Mapping peat thickness and carbon stocks of the central Congo Basin using field data. *Nat. Geosci.* 15 (8), 639–644. doi:10.1038/s41561-022-00966-7

Denning, A. S. (2022). Where has all the carbon gone? *Annu. Rev. Earth Planet. Sci.* 50 (1), 55–78. doi:10.1146/annurev-earth-032320-092010

Duffy, K. A., Schwalm, C. R., Arcus, V. L., Koch, G. W., Liang, L. L., and Schipper, L. A. (2021). How close are we to the temperature tipping point of the terrestrial biosphere? *Sci. Adv.* 7 (3), eaay1052. doi:10.1126/sciadv.aay1052

Fankhauser, S., Smith, S. M., Allen, M., Axelsson, K., Hale, T., Hepburn, C., et al. (2021). The meaning of net zero and how to get it right. *Nat. Clim. Change* 12 (1), 15–21. doi:10.1038/s41558-021-01245-w

Fernández-Martinez, M., Penuelas, J., Chevallier, F., Ciais, P., Obersteiner, M., Rodenbeck, C., et al. (2023). Diagnosing destabilization risk in global land carbon sinks. *Nature* 615, 848–853. doi:10.1038/s41586-023-05725-1

Fernández-Martínez, M., Sardans, J., Chevallier, F., Ciais, P., Obersteiner, M., Vicca, S., et al. (2018). Global trends in carbon sinks and their relationships with CO2 and temperature. *Nat. Clim. Change* 9 (1), 73–79. doi:10.1038/s41558-018-0367-7

Friedlingstein, P., Jones, M. W., O'Sullivan, M., Andrew, R. M., Bakker, D. C. E., Hauck, J., et al. (2022). Global carbon budget 2021. *Earth Syst. Sci. Data* 14 (4), 1917–2005. doi:10.5194/essd-14-1917-2022

Friedlingstein, P., O'Sullivan, M., Jones, M. W., Andrew, R. M., Bakker, D. C. E., Hauck, J., et al. (2023). Global carbon budget 2023. *Earth Syst. Sci. Data* 15 (12), 5301–5369. doi:10.5194/essd-15-5301-2023

Gatti, L. V., Basso, L. S., Miller, J. B., Gloor, M., Gatti Domingues, L., Cassol, H. L. G., et al. (2021). Amazonia as a carbon source linked to deforestation and climate change. *Nature* 595 (7867), 388–393. doi:10.1038/s41586-021-03629-6

Gidden, M. J., Gasser, T., Grassi, G., Forsell, N., Janssens, I., Lamb, W. F., et al. (2023). Aligning climate scenarios to emissions inventories shifts global benchmarks. *Nature* 624 (7990), 102–108. doi:10.1038/s41586-023-06724-y

Goldstein, A., Turner, W. R., Spawn, S. A., Anderson-Teixeira, K. J., Cook-Patton, S., Fargione, J., et al. (2020). Protecting irrecoverable carbon in Earth's ecosystems. *Nat. Clim. Change* 10 (4), 287–295. doi:10.1038/s41558-020-0738-8

Grassi, G., House, J., Dentener, F., Federici, S., den Elzen, M., and Penman, J. (2017). The key role of forests in meeting climate targets requires science for credible mitigation. *Nat. Clim. Change* 7 (3), 220–226. doi:10.1038/nclimate3227

Grassi, G., House, J., Kurz, W. A., Cescatti, A., Houghton, R. A., Peters, G. P., et al. (2018). Reconciling global-model estimates and country reporting of anthropogenic

forest CO2 sinks. *Nat. Clim. Change* 8 (10), 914–920. doi:10.1038/s41558-018-0283-x

Grassi, G., Schwingshackl, C., Gasser, T., Houghton, R. A., Sitch, S., Canadell, J. G., et al. (2023). Harmonising the land-use flux estimates of global models and national inventories for 2000–2020. *Earth Syst. Sci. Data* 15 (3), 1093–1114. doi:10.5194/essd-15-1093-2023

Grassi, G., Stehfest, E., Rogelj, J., van Vuuren, D., Cescatti, A., House, J., et al. (2021). Critical adjustment of land mitigation pathways for assessing countries' climate progress. *Nat. Clim. Change* 11 (5), 425–434. doi:10.1038/s41558-021-01033-6

Gumbricht, T., Roman-Cuesta, R. M., Verchot, L., Herold, M., Wittmann, F., Householder, E., et al. (2017). An expert system model for mapping tropical wetlands and peatlands reveals South America as the largest contributor. *Glob. Chang. Biol.* 23 (9), 3581–3599. doi:10.1111/gcb.13689

Gurgel, A., Morris, J., Haigh, M., Robertson, A. D., Van der Ploeg, R., and Paltsev, S. (2024). Land-Use Competition in 1.5C Climate Stabilization: is there enough land for all potential needs? *Front. Environ. Sci. [Preprint]*.

Hansen, M. C., Potapov, P. V., Moore, R., Hancher, M., Turubanova, S. A., Tyukavina, A., et al. (2013). High-resolution global maps of 21st-century forest cover change. *Science* 342 (6160), 850–853. doi:10.1126/science.1244693

Hasegawa, T., Fujimori, S., Frank, S., Humpenöder, F., Bertram, C., Després, J., et al. (2021). Land-based implications of early climate actions without global net-negative emissions. *Nat. Sustain.* 4 (12), 1052–1059. doi:10.1038/s41893-021-00772-w

Hughes, T. P., Anderson, K. D., Connolly, S. R., Heron, S. F., Kerry, J. T., Lough, J. M., et al. (2018). Spatial and temporal patterns of mass bleaching of corals in the Anthropocene. *Science* 359 (6371), 80–83. doi:10.1126/science.aan8048

Hurtt, G. C., Chini, L., Sahajpal, R., Frolking, S., Bodirsky, B. L., Calvin, K., et al. (2020). Harmonization of global land use change and management for the period 850–2100 (LUH2) for CMIP6. *Geosci. Model. Dev.* 13 (11), 5425–5464. doi:10.5194/gmd-13-5425-2020

Jung, M., Reichstein, M., Schwalm, C. R., Huntingford, C., Sitch, S., Ahlstrom, A., et al. (2017). Compensatory water effects link yearly global land CO(2) sink changes to temperature. *Nature* 541 (7638), 516–520. doi:10.1038/nature20780

Keenan, T. F., Luo, X., Stocker, B. D., De Kauwe, M. G., Medlyn, B. E., Prentice, I. C., et al. (2023). A constraint on historic growth in global photosynthesis due to rising CO2. *Nat. Clim. Change* 13 (12), 1376–1381. doi:10.1038/s41558-023-01867-2

Keenan, T. F., and Williams, C. A. (2018). The terrestrial carbon sink. *Annu. Rev. Environ. Resour.* 43 (1), 219–243. doi:10.1146/annurev-environ-102017-030204

Keith, H., Kun, Z., Hugh, S., Svoboda, M., Mikoláš, M., Adam, D., et al. (2024). Carbon carrying capacity in primary forests shows potential for mitigation achieving the European Green Deal 2030 target. *Commun. Earth Environ.* 5 (1), 256. doi:10.1038/s43247-024-01416-5

Keith, H., Vardon, M., Obst, C., Young, V., Houghton, R. A., and Mackey, B. (2021). Evaluating nature-based solutions for climate mitigation and conservation requires comprehensive carbon accounting. *Sci. Total Environ.* 769, 144341. doi:10.1016/j.scitotenv.2020.144341

Longbottom, T., Wahab, L., Min, K., Jurusik, A., Moreland, K., Dolui, M., et al. (2022). What's soil got to do with climate change? *GSA Today* 32 (5), 4–10. doi:10.1130/gsatg519a.1

Mo, L., Zohner, C. M., Reich, P. B., Liang, J., de Miguel, S., Nabuurs, G. J., et al. (2023). Integrated global assessment of the natural forest carbon potential. *Nature* 624 (7990), 92–101. doi:10.1038/s41586-023-06723-z

Page, S. E., Rieley, J. O., and Banks, C. J. (2011). Global and regional importance of the tropical peatland carbon pool. *Glob. Change Biol.* 17 (2), 798–818. doi:10.1111/j.1365-2486.2010.02279.x

Paltsev, S., Sokolov, A., Haigh, M., Hone, D., and Morris, J. (2021). Changing the global energy system: temperature implications of the different storylines in the 2021 Shell energy transformation scenarios. *Jt. Program Rep. Ser. Rep.* 348 (February), 20.

Penuelas, J., Ciais, P., Canadell, J. G., Janssens, I. A., Fernandez-Martinez, M., Carnicer, J., et al. (2017). Shifting from a fertilization-dominated to a warming-dominated period. *Nat. Ecol. Evol.* 1 (10), 1438–1445. doi:10.1038/s41559-017-0274-8

Regnier, P., Resplandy, L., Najjar, R. G., and Ciais, P. (2022). The land-to-ocean loops of the global carbon cycle. *Nature* 603 (7901), 401–410. doi:10.1038/s41586-021-04339-9

Ritchie, P. D. L., Clarke, J. J., Cox, P. M., and Huntingford, C. (2021). Overshooting tipping point thresholds in a changing climate. *Nature* 592 (7855), 517–523. doi:10.1038/s41586-021-03263-2

Roe, S., Streck, C., Beach, R., Busch, J., Chapman, M., Daioglou, V., et al. (2021). Land-based measures to mitigate climate change: potential and feasibility by country. *Glob. Chang. Biol.* 27 (23), 6025–6058. doi:10.1111/gcb.15873

Roe, S., Streck, C., Obersteiner, M., Frank, S., Griscom, B., Drouet, L., et al. (2019). Contribution of the land sector to a 1.5 °C world. *Nat. Clim. Change* 9 (11), 817–828. doi:10.1038/s41558-019-0591-9

Rogelj, J., Geden, O., Cowie, A., and Reisinger, A. (2021). Net-zero emissions targets are vague: three ways to fix. *Nature* 591 (7850), 365–368. doi:10.1038/d41586-021-00662-3

Ruehr, S., Keenan, T. F., Williams, C., Zhou, Y., Lu, X., Bastos, A., et al. (2023). Evidence and attribution of the enhanced land carbon sink. *Nat. Rev. Earth Environ.* 4 (8), 518–534. doi:10.1038/s43017-023-00456-3

Schwingshackl, C., Obermeier, W. A., Bultan, S., Grassi, G., Canadell, J. G., Friedlingstein, P., et al. (2022). Differences in land-based mitigation estimates reconciled by separating natural and land-use CO2 fluxes at the country level. *One Earth* 5 (12), 1367–1376. doi:10.1016/j.oneear.2022.11.009

Sokolov, A., Kicklighter, D., Schlosser, A., Wang, C., Monier, E., Brown-Steiner, B., et al. (2018). Description and evaluation of the MIT earth system model (MESM). *J. Adv. Model. Earth Syst.* 10 (8), 1759–1789. doi:10.1029/2018ms001277

Sokolov, A., Paltsev, S., Gurgel, A., Haigh, M., Hone, D., and Morris, J. (2023). Temperature implications of the 2023 Shell energy security scenarios: Sky 2050 and Archipelagos. *Jt. Program Rep. Ser. Rep.* 364 (3), 17.

Tsai, W.-T. (2020). Forest resource management and its climate-change mitigation policies in taiwan. *Climate* 9 (1), 3. doi:10.3390/cli9010003

Upton, S., Reichstein, M., Gans, F., Peters, W., Kraft, B., and Bastos, A. (2024). Constraining biospheric carbon dioxide fluxes by combined top-down and bottom-up approaches. *Atmos. Chem. Phys.* 24 (4), 2555–2582. doi:10.5194/acp-24-2555-2024

Walker, A. P., De Kauwe, M. G., Bastos, A., Belmecheri, S., Georgiou, K., Keeling, R. F., et al. (2021). Integrating the evidence for a terrestrial carbon sink caused by increasing atmospheric CO2. *New Phytol.* 229 (5), 2413–2445. doi:10.1111/nph.16866

Walker, X. J., Baltzer, J. L., Cumming, S. G., Day, N. J., Ebert, C., Goetz, S., et al. (2019). Increasing wildfires threaten historic carbon sink of boreal forest soils. *Nature* 572 (7770), 520–523. doi:10.1038/s41586-019-1474-y

Xu, (2021). Changes in global terrestrial live biomass over the 21st century. *Sci. Adv.* 7, eabe9829. doi:10.1126/sciadv.abe9829

Xu, J., Morris, P. J., Liu, J., and Holden, J. (2018). PEATMAP: refining estimates of global peatland distribution based on a meta-analysis. *Catena* 160, 134–140. doi:10.1016/j.catena.2017.09.010

Yue, C., Ciais, P., Houghton, R. A., and Nassikas, A. A. (2020). Contribution of land use to the interannual variability of the land carbon cycle. *Nat. Commun.* 11 (1), 3170. doi:10.1038/s41467-020-16953-8

frontiers | Frontiers in Environmental Science

TYPE Original Research
PUBLISHED 12 November 2024
DOI 10.3389/fenvs.2024.1393327

OPEN ACCESS

EDITED BY
Chenxi Li,
Xi'an University of Architecture and Technology, China

REVIEWED BY
Maurizio Tiepolo,
Polytechnic University of Turin, Italy
Eve Bohnett,
University of Florida, United States

*CORRESPONDENCE
Sergey Paltsev,
paltsev@mit.edu

RECEIVED 28 February 2024
ACCEPTED 28 October 2024
PUBLISHED 12 November 2024

CITATION
Gurgel A, Morris J, Haigh M, Robertson AD, van der Ploeg R and Paltsev S (2024) Land-use competition in 1.5°C climate stabilization: is there enough land for all potential needs? *Front. Environ. Sci.* 12:1393327. doi: 10.3389/fenvs.2024.1393327

Land-use competition in 1.5°C climate stabilization: is there enough land for all potential needs?

Angelo Gurgel[1], Jennifer Morris[1], Martin Haigh[2], Andy D. Robertson[3], Robin van der Ploeg[4] and Sergey Paltsev[1]*

[1]MIT Center for Sustainability Science and Strategy, Massachusetts Institute of Technology, Cambridge, MA, United States, [2]Shell Scenarios Team, Shell International, London, United Kingdom, [3]Shell International Exploration and Production B. V., The Hague, Netherlands, [4]Shell Global Solutions International B.V., Amsterdam, Netherlands

Achieving a low-carbon future requires a comprehensive approach that combines emission mitigation options from economic activities with the sustainable use of land for numerous needs: food production, energy production, carbon sequestration, nature preservation and broad ecosystem services. Using the MIT Integrated Global System (IGSM) framework we analyze land-use competition in a 1.5°C climate stabilization scenario, in which demand for bioenergy and natural sinks increase along with the need for sustainable farming and food production. We find that to address the numerous trade-offs, effective approaches to nature-based solutions (NBS) and agriculture practices are essential. With proper regulatory policies and radical changes in current practices, global land is sufficient to provide increased consumption of food *per capita* (without large diet changes) over the century while also utilizing 2.5–3.5 billion hectares (Gha) of land for NBS practices that provide a carbon sink of 3–6 gigatonnes (Gt) of CO_2 per year as well as 0.4–0.6 Gha of land for energy production—0.2–0.3 Gha for 50–65 exajoules (EJ) per year of bioenergy and 0.2–0.35 Gha for 300–600 EJ/year of wind and solar power generation. We list the competing uses of land to reflect the trade-offs involved in land use decisions, and note that while there is sufficient land in our scenario, attaining this outcome, capable of delivering a 1.5°C future, requires effective policies and measures at national and global levels that promote efficient land use for food, energy and nature (including carbon sequestration) and ensure long-term commitments by decision makers from governments and industry in order to realize the benefits of climate change mitigation.

KEYWORDS

land use, decarbonization, sustainability, climate, greenhouse gas, nature-based solutions, carbon removals

1 Introduction

A transformation of both the energy system and land use are necessary in order to limit global warming to 1.5°C while also meeting needs for food and environmental sustainability (IPCC, 2023). This has led to widespread concern that there may not be enough land to meet all the needs for food and nature whilst providing land for urban environments, energy production, and nature-based carbon sequestration (e.g., Searchinger and Heimlich, 2015;

Rulli et al., 2016; Fehrenbach et al., 2023). Following the goals of the Paris Agreement (UN, 2015), numerous governments, international organizations and companies advocate for and explore sustainable pathways to net-zero emissions. Achieving the net-zero targets requires not only reducing anthropogenic greenhouse gas (GHG) emissions, but also increasing removals of GHG from the atmosphere (IPCC, 2023; Morris et al., 2023).

Recent studies have shown that the land sector plays an especially important role in such low-emissions pathways, particularly through land-based carbon dioxide removal (e.g., bioenergy with carbon capture and storage (BECCS), afforestation/reforestation and other nature-based solutions (NBS)), energy crops and changing agricultural practices (Roe et al., 2019; Hasegawa et al., 2021; Morris et al., 2024). Land for the expansion of wind and solar generation, and potentially direct air capture facilities, adds further pressure for land (e.g., MIT Joint Program, 2023; van de Ven et al., 2021). Given the broad range of climate change mitigation options that rely on land, careful consideration of trade-offs between those options is needed. For example, those options vary in terms of the amount of land required, their mitigation/sequestration potential, their energy production, their implications for food security, and their impact on wider ecosystem services such as the ability to improve biodiversity or combat desertification and land degradation.

Particular attention has been given to trade-offs between using land for BECCS and/or NBS vs. for food production and/or nature preservation (e.g., Boysen et al., 2017; Busch et al., 2019; IPCC, 2020; Donnison et al., 2020; Seddon et al., 2020; Seddon et al., 2021; Vera et al., 2022). While globally, the sheer amount of useable land (see Section 2) does not appear to be a limiting factor for multiple uses of land, it is not clear how realistic it is to pursue all potential options at once. Lastly, increasing land competition may impact the resilience of natural land carbon sinks that play a crucial role in partially mitigating anthropogenic climate change (Ruehr et al., 2023).

Decisions will need to be made about how to best use land in any given location for a sustainable low-carbon future. Toward that end, there are many estimates of the amount of land that could be demanded for different purposes. The Food and Agriculture Organization (FAO) of the United Nations estimated that the global arable land area must increase by 165 million hectares (Mha)[1] to guarantee food and material supplies by 2050, which corresponds to an expansion of arable land by 11% (FAO, 2018). FAO stated that the additional land requirement may increase to 325 Mha (or 21% expansion) under less favorable prospects for population growth, dietary changes, climate impacts on yields, rate of technological progress and institutional aspects (FAO, 2018). For the high warming scenarios, several studies project substantial crop yield losses of 10% or more (Hsiang et al., 2017; Robertson et al., 2018; Sue Wing et al., 2021; Hasegawa et al., 2022; IPCC, 2023; Rezaei et al., 2023). Climate change mitigation helps to alleviate these damages. For 1.5°C stabilization, crop yield impacts are estimated to be close to zero (Rezaei et al., 2023; Hasegawa et al., 2022), which provides another incentive for rapid global emission reduction actions.

Emission mitigation scenarios often envision substantial increases in bioenergy production. Fajardy et al. (2021) evaluated that land needs for bioenergy by 2100 under 1.5°C or 2°C stabilization may require between 80 Mha (to produce only 22 EJ/yr of primary energy) and more than 500 Mha (to achieve 300–400 EJ/yr), depending on BECCS availability, biomass yields and climate stabilization targets. Falling within that range, Smith et al. (2016) estimated 380 Mha of land required for 170 EJ/yr of bioenergy in 2100. To provide context, the current global total energy consumption is about 630 EJ/year, of which about 10% is from bioenergy and traditional use of biomass (IEA, 2023).

The use of NBS, sometimes also referred as Natural Climate Solutions (NCS; Environmental Defense Fund, 2024), has been estimated to require active management of more than 4 billion hectares (Gha) to achieve their maximum potential contribution of ~30 $GtCO_2e$/yr in mitigation (Roe et al., 2021). However, that is a technical maximum combining all NBS activities at once, and a more feasible estimate is in the range of 2 Gha to achieve a cost-effective potential contribution to mitigation. For context, the global land area dedicated to agriculture (crops and livestock) exceeds 4 Gha and estimates of additional land area available for reforestation are 678–900 Mha (Griscom et al., 2017; Bastin et al., 2019). At the same time, estimates of global area of abandoned agriculture are quite sizeable, between 390 Mha and 475 Mha (Campbell et al., 2008).

With many competing demands for land, the question arises whether there is enough land to meet climate goals and agricultural/food needs while preserving and restoring ecosystem functions, including biodiversity. Is it possible to allocate land for food, carbon sequestration, energy and nature globally and regionally to address both human and environmental needs? What are the required actions and changes in land use to achieve these needs?

The goal of this paper is to assess the land competition that arises while achieving a 1.5°C temperature stabilization target. In particular, this paper seeks to determine whether global land can meet competing needs for food, carbon sequestration, energy, and nature preservation. To quantify the trajectories of land use and its implications, we use a tool that provides an interconnected representation of the physical and socio-economic systems, the MIT Integrated Global System Modeling (IGSM) framework (Sokolov et al., 2018). We employ MIT IGSM and its socio-economic component, the MIT Economic Projection and Policy Analysis (EPPA) model, to assess the land implications of the Sky 2050 scenario (Shell, 2023), where the world is developing in increasingly sustainable directions across both land and energy systems. Sky 2050 is a 1.5°C scenario with an overshoot (category C2 by the definition of the IPCC (IPCC, 2023)) which was designed to achieve a global net-zero target for total anthropogenic CO_2 emissions (i.e., energy + industry + land use) in the year 2050. When including non-CO_2 GHGs, net emissions in this scenario decline to zero in 2062 and stay below zero until 2100. The profiles for GHG emissions and the temperature implications of this scenario are described in Sokolov et al. (2023). While for illustrative purposes we focus on Sky 2050 (namely because it involves a detailed consideration of NBS and provides public information for many relevant energy and land characteristics), similar land competition and trade-offs will be required in other scenarios that target 1.5°C stabilization, such as those summarized by IPCC (2023) or those

1 1 square kilometer (sq km) = 100 hectares (ha).

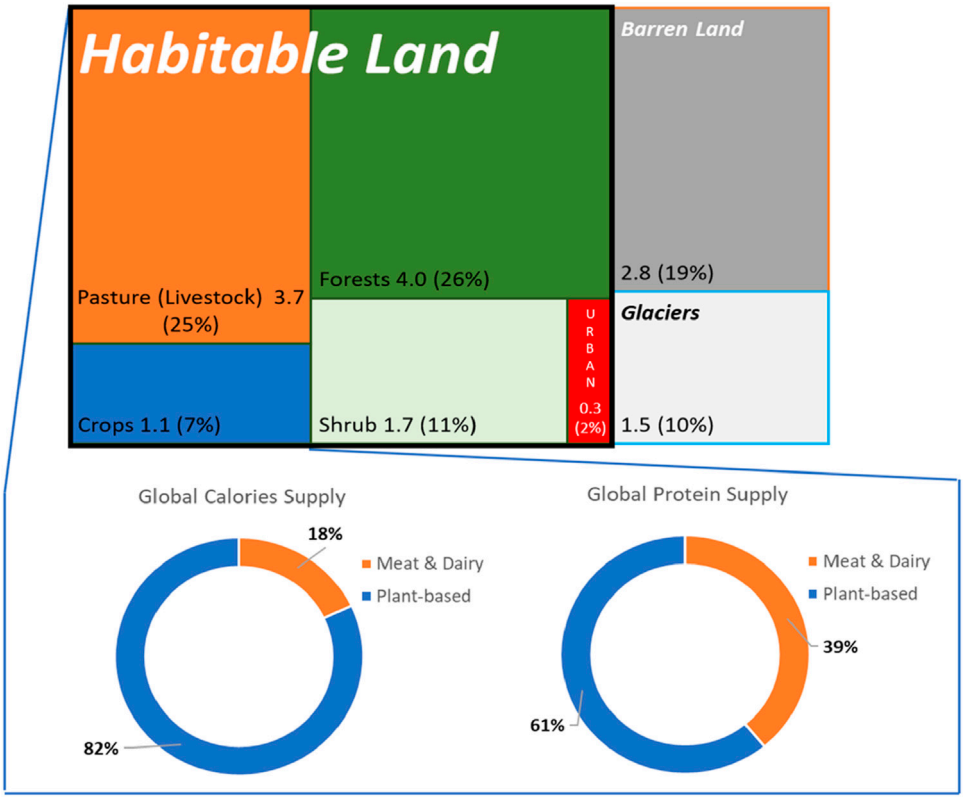

FIGURE 1
Current global land use (in gigahectares, Gha, and percentage of total) by land category and shares of animal and plant-based sources in global supply of calories and protein. Data source: Ritchie and Roser (2013), FAO (2019).

developed by other entities (e.g., IEA, 2023; MIT Joint Program, 2023).

In the following sections, this paper: i) summarizes current global land use, ii) describes the methods we use for assessing future trajectories for land use, iii) discusses global and regional land-use implications, iv) evaluates the feasibility of achieving the land-use optimization needed by such a 1.5°C scenario, and v) discusses the needs for fast and radical changes to achieve climate stabilization goals.

2 Current global land use and land-use emissions

Land covers almost 15 Gha of our planet's surface, distributed among habitable land, glaciers (ice covered areas), and barren areas (FAO, 2019). As we discuss later, different sources (e.g., FAO, IPCC) use different land use/land cover categorization, and, as a result, the total 15 Gha is sometimes divided in a different fashion between several land use classes. In Figure 1, we use the data from FAO (2019) to illustrate how the current use of the 10.4 Gha of habitable land is split between five major categories: two categories are related to agriculture (crops and livestock) and three categories are related to other uses and covers (forests, shrubland, and urban areas).

As shown, the global area dedicated to livestock production occupies 3.7 Gha and global cropland uses another 1.1 Gha. These categories of agricultural land provide different contributions for the global supply of calories and protein. Although the global area dedicated to crops is only one third of the area for livestock and dairy, crops provide 82% of the total calories and 61% of the global protein supply (FAO, 2023). As for other land uses, forests and shrublands account for 4.0 Gha and 1.7 Gha, respectively. Urban areas and freshwater areas occupy additional 0.3 Gha.

Land used for energy production is not typically a land use/land cover category estimated in most global data sources, and therefore needs to be estimated. To evaluate the land areas used for energy production, we apply the estimates from Shell (2023) for wind and solar and the EPPA model estimates for bioenergy based on the approach from Winchester and Reilly (2015). The 2020 land requirements for wind and solar are consistent with the estimates from the U. S. National Renewable Laboratory (NREL, 2019), where 1 MW of solar generating capacity requires about 1 ha of land, and 1 MW of wind capacity requires 15–20 ha of land. For wind, only 1%–2% of that area is used directly by turbines and other supporting infrastructure, and the remaining area might be used for other purposes (e.g., farming). However, in this study we are interested in the upper bound for a potential land use. Hence, in our estimates we assign the full area to wind generation. We also separate onshore and offshore wind based on the BNEF 2022 Energy Outlook (BloombergNEF, 2022), and our wind-related reporting reflects only the areas for onshore generation. Over time, the amount of wind and solar energy produced on a particular land area is prescribed to increase due to improved packing density and conversion efficiency. We follow Shell (2023) and use the

TABLE 1 Land area (Mha) used for bioenergy, wind generation and solar generation in 2020.

	Land for			Total land	Share of land for energy (%)
	Bioenergy	Wind	Solar		
United States	22.6	1.6	0.1	930	2.6
Europe	8.8	1.8	0.1	486	2.2
China	12.0	2.9	0.2	933	1.6
India	2.2	0.5	0.0	296	0.9
Brazil	13.9	0.3	0.0	855	1.7
Rest of the World	36.4	1.3	0.2	9,950	0.4
World	95.9	8.0	0.6	13,450	0.8

following trajectories for energy generated per year per ha: 3.4 TJ/ha for solar and 0.57 TJ/ha for wind in 2020, 7.4 TJ/ha for solar and 0.58 TJ/ha for wind in 2050, and 9.5 TJ/ha for solar and 0.58 TJ/ha for wind in 2100.

Table 1 shows the resulting estimates of global and regional land use for energy. In the regions with substantial bioenergy production (Brazil, Europe, United States), the share of land used for energy is between 1.7% and 2.6%. However, the global share of land dedicated to energy is less than 1%. Note that we do not include the land areas for fossil fuel production and mining of critical materials.

Changes in the uses of land induce changes in related emissions. According to IPCC (2023), the corresponding net anthropogenic GHG emissions from land use, land-use change and forestry (LULUCF) are subject to large uncertainties and high annual variability. Global LULUCF CO_2 emissions (annual average for 2010–2019) are estimated to be in the range of 5.9 ± 4.1 $GtCO_2e/yr$ (IPCC, 2023). The Global Carbon Project in its 2023 edition estimates the 2022 global net anthropogenic land-use change emissions to be 4.2 $GtCO_2e/yr$ (Friedlingstein et al., 2023). While different editions of the Global Carbon Project provide different estimates for historic land-use change emissions, the recent estimates seem to settle at a number around 4 $GtCO_2e/yr$.

It is worth to note that alternative methodological approaches for estimating emissions from Agriculture, Forestry and Other Land Uses (AFOLU) lead to different values. National GHG inventory reporting separates the net flux from LULUCF and the net flux from Agriculture (IPCC, 2023). They include direct human-induced effects and, in most cases, indirect effects due to anthropogenic environmental change. These include changes in biomass carbon stock in forest land that may include unmanaged natural forest. Food and Agriculture Organization of the United Nations (FAO) follows the similar approach in reporting emissions from agri-food systems that include land use and land use change emissions. However, according to IPCC (2023), for calculating anthropogenic land CO_2 in integrated assessment models and book-keeping models, such as Global Carbon Project, only the impacts of direct effects and only for those areas that are subject to intense and direct management are considered. These models also estimate non-anthropogenic land CO_2 flux, and separations between anthropogenic and non-anthropogenic land CO_2 fluxes are not always consistent (IPCC, 2023). Typically, national GHG inventories report lower net land-use emissions with a global total between 1 and 1.5 $GtCO_2e/yr$ in 2016–2019 (IPCC, 2023). For the Sky 2050 scenario, we have used the data consistent with the Global Carbon Budget estimates with historic land-use change CO_2 emissions around 4 $GtCO_2e/yr$ (Sokolov et al., 2023).

How LULUCF emissions will change in the future depends on future decisions about how to use land, given competition for multiple uses. The IPCC (2023) points to the potential for anthropogenic land-use to transition from being a net-source of GHG emissions today to a large net-sink (8–14 $GtCO_2e/yr$) by mid-century, if land-use carbon mitigation is supported at the level of 100 USD/tCO_2e. In addition, IPCC's illustrative mitigation pathways include net CO_2 removal on managed land with a range of 0.23–6.38 $GtCO_2/yr$ in 2050. On such timescales, the natural land carbon sink also acts to partially buffer CO_2 exchange between the atmosphere and biosphere through CO_2 fertilization of photosynthesis (see Ruehr et al. (2023) for a comprehensive review).

3 Methods

To explore potential future land competition, we combine detailed bottom-up modeling/estimates (i.e., an approach that considers specific activities, pathways, and challenges at a detailed level) of land uses from the Sky 2050 scenario with the top-down modeling (i.e., an aggregate-level representation of the main driving forces and their impacts) of land use change using the MIT Economic Projection and Policy Analysis (EPPA) model, each of which is described below.

3.1 Bottom-up modeling of the potential for nature-based solutions (NBS)

The Sky 2050 scenario is designed to meet the goal of net-zero (anthropogenic) CO_2 by 2050; it is a "high overshoot" 1.5°C pathway (i.e., C2 category), based on IPCC's definition, sitting in the middle of the IPCC scenarios' C2 range (Sokolov et al., 2023). The scenario is unique among 1.5°C scenarios due to its detailed consideration of NBS, using country level modeling for both energy and the development of NBS, in an integrated narrative. NBS achieve atmospheric CO_2 reduction through the conservation,

restoration, or altered management of natural ecosystems (Waring et al., 2023). The Sky 2050 scenario seeks to recognize that implementing change, scaling up technologies or rolling out changes in land-use takes time to build when they are in their infancy today. The land-use analysis in the scenario draws heavily on the academic literature reviewed by the latest assessment of scientific findings (Sixth Assessment Report) by the Intergovernmental Panel on Climate Change (IPCC, 2023) for the long-term and cumulative potentials for NBS.

In particular, data developed by Cook-Patton et al. (2020) and the underlying references of Roe et al. (2021) are used for the modeling of the scale-up of NBS and the total ultimate potential land areas and cumulative CO_2 impact for protection, improved management or restoration. While the Sky 2050 scenario is highly ambitious, it does apply cost constraints for all NBS activities that require a change in land use or management (e.g., reforestation, regenerative agriculture, peatland/forest management). In related literature this is commonly referred to as the "cost-effective" available area and implies that implementing the NBS activity would require no more than 100 USD/tCO_2 (Roe et al., 2021; IPCC, 2023). The analysis is built up from a combination of changing land areas under management together with profiles of CO_2 stored and taken up through time in different ecosystems. Temporal profiles are based on an analysis that uses country-, NBS pathway-, and scenario-specific profiles of how hectares under management (i.e., "enrolled") scale up.

The approach assesses how five categories of barriers (economic, political, technological, socio-cultural and environmental) will affect the deployment rate, separately across 19 different NBS pathways for 200+ countries, for each scenario. For simplicity, all pathways start this enrollment in 2023, but many do not reach material scale for several years or even decades, dependent on the pathway and country. The greater the number of barriers to overcome, the slower the scale-up to the peak rate (ha/yr) of enrollment. The calibration of peak rates is based on a combination of expert elicitation, comparison with historic enrollment rates of ambitious NBS projects (e.g., US national forest expansion in the 1930s, large-scale reforestation campaigns in China in recent years) and validation against current ambitions (e.g., United Kingdom net-zero reforestation ambitions – Committee of Climate Change, 2020). The resulting anthropogenic land-use emissions fall from a net source of 4 $GtCO_2$/yr today to a net sink of −6.1 $GtCO_2$/yr in 2050 (Sokolov et al., 2023). The cumulative anthropogenic land-use emissions in 2023–2100 in the Sky 2050 scenario are −312 $GtCO_2$.

The second part of the calculation uses existing literature (Roe et al., 2019) to distribute rates of CO_2 removal and avoidance on a unit area and time basis (i.e., tCO_2/ha/yr). This uses country-specific rates for each different NBS type and applies a temporal distribution that describes that activity's temporal impact on mitigation (e.g., 1 hectare of avoided deforestation generates all emission reductions at the time the area is protected, whereas emission reductions generated by reforestation follow a lognormal distribution starting from the year trees are planted). For more detail on this calculation, see Barros et al. (2023). Many of these temporal profiles are generalized across several countries or climatic zones, but do represent the fact that reforestation in tropical zones may reach peak CO_2 sequestration rates within 6 years whereas reforestation in mid or high latitudes may take 10+ years after saplings have been planted.

Additionally, forests in different regions may reach equilibrium and limit additional sequestration over different time horizons (Cook-Patton et al., 2020). Avoidance pathways use the most recent assessment of current carbon stock levels. For some, such as avoided deforestation, if a hectare is protected then the emission reductions are accounted for in the year in which the hectares are enrolled, but the land area is considered enrolled and managed indefinitely, despite no longer generating any emission reductions. For other NBS activities, such as fire management in savannahs, avoided emissions can be ongoing. An important result from the two steps of the calculation is that both the scaling up of capacity to enroll hectares in land management programs, and factoring in the time from enrollment to CO_2 uptake, act as lags in removing CO_2 from the atmosphere. This bottom-up approach produces projections of land use that account for realistic constraints to the deployment of NBS.

3.2 Top-down modeling: the economic projection and policy analysis (EPPA) model

To assess land-use competition between different categories of land, we use the MIT Economic Projection and Policy Analysis (EPPA) model. EPPA is a dynamic multi-sector, multi-region computable general equilibrium (CGE) model of the world economy (Paltsev et al., 2005; Chen et al., 2022). It is designed to develop projections of economic growth, energy transitions and anthropogenic emissions of greenhouse gas and air pollutants. Land use changes in EPPA are explicitly modeled by land use transitions among five major land categories (cropland, pasture, managed forest, natural grassland and natural forest) taking into account costs of transitions and associated emissions and maintaining consistent supplemental physical accounts of land (Gurgel et al., 2016; Gurgel et al., 2021).

Conversion of natural areas to agriculture follows a land supply response based on land conversions observed over the past few decades. Land can move to a less intensely managed use (e.g., from cropland to pasture or forest) or be abandoned completely and return to "natural" grass or forest land if investment in managed land is not maintained. Direct and indirect emissions associated with land use changes are represented in the model. Agricultural goods (e.g., crops, livestock, forestry) are produced by combining land, capital, labor, energy and intermediate inputs under multi-nested Constant Elasticity of Substitution (CES) functions. Alternative bioenergy technologies (e.g., liquid biofuels, bioelectricity, BECCS) are considered in EPPA, and require cropland areas to be deployed.

Future projections in the EPPA model are driven by economic decisions related to savings and investments, productivity improvements in labor, capital, land and energy, changing demand for goods and services due to income growth and international trade, and depletion of natural resources. These economic drivers, combined with imposed policies such as GHG emissions constraints, determine the economic trajectories over time and across scenarios and, consequently, land use changes. In terms of policies, EPPA uses a 1.5°C increase by the end-of-century with a 50% likelihood given an assessment of uncertainty in climate response to greenhouse gas forcing in the MIT Earth System Model (MESM). Global GHG emissions are driven by regional emissions caps based on the existing NDC commitments by

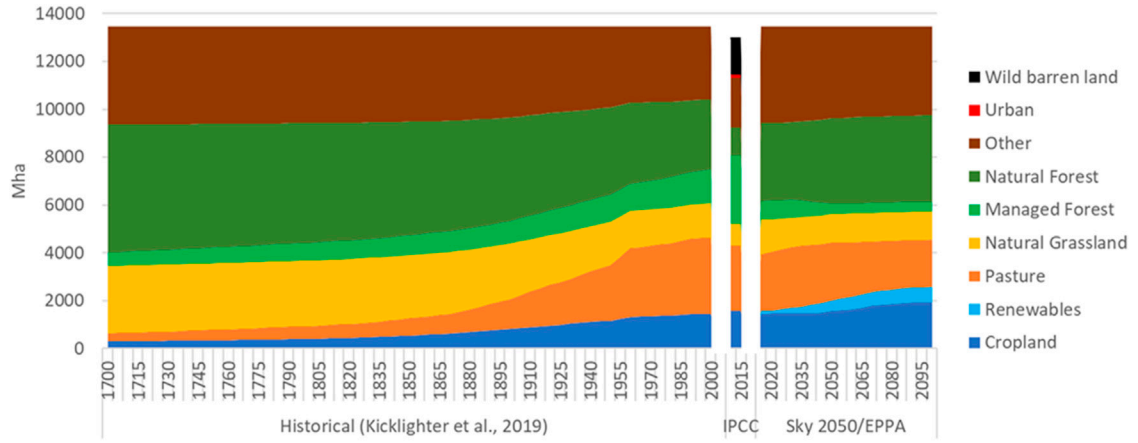

FIGURE 2
Historical global land use and future projections by broad categories (in Mha). Data source: Kicklighter et al. (2019) for 1700–2000, IPCC (2020) for 2015, EPPA model projections for 2020–2100.

2030 and proportional historical contributions to GHG concentrations beyond that, assuming differentiated responsibilities across regions. In order to capture the potential contribution and land use competition from large adoption of NBS, in EPPA emissions from land use changes are included under the cap and afforestation/reforestation activities can generate carbon credits toward the climate stabilization goal.

A strength of the EPPA model is its economy-wide representation, which captures economic dynamics across multiple sectors of the economy, driving market-based demand for land. However, as a top-down model, EPPA is limited to aggregated representations of land types and land management/mitigation options. It lacks the level of detail considered in the Sky 2050 scenario, particularly details related to NBS. Therefore, to assess potential future land competition among food production, energy production, and carbon sequestration via NBS, we combine the detailed bottom-up estimates of land uses from the Sky 2050 scenario with the top-down modeling of land use change using the EPPA model.

We do this by overlaying the demanded areas for alternative land uses from Sky 2050 in EPPA and evaluating the consistency between them. More specifically, assuming the same climate stabilization target, we combine the NBS adoption rates and projections of land used for renewable energy sources from Sky 2050 with land use projections from EPPA which account for changes in income, food and energy consumption and prices due to the climate stabilization target and future development of societies. We then verify if the detailed bottom-up Sky 2050 land use requirements are compatible with the top-down EPPA market mediated projections on land demand to achieve the 1.5°C target while also satisfying future demand for food, energy and other land-intensive materials.

4 Results

4.1 Global land use: 1700–2100

Global land use was quite stable among broad land use categories before the Industrial Revolution (Figure 2). In the middle of the nineteenth century, changes in land use from natural vegetation to pasture and cropland accelerated—1.08 Gha of natural forests and natural grassland that existed in 1800 became agricultural areas by 1900, and had risen to 3.41 Gha converted by 2000. The most recent 50 years have experienced declining rates of land use conversion worldwide. As shown in Figure 2, strong decarbonization efforts in the 21st century require a halt of historical deforestation trends and a movement toward forest regrowth and more efficient management of existing pasture and grassland areas. It also requires increasing amounts of land used for renewables (bioenergy, wind and solar). At the same time, even with productivity increases, the total amount of cropland must grow somewhat for food production to keep up with population and economic growth, while the significant potential for pasture productivity increases allows land for pasture to slightly decline while still meeting growing demand for products from livestock. Our results are consistent with the IPCC (2023) summary of 1.5°C scenarios that require substantial action on both land and energy.

A relevant aspect of the land use change assessment is the fact that different databases use alternative classifications of land use categories, which poses challenges in comparing specific land use types, as can be noticed by the three alternative datasets displayed in Figure 2. Major differences among the datasets are due to land use/land cover categorization and the number of land use types. Kicklighter et al. (2019) land use is based on land use transitions from Hurtt et al. (2011) from the year 1500 to the year 2100. IPCC land use areas rely on the data and approaches described in Lambin and Meyfroidt (2011), Luyssaert et al. (2014), and Erb et al. (2016).

While a consistent alignment between different land datasets remains challenging, in our modeling we combine the data from FAO (2019) and Kicklighter et al. (2019) to disaggregate total forest into natural and managed forest and to split grasslands into pastures and natural grasslands. We map land use categories from alternative databases to the categories used in the EPPA model (see Supplementary Table SA1 in the Supplemental Material) to allow a proper comparison. The total land area in Kicklighter et al. (2019) and EPPA is consistent and equals to 13.46 Gha, while IPCC reports the global ice-free area as 13 Gha. These numbers are close to the

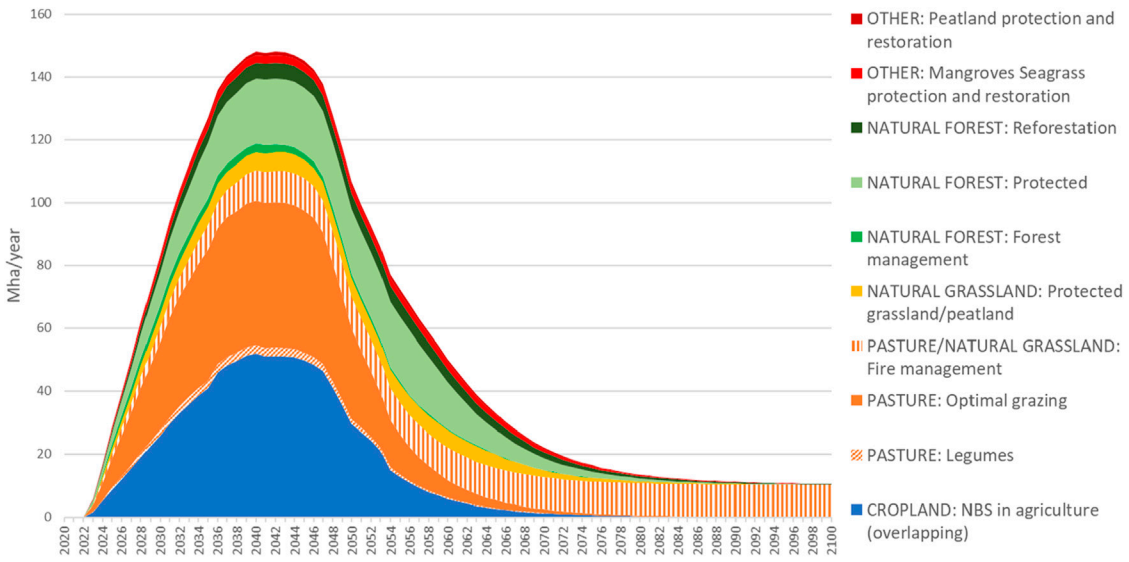

FIGURE 3
Annual increments in land areas for different categories of nature-based solutions. Source: authors calculations.

global area reported in Figure 1 (13.5 Gha), when glaciers are removed from the overall number. Overall, the general historical trends are similar in direction and relative size across most databases and in our representation.

4.2 Nature-based solutions

Under the decarbonization ambitions of a 1.5°C scenario, there is significant potential for NBS to be deployed at large scale. Figure 3 presents the required annual adoption of NBS projections in the Sky 2050 scenario. The two largest adopted options are related to agricultural areas, such as NBS in cropland (including both biochar and a broad suite of regenerative agricultural practices to reduce emissions and increase soil carbon sequestration) and optimal grazing in pasture areas, which grow fast after 2023, achieve adoption peak rates above 50 Mha per year by 2040, and saturate at the beginning of the 2070s. Natural forest protection also increases, experiencing annual maximum deployment rates of 21 Mha by 2040s and declining thereafter, ceasing completely by 2080. Fire management deployment for grasslands and savannahs expands to 10 Mha by 2040 and keeps this rate of adoption until the end of the century. While this pathway is expressed as 10 Mha/yr, it does not necessitate the enrollment of new area each year; emission reductions can be derived from reducing the intensity/severity of fires in the same area each year. Other relevant NBS practices do not achieve such large rates of adoption, but may accumulate to sizeable amounts by the end of the century, which is the case of reforestation of natural forest areas, achieving 202 Mha, and grassland protection, which covers 246 Mha.

As NBS areas increase through the end of the century, they will compete with other land uses, such as food production, bioenergy and other renewable sources. Figure 4 shows how these competing uses can fit in EPPA's projections of land requirements under 1.5°C stabilization. Adoption of NBS practices in crop production accelerates after 2030 and covers more than 60% of total cropland area by the end of the century. Bioenergy production requires 286 Mha by the end of the century, while land dedicated to solar and onshore wind generation achieves 347 Mha. Natural forest areas grow by 355 Mha from 2015 to 2100, which is larger than the 202 Mha projected reforestation areas in Sky 2050, since in the EPPA model we also represent market incentives, such as carbon offsets, in reforestation projects that leads to a larger increase in natural forest areas. Almost half of the natural forest area is explicitly convening some NBS by 2100, including forest protection and improved management, and only a very small amount is attributed to reforestation. Despite the expansion of NBS, forest protection and restoration, between 2020 and 2100 forestry products *per capita* are increased by 213%.

Cropland and forest expansion are possible due to a sharp contraction of 13% (−420 Mha) in pasture areas from 2015 to 2100, as well as some loss of natural grassland areas (−282 Mha). Such strong conversion of pasture areas is driven by increasing GHG prices on land use changes and methane-intensive livestock activities, but also due to current low productivity in grazing activities in several developing countries around the world, which makes the intensification of livestock practices relatively cheap when GHG emissions are constrained. The remaining pasture area by 2100 is still large enough to accommodate the NBS projections from Sky 2050, which covers 42% of the total pasture area. Sky 2050's projection of NBS related to cropland covers 61% of total cropland by the end of the century, and improved grazing practices are adopted by 42% of total grasslands. We allocate several NBS opportunities not directly related to major agricultural and natural land use types represented in EPPA, such as protection and restoration of peatland, mangrove, seagrass and salt marshes, on EPPA's "other" land use category, since these are quite small areas compared to other NBS options.

Focusing specifically on agriculture, NBS is projected to grow significantly. The 4.7 Gha of land dedicated to agriculture and

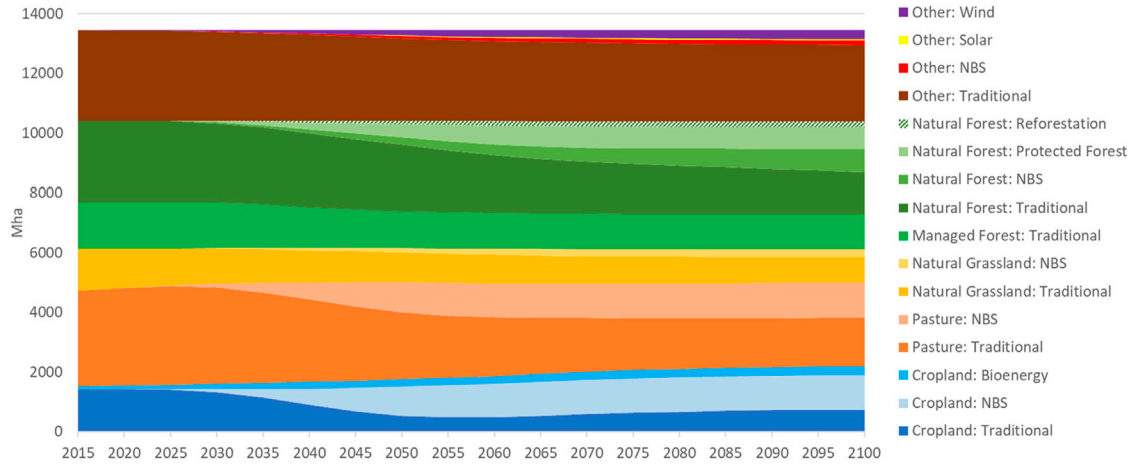

FIGURE 4
Global land use by categories. Source: Authors calculations.

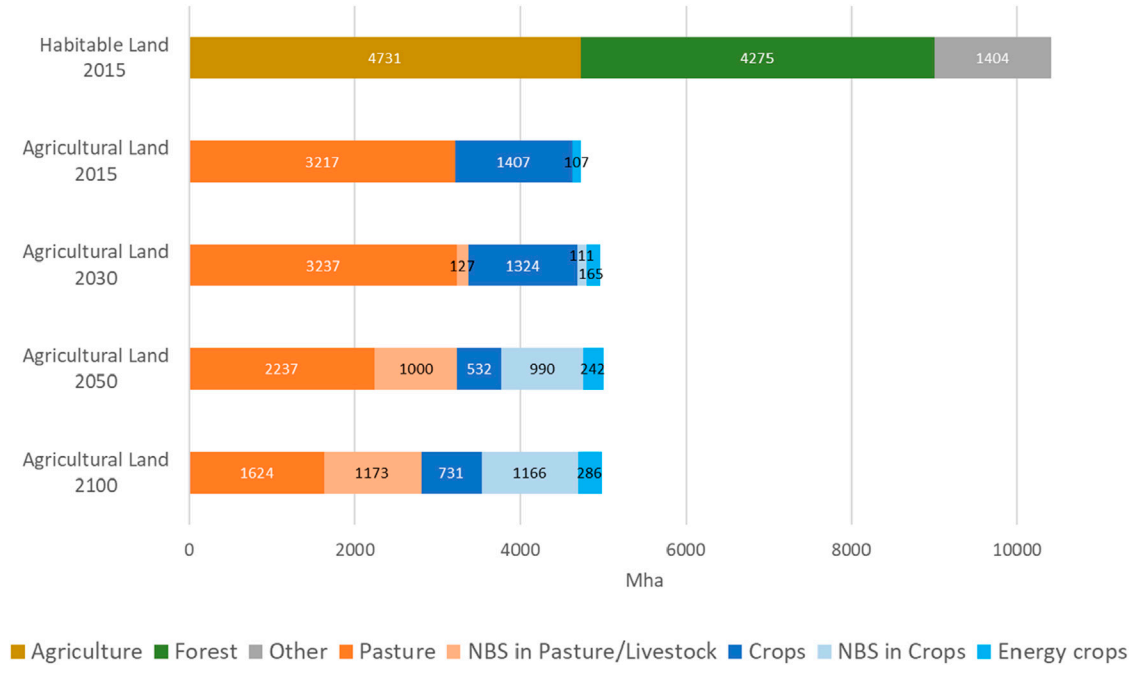

FIGURE 5
Projections for agricultural land use in the sky scenario. Source: authors calculations.

bioenergy in 2015 is projected to reach 5.0 Gha by 2030, and then stabilize throughout the period to 2100 (Figure 5), according to EPPA projections under a 1.5°C stabilization scenario. The allocation of agricultural land among different uses will be very different by 2100 from today, and will include large areas of NBS. NBS in pasture areas will grow from 127 Mha in 2030 to 1.0 Gha by 2050 and 1.2 Gha by 2100, while NBS in cropland will evolve from 111 to 990 Mha by mid-century and 1.2 Gha by 2100.

Total land managed for NBS by the end of the century is projected to be about 3.5 Gha, of which 0.77 Gha is related to forest, 1.17 Gha to cropland, 1.17 Gha to pasture, 0.26 Gha to grassland and 0.15 Gha to other land types. Globally, there is enough land in each category to accommodate the NBS projections from Sky 2050, while also ensuring growing demand for food and other land-based products is met. In particular, our results show that despite economic and population growth (MIT Joint Program, 2023) and increasing demand for food, NBS does not interfere with the provision of food, and in fact, between 2020 and 2100 the consumption of total nutrients *per capita* (based on the overall changes in agriculture and food production) are increased by 161%. Still, it is important to note again that this scenario represents an ambitious expansion of NBS, which can present challenges at the

TABLE 2 Land area (Mha) used for bioenergy, wind generation and solar generation in 2050.

Mha	Land for			Total land	Share of land for energy (%)
	Bioenergy	Wind	Solar		
United States	50.2	16.8	1.1	930	7.3
Europe	13.5	12.6	1.0	486	5.6
China	39.0	33.6	5.3	933	8.3
India	2.7	19.5	3.1	296	8.5
Brazil	16.8	2.7	0.4	855	2.3
Rest of the World	119.8	94.0	10.1	9,950	2.3
World	242.0	179.1	21.0	13,450	3.3

TABLE 3 Land area (Mha) used for bioenergy, wind generation and solar generation in 2100.

Mha	Land for			Total land	Share of land for energy (%)
	Bioenergy	Wind	Solar		
United States	58.0	26.2	2.1	930	9.3
Europe	13.5	14.5	1.0	486	6.0
China	45.4	18.3	5.6	933	7.4
India	3.4	17.2	6.8	296	9.3
Brazil	16.7	3.5	0.7	855	2.4
Rest of the World	149.3	222.9	28.3	9,950	4.0
World	286.2	302.7	44.5	13,450	4.7

regional scale (see Section 4.5). An increase in total nutrients means that supply of some specific nutrients (such as high-calories energy-yielding nutrients) will grow slower than other nutrients (such as vitamins, minerals, dietary fibers and proteins), but that the overall *per capita* needs are improving over time if a proper food distribution for healthier diets is in place, especially in developing regions of the world.

4.3 Land for energy

Table 2 shows the projected land areas used for bioenergy, onshore wind and solar power generation in 2050 for the selected regions in the Sky 2050 scenario. Table 3 provides the corresponding information for 2100. Global land area dedicated to bioenergy is projected to more than double by mid-century. It grows from about 100 Mha in 2020 (see Table 1) to 242 Mha in 2050 and 286 Mha by 2100. Dedicated biomass growing areas enable growing bioenergy consumption. The total commercial bioenergy use (i.e., including first-generation biofuels, second-generation biofuels and commercial solid biomass, but excluding traditional bioenergy used for heating and cooking) grows from about 20 EJ in 2020 to about 50 EJ in 2050, and about 70 EJ in 2100. We consider this as a conservative projection for bioenergy demand growth, because some alternative scenarios project a larger role for bioenergy with carbon capture (IPCC, 2018; Fajardy et al., 2021). In the Sky 2050 scenario, we take into account sustainability criteria preventing unintended consequences on global food security and environmental quality.

Land used for wind and solar generation grows much faster because of accelerated deployment of these sources of energy in a decarbonized world. In 2020, the global areas for wind and solar generation were 8 Mha and 0.6 Mha, respectively. By 2050, they are projected to grow to 180 Mha and 21 Mha. By the end of the century, the areas grow further to about 300 Mha for wind power and to 45 Mha for solar power. As shown in Tables 2, 3, total energy-dedicated land areas are reaching 7%–9% of the total land areas in the United States, China and India. Globally, land for energy is increasing from less than 1% of total land area in 2020, to about 3% in 2050, and to about 5% in 2100 (about 0.6 Gha). To achieve this scale of transition would require regulatory incentives from policy makers that not only bring the substantial investments needed to scale up low-carbon energy sources, but also address the social and environmental justice issues related to the associated land implications.

The amount of renewable energy in the Sky 2050 scenario is consistent with similar scenarios in other energy outlooks. For example, the International Energy Agency in its net-zero scenario (IEA, 2023) projects that in 2050 the share of wind and solar in global primary energy will be 41% and the corresponding share for

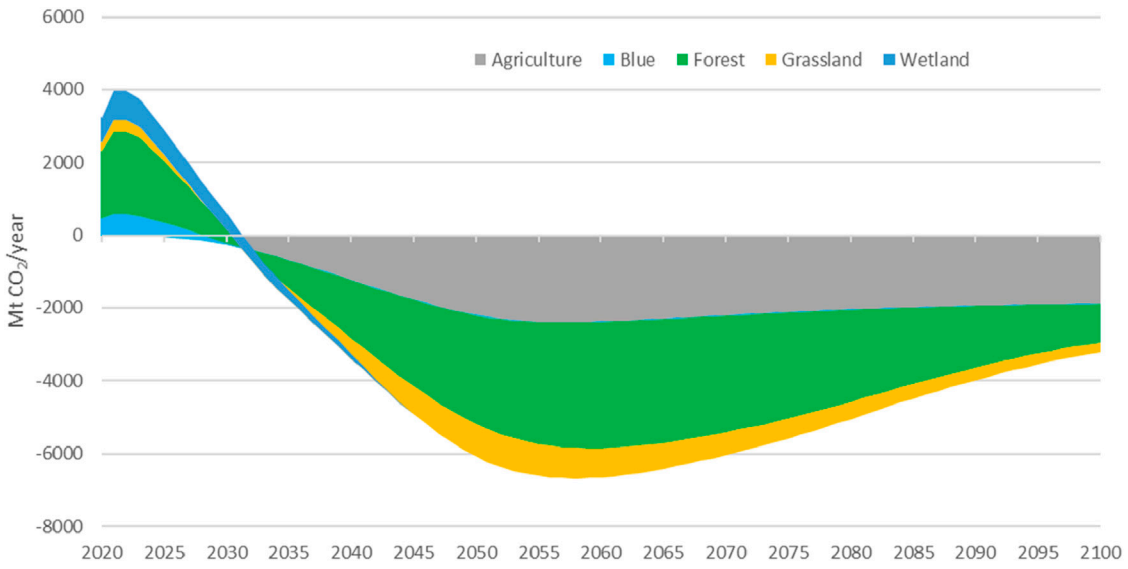

FIGURE 6
Annual carbon emissions and sequestration from different NBS types (agriculture, blue, wetland, grassland, forest). Source: authors calculations.

bioenergy is 18%. The Sky 2050 scenario is slightly more optimistic about wind and solar generation with their 2050 combined share of 43%, and slightly less optimistic about bioenergy with its share at about 10% of total primary energy. The differences in bioenergy are mostly related to different assumptions about traditional biomass and solid commercial biomass.

4.4 CO_2 sequestration

Figure 6 presents the CO_2 sequestration contributions from NBS deployed in major land use types in the Sky 2050 scenario. The correspondence between land use types and NBS categories for CO_2 sequestration is provided in Supplementary Table SA2 of the Supplemental Material. Forest NBS opportunities provide the largest contribution and can reach more than 3.7 $GtCO_2$/year by mid-century, but decline thereafter due to several reforested areas approaching or reaching a maturation age at which point the net sequestration of carbon on living biomass is small. NBS in agricultural activities is the second largest CO_2 sink and may sequester around 2 $GtCO_2$/year for several decades. NBS in Grassland contributes to sequestering at most 1 $GtCO_2$/year by mid-century.

Among the NBS options in agriculture areas (Figure 7), biochar provides the largest sequestration from a single activity and is the only one where emission reductions are continuing to increase at the end of the century. Other options, such as optimal grazing practices, legumes in pastures, regenerative arable agriculture, and agroforestry may contribute with substantial CO_2 removals at mid-century, but as carbon in soils reach a saturation level and adopted areas stabilize around equilibrium carbon stocks approaching the end of the century, their contribution to sequester additional CO_2 reduces.

For biochar, there is uncertainty in the literature about application rates, the effects of repeated application and long terms stability (e.g., Jeffery et al., 2017; Tisserant and Cherubini, 2019; Lehmann et al., 2021; Woolf et al., 2021). In our study, we assume that biochar is applied to soils or sediments and no additional impact of the biochar on plant growth or "additional" soil carbon sequestration is factored in. The biochar is applied to land at appropriate rates and in appropriate contexts to ensure negligible effects on existing carbon cycling in that site/ecosystem. It should be noted that we aim to be conservative for the overall NBS estimates and we only include pathways that have more robust scientific evidence. Some researchers are working on other pathways (such as improved aquaculture, enhanced rock weathering, permafrost protection, advanced rice management, advanced manure management and change in cattle diets, etc.), and some of these may well come to fruition. This would potentially increase our overall NBS estimates.

4.5 Regional land-use changes

Land use at the global level can accommodate the multiple demands expected under a 1.5°C climate stabilization scenario. At the regional level, however, challenges to integrate all land uses may arise. We explore such potential challenges by considering land use allocation in a set of selected major countries and regions in the world (Figure 8).

In the United States, NBS related to livestock activities occupies 88% of total available pasture land by 2100. Almost half of the other land use category is needed to accommodate other types of NBS and solar energy, while we assume onshore-wind is placed on cropland areas. In the case of Europe, the placement of wind, solar and some NBS on Other land is even more challenging, requiring 74% of it, which means a possible competition with urban and infrastructure areas. NBS in cropland and pastures also may raise concerns, since only 16% and 12% of these land categories, respectively, are not adopting some kind of NBS by 2100.

In emerging economies, we observe mixed outcomes. In China, the amount of required NBS in crops to achieve 1.5°C needs to cover the total cropland available plus most of the area dedicated to

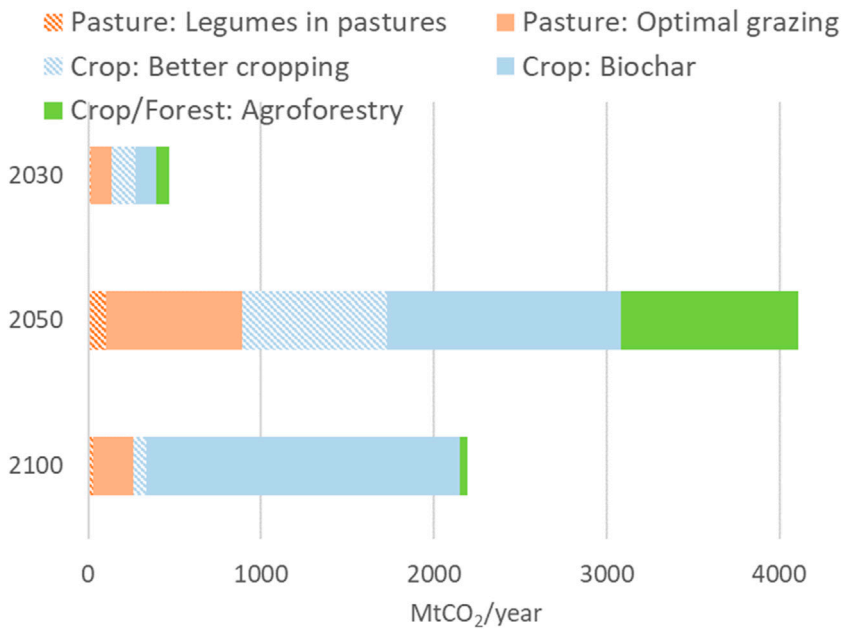

FIGURE 7
Projections for CO_2 sequestration in crops and livestock. Source: authors calculations.

bioenergy crops. India faces several land use competition issues: wind, solar and some NBS will require 80% of the Other land category by 2100, around 70% of the already limited pasture areas need to adopt some NBS, and 73% of the 150 Mha of cropland will be required to produce crops using NBS approaches.

Among the major food and bioenergy producers in the world, only Brazil seems to face moderate pressures on land use constraints due to NBS adoption in agriculture and major natural land use categories. However, the country has a very small area of the Other land use category, and the deployment of solar, wind and other NBS types will require the equivalent of 65% of this area, which poses questions about feasibility and competition with urban and infrastructure uses, which may be alleviated if wind, solar and other NBS are placed elsewhere.

Figure 9 provides a snapshot for the shares of land in a particular use in 2050 for the selected major regions and the globe. The figure shows the shares for traditional practices, land for energy, NBS, and proactive land management, such as restoration and protection. Our projections for 2050 illustrate a substantial deployment of advanced land practices, especially for NBS in cropland in Europe and India, NBS in pasture in United States, Europe, China, Brazil, and Africa, and NBS in natural forests in Brazil. At the same time, some regions still rely heavily on traditional land uses, such as pasture in China and Africa, and natural grassland and natural forests in most of the regions.

5 Discussion

Achieving the climate stabilization goal of 1.5°C by the end of the century will require transformative societal changes in policy, consumption patterns, and land management practices, including a reversal of current trends on land use changes and a reconfiguration of land cover distribution and agricultural activities. There are many opportunities to mitigate emissions and sequester carbon in soils through nature-based solutions (such as agroforestry or soil carbon sequestration), but also, many challenges to accommodate such practices in synergistic ways with food provision and renewable energy requirements. We assessed the potential competition and complementarity of land use demands among NBS practices, agricultural production and renewable energy by combining a detailed bottom-up scenario of future deployment of NBS and renewables to achieve the 1.5°C stabilization goal with a global integrated assessment model projecting the economics of land use changes and overall GHG mitigation to achieve the same climate goal.

We show that the global land system can accommodate the 3.5 Gha of NBS projected, which helps to remove about 6 $GtCO_2$/year. However, we identify several perceived trade-offs related to land use competition. First, there are concerns that NBS activities may affect agricultural output and food production. Our modelling shows that ambitious NBS deployment does not need to threaten the provision of food, with results showing a 161% increase in nutrients *per capita* between 2020 and 2100 despite the deployment of NBS. This is in line with the consensus that effective adoption of regenerative agricultural practices does not negatively impact yields, and typically increases nutrient cycling efficiencies (Van Balen et al., 2023; Tonitto et al., 2006; Allam et al., 2023).

The second potential concern is related to land required for energy production (primarily for wind, solar, and biomass) and its competition with the land for food and preserving nature. The Sky 2050 scenario was deliberately designed to limit bioenergy demand to levels well below published potential resource base estimates. We show that land for bioenergy and renewable energy takes only about 3%–5% of total land even under aggressive assumptions about solar and wind energy deployment. Another concern is related to forest

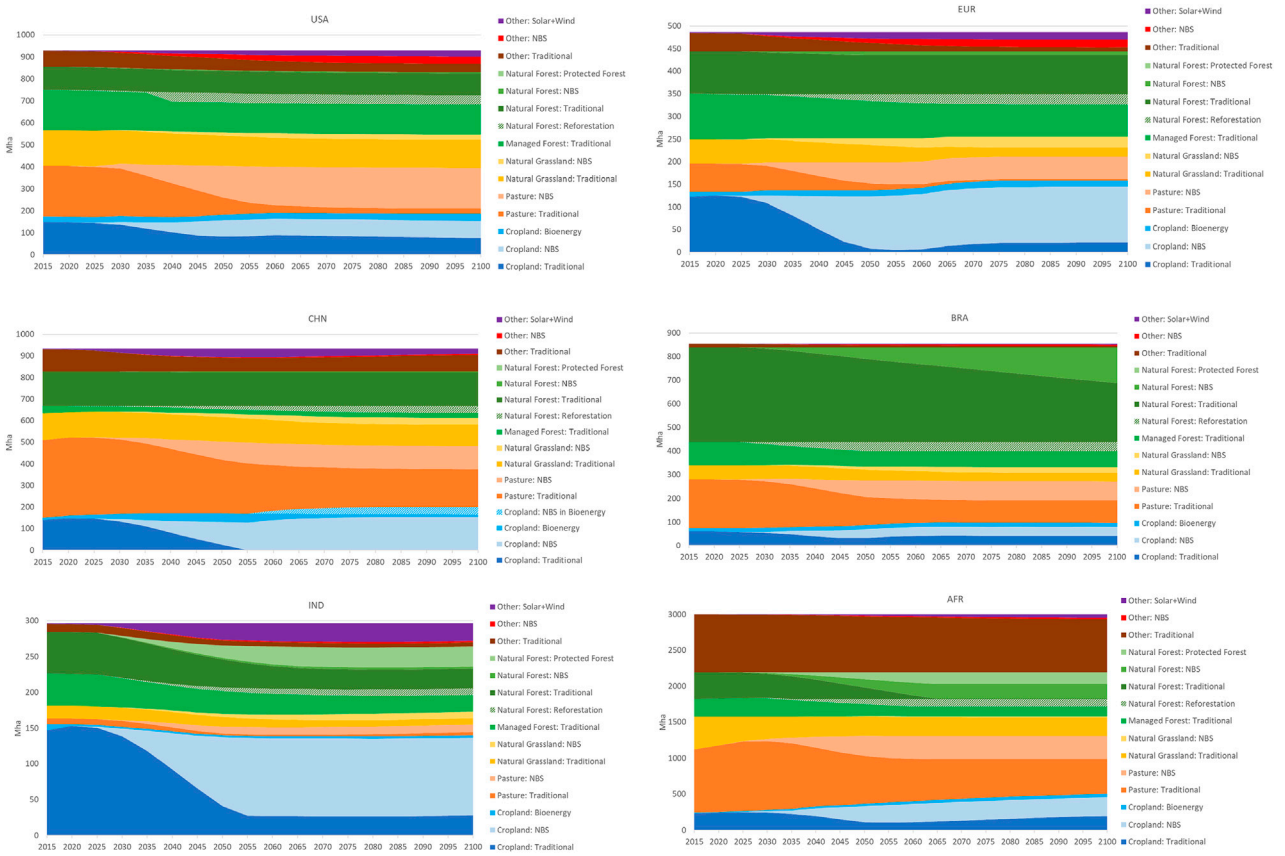

FIGURE 8
Land use evolution (2015–2100) in selected regions (United States, Europe, China, India, Brazil, Africa). Source: authors calculations.

products, in particular to the trade-offs between timber production (that can lead to such outcomes as destruction of forest cover, loss of biodiversity, soil erosion, ecological imbalance and other negative impacts) and forest protection and reforestation. Our results show that between 2020 and 2100 forestry products *per capita* are increased by 213%, while we also represent NBS, forest protection and restoration.

A trade-off with biodiversity has been gaining substantial attention recently (Environmental Defense Fund, 2024), as well as impacts on water availability (Schlosser et al., 2014; MIT Joint Program, 2023). While in our current study we do not capture the impacts on biodiversity and water, we fully support the need for further examination of the issue. A principle of the Sky 2050 scenario is that the NBS is not just optimizing for CO_2, but taking a more holistic view of appropriate ecosystem restoration, of which just one of the benefits is increasing the land stock of CO_2. However, putting the regulations in place to deliver this is far from straightforward. In particular, there is a need for systematic biodiversity indicators (Rouge and Schlosser, 2023) that would help to understand and predict the fate of global biodiversity amidst an increasingly complex and changing world. Among the objectives is the ability to construct a comprehensive metric that not only quantifies the current state of biodiversity, but also captures future trends that are driven by a variety of stressors across environmental, social, and economic systems.

In this study we focus on nature-based solutions rather than on engineering carbon capture solutions, such as bioenergy with carbon capture and storage (BECCS) or direct air CO_2 capture and storage (DACCS). An additional trade-off with engineered carbon dioxide removal (CDR) options would put additional pressure on land, however, these options should be deployed as an addition to the efforts for emission mitigation. While the cost of these engineered CDR options appears to be higher than most NBS, they could compete with NBS for land in the future, depending on how their costs evolve, the rate of carbon sequestration per ha they can achieve, demand for negative emissions and policies around using offsets, particularly international offsets.

While we share concerns (e.g., Searchinger and Heimlich, 2015; Rulli et al., 2016; Fehrenbach et al., 2023) about the urgent need for advancing sustainable approaches to land management for food and nature, our results suggest that, at global level, in the second half of the 21st century land is available to provide 3-6 $GtCO_2$/year sink through 2.5–3.5 Gha of NBS practices of protecting, managing, and restoring land, and, at same time, providing 325–650 EJ/year of renewable energy, using 0.4–0.6 Gha of land, including 0.2–0.3 Gha for bioenergy and 0.2–0.35 Gha for wind and solar power generation. Our regional exploration of land competition between different uses suggests that it is possible to fit the land for major human needs, while protecting and restoring land. These ranges of NBS deployment over time would not disturb food and primary goods production from agriculture more than the multiple

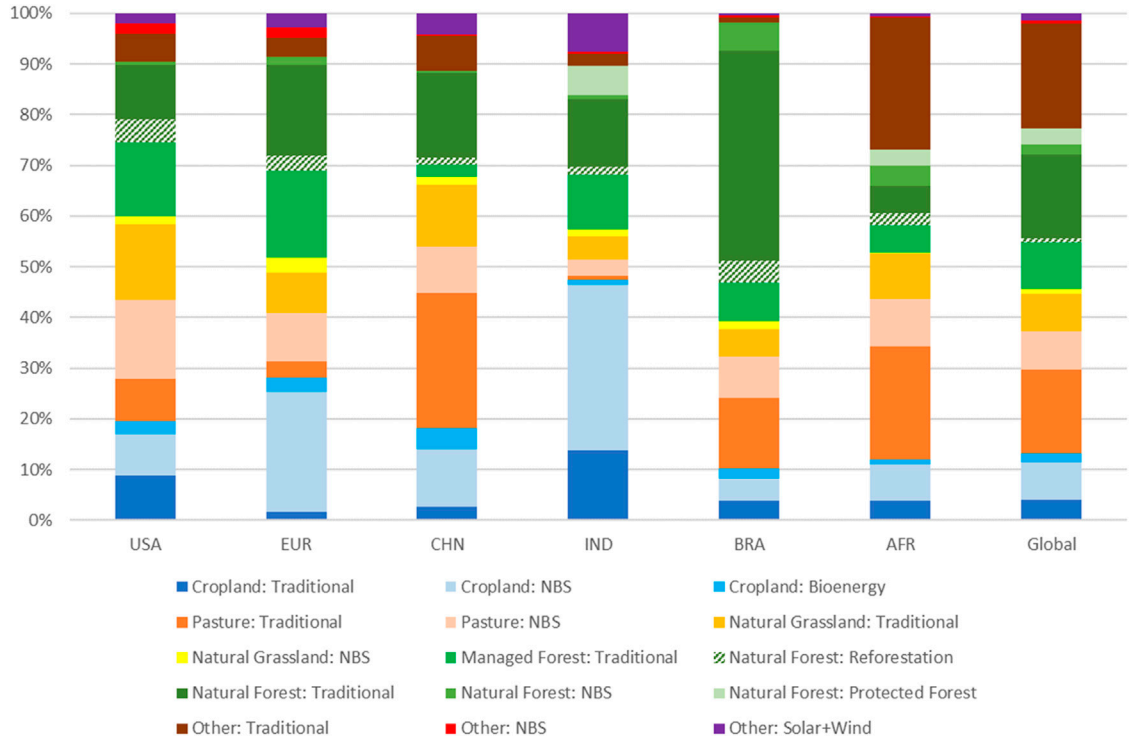

FIGURE 9
Comparison of 2050 land use shares (%) in selected regions (United States, Europe, China, India, Brazil, Africa, and The World). Source: authors calculations.

economic pressures which are associated with a 1.5°C stabilization target, such as changes in energy and good prices and impacts on income and overall demand.

However, to achieve such an outcome, NBS practices in agriculture need to be massively adopted by farmers, mostly by mid-century, and in such a way that will maintain observed trends in crop yield improvements. In the case of the livestock sector, pasture yields and productivity gains must accelerate, at the same time as NBS is adopted, in order to free up land for other uses, such as the regrowth of forest areas. Such deployment of NBS requires engagement of local communities, especially in places where the majority of land is owned by small landholders. Special attention needs to be paid to protection of indigenous communities, whose rights to the land they occupy are often not formally recognized (Waring et al., 2023). In addition to engagement and communication, adoption of NBS will likely also require incentives, which can have different implications for equity depending on how those incentives are designed.

In the face of competition for relatively limited "cheap and easy" land for various options, it will be crucial to have the right policies and incentives in place to ensure that the land is used in ways that is best for both human and environmental goals. It will be crucial to ensure that policies that encourage certain land uses (such as for carbon sequestration or energy) do not negatively impact land uses needed to meet other societal goals, such as food security to biodiversity. It is also important to understand that future competition between the different land uses critically depends on a number of factors, including economic and population growth, land productivity, crop value, and how it may be impacted by changing climate, land and technology costs, and policy design and stringency.

For NBS to contribute to achieving climate targets, policies are needed to appropriately price land use emissions/sequestration and/or require certain practices. This can be achieved by covering the land sector under an emissions policy, by creating separate offset markets for sequestered carbon, or other regulatory policies such as NBS requirements or targets for carbon removal. Regardless of the policy approach for NBS, careful monitoring, accounting and crediting of emissions is needed, which requires agreement on important questions related to permanence, additionality and leakage. We can learn from existing voluntary offset markets as well as policies being implemented in various countries.

While our analysis is intended to provide the "big picture" regarding land competition in a world that is developing in increasingly sustainable directions across both land and energy systems and as such many aspects of energy and agricultural operations are beyond the scope of our modeling (and therefore the exact numerical values should be treated with a great degree of caution), several recommendations can be offered based on our assessment. The novelty of our study is in providing a clear message that it is possible to fit the land for major human needs, while protecting and restoring land. Our study shows the feasibility of achieving the land-use optimization needed for a climate stabilization scenario. With all inherent uncertainty about the potential cost reductions for existing technologies and deployment of new regulatory and technological options, one message is clear: there is an urgent need for advancing sustainable land management for food and nature.

We also stress the crucial importance of detailed regional and local evaluations of the pathways for achieving sustainability. Government authorities and industry participants should encourage these studies and involve local and international experts. Such studies will provide a valuable framework for understanding the challenges and opportunities ahead, guiding the world toward a sustainable future.

Data availability statement

The original contributions presented in the study are included in the article/Supplementary Material, further inquiries can be directed to the corresponding author.

Author contributions

AG: Conceptualization, Formal Analysis, Investigation, Methodology, Software, Writing–original draft, Writing–review and editing. JM: Data curation, Investigation, Validation, Writing–original draft, Writing–review and editing. MH: Conceptualization, Data curation, Formal Analysis, Methodology, Validation, Writing–original draft, Writing–review and editing. AR: Data curation, Formal Analysis, Investigation, Methodology, Writing–original draft, Writing–review and editing. RP: Data curation, Investigation, Writing–original draft, Writing–review and editing. SP: Conceptualization, Data curation, Formal Analysis, Investigation, Methodology, Supervision, Writing–original draft, Writing–review and editing.

Funding

The author(s) declare that no financial support was received for the research, authorship, and/or publication of this article.

Acknowledgments

The authors gratefully acknowledge David Hone and Solene Chiquier for their valuable inputs to the analysis. Development of the EPPA-IGSM framework used in the analysis is supported by an international consortium of government, industry and foundation sponsors of the MIT Center for Sustainability Science and Strategy. For a complete list, see: https://cs3.mit.edu/sponsors/current. Whilst Shell has provided no direct financial support to this research, Shell does support the MIT Center for Sustainability Science and Strategy (formerly the MIT Joint Program on the Science and Policy of Global Change) with an annual sponsorship and occasional supplementary donations. The last supplementary donation was in 2021 to defray costs exploring issues around scenarios and land-use implications. Shell participated actively in this study, supplying the background data behind their scenarios. MIT remains responsible for all analysis and conclusions.

Conflict of interest

Author MH was employed by Shell International. Author AR was employed by Shell International Exploration and Production B. V. Author RP was employed by Shell Global Solutions International B.V.

The remaining authors declare that the research was conducted in the absence of any commercial or financial relationships that could be construed as a potential conflict of interest.

Publisher's note

Supplementary material

The Supplementary Material for this article can be found online at: https://www.frontiersin.org/articles/10.3389/fenvs.2024.1393327/full#supplementary-material

References

Allam, M., Radicetti, E., Ben Hassine, M., Jamal, A., Abideen, Z., and Mancinelli, R. (2023). A meta-analysis approach to estimate the effect of cover crops on the grain yield of succeeding cereal crops within European cropping systems. *Agriculture* 13 (9), 1714. doi:10.3390/agriculture13091714

Barros, F., Lewis, K., Robertson, A., Pennington, R. T., Hill, T., Matthews, C., et al. (2023). Cost-effective restoration for carbon sequestration across Brazil's biomes. *Sci. Total Environ.* 876, 162600. doi:10.1016/j.scitotenv.2023.162600

Bastin, J., Finegold, Y., Garcia, C., Mollicone, D., Rezende, M., Routh, D., et al. (2019). The global tree restoration potential. *Science* 365 (6448), 76–79. doi:10.1126/science.aax0848

BloombergNEF (2022). New energy Outlook. Available at: https://about.bnef.com/new-energy-outlook/.

Boysen, L., Lucht, W., and Gerten, D. (2017). Trade-offs for food production, nature conservation and climate limit the terrestrial carbon dioxide removal potential. *Glob. Change Biol.* 23 (10), 4303–4317. doi:10.1111/gcb.13745

Busch, J., Engelmann, J., Cook-Patton, S., Griscom, B., Kroeger, T., Possingham, H., et al. (2019). Potential for low-cost carbon dioxide removal through tropical reforestation. *Nat. Clim. Change* 9, 463–466. doi:10.1038/s41558-019-0485-x

Campbell, J., Lobell, D., Genova, R., and Field, C. (2008). The global potential of bioenergy on abandoned agriculture lands. *Environ. Sci. Technol.* 42, 5791–5794. doi:10.1021/es800052w

Chen, Y., Paltsev, S., Gurgel, A., Reilly, J., and Morris, J. (2022). A multisectoral dynamic model for energy, economic, and climate scenario analysis. *Low Carbon Economy* 13, 70–111. doi:10.4236/lce.2022.132005

Committee on Climate Change (2020). Land use: policies for a net zero UK. Available at: https://www.theccc.org.uk/publication/land-use-policies-for-a-net-zero-uk/.

Cook-Patton, S., Leavitt, S., Gibbs, D., Harris, N. L., Lister, K., Anderson-Teixeira, K. J., et al. (2020). Mapping carbon accumulation potential from global natural forest regrowth. *Nature* 585, 545–550. doi:10.1038/s41586-020-2686-x

Donnison, C., Holland, R. A., Hastings, A., Armstrong, L. M., Eigenbrod, F., and Taylor, G. (2020). Bioenergy with Carbon Capture and Storage (BECCS): finding the

win–wins for energy, negative emissions and ecosystem services—size matters. *GCB Bioenergy* 12 (8), 586–604. doi:10.1111/gcbb.12695

Environmental Defense Fund (2024). Natural climate solutions crediting handbook. Available at: https://www.edf.org/natural-climate-solutions/handbook.

Erb, K.-H., Lauk, C., Kastner, T., Mayer, A., Theurl, M., and Haberl, H. (2016). Exploring the biophysical option space for feeding the world without deforestation. *Nat. Commun.* 7, 11382. doi:10.1038/ncomms11382

Fajardy, M., Morris, J., Gurgel, A., Herzog, H., Mac Dowell, N., and Paltsev, S. (2021). The economics of bioenergy with carbon capture and storage (BECCS) deployment in a 1.5°C or 2°C world. *Glob. Environ. Change* 68, 102262. doi:10.1016/j.gloenvcha.2021.102262

FAO (2018). *The future of food and agriculture – alternative pathways to 2050*. Rome, Italy: Food and Agricultural Organization of the United Nations. Available at: https://www.fao.org/global-perspectives-studies/resources/detail/en/c/1157074/.

FAO (2019). Land use. Available at: https://www.fao.org/faostat/en/#data/RL.

FAO (2023). Food balances. Available at: https://www.fao.org/faostat/en/#data/FBS.

Fehrenbach, H., Burck, S., and Wehrle, A. (2023). *The carbon and food opportunity costs of biofuels in the EU27 plus UK*. Institute for Energy – Heidelberg. Available at: https://www.transportenvironment.org/wp-content/uploads/2023/03/ifeu-study-COC-biofuels-EU_for-TE-2023-03-02_clean.pdf.

Griscom, B., Adams, J., Ellis, P., Houghton, R., Lomax, G., Miteva, D. A., et al. (2017). Natural climate solutions. *Proc. Natl. Acad. Sci. U. S. A.* 114 (44), 11645–11650. doi:10.1073/pnas.1710465114

Gurgel, A., Chen, Y.-H. H., Paltsev, S., and Reilly, J. (2016). "CGE models: linking natural resources to the CGE framework," in *The WSPC reference on natural resources and environmental policy in the era of global change: v. 3 – computable general equilibrium models of society*. Editors A. Dinar, and T. Briant (New Jersey: World Scientific Publishing), 57–98.

Gurgel, A., Reilly, J., and Blanc, E. (2021). Challenges in simulating economic effects of climate change on global agricultural markets. *Clim. Change* 166, 29. doi:10.1007/s10584-021-03119-8

Hasegawa, T., Fujimori, S., Frank, S., Humpenöder, F., Bertram, C., Després, J., et al. (2021). Land-based implications of early climate actions without global net-negative emissions. *Nat. Sustain.* 4 (12), 1052–1059. doi:10.1038/s41893-021-00772-w

Hasegawa, T., Wakatsuki, H., Ju, H., Vyas, S., Nelson, G. C., Farrell, A., et al. (2022). A global dataset for the projected impacts of climate change on four major crops. *Sci. Data* 9 (1), 58. doi:10.1038/s41597-022-01150-7

Hsiang, S., Kopp, R., Jina, A., Rising, J., Delgado, M., Mohan, S., et al. (2017). Estimating economic damage from climate change in the United States. *Science* 356 (6345), 1362–1369. doi:10.1126/science.aal4369

Hurtt, G., Chini, L., Frolking, S., Betts, R., Feddema, J., Fischer, G., et al. (2011). Harmonization of land-use scenarios for the period 1500–2100: 600 years of global gridded annual land-use transitions, wood harvest, and resulting secondary lands. *Climatic Change* 109, 117. doi:10.1007/s10584-011-0153-2

IEA (International Energy Agency) (2023). World energy Outlook. Available at: https://www.iea.org/reports/world-energy-outlook-2023.

IPCC (Intergovernmental Panel on Climate Change) (2018). Special report. *Glob. Warming*. Available at: https://www.ipcc.ch/sr15/.

IPCC (Intergovernmental Panel on Climate Change) (2020). Special report. *Clim. Change Land*. Available at: https://www.ipcc.ch/srccl/.

IPCC (Intergovernmental Panel on Climate Change) (2023). AR6 synthesis report: climate change 2023. Available at: https://www.ipcc.ch/report/ar6/syr/.

Jeffery, S., Abalos, D., Prodana, M., Bastos, A., Groenigen, J., Hungate, B., et al. (2017). Biochar boosts tropical but not temperate crop yields. *Environ. Res. Lett.* 12, 053001. doi:10.1088/1748-9326/aa67bd

Kicklighter, D. W., Melillo, J. M., Monier, E., Sokolov, A. P., and Zhuang, Q. (2019). Future nitrogen availability and its effect on carbon sequestration in Northern Eurasia. *Nat. Commun.* 10 (1), 1–19. doi:10.1038/s41467-019-10944-0

Lambin, E., and Meyfroidt, P. (2011). Global land use change, economic globalization, and the looming land scarcity. *PNAS* 108 (9), 3465–3472. doi:10.1073/pnas.1100480108

Lehmann, J., Cowie, A., Masiello, C., Kammann, C., Woolf, D., Amonette, J., et al. (2021). Biochar in climate change mitigation. *Nat. Geosci.* 14, 883–892. doi:10.1038/s41561-021-00852-8

Luyssaert, S., Jammet, M., Stoy, P., Estel, S., Pongratz, J., Ceschia, E., et al. (2014). Land management and land-cover change have impacts of similar magnitude on surface temperature. *Nat. Clim. Change* 4 (5), 389–393. doi:10.1038/nclimate2196

MIT Joint Program (2023). *Glob. Change Outlook*. Available at: https://globalchange.mit.edu/news-media/jp-news-outreach/accelerated-climate-action-needed-sharply-reduce-current-risks-life-and.

Morris, J., Chen, H., Gurgel, A., Reilly, J., and Sokolov, A. (2023). Net zero emissions of greenhouse gases by 2050: achievable and at what cost?. *Clim. Change Econ.* 14 (4), 2340002. doi:10.1142/s201000782340002x

Morris, J., Gurgel, A., Mignone, B., Kheshgi, H., and Paltsev, S. (2024). Mutual reinforcement of land-based carbon dioxide removal and international emissions trading in deep decarbonization scenarios. *Nat. Commun.* 15, 7160. doi:10.1038/s41467-024-49502-8

NREL (2019). Golden, CO: National Renewable Energy Laboratory. Available at: https://www.energy.gov/sites/default/files/2019/05/f63/gagne-rule-thumb-ppt.pdf.

Paltsev, S., Reilly, J., Jacoby, H., Eckaus, R., McFarland, J., Sarofim, M., et al. (2005). The MIT emissions prediction and policy analysis (EPPA) model: version 4. MIT Joint program report 125. Available at: https://globalchange.mit.edu/publication/14578.

Rezaei, E. E., Webber, H., Asseng, S., Boote, K., Durand, J. L., Ewert, F., et al. (2023). Climate change impacts on crop yields. *Nat. Rev. Earth & Environ.* 4 (12), 831–846. doi:10.1038/s43017-023-00491-0

Ritchie, H., and Roser, M. (2013). Land use. Available at: https://ourworldindata.org/land-use.

Robertson, A., Zhang, Y., Sherrod, L., Rosenzweig, S., Ma, L., Ahuja, L., et al. (2018). Climate change impacts on yields and soil carbon in row crop dryland agriculture. *J. Environ. Qual.* 47, 684–694. doi:10.2134/jeq2017.08.0309

Roe, S., Streck, C., Beach, R., Busch, J., Chapman, M., Daioglou, V., et al. (2021). Land-based measures to mitigate climate change: potential and feasibility by country. *Glob. Change Biol.* 27 (23), 6025–6058. doi:10.1111/gcb.15873

Roe, S., Streck, C., Obersteiner, M., Frank, S., Griscom, B., Drouet, L., et al. (2019). Contribution of the land sector to a 1.5 °C world. *Nat. Clim. Change* 9 (11), 817–828. doi:10.1038/s41558-019-0591-9

Rouge, K., and Schlosser, A. (2023). *Building a composite indicator for biodiversity through supervised learning and linked indicator sets*. Cambridge, MA: MIT Joint Program on the Science and Policy of Global Change. Available at: http://globalchange.mit.edu/publication/17984.

Ruehr, S., Keenan, T. F., Williams, C., Zhou, Y., Lu, X., Bastos, A., et al. (2023). Evidence and attribution of the enhanced land carbon sink. *Nat. Rev. Earth & Environ.* 4 (8), 518–534. doi:10.1038/s43017-023-00456-3

Rulli, M., Bellomi, D., Cazzoli, A., De Carolis, G., and D'Odorico, P. (2016). The water-land-food nexus of first-generation biofuels. *Sci. Rep.* 6, 22521. doi:10.1038/srep22521

Schlosser, A., Strzepek, K., Gao, X., Fant, C., Blanc, E., Paltsev, S., et al. (2014). The future of global water stress: an integrated assessment. *Earth's Future* 2 (8), 341–361. doi:10.1002/2014EF000238

Searchinger, T., and Heimlich, R. (2015). *Avoiding bioenergy competition for food crops and land*. Washington, DC: World Resources Institute. Available at: https://www.wri.org/research/avoiding-bioenergy-competition-food-crops-and-land.

Seddon, N., Chausson, A., Berry, P., Girardin, C. A., Smith, A., and Turner, B. (2020). Understanding the value and limits of nature-based solutions to climate change and other global challenges. *Philosophical Trans. R. Soc. B* 375 (1794), 20190120. doi:10.1098/rstb.2019.0120

Seddon, N., Smith, A., Smith, P., Key, I., Chausson, A., Girardin, C., et al. (2021). Getting the message right on nature-based solutions to climate change. *Glob. Change Biol.* 27 (8), 1518–1546. doi:10.1111/gcb.15513

Shell (2023). The energy security scenarios. Available at: https://www.shell.com/energy-and-innovation/the-energy-future/scenarios/the-energy-security-scenarios.html.

Smith, P., Davis, S. J., Creutzig, F., Fuss, S., Minx, J., Gabrielle, B., et al. (2016). Biophysical and economic limits to negative CO_2 emissions. *Nat. Clim. Change* 6 (1), 42–50. doi:10.1038/nclimate2870

Sokolov, A., Kicklighter, D., Schlosser, A., Wang, C., Monier, E., Brown-Steiner, B., et al. (2018). Description and evaluation of the MIT Earth system model (MESM). *AGU J. Adv. Model. Earth Syst.* 10 (8), 1759–1789. doi:10.1029/2018ms001277

Sokolov, A., Paltsev, S., Gurgel, A., Haigh, M., Hone, D., and Morris, J. (2023) *Temperature implications of the 2023 Shell energy security scenarios: Sky 2050 and archipelagos*. Cambridge, MA: MIT Joint Program Report. Available at: http://globalchange.mit.edu/publication/17983.

Sue Wing, I., De Cian, E., and Mistry, M. N. (2021). Global vulnerability of crop yields to climate change. *J. Environ. Econ. Manag.*, 109, 102462. doi:10.1016/j.jeem.2021.102462

Tisserant, A., and Cherubini, F. (2019). Potentials, limitations, co-benefits, and trade-offs of biochar applications to soils for climate change mitigation. *Land*, 8 (12), 179. doi:10.3390/land8120179

Tonitto, C., David, M., and Drinkwater, L. (2006). Replacing bare fallows with cover crops in fertilizer-intensive cropping systems: a meta-analysis of crop yield and N dynamics. *Agric. Ecosyst. Environ.* 112 (1), 58–72. doi:10.1016/j.agee.2005.07.003

UN (United Nations) (2015). The Paris Agreement. Available at: https://unfccc.int/process-and-meetings/the-paris-agreement.

Van Balen, D., Cuperus, F., Haagsma, W., De Haan, J., Van Den Berg, W., and Sukkel, W. (2023). Crop yield response to long-term reduced tillage in a conventional and organic farming system on a sandy loam soil. *Soil Tillage Res.* 225, 105553. doi:10.1016/j.still.2022.105553

Van de Ven, D., Capellan-Peréz, I., Arto, I., Cazcarro, I., de Castro, C., Patel, P., et al. (2021). The potential land requirements and related land use change emissions of solar energy. *Sci. Rep.* 11 (1), 2907. doi:10.1038/s41598-021-82042-5

Vera, I., Wicke, B., Lamers, P., Cowie, A., Repo, A., Heukels, B., et al. (2022). Land use for bioenergy: synergies and trade-offs between sustainable development goals. *Renew. Sustain. Energy Rev.* 161, 112409. doi:10.1016/j.rser.2022.112409

Waring, B., Gurgel, A., Koberle, A., Paltsev, S., and Rogelj, J. (2023). Natural Climate Solutions must embrace multiple perspectives to ensure synergy with sustainable development. *Front. Clim.* 5, 1216175. doi:10.3389/fclim.2023.1216175

Winchester, N., and Reilly, J. (2015). The feasibility, costs, and environmental implications of large-scale biomass energy. *Energy Econ.* 51, 188–203. doi:10.1016/j.eneco.2015.06.016

Woolf, D., Lehmann, J., Ogle, S., Kishimoto-Mo, A., McConkey, B., and Baldock, B. (2021). Greenhouse gas inventory model for biochar additions to soil. *Environ. Sci. Tech.* 55, 14795–14805. doi:10.1021/acs.est.1c02425

frontiers | Frontiers in Environmental Science

TYPE Original Research
PUBLISHED 15 November 2024
DOI 10.3389/fenvs.2024.1433491

OPEN ACCESS

EDITED BY
Bao-Jie He,
Chongqing University, China

REVIEWED BY
Peter Eckersley,
Nottingham Trent University, United Kingdom
Shengqing Xu,
Jiangsu Ocean Universiity, China

*CORRESPONDENCE
Fiona Köhnke,
fiona.koehnke@hereon.de

RECEIVED 16 May 2024
ACCEPTED 31 October 2024
PUBLISHED 15 November 2024

CITATION
Köhnke F, Steuri B, Baetcke L, Borchers M, Brinkmann T, Dittmeyer R, Dornheim M, El Zohbi J, Förster J, Gawel E, Görl K, Herbst M, Heß D, Kalhori A, Korte K, Li Z, Markus T, Mengis N, Monnerie N, Oschlies A, Prats-Salvado E, Reusch TBH, Rhoden I, Sachs T, Schaller R, Schill E, Simon S, Stevenson A, Thoni T, Thrän D, Xiao M and Jacob D (2024) A storyline approach: integrating comprehensive, interdisciplinary research results to create narratives – in the context of the net-zero target in Germany. *Front. Environ. Sci.* 12:1433491. doi: 10.3389/fenvs.2024.1433491

A storyline approach: integrating comprehensive, interdisciplinary research results to create narratives – in the context of the net-zero target in Germany

Fiona Köhnke[1]*, Bettina Steuri[1], Lars Baetcke[2], Malgorzata Borchers[3], Torsten Brinkmann[4], Roland Dittmeyer[5], Martin Dornheim[6], Juliane El Zohbi[1], Johannes Förster[7], Erik Gawel[8,9], Knut Görl[1], Michael Herbst[10], Dominik Heß[5], Aram Kalhori[11], Klaas Korte[8], Zhan Li[11], Till Markus[12], Nadine Mengis[13], Nathalie Monnerie[14], Andreas Oschlies[13], Enric Prats-Salvado[14,15], Thorsten B. H. Reusch[16], Imke Rhoden[17], Torsten Sachs[11], Romina Schaller[12], Eva Schill[5,18], Sonja Simon[19], Angela Stevenson[16], Terese Thoni[7,20], Daniela Thrän[3,21], Mengzhu Xiao[19] and Daniela Jacob[1]

[1]Climate Service Center Germany (GERICS), Helmholtz-Zentrum Hereon, Hamburg, Germany, [2]Institute for Maritime Energy Systems, German Aerospace Center (DLR), Geesthacht, Germany, [3]Department of Bioenergy, Helmholtz Centre for Environmental Research - (UFZ), Leipzig, Germany, [4]Institute of Membrane Research, Helmholtz-Zentrum Hereon, Geesthacht, Germany, [5]Institute for Micro Process Engineering, Karlsruhe Institute of Technology (KIT), Karlsruhe, Germany, [6]Faculty of Engineering, University of Nottingham, Nottingham, United Kingdom, [7]Department of Environmental Politics, Helmholtz Centre for Environmental Research (UFZ), Leipzig, Germany, [8]Department of Economics, Helmholtz Centre for Environmental Research—(UFZ), Leipzig, Germany, [9]Institute of Infrastructure and Resources Management, Faculty of Economics and Business Management, Leipzig University, Leipzig, Germany, [10]Agrosphere Institute, Institute of Bio- and Geosciences (IBG-3), Forschungszentrum Jülich GmbH, Jülich, Germany, [11]Remote Sensing and Geoinformatics, GFZ German Research Centre for Geosciences, Potsdam, Germany, [12]Department of Environmental and Planning Law, Helmholtz Centre for Environmental Research (UFZ), Leipzig, Germany, [13]Biogeochemical Modelling, GEOMAR Helmholtz Centre for Ocean Research Kiel, Kiel, Germany, [14]Institute of Future Fuels, German Aerospace Center (DLR), Cologne, Germany, [15]Chair for Solar Fuel Production, RWTH Aachen University, Aachen, Germany, [16]Marine Evolutionary Ecology, GEOMAR Helmholtz Centre for Ocean Research Kiel, Kiel, Germany, [17]Institute for Energy and Climate Research – Jülich Systems Analysis (JSA/IEK-3), Forschungszentrum Jülich GmbH (FZJ), Jülich, Germany, [18]Energy Geosciences, Lawrence Berkeley National Laboratory, Berkeley, CA, United States, [19]Programm Directorate Energy, German Aerospace Center (DLR), Stuttgart, Germany, [20]Centre for Environmental and Climate Science (CEC), Lund University, Lund, Sweden, [21]Bioenergy Systems Department, Deutsches Biomasseforschungszentrum gGmbH, Leipzig, Germany

With the amendment to the German Climate Change Act in 2021, the Federal Government of Germany has set the target to become greenhouse gas neutral by 2045. Reaching this ambitious target requires multisectoral efforts, which in turn calls for interdisciplinary collaboration: the *Net-Zero-2050* project of the *Helmholtz Climate Initiative* serves as an example of successful, interdisciplinary collaboration with the aim of producing valuable recommendations for action to achieve net-zero CO_2 emissions in Germany. To this end, we applied an interdisciplinary approach to combining comprehensive research results from ten German national research centers in the context of carbon neutrality in Germany. In this paper, we present our

approach and the method behind the interdisciplinary storylines development, which enabled us to create a common framework between different carbon dioxide removal and avoidance methods and the bigger carbon neutrality context. Thus, the research findings are aggregated into narratives: the two complementary storylines focus on technologies for net-zero CO_2 emissions and on different framing conditions for implementing net-zero CO_2 measures. Moreover, we outline the *Net-Zero-2050* results emerging from the two storylines by presenting the resulting narratives in the context of carbon neutrality in Germany. Aiming at creating insights into how complementary and related expertise can be combined in teams across disciplines, we conclude with the project's lessons learned. This paper sheds light on how to facilitate cooperation between different science disciplines with the purpose of preparing joint research results that can be communicated to a specific audience. Additionally, it provides further evidence that interdisciplinary and diverse research teams are an essential factor for defining solution spaces for complex, interdisciplinary problems.

KEYWORDS

interdisciplinary research, storyline approach, net-zero, carbon dioxide removal, circular carbon approach

1 Introduction

Against the background of the urgency to act on the climate crisis and Europe's promise to achieve net-zero CO_2 emissions[1] by 2050, the project *Net-Zero-2050* was initiated in the framework of the *Helmholtz Climate Initiative*. *Net-Zero-2050* consisted of an intercultural and interdisciplinary team of 80 researchers from ten research centers within the German Helmholtz Association, the largest scientific research organization in Germany. Interdisciplinary and diverse research teams that join forces have been found to be beneficial to achieve holistic outcomes with increased scrutiny (Bates et al., 2024; Kreuter et al., 2020). The goal of the project was the integration of the extensive scientific expertise within the Helmholtz centers to carry out a comprehensive assessment of options and the development of possible recommendations for action that contribute to achieving the net-zero target in Germany. Thus, *Net-Zero-2050* generated knowledge in the context of national carbon neutrality, covering a wide range of associated research topics. The year 2050 was used as this was the target year in the German climate law at the time the project was launched. In research phase 1, which ran from July 2019 until March 2022, the project combined an overarching assessment of CO_2 reduction options, complemented by two case studies to bridge science and practice, with the assessment of options for Carbon Dioxide Removal (CDR) presented in Box 1 (Net-Zero-2050, 2022). In this context, a strong focus lay on new technologies to tackle hard-to-abate emission sectors as well as removing CO_2 from the atmosphere.

To summarize and to narrate the multi-faceted spectrum of this interdisciplinary collaboration, we used the storyline method and customized it to integrate the research results of the project. Aiming at providing a structured overview of the vast research findings, they were combined in two interlinked storylines. The choice of the storylines' focus and content was based on the expertise of the project team on the one hand and the need for scientific knowledge on the implementation possibilities of net-zero CO_2 emissions measures in Germany on the other. The specific occasion and primary purpose for creating the storylines was a main *Helmholtz Climate Initiative* conference where the interim research results were presented to high-level representatives of the German research community as well as to external stakeholders. Thus, the target group for the storylines was firstly only the scientific community. The subsequent step, which falls outside the scope of this paper, was to prepare the storylines in a format that is relevant and useable for different practitioners. One example of this is the final study of the project (Jacob et al., 2023), which used the storylines as a basis. Hence, creating these storylines also served as a test run to rehearse the later communication of the results, e.g., to policy makers.

In the literature, there is a number of examples in different research areas and sectors (e.g., education, health and policy) where the authors found that using narratives and stories can be an effective approach to communicate scientific evidence (e.g., Shanahan et al., 2018; Shaffer et al., 2018; Schlaufer et al., 2022). Jones and Anderson Crow (2017) explored the "science of stories" and argued that narratives are highly influential elements in the social realities of human beings, which is why it is beneficial to address and connect with audiences by means of gripping stories. This way of communicating can increase the importance of the issue for people as well as their connection to the topic. For these reasons and to emphasize the interdisciplinary nature of the project, we opted for developing intertwined and at the same time overarching storylines: a storyline on the framing conditions for implementing measures for net-zero CO_2 emissions "Accelerating Action" and a technology-based storyline "From Source to Sink" (see Figure 1). The scientific content of the wide-ranging *Net-Zero-2050* sub-projects was complemented with a qualitative context by means of the storylines. In this way, we could pave the way to integrate individual and often single-disciplinary sub-project results into a

1 Net-zero CO_2 emissions signifies that anthropogenic sources of CO_2 to the atmosphere are balanced by anthropogenic activities that either enhance natural carbon sinks or remove CO_2 from the atmosphere by means of different technologies.

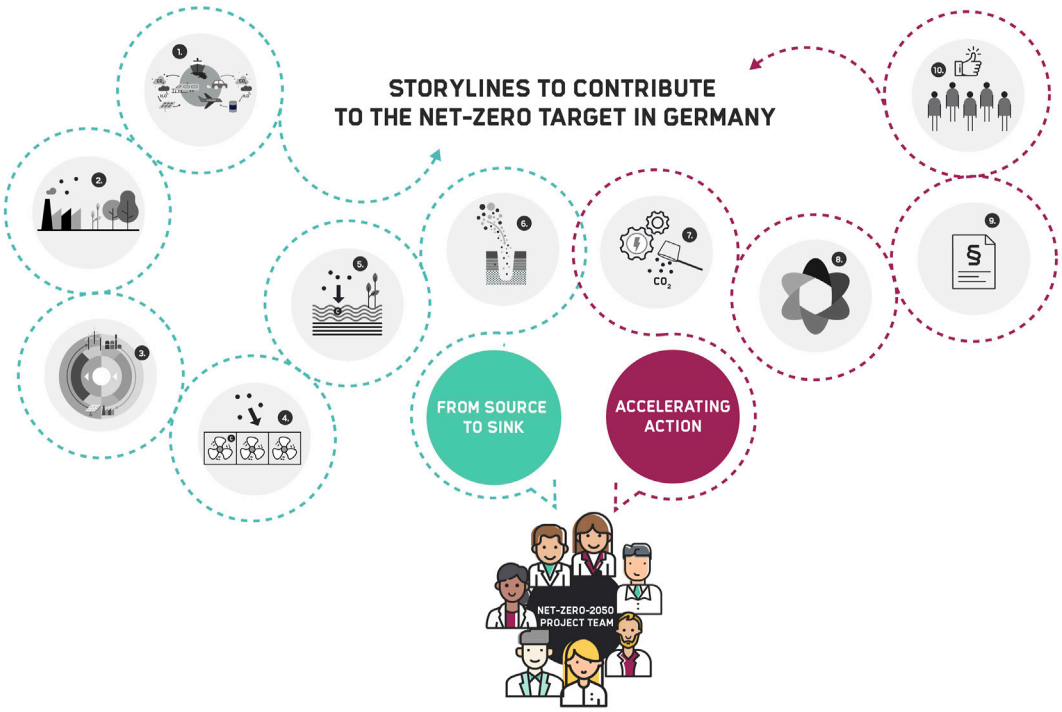

FIGURE 1
The figure visualizes the two intertwined *Net-Zero-2050* storylines that are based on the interdisciplinary, interim research results of *Net-Zero-2050* phase 1. The storyline "From Source to Sink" consists of the six central topics: 1) Conversion of CO_2 into fuels, 2) Bioenergy with carbon capture and storage (BECCS), 3) Carbon loop concept for energy storage, 4) Direct air carbon capture (DAC), 5) Biological CDR options, and 6) CO_2 distribution networks. The "Accelerating Action" storyline includes four central areas: 7) Combined CDR options and energy scenario approach, 8) Feasibility assessment of CDR options, 9) Regulatory framework for deploying CDR options, and 10) Societal acceptability of CDR deployment. (Source and copyright: Helmholtz Climate Initiative/Julia Blenn).

bigger picture and thus create an added value which results in more than the sum of its individual parts.

The present study describes the method to achieve this objective and the content of the storylines in three sections. First, the storylines methodology and key options for net-zero CO_2 emissions reduction, avoidance and removal are explained, linking them to *Net-Zero-2050*'s areas of activity (see Section 2.2). This includes a brief outline of the relevant system with which the project is linked: it considers the multiple facets of reaching net-zero from a systemic perspective as comprehensively as possible (Köhnke et al., 2023). Second, the storylines, with a focus on technological options (biological and chemical) and the framing implementation conditions, are presented as the result of the method. Third, key aspects of the working processes and the lessons learned are described to provide useful insights, success factors and recommendations for similar interdisciplinary approaches and future project phases.

2 Materials and methods

2.1 The interdisciplinary storyline approach

The storyline method is used in different contexts and is hence defined in several ways. In the context of representing uncertainty in physical aspects of climate change, Shepherd et al. (2018) explained a storyline as "a physically self-consistent unfolding of past events, or of plausible future events or pathways". Alcamo (2008) defines storylines as qualitative scenarios, which are generally narrative texts. In addition, Alcamo (2008), p. 124) states that "well-written storylines can be an understandable and interesting way of communicating information about the future, at least as compared to dry tables of numbers or confusing graphs". Hence, the focus of this method lies on a qualitative understanding of the given element and the corresponding context instead of on quantitative precision. In line with this, Shepherd et al. (2018) explain the importance of episodic information, i.e., qualitative information, for humans to grasp information and turn it into action. Difficulties to take and act on information rather occur if solely information that is outside their experience is used, i.e., quantitative, precise information. Thus, episodic information is to be included when scientifically developed storylines are used to communicate information that is tangible. Beyond this, storylines with qualitative components enable to present the findings of several different experts simultaneously (Shepherd et al., 2018). Jones and Anderson Crow (2017) illustrate in particular the necessity of a story's moral, i.e., the main piece of information that the audience learns from the story. The authors specify the existence of good morals as a prerequisite for the content to be implemented later (in this case in a policy context). The better the story is told, the more likely it is that the audience will remember the moral afterwards. In view of these characteristics and benefits, the storyline approach was selected and customized to integrate the *Net-Zero-2050* results.

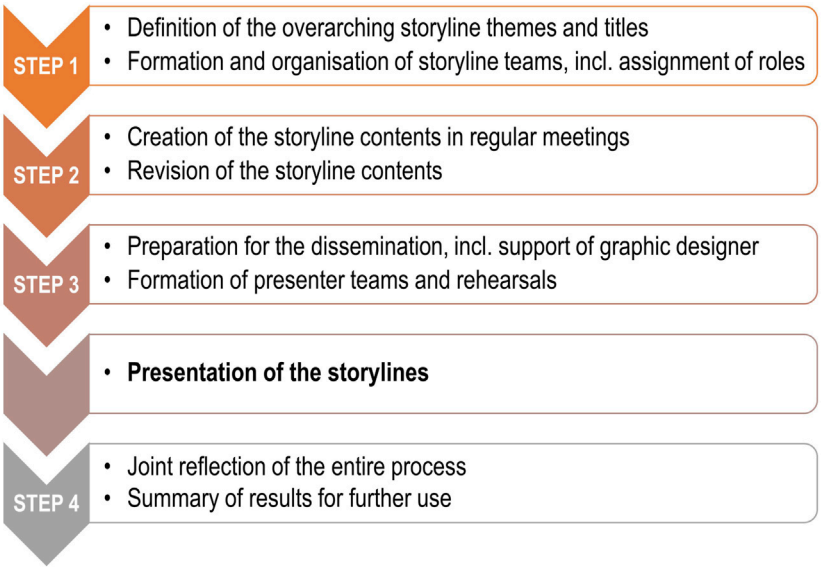

FIGURE 2
The four steps of the interdisciplinary storyline approach.

Hence, an approach was designed that was specific to the research team as well as to their findings and integrated both. The collaborative nature of this method also supported the interdisciplinary approach in the diverse team (i.e., age, gender, culture, disciplinarity). The interdisciplinarity of the *Net-Zero-2050* team was deemed important, because bringing together diverse perspectives, skills and other aspects is a key factor to successfully meet the project's research objective (Bammer, 2008). The process was therefore designed and structured in a way that offers a supportive context and that prevents participants from feeling overwhelmed or overburdened (Bates et al., 2024). We refer to our approach as 'interdisciplinary storyline approach', which we define as follows: individual elements, which are based on interdisciplinary, quantitative, and qualitative research results, have been coherently combined into storylines. The interdisciplinary storyline approach can be divided into four steps, which are described hereafter (see Figure 2).

The first step was to discuss and define the overarching storyline themes with the whole team of 80 researchers. Given the project's research areas (earth and environment, matter, key technologies, energy, information, and data science), it was jointly decided to develop two storylines: a technology-based storyline and a storyline on the framing conditions for implementing net-zero CO_2 emissions measures. Thus, two teams of about ten researchers – predominantly consisting of early-career researchers – were then formed and their collaboration organized. Among other things, this meant communicating the rules of participation and the expectations as well as jointly defining the individual tasks, responsibilities, and deadlines. In both teams, the researchers were able to enrich the respective focal points of the two storylines with content based on their skill sets and research results. Furthermore, three stewards per storyline were identified who coordinated the teams, i.e., they were responsible for schedules, the exchange with the other team, the distribution of responsibilities and for the compilation of submitted storyline contributions. Since the participating researchers were spread across Germany, the storylines were created using online tools.

In the second step, the storylines were created in regular large collaboration meetings. This step involved an idea generation process, content creation and a revision process. During the content creation, the storylines' manuscripts were constructed in an iterative fashion. A draft was created by the storyline teams, which was then adjusted and completed during and between meetings. For the revision process, each storyline was presented to and iterated with the entire consortium twice. The aim of the first revision meeting with the principal investigators was to identify and clarify the strategic cornerstones of the storylines. The purpose of the second revision meeting with the early-career researchers was to ensure that all relevant content was part of the storylines, including the storylines' key messages (morals). Subsequently to these meetings, the storylines were further adapted and refined according to the feedback from the revision.

The third step consisted of the preparation for the dissemination. The storylines were primarily used to present the research results at a conference with representatives of the research community. A graphic designer received the final presentations and ensured that the scientific content could be communicated in a visually appealing and consistent manner, establishing a brand. Additionally, presenter teams, including replacement speakers, were formed for both storylines, consisting of one person from each storyline team. These teams met with each expert of their storyline teams to guarantee that all storyline elements were communicated appropriately. As a final step, the overall presentations were rehearsed several times with a test audience, which ensured that the guiding thread of the storylines ran through the entire presentations. This was followed by the presentation at the major conference.

The fourth step was to reflect on the whole process of creating and presenting the storylines. For this purpose, a joint meeting was organized about a week after the conference. The following questions were discussed at the meeting: 1) Was the purpose of the storylines clear to all of us? 2) Were our roles and responsibilities well defined, understood and followed? 3) Did we have the tools and resources we needed to achieve our objectives? 4) Did we learn from each other? 5) What are our most important lessons learned?

The joint reflection was important because it was already clear at this point that overarching storylines should also be developed for the final conference of the research initiative. This was decided by the project management after the event, as the audience's feedback on the storylines was extremely positive. Hence, the results of the meeting were recorded in writing, made available to the entire team and used again as part of the preparations for the final conference about a year later. The exercise furthermore motivated the research team to compile a scientific publication that was to incorporate all the elements of the two storylines bringing it all together, led by two of the early-career research stewards of the exercise (Mengis et al., 2022)

2.2 Definition of the considered systems

To remove CO_2 from the atmosphere, several options have been proposed that entail either biological, chemical, or combined processes. In addition, the captured CO_2 can also be used, creating a so-called circular carbon approach where the CO_2 is eventually released back into the atmosphere. In the following, the main options that were included in the research of *Net-Zero-2050* are briefly summarized.

1) Direct air carbon capture and storage (DACCS) combines technologies that first capture CO_2 out of the ambient air through chemical processes with carbon dioxide absorbing materials. Subsequently, the CO_2 is purified, concentrated, and sequestered in geological storage sites. Quality of storage in the underground ranges from recoverable CO_2 to chemically fixed carbon over geological times in minerals (Helmholtz-Klima-Initiative, 2020; Smith et al., 2023).
2) Bioenergy with carbon capture and storage (BECCS) combines biological and chemical processes: First the natural process of photosynthesis to remove carbon from the atmosphere is used, afterwards the carbon is captured using chemical processes. If the emitted carbon dioxide is captured and then stored in geological storage sites, CO_2 is removed from the atmosphere (Borchers et al., 2022).
3) CO_2 can also be removed from the atmosphere by means of biological CO_2 removal options. This includes, *inter alia*, increasing the terrestrial or marine biological carbon sink, e.g., rewetting peatlands, restoring seagrasses or changing agricultural practices in a way that the soil carbon content is increased (Helmholtz-Klima-Initiative, 2023a; Smith et al., 2023).
4) In a circular carbon approach, CO_2 is firstly removed from the atmosphere using DAC or BECC options. In contrast to storing the CO_2, it is re-used and afterwards it re-enters the atmosphere. To use the CO_2, it is transformed with renewable energy and hydrogen to be utilized as an energy carrier or chemical feedstock. Point source carbon capture and use (CCU) is a further example for a circular carbon approach where sources of exhaust gases are used as a source of CO_2. Here, the CO_2 concentration is high compared to the concentration in the ambient air. In particular, in the process of direct air carbon capture and use (DACCU), the captured CO_2 is converted together with H2 into materials that can be used in industrial processes as substitutes for fossil carbon materials. Thereby, emissions that would have occurred are either avoided or the CO_2 is converted, with H_2 and energy input, into alternative fuels for "hard-to-abate" sectors (Helmholtz-Klima-Initiative, 2023b; Prats-Salvado et al., 2022).

3 Results and discussion

As described in the section about the method, the focus in the following two *Net-Zero-2050* storylines towards national carbon neutrality was set on providing qualitative information. These are primarily based on numerical research results as well as on qualitative findings. In addition to that, the purpose of creating two complementary storylines was to emphasize the importance of both topics: the different technologies for net-zero CO_2 emissions and the framing conditions. The project findings were thematically divided among both storyline topics to thus clearly demonstrate the importance of both topics. The framework requirements mentioned in Storyline one must be met to be able to implement the technologies mentioned in Storyline 2. The storylines as shown in the following two sections (in italics) correspond to the spoken texts of the presentations of the storylines.

3.1 Storyline 1: "Accelerating Action"

In the first storyline "Accelerating Action", the focus is set on the aim to accelerate climate action in Germany. The title and the content of the storyline were identified by the storyline teams to provide a connecting analytical framework. To link the individual project results, they were placed in a common context and thus, their relative importance and their relationship to each other could be demonstrated. This storyline focuses on specific aspects related to the framing conditions. It does not include a discussion of all related aspects because they were out of the scope of the *Net-Zero-2050* project.

In a first step, the project's system boundaries and systems approach for assessing CO_2 emissions were specified (Köhnke et al., 2023; Thrän et al., 2021). *These included the geographic limit of Germany within the European context, the time frame until 2050 and the CO_2 budget after 2021 for Germany that is in line with a 1.5°C trajectory for global mean temperature change* (Mengis et al., 2021). *The importance of considering contributions from all sectors to achieve a net-zero trajectory as well as the need to give tangible form and limitations to the CO_2 emission budget led to an interdisciplinary assessment of the system capacity on how net-zero can be achieved in Germany. In line with this, Net-Zero-2050 combined the expertise on single CO_2 removal options with*

the expertise on how actions on climate change can be accelerated in the German framework. Four central areas for urgent action were identified:

The regulatory framework for the deployment of CO_2 removal options in Germany: It is crucial to investigate and assess how the regulatory framework at international, European and national levels can hinder or support the market uptake of CDR measures and take account of the related risks and co-benefits. In Net-Zero-2050, the focus is set on investigating how CO_2 removal options are governed in the existing climate regime (Markus et al., 2021a; b) *and how regulations should be designed to enable the deployment of these options* (Markus et al., 2020). *The results included a comprehensive set of aspects that need to be addressed by legislatures. The results also indicate that the existing regulatory frame at the national and EU level is not adequately prepared to guide the deployment of CO_2 removal options* (Markus et al., 2021b; Schaller et al., 2022). *Further improvement, however, requires both sound conceptualizing and balancing measures of mitigation, CDR and adaptation* (Markus et al., 2021b).

The societal acceptability of CDR deployment: One of the project's priorities is to investigate the needs and concerns of stakeholders by involving key actors. Different engagement approaches were identified. The stakeholder activities can be assigned into three levels, i.e., 1) understand: this level is based on a one-way communication channel. We gather information from stakeholders; 2) exchange: this level is based on a two-way communication channel. At a certain point of time, the status of work within Net-Zero-2050 is discussed with stakeholders and feedback is incorporated; and 3) co-development: this level is based on a regular two-way communication channel. The exchange with stakeholders takes place several times in a row on the same topic (El Zohbi et al., 2021). *It is assumed that a potential market uptake of CDR options can be accelerated if the resistance from stakeholders can be identified in advance. The project's analysis shows that co-development can allow for acceleration of the implementation of related infrastructure by providing the possibility of addressing concerns early in the planning phase. A co-design for a comparable heat storage project that is equally subjected to the German mining law reveals major criteria for storage in the deep subsurface such as transparency, assessment of alternatives, economic viability, and groundwater and seismic monitoring. Addressing these criteria together with the public in an early planning phase has proven to accelerate the permitting process.*

Following the hypothesis that a feasibility assessment of CO_2 removal options needed to compensate for residual emissions for a net-zero target can accelerate the climate action, feasibility was assessed along six dimensions: system utility, technological, economic, institutional, environmental and societal dimension. In this context, Net-Zero-2050 has developed the Technology Assessment Framework (TAF), a new tool that is contextualized, scaled-down and comprehensive in terms of aspects covered and tailored to the national context (Förster et al., 2022). *The primary objective is to inform and catalyze a discussion with and for national policy. Furthermore, 16 CO_2 removal concepts were designed that provide promising options for carbon removal in the German context (thirteen of which have been described in* Borchers et al. 2022*). These concepts of CO_2 removal options were evaluated concerning their feasibility across the different categories of the Technology Assessment Framework* (Förster et al., 2022) *and tailored to the G. context* (Borchers et al., 2024). *This assessment accordingly brings together the expertise from the entire project to provide a comprehensive evaluation and comparison of possible CO_2 removal measures that are in addition to CO_2 emission reduction options necessary to achieve net-zero CO_2 emission in Germany.*

In addition, Net-Zero-2050 worked on a combined CO_2 removal options and energy scenario approach. It complemented the CO_2 removal options with a comprehensive outlook on the necessary emission reductions from the main CO_2 emitting sector, the energy sector, which encompasses generation, distribution, storage, infrastructure, and supply of electricity as well as heat. Here, starting from the normative target scenario "Net-Zero Germany" by 2050 under a limited total CO_2 budget, the backcasting approach identifies actions in all energy sectors (buildings, industry, transport, and energy conversion) needed to contribute on the way to reach this scenario (Harpprecht et al., 2022; Simon et al., 2022). *This quantifies on the one hand the necessary effort and investment to mitigate CO_2 emissions and the additional requirements on energy infrastructures (*Simon et al., 2022*). On the other hand, it identifies the order of magnitude of hard to abate or residual CO_2 emissions* (Harpprecht et al., 2022), *which still need to be compensated for by CO_2 removal options. Summarizing, one main finding was that the implementation of CO_2 removal options in Germany will only be successful if the energy system is drastically transformed, including the deployment of carbon neutral technologies.*

3.2 Storyline 2: "From Source to Sink"

The second *Net-Zero-2050* storyline "From Source to Sink", comprised the results obtained in the area of CO_2 mitigation approaches. This included chemical, biological and hybrid options for CO_2 capture, storage and usage as well as CO_2 mitigation approaches related to energy production, e.g., fuels synthesis with CO_2, H_2 and renewable energy (Sun-to-Liquid, 2021). The context for storyline 2 was that 1) the use of fossil carbon has to be limited to a total CO_2 budget and 2) circular carbon approaches need to be established (see Section 2.2). The broad concept of the storyline was to provide a narrative explanation from completely chemical to exclusively biological CO_2 removal options. The aim was to show where major differences and similarities exist, resulting in synergies and trade-offs in the conclusion of the storyline. In the following, the details on these priority topics that form this storyline and its conclusions are summarized (for details compare also Mengis et al., 2022).

Direct Air Capture (DAC) was investigated by Net-Zero-2050. In particular, the technology readiness level (TRL) of DAC, the energy demand and the cost of DAC technologies were assessed. In this context, it was found that there is scope for improvement in terms of energy demand especially for DAC. Hereby, the most potential for improvement lies in the scale up of the production and innovations in the sorbent material. Furthermore, Net-Zero-2050 started research on the recently developed technology electro-swing-adsorption (ESA), which is more energy-efficient compared to established Low and High-Temperature-DAC plants. Those ESA-modules offer a great variability in sizing and could potentially be employed in a wide variety of applications. Integrating DAC-technologies directly into a

heating, ventilation, and air conditioning (HVAC) system, for example, could generate synergies between the building services engineering and DAC. Additionally, unutilized areas are capitalized and small players could participate in a future carbon dioxide market, creating new business opportunities, especially if the CO_2 is then converted into valuable products like hydrocarbons. Net-Zero-2050 assumes this method – for which it has coined the term "crowd-oil" – to be a pioneering technology. Due to a relatively low concentration of CO_2 in the ambient air the DAC processes are very energy consuming. In contrast to that, CO_2 capture at concentrated point sources is less energy consuming, as the concentrations of CO_2 in the exhaust gases are higher. The point sources can be fossil-based, like coal power plants, or renewable, e.g., biogas plants (see BECCS-related section below). Newer developments such as membrane separators could increase the efficiency further.

Within the framework of Net-Zero-2050, eight technologies for Bioenergy with Carbon Capture and Storage (BECCS) have been analyzed: three pathways for biogas production with combined heat and power (CHP) generation (each based on different type of feedstock), biogas upgrading to biomethane, biomass combustion for CHP, gasification for synthetic fuels, and fast/slow pyrolysis for bio-oil/biochar production. All these options are characterized by relatively high TRL (TRL 7–9), promising their possible near-term deployment. An important attribute of BECCS is its ability to generate energy (e.g., heat, electricity, fuels), which is particularly useful in the advancing decarbonization and energy transition as it supplies the demand for flexible renewable energy sources. However, BECCS as a land-based concept, faces concerns related to its possible negative impacts on land use and biodiversity, especially when deployed on large-scales. To address these issues in Net-Zero-2050, particular attention has been given to sustainably sourced biomass, including novel approaches like paludiculture and macroalgae farming (Borchers et al., 2024).

Net-Zero-2050 includes research activities on a novel carbon loop concept for energy storage, which is based on the Power-to-X-to-Power approach. Applying this concept, two scenarios for a CO_2 neutral German power sector in 2050 were analyzed. The difference between both is that, in one case, the net electrical energy consumption is covered by a residual share of natural gas. The CO_2 that is emitted must be stored permanently in deep subsurface storage. In the other scenario, the net electrical energy consumption is provided by renewable energies. The latter system does not need storage of CO_2 that is permanent because the amount of CO_2 stored matches the amount of CO_2 extracted. However, the demand for temporary storage is higher in this scenario. All this includes the supply of hydrogen, since a large electrolyzer is integrated to supply H2 for the PtX methane production. Therefore, this system also includes hydrogen production, storage, and distribution. Also, it is possible to use this electrolyzer to supply other hydrogen consumers, which directly avoids CO_2 emissions (Fogel et al., 2022).

For the conversion of CO_2 into fuels, two basic steps were identified. First, CO_2 and H_2O must be converted into CO and H_2 respectively. Second, the mixture of these two chemicals (which is often referred to as synthesis gas) is processed into the final fuel. In the frame of the Net-Zero-2050, three pathways were analyzed for the production of synthesis gas: the solar thermochemical cycle, the PEM electrolysis with rWGS and the co-electrolysis with a SOEC. Similarly, methane, methanol and hydrocarbon mixtures produced with the Fischer-Tropsch process were considered as the three possible final fuels. The results showed that the solar thermochemical cycle was the most energetically efficient process since it can directly convert heat into fuel with a minimal electricity input (Prats-Salvado et al., 2022). *This is important because significant energy losses occur in the conversion of primary energy into electricity, which is the main energy input of the electrolysis pathways* (Dittmeyer et al., 2021).

Another focus of the Net-Zero-2050 was the integration of the fuel production with the available renewable energy infrastructure. For this reason, a decentralized unit integrated with a building was designed and modelled. For this case study, a solar thermochemical cycle was considered to produce synthesis gas and the chosen final product was Fischer-Tropsch oil containing hydrocarbons between C5 and C50. To meet the heat demand of the process, a parabolic dish that could be installed on the rooftop of a building was sized and the required area of PV panels integrated with the buildings' façade was determined for the calculated electricity needs. The results confirmed the viability of these decentralized systems and the remarkable synergies with the DAC when integrated with the buildings' HVAC system (Prats-Salvado et al., 2021).

In the research field of CO_2 distribution networks, Net-Zero-2050 analyzed a CO_2 pipeline network connecting industrial point sources in Germany to permanent and temporary CO_2 storage sites in porous aquifers. The focus is set on a CO_2 distribution network, which is cost-efficient and based on the idea of regionally clustering large industrial CO_2 sources. In particular, this implied that CO_2 pipeline costs can be reduced if regional clustering is optimized.

Three biological CO_2 removal options that contribute to achieving carbon neutrality were assessed in the Net-Zero-2050: Land use management, peatland rewetting and seagrass blue carbon. Biological CO_2 removal differs mainly from chemical and hybrid options because it does not require additional energy input. Regarding the management of agricultural soils, a modelling approach on the emission reduction potential in agricultural topsoil was used to spatially estimate how much emissions from top soils can be reduced. The most promising soil management scenario includes temporal intercropping, changing crop rotation, conversion to grassland and increasing organic fertilizer applications. Such details are made accessible to farmers and stakeholders via the Soil Carbon App developed by Net-Zero-2050 (Net-Zero-2050, 2022). *Peatlands store millennia of accumulated organic carbon, but when drained for agricultural use, these systems emit large amounts of CO_2. To avoid these emissions, drained peatlands need to be rewetted. Net-Zero-2050 quantified the annual CO_2 emissions of peatlands in northeastern Germany after rewetting* (Kalhori et al., 2024). *These vary by sites and depending on site history and water table management, the transition from CO_2 source to sink will happen sooner or later. In one of the experimental sites, CO_2 emissions initially continued after rewetting and decreased a decade after rewetting, resulting in a source-to-sink transition 16 years after rewetting* (Kalhori et al., 2024). *The other rewetted site turned to a larger CO_2 sink immediately after rewetting. Seagrasses are marine plants that have an exceptional ability to capture CO_2 that has dissolved into the oceans from the atmosphere and sequester it long term as organic carbon below ground. Net-Zero-2050 quantified the carbon stock and sequestration rates of seagrass meadows along the German Baltic Sea coast via field measurements. The organic carbon*

stock stored beneath seagrasses in the Baltic S. coast of Germany is substantial and re-emission of this stock can be prevented via the conservation of existing seagrass meadows (Stevenson et al., 2023). *Carbon dioxide removal by these habitats can be enhanced by expanding the seagrass area via restoration activities, thereby gaining negative emissions* (SeaStore, 2023).

3.3 *Net-Zero-2050* storylines summary and discussion

Summarizing storyline 1, the *Net-Zero-2050* cluster concluded that, to accelerate action in Germany, it is necessary to 1) provide an assessment of the regulatory framework for CO_2 removal options, 2) support the implementation of CO_2 removal options by considering the concerns and needs of key actors, 3) provide an impartial assessment of CO_2 reduction and removal measures that need to be taken into account to achieve net-zero by 2050.

The second storyline shows that a large number of different CO_2 avoidance, reduction and removal options are available in Germany and that each can contribute to achieving the net-zero target. This means that these approaches need to coexist in their respective applications and that a sensible combination of them is necessary. However, such a portfolio must take into account the synergies and trade-offs between the different approaches to CO_2 removal, which was addressed in Borchers et al. (2024).

The two storylines concluded with the following key statements: Developing the scientific knowledge of technologies for circular carbon approaches and decreasing the energy demand of CO_2 capture by new approaches were prioritized within *Net-Zero-2050*. By comparing and identifying CO_2 reduction and removal potentials and benefits, *Net-Zero-2050* aimed to provide knowledge to support increasing the acceptance and the successful implementation of the identified options in society. The project's analysis showed that Germany will not be able to achieve net-zero CO_2 emissions by 2050 within national borders without compensation of residual emissions (Simon et al., 2021; Simon et al., 2022; Mengis et al., 2022). For a maximum reduction, a significant expansion of renewable power capacity, including power grid and hydrogen infrastructure is necessary (Xiao et al., 2021a; Xiao et al., 2021b). It is thus also necessary to import sustainable chemical energy carriers (e.g., green hydrogen, synthetic methane or synthetic fuels). In addition, the *Net-Zero-2050* recommendations included reaching out to national and international science partners, involving stakeholders and industry partners, improving the overall impact and visibility of Helmholtz research in the climate field and helping overcome the usual institutional barriers within the science community. The storylines ended with the final message: An integrated solution is necessary, taking CO_2 out of the atmosphere, back into use and storage – sustainably.

4 Conclusion

In this paper, we have presented our approach to combine and outline the interdisciplinary *Net-Zero-2050* results from ten national research centers in two complementing storylines as contributions to achieving the net-zero target in Germany. Rather than merely communicating the pure facts, we wanted to generate knowledge by combining the results, putting them into a bigger picture and – by using a narrative explanation approach – addressing a specific target group. The interdisciplinary storyline approach enabled us to create the connection between emissions reduction, avoidance, and the implementation of different CDR methods, to create a greater context and two storylines that encompass all research results.

With our approach, we have provided further evidence that interdisciplinary and diverse research teams are an essential factor for solution-oriented collaborative research. An internal, joint discussion and reflection on the working processes revealed that the project partners considered the collaborative effort on the storylines highly successful and helpful to meet challenges unique to interdisciplinary research projects. As a result, several lessons were drawn for future collaborations. Concerning the storyline teams, the continuous support by all project partners was identified as an essential success factor. Another important factor was to assure the sufficient visibility of each contributor. In addition, the support of the graphic designer was considered advantageous for preparing outreach and improving communication, but it should have been provided right from the start. Moreover, specific communication needs of the project team must be considered, e.g., researchers from different research fields had different understandings of the same terms because the same words can be used differently in different contexts (e.g., CO_2 with a positive or negative connotation). Regarding time and human resources, the role of the stewards was very time consuming, which is why time availability should be a consideration in the role allocation process. Given that the development of storylines was not part of the *Net-Zero-2050* project proposal, we found that future proposals should ensure that adequate resources are allocated to such formats. Overall, our approach showed that 6 weeks preparation time is sufficient after having identified the purpose and target groups. Finally, the process reflection as well as reflecting on personal roles was found to be helpful.

In view of the added value of developing the interdisciplinary storylines, the knowledge transfer between experts from different entities, who rather rarely exchange and share knowledge in such detail, was considered one of the key accomplishments from this process and from working in an interdisciplinary context. Thus, the storyline development was a comprehensive learning experience in terms of capacity building and conducting interdisciplinary research and future outreach. Another special feature of the process was that many linkages between the single work packages were created. As a result, a joint identification for all researchers with the overarching project goals was created, which in turn enabled a productive collaboration. In particular, the project partners were more willing to join forces and contribute to joint products (Jacob et al., 2023; Mengis et al., 2022; Förster et al., 2022; Borchers et al., 2022 & 2024), including this paper. As a significant improvement for large projects relevant for the future project period and beyond, the storylines were also enablers of mutual continuous support by all partners. While these are useful findings, the interdisciplinary storyline approach was used once under the specific conditions. This does not ensure that it would be as effective in other research settings. To this end, the following possible challenges that research teams may face need to be considered: The development of storylines can take a considerable amount of

time, it requires commitment by the entire research team and the storyline content cannot include detailed results. Future studies on the application of the interdisciplinary storyline approach would help to further clarify the approach.

In summary, the interdisciplinary storyline approach was found to be an appropriate and innovative way to combine and present overarching topics and findings of the interdisciplinary and diverse research activities in narrative form. It supports integrating detailed in-depth studies with overarching systemic results. Moreover, this concept can also be useful in the context of diverse outreach activities and communicating scientific results to different and broader target groups. To tackle major societal challenges like climate change and the transformation of society and industry on the way to a net-zero Germany, large and interdisciplinary projects and research programs are urgently needed and we hope that our findings will be valuable in enabling and facilitating such cooperations.

Data availability statement

The original contributions presented in the study are included in the article/supplementary material, further inquiries can be directed to the corresponding author.

Author contributions

FK: Writing–original draft, Writing–review and editing. BS: Writing–original draft, Writing–review and editing. LB: Writing–original draft, Writing–review and editing. MB: Writing–original draft, Writing–review and editing. TB: Writing–original draft, Writing–review and editing. RD: Writing–original draft, Writing–review and editing. MD: Writing–original draft, Writing–review and editing. JE: Writing–original draft, Writing–review and editing. JF: Writing–original draft, Writing–review and editing. EG: Writing–original draft, Writing–review and editing. KG: Writing–original draft, Writing–review and editing. MH: Writing–original draft, Writing–review and editing. DH: Writing–original draft, Writing–review and editing. AK: Writing–original draft, Writing–review and editing. KK: Writing–original draft, Writing–review and editing. ZL: Writing–original draft, Writing–review and editing. NdM: Writing–original draft, Writing–review and editing. NtM: Writing–original draft, Writing–review and editing. AO: Writing–original draft, Writing–review and editing. EP-S: Writing–original draft, Writing–review and editing. TR: Writing–original draft, Writing–review and editing. IR: Writing–original draft, Writing–review and editing. TS: Writing–original draft, Writing–review and editing. RS: Writing–original draft, Writing–review and editing. ES: Writing–original draft, Writing–review and editing. SS: Writing–original draft, Writing–review and editing. AS: Writing–original draft, Writing–review and editing. TT: Writing–original draft, Writing–review and editing. DT: Writing–original draft, Writing–review and editing. MX: Writing–original draft, Writing–review and editing. DJ: Writing–original draft, Writing–review and editing.

Funding

The author(s) declare that financial support was received for the research, authorship, and/or publication of this article. The Helmholtz-Climate-Initiative (HI-CAM) is funded by the Helmholtz Associations Initiative and Networking Fund. The authors are responsible for the content of this publication.

Acknowledgments

We thank our project partners from German Aerospace Center (DLR), Karlsruhe Institute of Technology (KIT), Forschungszentrum Jülich, GEOMAR Helmholtz Centre for Ocean Research Kiel, Helmholtz Centre Potsdam – GFZ German Research Centre for Geosciences, Helmholtz-Zentrum Hereon and Helmholtz Centre for Environmental Research – UFZ, who provided great insight and expertise over the course of the project and in particular, for collectively working on the *Net-Zero-2050* storylines. We also thank J. Gehrke and R. Valencia Cotera for their assistance in writing the manuscript and their valuable comments.

Conflict of interest

The authors declare that the research was conducted in the absence of any commercial or financial relationships that could be construed as a potential conflict of interest.

Publisher's note

All claims expressed in this article are solely those of the authors and do not necessarily represent those of their affiliated organizations, or those of the publisher, the editors and the reviewers. Any product that may be evaluated in this article, or claim that may be made by its manufacturer, is not guaranteed or endorsed by the publisher.

References

Alcamo, J. (2008). "Chapter six the SAS approach: combining qualitative and quantitative knowledge in environmental scenarios,". *Chapter 6 of environmental futures—the practice of environmental scenario analysis*. Editor J. Alcamo (Amsterdam: Elsevier), 2, 123–150. doi:10.1016/s1574-101x(08)00406-7

Bammer, G. (2008). Enhancing research collaborations: three key management challenges. *Res. policy* 37 (5), 875–887. doi:10.1016/j.respol.2008.03.004

Bates, A. E., Davies, M. A., Stuart-Smith, R. D., Lazzari, N., Lefcheck, J. S., Ling, S. D., et al. (2024). Overcome imposter syndrome: contribute to working groups and

build strong networks. *Biol. Conserv.* 293, 110566. doi:10.1016/j.biocon.2024.110566

Borchers, M., Förster, J., Thrän, D., Beck, S., Thoni, Mengis, N., et al. (2024). A comprehensive assessment of carbon dioxide removal options for Germany. *Earth's Future* 12, e2023EF003986. doi:10.1029/2023EF003986

Borchers, M., Thrän, D., Chi, Y., Dahmen, N., Dittmeyer, R., Dolch, T., et al. (2022). Scoping carbon dioxide removal options for Germany–What is their potential contribution to Net-Zero CO2? *Front. Clim.* 4. doi:10.3389/fclim.2022.810343

Dittmeyer, R., Dahmen, N., Heß, D., Chi, Y., Monnerie, N., Prats-Salvado, E., et al. (2021). Preferred technology options for DAC and BECCS schemes based on results of assessment. Helmholtz klima initiative. Available at: https://www.helmholtz-klima.de/sites/default/files/medien/dokumente/P1.2_Delivarable_JB-08.pdf (Accessed May 02, 2024).

El Zohbi, J., Steuri, B., Ball, C., Bernitt, U., Blome, T., Born, A., et al. (2021). Stakeholder activities within the net-zero-2050 cluster in HI-cam. Available at: https://www.netto-null.org/imperia/md/assets/net_zero/dokumente/9_stakeholder_activities_final.pdf (Accessed May 02, 2024).

Fogel, S., Yeates, C., Unger, S., Rodriguez-Garcia, G., Baetcke, L., Dornheim, M., et al. (2022). SNG based energy storage systems with subsurface CO2 storage. *Energy Adv.* 1, 402–421. doi:10.1039/d1ya00035g

Förster, J., Beck, S., Borchers, M., Gawel, E., Korte, K., Markus, T., et al. (2022). Framework for assessing the feasibility of carbon dioxide removal options within the national context of Germany. *Front. Clim.* 4, 758628. doi:10.3389/fclim.2022.758628

Harpprecht, C., Naegler, T., Steubing, B., Tukker, A., and Simon, S. (2022). Decarbonization scenarios for the iron and steel industry in context of a sectoral carbon budget: Germany as a case study. *J. Clean. Prod.* 380 (2), 134846. doi:10.1016/j.jclepro.2022.134846

Helmholtz-Klima-Initiative (2020). Factsheet No. 4 direct air capture. Available at: https://www.helmholtz-klima.de/sites/default/files/medien/dokumente/factsheet_direct-air-capture_dina4_de_screen.pdf (Accessed May 02, 2024).

Helmholtz-Klima-Initiative (2023a). Factsheet No. 10 moore. Available at: https://www.helmholtz-klima.de/sites/default/files/medien/dokumente/factsheet_feuchtgebiete_moore_dina4_de_screen.pdf (Accessed May 02, 2024).

Helmholtz-Klima-Initiative (2023b). Factsheet No. 13 kohlenstoffdioxid. Available at: https://www.helmholtz-klima.de/sites/default/files/medien/dokumente/factsheet_kohlendioxid_dina4_de_screen.pdf (Accessed May 02, 2024).

Jacob, D., El Zohbi, J., Köhnke, F., Abetz, V., Baetcke, L., Ball, C., et al. (2023). Netto-Null-2050 Wegweiser - Strategische Handlungsempfehlungen und mögliche Wege für ein CO2-neutrales Deutschland bis 2050. Available at: https://www.netto-null.org/cms61/Projektergebnisse/Reports/order/index.php.de (Accessed May 02, 2024).

Jones, M. D., and Anderson Crow, D. (2017). How can we use the 'science of stories' to produce persuasive scientific stories? *Palgrave Commun.* 3 (1), 1–9. doi:10.1057/s41599-017-0047-7

Kalhori, A., Wille, C., Gottschalk, P., Li, Z., Hashemi, J., Kemper, K., et al. (2024). Temporally dynamic carbon dioxide and methane emission factors for rewetted peatlands. *Commun. Earth Environ.* 5, 62. doi:10.1038/s43247-024-01226-9

Köhnke, F., Steuri, B., El Zohbi, J., Görl, K., Borchers, M., Förster, J., et al. (2023). On the path to net-zero: establishing a multi-level system to support the complex endeavor of reaching national carbon neutrality. *Front. Clim.* 5. doi:10.3389/fclim.2023.1056023

Kreuter, J., Matzner, N., Baatz, C., Keller, D. P., Markus, T., Wittstock, F., et al. (2020). Unveiling assumptions through interdisciplinary scrutiny: observations from the German priority program on climate engineering (SPP 1689). *Clim. Change* 162, 57–66. doi:10.1007/s10584-020-02777-4

Markus, T., Schaller, R., Gawel, E., and Korte, K. (2021a). Negativemissionstechnologien als neues Instrument der Klimapolitik. Charakteristiken und klimapolitische Hintergründe. *Nat. Recht* 43 (2), 90–99. doi:10.1007/s10357-021-3804-8

Markus, T., Schaller, R., Gawel, E., and Korte, K. (2021b). Negativemissionstechnologien und ihre Verortung im Regelsystem internationaler Klimapolitik. *Nat. Recht* 43 (3), 153–158. doi:10.1007/s10357-020-3755-5

Markus, T., Schaller, R., Korte, K., and Gawel, E. (2020). Zum regulatorischen Rahmen direkter Abscheidung von Kohlendioxid aus der Luft (Direct air capture – DAC). Projekt 2 | M-P2.1: Rechtliche und ökonomische Anforderungen im europäischen und deutschen Recht Helmholtz-Klima-Initiative (HI-CAM). Available at: https://www.netto-null.org/imperia/md/assets/net_zero/dokumente/2020_netto-null-2050_deliverable_m-p2.1_web.pdf (Accessed May 02, 2024).

Mengis, N., Kalhori, A., Simon, S., Harpprecht, C., Baetcke, L., Prats-Salvado, E., et al. (2022). Net-zero CO2 Germany—a retrospect from the year 2050. *Earth's Future* 10 (2). doi:10.1029/2021EF002324

Mengis, N., Simon, S., Thoni, T., Stevenson, A., Görl, K., Steuri, B., et al. (2021). Defining the German carbon budget. Available at: https://www.netto-null.org/imperia/md/assets/net_zero/dokumente/2_carbonbudget_2021_10_web.pdf (Accessed May 02, 2024).

Net-Zero-2050 (2022). About net-zero-2050. Available at: https://netto-null.org/about_us/index.php.en (Accessed May 02, 2024).

Prats-Salvado, E., Monnerie, N., and Roeb, M. (2022). *Project briefing #10: solar thermochemical cycles*. Helmholtz Klima Initiative. Available at: https://www.netto-null.org/imperia/md/assets/net_zero/dokumente/netto-null_tcc_project_briefing_enric_prats_et_al.pdf (Accessed May 02, 2024).

Prats-Salvado, E., Monnerie, N., and Sattler, C. (2021). Synergies between direct air capture technologies and solar thermochemical cycles in the production of methanol. *Energies* 14 (16), 4818. doi:10.3390/en14164818

Schaller, R., Markus, T., Korte, K., and Gawel, E. (2022). Atmospheric CO2 as a resource for renewable energy production: a European energy law appraisal of direct air capture fuels. *RECIEL* 31, 258–267. doi:10.1111/reel.12434

Schlaufer, C., Kuenzler, J., Jones, M. D., and Shanahan, E. A. (2022). The narrative policy framework: a traveler's guide to policy stories. *Polit. Vierteljahr.* 63, 249–273. doi:10.1007/s11615-022-00379-6

SeaStore (2023). Seegras für den Klimaschutz - Seegraswiesen-Forschungsprojekt. Available at: https://www.seegraswiesen.de/en/(Accessed May 02, 2024).

Shaffer, V. A., Focella, E. S., Hathaway, A., Scherer, L. D., and Zikmund-Fisher, B. J. (2018). On the usefulness of narratives: an interdisciplinary review and theoretical model. *Ann. Behav. Med.* 52 (5), 429–442. doi:10.1093/abm/kax008

Shanahan, E. A., Jones, M. D., Mcbeth, M. K., and Radaelli, C. M. (2018). "The narrative policy framework," in *Routledge eBooks*, 173–213. doi:10.4324/9780429494284-6

Shepherd, T. G., Boyd, E., Calel, R. A., Chapman, S. C., Dessai, S., Dima-West, I. M., et al. (2018). Storylines: an alternative approach to representing uncertainty in physical aspects of climate change. *Clim. Change* 151, 555–571. doi:10.1007/s10584-018-2317-9

Simon, S., Xiao, M., Harpprecht, C., Sasanpour, S., Gardian, H., and Pregger, T. (2022). A pathway for the German energy sector compatible with a 1.5 °C carbon budget. *Sustainability* 14 (2), 1025. doi:10.3390/su14021025

Simon, S., Xiao, M., Pregger, T., Harpprecht, C., Gardian, H., and Sasanpour, S. (2021). Energy scenario for net-zero-2050 in Germany. Net. *Zero-2050 Web Atlas*. Available at: https://atlas.netto-null.org/contribution/92 (Accessed May 02, 2024).

Smith, S. M., Geden, O., Nemet, G., Gidden, M., Lamb, W. F., Powis, C., et al. (2023). The state of carbon dioxide removal - 1st edition. The state of carbon dioxide removal. doi:10.17605/OSF.IO/W3B4Z

Stevenson, A., Ó Corcora, T. C., Hukriede, W., Schubert, P. R., and Reusch, T. B. H. (2023). Substantial seagrass blue carbon pools in the southwestern Baltic Sea include relics of terrestrial peatlands. *Front. Mar. Sci.* 10. doi:10.3389/fmars.2023.1266663

Sun-to-Liquid (2021). Available at: www.sun-to-liquid.eu (Accessed May 02, 2024).

Thrän, D., Mengis, N., Mayer, M., Steuri, B., Oschlies, A., Simon, S., et al. (2021). Project briefing #1. *Struct. Proj. 1 within Clust.* | *Net-Zero-2050*. Available at: https://www.netto-null.org/imperia/md/assets/net_zero/dokumente/1_p1-structure_2021_10_web.pdf (Accessed May 02, 2024).

Xiao, M., Gardian, H., Pregger, T., Sasanpour, S., Simon, S., and Harpprecht, C. (2021a). Necessary expansion of the power grid for a CO2-neutral Germany. *Net-Zero-2050 Web-Atlas*. Available at: https://atlas.netto-null.org/contribution/84 (Accessed May 02, 2024).

Xiao, M., Gardian, H., Pregger, T., Sasanpour, S., Simon, S., and Harpprecht, C. (2021b). Hydrogen and synthetic methane infrastructure in net-zero-2050. *Net-Zero-2050 Web-Atlas*. Available at: https://atlas.netto-null.org/contribution/109 (Accessed May 02, 2024).

Frontiers in Environmental Science

Explores the anthropogenic impact on our natural world

An innovative journal that advances knowledge of the natural world and its intersections with human society. It supports the formulation of policies that lead to a more inhabitable and sustainable world.

Discover the latest Research Topics

See more →

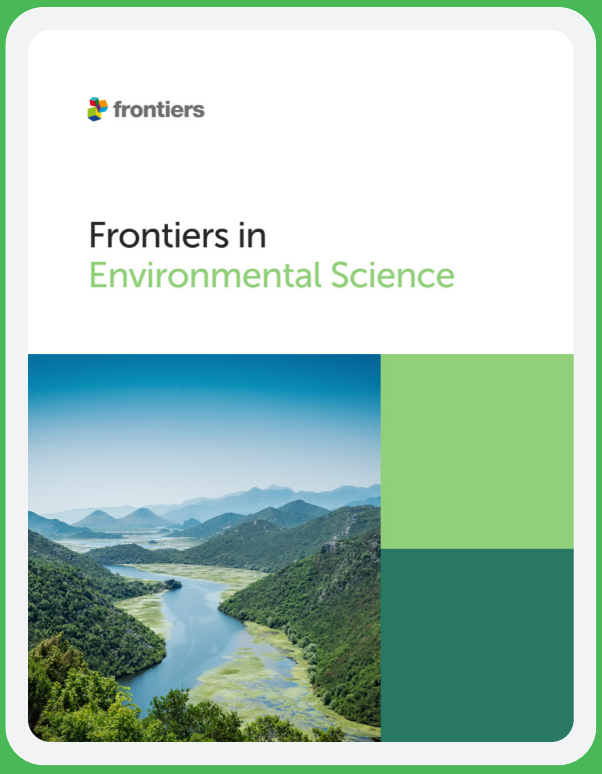

Frontiers

Avenue du Tribunal-Fédéral 34
1005 Lausanne, Switzerland
frontiersin.org

Contact us

+41 (0)21 510 17 00
frontiersin.org/about/contact